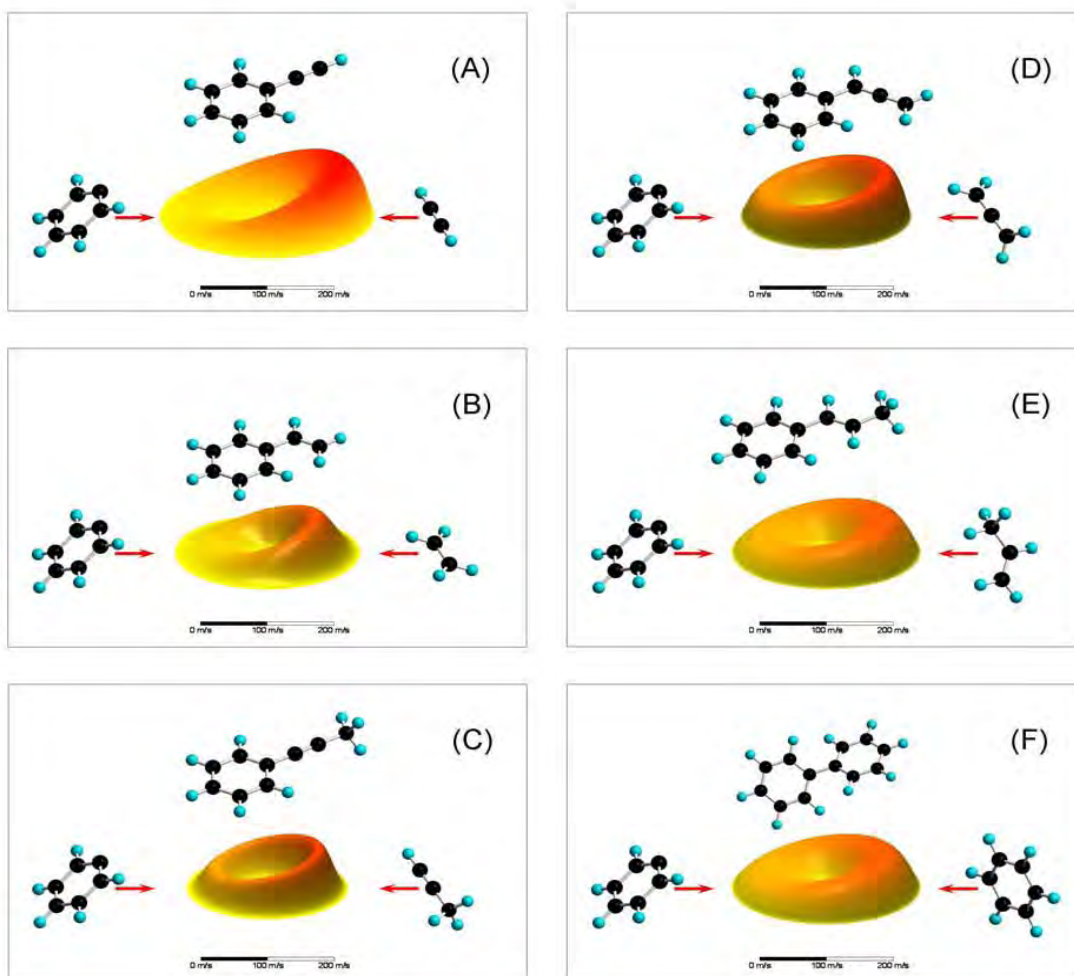


30th Annual Combustion Research Meeting

Airlie Conference Center
Warrenton, Virginia
May 26 – May 29, 2009



U.S. DEPARTMENT OF
ENERGY

Office of Science, Office of Basic Energy Sciences
Chemical Sciences, Geosciences & Biosciences Division

30th Annual Combustion Research Meeting

DOE Contractors' Meeting Program and Abstracts

Airlie Conference Center
Warrenton, Virginia
May 26 – May 29, 2009

Chemical Sciences, Geosciences, and Biosciences Division
Office of Basic Energy Sciences
Office of Science
U.S. Department of Energy

Cover Graphics:

Selected center-of-mass velocity contour flux maps for the reaction of phenyl radicals (left; 0°) with acetylene (A), ethylene (B), methylacetylene (C), allene (D), propylene (E), and D6-benzene (F) to form phenylacetylene (A), styrene (B), 1-phenylmethylacetylene (C), phenylallene (D), 1,- and 3-phenylpropylene (E), and diphenyl (F) (right; 180°). The colors connect data points with an identical flux and range from red (highest flux) to yellow (lowest flux). The units of axis are given in ms^{-1} .

Adapted from X. Gu, R.I. Kaiser, *Reaction Dynamics of Phenyl Radicals in Extreme Environments - A Crossed Molecular Beam Study*. Acc. Chem. Res. 42, 290-302 (2009).

This document was produced under contract number DE-AC05-06OR23100 between the U.S. Department of Energy and Oak Ridge Associated Universities.

The research grants and contracts described in this document are supported by the U.S. DOE Office of Science, Office of Basic Energy Sciences, Chemical Sciences, Geosciences and Biosciences Division.

Foreword

This abstract booklet provides a record of the thirtieth U.S. Department of Energy contractors' meeting focused on gas-phase chemical physics. The reports appearing in this volume present work in progress in basic research contributing to the development of a predictive capability for combustion processes. The work reported herein is supported by the Department of Energy's Office of Basic Energy Sciences (BES) and, in large measure, by the chemical physics program. The long-term objective of this effort is the provision of theories, data, and procedures to enable the development of reliable computational models of combustion processes, systems, and devices.

The objective of this meeting is to provide a fruitful environment in which researchers with common interests will present and exchange information about their activities, will build collaborations among research groups with mutually reinforcing strengths, will identify needs of the research community, and will uncover opportunities for future research directions. The agenda consists of an invited keynote talk, oral presentations by program PIs and for the first time invited poster presentations from junior level researchers in an effort to increase the awareness of the Gas Phase Chemical Physics program. Approximately one third of the PIs in the program speak each year in rotation. With ample time for discussion and interactions, we emphasize that this is an informal meeting for exchange of information and building of collaborations; it is not a review of researchers' achievements or a forum to define the future direction of the program.

We appreciate the privilege of serving in the management of this research program. In carrying out these tasks, we learn from the achievements and share the excitement of the research of the many sponsored scientists and students whose work is summarized in the abstracts published on the following pages.

We thank all of the researchers whose dedication and innovation have advanced DOE BES research and made this meeting possible and productive. We hope that this conference will help you will build on your successes and we look forward to our assembly next year for our 31st annual meeting.

We thank Diane Marceau of the Chemical Sciences, Geosciences and Biosciences Division, and Margaret Lyday and Connie Lansdon of the Oak Ridge Institute for Science and Education for their important contributions to the technical and logistical features of this meeting.

Michael Casassa
Larry A. Rahn
Wade Sisk

Agenda

30th Annual Combustion Research Meeting
U.S. Department of Energy
Office of Basic Energy Sciences

Agenda

Tuesday, May 26, 2009

3:00 pm *Registration*
5:00 pm *No-host Reception at The Whistling Swan Pub*
7:00 pm *Dinner*

Wednesday, May 27, 2009

7:00 am *Breakfast*

Session I
George Flynn, Chair

8:00 am Welcome and Introduction, Eric Rohlfing, Michael Casassa, Wade Sisk

8:30 am “*Kinetics of Roaming Radical Reactions,*”
Stephen J. Klippenstein.....139

9:00 am “*Theoretical studies of chemical reactions related to the formation and growth*
of polycyclic aromatic hydrocarbons,”
Alexander Mebel.....167

9:30 am “*Mechanism and Detailed Modeling of Soot Formation,*”
Michael Frenklach.....79

10:00 am *Break*

Session II
Floyd Davis, Chair

10:30 am “*Vibrationally Mediated Photodissociation Dynamics of Phenol and Phenol*
Complexes,” F. Fleming Crim.....51

11:00 am “*Non-Born–Oppenheimer Molecular Dynamics and Theoretical Kinetics,*”
Ahren Jasper.....119

11:30 am “*Dynamical Analysis of Highly Excited Molecular Spectra,*”
Michael E. Kellman.....127

12:00 pm *Lunch*

Session III
Anna Krylov, Chair

4:00 pm “*Theoretical Studies of Molecular Systems,*”
William A. Lester Jr.....155

4:30 pm “*Toward the exact solutions of the Schrödinger equations for polyatomic molecules,*” So Hirata.....115

5:00 pm “*New Single- and Multi-Reference Coupled-Cluster Methods for High Accuracy Calculations of Ground and Excited States,*”
Piotr Piecuch.....227

5:30 pm *Reception*

6:00 pm *Dinner*

Session IV
Branko Ruscic, Chair

7:00 pm “*Chemical Kinetic Data Base for Combustion Modeling,*” Wing Tsang.....293

7:30 pm “*Ultrafast Structural Dynamics as seen through Rydberg Electrons,*”
Peter M. Weber.....297

8:00 pm “*Threshold Photoelectron Photoion Coincidence (TPEPICO) Studies: The Road to ± 0.1 kJ/mol Thermochemistry,*” Tomas Baer.....15

Thursday, May 28, 2009

7:00 am *Breakfast*

Session V
Hope Michelsen, Chair

8:00 am **Keynote Speaker** “*Combustion Chemistry Diagnostics,*”
Katharina Kohse-Hoinghaus, Universität Bielefeld.....1

9:00 am “*Spectroscopy and Kinetics of Combustion Gases at High Temperatures,*”
Ronald K. Hanson.....99

9:30 am	<i>“Quantitative Imaging Diagnostics for Reacting Flows,”</i> Jonathan H. Frank.....	75
10:00 am	<i>Break</i>	
	Session VI <i>Timothy Zwier, Chair</i>	
10:30 am	<i>“Gas-Phase Molecular Dynamics: Theoretical Studies in Spectroscopy and Chemical Dynamics,”</i> James Muckerman.....	191
11:00 am	<i>“Spectroscopic Investigations of Reactive Organic Peroxy Radicals,”</i> Terry A. Miller.....	183
11:30 am	<i>“Gas-Phase Molecular Dynamics: High Resolution Spectroscopy and Collision Dynamics of Transient Species,”</i> Gregory E. Hall.....	91
12:00 pm	<i>Lunch</i>	
	Session VII <i>Stephen Leone, Chair</i>	
4:00 pm	<i>“Flame Chemistry and Diagnostics,”</i> Nils Hansen.....	95
4:30 pm	<i>“Probing Flame Chemistry with MBMS, Theory, and Modeling,”</i> Phillip R. Westmoreland.....	301
5:00 pm	<i>“Reacting Flow Modeling with Detailed Chemical Kinetics,”</i> Habib N. Najm.....	199
5:30 pm	<i>“Combustion Chemistry,”</i> Nancy Brown.....	27
6:00 pm	<i>Poster Session/Reception</i>	
7:30 pm	<i>Dinner at the Pavilion</i>	

Friday, May 30, 2009

7:00 am

Breakfast

Session VIII

Hua-Gen Yu, Chair

8:00 am

“Photoinitiated Reactions of Radicals and Diradicals in Molecular Beams,”
Hanna Reisler.....243

8:30 am

“Universal and State Resolved Imaging of Chemical Reaction Dynamics,”
Arthur G. Suits.....273

9:00 am

*“Probing the Reaction Dynamics of Hydrogen-Deficient Hydrocarbon
Molecules and Radical Intermediates via Crossed Molecular Beams,”*
Ralf Kaiser.....123

9:30 am

Break

Session IX

David Perry, Chair

10:00 am

“Kinetics of Combustion-Related Processes at High Temperatures,”
John H. Kiefer.....135

10:30 am

“Dynamics of Activated Molecules,” Amy S. Mullin.....195

11:00 am

“Vibronic Interactions in Autoionization and Dissociative Recombination,”
Stephen Pratt.....239

11:30 am

Closing Remarks

12:00 pm

Lunch

Table of Contents

Table of Contents

Foreword	iii
Agenda	v
Table of Contents	ix
Abstracts	1
<u>Invited Presentations</u>	
Katharina Kohse-Hoeinghaus - Combustion Chemistry Diagnostics.....	1
Spiridoula Matsika - Two- and Three-State Conical Intersections in Molecular Systems.....	3
Matt Oehlschlaeger - Ignition of Jet Fuel Relevant Hydrocarbons at Engine Conditions.....	5
Edward F. Valeev - Practical Explicitly Correlated Many-Body Methods.....	9
Angela Violi- Multiscale Simulations of Nanoparticle Formation in High Temperature Conditions.....	11
J. Mathias Weber - Vibrational Autodetachment - A New Experimental Approach to Intramolecular Vibrational Relaxation.....	13
<u>Principal Investigator Presentations</u>	
Tomas Baer - Threshold Photoelectron Photoion Coincidence (TPEPICO) Studies: The Road to ± 0.1 kJ/mol Thermochemistry.....	15
Robert S. Barlow - Turbulence-Chemistry Interactions in Reacting Flows.....	19
Joel M. Bowman - Theoretical Studies of Combustion Dynamics.....	23
Nancy J. Brown - Combustion Chemistry.....	27
Laurie J. Butler - Dynamics of Product Branching in Elementary Combustion Reactions.....	31
David W. Chandler - Production and Study of Ultra-cold Molecules Produced by Kinematic Cooling.....	35
Jacqueline H. Chen - Petascale Direct Numerical Simulation and Modeling of Turbulent Combustion.....	39
Robert E. Continetti - Dynamics and Energetics of Elementary Combustion Reactions and Transient Species.....	43
Terrill A. Cool - Studies of the Chemistry of Oxygenated Fuels with Photoionization Mass Spectrometry.....	47
F.F. Crim - Dissociation Pathways and Vibrational Dynamics in Excited Molecules and Complexes.....	51
H. Floyd Davis - Bimolecular Dynamics of Combustion Reactions.....	55
Michael J. Davis - Global Combustion Modeling and Potential Energy Surface Fitting.....	59
Kent M. Ervin - Hydrocarbon Radical Thermochemistry: Gas-Phase Ion Chemistry Techniques.....	63

Robert W. Field - Spectroscopic and Dynamical Studies of Highly Energized Small Polyatomic Molecules.....	67
George Flynn - Scanning Tunneling Microscopy Studies of Chemical Reactions on Surfaces.....	71
Jonathan H. Frank - Quantitative Imaging Diagnostics for Reacting Flows.....	75
Michael Frenklach - Mechanism and Detailed modeling of Soot Formation.....	79
William H. Green - Computer-Aided Construction of Chemical Kinetic Models.....	83
Hua Guo - Quantum Dynamics of Elementary Combustion Reactions.....	87
Gregory E. Hall and Trevor J. Sears - Gas-Phase Molecular Dynamics: Experimental Studies of the Spectroscopy and Dynamics of Transient Species.....	91
Nils Hansen - Flame Chemistry and Diagnostics.....	95
Ronald K. Hanson and Craig T. Bowman - Spectroscopy and Kinetics of Combustion Gases at High Temperatures.....	99
Lawrence B. Harding - Theoretical Studies of Potential Energy Surfaces.....	103
Martin Head-Gordon - Chemical Accuracy from Ab-Initio Molecular Orbital Calculations..	107
John F. Hershberger - Laser Studies of Combustion Chemistry.....	111
So Hirata - Breakthrough Design and Implementation of Electronic and Vibrational Many-Body Theories.....	115
Ahren W. Jasper - Non-Born–Oppenheimer Molecular Dynamics and Theoretical Kinetics..	119
Ralf I. Kaiser - Probing the Reaction Dynamics of Hydrogen-Deficient Hydrocarbon Molecules and Radical Intermediates via Crossed Molecular Beams.....	123
Michael E. Kellman - Dynamical Analysis of Highly Excited Molecular Spectra.....	127
Alan R. Kerstein - Theory and Modeling of Small Scale Processes in Turbulent Flow.....	131
J. H. Kiefer - Kinetics of Combustion-Related Processes at High Temperatures.....	135
Stephen J. Klippenstein - Theoretical Chemical Kinetics.....	139
Anna I. Krylov - Theoretical Modeling of Spin-Forbidden Channels in Combustion Reactions.....	143
Stephen R. Leone - Synchrotron Studies of Combustion Radical Reactions and Aerosol Chemistry.....	147
Marsha I. Lester - Intermolecular Interactions of Hydroxyl Radicals on Reactive Potential Energy Surfaces.....	151
William A. Lester, Jr. - Theoretical Studies of Molecular Systems.....	155
Robert P. Lucht - Advanced Nonlinear Optical Methods for Quantitative Measurements in Flames.....	159
R. G. Macdonald - Time-Resolved Infrared Absorption Studies of Radical Reactions.....	163
Alexander M. Mebel - Theoretical Studies of Chemical Reactions Related to the Formation and Growth of Polycyclic Aromatic Hydrocarbons and Molecular Properties of Their Key Intermediates.....	167
Joe V. Michael - Flash Photolysis-Shock Tube Studies.....	171
H. A. Michelsen - Multiphase Combustion Diagnostics Development.....	175
James A. Miller - Chemical Kinetics and Combustion Modeling.....	179

Terry A. Miller - Detection and Characterization of Free Radicals Relevant to Combustion Processes.....	183
William H. Miller - Reaction Dynamics in Polyatomic Molecular Systems.....	187
James T. Muckerman and Hua-Gen Yu - Gas-Phase Molecular Dynamics: Theoretical Studies in Spectroscopy and Chemical Dynamics.....	191
Amy S. Mullin - Dynamics of Activated Molecules.....	195
Habib N. Najm - Reacting Flow Modeling with Detailed Chemical Kinetics.....	199
David J. Nesbitt - Spectroscopy, Kinetics and Dynamics of Combustion Radicals.....	203
Daniel M. Neumark - Radical Photochemistry and Photophysics.....	207
C. Y. Ng - Determination of Accurate Energetic Database for Combustion Chemistry by High-Resolution Photoionization and Photoelectron Methods.....	211
Joseph C. Oefelein - Large Eddy Simulation of Turbulence-Chemistry Interactions in Reacting Multiphase Flows.....	215
David L. Osborn - Kinetics and Dynamics of combustion Chemistry.....	219
David S. Perry - The Dynamics of Large-Amplitude Motion in Energized Molecules.....	223
Piotr Piecuch - New Single- and Multi-Reference Coupled-Cluster Methods for High Accuracy Calculations of Ground and Excited States.....	227
William J. Pitz and Charles K. Westbrook - Chemical Kinetic Modeling of Combustion Chemistry.....	231
Stephen B. Pope - Investigation of Non-Premixed Turbulent Combustion.....	235
S.T. Pratt - Optical Probes of Atomic and Molecular Decay Processes.....	239
Hanna Reisler - Photoinitiated Reactions of Radicals and Diradicals in Molecular Beams.....	243
Klaus Ruedenberg - Accurate Calculations and Analyses of Electronic Structure, Molecular Bonding and Potential Energy Surfaces.....	247
Branko Ruscic - Active Thermochemical Tables – Progress Report.....	251
Henry F. Schaefer III and Wesley D. Allen - Theoretical Studies of Elementary Hydrocarbon Species and Their Reactions.....	255
Thomas B. Settersten - Picosecond Nonlinear Optical Diagnostics.....	259
Ron Shepard - Theoretical Studies of Potential Energy Surfaces and Computational Methods.....	263
M. D. Smooke and M. B. Long - Computational and Experimental Study of Laminar Flames.....	267
John F. Stanton - Quantum Chemistry of Radicals and Reactive Intermediates.....	271
Arthur G. Suits - Universal and State-Resolved Imaging Studies of Chemical Dynamics.....	273
Craig A. Taatjes - Elementary Reaction Kinetics of Combustion Species.....	277
Donald L. Thompson - Theoretical Chemical Dynamics Studies of Elementary Combustion Reactions.....	281
Robert S. Tranter - Elementary Reactions of PAH Formation.....	285
Donald G. Truhlar - Variational Transition State Theory.....	289
Wing Tsang - Chemical Kinetic Data Base for Combustion Modeling.....	293
Peter M. Weber - Ultrafast Structural Dynamics as seen through Rydberg Electrons.....	297

T.J. Mountziaris, P. R. Westmoreland - Probing Flame Chemistry with MBMS, Theory, and Modeling.....	301
David R. Yarkony - Theoretical Studies of the Reactions and Spectroscopy of Radical Species Relevant to Combustion Reactions and Diagnostics.....	305
Timothy S. Zwier - Experimental Characterization of the Potential Energy Surfaces for Conformational and Structural Isomerization in Aromatic Fuels.....	309
Participant List	313

*Abstracts
of
Invited Presentations*

Combustion chemistry diagnostics

Katharina Kohse-Höinghaus

Chemistry Department, Bielefeld University, Germany

The need for clean energy drives many recent studies in combustion research and applications. Use of alternative fuels with different chemical functions, restrictions on harmful emissions, and introduction of novel combustion strategies stimulate an increasing demand for information on combustion chemistry. Details of the reaction networks, of important pathways, of sensitivities to specific conditions are crucial for the formation of certain intermediates and of undesired products.

The presentation is planned to stimulate discussion by providing selected recent results in five areas where diagnostics can be used to obtain insight into the combustion chemistry.

- Some specific features in the combustion of oxygenate fuels and hydrocarbon/oxygenate blends will be highlighted. Still far from assembling a complete picture, important contributions have been made by many groups in the US and overseas to establish a basis for predictive modeling of the combustion of esters, ethers, alcohols and their blends with conventional hydrocarbon fuels. A more general approach for estimating structure-product relations from chemically complex fuel molecules would be desirable.
- Diagnostic tools that have been used in the context of oxygenate fuels, including especially mass spectrometric techniques, have also been applied to study the chemistry of fuel-bound nitrogen when burning model alternative fuel compounds with, for example, amine functions. Such nitrogen-containing compounds may originate from pyrolysis of plant matter, such as wood bark, or from other biological waste. The combustion chemistry of such fuel components must be considered as largely unstudied.
- When analyzing the intermediate and product species pool in combustion processes, especially in situations where the available information is incomplete, mass spectrometry – although intrusive – is indispensable, and mechanisms are validated by such techniques. Following earlier investigations of molecular beam sampling with probes, accurate laser measurements today offer the potential to revisit such perturbation effects. Some recent results will be highlighted to discuss useful strategies.
- Sensing and controlling the combustion status under practical conditions will potentially have to rely on optical information. Laser tools offer a broad wavelength range and many options for the detection of radicals, and alternative fuels may warrant to look at different species than would be measured when addressing conventional hydrocarbon flames. Also, chemiluminescence is widely advocated as an intrinsic combustion sensor, and some aspects will be presented of using this information quantitatively.
- Finally, combustion regimes are becoming attractive where high efficiency and low emission might be beneficially combined. As one of these approaches, low-temperature combustion will be addressed using both a novel burner and a homogeneous or catalytic flow reactor, and issues for analysis of the combustion chemistry under such conditions will be discussed.

Two- and three-state conical intersections in molecular systems

Spiridoula Matsika
Department of Chemistry
Temple University
Philadelphia, PA 19122
smatsika@temple.edu

Conical intersections between two and three states of the same symmetry have been found to play a key role in nonadiabatic processes. Two-state conical intersections have been known for a while and their importance is now widely recognized. Three-state conical intersections, actual degeneracies between three electronic states that are not imposed by symmetry, are less known, but they have been shown in recent years to be present in many polyatomic molecules. These features may exist when there are at least five degrees of freedom present in the molecule. Their importance and effect on nonadiabatic dynamics are not well understood.

The importance of conical intersections is being investigated in a variety of photoinitiated processes. Large scale ab initio multireference configuration interaction methods are being used to locate and characterize conical intersections and examine how they influence the excited state properties of molecular systems. We will present studies on biologically relevant systems, and particularly the nucleobases and their analogs, where we have found many seams of two- or three-state conical intersections that can complicate the potential energy surfaces and dynamics of these systems.¹⁻⁴ It is shown that the accessibility of conical intersections is a key factor in determining their fluorescence properties. Implicit effects of three-state conical intersections are investigated by calculating nonadiabatic coupling terms, and it is demonstrated how the phase of the nonadiabatic coupling terms can be a diagnostic for the presence and location of additional seams.⁴

The topography of the conical intersection region that couples the electronically excited and ground state potential energy surfaces can affect the product distributions of photoinitiated reactions. We will demonstrate this in collisional quenching of electronically excited OH $A^2\Sigma^+$ by N_2 or H_2 . The rotational excitation of the OH $X^2\Pi$ products and branching fraction are found to be dynamical signatures of nonadiabatic passage through the conical intersection region.⁵

1. "Radiationless Decay of Excited States of Uracil through Conical Intersections", S. Matsika, *J. Phys. Chem. A*, **108**, 7584-7590, (2004)
2. "Three-State Conical Intersections in Nucleic Acid Bases", S. Matsika, *J. Phys. Chem. A*, **109**, 7538 - 7545, (2005)
3. "Radiationless Decay Mechanism of Cytosine: An Ab Initio Study with Comparisons to the Fluorescent Analogue 5-Methyl-2-Pyrimidinone", K. A. Kistler and S. Matsika, *J. Phys. Chem. A*, **111**, 2650-2661, (2007)
4. "Three-State Conical Intersections in Cytosine and Pyrimidinone Bases", K. A. Kistler and S. Matsika, *J. Chem. Phys.*, **128**, 215102, (2008)
5. "State-resolved distribution of OH $X^2\Pi$; products arising from electronic quenching of OH $A^2\Sigma^+$ by N_2 ", L. P. Dempsey, T. D. Sechler, C. Murray, M. Lester, and S. Matsika *J. Chem. Phys.*, **130**, 104307, (2009)

The Ignition of Jet Fuel Relevant Hydrocarbons at Engine Conditions

Matthew A. Oehlschlaeger

Rensselaer Polytechnic Institute, Troy, NY
oehism@rpi.edu

Overview

This AFOSR sponsored project is aimed at understanding the oxidation and ignition kinetics for jet fuels through shock tube studies. Our group has recently constructed a heated shock tube facility capable of elevated pressure homogenous gas-phase kinetic measurements of the ignition and oxidation characteristics of low vapor pressure hydrocarbon compounds such as those found in current (gasoline, diesel, and jet fuels) and future transportation fuels (Fischer-Tropsch fuels, biofuels, oil sands fuels, and others). Shock tube measurements of the ignition delay times of individual hydrocarbons found in and representative of those found in jet fuels at conditions of relevance to aero-propulsion devices are in progress. To date, a large range of compounds have been studied from the various classes of hydrocarbons found in high concentrations in jet fuels (n-alkanes, iso-alkanes, cyclo-alkanes, and aromatics). These measurements provide: 1) kinetic targets for the development and assessment of oxidation mechanisms for many compounds for which targets are sparse or do not exist in the literature, 2) an assessment of the influence of organic structure on reactivity, and 3) data needed for the development of surrogate mixtures for jet fuels and their detailed kinetic mechanisms.

Recent Progress

New Shock Tube: A new shock tube has been designed and constructed for the investigation of fuel chemistry at elevated pressures (reflected shock pressures up to 200 atm). The stainless steel shock tube has a 5.7 cm inner diameter, a 4.1 m long driven section, and a 2.6 m long driver. The shock tube, mixing vessel, and filling manifold can be heated with an electronically controlled electrical resistance heating system to temperatures up to 180 °C. Measurements of temperature on the inner wall of the shock tube indicate that the temperature is uniform within ± 2 °C, the thermocouple measurement uncertainty. This facility allows the investigation of low vapor pressure fuels, for which limited kinetic targets are available, at pressures and mixture compositions (fuel and air mixtures) relevant to aero-propulsion and internal combustion engines. The shock tube has been fully characterized and uncertainties in post-shock temperature and pressure are estimated at 1-1.5%. Ignition measurements were made for iso-octane mixtures at a wide range of conditions for comparison to previous well established literature data from the groups at Aachen, Fieweger et al. (1997) [1], and Stanford, Davidson et al. (2005) [2], for validation of the shock tube and measurement techniques.

Ignition of jet fuel relevant compounds: Ignition delay time studies have been carried out for a large number of individual hydrocarbon compounds in reflected shock experiments for conditions that range from 750-1500 K, 7-60 atm, and $\Phi = 0.25-1.5$ in air. The focus of our work thus far has been on ignition measurements for individual hydrocarbon compounds from a variety of organic classifications that are found in relatively high concentrations in jet fuels or are representative of compounds found in jet fuels. Some of the compounds investigated have been the subject of previous shock tube and/or rapid compression machine ignition studies. However, for many of the compounds these ignition studies represent the first measurements or

the first measurements at conditions relevant to aero-propulsion and internal combustion engines. Measurements have been completed for the following: C₇-C₁₄ n-alkanes, iso-octane (2,2,4-trimethylpentane, a reference fuel for octane number), iso-cetane (2,2,4,4,6,8,8- heptamethylnonane, a reference fuel for cetane number), cyclopentane, cyclohexane, methylcyclohexane, ethylcyclohexane, decalin, toluene, the three xylene isomers, ethylbenzene, and α -methylnaphthalene. Ignition delay times for these compounds have been made using simultaneous pressure and electronically excited OH emission measurements near the shock tube end wall; see Fig. 1 for an example ignition time measurement.

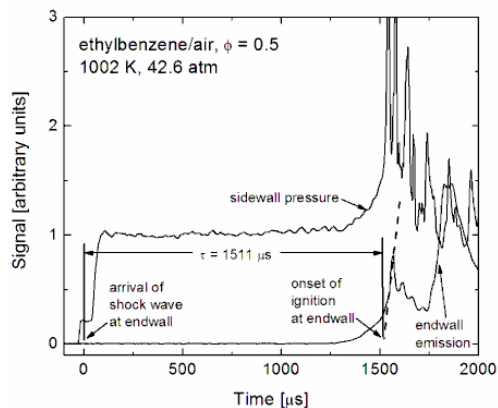


Fig. 1. Example ignition time measurement.

N-Alkanes: As an example of our work on hydrocarbon ignition, a brief description of the major kinetic conclusions from our work on n-alkanes is given. Figure 2 shows a comparison of ignition time measurements made near 12 atm for stoichiometric n-alkane/air mixtures. The graph includes data for n-heptane, n-decane, n-dodecane, and n-tetradecane ignition measurements obtained in our heated shock tube facility and results from other shock tube and rapid compression machine studies for these compounds. This comparison and comparisons made at other conditions (pressures and equivalence ratio) show experimentally, for the first time, that the reactivity of n-alkane/air mixtures for C₇ and larger n-alkanes vary little with n-alkane chain length, for mixtures with approximately common carbon content at elevated pressure conditions. The similarity in reactivity for n-alkanes observed experimentally is in good agreement with the recent predictions of LLNL (Westbrook et al., 2009 [3]) and Milano (Ranzi et al., 2005 [4]) kinetic modeling studies but is in disagreement with the kinetic modeling of the Nancy group (Biet et al., 2008 [5]). Hence, this data has cleared up, to some degree, disagreement within the kinetic modeling community as to influence of n-alkane length on reactivity. The similarity in reactivity for long n-alkanes can be explained by examining the primary reaction pathways and intermediates, which obviously vary significantly with temperature.

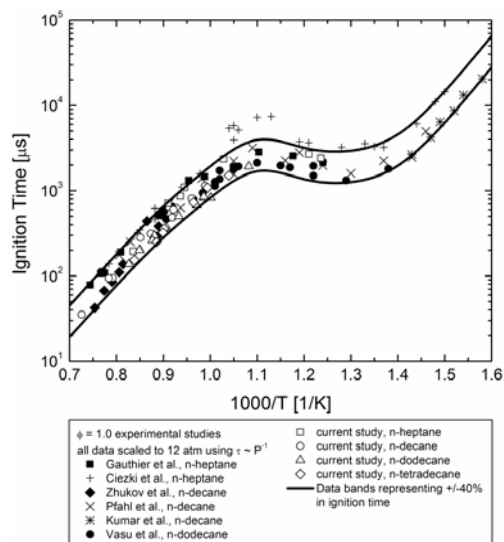


Fig. 2. Measured ignition times for $\Phi = 1.0$ n-alkane/air mixtures at 40 atm.

For shock tube experiments at temperatures below 1400 K the n-alkanes are primarily consumed via H-atom abstraction by small radicals (O, H, OH, HO₂, CH₃, and others) to produce alkyl radicals; at T > 1400 K n-alkane thermal decomposition competes. At higher temperatures (T > 900-1000 K) these alkyl radicals primarily decompose, which can be preceded by isomerization (H-atom transfer), to produce olefins, most of which are ethylene and propene for all n-alkanes regardless of chain length. Therefore, at higher temperatures the intermediate olefin pool for all

n-alkanes is very similar, provided that the mixtures are of common carbon content, and therefore the ignition times are very similar.

At moderate to lower temperatures the explanation for the similarity in reactivity is different. At lower temperatures ($T < 900\text{-}1000\text{ K}$) alkyl radicals can add directly to O_2 to form alkylperoxy radicals (RO_2) which can dissociate back to alkyl and O_2 or isomerize to form hydroperoxy alkyl radicals (QOOH). The QOOH can add an additional O_2 to form hydroperoxy peroxy (OOQOOH) which can quickly isomerize to a ketohydroperoxide and an OH radical. The ketohydroperoxide can decompose to form a second OH radical and another radical. In total, this reaction sequence produces three radicals from the original alkyl radical and thus chain low-temperature radical branching. At moderate temperatures (700-1000 K) this low-temperature branching reaction pathway competes with the dissociation of QOOH to form different products: olefins and HO_2 , cyclic ethers and OH, and β -scission products and alkyl radicals. This moderate temperature pathway results in no radical branching and thus lower reactivity is observed in the moderate-temperature negative-temperature-coefficient (NTC) regime than at lower temperatures where $\text{QOOH} + \text{O}_2$ is faster than QOOH decomposition.

The similarity of the measured ignition times in all the experimental studies shown in Fig. 2 for temperatures less than 1000 K implies that the moderate- and low- temperature reaction pathways, described above, and rate coefficients are not strongly influenced by n-alkane chain length for C_7 and larger n-alkanes. In particular, reactions involving internal isomerization ($\text{RO}_2 \rightarrow \text{QOOH}$ and $\text{OOQOOH} \rightarrow \text{OH} + \text{ketohydroperoxide}$), the rates of which are dependent on the length of R for smaller molecules, must not be strongly dependent on length, for C_7 and larger alkyls. This conclusion is consistent with the premise that reactions proceeding through cyclic transition states typically proceed through 5-8 member rings and in the case of larger alkanes the addition of chain length does not add probable isomerization pathways.

Future Work

Future work will expand our ignition time measurements to multi-component hydrocarbon mixtures to provide insight into the influence of fuel-fuel interactions on reactivity. We will also begin evaluating surrogate mixtures and distillate jet fuels (Jet A and JP-8) to determine which surrogates suitably mimic the reactivity characteristics of commercial and military use jet fuels. Additionally, we have recently developed a ppm-sensitive mid-IR quantum cascade laser absorption sensor for carbon monoxide which will be used to study both high- and low-temperature fuel oxidation in shock tubes.

References

- [1] K. Fieweger, R. Blumenthal, G. Adomeit, *Combust. Flame* 109 (1997) 599-619.
- [2] D.F. Davidson, B.M. Gauthier, R.K. Hanson, *Proc. Combust. Inst.* 30 (2005) 1175-1182.
- [3] C.K. Westbrook, W.J. Pitz, O. Herbinet, H.J. Curran, E.J. Silke, *Combust. Flame* 156 (2009) 181-199.
- [4] E. Ranzi, A. Frassoldati, S. Granata, T. Faravelli, *Ind. Eng. Chem. Res.* 44 (2005) 5170-5183.
- [5] J. Biet, M.H. Hakka, V. Warth, P.-A. Glaude, F. Battin-Leclerc, *Energy Fuels* 22 (2008) 2258-2269.

Recent Publications

1. M.A. Oehlschlaeger, J. Steinberg, C.K. Westbrook, and W.J. Pitz, "The Autoignition of Iso-Cetane: Shock Tube Experiments and Kinetic Modeling," *Combustion and Flame*, submitted.
2. H.-P.S. Shen, J. Steinberg, J. Vanderover, and M.A. Oehlschlaeger, "A Shock Tube Study of the Ignition of n-Heptane, n-Decane, n-Dodecane, and n-Tetradecane at Elevated Pressures," *Energy and Fuels*, to appear; DOI: 10.1021/ef8011036.
3. M.A. Oehlschlaeger, H.-P.S. Shen, A. Frassoldati, S. Pierucci, and E. Ranzi, "An Experimental and Kinetic Modeling Study of the Pyrolysis and Oxidation of Decalin," *Energy and Fuels*, 23, 1464-1472 (2009).
4. H.-P.S. Shen and M.A. Oehlschlaeger, "The Ignition of C₈H₁₀ Aromatics at Elevated Pressures," *Combustion and Flame* 156, 1053-1062 (2009).
5. H.-P.S. Shen, J. Vanderover, and M.A. Oehlschlaeger, "A Shock Tube Study of the Auto-Ignition of Toluene/Air Mixtures at High Pressures," *Proceedings of the Combustion Institute* 32, 165-172 (2009).
6. J. Vanderover and M.A. Oehlschlaeger, "Ignition Time Measurements for Methylcyclohexane- and Ethylcyclohexane-Air Mixtures at Elevated Pressures," *International Journal of Chemical Kinetics* 41, 82-91 (2009).
7. H.-P.S. Shen, J. Vanderover, and M.A. Oehlschlaeger, "A Shock Tube Study of Iso-Octane Ignition at Elevated Pressures: the Influence of Diluent Gases," *Combustion and Flame* 155, 739-755 (2008).
8. J.T. Moss, A.M. Berkowitz, M.A. Oehlschlaeger, J. Biet, V. Warth, P.-A. Glaude, and F. Battin-Leclerc, "An Experimental and Kinetic Modeling Study of the Oxidation of the Four Isomers of Butanol" *Journal of Physical Chemistry A* 112, 10843-10855 (2008).
9. S.M. Daley, A.M. Berkowitz, and M. A. Oehlschlaeger, "A Shock Tube Study of Cyclopentane and Cyclohexane Ignition at Elevated Pressures," *International Journal of Chemical Kinetics* 40, 624-634 (2008).

Practical Explicitly Correlated Many-Body Methods

Edward F. Valeev

Department of Chemistry, Virginia Tech, Blacksburg, VA 24061

Abstract

Predictive computation of energy differences and properties related to them (equilibrium constants, reaction rates, rovibrational spectra) demand convergent series of high-level wave function models in combination with specially-designed basis set sequences. Unfortunately, the use of practical basis sets results in unacceptably-large basis set errors. For example, the mean absolute and maximum basis set error of heats of formations of small closed and open-shell molecules in the HEAT testset¹ are 9.1 and 25.2 kJ/mol when using the correlation-consistent triple-zeta basis set. Reliable predictions of chemical accuracy (defined as 1 kcal/mol = 4.2 kJ/mol) clearly requires more extensive basis sets and computational costs increased by orders of magnitude. The cause of the large basis set errors is **fundamental**: *the qualitatively incorrect behavior of the standard wave functions when electrons approach each other closely*. Although carefully designed basis set sequences allow to reduce the basis set error of molecular energies by empirical extrapolation, such approaches are often not reliable and cannot be easily extended to properties.

To account for the basis set challenge from first principles we employ *explicitly correlated* R12 wave function methods. In R12 methods^{2,3} the two-electron basis includes products $f(r_{12})|ij\rangle$, where $f(r_{12})$ is an appropriate function of the interelectronic distances known as the correlation factor. The many-electron integrals that appear in explicitly correlated methods are simplified by systematic approximations^{4,5} based on the resolution of the identity (RI).⁶ At the MP2 level the use of R12 approach allows to reduce the basis set error by an order of magnitude, with a disproportionately-small increase in computational cost.

Here we will discuss our recent progress in extension of R12 approach to the highly-accurate coupled-cluster (CC) methods for ground and excited states using the rigorous and perturbative routes. The rigorous R12 extension of the CC method is formally straightforward but the resulting equations are immensely complex and are not suited for manual implementation. To derive, manipulate, and implement these equations we employed an automated compiler that can handle the more general algebraic structure of the CC-R12 equations, isolate the special R12 intermediates, factorize the resulting tensor expressions, and generate efficient computer codes. Evaluation of the nonstandard two-electron integrals is also carried out by a high-performance computer code generated by a specialized compiler. These developments have allowed us for the first time to investigate a range of unprecedented ground-state CC-R12 methods through CCSDTQ-R12. Application of these novel methods to small polyatomic molecules results in absolute electronic energies of chemical accuracy and without any extrapolation.⁷ The work is underway to develop excited state and response CC-R12 capabilities.⁸

A more practical approach to R12 coupled-cluster methods is to introduce explicit correlation by perturbation theory. We have developed a family of CC-R12 methods that treat geminal terms alone (CCSD(2)_{R12}),^{9,10} or in conjunction with triple excitations (CCSD(T)_{R12}),¹¹ in a manner similar the workings of the "gold standard" CCSD(T) method. The advantage of the perturbative route is that the standard CC equations are not modified, and technical changes to the MP2-R12 code are minor. We demonstrate that the CCSD(T)_{R12} method is a practical R12 variant of the CCSD(T) method with performance similar to the rigorous CCSD(T)-R12 counterpart. For the aforementioned HEAT example,

the use of the $\text{CCSD}(T)_{\text{R12}}$ method allows to reduce the basis set error to 2.8 kJ/mol in mean absolute sense and to 7.2 kJ/mol at most, all with the same triple-zeta basis set. Thus, *the $\text{CCSD}(T)_{\text{R12}}$ method with only a triple-zeta basis set seems to reach chemical accuracy on average.*

We will finally investigate how the R12 approach can be applied in a universal fashion to any electronic structure model (wave function or density-based).¹² Our approach is formally similar to the perturbative CC route described above. We hope to apply such universal correction in conjunction with multireference CC or CI models to quantitatively describe potential energies of bond breaking processes, in ground and excited states, and other phenomena involving near-degenerate electronic structures.

References

- [1] A. Tajti, P. G. Szalay, A. G. Császár, M. Kállay, J. Gauss, E. F. Valeev, B. A. Flowers, J. Vázquez, and J. F. Stanton, *J. Chem. Phys.*, **121**, 11599 (2004). HEAT: High Accuracy Extrapolated Ab Initio Thermochemistry.
- [2] W. Kutzelnigg, *Theor. Chim. Acta*, **68**, 445 (1985). r_{12} -Dependent terms in the wave function as closed sums of partial wave amplitudes for large l .
- [3] W. Klopper, F. R. Manby, S. Ten-no, and E. F. Valeev, *Int. Rev. Phys. Chem.*, **25**, 427 (2006). R12 methods in explicitly correlated molecular electronic structure theory.
- [4] A. J. May, E. Valeev, R. Polly, and F. R. Manby, *Phys. Chem. Chem. Phys.*, **7**, 2710 (2005). Analysis of the errors in explicitly correlated electronic structure theory.
- [5] S. Kedžuch, M. Milko, and J. Noga, *Int. J. Quantum Chem.*, **105**, 929 (2005). Alternative formulation of the matrix elements in MP2-R12 theory.
- [6] E. F. Valeev, *Chem. Phys. Lett.*, **395**, 190 (2004). Improving on the resolution of the identity in linear R12 ab initio theories.
- [7] T. Shiozaki, M. Kamiya, S. Hirata, and E. F. Valeev, *J. Chem. Phys.*, **130**, 054101 (2009). Higher-order explicitly correlated coupled-cluster methods.
- [8] T. Shiozaki, M. Kamiya, S. Hirata, and E. F. Valeev, *Phys. Chem. Chem. Phys.*, **10**, 3358 (2008). Equations of explicitly-correlated coupled-cluster methods.
- [9] E. F. Valeev, *Phys. Chem. Chem. Phys.*, **10**, 106 (2008). Coupled cluster methods with perturbative inclusion of explicitly correlated terms: A preliminary investigation.
- [10] M. Torheyden and E. F. Valeev, *Phys. Chem. Chem. Phys.*, **10**, 3410 (2008). Variational formulation of perturbative explicitly correlated coupled-cluster methods.
- [11] E. F. Valeev and T. D. Crawford, *J. Chem. Phys.*, **128**, 244113 (2008). Simple coupled-cluster singles and doubles method with perturbative inclusion of triples and explicitly correlated geminals: The $\text{CCSD}(T)_{\text{R12}}$ model.
- [12] M. Torheyden and E. F. Valeev, in preparation. Universal perturbative explicitly-correlated basis set incompleteness correction.

Multiscale simulations of nanoparticle formation in high temperature conditions

Angela Violi

*Departments of Mechanical Engineering, Chemical Engineering and Biomedical Engineering
University of Michigan
Ann Arbor, MI, USA*

Abstract

The process of combustion is the dominant pathway through which mankind continuously injects particulate matter into the atmosphere. These combustion-generated particles are present not only in very large amounts, but they are produced, at the smallest scale, in the form of clusters with nanometric dimensions. Although the total mass of particulate emissions has been significantly reduced with improvement of combustion efficiency and emissions control systems, the very small nanoparticles are exceedingly difficult to control by the emission systems typically installed on vehicles. In addition, the current emissions regulations are mass-based and do not address the presence of nanoparticles. Predictive models of nanoparticle formation and oxidation that provide detailed chemical structures of the particles currently do not exist, a fact that greatly limits our ability to control this important chemical process.

The objectives of this work are focused on gaining a clear understanding of the chemical and physical processes occurring during the formation of carbon nanoparticles in combustion conditions and their fate in the environment. Starting from the chemistry of novel fuels, including esters, the primary focus is to provide a detailed multi-scale characterization of nanoparticle formation in combustion environments, through the use of novel simulation methodologies operating across disparate (spatial/temporal) regimes. The use of *ab initio* simulations to describe the reaction pathways for the breakdown of the fuel molecules, together with atomistic models, such as Molecular Dynamics simulations, provides information on the reaction pathways from fuel decomposition to nanoparticle formation in a chemically specific way. This approach establishes a connection between the various time scales in the nanoparticle self-assembly problem, together with an unprecedented opportunity for the understanding of the atomistic interactions underlying carbonaceous nanoparticle structures and growth.

Vibrational Autodetachment –
A New Experimental Approach to Intramolecular Vibrational Relaxation

J. Mathias Weber

*JILA, NIST, and Department of Chemistry and Biochemistry, University of Colorado,
Boulder, Colorado 80309, USA*

Abstract

The distribution and relaxation of vibrational energy through molecules is a process that is very important in many chemical phenomena. Consequently, understanding internal vibrational redistribution / relaxation (IVR) of energy is critical for obtaining predictive power in modeling of processes in complex chemical environments. In this work, we use vibrational autodetachment (VAD) as a new experimental approach to studying IVR.

If the binding energy of an excess electron to a molecule is less than the energy of a certain vibrationally excited state, excitation into that state can lead to VAD. If the lifetime of the excited anion with respect to VAD is short compared to the experimental timescale, the absorption of a photon leads to the formation of neutral products and free electrons with near unit efficiency.

Unless there is a direct coupling mechanism between the excited vibrational state and the detaching mode(s), VAD relies to a large extent on IVR, resulting in the excitation of vibrational modes that couple the anionic and neutral potential energy surfaces. In the context of IVR, the situation of vibrational autodetachment (VAD) is similar to the use of vibrational predissociation in that the initially excited zero-order bright state is embedded in a continuum of dark states (the dissociation continuum and the electron emission continuum, respectively). For VAD from polyatomic anions, an excited vibrational mode is often not directly coupled to electron emission, and energy needs to be redistributed into a mode that is.

Our model systems in this study are nitroalkanes, which have electron affinities of about 1400 cm^{-1} [1], well below the excitation energies for CH stretching modes, with the excess charge localized mostly on the nitro group. The low electron binding energy facilitates VAD as well as direct photodetachment in the energy region of the CH stretching fundamentals ($2700 - 3000\text{ cm}^{-1}$). The absorption bands of the CH stretching vibrations in the hydrocarbon are the zero-order bright states, while the nitro group serves as a localized energy acceptor, as the most important vibrational modes coupling the anionic and neutral potential energy surfaces are the NO_2 wagging modes.

The coupling of vibrational energy to electronic motion manifests itself in macroscopic systems e.g. as thermionic emission. In a molecular description, the coupling of vibrational and electronic motion constitutes a breakdown of the Born-Oppenheimer approximation. Ro-vibrational autodetachment (AD) has first been reported by Lineberger and coworkers [2], where the excess electron on NH^- was ejected after ro-vibrational excitation of the anion. The VAD approach has not been widely used for spectroscopic purposes, and the only time it has been employed with a (partial) focus on IVR was a few years ago by Johnson and coworkers, in the case of bare and Ar solvated nitromethane anions [3].

In the present work, VAD spectra are compared to Ar-predissociation spectra of Ar solvated nitroalkane anions [4]. In addition, low-energy velocity map photoelectron imaging results for nitromethane anions without and with vibrational excitation are shown. The “regular” photoelectron spectrum is interpreted with the aid of *ab initio* theory and Franck–Condon factor calculations [1]. From photoelectron spectra resulting from electron loss after vibrational excitation and comparison to the calculated density of states of the neutral and the anion, we can draw conclusions on how vibrational energy is coupled into the electron loss channel.

1. C.L. Adams, H. Schneider, K.M. Ervin, and J.M. Weber, "Low-energy photoelectron imaging spectroscopy of nitromethane anions: Electron affinity, vibrational features, anisotropies and the dipole-bound state," *J. Chem. Phys.* **130**, 074307-1 - 10 (2008).
2. D.M. Neumark, K.R. Lykke, T. Andersen, and W.C. Lineberger, "Infrared-Spectrum and Autodetachment Dynamics of NH^- ," *Journal of Chemical Physics* **83**, 4364-4373 (1985).
3. J.M. Weber, W.H. Robertson, and M.A. Johnson, "Argon predissociation and electron autodetachment spectroscopy of size-selected $\text{CH}_3\text{NO}_2^- \cdot \text{Ar}_n$ clusters," *J. Chem. Phys.* **115**, 10718-10723 (2001).
4. H. Schneider, K.M. Vogelhuber, F. Schinle, J.F. Stanton, and J.M. Weber, "Vibrational spectroscopy of nitroalkane chains using electron detachment and Ar predissociation," *J. Phys. Chem. A* **112**, 7498-7506 (2008).

*Abstracts
of
Principal Investigator
Presentations*

Annual Progress report April 2009
**Threshold Photoelectron Photoion Coincidence (TPEPICO) Studies:
The Road to ± 0.1 kJ/mol Thermochemistry**

Tomas Baer (baer@unc.edu)
Department of Chemistry
University of North Carolina
Chapel Hill, NC 27599-3290
DOE Grant DE-FG02-97ER14776

Program Scope

The threshold photoelectron photoion coincidence (TPEPICO) technique is utilized to investigate the dissociation dynamics and thermochemistry of energy selected medium to large organic molecular ions. The reactions include parallel and consecutive steps that are modeled with the statistical theory in order to extract dissociation onsets for multiple dissociation paths. These studies are carried out with the aid of molecular orbital calculations of both ions and the transition states connecting the ion structure to their products. The results of these investigations yield accurate heats of formation of ions, free radicals, and stable molecules. In addition, they provide information about the potential energy surface that governs the dissociation process. Isomerization reactions prior to dissociation are readily inferred from the TPEPICO data.

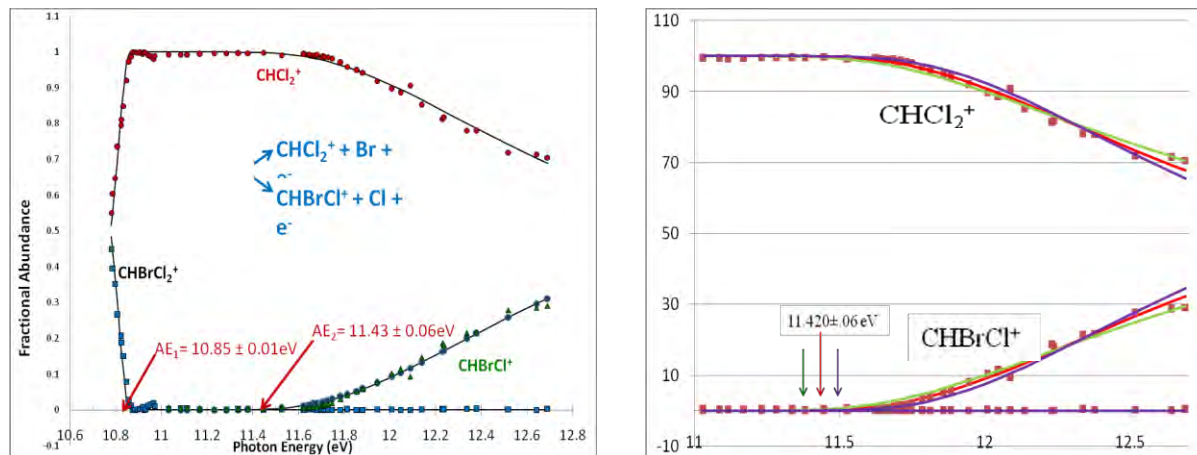
The TPEPICO Experiment

The threshold photoelectron photoion coincidence (TPEPICO) experiment in Chapel Hill is carried out with a laboratory H₂ discharge light source. Threshold electrons are collected by velocity focusing them into a 1.5 mm hole on a mask located at the end of the 12 cm drift tube. Some hot electrons pass through a 2x5 mm opening located next to the central 1.5 mm hole. In this fashion, two TPEPICO spectra are simultaneously collected, one for threshold and one for hot electrons. Hot electron free data are obtained by subtracting a fraction of the hot from the threshold TPEPICO data. The ion TOF is either a linear version or a reflectron for studying H loss processes. The electrons provide the start signal for measuring the ion time of flight distribution. When ions dissociate in the microsecond time scale, their TOF distributions are asymmetric. The dissociation rate constant can be extracted by modeling the asymmetric TOF distribution. A high-resolution version of this experiment with a molecular beam source and an electron imaging detector at the Swiss Light Source (SLS) has been constructed and has been collecting data since August, 2008. Because of the high photon flux, we have implemented the first multi-start multi-stop coincidence scheme using a master clock as the time base. The maximum photon resolution and flux have not yet been achieved due to some alignment issues. However, 2 meV resolution has been demonstrated, which will yield onset energies accurate to 0.2 kJ/mol.

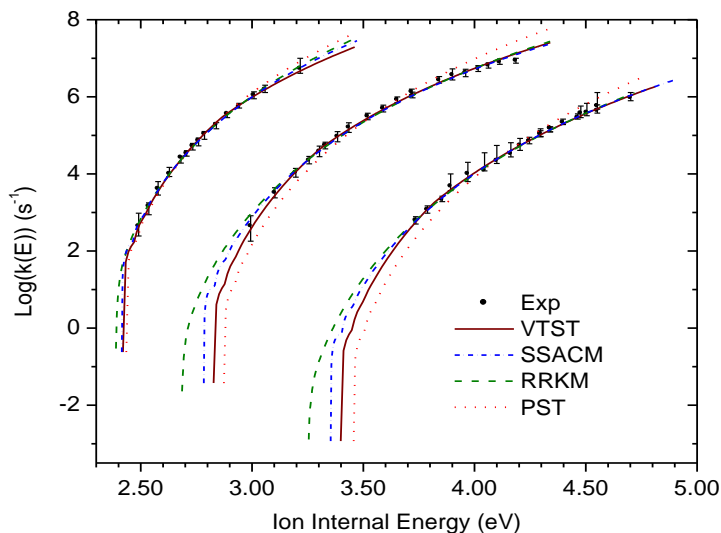
Recent Results

The Heats of Formation of HCCl₃, HCCl₂Br, HCClBr₂, HCB₃, and Their Fragment Ions Studied by Threshold Photoelectron Photoion Coincidence: The parallel onsets for Cl and Br loss were measured for the following mixed tri-halide ions, HCCl₃, HCCl₂Br, HCClBr₂, and HCB₃ by threshold photoelectron photoion coincidence (TPEPICO) in order to establish the heats of formation of the mixed halides as well as the following fragment ions: HCCl₂⁺, HCClBr⁺, HCB₂⁺. The first zero Kelvin onsets were measured with a precision of 10 meV.

The second onsets, which are in competition with the lower energy onsets, were established with a precision of 60 meV. Because both the chloroform and bromoform have relatively well established heats of formation, these measurements provide a route for establishing the heats of formation of the mixed halomethanes within uncertainties of less than 5 kJ mol⁻¹. A particular effort was made to establish believable error limits in second onset energies (see figure below).



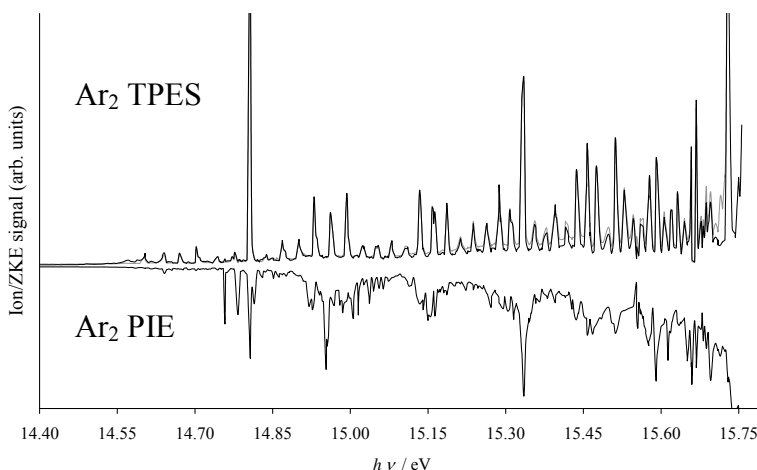
Specific Rate Constants $k(E)$ of the Dissociation of the Halobenzene Ions: Analysis by Statistical Unimolecular Rate Theories Specific rate constants $k(E)$ of the dissociation of the halobenzene ions $C_6H_5X^+ \rightarrow C_6H_5^+ + X$ ($X = Cl, Br, \text{ and } I$) were measured over a range of 10^3 to 10^7 s⁻¹ by threshold photoelectron-photoion coincidence (TPEPICO) spectroscopy. The experimental data were analyzed by various statistical unimolecular rate theories in order to derive the threshold energies E_0 . Although rigid activated complex RRKM theory fits the data in the experimentally measured energy range, it significantly underestimates E_0 for chloro- and bromobenzene. Phase space theory (PST) does not fit the experimentally measured rates. A parameterized version of the variational transition state theory (VTST) as well as a simplified version of the statistical adiabatic channel model (SSACM) incorporating an energy dependent rigidity factor provide excellent fits to the experimental data and predict the correct dissociation energies. Although both approaches have just two adjustable parameters, one of which is E_0 , SSACM is effective and particularly simple to apply.



This is an important study for us because it clearly demonstrates the necessity of using theories more sophisticated than RRKM to extrapolate the measured rate constants down to the 0 K dissociation limit. The Chapel Hill opinion of SSACM is that it is simply a first order correction to PST and thus ideally suited for ionic dissociations. There does not appear to be much physical meaning to the adjustable parameter, though. The VTST is intuitively more appealing, but the fitting parameters are difficult to predict and not unique.

Progress at the Swiss Light Source (SLS)

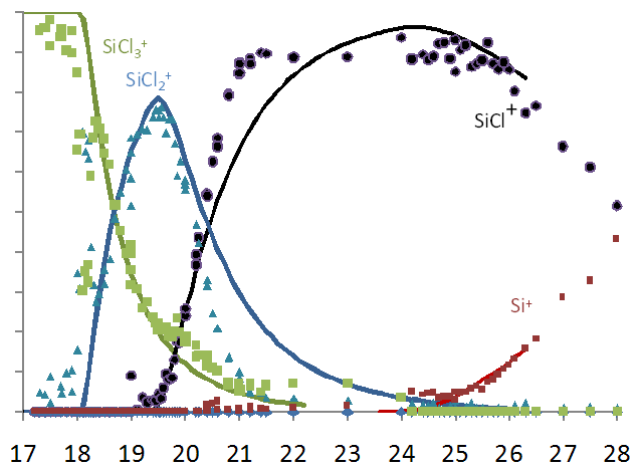
The VUV beamline at the SLS is rapidly becoming a smoothly running facility.



TPES and total ion scans in an Ar beam below the Ar IE (15.760 eV). TPES was obtained in coincidence with Ar₂⁺ ions. The TPES peaks are about 7 meV wide. Electron velocity map images at each photon energy reveal the autoionization paths of the Ar₂ Rydberg states. This scan was run overnight on autopilot.

Below is the breakdown diagram of SiCl₄⁺ between 17 and 26 eV obtained at the SLS.

The best photon resolution obtained so far has been 2 meV, which should also be the best electron resolution. More work is required to reduce Stark broadening of electron peaks due to the 40 V/cm extraction field. The machine runs on autopilot so that 2 people can work 24/7 for two weeks without wearing themselves out. So far, the focus has been on collecting breakdown diagrams for molecular ions that sequentially lose ligands, e.g. SiCl₄⁺, until we see the bare Si⁺ ion above 25 eV. The loss of Cl from SiCl₄⁺ at 10 eV is not shown. By modeling the energy partitioning in the various sequential dissociation steps, we can semi-quantitatively reproduce the entire breakdown diagram (solid lines). The only adjustable parameters are the onset energies. The slopes of the lines are given by the statistical energy partitioning. We have similar data for SnCl₄, GeCl₄, and BBr₃. Deviations of the data from the statistical model probably reflect non-statistical energy partitioning, which needs investigating.



Work in Progress and Future Plans

Some papers in progress include an accurate and reliable measurement of the t-butyl ion heat of formation. This is being done with variable temperature TPEPICO apparatus in Chapel Hill using CH₃ loss from neopentane ions as the precursor. The challenge is to extract an accurate onset for the methyl loss channel in the presence of a slightly lower energy CH₄ loss onset. With this in hand, we can determine the heats of formation of t-butyl iodide, and t-butyl peroxide, both of which yield the t-butyl ion as an ionic product. Another study involves the determination of the t-butyl-OO radical heat of formation by photoionization of di-t-butyl peroxide. This reaction is very metastable and its analysis has shown that simple RRKM and SSACM yield different onset energies. Our calculations suggest that the SSACM onset is the correct one. This study depends on the accurate t-butyl ion heat of formation obtained from the neopentane study. A third paper in progress involves the heat of formation of the C₃H₅⁺ ion.

The challenge here is that H loss from propene involves a slow reaction, whose rates must be measured. Because of the small mass loss, the data analysis is challenging.

Future plans include further testing of the VTST and SSACM models for ionic reactions that involve the loss of dipolar species. These are ones that have non-spherical potentials, which often require special care. But, there are not many examples of such reactions. A study of $C_6H_5NO^+ \rightarrow C_6H_5^+ + NO$ is in progress. In addition, we will continue our study of peroxides in order to obtain heats of formation of other peroxy radicals.

Publications from DOE supported work 2007 – 2009

James P. Kercher, Zsolt Gengeliczki, Bálint Sztáray, and Tomas Baer, Dissociation dynamics of sequential ionic reactions: Heats of formation of tri-, di- and monoethyl phosphines, *J. Phys. Chem. A* **111**, 16-26 (2007)

James P. Kercher, Will Stevens, Zsolt Gengeliczki, and Tomas Baer, Modeling Ionic Unimolecular Dissociations from a Temperature Controlled TPEPCIO Study on $I-C_4H_9I$ Ions, *Int. J. Mass Spectrom.* **267**, 159-166 (2007)

Zsolt Gengeliczki, László Szepes, Bálint Sztáray, and Tomas Baer, Photoelectron spectroscopy and thermochemistry of tert-butylisocyanide substituted cobalt tricarbonyl nitrosyl, *J. Phys. Chem. A* **111**, 7542-7550 (2007)

Andras Bodi, Bálint Sztáray, Tomas Baer, Melanie Johnson and Thomas Gerber, Data acquisition schemes for continuous two-particle time-of-flight coincidence experiments, *Rev. Sci. Instrum.* **78**, 084102/1 – 7 (2007)

Nicholas S. Shuman, Melony A. Ochieng, Bálint Sztáray, Tomas Baer, TPEPICO Spectroscopy of Vinyl Chloride and Vinyl Iodide: Neutral and Ionic Heats of Formation and Bond Energies, *J. Phys. Chem. A* **112**, 5647-5652 (2008)

Nicholas S. Shuman, James P. Kercher, and Tomas Baer, The Dissociation Dynamics of Energy-Selected Neopentylamine Ions: Heats of Formation of Neopentylamine and Neopentyl Alcohol, *Int. J. Mass Spectrom.* **287** 26-31 (2008)

Nicholas S. Shuman, Linda Ying Zhao, Michael Boles, Bálint Sztáray, and Tomas Baer, The Heats of Formation of $HCCl_3$, $HCCl_2Br$, $HCClBr_2$, $HCBBr_3$, and their ions studied photoelectron photoion coincidence. *J. Phys. Chem.A* **112**, 10533-10538 (2008)

William Stevens, Bálint Sztáray, Nicholas S. Shuman, Tomas Baer, and Jürgen Troe, Specific Rate Constants $k(E)$ of the Dissociation of Halobenzene Ions: Analysis by Statistical Unimolecular Rate Theories. *J. Phys. Chem. A* **113** 573-582 (2009)

Andras Bodi, Melanie Johnson, Thomas Gerber, Zsolt Gengeliczki, Bálint Sztáray, and Tomas Baer, Imaging photoelectron photoion coincidence spectroscopy with velocity focusing electron optics, *Rev. Sci. Instrum.* **80** 034101/1-7 (2009)

Balázs Hornung Andras Bodi Csaba I. Pongor, Zsolt Gengeliczki Tomas Baer and Bálint Sztáray, Dissociative photoionization of $X(CH_3)_3$ ($X = N, P, As, Sb, Bi$): mechanism, trends and accurate energetics, *J. Phys. Chem.* (2009) in press

Turbulence-Chemistry Interactions in Reacting Flows

Robert S. Barlow
Combustion Research Facility
Sandia National Laboratories, MS 9051
Livermore, California 94550
barlow@sandia.gov

Program Scope

This program is directed toward achieving a more complete understanding of turbulence-chemistry interactions in flames and providing detailed measurements for validation of combustion models. In the Turbulent Combustion Laboratory (TCL) at the CRF, simultaneous line imaging of spontaneous Raman scattering, Rayleigh scattering, and two-photon laser-induced fluorescence (LIF) of CO is applied to obtain spatially and temporally resolved measurements of temperature, the concentrations of all major species, mixture fraction, and reaction progress, as well as gradients in these quantities in hydrocarbon flames. The instantaneous three-dimensional orientation of the turbulent reaction zone is also measured by imaging of OH LIF in two crossed planes, which intersect along the laser axis for the multiscale measurements. These combined data characterize both the thermo-chemical state and the instantaneous flame structure, such that the influence of turbulent mixing on flame chemistry may be quantified. Our experimental work is closely coupled with international collaborative efforts to develop and validate predictive models for turbulent combustion. This is accomplished through our visitor program and through the TNF Workshop series. Although the past emphasis has been on nonpremixed combustion, the workshop and this program are in the process of expanding their scope to address a broad range of combustion regimes, including premixed and stratified flames. We are also working to extend our quantitative multiscale diagnostics to more complex fuels by implementing a polarization separation technique for single shot measurements. Within the CRF we collaborate with Joe Oefelein to use highly-resolved large-eddy simulations (LES) of our experimental flames in order to gain greater fundamental understanding of the dynamics of multi-scale flow-chemistry interactions. We also collaborate with Tom Settersten and Jonathan Frank to refine our quantitative LIF methods and to apply complementary imaging diagnostics to selected turbulent flames.

Recent Progress

Work during the past year has focused on four areas closely linked to the new directions of the TNF Workshop: 1) stratified flame experiments and data analysis (collaboration with Cambridge University, UK), 2) development of a new processing approach for processing Raman scattering data from hydrocarbon flames (collaboration with the Technical University of Darmstadt, Germany) 3) exploratory measurements in laminar and turbulent flames of ethane, ethylene, propane, and dimethyl ether (DME), and 4) buildup of collection optics and detection hardware for polarized/depolarized Raman measurements and for improved OH PLIF imaging.

Stratified Flame Experiments and Data Analysis

In stratified combustion a turbulent flame propagates through a nonuniform mixture of fuel and oxidizer. This mode of combustion is common on practical systems but is not well understood at a fundamental level, and it represents an important challenge for combustion models. Stratified combustion is also challenging for laser diagnostics because high precision in the measurement of the local equivalence ratio, ϕ , is required and thin reaction zones demand high spatial

resolution. In collaboration with Prof. Simone Hochgreb and Mr. Mark Sweeney of Cambridge, we investigated two stratified burners using line-imaged Raman/Rayleigh/CO-LIF in combination with crossed planar LIF imaging of OH. The first burner (Fig. 1a) uses parallel slots and mesh to create a turbulent mixing layer between two streams to different equivalence ratio. Data from this burner have been analyzed to extract statistics on the instantaneous dissipation of reaction progress variable, which is an important quantity for some modeling approaches and which had not previously been measured in any turbulent stratified flame. Statistics of the flame surface density, curvature, and orientation have also been reported. We recently conducted experiments on a new stratified burner (Fig. 1c) that operates at significantly higher turbulence levels than the slot burner. This burner is intended as a target for validation of RANS and LES combustion models. It has a central bluff body for flame stabilization and two annular flow passages. Variable swirl may be applied to the outer annular flow. This swirl burner was designed to complement a burner from TU Darmstadt. (See abstract by J. Frank.)

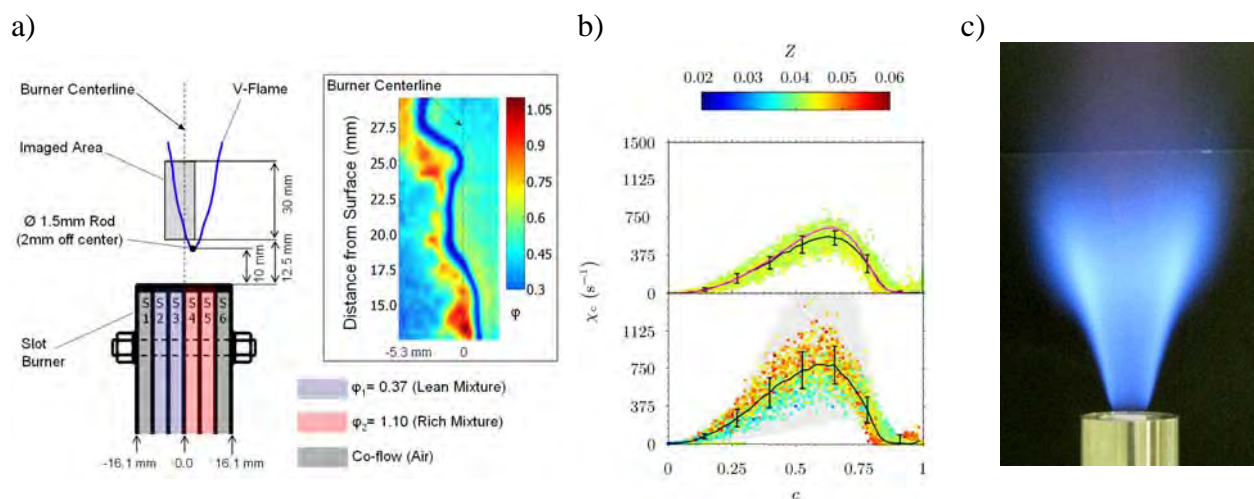


Figure 1. a) Cambridge stratified slot burner diagram and example image combining acetone and OH imaging [1]; b) measured results for 3D (angle corrected) scalar dissipation χ_c plotted vs. instantaneous progress variable c with color indicating mixture fraction Z [2]; and c) photograph of the new annular burner for investigation of stratified flames at higher turbulence levels.

'Hybrid' Processing of Raman Measurements

We collaborated with the group of Prof. Andreas Dreizler at TU Darmstadt, Germany to develop a method of analysis of Raman scattering measurements that combines the best aspects of the separate methods used by the two groups. This 'hybrid' method applies a matrix inversion approach but uses lookup tables based on integration of regions of theoretically calculated Raman spectra instead of polynomial curves based upon extensive calibration. The new method offers significant advantages for processing of data from our low f -number transmission spectrometer because the effects of optical bowing of the line image and beam steering within turbulent flames can be corrected automatically.

Flames of Ethane, Propane, Ethylene, and DME

In order to evaluate the potential for extending high-quality multiscalar measurements to turbulent flames burning more complex fuels, we measured Raman scattering spectra in heated flows (up to $\sim 850K$) and in laminar partially-premixed jet flames of ethane, propane, ethylene, and DME. Measurements were conducted in collaboration with TU Darmstadt during a visit by

PhD student, Frederik Fuest (Jan-Feb 2009), and they included both high-resolution spectra and spectrally binned (on-chip) data separated into two polarization components. The high resolution results will be used to develop synthetic spectral libraries, which will subsequently be used to extend the ‘hybrid’ Raman processing method to address these fuels. Some exploratory measurements were also obtained in piloted turbulent jet flames of each fuel, so that relative levels of fluorescence interference may be evaluated.

Enhancement of Measurement Capabilities

We are in the process of duplicating (in mirror image) the complete three-camera (Raman/Rayleigh/CO-LIF) detection system that was brought on line in June 2007. The second system will allow simultaneous detection of the separate polarization components of signal from the test section, so that fluorescence interference and flame luminosity may be subtracted from the Raman scattering signal. Implementation of this polarization separation technique as a quantitative, single-shot method for turbulent flames is the critical path toward extending model validation experiments to more complex fuels, including some alternative transportation fuels. We have also upgraded the UV imaging optics for our crossed OH PLIF measurements. Light collection has been increased by an order of magnitude, yielding significant improvement in spatial resolution and accuracy of measurements of flame curvature in premixed and stratified flames.

Future Plans

Research plans are closely aligned with two of the major priorities identified at the TNF9 Workshop (Montreal, August 2008). The first is to extend our work on stratified combustion to flames with higher levels of turbulence. This is being done in collaboration with the University of Cambridge (UK) and the Technical University of Darmstadt (Germany). In both cases, burner designs emphasize well-defined boundary conditions for turbulent combustion models, such that unambiguous comparisons of measured and modeled results may be achieved. Strong coupling of the experimental and computational work on stratified combustion at Cambridge, TU Darmstadt, and Sandia will be facilitated by funding from the Leverhulme Trust (UK) for establishment of a research network. This three year grant to Prof. Hochgreb allows for research exchanges (travel expenses) and annual workshops. The intent is to accelerate progress in this research area and feed the larger (and less focused) model validation framework of TNF series.

Our second thrust will be to extend multiscale measurements to turbulent flames of more complex fuels. We expect to complete construction and installation of our second three-camera detection system during the coming year. In parallel, we will work with TU Darmstadt to develop synthetic libraries representing the temperature dependence of Raman scattering spectra for methane, ethane, propane, ethylene, and DME, so that the hybrid processing method may also be applied to fuels. It is hoped that detailed multiscale results on the first turbulent flames of the new fuels will be available within the next year.

- [1] P. Anselmo-Filho, S. Hochgreb, R.S. Barlow, R.S. Cant, “Experimental Measurements of Geometric Properties of Turbulent Stratified Flames,” *Proc. Combust. Inst.* **32**, 1763-1770 (2009).
- [2] M.S. Sweeney, O.R. Darbyshire, S. Hochgreb, R.S. Barlow, “Experiments on the Structure of Stratified Flames in Low Turbulence,” US National Combustion Mtg., Ann Arbor, May 2009.

BES Supported Publications (2007 - present)

R.S. Barlow, "Laser Diagnostics and Their Interplay with Computations to Understand Turbulent Combustion," invited plenary paper, *Proc. Combust. Inst.* **31**, 49-75 (2007).

D. Wang, C. Tong, R.S. Barlow, A.N. Karpetis, "Experimental Study of Scalar Filtered Mass Density Function in Turbulent Partially Premixed Flames," *Proc. Combust. Inst.* **31**, 1533-1541 (2007).

G.H. Wang, R.S. Barlow, N.T. Clemens, "Quantification of Resolution and Noise Effects on Thermal Dissipation Measurements in Turbulent Non-premixed Jet Flames," *Proc. Combust. Inst.* **31**, 1525-1532 (2007).

G.H. Wang, A.N. Karpetis, R.S. Barlow, "Dissipation Length Scales in Turbulent Nonpremixed Jet Flames" *Combust. Flame*, **148**, 62-75 (2007).

R.P. Lindstedt, H.C. Ozarovsky, R.S. Barlow, A.N. Karpetis, "Progression of Localised Extinction in High Reynolds Turbulent Jet Flames," *Proc. Combust. Inst.* **31**, 1551-1558 (2007).

A.R. Masri, P.A.M. Kalt, Y.M. Al-Abdeli, R.S. Barlow, "Turbulence-Chemistry Interactions in Non-Premixed Swirling Flames," *Combust. Theory Modelling*, **11**, 653-673 (2007).

G.H. Wang, N.T. Clemens, R.S. Barlow, P.L. Varghese, "A System Model for Assessing Scalar Dissipation Measurement Accuracy in Turbulent Flows" *Meas. Sci. Technol.* **18**, 1287-1303 (2007).

G.H. Wang, N.T. Clemens, P.L. Varghese, R.S. Barlow, "Turbulent Time Scales in a Nonpremixed Turbulent Jet Flame by Using High-Repetition Rate Thermometry," *Combust. Flame*, **152**, 317-335 (2008).

T.G. Drozda, G.H. Wang, V. Sankaran, J.R. Mayo, J.C. Oefelein, R.S. Barlow, "Scalar Filtered Mass Density Functions in Nonpremixed Turbulent Jet Flames," *Combust. Flame*, **155**, 54-96 (2008).

R.S. Barlow, G.H. Wang, P. Anselmo-Filho, M.S. Sweeney, S. Hochgreb, "Application of Raman/Rayleigh/LIF Diagnostics in Turbulent Stratified Flames," *Proc. Combust. Inst.* **32**, 945-953 (2009).

P. Anselmo-Filho, S. Hochgreb, R.S. Barlow, R.S. Cant, "Experimental Measurements of Geometric Properties of Turbulent Stratified Flames," *Proc. Combust. Inst.* **32**, 1763-1770 (2009).

M.J. Dunn, A.R. Masri, R.W. Bilger, R.S. Barlow, G.H. Wang, "The Compositional Structure of Highly Turbulent Piloted Premixed Flames Issuing into Hot Coflow," *Proc. Combust. Inst.* **32**, 1779-1786 (2009).

R.S. Barlow, H.C. Ozarovsky, A.N. Karpetis, R.P. Lindstedt, "Piloted Jet Flames of CH₄/H₂/Air: Experiments on Localized Extinction in the Near Field at High Reynolds Numbers," *Combust. Flame* (accepted).

TNF Workshop Information: <http://www.ca.sandia.gov/TNF>

Theoretical Studies of Combustion Dynamics (DE-FG02-97ER14782)

Joel M. Bowman

Cherry L. Emerson Center for Scientific Computation and Department of Chemistry,
Emory University Atlanta, GA 30322, jmbowma@emory.edu

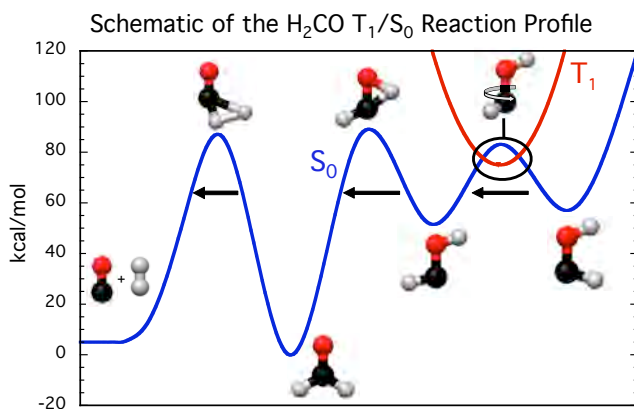
Program Scope

The research program supported by this Department of Energy grant centers on developing rigorous, predictive and insightful computational methods to model the basic dynamics of chemical and physical processes of importance in gas-phase combustion. We have focused in recent years on developing full-dimensional global *ab initio*-based potential energy surfaces (PESs) that describe complex unimolecular and bimolecular reactions. These PESs are fits to tens of thousands or more of *ab initio* energies using special polynomial bases that are manifestly invariant with respect to all permutations of like nuclei. Dynamics calculations using these potentials, which may contain multiple minima and saddle points, can be done for long times and can reveal new pathways and mechanisms of chemical reactions. The choice of reaction system to study is always motivated by experiments that challenge and ultimately advance basic understanding of combustion reaction dynamics.

Recent Progress in "Roaming" Dynamics

H₂CO photodissociation

We have extended our studies of the so-called "roaming dynamics" in H₂CO photodissociation by explicit consideration of aspects of the interaction between the



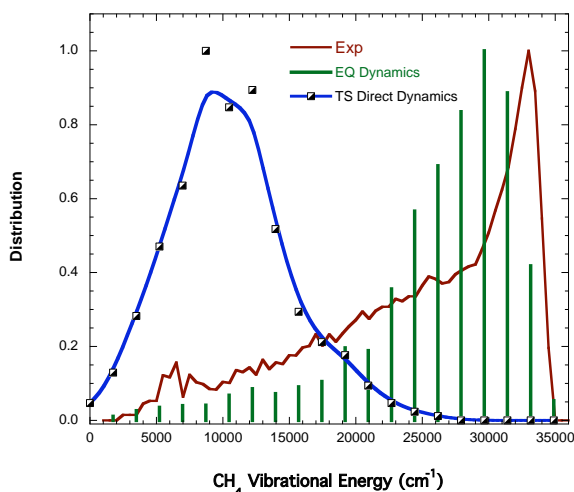
the T₁ and S₀ electronic states in a collaboration with the groups of Anna Krylov and Keiji Morokuma, who used using different electronic structure methods to characterized these intersections.^{P1} (Note: "Pn" refers to publication no. n in list "PUBLICATIONS SUPPORTED BY THE DOE (2007-present).") The lowest energy intersections between T₁ and S₀, determined by these groups, are located in the hydromethylene region

of the potential energy surface as indicated in the schematic figure shown above. The configurations of these intersections are close to the geometry of the *cis/trans*-HOCO isomerization saddle point. We performed extensive quasiclassical trajectory (QCT) calculations initiated at these intersection geometries using an updated global potential energy surface. The new PES contains a high-energy saddle point connecting the molecular channel H₂+CO to the HOCO region of the PES. (At the energies of relevance to present photodissociation experiments this channel is classically closed; however, configurations near this saddle point are sampled in the dynamics calculations.) The QCT calculations find that isomerization occurs from the HOCO region of the PES to the H₂CO (as indicated in the figure), which then proceeds to the molecular products by both the conventional molecular saddle-point pathway

and the roaming pathway. The results of these new calculations, i.e., the H₂ and CO ro-vibrational distributions, are virtually identical to those obtained from trajectories initiated at the S₀ global minimum, which were reported recently.^{1,P2-P5} The roaming mechanism, first uncovered by running QCTs from the global minimum continues to apply to the trajectories initiated from the T1/S0 crossing configurations.

CH₃CHO Photodissociation

We reported a global PES for CH₃CHO based on roughly 130 000 CCSD(T)/cc-pVTZ electronic energies in the single-reference regions of the potential and augmenting those energies with accurate CCSD(T)/cc-pVTZ and aug-cc-pVTZ energies for many fragments, e.g., CH₄+CO, CH₃+HCO, CH₂CO+H₂, C₂H₂+H₂O, etc.^{P6} This potential was



used in QCT calculations of the photodissociation of CH₃CHO, which initially were done at a total energy corresponding to the 308 nm experiment of Houston and Kable.² New calculations were done as part of a collaboration with the groups of Scott Kable and David Osborn, who measured the IR emission from the vibrationally very hot CH₄ product, shown in the figure to the left.^{P7} QCT calculations were performed on the global PES and initiated at the CH₃CHO equilibrium (EQ) geometry. In addition "Direct-Dynamics" QCT calculations were performed at the

MP2/ccpVDZ level of theory and basis. These were initiated at the conventional molecular saddle-point transition state corresponding to the dissociation of acetaldehyde to the CH₄+CO products. As seen in the figure there is good agreement between the measured CH₄ vibrational energy distribution and QCT trajectories initiated at the equilibrium configuration, denoted "EQ Dynamics", but poor agreement with trajectories initiated at the conventional TS, denoted "TS Direct Dynamics". Based primarily on this results shown in this figure we estimated that the dissociation dynamics to the molecular products is roughly 85% non-conventional TS. Animations of a number of trajectories indicate that there is significant "roaming" of the CH₃ group.

Ab initio IR Spectroscopy of *cis/trans*-HOCO

In collaboration with Anna Krylov (USC) a semi-global PES was developed for the *cis* and *trans* isomers of H₂CO, based on fitting 17 262 CCSD(T)/cc-pVTZ (frozen core) energies.^{P8} A dipole moment surface (DMS) was also obtained by fitting the dipole moment obtained with CCSD/6-311G** (all electrons correlated) calculations. The PES and DMS were used in rigorous vibrational calculations using the code MULTIMODE,³ to obtain vibrational energies and intensities. The results are in very good agreement with the recently measured matrix-isolation spectrum of *trans*-HOCO.⁴

F+CH₄ reaction

We reported a full-dimensional, *ab initio*-based PES for the F+CH₄ reaction,^{P9} based on an accurate composite method. This PES is the most accurate one currently available. The first set of comparisons with experiments focused on those from Nesbitt and co-workers⁵ who determined the HF(*v'*,*j'*) product distributions at one initial relative kinetic energy. Excellent agreement was found.

Future Plans

(1) We plan to extend the study of multi-electronic state dynamics calculations of H₂CO photodissociation by explicitly considering the non-adiabatic coupling. (2) We plan further calculations of the F+CD₃H reaction in order to make direct comparisons with the experiments of Kopin Liu and co-workers,⁶ who presented some evidence of a possible resonance in this reaction. Liu's experiments detect the correlated products CD₃(*v*=0)+HF(*v'*) and CD₂H(*v*=0)+DF(*v'*). To model this quasiclassically some method development will be needed so that the assignment of the ground vibrational state of the methyl fragment is done as rigorously as possible. One approach that we will investigate is to analyze the final vibrational energy distribution of the methyl fragment by projecting the vibrational motion onto normal modes and then perhaps using "Gaussian Binning"⁷ to obtain the mode-specific final states.

References

1. D. Townsend, S. A. Lahankar, S. K. Lee, S. D. Chambreau, A. G. Suits, X. Zhang, J. Rheinecker, L. B. Harding, and J. M. Bowman, *Science* **306**, 1158 (2004).
2. P. L. Houston and S. H. Kable, *Proc. Natl. Acad. Sci. USA*, **103**, 16079 (2006).
3. J. M. Bowman, S. Carter, and X. Huang, *Int. Rev. Phys. Chem.* **22**, 533 (2003).
4. P. R. Schreiner, H. P. Reisenauer, F. Pickard, A. C. Simmonett, W. D. Allen, E. Mátyus, and A. G. Császár, *Nature*, **453**, 906 (2008).
5. W. W. Harper, S. G. Nizkorodov, and D. J. Nesbitt, *J. Chem. Phys.* **113**, 3670 (2000).
6. (a) W. Shiu, J. Lin, and K. Liu, *Phys. Rev. Lett.* **92**, 103201 (2004); (b) J. Zhou, J. J. Lin and K. Liu *J. Chem. Phys.* **119**, 8289 (2003).
7. L. Bonnet and J.C. Rayez, *Chem. Phys. Lett.* **277** (1997) 183.

PUBLICATIONS SUPPORTED BY THE DOE (2007-present)

1. Photodissociation dynamics of formaldehyde initiated at the T₁/S₀ minimum energy crossing configurations (Letter), B. Shepler, E. Epifanovsky, P. Zhang, J. M. Bowman, A. I. Krylov, and K. Morokuma, *J. Phys. Chem. A* **112**, 13267 (2008).
2. Further aspects of the roaming mechanism in formaldehyde dissociation, S. A. Lahankar, V. Goncharov, F. Suits, J. D. Farnum, J. M. Bowman, and A. G. Suits, *Chem. Phys.* **347**, 288 (2008).
3. Energy dependence of the roaming atom pathway in formaldehyde decomposition, S. A. Lahankar, S. D. Chambreau, X. Zhang, J. M. Bowman, and A. G. Suits, *J. Chem. Phys.* **126**, 044314 (2007).
4. Phase-Space Analysis of Formaldehyde Dissociation Branching and Comparison with Quasiclassical Trajectory Calculations, J. D. Farnum, and J. M. Bowman, *J. Phys. Chem. A* **111**, 10376 (2007).

5. Formaldehyde photodissociation: Dependence on total angular momentum and rotational alignment of the CO product, J. Farnum, X. Zhang, and J.M. Bowman, *J. Chem. Phys.* **126**, 134305 (2007).
6. Quasiclassical Trajectory Calculations of Acetaldehyde Dissociation on a Global Potential Energy Surface Indicate Significant Non-transition State Dynamics, B.C. Shepler, B. J. Braams, and J. M. Bowman, *J. Phys. Chem. A (Letter)* **111**, 8282 (2007).
7. Roaming is the dominant mechanism for molecular products in acetaldehyde photodissociation, B. R. Heazlewood, M. J. T. Jordan, S. H. Kable, T. M. Selby, D. L. Osborn, B. C. Shepler, B. J. Braams, and J. M. Bowman, *Proc. Natl. Acad. Sci. USA* **105**, 12719 (2008).
8. The theoretical prediction of infrared spectra of *trans*- and *cis*-hydroxycarbene calculated using full dimensional *ab initio* potential energy and dipole moment surfaces, L. Koziol, Y. M. Wang, B. J. Braams, J. M. Bowman, and A. I. Krylov, *J. Chem. Phys.* **128**, 204310 (2008).
9. Accurate *ab initio* potential energy surface, dynamics, and thermochemistry of the $F + CH_4 \rightarrow HF + CH_3$ reaction, G. Czako, B. C. Shepler, B. J. Braams, and J. M. Bowman, *J. Chem. Phys.* **130** 084301 (2009).
10. Three Reaction Pathways in the $H+HCO \rightarrow H_2+CO$ reaction, K. M. Christoffel and J. M. Bowman, *J. Phys. Chem.* ASAP DOI: 10.1021/jp810517e (2009).
11. Quasiclassical Trajectory Calculations of the HO_2+NO Reaction on a Global Potential Surface, C. Chen, B. C. Shepler, B. J. Braams and J. M. Bowman, *Phys. Chem. Chem. Phys.*, accepted for publication.
12. Production of vibrationally excited H_2O from charge exchange of H_3O^+ with cesium, J. E. Mann, Z. Xie, J. D. Savee, J. M. Bowman, and R. Continetti, *J. Chem. Phys.* **130**, 041102 (2009).
13. Accurate *ab initio* structure, dissociation energy, and vibrational spectroscopy of the $F--CH_4$ anion complex, G. Czako, B. J. Braams, and J. M. Bowman, *J. Phys. Chem. A* **112**, 7466 (2008).
14. "Roaming" dynamics in CH_3CHO photodissociation revealed on a global potential energy surface, B. C. Shepler, B. J. Braams, and J. M. Bowman, *J. Phys. Chem. A* **112**, 9344 (2008).
15. Probing the structure of CH_5^+ by dissociative charge exchange, J. E. Mann, Z. Xie, J. D. Savee, B. J. Braams, J. M. Bowman, and R. E. Continetti, *J. Am. Chem. Soc.* **130**, 3730 (2008).
16. Combined Experimental and Computational Study on the Ionization Energies of the Cyclic and Linear C_3H Isomers. R. I. Kaiser, L. Belau, S. R. Leone, M. Ahmed, Y. Wang, B. J. Braams, and J. M. Bowman, *Chem Phys Chem* **8**, 1236 (2007).
17. *Ab initio*-Based Potential Energy Surfaces and Franck-Condon Analysis of Ionization Thresholds of cyclic- C_3H and linear- C_3H , Y. Wang, B. J. Braams, and J. M. Bowman, *J. Phys. Chem. A* **111**, 4056 (2007).
18. Potential Energy Surface and Reaction Dynamics of the $OH+NO_2$ Reaction, C. Chen, B. Schepler, B. Braams, and J. M. Bowman, *J. Chem. Phys.* **127**, 104310 (2007).

COMBUSTION CHEMISTRY
Principal Investigator: Nancy J. Brown
Environmental Energy Technologies Division
Lawrence Berkeley National Laboratory
Berkeley, California, 94720
510-486-4241
NJBrown@lbl.gov

Project Scope

Combustion processes are governed by chemical kinetics, energy transfer, transport, fluid mechanics, and their complex interactions. Understanding the fundamental chemical processes offers the possibility of optimizing combustion processes. The objective of our research is to address fundamental issues of chemical reactivity and molecular transport in combustion systems. Our long-term research objective is to contribute to the development of reliable combustion models that can be used to understand and characterize the formation and destruction of combustion-generated pollutants. We emphasize studying chemistry at both the microscopic and macroscopic levels. Our current work is concerned with improving the calculation of transport properties for combustion modeling.

Recent Progress

A review of transport property formalisms and their underlying parameterizations has been conducted (In collaboration with Lucas Bastien and Phillip Price).

Diffusion, viscosity, thermal conductivity, and thermal diffusion are critically important in combustion processes. They affect profile shapes, flame velocities, and pollutant production. Relative to efforts directed toward improving chemistry, little effort has been directed toward improving the description of transport in combustion models since the work of Kee et al. [1986]. The state of the art is described adeptly by Wakeham et al. [2007]: “there was considerable development in both transport property theory and experimentation between 1950 and 1970; between 1970 and 1986, these efforts were extended to more complex molecular systems, and currently the field has stagnated with little new development and is driven by specific application needs.” Sensitivity analysis [Brown and Revzan, 2005] revealed that influential transport properties are as important in flame modeling as influential reaction rates, and both should be taken into account when building chemical mechanisms. Major products of this review are suggestions of the best approaches for improving transport property evaluations under combustion conditions as well as improvements in their underlying parameterizations.

Our first task was to assemble a large amount of viscosity data because it is the most accurately measured of the properties, and experimentally determined viscosity coefficients for pure substances and binary mixtures can serve as benchmarks for different theoretical approaches. This is possible because there were large improvements in the instrumentation for measuring viscosity during the 1970s, and measurements were made in the temperature regime 70 to 2000 K, with the majority of these under 1000 K, with errors less than 0.5 %. We are currently evaluating transport properties using different formalisms and comparing

them with each other and to experimental values for the temperature range $1 < T^* < 10$, where $T^* = kT/\epsilon$ and ϵ is the well depth. We have compared: **Tranlib** (CHEMKIN) of Kee et al. [1986] that has been corrected for coding errors, the approach of Mason, Kestin, and colleagues, **MKC** [Mason and Uribe, 1996 and Bzowski et al., 1990], with the Dipole Reduced Formalism, **DRFM**, [Paul 1997 and Paul and Warnatz 1998]. Collision integrals for the latter two are identical except for the case of molecules with dipole moments. We calculated viscosities for pure substances that are simple non-polar molecules like rare gases and CO_2 using the same sets of potential parameters (from Paul and Warnatz) for each approach, and they agree excellently with each other-indicating that each approach to collision integral evaluation leads to the same values for $1 < T^* < 10$ where $T^* = kT/\epsilon$. We also compared predicted viscosities calculated with Tranlib and DRFM –each with their supporting data for each of the representative molecules over a range of temperatures. Rare gas and “simple non-polar molecules” (Ar , O_2 , N_2 , CO_2 , CH_4) viscosities calculated with Tranlib, MKC, and DRFM agree with each other and with experimentally determined values as well (relative errors usually less than 2 % and as high as 4 %).

Many molecules important in combustion including radical species have dipole moments and all have polarizabilities. Values for these parameters are often incorrect in the Tranlib data base. Errors in viscosities calculated with Tranlib are 3 % for H_2O and 17 % for NH_3 while those calculated with DRFM are 2 and 3 %, respectively. This indicates that the two approaches to correcting for dipoles are reasonable [DRFM approach is from Hirschfelder et al., 1954], and argues for having correct values of dipole moments and polarizabilities. Unfortunately, there are very few measurements of the transport properties of radical species, and their supporting data are frequently incorrect. MKC only treats rare gases and simple molecules and does not attempt any special treatment for properties involving polar molecules and DRFM uses their dipole correction with newly estimated values of potential length and energy scaling parameters. Figure 1 provides an illustration of how far apart Tranlib and DRFM are for radicals and a “not so simple” polyatomic molecule.

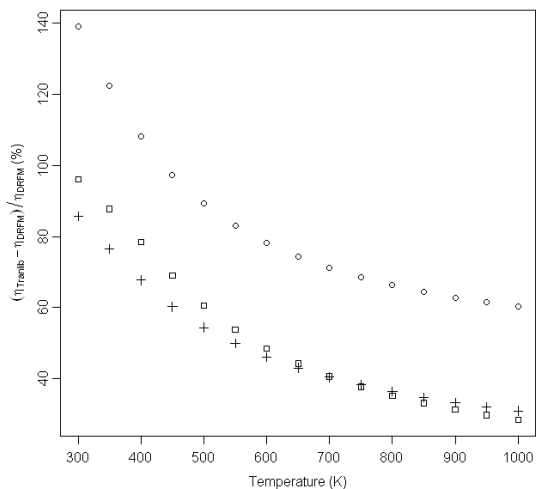


Figure 1: Difference between the viscosities of OH (\circ), HO_2 (\square) and H_2O_2 ($+$) predicted with Tranlib and DRFM versus temperature.

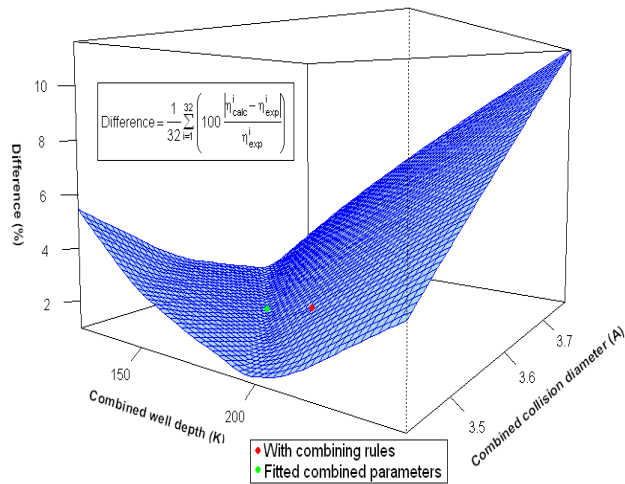


Figure 2: Difference between computed and experimental viscosities (32 values) over the space of possible combined parameters: O_2 - CO_2 mixtures.

Note that the differences are in the range 50 to 140 % at temperature where radical transport processes are especially important in flames. Measurements of the diffusion coefficients of OH and HO₂ at ambient temperature by Ivanov et al. [2007] agree better with the DRFM values, which are 20 to 33 % higher than with Tranlib values, which are over a factor of two larger. There needs to be further research on transport properties of radical species because they are extremely important in combustion modeling.

Considerable literature exists regarding the importance of different combining rules that attempt to infer binary interactions of unlike molecules from like ones, as well as a body of literature regarding various approximation that are useful for treating mixture transport properties. We used a multi component transport approach to calculate viscosities of several binary mixtures each having a set of good experimental data for the pure species as well as for the binary mixtures. Pure species viscosity data were used to fit pure species parameters, ϵ_{ii} and σ_{ii} . We fixed the pure species parameters and fitted the combined parameters (ignoring all combining rules) such that agreement between computed and experimental viscosities is optimized. We found that there is no unique solution to this problem; but rather, there is a whole set of couples ($\epsilon_{ij}, \sigma_{ij}$) such that the error between calculated and experimental values is minimized along a line (trough) as shown in Figure 2. Two very different sets of parameters yield nearly the same accuracy. Further investigation revealed that there is one set of potential parameters such that the agreement between experiment and calculation is almost perfect (within experimental uncertainty) at every temperature over which the fit was conducted. This is true for both pure substances and binary mixtures.

There are many combining rules, and several of these appear to be quite ad hoc without much physical basis. We considered five combining rules that are frequently used. Each rule yields values that are different from the optimum parameters determined from fitting, and generally the geometric mean (GM) and the harmonic mean (HM) rules underestimated the ϵ_{ij} value. Although the various rules yield parameters that are quite different from the best combined parameters, they are surprising close to the line (trough) describing the acceptable fits for various couples of potential parameters, and are therefore able to provide reasonable, non-optimal results. The harmonic mean rule works best in most cases, and the commonly used arithmetic combining rule for σ_{ij} tends to overestimate the value.

Current Research

We have also conducted sensitivity analysis of the deflection function, the cross sections, and collision integrals with respect to a Lennard-Jones potential energy surface to understand the sensitivity of molecular transport properties to the potential energy surface. We have determined cross sections with a square well potential to further explore this.

We are also extending the transport property evaluation to temperatures beyond $T^* = 10$. We are using correlation formulae derived by Tang and Toennies to determine parameters for an exponential repulsive potential from those of the Lennard-Jones potential for various molecules. We are using MOLPRO within the SCF approximation to estimate molecular polarizabilities, many of which can be compared with experimental values. By using the correlations introduced by Cambi et al. [1991] and Pirani et al. [2008] and the computed polarizabilities, we are estimating L-J parameters for transport property evaluation.

References

- Brown, N.J., K.L. Revzan, *Int. J. Thermophys.*, 37 (2005) 538-553.
- Brown, N.J., L. Bastien, P.N. Price, "PRiME: Transport Properties for combustion Modeling." 32nd International Symposium on Combustion in Montreal, Canada Montreal, Canada, 2008.
- Bzowski, J., J. Kestin, E. Mason, F.J. Uribe, *J. Phys. Chem. Ref. Data*, 19 (1990) 1179-1232.
- Cambi, R. D. Cappelletti, G. Liuti and F. Pirani, *J. Chem. Phys.* 95, (1991), 1852
- Hirschfelder, J.O., C.F. Curtiss, R.B. Bird, *Molecular Theory of Gases and Liquids*, Wiley, New York, 1954.
- Ivanov, A.V., S. Trakhtenberg, A.K. Bertram, Y.M. Gershenzon, M.J. Molina, *J. Phys. Chem.*, A111 (2007) 1632-1637.
- Kee, R.J., G. Dixon-Lewis, J. Warnatz, M.E. Coltrin, J.A. Miller, *A FORTRAN Computer Package for the Evaluation of Gas-Phase Multicomponent Transport Properties*, SANDIA, 1986.
- Mason, E.A., F.J. Uribe, in: *Transport Properties of Fluids (Their Prediction, Estimation, and Correlations)*, Cambridge University Press, 250-283, 1996.
- Paul P.H., *DRFM: A New Package for the Evaluation of Gas-Phase Transport Properties*, Sandia, 1997.
- Paul, P.H., J. Warnatz, Boulder, Colorado, 1998, pp. 495-504.
- Pirani, F., S. Brizi, L.F. Roncaratti, Z.P. Casavecchia, D. Cappelletti, and F. Vecchiocattivi, *Phys. Chem. Chem Phys.*, **10**, 5489-5503 (2008)
- Tang, K.T., and P. Toennies, *J. Chem. Phys.* 66, 1496 (1977)
- Wakeham, W.A., M.A. Assael, J.K. Atkinson, J. Bilek, J.M.N.A. Fareleira, A.D. Fitt, A.R.H. Goodwin, C.M.B.P. Oliveira, *Int. J. Thermophys.*, 28 (2007) 372-416.

Publications since 2007:

- Tonse, S.R., M.S. Day, and N.J. Brown. Dynamic Reduction of a CH₄/Air Chemical Mechanism Appropriate for Investigating Vortex Flame Interactions. *International Journal of Chemical Kinetics* 39, pp 204-220, 2007. LBNL Report No. 59750.
- Brown, N.J., L. Bastien, P.N. Price, "PRiME: Transport Properties for combustion Modeling." 32nd International Symposium on Combustion in Montreal, Canada Montreal, Canada, 2008.

Dynamics of Product Branching in Elementary Combustion Reactions

Laurie J. Butler

The University of Chicago, The James Franck Institute
5640 South Ellis Avenue, Chicago, IL 60637
L-Butler@uchicago.edu

I. Program Scope

The elementary reactions that determine the performance of a combustion system range from direct H-atom abstraction reactions to complex reactions involving competing addition/elimination mechanisms. The reaction rate and the branching to multiple product channels can evidence a strong temperature and pressure dependence. While the total rate constant for many elementary reactions is well-characterized, understanding the product branching in complex reactions presents a formidable challenge. To gain an incisive probe of such reactions, our experiments directly probe the dynamics of the product channels that arise from long-lived radical intermediates along the bimolecular reaction coordinates. The work uses the methodology developed in my group in the last eight years, using both imaging and scattering apparatuses. The experiments generate a particular isomeric form of an unstable radical intermediate along a bimolecular reaction coordinate and investigate the branching between the ensuing product channels of the energized radical as a function of its internal energy under collision-less conditions. They probe the reaction from each radical intermediate to the competing product channels and determine the energetic barriers in both the entrance and the product channels. When one of the competing product channels produces a heavy and a light co-fragment, such as in the acrolein + H product channel from the O + allyl reaction described below, the experiments offer a direct measurement of the microcanonical rate, $k(E)$, of that product channel relative to the other competing product channels from the addition mechanism.

The experiments use a combination of: 1) measurement of product velocity and angular distributions in a crossed laser-molecular beam apparatus, with electron bombardment detection in my lab in Chicago or 2) with tunable vacuum ultraviolet photoionization detection in collaboration with Jim Lin at Taiwan's National Synchrotron Radiation Research Center (NSRRC), and 3) velocity map imaging using state-selective REMPI ionization and single photon VUV ionization of radical intermediates and reaction products. Our efforts this year continued our study of the O + allyl reaction, probing the product channels that result from addition of the O atom at an end carbon atom, and initiated new studies on a radical intermediate of the OH + ethene reaction. In summary, the results develop insight on product channel branching in such reactions and provide a key benchmark for emerging electronic structure calculations on polyatomic reactions that proceed through unstable radical intermediates.

II. Recent Progress and Ongoing Work

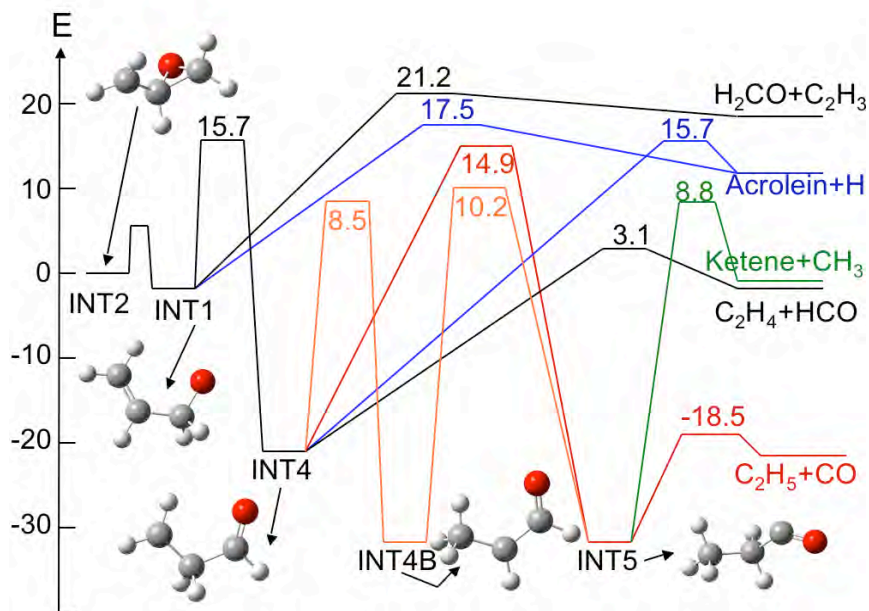
A. O + Allyl

Our primary work this year focused on a continuation of our studies on the complex dynamics of the O + allyl reaction. The work includes imaging experiments and scattering experiments in our lab at Chicago, CCSD(T) calculations on the relevant radical intermediates and transition states on the path to the energetically allowed product channels, and extensive scattering experiments at the NSRRC in Taiwan in collaboration with J. J. Lin on the product

channels accessed from the radical intermediate formed when the O atom adds to an end C atom. Our work identifies all the product channels accessed from that radical intermediate and experimentally determines the product branching fractions. (The latter requires measuring the relative signal levels and calibrating, in separate experiments, the photoionization cross sections of some of the radical and molecular products with respect to Cl atoms or standards like ethene.)

Before our work, a few key studies on the O + allyl reaction had attempted to probe the product branching and dynamics of this reaction. The early bulk kinetics work of Gutman et al (J. Phys. Chem. 94, 3652 (1990)) identified only the acrolein + H product channel as a primary one, putting a <20% upper limit on the H₂CO + C₂H₃ product channel. Later crossed molecular beam experiments by Choi et al (J. Chem. Phys. 116, 2675 (2002); 117, 2017 (2002); 120, 7976 (2004)) focused on detecting only OH and H atom products; they also computationally characterized (J. Chem. Phys. 119, 8966 (2003)) the multiple reaction pathways that can result from the addition of O atoms to an end vs. the central C atom. Most recently, Casavecchia et al (Phys. Chem. Chem. Phys. 9, 1307 (2007)) used soft-electron impact ionization in a crossed-molecular beams experiment to try to identify all the product channels. The data evidenced that acrolein + H is a major product channel, but they were unable to definitively assign the product channels resulting in their signal at m/e=29 and 27, concluding that “one or more C-C fission product channels” contribute to the product branching.

Our first experiments, published this year,¹ photolytically generated the radical intermediate formed when an O atom adds to the end C atom of allyl and then definitively identified all three major product channels resulting from this radical intermediate. The photodissociation of epichlorohydrin at 193 nm produces chlorine atoms and c-OCH₂CHCH₂ radicals; these undergo a facile ring opening to the OCH₂CHCH₂ radical intermediate. State-selective REMPI detection resolves the velocity distributions of ground and spin-orbit excited state chlorine independently, allowing for a more accurate determination of the internal energy distribution of the nascent radicals. To elucidate the product channels resulting from the OCH₂CHCH₂ radical intermediate, the crossed laser-molecular beam experiment uses VUV photoionization and detects the products' velocity distributions. The data identified the three dominant channels that contribute to the product branching: acrolein + H, ethene + HCO, and H₂CO + C₂H₃. A small signal from ketene product is also detected. The measured velocity distributions and relative signal intensities at m/e = 27, 28, and 29 at two photoionization energies show that the most exothermic product channel, C₂H₅ + CO, does not contribute significantly to the product branching. The higher internal energy onset of the acrolein + H product channel, detected in the velocity measurements of the acrolein product, is consistent with the relative barriers en route to each of these product channels calculated at the CCSD(T)/aug-cc-pVQZ level of theory, though a clean determination of the barrier energy to H + acrolein is precluded by the substantial partitioning into rotational energy during the photolytic production of the nascent radicals. The measured branching fraction to the H + acrolein product channel of 18% almost half that predicted using RRKM theory and the calculated transition states. This suggests that the barrier for the 1,2 H-atom shift en route to the ethene + HCO product channel calculated at the CBS-QB3 and CCSD(T) levels of theory may be too high (this isomerization competes with the acrolein + H and H₂CO + C₂H₃ product channels). Interestingly, it may also reflect the fact that the transition state for isomerization and the transition state for C-H fission are not dynamically separated; trajectory calculations are needed to understand this possibility.



Our work this year has focused on the dynamics of the C-C fission product channels and their branching fractions. We can determine the branching fraction to the $\text{H}_2\text{CO} + \text{C}_2\text{H}_3$ product channel from the measured signal intensity at $m/e=27$, C_2H_3^+ , dividing by the total number of radicals formed, determined by detecting the momentum-matched Cl atoms, and correcting for the appropriate kinematic factors and photoionization cross sections of each. (The photoionization cross section for vinyl radicals measured by Neumark et al. and Taatjes et al. play a role here.) The relative signal intensities at $m/e=28$ and $m/e=35$ similarly allow us to determine the branching fraction to the ethene + HCO product channel (using photoionization cross sections measured by Person and Nicole, *J. Chem. Phys.* **49**, 5421 (1968), and put on an absolute scale by Cool et al., *Int. J. Mass Spectrom.* **247**, 18 (2005)). Our data can also allow us to determine the absolute photoionization cross section of HCO radicals. This is a key unknown in analyzing kinetics experiments in other labs. The data we have at 12.1 eV is subject to contamination by daughter fragmentation of H_2CO to HCO^+ , so our work in April at the NSRRC measures the HCO signal relative to ethene at a lower energy and the photoionization yield curve from there to the low ionization energies used by other workers (thus those measurements can be put on a absolute scale using our data). We also are taking data at $m/e=55$ as our calculations of the $\text{OCH}_2\text{CHCH}_2$ cation suggest it may be unstable relative to H_2 elimination (the vertical IE is 10.3 eV while the structure at the adiabatic IE of 6.8 eV reveals a loosely bound $\text{H}_2^{\cdots}\text{CH}_2\text{CHCO}$ cation). Signal from the $\text{OCH}_2\text{CHCH}_2$ radicals formed with vibrational energy below the barrier for isomerization to INT4 directly determines the energy of this barrier, which is key to accurate predictions of the product branching.

Our computational efforts on this system include calculating all the relevant isomerization and dissociation channels of the key radical intermediates in the O + allyl reaction at the CCSD(T)/aug-cc-pVQZ level of theory, followed by predictions of the product branching fractions using master equation modeling and RRKM microcanonical rate constants. Braams has calculated a global potential energy at the B3LYP level of theory; trajectories on that surface offer a valuable test of the statistical predictions.

B. OH + Ethene

Our other major effort this year centered on the radical intermediate formed when an OH radical adds to ethene. There has been extensive experimental and theoretical work on the OH + ethene reaction: thirteen prior theoretical studies and a shocking thirty-eight prior experimental studies, many focusing on the temperature and pressure dependence of the total rate constant. The experiments evidence stabilized radical adduct at high pressure and low temperatures, but become dominated by the H atom abstraction channel to form H₂O + vinyl at high temperatures. Our work investigates the products from the addition of OH to the C=C bond of ethene, forming the HOCH₂CH₂ radical intermediate. Upon forming this adduct, one can expect a competition between collisional stabilization of the adduct in the bulk and, if the adduct is formed with high enough internal energy, its direct dissociation to ethenol + H, and its isomerization, via H-atom transfer, to a second radical intermediate, OCH₂CH₃. This second radical intermediate leads to the formaldehyde + CH₃ and acetaldehyde + H product channels. Interestingly, there has been two recent reports (Taatjes et al, *Science* **308**, 1887 (2005) and *J. Phys. Chem. A* **110**, 3254 (2006) and Cool et al, *J. Chem. Phys.* **119**, 8356 (2003)) of ethenol production in ethene flames; this observation is attributed to the ethenol + H product channel in the OH + ethene reaction.

We used bromoethanol to generate the HOCH₂CH₂ radical intermediate and measured the velocity distributions of the Br(²P_{3/2}) and Br(²P_{1/2}) co-fragments in our imaging experiments with state selective REMPI detection. This accurately determines the internal energy distribution of the nascent HOCH₂CH₂ radicals. We built a new photoionization detection system (using tripled 355 nm light with a photon energy of 10.5 eV) to detect the velocities of the HOCH₂CH₂ radicals that are stable to dissociation. This combined with the measurement of the ethenol velocity distribution that we plan to take in our upcoming trip to the NSRRC should allow us to directly determine the relative energies of the isomerization barrier to the OCH₂CH₃ radical, which leads to the formaldehyde + CH₃ and acetaldehyde + H product channels, and the barrier for direct dissociation of the HOCH₂CH₂ radical intermediate to ethenol + H. The most recent theoretical work (Senosiain et al, *J. Phys. Chem. A* **110**, 6960 (2006)) predicted the barrier to ethenol + H is higher by 1.2 kcal/mol than the isomerization barrier. In contrast other recent theoretical work by M. C. Lin et al (*Chem. Phys. Lett.* **408**, 25 (2005)) predicts the barrier to isomerize to OCH₂CH₃ is higher, not lower, than the barrier for the HOCH₂CH₂ radical intermediate to dissociate to ethenol + H. They conclude that the ethenol + H product channel would be the only significant product channel to compete with the direct abstraction reaction that forms H₂O + C₂H₃. Thus, our experiments are designed to determine the barrier energies for the HOCH₂CH₂ radical adduct to dissociate to ethenol + H and to isomerize to OCH₂CH₃. The velocity distribution of the ethenol product can also determine the energy dependent branching fraction to the ethenol + H channel.

IV. Publications Acknowledging DE-FG02-92ER14305 (2007 or later)

1. Characterization of the Methoxy Carbonyl Radical Formed via Photolysis of Methyl Chloroformate at 193.3 nm, M. J. Bell, K.-C. Lau, M. J. Krisch, D. I. G. Bennett, L. J. Butler and F. Weinhold, *J. Phys. Chem. A*, **111**, 1762-1770 (2007).
2. Investigation of the O + allyl addition/elimination reaction pathways from the OCH₂CHCH₂ radical intermediate, B. L. FitzPatrick, K. -C. Lau, L. J. Butler, S. -H. Lee, and J. J. Lin, *J. Chem. Phys.* **129**, 084301 (2008).

Production and Study of Ultra-Cold Molecules Produced by Kinematic Cooling

David W. Chandler
Combustion Research Facility
Sandia National Laboratory
Livermore, CA 94551-0969
Email:chand@sandia.gov

Program Scope

The study of Chemical Dynamics is the observation and analysis of atomic and molecular action. Both unimolecular and bimolecular action reveals information about the forces that dictate the interactions. These forces are captured in the form of potential energy surfaces. In general inelastic scattering reveals information about the repulsive wall of the potential energy surface, in contrast long-range attractive forces dictate low-energy collision dynamics. It is these long-range attractive forces that we hope to study in greater detail. Previously we have done this by studying near threshold photodissociation events and in the future hope to perform low collision energy inelastic scattering studies. During the last period we have finished our study of near threshold (between 1 and 25 cm⁻¹ above threshold) dissociation of NO-Ar van der Waals clusters. This is equivalent of a low-temperature half collision. If we are able to trap samples of cold molecules in electrostatic and magnetic traps we will be able to determine their collision energy transfer characteristics at low temperature. This information is sensitive to the long range part of the interaction potential. To compliment these studies we propose a new line of study of quantum-state selective diffraction or Fraunhofer scattering. In the past, our inelastic scattering study revealed to us a new technique for cooling molecules to sub Kelvin temperatures, Kinematic Cooling. Kinematic Cooling is the use of a single collision between a molecule and an atom that brings a subset of the molecules to rest in the laboratory reference frame. We have recently studied the scattering of NH₃ and ND₃ from Ne and Kr atom from Kr atom as these systems are mass degenerate and produce the coldest samples.

We have spent effort of the last year investigating Kinematic cooling and trying to bring it to a state where it can be used to study new collisional and spectroscopic regimes. In the next period we plan on continuing our improvements in the technique and demonstrate both high-resolution double-resonant spectroscopy and trapping of molecules utilizing Kinematic cooling. Further we have in development a new cooling technique that takes advantage of the same collision physics to slow molecules. This new technique relies upon a collision between a molecule and an ultra-cold atom inside a magneto optical trap (MOT). We believe this experimental arrangement will allow us to make samples at microKelvin temperatures. Our first experiments are presently underway. In addition, in the last year a radically new (and cheaper) design for a miniature crossed molecular beam apparatus is also being developed for the study of molecular beam scattering and photodissociation. This new design is the subject of a Review of Scientific instruments paper.

Progress report:

During the last year we have developed the Kinematic cooling technique for the “routine” production of samples of millikelvin temperature molecules. One manifestation of this physics has been the crossed molecular beam scattering of a molecular beam from an atomic beam at 90° geometry. By picking the masses of the particles and the velocity of the molecule one can dictate that molecules populating a particular quantum state come to rest in the laboratory. We have produced measurable amounts of cold (milliKelvin temperature range) molecules (NO, NH₃, HCl) as well as cold atoms, Kr and Ne using this technique. Recently we reported on a redesign of our molecular beam apparatus has allowed us to not only produce kinematically cooled molecules but to also extract them from the high density molecular and atomic beams. This is a major advancement in the kinematic cooling technique and will be described below.

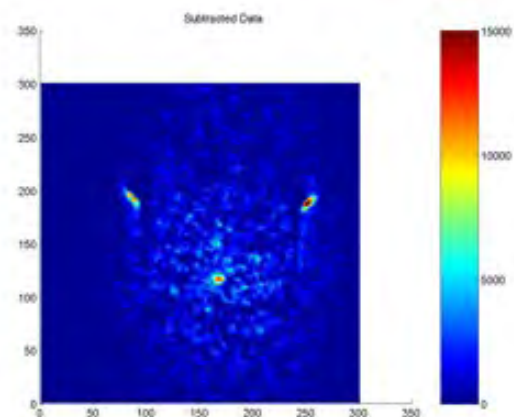


Figure 1: Image of Kr scattering off of Kr producing cold Kr atoms. Because the system is mass degenerate the cold atoms are centered at zero velocity in the laboratory.

The major obstacle in kinematic cooling has been that only a small number of the total collisions results in the formation of cold molecules, and the cold molecules are necessarily formed in the interaction volume of the atomic and molecular beams. As a result, cold molecules have a high probability of secondary glancing collisions with the atomic and molecular beams that re-heat them. In the past year we have reported on our success at reducing the destructive re-heating collisions for the cold molecules such that our observation time is consistent with being limited by diffusion of the cold molecules from our interaction region and not secondary collisions. Under these conditions we are able to observe unconfined kinematically cooled ground vibrational Nitric Oxide (NO), in the $j=7.5$ rotational state for over $150 \mu\text{s}$. An upper limit for the final average velocity is estimated from the diffusion time of the cold molecules from the observation region defined by the intersection of the atomic and molecular beams with the detection laser. The diffusion of the cold molecules is modeled using a three-dimensional Monte-Carlo simulation to account for the size of the interaction region and laser beam overlap. These simulations are consistent with the data and give an average final velocity of approximately, 4.5 m/s for the $\text{NO}(X)_{j=7.5}$. We are now able to observe a single sample of cold molecules in a field free region for up to $150 \mu\text{s}$ that allows for the possibility of trapping of the cold molecules.

This important result is graphically summarized in figure 2 we have, for the first time, been able to establish a set of experimental conditions such that the cold molecules

produced via Kinematic cooling are temporally separated from the parent atomic and molecular beams. This conclusion is supported by our observations of the quantum state dependence of the bi-modal decays for both the $\text{NO}(X) j=7.5$ and $j=10.5$ rotational states. The temporally separated cold molecules can now serve as a starting point for several new experiments including trapping and storing molecules allowing for cold collisional studies and high resolution molecular spectroscopy. We have recently reported on utilizing this technique for the cooling of ammonia molecules in collision with Ne. the $\text{ND}_3 + \text{Ne}$ system as this should result in even colder molecules than the $\text{NO} + \text{Ar}$ system due to the mass match between the atom and molecule.

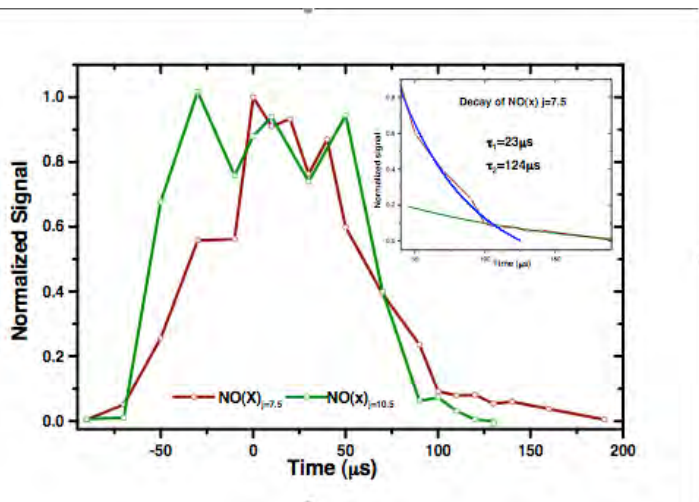


Figure 2: Normalized production and decay of the $\text{NO}(X)j=7.5$ compared with the $\text{NO}(X)j=10.5$. The $\text{NO}(X)j=10.5$ data is given by the marked with the square points and colored green while the $\text{NO}(X)j=7.5$ is marked with the circular points and colored red.

The scattering of a molecular beam perpendicular to an atomic beam is only one geometry that can be utilized for cooling by kinematic collisions. If one imagines that the atomic beam is moving very slowly, then one can see how the scattering of a molecular beam from a continuously loaded MOT of alkali atoms is a special case of Kinematic Cooling. If the molecule of interest has a mass very close to that of the alkali atom then some fraction of the collisions will result in a transfer a significant enough portion of the momentum to the alkali atom to slow the molecule in the vicinity of the MOT. This can be thought of as a billiard like collisions of a fast molecule hitting a “stopped” atom and transferring enough of its momentum to the “stopped” atom for it to be slowed sufficiently and further cooled with glancing collisions with the cold atoms. When an additional optical or electrostatic trap is superimposed upon the MOT then the cold molecules, generated from the effective collisions, can be collected in the trap. Molecules trapped in this manner will subsequently undergo collisional cooling with the ultracold atoms that will further cool them to their temperature of around 100 microKelvin. Experiments are presently underway to demonstrate this technique

Future Work:

We propose to both further the development of our crossed molecular beam scattering program for the study of potential energy surfaces and to further develop the process of kinematically cooling molecules by a single collision with an atom for the production of ultracold molecules. The utilization of those cold, state selected and oriented molecules in unimolecular and bimolecular interaction experiments will be the culmination of this research. Trapping molecules and holding them for long periods of time inside electrostatic or magnetic traps will give us the ability to study both collision dynamics of oriented molecules at low collision energy and photochemistry of unique m_j selected molecular samples. The Kinematic cooling experiments that are of highest priority are the trapping of ammonia utilizing a quadrupole electrostatic trap, the trapping of $\text{NO}(^2\Pi_{3/2})$ by a magnetic trap, demonstration of the MOT cooling technique, and demonstration of Kilohertz-resolution double-resonance spectroscopy with cold molecules. Over the next period we will also extend our work on Kinematic cooling in several areas and add a new effort in the high velocity-resolution scattering detection of near side-far side interference scattering.

BES Supported Publications 2007- 2009

- 1) D. W. Chandler and S. Stolte “ Inelastic Energy Transfer: The NO-rare gas system” **2007**, *Gas Phase Molecular Reaction and Photodissociation Dynamics*, editors K. C. Lin and P. D. Kleiber, Trans World Research Network publishing.
- 2) K. E. Strecker, D. W. Chandler *Physical Review A*. “Kinematic production of isolated milli-Kelvin molecules” **2008**, 78, 063406
- 3) K. E. Strecker, D. W. Chandler “Kinematic Cooling of Molecules” *Low Temperatures and Cold Molecules*. **2008**, Imperial College Press, Editor Ian Smith.
- 4) J. J. Kay, S. Y. T. v. d. Meerakker, K. E. Strecker, D. W. Chandler “Production of Cold ND_3 by Kinematic Cooling” *Transactions of the Faraday Society*. **2009**, Cold and Ultracold Molecule Production Faraday meeting 142.
- 5) W. G. Roeterdink, K. E. Strecker, C. C. Hayden, M. H. M. Janssen, D. W. Chandler “Imaging the rotationally state-selected $\text{NO}(A,n)$ product from the predissociation of the A state of the NO-Ar van der Waals cluster” *J. Chem. Phys.* **2009**, Accepted for publication.
- 6) D. W. Chandler and S. Stolte “ Inelastic Collisions”, *Tutorials in Molecular Reaction Dynamics*, edited Mark Brouard and Claire Vallance, **2009**, Royal Society of Chemistry, in press.
- 7) D. W. Chandler and K. E. Strecker “The Quest for Cold and Ultracold Molecules” *ChemPhysChem*, **2009**, Volume 10 Issue 5, Pages 751 - 754.
- 8) K. E. Strecker and D. W. Chandler “A New Miniature Crossed Molecular Beam Apparatus” *Rev. Sci. Instr.*, **2009**, Submitted for Publication.

Petascale Direct Numerical Simulation and Modeling of Turbulent Combustion

Jacqueline H. Chen (PI) and Ed Richardson
Sandia National Laboratories, Livermore, California 94551-0969
Email: jhchen@sandia.gov

Program Scope

In this research program we have developed and applied massively parallel three-dimensional direct numerical simulation (DNS) of building-block, laboratory scale flows that reveal fundamental turbulence-chemistry interactions in combustion. The simulation benchmarks are designed to expose and emphasize the role of particular physical subprocesses in turbulent combustion. The simulations address fundamental science issues associated with chemistry-turbulence interactions that underly most practical combustion devices: extinction and reignition, flame propagation and structure, flame stabilization in autoignitive flows, autoignition under homogeneous charge compression ignition (HCCI) environments, stratified combustion, and differential transport of soot in turbulent jet flames. In addition to the new understanding provided by these simulations, the resultant data are being used to develop and validate predictive models required in engineering simulations.

Recent Progress

In the past year, significant computer allocations from INCITE grants and from the 250 Tflop Transition-to-Operations at ORNL have enabled us to perform large 3D DNS of: 1) Mixture stratification effects on the structure and propagation of stratified methane-air turbulent jet flames; 2) Intermediate species mixing frequencies in turbulent premixed flames; 3) Stabilization of lifted turbulent ethylene/air jet flames in heated coflow; and 4) Modeling of differential soot transport in a turbulent sooting ethylene-air jet flame. Highlights of our accomplishments in the past year are summarized below, followed by a summary of future research directions.

Mixture Stratification Effects on Propagation in a Turbulent CH₄/Air Flame^{1,2}

Three-dimensional DNS was performed of a stratified methane-air turbulent slot Bunsen fuel jet issuing into a co-flow of burnt products. This configuration allows for intense turbulence to interact with the flame front while preventing the flame from blowing out. Stratification is achieved by varying the equivalence ratio along the span-wise (z) direction. The stratification levels studied are centered about the perfectly premixed $\phi=0.7$ case (Sankaran et al. 2007), extending via a low stratification case $0.4 < \phi < 1.0$, to a highly stratified case with equivalence ratio ranging from zero (pure air) to 1.4. The flame is highly wrinkled with significant flame-flame interactions. Under these conditions the flame is characterized by the thin reaction zones regime in which turbulent eddies penetrate the flame's preheat layer but are too large to disrupt the reaction zone. The result is a thickened preheat layer identified by the reduction of the conditionally averaged progress variable gradient, compared to the laminar flame gradient. As the equivalence ratio falls to $\phi=0.4$ and subsequently drops below the lean flammability limit there is a dramatic reduction in the heat release rate. The areas of weakly burning flame are disrupted by the turbulent motions, permitting study of the broken reaction zones combustion regime.

As the initial fuel-air stratification dissipates due to turbulent mixing, the flames are subjected to steep, time varying equivalence ratio gradients. Locations where the equivalence ratio gradients align normal to the flame exhibit greatly modified burning rates and flame propagation speeds, compared to the perfectly premixed case. Variation of propagation speed with the flame normal equivalence ratio gradient, shows enhanced flame speeds when the products are richer than the reactants, with the reverse also true. The strain rate normal to the flame is strongly correlated with the magnitude of the equivalence ratio gradient, but not its orientation. Studying this effect using computations of both steady and unsteady strained one-dimensional counterflow flames in the presence of equivalence ratio gradients (Richardson et al., 2009) reveals the thermo-chemical basis for this observation. Specifically, equivalence ratio gradients resulting in flames with richer, higher temperature products lead to enhanced equilibrium concentrations of species such as the hydroxyl radical in the flame's carbon monoxide-hydrogen recombination layer. Diffusion of these highly reactive intermediate species towards the reactant side of the flame, as opposed to thermal diffusion, are the main source of the increased reaction rate. Close agreement with the one-

dimensional counterflow simulations with the DNS data establishes the stratified counterflow configuration as a valid paradigm for understanding and modeling turbulent combustion with fuel-air stratification. The presence of equivalence ratio variation through the flame implies that flame speed, flame thickness or reaction rate can not be modeled accurately as functions of only the progress variable and equivalence ratio. Models accounting for temporal and spatial equivalence ratio variation may be advantageous.

Reaction-Diffusion Effects on Species Mixing Rates in Turbulent Premixed CH_4 -Air Combustion³

Advanced turbulent reactive flow models needed for the design of practical applications typically require turbulent mixing frequencies or scalar dissipation rates. In the transported probability density function (PDF) approach, for example, the chemical reaction rate appears in closed form and closure must be achieved by modeling the molecular mixing processes. Reactive scalar mixing time scales have been determined from DNS data for turbulent premixed Bunsen flames in the thin reaction zones regime with reduced methane-air chemistry. Previous conclusions from single step chemistry studies are confirmed regarding the role of dilatation and turbulence-chemistry interactions on the progress variable dissipation rate. In particular, the dissipation rate is controlled by a balance between molecular dissipation and gradient generation due to flame propagation, dilatation and compression of scalar gradients by turbulent strain. The mixing rates of intermediate species which do not vary monotonically with progress variable were up to a factor of ten greater than those of progress variable. They are not well modeled by existing models for mixing rates of either the progress variable or of passive scalars. Effects of the so-called dilatation term appear to be negligible for the intermediates. The effect of turbulent straining is also of reduced importance, becoming negligible for the highest Damköhler number species, H atom. Instead, a reaction-dissipation balance dominates the intermediate scalar gradients, driven by the premixed flame structure. A new model for the ratio of intermediate species and progress variable mixing rates is presented. The model employs the species gradients obtained from laminar flames to estimate the relative magnitude of the species dissipation rates in the turbulent flame. The implied alignment of the species and progress variable provides a good approximation since scalar gradients parallel to the flame make only small contributions to the dissipation rate. The use of laminar flame data also provides a good approximation for the relative magnitude of the species gradients, even in the thin reaction zones regime. Overall, the new model accurately predicts the variation of the intermediate-progress variable mixing frequencies for premixed flame Damköhler numbers greater than 0.5.

Stabilization of Lifted Turbulent Ethylene/Air Jet Flames in Heated Coflow⁴

Direct numerical simulation (DNS) of the near field of a three-dimensional spatially-developing turbulent lifted jet flame in heated coflow is performed with a reduced ethylene-air mechanism to determine the stabilization mechanism and the flame structure. The DNS was performed at a jet Reynolds number of 10,000 with over 1.3 billion grid points. The results show that auto-ignition in a fuel-lean mixture immediately upstream of the flame base is the main source of stabilization of the lifted jet flame. This is verified by the presence of formaldehyde and hydroperoxy upstream of the flame. The dynamics between the instantaneous stabilization point and the large-scale coherent jet motions are investigated by comparing power spectra of the fluctuations of the stabilization point and the two-point correlation function of axial velocity fluctuations over a transverse separation distance of the jet width at the mean stabilization point. Both power spectra show a dominant frequency at a similar Strouhal number of 0.035 showing the fluctuations of the stabilization point are indeed correlated with the passage of large-scale coherent jet motions near the flame base.

Apriori Conditional Moment Modeling of a Temporal Ethylene Jet Flame with Soot¹³

Modeling soot formation in turbulent nonpremixed combustion is a difficult problem. Unlike most gaseous combustion species, soot lacks a strong state relationship with the mixture fraction due to unsteady formation rates which overlap transport timescales, and strong differential diffusion between gaseous species and soot. The conditional moment closure model (CMC) has recently been applied to the problem of turbulent soot formation. A challenge in CMC modeling is the treatment of differential diffusion. 3D DNS of a nonpremixed ethylene jet flame with soot formation has been performed using a nineteen species reduced ethylene mechanism and a four-step, three-moment, semi-empirical soot model.

The DNS provides full resolution of the turbulent flow field and is used to perform a-priori analysis of a recent CMC model derived from the joint scalar PDF transport equation. Unlike other approaches, this CMC model does not require additional transport equations to treat differentially diffusing species. A budget of the terms of the CMC equation for both gaseous species and soot is presented. In particular, exact expressions for unclosed terms are compared to typical closure models for scalar dissipation, cross dissipation, differential diffusion, and reactive source terms. The differential diffusion model for gaseous species is found to be quite accurate, while that for soot requires an additional model for the residual term.

Future Plans

Stabilization of a N-Heptane Jet Flame in Hot Coflow at Diesel Pressures

Lifted turbulent jet flames in heated co-flows provide an excellent test case for chemical kinetics and the modeling of the turbulence/chemistry interactions in turbulent flows. Recent DNS and PDF models have revealed that the stabilization mechanism is primarily auto-ignition, but with turbulent mixing also playing a role. Hence the kinetics of auto-ignition – relevant to IC engines can be studied in detail in this configuration. DNS are planned at diesel pressures (~40 atm) to investigate the role of ‘cool flame’ chemistry and low-temperature heat release on lifted flame stabilization. Parametric studies will be performed varying the co-flow temperature, jet velocity, pressure, and ignition quality of the fuel. Fuels under consideration include n-heptane and oxygenated fuels like dimethyl ether. Previous strained counterflow n-heptane ignition studies at diesel pressures show strong sensitivity of the thermal dissociation reaction $\text{H}_2\text{O}_2 \rightarrow \text{OH} + \text{OH}$ to fluctuations in local mixing conditions, and hence differences in the ignitability of fuels in a dissipative environment may influence ignition delays and lift-off heights.

Controlling Ignition Timing and Combustion Rates under HCCI Conditions through Stratification

HCCI combustion offers the potential of high diesel-like efficiencies with low NO_x and particle emissions. It achieves this by burning overall lean and dilute, largely through volumetric autoignition in the absence of flames. As a viable alternative to spark-ignited engines, an important issue that needs to be resolved is controlling the rapid rate of pressure rise and energy release at high loads. One strategy is to control the rate of pressure rise through mixture and thermal stratification. The objective of the proposed study is to determine the effect of different mean and root-mean-square temperature and concentration distributions, particularly spanning the negative temperature coefficient (NTC) region, on the transient evolution of ignition of fuel-lean n-heptane and dimethyl ether mixtures at high pressure in a constant volume. In particular, the influence of scalar gradients, and dilution with exhaust gas recirculation (EGR) on ignition front propagation and structure will be determined as a function of the level of stratification and turbulence characteristics. A priori evaluation of ODT/LEM models for HCCI will also be performed.

A priori Lagrangian Particle Analysis of Reactive Scalar Mixing Models

Building on the latest study of mixing timescales in premixed combustion³, turbulent combustion timescales will be analyzed in stratified and autoigniting non-premixed DNS data sets. The use of detailed models for reaction and diffusion permits the effects of realistic thermal expansion (dilatation), differential transport, and strain-scalar alignments to be investigated. In particular the results of the modified flame structures arising due to mixture stratification will be assessed in comparison to premixed flame mixing. The autoigniting non-premixed particle data will be probed to explore the transition from passive low temperature mixing processes to flamelet dominated combustion. Having shown that the reactive species all mix at different rates, depending on both the combustion mode and regime, it is necessary to develop and validate mixing models capable of expressing the full range of mixing behavior.

DNS and Modeling of Stratified Turbulent Flame Propagation and Structure

The library of benchmark data on turbulent stratified jet flames will be expanded by varying the initial orientation of the fuel stratification such that the stratification is aligned with the direction of mean shear. The instantaneous flame structure and propagation rates will be compared to new asymptotic and laminar one-dimensional representations of stratified combustion, validating their use as a paradigm for turbulent stratified combustion. Effects of fuel stratification on turbulent flame speed and flame surface area will be analyzed in comparison to premixed flame data.

References:

1. E. S. Richardson and J. H. Chen, "DNS of Stratified Turbulent CH₄-Air Flames," TNF9, Montreal, 2008.
2. E. S. Richardson, V. E. Granet, A. Eyssartier, and J. H. Chen, "Effects of Equivalence Ratio Variation on Lean Stratified CH₄-Air Laminar Counterflow Flames, Mediterranean Combustion Symposium 6, 2009.
3. E. S. Richardson, R. Sankaran, R. W. Grout, and J. H. Chen, "A Numerical Analysis of Reaction-Diffusion Effects on Species Mixing Rates in Turbulent Premixed Methane-Air Combustion," Paper #21D4, US Joint Sections Meeting, 2009.
4. J. H. Chen, C. S. Yoo, R. Grout, A. Mascarenhas, P.T. Bremer and V. Pascucci, "Terascale Simulations of Turbulent Jet Flames and the Morphology of High Scalar Dissipation Rate Regions," DNS/LES of Reacting Flows, October 22-24, 2008 Eindhoven, Netherlands.

BES Publications (2007-2009)

1. R. Sankaran, E. R. Hawkes, J. H. Chen, T. Lu, and C. K. Law, "Structure of a Spatially-Developing Lean Methane-Air Turbulent Bunsen Flame," *Proceedings of the Combustion Institute*, **31**:1291-1298, (2007).
2. E. Hawkes, R. Sankaran, J. Sutherland, and J. H. Chen, "Scalar Mixing in DNS of Temporally-Evolving Plane Jet Flames with Detailed CO/H₂ Kinetics," *Proc. of the Combustion Institute*, **31**:1633-1640, (2007).
3. D. J. Cook, H. Pitsch, J. H. Chen, and E. R. Hawkes, "Flamelet-Based Modeling of Autoignition with Thermal Inhomogeneities for Application to HCCI Engines," *Proc. of the Combust. Inst.*, **31**: 2903-2911, (2007).
4. J. C. Sutherland, P. J. Smith, and J. H. Chen, "A quantitative method for a priori evaluation of combustion reaction models," *Combust. Theory and Modelling*, **11**, 287-303, (2007).
5. D. Lignell, J. H. Chen, P. J. Smith, T. Lu and C. K. Law, "The effect of flame structure on soot formation and transport in turbulent nonpremixed flames using DNS," *Combust. Flame* 151:2-28 (2007).
6. D. Lignell, J. H. Chen, and P. J. Smith, "Three-dimensional DNS of Soot Formation and Transport in a Temporally-Evolving Non-premixed Ethylene Jet Flame," *Combust. Flame* 155:316-333 (2008).
7. N. Chakraborty, E. R. Hawkes, J. H. Chen, and S. Cant, "The Effects of Strain Rate and Curvature on Surface Density Function Transport in Turbulent Premixed Methane-Air and Hydrogen-Air Flames: A Comparative Study," *Combust. Flame* **154**: 259-280 (2008).
8. F. Bisetti, J. Y. Chen, E. R. Hawkes, and J. H. Chen, "Probability Density Function Treatment of Turbulence-Chemistry Interactions during the Ignition of a Temperature-Stratified Mixture for Application to HCCI Engine Modeling," *Combust. Flame* **155**:571-584 (2008).
9. C. S. Yoo, J. H. Chen, J. H. Frank, "A Numerical Study of Transient Ignition and Flame Characteristics of Diluted Hydrogen Versus Heated Air in Counterflow," *Combust. Flame* **156**:140-151 (2009).
10. E. R. Hawkes, R. Sankaran, J. H. Chen, S. Kaiser, and J. H. Frank, "An Analysis of Lower-Dimensional Approximations to the Scalar Dissipation Rate using DNS of Plane Jet Flames," *Proc. of the Combust. Inst.*, **32**, **1**, 1455-1463 (2009).
11. E. S. Richardson, C. S. Yoo, and J. H. Chen, "Analysis of Second-Order Conditional Moment Closure Applied to an Autoignitive Lifted Hydrogen Jet Flame," *Proc. of the Combust. Inst.*, **32**, **2**, 1695-1703 (2009).
12. U. D. Lee, C. S. Yoo, J. H. Chen, and J. H. Frank, "Effects of H₂O and NO on Extinction and Reignition of Vortex-Perturbed Hydrogen Counterflow Flames," *Proc. of the Combust. Inst.*, **32**, **1**, 1059-1066 (2009).
13. D. Lignell, J. C. Hewson, and J. H. Chen, "A priori Analysis of Conditional Moment Closure Modeling of a Temporal Ethylene Jet Flame with Soot Formation using DNS," *Proc. of the Combust. Inst.*, **32**, **1**, 1491-1498 (2009).
14. F. Bisetti, J. Y. Chen, E. R. Hawkes, and J. H. Chen, "Differential Diffusion Effects During the Ignition of a Thermally Stratified Premixed Hydrogen-Air Mixture Subject to Turbulence," *Proc. of the Combust. Inst.*, **32**, **1**, 1465-1472 (2009).
15. T. Lu, C. S. Yoo, J. H. Chen, and C. K. Law, "On-the-fly Stiffness Removal for DNS," to appear *Combust. Flame*, 2009.
16. C. S. Yoo, J. H. Chen, and R. Sankaran, "Three-Dimensional Direct Numerical Simulation of a Turbulent Lifted Hydrogen Jet Flame in Heated Coflow: Flame Stabilization and Structure," submitted to *J. Fluid Mech.* (2008).
17. T. Lu, C. S. Yoo, J. H. Chen, and C. K. Law, "Analysis of a Turbulent Lifted Hydrogen/Air Jet Flame from DNS with Computational Singular Perturbation," submitted to *J. Fluid Mech.* (2008).
18. U. D. Lee, S. A. Kaiser, C. S. Yoo, J. H. Chen, and J. H. Frank, "Effects of NO on Extinction and Reignition of Vortex-Perturbed Hydrogen Flames," submitted to *Combust. Flame* (2008).
19. A. Gruber, R. Sankaran, E. R. Hawkes, and J. H. Chen, "Turbulent Flame-Wall Interaction at Low Reynolds Number: A DNS Study," submitted to *J. Fluid Mech.* (2009).

Dynamics and Energetics of Elementary Combustion Reactions and Transient Species Grant DE-FG03-98ER14879

Robert E. Continetti
Department of Chemistry and Biochemistry
University of California San Diego
9500 Gilman Drive
La Jolla, CA 92093-0340
rcontinetti@ucsd.edu

March 30, 2009

I. Program Scope

This research program continues to focus on the preparation and study of transient neutral species and collision complexes relevant to combustion phenomena. In the past year, the primary focus has been on the design and construction of a new cryogenically cooled ion trap to allow the preparation of negative ion precursors to important neutral combustion intermediates with well-characterized internal temperatures. This new apparatus will allow us to extend our studies of the HOCO free radical and the potential energy surface that governs the $\text{OH} + \text{CO} \rightarrow \text{H} + \text{CO}_2$ reaction, by removing any ambiguity owing to internal excitation of the precursor HOCO^- anion, and allowing a more definitive determination of the direct and tunneling contributions to the $\text{H} + \text{CO}_2$ product channel. Our goal is to provide detailed information on the energetics and reaction dynamics of important combustion intermediates such as HOCO, allowing more quantitative evaluation of the roles they play in combustion and the validation of theoretical approaches to predicting the dynamics of combustion reactions.

With the construction of the fast beam linear electrostatic ion trap, this research program will take the technique of photoelectron-photofragment coincidence (PPC) spectroscopy to a new level. As we have shown in prior work, photodetachment of precursor anions in a mass-selected negative ion beam allows the preparation of mass- and energy-selected neutral species if the parent anions are internally cold. Particularly for high frequency vibrations, this is sometimes difficult to establish, in particular with the kHz ion sources required for the single-pass experiments carried out to date. By trapping and cooling molecular anions then synchronizing the ions oscillating in the trap with our photodetachment laser, we will be able to study the dissociation pathways of the unstable neutral products using current coincidence imaging techniques. The detection methods in use also enable measurement of angular distributions for both the photoelectrons and photofragments, providing further insights into the dissociative photodetachment (DPD) dynamics. We anticipate that with the trap in use, a new generation of transition-state dynamics experiments on hydroxyl radical reactions such as $\text{OH} + \text{OH}$, $\text{OH} + \text{F}$, $\text{OH} + \text{Cl}$ and $\text{OH} + \text{H}_2$ will become possible. In addition, our effort to carry out studies of larger oxygenated radicals initiated last year will benefit considerably as well, owing to the fact that in these larger polyatomic systems uncertainty in the internal energy become even more significant.

II. Recent Progress

A. Probing the $\text{OH} + \text{CO} \rightarrow \text{HOCO} \rightarrow \text{H} + \text{CO}_2$ reaction by photodetachment of HOCO^-

In the last year we completed publishing the initial phase of our efforts to study the $\text{OH} + \text{CO} \rightarrow \text{HOCO} \rightarrow \text{H} + \text{CO}_2$ reaction by photodetachment of HOCO^- with a manuscript in *Molecular Physics* focusing on finer details of the recoil-frame photoelectron and photofragment angular

distributions in the dissociative photodetachment of HOCO^- as it proceeds via unimolecular decomposition of the energized HOCO free radical. This work builds on our earlier studies of the $\text{OH} + \text{CO} \rightarrow \text{H} + \text{CO}_2$ potential energy surface.^{1,2,3} Anisotropic photofragment angular distributions were observed in the $\text{HOCO}^-/\text{DOCO}^- + h\nu \rightarrow \text{OH}/\text{OD} + \text{CO} + e^-$ channel. The anisotropy parameters were obtained for the laboratory frame (LF) angular distributions of photoelectrons for all three photodetachment channels ($\text{HOCO} + e^-$, $\text{OH} + \text{CO} + e^-$ and $\text{H} + \text{CO}_2 + e^-$) at 388 and 775 nm and the photofragment angular distribution was also obtained for $\text{OH} + \text{CO}$. The photoelectron angular distributions (PAD) were also studied within the photofragment recoil frame (RF) using the coincidence data. The comparison of LF- and RF-PAD in the $\text{OH} + \text{CO} + e^-$ channel shows the latter one is more isotropic, indicating that lifetimes of the neutral HOCO free radicals that dissociate into $\text{OH} + \text{CO}$ are commensurate with the period of molecular rotation. Estimated upper limits of 9×10^{-13} sec and 1.3×10^{-12} sec were found for HOCO and DOCO dissociation into $\text{OH}/\text{OD} + \text{CO}$, respectively. Our ability to study the RF-PADs for the $\text{H} + \text{CO}_2 + e^-$ channel was limited by the small solid angle for detection of the light H atoms. This is a limitation that can be overcome in the future by implementation of a larger area detector for the neutral photofragments.

This initial study of the more detailed dynamics of DPD in the HOCO^- system provides some insight into what could be obtained in a next generation experiment: detailed lifetimes as a function of internal energy for HOCO. We have yet to record the huge data set required for this next step owing to some open questions about the internal energy of the HOCO^- and DOCO^- parent anions. In work published in 2007, we focused on isotope effects in the product energy distributions and branching ratios obtained by the DPD of HOCO^- and DOCO^- at a photon energy of 3.21 eV.² These experiments confirmed that the $\text{H} + \text{CO}_2 + e^-$ channel is open below the calculated dissociation barrier,⁴ indicating that quantum mechanical tunneling is important for this channel. The tunneling effect was found to be essentially removed by deuteration of the system. Furthermore, it was found at all wavelengths that the $\text{OH} + \text{CO}$ product channel is observed at and slightly *below* the calculated energetic limit. In this case, tunneling is not possible and the most likely explanation are hot bands in the HOCO^- anion, assuming the quantum chemical calculations on the energetics of this system are accurate. These results were compared with six-dimensional quantum dynamics simulations of the DPD of HOCO^- by Gray, Goldfield and co-workers.⁵ Good qualitative agreement was found with theory, with the exception of the absence of significant tunneling in the $\text{HOCO} \rightarrow \text{H} + \text{CO}_2$ pathway on the LTSH potential energy surface⁶ used in the calculations. The LTSH surface was optimized for reproducing kinetic data, and has been found to have a relatively poor description of the HOCO well and the barrier between the well and the $\text{H} + \text{CO}_2$ product channel. Theoretically, a refined potential energy surface for both the neutral and the parent anion are required for more accurate quantum dynamics predictions. Experimentally, in light of the discrepancies of the $\text{OH}/\text{OD} + \text{CO}$ product channel results with theory, it is incumbent upon us to resolve the outstanding issue of the parent anion vibrational temperature. This critical issue will be addressed with the new cryogenic ion trap that is now being brought online as discussed in the next section.

B. Cryogenically cooled linear electrostatic ion beam trap

An important focus of the project is to develop methods to allow greater control and better characterization of the internal energies in the parent anions used to study the neutral reaction dynamics relevant to combustion. To this end, we are constructing an electrostatic ion beam trap of the type developed by Zajfman and co-workers.⁷ This trap will enable the study of internally cold ions, leading to more precise determinations of the energies of molecular dissociation processes and the internal states of various species, as well as remove ambiguities in dissociation processes due to potential internal excitation.

The trap consists of two electrostatic mirrors surrounded by cold shields held at 10K, as shown schematically in Figure 1. Ions are injected through one of the mirrors, which is then switched to the reflection potential prior to the first round trip, trapping an ion bunch. Ions oscillating in the trap have well defined and consistent momenta, which makes it ideal for the photoelectron-photofragment coincidence experiments carried out in this lab. There is a large field-free region at the center of the trap where a pulsed laser can interact with the trapped ions. This interaction produces an electron which will be detected by an imaging detector placed above the center of the trap cavity, and multiple neutral products that will continue downstream along the center-of-mass trajectory and impact a second time-and-position sensitive detector, achieving the kinematically complete measurement that constitutes photoelectron-photofragment coincidence spectrometry. The ions in the trap will have nearly no exposure to room temperature radiation, ensuring that they can radiatively cool over periods of milliseconds to seconds.^{8,9}

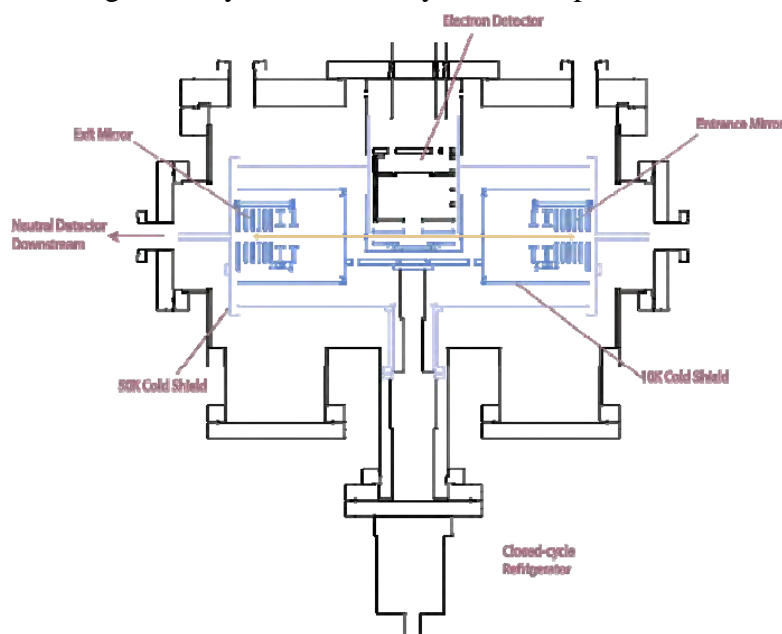


Figure 1. Schematic diagram of the cryogenically cooled linear ion beam trap configured for carrying out photoelectron-photofragment coincidence spectroscopy.

The trap has been installed on an existing translational spectrometer. A closed-cycle cryogenic refrigeration and vacuum pumping system is now in place to maintain the trap chamber at low pressures and to cool the cold shields. Electronic systems and software to monitor and modify the parameters of trapped ions have been developed and are currently either implemented or in testing. Finally, a new data acquisition system which records not only particle hits from electron and neutral detectors, but also the cooling time for a given event is under development in order to quantitatively investigate cooling dynamics of trapped ions. We have successfully trapped O_2^+ and Ar^+ ions at 7 keV beam energy and are now

prepared to assemble and install the shields so we can commence to run at cryogenic temperatures. In the meantime, we have been exploring the parameter space of the trap and optimizing trapping lifetimes. Initial results are very positive relative to reported lifetimes by other groups. Lifetimes are primarily characterized by two exponential factors, a fast component that represents loss of ions not on proper trajectories, and a slow component due to collisions with background gas.¹⁰ Conditions have been found to minimize the effect of the first decay, and provide for the slowest rate of decay in the second component. Presently, ion density in the trap as a function of time is being measured by the detection of fast neutrals on a microchannel plate detector downstream of the trap, however, a ring pickup electrode has also been demonstrated that allows nondestructive measurement of the oscillating trapped ions. The best lifetimes ($1/e$ relaxation times) achieved to date are 202 ms for Ar^+ and 126 ms for O_2^+ at a background pressure of 2×10^{-9} . Scaling the Ar lifetime to compare with reported numbers shows that these lifetimes are $\sim 30\%$ longer than previously demonstrated.⁷ The vacuum chamber has been proven to 1×10^{-11} torr, so it is expected that ultimately trapping times in excess of 10 s can be obtained given the inverse dependence of trapping lifetime and ambient pressure.

Initial indications of bunching dynamics suggest a dephasing of ions from the injected bunch over the first 5 - 10 ms of trapping, with bunch signal disappearing completely around 12 ms after injection. These relatively long natural bunching lifetimes suggest forced bunching by application of an RF field with a frequency nearly equal to the trap frequency should be successful.¹¹ By tuning the trap frequency to approximately an integer multiple of the laser repetition rate, forced bunching by an RF frequency phaselocked exactly to the laser output will ensure laser-ion overlap for each laser shot. This system has been tested on the bench and promises to be very stable.

III. Future plans

Once trapping is demonstrated and optimized for cryogenic operation, an analysis of the cooling rates may first be carried out by photodissociation of a well-characterized molecular cation such as H_3^+ . We anticipate, however, moving expeditiously to convert to negative ion mode of operation so we can carry out this year the important study of the HOCO^- anion internal energy needed to resolve the outstanding questions concerning the benchmark $\text{OH} + \text{CO} \rightarrow \text{H} + \text{CO}_2$ reaction. In addition, we will then be in a position to pursue completion of our studies of carboxyl radicals and reaction complexes involving the hydroxyl radical with polyatomic molecules starting with ionic complexes such as $\text{OH}^-(\text{CH}_3)$ and $\text{OH}^-(\text{CH}_3\text{COCH}_3)$.

IV. DOE Publications: 2007 – 2009

1. Z. Lu, Q. Hu, J.E. Oakman and R.E. Continetti, "Dynamics on the HOCO potential energy surface studied by dissociative photodetachment of HOCO^- and DOC O^- .", *J. Chem. Phys.* **126**, 194305-1 – 194305-11 (2007).
2. Z. Lu and R.E. Continetti, "Alignment of a molecular anion via a shape resonance in near-threshold photodetachment.", *Phys. Rev. Lett.* **99**, 113005-1 – 113005-4 (2007). Featured in the Virtual Journal of Ultrafast Science, vol. 6, No. 10, 2007. <http://www.vjulfrafast.org/>
3. Z. Lu, J.E. Oakman, Q. Hu and R.E. Continetti, "Photoelectron-photofragment angular correlations in the dissociative photodetachment of HOCO^- .", *Molec. Phys.* **106**, 595-606 (2008).

V. References Cited

-
1. T.G. Clements, R.E. Continetti and J.S. Francisco, *J. Chem. Phys.* **117**, 6478 (2002).
 2. Z. Lu, Q. Hu, J. E. Oakman, and R. E. Continetti, *J. Chem. Phys.* **126**, 19305 (2007).
 3. Z. Lu and R.E. Continetti, *Phys. Rev. Lett.* **99**, 113005 (2007)
 4. H.-G. Yu, J.T. Muckerman and T. Sears, *Chem. Phys. Lett.* **349**, 547 (2001).
 5. S. Zhang, D. M. Medvedev, E. M. Goldfield, and S. K. Gray, *J. Chem. Phys.* **125**, 164312 (2006).
 6. M. J. Lakin, D. Troya, G. C. Schatz, and L. B. Harding, *J. Chem. Phys.* **119**, 5848 (2003).
 7. M. Dahan, *et al.*, *Rev. Sci. Instrum.* **69**, 76 (1998).
 8. Z. Amitay, D. Zajfman and P. Forck, *Phys. Rev. A* **50**, 2304 (1994)
 9. H. Kreckel, *et al.*, *Phys. Rev. A* **66**, 052509 (2002)
 10. H.B. Pedersen, *et al.*, *Phys. Rev. A* **65**, 042703 (2002)
 11. H.B. Pedersen, *et al.*, *Phys. Rev. Lett.* **87**, 055001 (2001)

Studies of the Chemistry of Oxygenated Fuels with Photoionization Mass Spectrometry

Terrill A. Cool

School of Applied and Engineering Physics
Cornell University, Ithaca, New York 14853
tac13@cornell.edu

I. Project Scope

Clean-burning renewable oxygenated bio-derived fuels are potentially important replacements for conventional gasoline and diesel fuels, which may reduce dependence on imported petroleum and lower net greenhouse-gas emissions. Our current research focuses on the chemistry of thirteen simple methyl and ethyl esters chosen as surrogates for the long-chain esters that are primary constituents of biodiesel fuels. Principal goals of these studies are: (1) show how fuel-specific structural differences including degree of unsaturation, linear vs branched chain structures, and methoxy vs ethoxy functions affect fuel-destruction pathways, (2) understand the chemistry leading to potential increases in the emissions of hazardous air pollutants including aldehydes and ketones inherent in the use of biodiesel fuels, and (3) define the key chemical reaction mechanisms responsible for observed reductions in polycyclic aromatic hydrocarbons, particulate matter, unburned hydrocarbons, and carbon monoxide when oxygenated fuels are used as replacements for conventional fuels. Experimental measurements of the composition of reaction intermediates for each of the thirteen selected model compounds, performed with flame-sampling molecular-beam synchrotron photoionization mass spectrometry, combined with comprehensive kinetic modeling, are key steps toward predictive descriptions of the combustion of practical biodiesel fuels.

II. Recent Progress

A. MBMS Study of Low-Pressure Premixed $C_5H_{10}O_2$ Ethyl and Methyl Ester Flames. B. Yang, J. Wang, T.A. Cool, T. Kasper, N. Hansen, K. Kohse-Höinghaus

Low-pressure premixed laminar flames fueled by three $C_5H_{10}O_2$ ester isomers: methyl butanoate (MB), methyl isobutanoate (MIB) and ethyl propanoate (EP), were studied using flame-sampling molecular beam synchrotron photoionization mass spectrometry. Most intermediates were identified using measurements of photoionization efficiencies (PIE) spectra and spatial mole fractions. Comparisons of the compositions of reaction intermediates revealed fuel-specific differences in the initial fuel destruction pathways.

Methyl ester versus ethyl ester:

For the low-pressure premixed flames studied here, primary fuel destruction pathways include H-atom abstractions and cyclic (four- and six-center) unimolecular dissociations. H-abstraction from the methoxy group, followed by β -scission, leads to substantial formation of formaldehyde in methyl ester flames, while abstraction of a secondary hydrogen from the ethoxy group, followed by β -scission, accounts for the relatively high concentration of acetaldehyde among ethyl esters. The maximum mole fraction for formaldehyde in the MB flame is four times larger than that in the EP flame, while the maximum mole fraction for acetaldehyde in the EP flame is about eight and ten times larger than that in MB and MIB flames, respectively. Similar trends were also observed in our previous study of the combustion of the $C_3H_6O_2$ ester isomers: methyl acetate and ethyl formate.

Moreover, the conclusion reached in previous work that, for ethyl ester flames, primary hydrogen abstraction from the ethoxy group and six-centered dissociation may lead to the formation of C_2H_4 and significant sequential yields of other C_2 species is confirmed by this study. The high concentrations of C_2 species in ethyl ester flames may potentially lead to higher benzene concentrations than for methyl esters. However, several possible routes involving not only C_2 but also C_3 and even C_5 species may contribute to benzene formation. H-abstraction from acyl ester groups may also be important pathways to formation of

unsaturated hydrocarbons. Indeed, we find that the MIB flame has a greater tendency to form benzene than the EP flame, despite the observation that benzene formation in ethyl formate flames exceeds that of methyl acetate flames under identical flame conditions.

Linear ester versus branched ester:

MB and MIB differ by the chain structure of the alkyl in the acyl group. H-abstraction reactions from this group may account for differences in the composition of intermediates caused by linear/branched effects. There are three and two sites, respectively, for H-abstraction in the acyl group for MB and MIB. As a consequence, ethyl ketene is formed in the MB flame while dimethyl ketene is observed in the MIB flame, which is the most notable difference between these two flames. As for the hydrocarbon species, MB favors the formation of methyl radical, ethylene and propene, while MIB only favors the formation of methyl radical and propene. On the whole, linear/branched influences are not as pronounced as the methoxy/ethoxy effects for these simple ester flames; however, this observation may not be applicable for larger esters with high degrees of chain branching.

B. Experimental and Kinetic Modeling Study of Methyl Formate Low-Pressure Flames S. Dooley, M. Chaos, F.L. Dryer, H.J. Curran, B. Yang, J. Wang, T. A. Cool, T. Kasper, N. Hansen

The high temperature oxidation of methyl formate was studied in low-pressure burner stabilized flames. A new comprehensive mechanism for methyl formate $\text{H}(\text{C}=\text{O})\text{OCH}_3$ oxidation has been developed, based upon expansion of a recent C_1 mechanism and an added C_2 subset. Predictions using this kinetic model were compared with new quantitative measurements of species concentrations in low-pressure (22-30 Torr) laminar flames performed with flame-sampling molecular-beam synchrotron photoionization mass spectrometry. These low-pressure flame measurements cover a broad range of equivalence ratios from $\Phi=1.0$ to 1.8 to complement previous high pressure (3 atm, 900 K) flow-reactor measurements for $\Phi=0.5$ to 1.6, shock tube ignition delay measurements (2-10 atm, 1000-2400 K, $\Phi = 0.5$ to 2.0) and burning velocities of outwardly propagating spherical $\text{H}(\text{C}=\text{O})\text{OCH}_3/\text{air}$ flames at atmospheric conditions for $0.6 < \Phi < 1.4$. The generally good agreement of model predictions with this diverse set of experiments provides a further validation of the proposed mechanism of methyl formate oxidation and contributes to the description of the analogous chemical kinetics of larger methyl esters.

Methyl formate is a small chemical system and as such its oxidation is devoid of the production of large intermediates. We have shown that the radicals formed by H-abstraction may beta-scission to form only small molecules that are common intermediates in any hydrocarbon system: CO , CO_2 , CH_2O and the radical species, CH_3 , CH_3O and HCO . Thus under the conditions of these low-pressure flames, any detectable intermediate species with the exception of methanol and methane, which are shown to form by direct elimination from MF, must result from radical recombination or addition reactions. As the molecular structure of MF does not contain any carbon to carbon bonds, one would expect that the formation of any C_2 species would be minimal. This conjecture fails to consider the effects of radical-radical recombination reactions. Besides methyl-methyl recombination leading to C_2H_5 common to all methyl ester flames, we suggest that close attention must be paid to other radical-radical recombination reactions in order to account for significant under-prediction of C_2H_4 and C_2H_2 mole fractions in the MF flames. The inclusion of this additional chemistry has practically no impact on the predicted profiles of the other species and does not interfere with the model verifications provided by the high pressure experiments, which have relatively small alkyl radical concentrations compared with the pools of intermediates found in low-pressure flames.

C. A detailed chemical reaction mechanism for oxidation of four small alkyl esters in laminar premixed flames, C. K. Westbrook, W. J. Pitz, P. R. Westmoreland, F.L. Dryer, M. Chaos, P. Oßwald, K. Kohse-Höinghaus, T. A. Cool, J. Wang, B. Yang, N. Hansen, T. Kasper

A detailed chemical kinetic reaction mechanism has been developed for a group of four small alkyl esters fuels, consisting of methyl formate, methyl acetate, ethyl formate and ethyl acetate. This mechanism is validated by comparisons between computed results and recently measured intermediate species mole fractions in fuel-rich, low-pressure, premixed laminar flames. The model development employs a principle of similarity of functional groups in constraining the H-atom abstraction and unimolecular decomposition reactions in each of these fuels. As a result, the reaction mechanism and

formalism for mechanism development are suitable for extension to larger oxygenated hydrocarbon fuels, together with an improved kinetic understanding of the structure and chemical kinetics of alkyl ester fuels that can be extended to biodiesel fuels. Variations in concentrations of intermediate species in these flames are traced to differences in molecular structure of the fuel molecules.

D. Composition of reaction intermediates for stoichiometric and fuel-rich dimethyl ether flames: Flame-sampling mass spectrometry and modeling studies. J. Wang, .Yang, T. A. Cool, M. Chaos, F. L. Dryer, T. Kasper, N. Hansen, P. Oßwald, K. Kohse-Höinghaus, P. R. Westmoreland

Molecular-beam synchrotron photoionization mass spectrometry and electron-ionization mass spectrometry are used for measurements of species mole fraction profiles for low-pressure premixed dimethyl ether (DME) flames with equivalence ratios ranging from near-stoichiometric conditions ($\Phi=0.93$) to fuel-rich flames near the limits of flat-flame stability ($\Phi=1.86$). The results are compared with predictions of a recently modified kinetic model for DME combustion [Zhao et al., *Int. J. Chem. Kinetics*, 2008, **40**, 1-18] that has been extensively tested against laminar flame speed measurements, jet-stirred reactor experiments, pyrolysis and oxidation experiments in flow reactors, species measurements for burner-stabilized flames and ignition delay measurements in shock tubes. The present comprehensive measurements of the composition of reaction intermediates over a broad range of equivalence ratios considerably extends the range of the previous experiments used for validation of this model and allows for an accurate determination of contributions of individual reactions to the formation or destruction of any given flame species. The excellent agreement between measurements and predictions found for all major and most intermediate species over the entire range of equivalence ratios provides a uniquely sensitive test of details of the kinetic model. The dependence on equivalence ratio of the characteristic reaction paths in DME flames is examined within the framework of reaction path analyses.

III. Future Plans

To date, we have completed experimental measurements and data analysis for 7 of 13 simple ester fuels. These 7 are methyl formate, methyl acetate, ethyl formate, ethyl acetate, methyl butanoate, methyl isobutanoate, and ethyl propanoate. Kinetic modeling is complete for the first 4 of these. During the next year we will finish all of our current proposed research on all 13 fuels. The remaining 6 fuels are methyl crotonate, ethyl propenoate, methyl methacrylate, methyl propenoate, vinyl acetate, and methyl propanoate. The experiments are performed for 30 Torr flat-flames with equivalence ratios of 1.2 and 1.56. Flames of fuel isomers are of particular interest because they can be studied under nearly identical flame conditions (flow rates, pressures, major species mole fractions, temperature profiles). These similarities facilitate the interpretation of the respective intermediate species compositions in terms of fuel-specific destruction mechanisms. For example, flames of the three $C_5H_{10}O_2$ $m/z=102$ isomers exhibit markedly different intermediate species compositions that reveal respective fuel-specific (methoxy vs ethoxy functions, and linear vs branched chain structure) fuel decomposition mechanisms. These flames can also be compared with those of three mono-unsaturated $C_5H_8O_2$ $m/z=100$ isomers to examine the effects of unsaturation on fuel decomposition. There are three pairs among these six fuels that have similar structures, differing only in degree of unsaturation (i.e., methyl butanoate vs methyl crotonate, methyl isobutanote vs methyl methacrylate, ethyl propanoate vs ethyl propenoate).

These molecules have relatively simple structures compared with the long hydrocarbon chains (up to 16-18 carbon atoms) of the component fatty acid esters of practical biodiesel fuels, which are precluded for use in laboratory flame studies because of their low volatility. Nevertheless, these molecules are well-suited for the proposed studies because they contain all of the structural functional groups expected to account for fuel-specific effects and their structural simplicity enables comprehensive quantitative kinetic modeling.

V. DOE Publications, 2007-present

1. N. Hansen, J. A. Miller, P. R. Westmoreland, T. Kasper, K. Kohse-Höinghaus, J. Wang, T. A. Cool, "Isomer-Specific Combustion Chemistry in Allene and Propyne Flames", *Combustion and Flame*, in press..

2. T. Kasper, P. Oßwald, U. Struckmeier, K. Kohse-Höinghaus, C. A. Taatjes, J. Wang, T. A. Cool, M. E. Law, A. Morel, P. R. Westmoreland, “Combustion chemistry of the propanol isomers—investigated by electron ionization and VUV-photoionization molecular-beam mass spectrometry, *Combustion and Flame*, in press..
3. J. Wang, M. Chaos, B. Yang, T. A. Cool, F. L. Dryer, N. Hansen, P. Oßwald, K. Kohse-Höinghaus, P. R. Westmoreland, “Composition of reaction intermediates for stoichiometric and fuel-rich dimethyl ether flames: Flame-sampling mass spectrometry and modeling studies”, *Physical Chemistry Chemical Physics*, **2009**, *11*, 1328-1339, DOI: 10.1039/B815988B.
4. N. Hansen, T.A. Cool, P.R. Westmoreland, K. Kohse-Höinghaus, “Recent Contributions of Flame-Sampling Molecular-Beam Mass Spectrometry to a Fundamental Understanding of Combustion Chemistry”, *Progress in Energy and Combustion Science*, **2009**, *35*, 168-191.
5. J. Wang, U. Struckmeier, B. Yang, T. A. Cool, P. Oßwald, K. Kohse-Höinghaus, T. Kasper, N. Hansen, P.R. Westmoreland, “Isomer-specific influences on the composition of reaction intermediates in dimethyl ether/propene and ethanol/propene flames”, *J. Phys. Chem. A*, **2008**, *112*, 9255-9265.
6. C. K. Westbrook, W. J. Pitz, P. R. Westmoreland, F. L. Dryer, M. Chaos, P. Oßwald, K. Kohse-Höinghaus, T. A. Cool, J. Wang, B. Yang, N. Hansen, T. Kasper, “A Detailed Chemical Kinetic Mechanism for Oxidation of Four Small Alkyl Esters in Laminar Premixed Flames”, *Proc. Combust. Inst.*, **2009**, *32*, 221-228.
7. A. Lucassen, P. Oßwald, U. Struckmeier, K. Kohse-Höinghaus, T. Kasper, N. Hansen, T.A. Cool, P. R. Westmoreland, “Species identification in a laminar premixed low-pressure flame of morpholine as a model substance for oxygenated nitrogen-containing fuels”, *Proc. Combust. Inst.*, **2009**, *32*, 1269-1276.
8. N. Hansen, J. A. Miller, T. Kasper, K. Kohse-Höinghaus, P. R. Westmoreland, J. Wang, T. A. Cool, “Benzene Formation in Premixed Fuel-Rich 1,3-Butadiene Flames”, *Proc. Combust. Inst.*, **2009**, *32*, 623-630.
9. C. A. Taatjes, N. Hansen, D. L. Osborn, K. Kohse-Höinghaus, T. A. Cool, P. R. Westmoreland, ““Imaging“ Combustion Chemistry via Multiplexed Synchrotron-Photoionization Mass Spectrometry”, *Phys. Chem. Chem. Phys.*, **2008**, *10*(1), 20-34.
10. J. Wang, B. Yang, T. A. Cool, N. Hansen and T. Kasper, “Near-threshold Absolute Photoionization Cross Sections of some Reaction Intermediates in Combustion”, *Int. J. Mass Spectrom.*, **2008**, *269*(3), 210-220.
11. N. Hansen, S. J. Klippenstein, P. R. Westmoreland, T. Kasper, K. Kohse-Höinghaus, J. Wang and T. A. Cool, “A Combined ab initio and Photoionization Mass Spectrometric Study of Polyynes in Fuel-Rich Flames”, *Phys. Chem. Chem. Phys.*, **2008**, *10*(3), 366-374.
12. N. Hansen, T. Kasper, S. J. Klippenstein, P. A. Westmoreland, M. E. Law, C. A. Taatjes, K. Kohse-Höinghaus, J. Wang, T. A. Cool, “Initial steps of aromatic ring formation in a laminar premixed fuel-rich cyclopentene flame”, *J. Phys. Chem. A*, **2007**, *111*(19), 4081-4092.
13. P. Oßwald, U. Struckmeier, T. Kasper, K. Kohse-Höinghaus, J. Wang, T. A. Cool, N. Hansen, P. R. Westmoreland, “Isomer-specific fuel destruction pathways in rich flames of methyl acetate and ethyl formate and consequences for the combustion chemistry of esters”, *J. Phys. Chem. A*, **2007**, *111*(19), 4093-4101.
14. M. E. Law, P. R. Westmoreland, T. A. Cool, J. Wang, Nils Hansen, Craig A. Taatjes, Tina Kasper and K. Kohse-Höinghaus, “Benzene precursors and formation routes in a stoichiometric cyclohexane flame”, *Proc. Combust. Inst.*, **2007**, *31*(1), 565-573.
15. K. Kohse-Höinghaus, P. Osswald, U. Struckmeyer, T. Kasper, N. Hansen, C. A. Taatjes, J. Wang, T. A. Cool, S. Gon, P. R. Westmoreland, “The influence of ethanol addition on a premixed fuel-rich propene-oxygen flame”, *Proc. Combust. Inst.*, **2007**, *31*(1), 1119-1127.
16. N. Hansen, J. A. Miller, C.A. Taatjes, J. Wang, T. A. Cool, M.E. Law, P.R. Westmoreland, T. Kasper, and K. Kohse-Höinghaus, “Photoionization mass spectrometric studies and modeling of fuel-rich allene and propyne flames”, *Proc. Combust. Inst.*, **2007**, *31*(1), 1157-1164.
17. T. A. Cool, J. Wang, N. Hansen, P. R. Westmoreland, F. L. Dryer, Z. Zhao, A. Kazakov, T. Kasper and K. K.-Höinghaus, “Photoionization mass spectrometry and modeling studies of the chemistry of fuel-rich dimethyl ether flames”, *Proc. Combust. Inst.*, **2007**, *31*(1), 285-293.

Dissociation Pathways and Vibrational Dynamics in Excited Molecules and Complexes

F.F. Crim
Department of Chemistry
University of Wisconsin–Madison
Madison, Wisconsin 53706
ffcrim@chem.wisc.edu

Our research investigates the chemistry of vibrationally excited molecules. The properties and reactivity of vibrationally energized molecules are central to processes occurring in environments as diverse as combustion, atmospheric reactions, and plasmas and are at the heart of many chemical reactions. The goal of our work is to unravel the behavior of vibrationally excited molecules and to exploit the resulting understanding to determine molecular properties and to control chemical processes. A unifying theme is the preparation of a molecule in a specific vibrational state using one of several excitation techniques and the subsequent photodissociation of that prepared molecule. Because the initial vibrational excitation often alters the photodissociation process, we refer to our double resonance photodissociation scheme as *vibrationally mediated photodissociation*. In the first step, fundamental or overtone excitation prepares a vibrationally excited molecule, and then a second photon, the photolysis photon, excites the molecule to an electronically excited state from which it dissociates. Vibrationally mediated photodissociation provides new vibrational spectroscopy, measures bond strengths with high accuracy, alters dissociation dynamics, and reveals the properties of and couplings among electronically excited states.

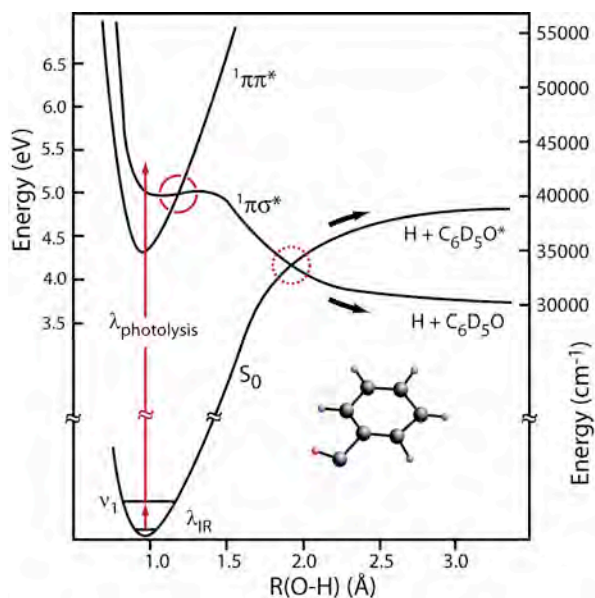
We have used ion imaging to follow the adiabatic and nonadiabatic dissociation pathways in ammonia, to make new measurements on the vibrationally mediated photodissociation of the hydrogen bonded dimer of formic acid, and to study the influence of vibrational excitation on the dynamics at conical intersections in phenol. Phenol is particularly interesting because of well-characterized one-photon photodissociation dynamics and clear theoretical predictions about changes arising from vibrational excitation prior to dissociation. Most recently, we have begun measurements on the complex of phenol with CO to understand how complexation alters the competition between adiabatic and nonadiabatic dissociation and, in particular, how it influences the vibrationally mediated photodissociation. In each of these cases, the goals are understanding and exploiting vibrations in the ground electronic state, studying the vibrational structure of the electronically excited molecule, and probing and controlling the dissociation dynamics of the excited state.

Ammonia and Phenol

Ammonia is a famously well-studied molecule that holds interesting opportunities for vibrationally mediated photodissociation experiments because it has both a nonadiabatic dissociation to yield ground state $\text{NH}_2 + \text{H}$ and an adiabatic dissociation to form excited state $\text{NH}_2^* + \text{H}$. We have demonstrated that NH_2^* , is the primary product from vibrationally mediated photodissociation through the antisymmetric N-H stretching state (3^1) because the vibrational excitation preferentially drives the system along the adiabatic dissociation path. Ion imaging has allowed us to detect the rotational structure of the products and to identify the electronically excited fragment.

The ion imaging experiments also provide the angular distributions of the recoiling fragments, and we have recently completed the analysis for the ground state NH_2 product from photodissociation through the excited symmetric N-H stretch (1^1) and through the excited antisymmetric N-H stretch (3^1). The angular distribution for the first case qualitatively resembles that for dissociation through the origin (0^0) and shows both parallel and perpendicular components depending on the rotational excitation in the NH_2 product. In general, the two-photon excitation scheme introduces higher order terms in the initial alignment, and the consequences are particularly clear in the NH_2^* products from dissociation through the antisymmetric (3^1) N-H stretching state. In that case, the first (vibrational) excitation step has a transition moment that is perpendicular to the C_3 axis of ammonia, and the second (electronic) excitation step has a parallel transition moment. The consequence is angular distributions that reflect these two alignments as well as the dynamics of the dissociation.

Phenol is one of several heteroaromatic molecules that has multiple conical intersections that are accessible at different excitation energies. Our goal in studying phenol is to discover the influence that vibrational excitation has on the passage through or around these crossings. We have performed both one-



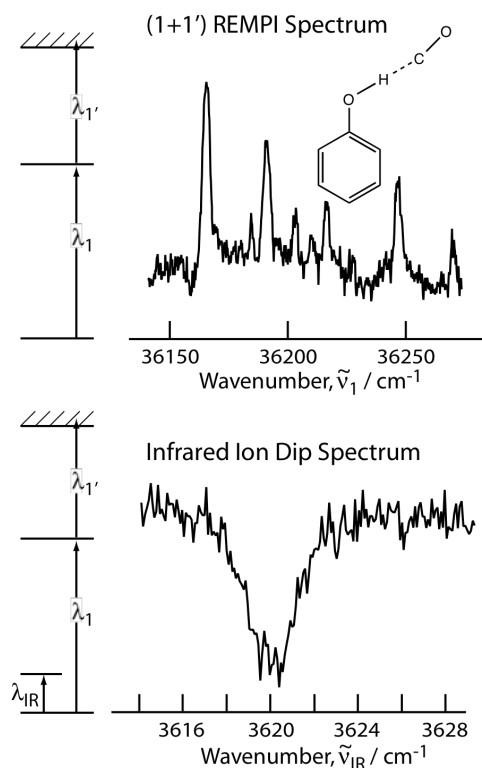
photon and vibrationally mediated photodissociation ion imaging experiments to extract the recoil energy distributions. The figure shows schematically diabatic potential curves for the ground (S_0) and first two excited states ($1^1\pi\pi^*$ and $1^1\pi\sigma^*$). The development of the wave function of the system as it passes through both intersections, $1^1\pi\pi^*-1^1\pi\sigma^*$ (solid circle) and $1^1\pi\sigma^*-S_0$ (dotted circle), determines the branching at the second intersection to form either ground state phenoxy by nonadiabatic dissociation or excited state phenoxy by adiabatic dissociation. Comparing the recoil energy distributions of the fragments from one-photon dissociation of phenol- d_5 with those from vibrationally mediated photodissociation shows that initial vibrational excitation strongly influences the disposal of energy into relative translation. Dissociation of phenol- d_5 molecules initially excited in the O-H stretching region produces significantly more fragments with low

recoil energies than does one-photon dissociation at the same total energy. The difference appears to come from the increased probability of adiabatic dissociation in which the initially vibrationally excited molecule passes around the conical intersection between the dissociative state and the ground state to produce electronically excited phenoxy- d_5 radicals.

Phenol-CO Complexes

Our experience with phenol, ammonia, and formic acid dimers prepares the way for our studies of the influence of an adduct on dissociation pathways and dynamics in vibrationally excited molecules. Because complexes can influence bimolecular reactions, our vibrationally mediated photodissociation studies potentially provide insights with consequences beyond excited state dissociation. We have begun studying one-photon dissociation in complexes of phenol with CO because we know that conical intersec-

tions are important in the dissociation of phenol and that vibrational excitation influences the course of that dissociation. We are in the position of studying both vibrational predissociation of the ground-state complex and vibrationally mediated photodissociation of the excited state complex. The figure shows



types of spectra that we have observed in the phenol-CO complex. The top part of the figure is the (1+1') REMPI spectrum obtained by observing the parent ion in an expansion of phenol with CO in a mixture of He and Ar. The features in the spectrum agree with a previous observation of the transitions (J. Chem. Phys. **111**, 1947 (1999)), and using this spectrum we have optimized the conditions for the production of the complex of phenol with only one CO molecule. Production of higher clusters, such as phenol-(CO)₂, is a competing channel that we have learned to diagnose and avoid. The lower part of the figure shows the infrared ion dip spectrum obtained by observing the depletion of the (1+1') REMPI signal upon excitation of the O-H stretching vibration of the complex. We observe ion dip spectra of both the bare phenol and the phenol-CO complex shifted from each other by about 30 cm⁻¹, in agreement with previous measurements (A. Fujii, T. Ebata, and N. Mikami, J. Phys. Chem. A **106**, 10124 (2002)). These two measurements set the stage for our next experiments. We intend to monitor the CO product of the vibrational predissociation and of the vibrationally mediated photodissociation to explore the effects of complexation on the dissociation dynamics.

Future Directions

The well-characterized ionization spectroscopy of phenol make it an attractive first target for vibrationally mediated photodissociation of complexes, but the NH₃-CO complex may be an even more interesting target, which we plan to pursue soon. The variety of complexes available, including ones with different bonding motifs, offer a rich array of possibilities in which to study the influence of an adduct and initial vibrational excitation.

PUBLICATIONS SINCE 2007 ACKNOWLEDGING DOE SUPPORT

Vibrational Action Spectroscopy of the C-H and C-D Stretches in Partially Deuterated Formic Acid Dimer, Y. Heidi Yoon, Michael L. Hause, Amanda S. Case, and F. Fleming Crim, J. Chem. Phys. **128**, 084305 (2008).

Dynamics at Conical Intersections: The Influence of O-H Stretching Vibrations on the Photodissociation of Phenol, Michael L. Hause, Y. Heidi Yoon, Amanda S. Case, and F. Fleming Crim, J. Chem. Phys. **128**, 104307 (2008).

Vibrationally Mediated Photodissociation of Ammonia: Product Angular Distributions from Adiabatic and Nonadiabatic Dissociation. Michael L. Hause, Y. Heidi Yoon, and F. Fleming Crim, Mol. Phys. **106**, 1127 (2008).

Bimolecular Dynamics of Combustion Reactions

H. Floyd Davis
Department of Chemistry and Chemical Biology
Baker Laboratory, Cornell University, Ithaca NY 14853-1301
hfd1@Cornell.edu

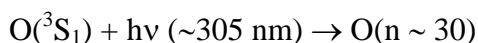
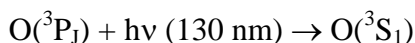
I. Program Scope:

The aim of this project is to better understand the mechanisms and product energy disposal in elementary bimolecular reactions fundamental to combustion chemistry. Using the crossed molecular beams method, a molecular beam containing highly reactive free radicals is crossed with a molecular beam. The angular and velocity distributions of the products from single reactive collisions are measured using Rydberg tagging methods or by single photon ionization using pulsed VUV light sources.

II. Recent Progress and Future Plans:

a) New VUV light source for HRTOF and ORTOF:

The $\text{H} + \text{O}_2 \rightarrow \text{OH} + \text{O}$ reaction is a prototype 3-atom reaction involving a deep HO_2 well. Although the reaction has received considerable theoretical attention¹ recently, dynamical experiments have been very limited.² The chief experimental difficulty is associated with the small reaction cross section, believed to be roughly an order of magnitude smaller than the hydrogen exchange reaction (e.g., $\text{H} + \text{D}_2 \rightarrow \text{HD} + \text{D}$). Several years ago we introduced the oxygen Rydberg TOF method³, which involves two-color excitation of ground state oxygen atoms $\text{O}(^3\text{P}_j)$ to high- n Rydberg levels via an intermediate $\text{O}(^3\text{S}_1)$ state:



The Rydberg O atoms drift with their nascent velocities ~ 30 cm through a field-free region to a rotatable detector where they are field ionized and collected. We have employed this method for studies of photodissociation reactions⁴ and bimolecular reactions⁵ of free radicals (e.g., $\text{CN} + \text{O}_2 \rightarrow \text{NCO} + \text{O}$). In our original experimental implementation, pulsed VUV light at 130 nm was generated by “2-1” four wave mixing of two 212 nm photons and one 582 nm photon in Kr. Although we found this approach was suitable for photodissociation or reactions with large cross sections, the sensitivity was limited because (unlike generation of Lyman- α , 121 nm), one cannot phase-match at this wavelength.⁴ Consequently, the sensitivity of the method was found to be insufficient to study the $\text{H} + \text{O}_2$ reaction.

Highly efficient VUV generation at 130 nm was first reported by Muller and coworkers using 4-wave mixing of transform-limited ns pulses in mercury (Hg) vapor.⁶ This approach is most general and efficient if *three* independent input laser beams are each tuned near Hg resonances at the precise wavelengths where index matching may be achieved. Pulsed beams in the VUV at the millijoule level⁶ and continuous wave (CW) Lyman- α (121 nm)⁷ have been produced using variants of this approach. During the past year, we have implemented this method in our laboratory on two separate machines.

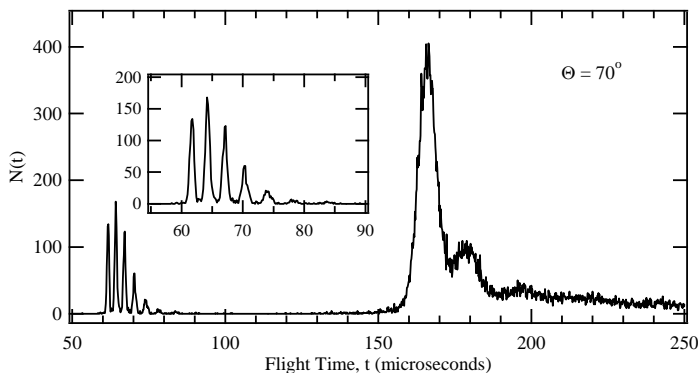


Fig. 1: Oxygen TOF spectra from N_2O photodissociation at 130 nm. Peaks at $t = 60$ -85 μs from $O(^1S_0) + N_2(X, v = 0-6)$; structure at $t = 160$ - 250 μs from $O(^3P_2) + N_2(A, v = 0-3)$.

method by a factor of ~ 100 relative to our original implementation.⁸ Somewhat surprisingly, we have found that the nascent $O(^1S)$ from the dominant $O(^1S) + N_2(X)$ channel can be detected directly (without further excitation) by our Rydberg detector. The structure in the TOF shown in Fig. 1 shows the vibrational progression in the ground electronic state $N_2(X)$ products, with $v = 0 - 6$ well-resolved; the second peak is due to the minor ($\sim 1\%$) $O(^3P_2) + N_2(A)$ channel. The spectrum shown in Fig. 1 corresponds to 3 minutes of data accumulation. A manuscript describing this recent work is currently in preparation.⁸

We believe that the sensitivity of our ORTOF setup is now sufficient to carry out a detailed study of the $H + O_2$ reaction. Because the thermal instability and the extremely high cost of HI ($> \$6000$ for a lecture bottle), an undergraduate student has set up a synthetic source of HI involving its catalytic production from the elements. A fast photolytic H atom beam has now been characterized in our laboratory and studies of the reaction will be underway shortly. In addition to studies of the $H + O_2$ reaction, we expect that ORTOF will be invaluable for studying the $O(^3P)$ channels from reactions of a number of hydrocarbon free radicals with molecular oxygen, e.g., $C_6H_5 + O_2 \rightarrow C_6H_5O_2 \rightarrow C_6H_5O + O(^3P)$.

The Lyman- α radiation for HRTOF experiments can also be generated free of residual UV radiation using an approach similar to that described above. This is of considerable importance to our program as it will greatly reduce background signals, particularly in studies involving polyatomic hydrocarbon free radicals that previously were found to fragment extensively upon absorption of residual UV at 212nm. We expect this will greatly expand the range of experiments that may be carried out using HRTOF in the future.

b) Universal “Soft” Photoionization Detection of Products from Bimolecular Reactions.

Cassavecchia has elegantly demonstrated the use of low energy electrons for “soft” electron impact ionization detection of products from bimolecular reactions in crossed molecular beams.⁹ One important feature of electron impact is that electrons are “universal” ionization detectors. However, because of small electron impact ionization cross sections and the continuous nature of this detector, this method generally requires continuous beams produced by discharge or by

For ORTOF, three unfocused input nanosecond pulses are simultaneously tuned near a one photon, two photon, and Rydberg resonance (i.e., 255 nm + 404 nm + 777 nm) in a 1 meter long Hg heat pipe, producing very intense 130 nm light. The VUV is spatially separated by off-axis transmission through a MgF_2 lens and reflected into the interaction region using a remotely-adjustable VUV mirror. To optimize and characterize the instrument, we photolyzed N_2O at 130 nm, producing $O(^3P) + N_2(A)$ as a minor channel which may be probed by ORTOF. Based on the signals obtained using our new configuration, we have increased the sensitivity of the ORTOF

pyrolysis. Pyrolytic *polyatomic* free radicals are typically produced with vibrational temperatures of several thousand degrees Kelvin. This degree of internal excitation complicates the determination of potential energy barrier heights and derivation of thermodynamic quantities in reactive scattering studies. The determination of branching ratios for competing reactions requires knowledge of electron impact ionization cross sections, which typically must be estimated using empirical methods. For polyatomic radical beams, photolytic sources have the potential advantage that in most cases the internal energy distributions are substantially colder. Therefore, it would be valuable to be able to carry out crossed beam reaction dynamics studies using pulsed photolytic beams. However, the fundamental mismatch in duty cycle between pulsed photolytic beams and continuous detection methods such as electron impact ionization or photoionization using synchrotron radiation has hampered the widespread implementation of this approach.

Over the past year, we have pursued two different approaches to “soft” photoionization detection of reaction products using pulsed VUV produced by tabletop light sources. The advantage of pulsed VUV light sources is that the duty cycles of reactant production and product detection are better matched, promising improved signal to noise ratios. In addition, by photodissociation of stable precursors, it is often possible to determine absolute or relative photoionization cross sections for different product channels.¹⁰ This should provide a potentially more direct route to the determination of branching ratios for competing channels from combustion reactions.

As in the ORTOF method described in the previous section, we have employed the use of 4-wave mixing of unfocussed laser beams in Hg for production of VUV in our rotatable source crossed beam apparatus. For example, by tuning to one of the Rydberg resonances in Hg, VUV pulses can be generated with conversion efficiencies exceeding 1% at wavelengths around 125 nm.¹¹ We believe this method is well-suited for photoionization detection of a number of polyatomic free radicals produced in bimolecular reactions in pulsed beams.

One class of reactions amenable to this approach involves reactions of various isomers of alkane radicals such as 1-butyl and 2-butyl radicals with molecular oxygen.¹² As a first step towards such studies, we have characterized the photodissociation dynamics of 1-iodobutane and t-butyl iodide using pulsed VUV photoionization detection in our rotatable source apparatus. Representative TOF spectra for the C₄H₉ and iodine atomic product channels, recorded using pulsed 125 nm photoionization are shown in Fig. 2. We find that for primary alkyl iodides, simple C-I bond fission is the dominant channel, whereas for secondary and tertiary iodides a competing pathway involving HI elimination producing an alkene plays an important role. Since one of the primary channels in alkane radical reactions with oxygen involves production of the alkene + HO₂, in cases where the alkene + HI channel from photolysis of the alkyl iodide is important, this source will likely *not* be an ideal source of alkyl radicals. Therefore, we are presently exploring alternative approaches to production of alkane radicals

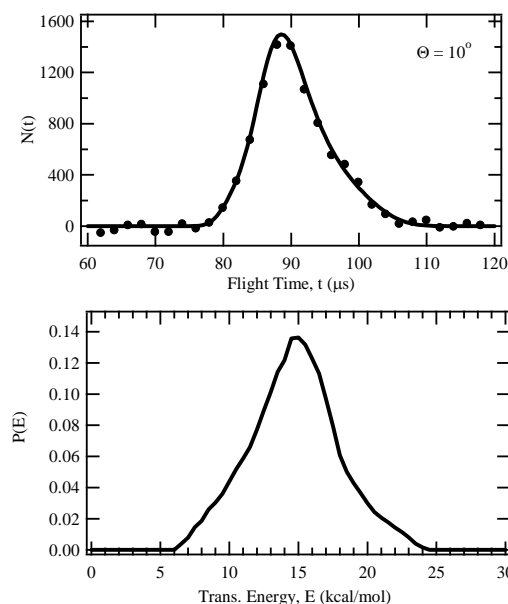


Fig. 2: Experimental TOF and resulting $P(E)$ for 1-butyl radicals at 10° produced by photolysis of 1-butyl iodide at 266nm using 125 nm pulsed photoionization detection.

such as 355 nm photolysis of mixtures of the appropriate hydrocarbons with molecular chlorine to initiate the Cl abstraction reaction.

We have also carried out a number of preliminary but very promising experiments using photoionization detection employing a home-built pulsed RF discharge-pumped Ar₂* excimer lamp operating at 128 nm. The lamp provides 250 μs long pulses at up to 200 Hz with peak photon fluxes comparable to that achievable using the raw undulator output from the ALS. We have found that the primary drawback of this type of light source is that the incoherent light beam is quite divergent, making it difficult to relay-image the radiation into the ionization region of our detector. After considerable effort, we have found that rather than trying to use refractive or reflective optics for this light source, it is best to miniaturize the source in order to facilitate placement very close to the ionization region of our detector.

III. Statement about DOE-supported publications for 2007-present:

Over the past 3 years, this DOE grant has supported the Ph.D. research of two students who have now graduated, Marivi Ortiz-Suarez and Steve Kroner. Their research primarily involved experimental studies of the quenching of electronically excited OH radicals by D₂ molecules,^{13,14} and the VUV photodissociation of OH radicals.¹⁴ They also carried out preliminary experiments laying the groundwork for our study of the H + O₂ and OH + D₂ (v = 1) reaction. Their work was summarized in previous DOE abstracts and has been presented at several national meetings. During the course of writing up their work, we found that some of this data was subject to interfering signals from photolysis by residual UV radiation associated with VUV generation. Using our newly-improved VUV light source, which allows separation of the VUV, we are presently rechecking some of this data. We expect this process to be completed shortly and the backlog of publications resulting from this DOE-supported research by these two students will be submitted prior to submission of our DOE grant renewal.

The grant has also partially supported the Ph.D. work of David Proctor, a student who has been working with the PI on the development of new pulsed VUV light sources as well as a novel narrowband OPO-based IR light source¹⁵ to be employed in future studies of the reaction dynamics of vibrationally excited species. David will be graduating in May 2009; the results of his thesis work including publications acknowledging DOE will be submitted for publication shortly.⁸

IV. References:

-
- ¹ Z. Sun, D.H. Zhang, C. Xu, S. Zhou, D. Xie, G. Lendvay, S-Y. Lee, Y. Shi, H. Guo, *J. Am. Chem. Soc.* **130**, 14962 (2008).
 - ² H. L. Kim, M.A. Wickramaaratchi, X. Zheng, G.E. Hall, *J. Chem. Phys.* **101**, 2033 (1994).
 - ³ C. Lin, M.F. Witinski, and H.F. Davis, *J. Chem. Phys.* **119**, 251 (2003).
 - ⁴ M.F. Witinski, M. Ortiz-Suarez, and H. F Davis, *J. Chem. Phys.* **122**, 174303 (2005).
 - ⁵ Mark F. Witinski, Mariví Ortiz-Suárez, and H. Floyd Davis, *J. Chem. Phys.*, **124**, 094307 (2006).
 - ⁶ C.H. Muller, D.D. Lowenthal, M.A. DeFaccio, and A. V. Smith, *Opt. Lett.* **13**, 651 (1988).
 - ⁷ K.S.E. Eikema, J. Walz, and T.W. Hansch, *Phys. Rev. Lett.* **83**, 3828 (1999).
 - ⁸ D. Proctor and H. F. Davis, manuscript in preparation.
 - ⁹ P. Casavecchia, F. Leonori, N. Balucani, R. Petrucci, G. Capozza, and E. Segoloni, *PCCP* **11**, 46 (2009).
 - ¹⁰ N. Sveum, S. J. Goncher, and D.M. Neumark, *PCCP* **8**, 592 (2006).
 - ¹¹ R. Hilbig and R. Wallenstein, *IEEE J. Quant. Elect.* QE-19, 1759 (1983).
 - ¹² J. D. Desain, S.J. Klippenstein, J.A. Miller and C.A. Taatjes, *J. Phys. Chem. A.* **107**, 4415 (2003).
 - ¹³ M. Ortiz-Suárez, M.F. Witinski, and H. F. Davis, *J. Chem. Phys.* **124**, 201106 (2006).
 - ¹⁴ S. Kroner, M. Ortiz-Suarez, M.F. Witinski and H.F. Davis, manuscript in preparation.
 - ¹⁵ D. Proctor and H.F. Davis, *Proc. Nat. Ac. Sci. Am.* **105**, 12673 (2008).

Global combustion modeling and potential energy surface fitting

Michael J. Davis

Chemistry Division
Argonne National Laboratory
Argonne, IL 60439
Email: davis@tcg.anl.gov

The focus of the research has shifted to the study of chemical-kinetic mechanisms and the fitting of potential energy surfaces. The study of reaction mechanisms is global, focusing on the composite phase space structure of the mechanisms and the chemical implications of that structure. Global sensitivity analysis has been implemented, and is being used to discern important reactions that need to be calculated more accurately, including their thermochemistry and rate parameters. The global sensitivity analysis uses two surrogates: HDMR (high-dimensional model representation) and the Gaussian process model. This latter surrogate is being used for fitting potential energy surfaces.

Recent Progress

Phase space structure of reaction mechanisms

The abstract focuses on the composite phase space structure¹ of CO/CH₂O/CH₃OH combustion (Li *et al*²). The procedure outlined here can be applied to any reaction mechanism and the phase space structure outlined here is generic, as is the information that can be gleaned from such an analysis. However, the quantitative details of the analysis depend on a particular physical situation. The case outlined here is for constant pressure, one-dimensional premixed flames.

The top panel of Fig. 1 shows results for 12 premixed flames, which have four distinct mixtures at the burner. The flame plots should be viewed from left to right in the panel and are coded by color and line type. Each of the mixtures was run for three different temperatures at the burner. Although there are 12 flames in the figure only eight curves are obvious in the plot as two of the temperature-dependent triplets have all three of their curves lying on top of each other. All the curves in the panel have asymptotes that lie on the thick black curve. All the flames in the panel were generated at $P = 40$ torr. For comparison the additional curves in the top

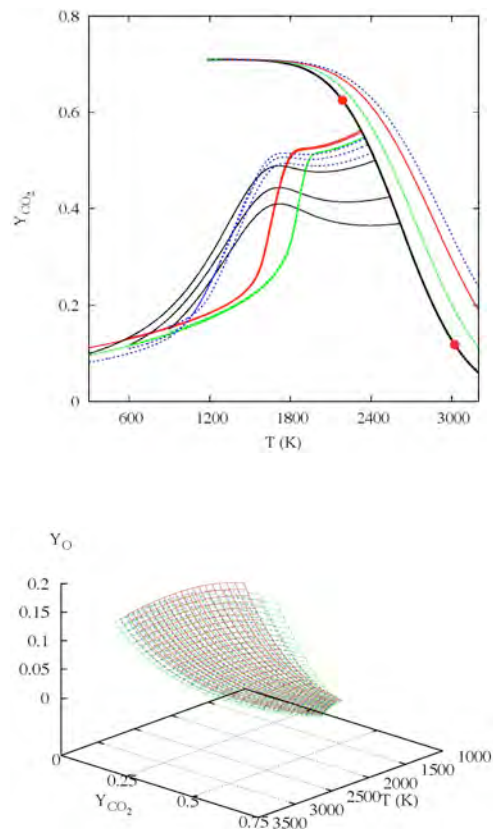


Fig. 1

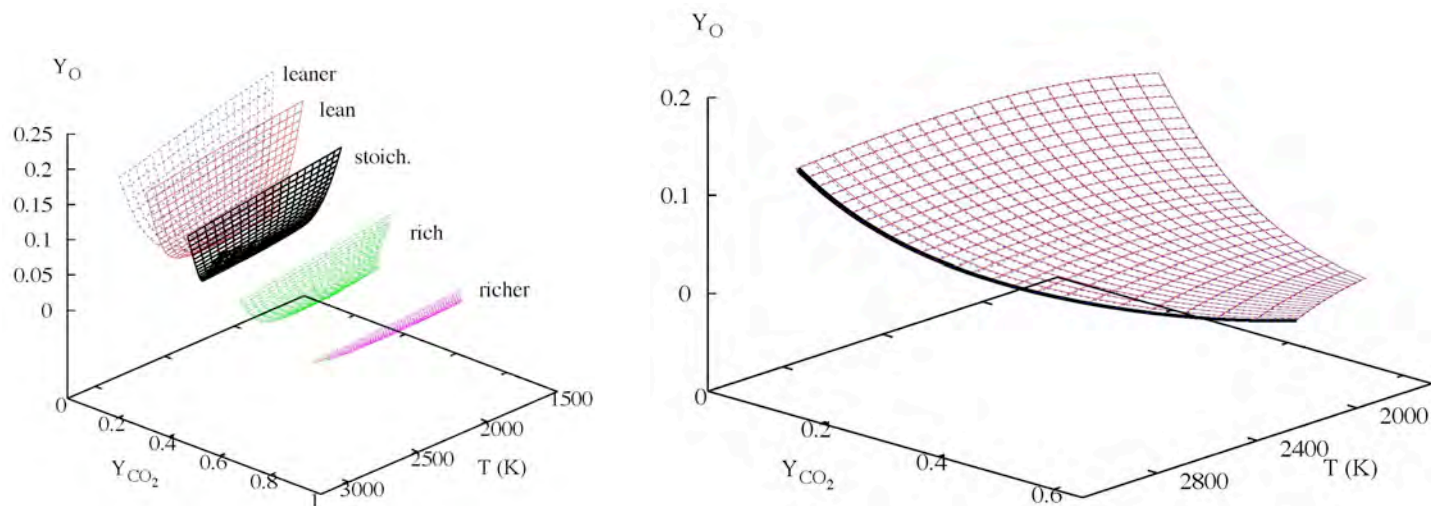


Fig. 2

panel that lie to the right of the black are shown for higher pressures (120, 400, and 760 torr). The flame profiles in the top panel of Fig. 1 approach one-dimensional curves between 1500 and 1800 K, depending on the flame. This behavior is a result of a phase space structure characterized by a set of one-dimensional manifolds, which form a 2D surface in the phase space, as demonstrated in the bottom panel of Fig. 1. These surfaces depend on pressure, with three pressures shown in the panel (40, 80, and 120 torr).

The surfaces shown in the bottom panel of Fig. 1 were generated for stoichiometric $\text{CH}_2\text{O} + \text{O}_2$ flames and mixtures of CO , H_2 , CH_3OH , which match the

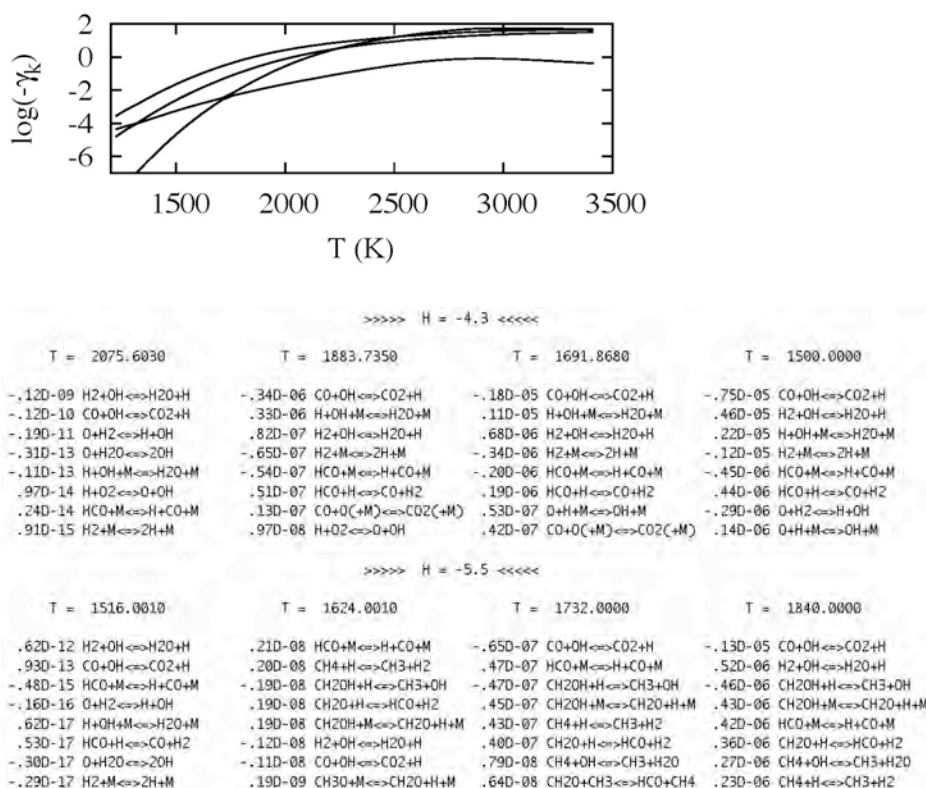


Fig. 3

elemental content of the stoichiometric flames. The flames in the top panel of Fig. 1, as well as the surfaces in the bottom panel are characterized by a set of asymptotic mixture enthalpies. The full phase space of the mechanism is further characterized by a range of elemental mixtures and the left panel of Fig. 2 shows surfaces for an additional set of mixtures characterized by $\text{CH}_2\text{O}/\text{O}_2$ content.

The surfaces in Figs. 1 and 2 allow for a global comparison of different mechanisms. The right panel in Fig. 2 compares the mechanism of Ref. 2 (blue, dashed lines) with the C_3 mechanism of Ref. 3 (red lines). It is clear from the right panel that the two mechanisms give almost identical behavior in this region of phase space. The analysis of the global phase space structure is a convenient way to monitor the changes in chemistry as conditions vary. The top panel of Fig. 3 shows the way the local eigenvalues change as the asymptotic enthalpy changes (characterized by temperature). This is accomplished by moving along the black curve in the top panel of Fig. 1. The top panel of Fig. 3 demonstrates that the eigenvalues cross, which indicates a change in the chemistry of the mechanism and are a result of changes in time scale for different reactions as conditions are varied. The results of this change are indicated in the bottom two panels of Fig. 3, where the production rates of the eight most productive reactions are shown along the one-dimensional manifold for a case to the right of the avoidance in the first set of reactions and to the left in the second set of reactions. In particular, the bottom set of reactions demonstrates that there is considerable production of hydrocarbon species for the one-dimensional manifolds compared to the first set.

Fitting potential energy surfaces using a Gaussian Process Model

The basic approach is outlined in Fig. 4 for a Morse oscillator. A set of random functions is sampled based on a Gaussian process (blue curves on the left top). The values of the potential function (bottom left) convert this joint distribution into a conditional distribution, conditioned on the sampled points (here there are 9). The red curves in the bottom panel are a sample from the new conditional distribution. The yellow curves give the 2σ error bounds of the conditional distribution. These bounds are

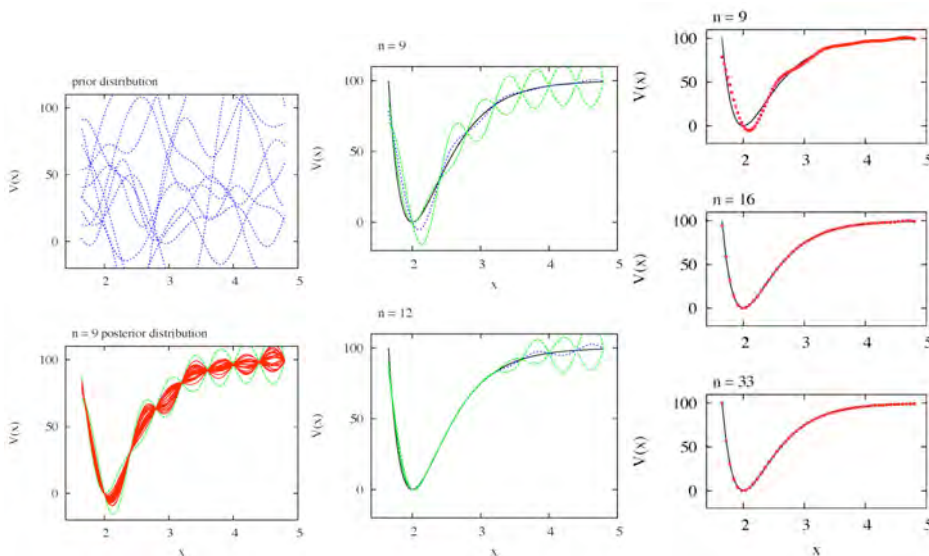


Fig. 4

repeated in the top middle curve along with the mean of the distribution (blue, dotted curve), which is the fit to the function. Three additional points are generated in regions of high error estimates, yielding a new conditional distribution and a new fit to the potential in the bottom middle plot. A summary of fits with the Gaussian process model is shown in the right most column of Fig. 4. The agreement with the exact potential is very good with 16 points and nearly perfect with 33 points.

Future Plans

Global sensitivity analysis is being implemented at this time. This will be applied to the methanol and C₃ mechanisms, as well as larger ones. This methodology will be used to highlight important reactions whose rate parameters and thermochemistry need to be calculated more accurately. We will use the Gaussian process model to fit potential surfaces of triatomic and tetra-atomic molecules.

References

- ¹ M. J. Davis, “Phase space structure for reaction mechanisms of hydrocarbon combustion: Basic formulation and chemical implications”, to be submitted.
- ² J. Li, Z. Zhao, A. Kazakov, M. Chaos, F. J. Dryer, and J. J. Scire, Jr., *Int. J Chem Kin* **39**, 109 (2007).
- ³ S. M. Gallagher, H. J. Curran, W. K. Metcalfe, D. Healy, J. M. Simmie, and G. Bourque, *Combustion and Flame* **153**, 306 (2008).
- ⁴ C. E. Rasmussen and C. K. I. Williams, “Gaussian Processes for Machine Learning”, MIT Press (2006).

Publications

- M. J. Davis, “Low-dimensional manifolds in reaction-diffusion equations. 1. Fundamental aspects”, *J. Phys. Chem. A* **110**, 5235-5256 (2006).
- M. J. Davis, “Low-dimensional manifolds in reaction-diffusion equations. 2. Numerical analysis and method development”, *J. Phys. Chem. A* **110**, 5257-5272 (2006).
- M. J. Davis and A. S. Tomlin, “Spatial dynamics of steady flames 1. Phase space structure and the dynamics of individual trajectories”, *J. Phys. Chem. A* **112**, 7768 -7783 (2008).
- M. J. Davis and A. S. Tomlin, “Spatial dynamics of steady flames 2. Low-dimensional manifolds and the role of transport processes”, *J. Phys. Chem. A* **112**, 7784-7805 (2008).
- M. J. Davis, “Phase space structure for reaction mechanisms of hydrocarbon combustion: Basic formulation and chemical implications”, to be submitted.

Hydrocarbon Radical Thermochemistry: Gas-Phase Ion Chemistry Techniques

Kent M. Ervin
Department of Chemistry and Chemical Physics Program
University of Nevada, Reno
Reno, NV 89557-0216
ervin@unr.edu

I. Program Scope

Gas-phase ion chemistry and mass spectrometry techniques are employed to determine energetics of hydrocarbon radicals that are important in combustion processes and to investigate the dynamics of ion–molecule reactions. Guided ion beam tandem mass spectrometry is used to measure the activation of endoergic ion-molecule reactions as a function of kinetic energy. Modeling the measured reaction cross sections using statistical rate theory [1] or empirical reaction models allows extraction of reaction threshold energies. These threshold energies yield relative gas-phase acidities, proton affinities, or hydrogen atom affinities, which may then be used to derive neutral R–H bond dissociation enthalpies using thermochemical cycles involving established electron affinities or ionization energies [2]. The reactive systems employed in these studies include endoergic bimolecular proton transfer reactions, hydrogen-atom transfer reactions, and collision-induced dissociation of heterodimer complex anions and cations. Electronic structure calculations are used to evaluate the possibility of potential energy barriers or dynamical constrictions along the reaction path, and as input for RRKM and phase space theory calculations.

II. Recent Progress

A. Threshold Collision-Induced Dissociation

We continue work to measure gas-phase acidities and other energetics of oxygen-containing hydrocarbons and of highly unsaturated hydrocarbons that are of interest in combustion kinetic systems. Energy-resolved collision induced dissociation is used to measure energetics of ion systems that can be related to neutral hydrocarbon molecules and radicals via thermochemical cycles.

Experimental work is in progress on the threshold collision-induced dissociation of peroxy-carboxylate anions, HCOOO^- and CH_3COOO^- . The goal is to measure the energy for loss of O atom to form the carboxylate RCOO^- . Combined with gas-phase acidities determined recently in Selected Ion Flow Tube experiments by the group of Prof. Veronica M. Bierbaum (University of Colorado) [3] and known values for the carboxylate anions, these measurements will yield the enthalpies of formation for the peroxy-carboxylate anions and the neutral peroxy-carboxylic conjugate acids, for which the thermochemistry is poorly established.

Bierbaum and coworkers developed a four-step reaction scheme to produce the peroxy-carboxylate anions with $\text{HOO}^- + \text{RCOOCH}_3$ as the final step. We have successfully produced the peroxyacetate anion with our flow tube reactor ion source and have conducted preliminary dissociation experiments in our guided ion beam tandem mass spectrometer [4].

We recently further developed multiwell and multiple transition state statistical rate theory (RRKM and phase-space theory) models to analyze the competitive collision-induced dissociation of proton-bound dimers of carboxylate anions [5], e.g., $[\text{RCOO}\cdots\text{H}\cdots\text{OOCR}']^-$, which possess multiple low-energy conformations in the doubly hydrogen-bonded complexes. The relative dissociation energies provide the gas-phase acidity difference between the two carboxylic acids. These methods are now being applied to analyze collision-induced dissociation experiments on polyynes anions, HC_{2n}^- ($n = 2, 3, 4$), hydrogen bonded with reference acids such as H_2S and CH_3CHO [6]. Because the polyynes carbon acids form weak hydrogen bonds, the potential energy surfaces of the proton-bound complexes typically have two minima, $[\text{RH}\cdots\text{X}]^-$ and $[\text{R}\cdots\text{HX}]^-$ with an intermediate barrier. Density functional theory calculations are used to characterize the potential energy surface along the two dissociation coordinates and multi-well transition state theory is used to characterize the sensitivity of the modeling of the product branching fractions on the barrier height. The goal of this work is to refine the gas-phase acidities of the polyynes, which will allow a better determination of the energies of the polyynyl radicals, $\text{HC}\equiv\text{C}-\text{C}\equiv\text{C}\cdot$, $\text{HC}\equiv\text{C}-\text{C}\equiv\text{C}-\text{C}\equiv\text{C}\cdot$, and $\text{HC}\equiv\text{C}-\text{C}\equiv\text{C}-\text{C}\equiv\text{C}-\text{C}\equiv\text{C}\cdot$, using previously measured electron affinities [7, 8].

B. Photoelectron Spectroscopy

Obtaining C–H or O–H bond dissociation energies, and the enthalpies of formation of the resulting radicals, from gas-phase acidities relies upon the negative ion thermochemical cycle [2],

$$D(\text{R}-\text{H}) = \Delta_{\text{acid}}H(\text{RH}) + \text{EA}(\text{R}\cdot) - \text{IE}(\text{H}),$$

and thus the electron affinity (EA) of the radical species. The electron affinities may be accurately determined by photoelectron spectroscopy of the anions (conjugate base of the neutral acid). Analysis of the negative ion photoelectron spectra is accomplished via Franck-Condon simulations of the vibronic transitions. Over the past year, we have collaborated with the groups of Prof. W. Carl Lineberger and Prof. J. Mathias Weber (both at JILA, University of Colorado, Boulder) in Franck-Condon modeling of photoelectron spectroscopy experiments. In particular, we extended and improved our PESCAL simulation program to allow (1) fitting of multiple electronic transitions simultaneously, (2) fits in the original time or velocity domains for time-of-flight spectrometer or velocity-mapped imaging experiments in addition to the electron kinetic energy domain for electrostatic energy analyzers, (3) simulation of threshold photoionization efficiency curves, (4) simulations of Franck-Condon intensities for hindered internal torsional modes, and (5) treatment of transitions with large geometry changes that require use of curvilinear coordinates.

In collaboration with the Weber group, we modeled the Franck-Condon intensities of their near-threshold photoelectron spectra of nitromethane, CH_3NO_2^- , which employed velocity-mapped imaging techniques [9]. Velocity-domain simulations were used to simulate the spectra and helped to verify the assignment of the electron origin and an electron affinity with improved precision. In the anion, the internal torsion around the C–N bond is hindered, while the neutral is essentially a free rotor. We determined the torsional energy levels from ab initio potential energy curves (solving the 1D Schrodinger equation with a free-rotor basis set [10]) and then

calculated the torsional Franck-Condon factors [11, 12] for comparison with the experimental spectra.

Our continuing collaboration with the Lineberger group has recently involved Franck-Condon analyses of new spectra of the CX_2^- and $H CX_2^-$ ($X = Cl, Br, I$) systems. For CX_2^- the experiments resolved a 10-year controversy regarding the singlet-triplet energy gaps of the neutral dihalomethylene radicals [13]. Simultaneous fitting of the singlet and triplet transition Franck-Condon profiles aided that effort. For $H CX_2^-$, the large geometry change between the pyramidal anion and the pseudo-planar neutral dihalomethyl radical results in a complete breakdown of the conventional computational techniques for treating normal mode vibrations in terms of mass-weighted Cartesian displacements and force fields [14]. We have modified PESCAL to use (non-orthogonal) curvilinear internal coordinates for the Franck-Condon simulations including the effects of Duschinsky rotation [15] between the normal mode coordinate systems of the anion and neutral electronic states. This work is currently in progress. Initial results show reasonable agreement in the case of $HC Cl_2^-$ with more sophisticated quantum mechanical treatments by additional collaborator Prof. Anne McCoy (Ohio State University) for the three strongly coupled CH pyramidal bending mode, CCl_2 symmetric bend, and CCl_2 symmetric bending vibrational modes [16]. Our PESCAL code has been used by several other groups recently, for example references [17-21].

III. Future Work

Experimental work will continue on the ion thermochemistry experiments detailed above and related work involving proton affinities in cationic systems. We are also further developing our quadrupole ion trap/time-of-flight mass spectrometer apparatus [22, 23] with future applications related to combustion systems.

IV. References

- ¹P. B. Armentrout, K. M. Ervin, and M. T. Rodgers, *J. Phys. Chem. A* **112**, 10071 (2008).
- ²K. M. Ervin, *Chem. Rev.* **101**, 391 (2001).
- ³S. M. Villano, N. Eyet, and V. M. Bierbaum, unpublished, (2009).
- ⁴A. Nickel and K. M. Ervin, work in progress, (2009).
- ⁵B. Jia, L. A. Angel, and K. M. Ervin, *J. Phys. Chem. A* **112**, 1773 (2008).
- ⁶S. Yang and K. M. Ervin, work in progress, (2009).
- ⁷T. R. Taylor, C. Xu, and D. M. Neumark, *J. Chem. Phys.* **108**, 10018 (1998).
- ⁸T. Pino, M. Tulej, F. Güthe, M. Pachkov, and J. P. Maier, *J. Chem. Phys.* **116**, 6126 (2002).
- ⁹C. L. Adams, H. Schneider, K. M. Ervin, and J. M. Weber, *J. Chem. Phys.* **130**, 073407 (2009).
- ¹⁰L. H. Spangler, *Annu. Rev. Phys. Chem.* **48**, 481 (1997).
- ¹¹K. C. Ingham and S. J. Strickler, *J. Chem. Phys.* **53**, 4313 (1970).
- ¹²L. H. Spangler and D. W. Pratt, *J. Chem. Phys.* **84**, 4789 (1986).
- ¹³S. W. Wren, K. M. Vogelhuber, K. M. Ervin, and W. C. Lineberger, *Phys. Chem. Chem. Phys.*, (2009).
- ¹⁴W. D. Gwinn, *J. Chem. Phys.* **55**, 477 (1971).
- ¹⁵F. Duschinsky, *Acta Physicochim. URSS* **7**, 551 (1937).

- ¹⁶K. Vogelhuber, S. W. Wren, A. McCoy, K. M. Ervin, and W. C. Lineberger, work in progress, (2009).
- ¹⁷G. Meloni, T. M. Selby, D. L. Osborn, and C. A. Taatjes, *J. Phys. Chem. A* **112**, 13441 (2008).
- ¹⁸A. J. Trevitt, F. Goulay, G. Meloni, D. L. Osborn, C. A. Taatjes, and S. R. Leone, *Int. J. Mass Spectrom.* **280**, 113 (2009).
- ¹⁹S. R. Miller, N. E. Schultz, D. G. Truhlar, and D. G. Leopold, *J. Chem. Phys.* **130**, 024304 (2009).
- ²⁰S. M. Sheehan, B. F. Parsons, J. Zhou, E. Garand, T. A. Yen, D. T. Moore, and D. M. Neumark, *J. Chem. Phys.* **182**, 034301 (2008).
- ²¹S. M. Sheehan, B. F. Parsons, T. A. Yen, M. R. Furlanetto, and D. M. Neumark, *J. Chem. Phys.* **128**, 174301 (2008).
- ²²N. A. Sassin, S. Everhart, J. I. Cline, and K. M. Ervin, *J. Chem. Phys.* **112**, 10071 (2008).
- ²³N. A. Sassin, S. Everhart, B. B. Dangi, K. M. Ervin, and J. I. Cline, *J. Am. Soc. Mass Spectrom.* **14**, 96 (2009).

V. Publications and submitted journal articles supported by this project 2007-2009

1. B. Jia and K. M. Ervin, "Threshold collision-induced dissociation of hydrogen-bonded dimers of carboxylic acids", *J. Phys. Chem. A*, **112**, 1773-1782 (2008).
2. Y. Shi and K. M. Ervin, "Hydrogen atom transfer reactions of C₂, C₄, and C₆. Bond dissociation energies of H-C_{2n} and H-C_{2n} (n = 1, 2, 3)", *J. Phys. Chem. A*, **112**, 1261-1267 (2008).
3. P. B. Armentrout, K. M. Ervin, and M. T. Rodgers, "Statistical rate theory and kinetic energy-resolved ion chemistry: Theory and applications", *J. Phys. Chem. A*, **112**, 10071-10085 (2008).
4. K. M. Ervin, PESCAL, Fortran program for Franck-Condon simulation of photoelectron spectra, <http://wolfweb.unr.edu/~ervin/pes/> (major revision 2008).
5. C. L. Adams, H. Schneider, K. M. Ervin, and J. M. Weber, "Low-energy photoelectron imaging spectroscopy of nitromethane anions: Electron affinity, vibrational features, anisotropies and the dipole-bound state." *J. Chem. Phys.* **130**, 074307:1-10 (2009).
6. S. W. Wren, K. M. Vogelhuber, K. M. Ervin, and W. C. Lineberger, "The photoelectron spectrum of CCl₂: The convergence of theory and experiment after a decade of debate", *Phys. Chem. Chem. Phys.* (in press, 2009).

Spectroscopic and Dynamical Studies of Highly Energized Small Polyatomic Molecules

Robert W. Field
Massachusetts Institute of Technology
Cambridge, MA 02139
rwfield@mit.edu

I. Program Scope

The fundamental goal of this program is to develop the experimental techniques, diagnostics, interpretive concepts, and pattern-recognition schemes needed to reveal and understand how large-amplitude motions are encoded in the vibration-rotation energy level structure of small, gas-phase, combustion-relevant polyatomic molecules. We are focusing our efforts on unimolecular isomerization in several prototypical systems, including the $\text{HNC} \leftrightarrow \text{HCN}$ and $\text{HCCH} \leftrightarrow \text{CCH}_2$ isomerization systems. We are developing chirped-pulse millimeter wave (CPmmW) spectroscopy as a technique that can be used in conjunction with Stimulated Emission Pumping (SEP) and the Stark effect to populate and identify molecular states with high excitation in *local* vibrational modes, which are of key importance in understanding isomerization processes.

II. Recent Progress

A. CPmmW Spectrometer and Acrylonitrile Photolysis

Chirped-Pulse Millimeter-Wave (CPmmW) spectroscopy is the first truly broadband technique for Fourier-transform spectroscopy in the millimeter wave region. We designed the technique in collaboration with the Brooks Pate research group at the University of Virginia, based on their pioneering Chirped-Pulse Fourier-Transform Microwave (CPMW) spectrometer, which operates at frequencies up to 20 GHz. We have built and tested a CPmmW spectrometer that operates in the 70–102 GHz frequency range. The spectrometer can acquire up to 12 GHz of spectral bandwidth in a single shot, and initial tests indicate significant advantage over existing millimeter-wave spectrometers in data acquisition speed.

The spectra in Figure 1 compare the CPmmW performance with that of the millimeter-wave absorption spectrometer previously used in the Field laboratory. The older spectrometer used a tunable W-band Gunn oscillator as the radiation source and a liquid-helium-cooled InSb bolometer to detect absorption of millimeter-wave power. In comparison with the scanned absorption spectrum in Figure 1.A, the Fourier-transform CPmmW spectrometer is capable of obtaining a spectrum (Figures 1.B and 1.C) of forty times greater spectral width with two times greater signal-to-noise ratio at comparable resolution in half the acquisition time.

The spectrum shown in Figure 1 can also be used to demonstrate the advantage of the CPmmW spectrometer over the previous state of the art, the millimeter-wave Fabry-Perot cavity spectrometer of Yamamoto, which would have required four times as long to collect a similar spectrum. Although the Yamamoto spectrometer requires only a few averages per ~ 2 MHz cavity bandwidth step to achieve comparable signal-to-noise, the collection rate of their spectrometer is limited by the time required to tune the cavity at each frequency step to a maximum scanning rate of 1 GHz / hour. The necessity for long averaging times in our CPmmW setup arises from the fact that we have insufficient power available to achieve optimal polarization of the sample. For a molecule with a 1 D transition dipole moment, ~ 1 W is required to achieve a $\pi/2$ polarization over a 4 GHz chirp bandwidth in 500 ns, but our spectrometer only generates 30 mW. We therefore expect that the sensitivity of the technique will improve significantly as the power available in the millimeter-wave region increases.

Another advantage of the CPmmW technique is that it can be used to obtain spectra with meaningful relative intensity information since all the frequency resolution elements of the spectrum are obtained and averaged in every shot. Fluctuations in laser intensity and other laboratory conditions made relative line intensities semi-quantitative at best in previous millimeter-wave spectrometers. We plan to put the accurate intensity information of our CPmmW spectrometer to use in our investigation of the photolysis dynamics of acrylonitrile at 193 nm. By measuring the nascent distribution of vibrational states in the photolysis products, we hope to shed light on the photolysis mechanism, and in particular on the controversy concerning the HCN/HNC product channels. The CPmmW spectrometer is a tool ideally suited to this investigation,

because it can be used to make simultaneous measurements of the $J = 1-0$ rotational transitions of many vibrational levels of both HCN and HNC that occur within a relatively narrow spectral region from 87–92 GHz. The intensities of all the lines will be averaged simultaneously over fluctuations in the photolysis laser power, allowing the determination of accurate relative intensities.

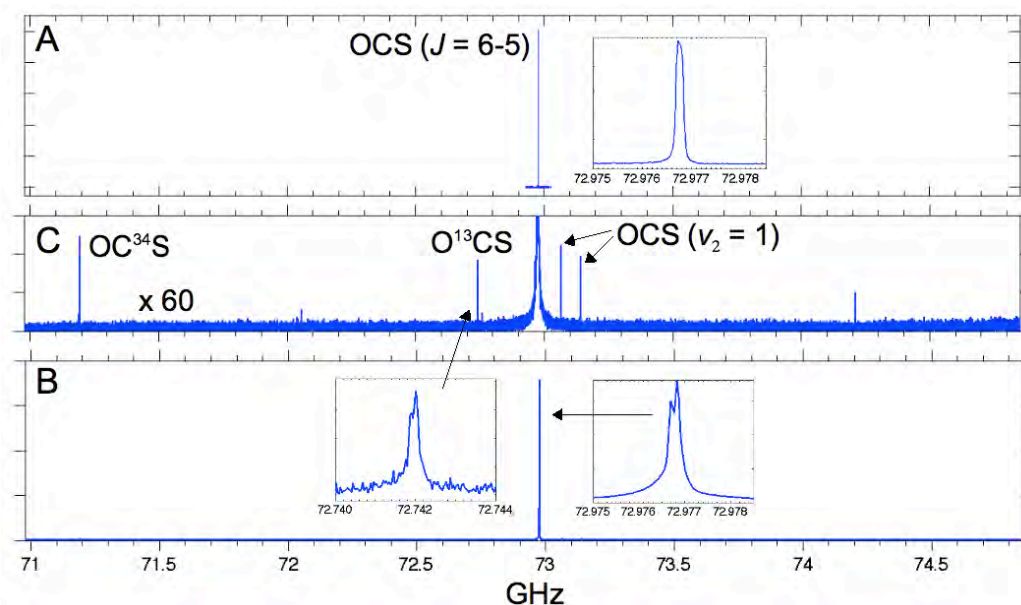


Figure 1: The performance of the CPmmW spectrometer is compared with that of the millimeter-wave absorption spectrometer previously used in the Field lab. Panel A displays a 100 MHz bandwidth spectrum centered on the OCS $J = 6 - 5$ transition recorded using the scanned absorption spectrometer. The signal-to-noise ratio is 670 and the acquisition time was 100 minutes. Panel B displays a 4 GHz bandwidth CPmmW spectrum centered on the same OCS transition. The signal-to-noise ratio is 1500 and the acquisition time was 50 minutes. Panel C shows a vertical zoom of the spectrum in which lines arising from isotopomers and excited vibrational states are labeled.

We have already made preliminary tests of the CPmmW experiment on acrylonitrile photolysis products. A survey spectrum of the photolysis products is shown in Figure 2. Rotational transitions of acrylonitrile, HCN, HNC and HCCCN are assigned in the figure. Note that after 1000 averages, only one line from vibrationally excited HCN is visible over the noise. However, many more lines are expected to be present below the noise threshold of the current spectrometer.

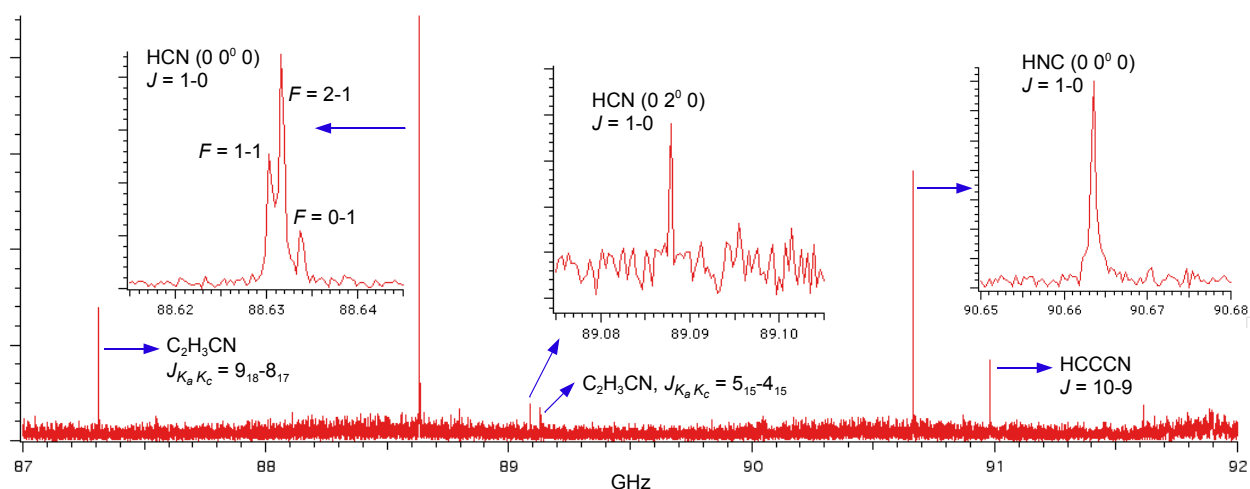


Figure 2: A survey CPmmW spectrum of the products of 193 nm photolysis of acrylonitrile. A mixture of 1% acrylonitrile in Ar is expanded in a supersonic jet and photolyzed at 193 nm by a focused beam from an ArF excimer laser (~ 4 mJ). ~ 20 μ s after the photolysis pulse, a chirped millimeter-wave pulse interacts with the molecular beam and the Fourier-transform spectrum is obtained after averaging the time-domain FID from 1000 pulses (~ 2 minutes).

B. High- and low-barrier unimolecular isomerization in S_0 and S_1 HCCH

The goal of our studies on the acetylene \leftrightarrow vinylidene system is to observe barrier-proximal states. Many studies have demonstrated that the vibrational eigenstates of acetylene and similar molecules undergo a normal-to-local transition in which the normal modes appropriate to describe small displacements from the equilibrium geometry evolve into local modes in which the excitation is isolated in a single C-H bond stretch or \angle CCH bend. The evolution of vibrational character is of particular interest in the acetylene bending system because the local bending vibration bears a strong resemblance to the reaction coordinate for isomerization from acetylene to vinylidene, with one hydrogen moving a large distance off of the C-C bond axis while the other hydrogen remains relatively stationary.

1. Experimental population of lowest energy local-bender eigenstates

While the existence of local bender eigenstates in S_0 acetylene has been predicted by a variety of theoretical models, including effective Hamiltonian fits to the available experimental data, experimental verification of the character of these states has been difficult to achieve. We recently observed the first direct evidence of the S_0 local bender states. Using local bender pluck states on the S_1 surface as SEP intermediates, we recorded spectra that show a degenerate pair of levels with g/u symmetries in the energy region where the local benders are predicted to emerge. The observed degeneracy corresponds with expectations for the local bender states. The large geometric distortions associated with these states should lead to large vibrationally-averaged dipole moments, which will distinguish them from ergodic states.

2. Observation and theoretical treatment of vibrational levels of S_1 *cis* acetylene

Aside from its utility as an intermediate for studying highly excited vibrational states of the S_0 surface, the S_1 state also presents the possibility of observing low-barrier isomerization from its *trans*-geometry minimum to a local energy minimum at a *cis* geometry. This process has been the focus of many theoretical studies, but it has been difficult to study experimentally because, though the *trans* minimum has been exhaustively characterized, the transition from the ground electronic state to the S_1 *cis* geometry is electronically forbidden and no transitions to this conformer have previously been observed. In the course of characterizing the S_1 surface, several vibrational levels were observed which could not be ascribed to S_1 -*trans* or other electronic states. S_1 -*cis* seems a likely candidate for explaining these interloper levels, which were, surprisingly, observed below the energy of the calculated barrier to *trans-cis* isomerization, and must therefore owe their intensity to mixing via tunneling with *trans*-geometry-localized states.

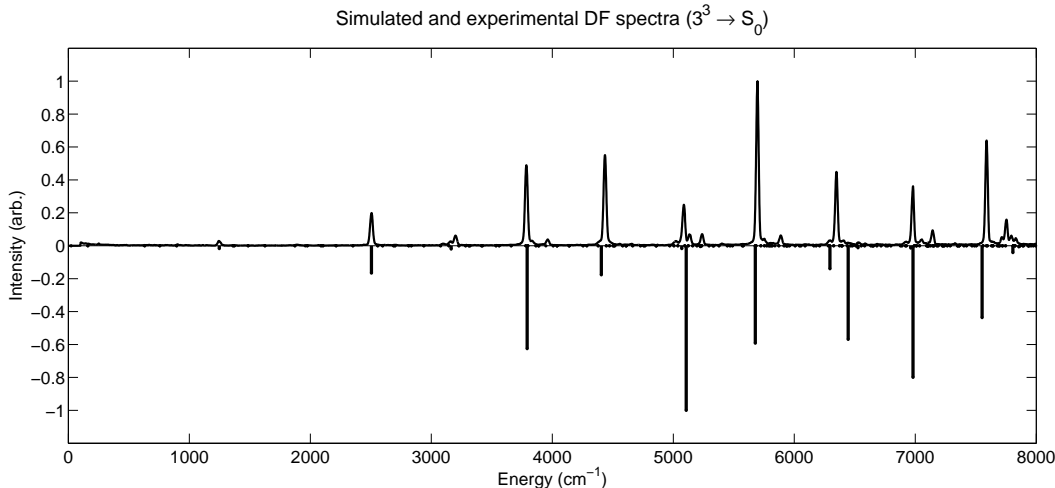


Figure 3: The dispersed fluorescence (DF) spectrum of the $3v_3$ level calculated from the 3D DVR wavefunctions (downward) is compared with the experimental spectrum (upward). The discrepancies in the intensities are due partially to the fractionation of bright states in the experimental spectrum into some eigenstates that are non-existent in the reduced dimension calculation, and partially to the neglect of the CH stretch coordinates when calculating the transition dipole moment.

As part of our investigation of the *cis*-well states, we undertook a discrete variable representation (DVR) calculation to obtain information about the delocalized wavefunctions of S_1 . Our reduced dimension

DVR was designed to capture the planar isomerization dynamics due to modes v_2 , v_3 , and v_6 . The initial results appear to corroborate our assignments of the interloper levels to the *cis* well. Since the same type of calculation can be performed for the S_0 state, we have also been able to simulate absorption, dispersed fluorescence, and SEP spectra (Fig. 3). We hope to use this capability to interpret and assign complicated experimental spectra, as well as identify appropriate intermediate states for experiments that will probe chemically interesting regions of the potential energy surface.

III. Future Work

We plan to continue to improve the sensitivity of our CPmmW spectrometer by taking advantage of new millimeter-wave technology and by incorporating a slit-jet molecular beam chamber. These enhancements will enable us to measure the populations of vibrationally-excited acrylonitrile photolysis products and locate the acetylene local bender states. Combining our S_1 DVR results with the survey capability of CPmmW/DF spectra will guide us towards conclusive SEP experiments. We will record Stark effect spectra of the S_0 highly vibrationally excited levels, in order to measure the large predicted vibrationally-averaged dipole moments of the barrier-proximal states. The accurate CPmmW intensity information will enable us to resolve the controversy over the photolysis mechanism of acrylonitrile.

Publications supported by this project 2007–2009

- [1] W.L. Virgo, K.L. Bittinger, A.H. Steeves, and R.W. Field. Contrasting singlet-triplet dynamical behavior of two vibrational levels of the acetylene S_1 $2^13^1B^2$ polyad. *J. Phys. Chem. A*, 111(49):12534–12537, 2007.
- [2] W. Bryan Lynch, Hans A. Bechtel, Adam H. Steeves, John J. Curley, and R. W. Field. Observation of the \tilde{A}^1A'' state of isocyanogen. *Journal of Chemical Physics*, 126(24), 2007.
- [3] B. H. Layne, L. M. Duffy, H. A. Bechtel, A. H. Steeves, and R. W. Field. Beam action spectroscopy via inelastic scattering. *J. Phys. Chem. A*, 111(31):7398–7403, 2007.
- [4] H. A. Bechtel, A. H. Steeves, B. M. Wong, and R. W. Field. Evolution of chemical bonding during HCN/HNC isomerization as revealed through nuclear quadrupole hyperfine structure. *Angewandte Chemie International Edition*, 47(16):2969–2972, 2008.
- [5] A. J. Merer, N. Yamakita, S. Tsuchiya, A. H. Steeves, H. A. Bechtel, and R. W. Field. Darling–Dennison resonance and Coriolis coupling in the bending overtones of the \tilde{A}^1A_u state of acetylene, C_2H_2 . *The Journal of Chemical Physics*, 129(5):054304, 2008.
- [6] A. H. Steeves, A. J. Merer, H. A. Bechtel, A. R. Beck, and R. W. Field. Direct observation of the symmetric stretching modes of \tilde{A}^1A_u acetylene by pulsed supersonic jet laser induced fluorescence. *Mol. Phys.*, 106(15):1867–1877, 2008.
- [7] A. J. Merer, Z. Duan, R. W. Field, and J. K. G. Watson. Perturbations in the $4\nu_3$ level of \tilde{A}^1A_u state of acetylene, C_2H_2 . *Canadian Journal of Physics*, in press, 2009.
- [8] A. H. Steeves, H. A. Bechtel, A. J. Merer, N. Yamakita, S. Tsuchiya, and R. W. Field. Stretch-bend combination polyads in the \tilde{A}^1A_u state of acetylene, C_2H_2 . *Journal of Molecular Spectroscopy*, submitted, 2009.

Scanning Tunneling Microscopy Studies of Chemical Reactions on Surfaces

George Flynn, Department of Chemistry, Columbia University

Mail Stop 3109, 3000 Broadway, New York, New York 10027

gwf1@columbia.edu

Introduction

A few years ago our work took a new direction and is now focused on fundamental chemical events taking place on carbon surfaces^{1,2} with the intent of shedding light on their role in mediating the formation of polycyclic aromatic hydrocarbons (PAHs) from small molecular precursors and the growth of soot particles.³ One of the exciting developments in this area of research has been the discovery of techniques for preparing and studying single graphite sheets or graphene, a two-dimensional material whose chemical reactivity is substantially greater than that of multi-sheet graphite.^{1,2,4,5} In addition the electronic and structural properties of graphene are quite unusual and depend on both the size and shape of the graphene flakes, which are themselves essentially giant PAHs. Graphene is, thus, an interesting model system in which to study the kind of carbon chemistry that is likely to shed light on the properties of soot-like materials. Interest in soot is ultimately driven by the environmental and health implications arising from its formation in combustion reactions (particularly those involving heavier, diesel fuels), which are nearly ubiquitous throughout our society.³

Scanning tunneling microscopy (STM) has become a powerful tool for interfacial studies of structure and chemistry mainly because of its ability to investigate surface structure and dynamics with molecular or even atomic resolution. For example, the same region of a surface can be investigated before and after exposure to reactive species using STM tip engagement techniques^{1,2}, thereby extracting information about reaction mechanisms localized at single atomic surface sites. In terms of chemical reactivity, the edges of large PAHs and the surfaces of soot particles in the third stage of growth are analogous to the edges of pits, defect sites and step edges on graphite and graphene. Exposure of well characterized, defected graphite and graphene surfaces to oxygen or hydrocarbon fuels (e.g. C₂H₂) in a controlled manner under ultra-high vacuum (UHV) conditions, thus, provides an opportunity to investigate the fundamental chemical steps involved in carbon chemistry and soot formation.

Results: Graphene on Metal Surfaces

Since many soot particles, especially those formed from diesel fuel, are impregnated with heavy metal atoms, which are virtually certain to affect particle reactivity,^{6,7} the interactions between carbon and metals or metal oxides are important for obtaining a full understanding of soot chemistry. We have pursued a number of experiments involving the interaction of PAHs and graphene with metals, for example, the chemistry of hexabenzocoronene on ruthenium metal.⁸ This large PAH molecule remains intact on ruthenium, even at high temperatures.

In quite remarkable contrast is the behavior of hexabenzocoronene (HBC) on a single crystal cobalt (0001) surface.⁹ After vacuum deposition on a clean Co surface, HBC decomposes with relatively mild heating to form flakes of graphene that are in excellent registry with the metal atoms on the Co surface. Experiments

were performed using a low-temperature scanning tunneling microscope in a UHV chamber, whose base pressure was 3×10^{-11} Torr. A cobalt single crystal with (0001) orientation was cleaned *in-situ* by repeated cycles of argon sputtering and subsequent thermal annealing at 570 K. Contorted hexabenzocoronene molecules^{8,9} were deposited onto a 300 K, clean Co(0001) surface by vacuum evaporation inside the UHV chamber. (Hexabenzocoronene (HBC) consists of a coronene core and 6 benzene rings around the outside. Because of steric hindrance the molecule is not flat, with alternate benzenes above and below the coronene plane.) Following this procedure, the substrate and sample were annealed *in-situ* at 600 K for 20 min in order to grow graphene flakes using HBC molecules as the carbon source. The graphene flakes were then characterized by Low Temperature-STM at 4.9 K. The low drift rate and stability of this device provides both superior quality images and a platform on which to perform STS experiments that have the potential to unravel the electronic structure and even the vibrational signature of molecular adsorbates.

These graphene on Co(0001) samples have an on-top overlayer structure wherein one of two carbon atoms in the graphene unit cell sits directly above an underlying metal atom (on-top position or A-site). The on-top registry along with the measured height of the graphene layer (~ 2.2 Å) is quite consistent with theoretical calculations for the similar system of graphene on Ni(111). It is also noteworthy that the inter-atomic distance between metal atoms on Co(0001) (and Ni(111)) almost perfectly matches the distance between every other carbon atom in graphene (lattice mismatch $< 2\%$), which favors epitaxial growth of graphene on these substrates.

Graphene flakes with zigzag edges and nearly triangular shapes, whose lateral dimensions are 2~4 nm, can be readily seen on the Co surface. At a voltage corresponding to tunneling at $E_F - 0.15$ eV, (E_F is the Fermi energy) triangular flakes with zigzag edges exhibit enhanced tunneling along the peripheries. This indicates that a high proportion of the density of electronic states (DOS) is spatially localized near the edge regions of these triangular soot nanoflakes at this specific energy level where there is a peak in the normalized STS conductance spectrum.

Soot nanoflakes with zigzag edges but having a hexagonal shape have also been observed in these experiments. Several of these flakes exhibit point-like defects inside the hexagonal graphene samples that are likely to be reactive sites for molecules such as acetylene. It will be interesting to compare the chemistry at these sites with that of defected graphite by performing experiments similar to those described in our earlier work involving defected graphite and acetylene.

As in the case of the triangular graphene nanoflakes, tunneling at a voltage corresponding to $E_F - 0.17$ eV shows relatively bright features along the periphery of hexagonal structures. However, this feature is less distinct than that of similar images for triangular flakes. It is interesting to note here that a recent theoretical argument¹⁰ suggests that the edge states of hexagonal graphene flakes have less edge character (more bulk character) than those of triangular flakes and leak more into the inner region of the sample.

These results show that soot-like graphene nanoflakes can be formed on Co surfaces. In addition the electronic structure of these samples differs depending on their geometric shape and can be readily probed by STM/STS. The coupling of the graphene flakes to the metal surface as well as the relative reactivity of different shaped flakes is presently under study. Nevertheless, the possibility of correlating the electronic state energies and their spatial distribution to subsequent chemistry is certainly a fruitful direction in which to pursue future experiments.

Present and Future Experimental Program

It should be possible to probe the reaction mechanism via which HBC breaks up and recombines on cobalt to form sizeable graphene flakes. Single molecule manipulation with the STM can be used to bring two HBC molecules in close proximity to each other, while temperature control can be used to mediate the rate of reaction leading to the formation of these large organized structures. Considerable insight into the mechanism for PAH chemistry on metals should be forthcoming from such a series of experiments.

References

1. Li Liu, Kwang Taeg Rim, Daejin Eom, Tony Heinz, and George W. Flynn "Direct Observation of Atomic Scale Graphitic Layer Growth," *Nanoletters*, **8**, 1872-1878 (2008)
2. Li Liu, Sunmin Ryu, Michelle R. Tomasik, Elena Stolyarova, Naeyoung Jung, Mark S. Hybertsen, Michael L. Steigerwald, Louis E. Brus, George W. Flynn, "Graphene Oxidation: Thickness-Dependent Etching and Strong Chemical Doping", *Nanoletters*, **8**, 1965-1970 (2008)
3. J. A. Miller and G. A. Fisk, "Combustion Chemistry", *Chem. & Eng. News*, **65** (35), 22-46, August 31, 1987
4. K. S. Novoselov, D. Jiang, F. Schedin, T. J. Booth, V. V. Khotkevich, S. V. Morozov, A. K. Geim", "Two-dimensional atomic crystals", *Proc. Nat'l Acad. of Sci. of the U.S.* **102**, 10451-10453 (2005)
5. Russell Whitesides, Dominik Domin, Romelia Salomon-Ferrer, William A. Lester, Jr., Michael Frenklach, "Graphene Layer Growth Chemistry: Five- and Six-Member Ring Flip Reaction", *Journal of Physical Chemistry A*, **112**, 2125-2130 (2008)
6. A. Braun, F. E. Huggins, N. Shah, Y. Chen, S. Wirick, S. B. Mun, C. Jacobsen, and G. P. Huffman, "Advantages of Soft X-ray Absorption Over TEM-EELS for Solid Carbon Studies—A Comparative Study on Diesel Soot with EELS and NEXAFS", *Carbon* **43**, 117-124 (2005)
7. I. E. Abdul-Khalek, D. B. Kittelson, B. R. Graskow and Q. Wei, "Diesel Exhaust Particle Size: Measurement Issues and Trends", *SAE 980525* (1998)
8. Kwang Taeg Rim, Mohamed Siaj, Shengxiong Xiao, Matthew Myers, Vincent D. Carpentier, Li Liu, Chaochin Su, Michael L. Steigerwald, Mark S. Hybertsen, Peter H. McBreen, George W. Flynn, and Colin Nuckolls, Forming Aromatic Hemispheres on Transition Metal Surfaces, *Angew. Chem. Int. Ed.* **46**, 7891-7895 (2007)
9. Daejin Eom, Deborah Prezzi, Kwang T. Rim, Hui Zhou, Michael Lefenfeld,

- Colin Nuckolls, Mark S. Hybertsen, Tony F. Heinz, and George W. Flynn, “Structure and Electronic Properties of Epitaxial Graphene on Co(0001)”, Physical Review Letters, submitted
10. R. Rosei, M. De Crescenzi, F. Sette, C. Quaresima, A. Savoia, and P. Perfetti, “Structure of graphitic carbon on Ni(111): A surface extended-energy-loss fine-structure study” Phys. Rev. B 28, 1161-1164 (1983).

DOE Publications: (2007-2009)

1. Kwang Taeg Rim, Mohamed Siaj, Shengxiong Xiao, Matthew Myers, Vincent D. Carpentier, Li Liu, Chaochin Su, Michael L. Steigerwald, Mark S. Hybertsen, Peter H. McBreen, George W. Flynn, and Colin Nuckolls, Forming Aromatic Hemispheres on Transition Metal Surfaces, Angew. Chem. Int. Ed. 46, 7891-7895 (2007)
2. Boaz Ilan, Gina M. Florio, Mark S. Hybertsen, Bruce J. Berne and George W. Flynn, “Scanning Tunneling Microscopy Images of Alkane Derivatives on Graphite: Role of Electronic Effects”, Nanoletters, 8, 3160-3165 (2008)
3. Elena Stolyarova, Daniil Stolyarov, Li Liu, Kwang T. Rim, Yuanbo Zhang, Melinda Han, Mark Hybertsen, Philip Kim and George Flynn, “STM Studies of Ultrathin Graphitic (Graphene) Films on an Insulating Substrate under Ambient Conditions”, J. Phys. Chem. C, 112, 6681-6688 (2008)
4. Li Liu, Kwang Taeg Rim, Daejin Eom, Tony Heinz, and George W. Flynn “Direct Observation of Atomic Scale Graphitic Layer Growth,” Nanoletters, 8, 1872-1878 (2008)
5. Li Liu, Sunmin Ryu, Michelle R. Tomasik, Elena Stolyarova, Naeyoung Jung, Mark S. Hybertsen, Michael L. Steigerwald, Louis E. Brus, George W. Flynn, “Graphene Oxidation: Thickness-Dependent Etching and Strong Chemical Doping”, Nanoletters, 8, 1965-1970 (2008)
6. E. Stolyarova, D. Stolyarov, K. Bolotin, S. Ryu, L. Liu, M. Klima, M. Hybertsen, I. Pogorelsky, I. Pavlishin, K. Kusche, J. Hone, P. Kim, L. Brus, H. L. Stormer, V. Yakimenko, G. Flynn, “Observation of Graphene Bubbles and Effective Mass Transport Under Graphene Films”, Nanoletters, 9, 332-337 (2009)
7. Daejin Eom, Deborah Prezzi, Kwang T. Rim, Hui Zhou, Michael Lefenfeld, Colin Nuckolls, Mark S. Hybertsen, Tony F. Heinz, and George W. Flynn, “Structure and Electronic Properties of Epitaxial Graphene on Co(0001)”, Phys. Rev. Letts., submitted
8. Kwang Taeg Rim, Daejin Eom, Li Liu, Elena Stolyarova, Joan Marie Raitano, Sui-Wei Chan, Maria Flytzani-Stepanopoulous, and George W. Flynn, “Catalytic Gold Nanoparticles on an Iron Oxide Surface: A Scanning Tunneling Microscopy/Spectroscopy Study”, J. Phys. Chem., submitted
9. Li Liu, Joshua Lui, Tony Heinz, Louis Brus, and George Flynn, “Probing Graphene on Mica: The Flattest 2-D Material ”, manuscript in preparation.

Quantitative Imaging Diagnostics for Reacting Flows

Jonathan H. Frank
Combustion Research Facility
Sandia National Laboratories
Livermore, CA 94551-0969
jhfrank@sandia.gov

Program Scope

The primary objective of this project is the development and application of laser-based imaging diagnostics for studying the interactions of fluid dynamics and chemical reactions in reacting flows. Imaging diagnostics provide temporally and spatially resolved measurements of species, temperature, and velocity distributions over a wide range of length scales. Multi-dimensional measurements are necessary to determine spatial correlations, scalar and velocity gradients, flame orientation, curvature, and connectivity. Current efforts in the Advanced Imaging Laboratory focus on planar laser-induced fluorescence and Rayleigh scattering techniques for probing the detailed structure of both isolated flow-flame interactions and turbulent flames. The investigation of flow-flame interactions is of fundamental importance in understanding the coupling between transport and chemistry in turbulent flames. These studies require the development of new imaging diagnostic techniques to measure key species in the hydrocarbon-chemistry mechanism as well as to image rates of reaction and dissipation. Recent advances in diagnostic capabilities enable us to probe the temporal evolution of turbulent flames as well.

Recent Progress

Dissipation length scales in turbulent jet flames and non-reacting jets

High-resolution imaging of laser Rayleigh scattering in turbulent jet flames has provided insights into the dynamic structure of the thermal dissipation field [1-3]. These insights motivated a series of studies on scalar dissipation in non-reacting jets. Detailed comparisons of measurements in the near field of a turbulent $\text{CH}_4/\text{H}_2/\text{N}_2$ jet flame with $\text{Re}=15,200$ and in non-reacting propane jets with Reynolds numbers from 7,200 to 21,700 reveal the effects of heat release on the turbulence dissipation structures. For example, Fig. 1 compares radial profiles of the cutoff length scale, λ_c , of the dissipation spectrum for the jet flame and the non-reacting jets. In the flame, λ_c has a distinctly different dependence on the radial location as a result of increased dissipation length scales and changes in the orientation of the dissipation structures at elevated temperatures. This jet flame is a target flame in the TNF Workshop, and the insights from these experiments are being used in the development of turbulent combustion models, as described in the following section.

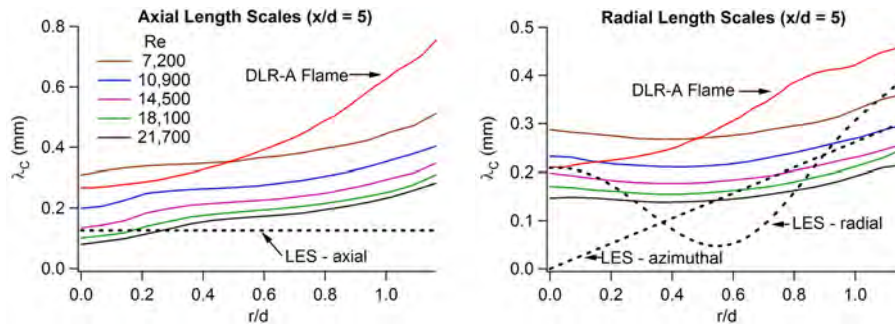


Figure 1. Radial profiles of the axial and radial dissipation cutoff scales at $x/d=5$. The red curve corresponds to the $\text{CH}_4/\text{H}_2/\text{N}_2$ jet flame (DLR-A), and the remaining solid curves correspond to the non-reacting propane jets. The dotted lines show the grid spacing of an 82M LES grid designed from the experimental results.

Coupling imaging diagnostics and large eddy simulations

Comparisons of experiments and large eddy simulations (LES) provide a unique opportunity for advancing our understanding of the spatial structures and temporal evolution of turbulent flames. We are developing a systematic approach for comparing laser-based imaging measurements and LES of turbulent non-premixed flames in collaboration with Joe Oefelein (Sandia). Experimental studies of turbulent jet flames and non-reacting jets are coupled with high-fidelity LES calculations to understand more clearly how LES represents small scale mixing and what the effect of resolution is on the time evolving dissipation fields. We are currently studying the effects of LES filter size on the evolution of scalar mixing processes and its implications for the development of improved turbulent combustion models. Figure 2 shows sample measurements of the instantaneous mixture fraction and scalar dissipation fields in the near field of a non-reacting turbulent propane jet with the LES computational domain that was designed using the measured cutoff length scales in Fig. 1.

We are investigating differences in spatial and temporal averaging in the experiments and simulations. One of the challenges of comparing LES calculations and measurements is that the simulations track the evolution of resolved-scale fields, which can lead to the development of very different turbulence structures than are observed in the instantaneous measurements. To demonstrate this point, we spatially filtered single-shot Rayleigh images such that the effective spatial resolution of the filtered measurements matched the resolved scale in a series of LES calculations with different grids. Figure 3 shows a sample single-shot measurement that was filtered using a progression of grids with subsequent refinements of a factor of two in each direction. The morphology of these filtered dissipation structures are very different from those predicted by LES (see abstract of J. Oefelein), indicating the effects of temporal coalescence and dispersion errors even when using a highly refined LES grid with cell sizes on the order of the dissipation cutoff length scales. Furthermore, a comparison of the relative dimensions of the dissipation structures and the grid cells indicates that LES calculations must account for the overlap of dissipation structures in the sub-grid and resolved scales. The limited quantity of dissipation structures in each LES grid cell indicates that widely used assumptions regarding the sampling of statistically significant quantities of turbulence structures within each grid cell must be carefully examined. The anisotropy of the dissipation structures, particularly in the jet flame, must also be considered. The results of these comparisons represent a first step in the development of a systematic approach for comparing imaging diagnostics and LES.

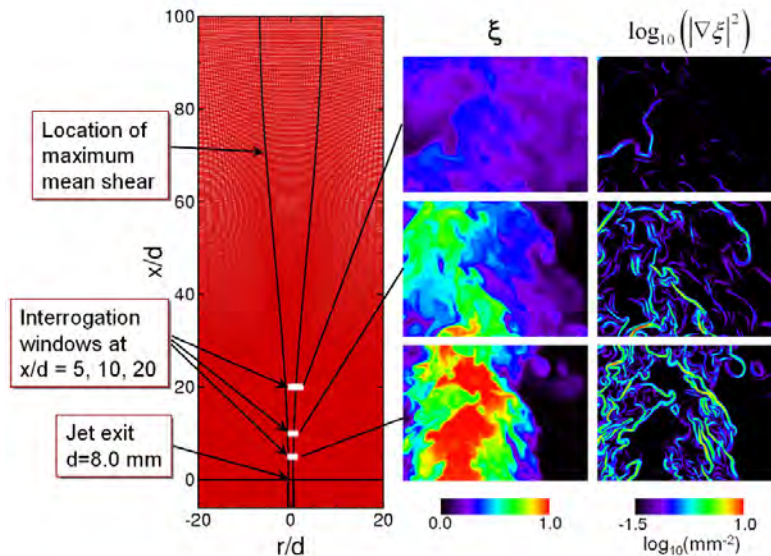


Figure 2. Single-shot laser Rayleigh scattering measurements of mixture fraction and scalar dissipation in a turbulent non-reacting propane jet at $x/d=5, 10, 20$. Jet Reynolds number is 14,200. The computational domain and grid for companion LES calculations are shown on the left.

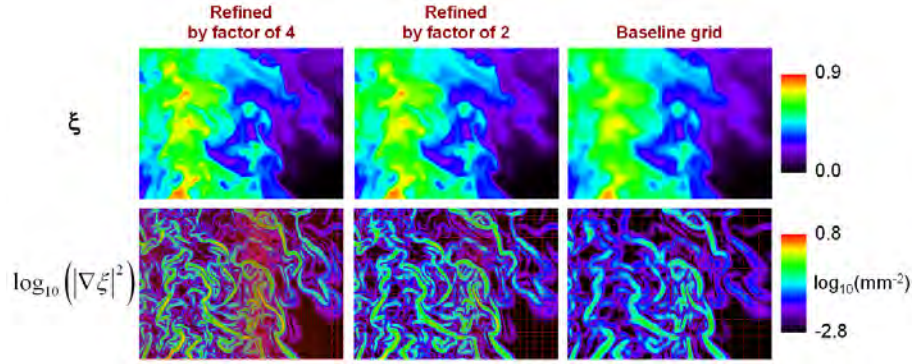


Figure 3. Effects of spatial filtering on single-shot measurements of mixture fraction (top row) and scalar dissipation (bottom row) in a non-reacting propane jet of $Re=14,200$ at $x/d = 10$. The image width is 16.1 mm. The dissipation images show the local grid distributions corresponding to three different LES calculations. The width of the smoothing kernel varies throughout the image according to the corresponding LES grids.

High-repetition rate imaging for studying temporal evolution of turbulent flames

We are developing a high-repetition rate imaging facility in the Advanced Imaging Laboratory to complement our current imaging approaches. This new capability will significantly enhance our research program by enabling us to probe the complex time history of interactions between turbulent flows and flames. Measurements of time history effects are particularly important for understanding intermittent phenomena, such as localized extinction and re-ignition. This information is not available from our other imaging systems, which provide ensemble statistics using instantaneous snapshot measurements that are temporally uncorrelated. As a first step in developing this new imaging facility, we recently added the capability of high-repetition rate laser-induced fluorescence imaging. This system consists of a 10 kHz tunable dye laser for LIF excitation and an intensified CMOS camera for detection. Initial investigations are focusing on OH-LIF measurements of the temporal evolution of turbulent non-premixed jet flames and lean premixed stratified CH_4 /air flames. We are leveraging our current capabilities through collaborations with other groups that have additional high-repetition rate imaging equipment, including W. Meier (DLR Stuttgart, Germany) and A. Dreizler (Technical University of Darmstadt, Germany).

Future Work

We plan to extend our studies of the effects of heat release on turbulent jets, and new results will be coupled with Joe Oefelein's LES calculations. Measurements of turbulence microscales will be used to develop accurate sub-grid scale models. Knowledge gained from comparisons of experiments and LES of passive scalar mixing will be incorporated into our studies of turbulent jet flames. Flame studies will address the challenges of modeling localized extinction and re-ignition. We also plan to investigate extinction and re-ignition in isolated flow-flame interactions with a focus on dimethyl ether and ethylene as fuels. Comparisons with DNS of Jackie Chen (Sandia) will be used to evaluate the coupling of transport and flame chemistry over a range of thermochemical conditions. These studies will include the use of picosecond two-photon LIF imaging of atomic hydrogen to study preferential diffusion of hydrogen in collaboration with Tom Settersten (Sandia).

The new high-repetition rate imaging capability will be coupled with high-resolution, low-repetition rate diagnostics. These combined approaches will be useful in determining the sequence of events that create and destroy the detailed structures that we observe with high-resolution single-shot measurements of turbulent flames. Events leading to localized extinction and re-ignition will be studied.

Studies of stratified combustion are a new component of our research. Local variations in fuel/air mixtures exist in practical combustion devices, and the effects of stratification on turbulent premixed flames are not well understood. We plan to conduct detailed studies of turbulent stratified flames in collaboration with experimental and computational groups from TU Darmstadt, Cambridge University, and Sandia. These collaborations are supported in part by the Leverhulme Trust of the UK.

References

- [1] J. H. Frank, S. A. Kaiser, *Exp. Fluids* **44** (2008) 221-233.
- [2] S. A. Kaiser, J. H. Frank, *Proc. Combust. Inst.* **31** (2007) 1515-1523.
- [3] S. A. Kaiser, J. H. Frank, *Proc. Combust. Inst.* **32** (2009) 1639-1646.

BES-Supported Publications (2007-present)

- G. Amantini, J. H. Frank, M. D. Smooke, A. Gomez, "Computational and experimental study of steady axisymmetric non-premixed CH₄ counterflow flames," *Combust. Theory and Modeling* **11**, 47-72 (2007).
- G. Amantini, J.H. Frank, B.A.V. Bennett, M.D. Smooke, A. Gomez, "Comprehensive study of the evolution of an annular edge flame during extinction and reignition of a counterflow diffusion flame perturbed by vortices," *Combust. Flame*, **150**, 292-319 (2007).
- J.H. Frank, A.D. Elder, J. Swartling, A.R. Venkitaraman, A.D. Jeyasekharan, C.F. Kaminski, "A white light confocal microscope for spectrally resolved multidimensional imaging," *J. Microscopy* **227**, 203-215 (2007).
- S.A. Kaiser and J.H. Frank,, "Imaging of dissipative structures in the near field of a turbulent non-premixed jet flame," *Proc. Combust. Inst.* **31**, 1515-1523 (2007).
- J.H. Frank and S.A. Kaiser, "High-resolution imaging of dissipative structures in a turbulent jet flame with Rayleigh scattering," *Exp. Fluids* **44**, 221-233 (2008).
- W.D. Kulatilaka, B.D. Patterson, J.H. Frank, and T.B. Settersten, "Comparison of nanosecond and picosecond excitation for interference-free two-photon laser-induced fluorescence detection of atomic hydrogen in flames," *Appl. Opt.* **47**, 4672-4683 (2008).
- S. Schlachter, A.D. Elder, J.H. Frank, A. Grudinin, and C.F. Kaminski, "Spectrally resolved confocal fluorescence microscopy with a supercontinuum laser," *Microscopy and Analysis* **22**, 11-13 (2008)
- C.F. Kaminski, R.S. Watt, A.D. Elder, J.H. Frank, and J. Hult, "Supercontinuum radiation for applications in chemical sensing and microscopy," *Appl. Phys. B* **92**, 367-378 (2008).
- C.S. Yoo, J.H. Chen, and J.H. Frank, "A numerical study of transient ignition and flame characteristics of diluted hydrogen versus heated air in counterflow," *Combust. Flame* **155**, 450-461 (2008).
- U.D. Lee, C.S. Yoo, J.H. Chen, J.H. Frank, "Effects of H₂O and NO on extinction and re-ignition of vortex-perturbed hydrogen counterflow flames," *Proc. Combust. Inst.* **32**, 1059-1066 (2009).
- E.R. Hawkes, R. Sankaran, J.H. Chen, S.A. Kaiser, J.H. Frank, "An analysis of lower-dimensional approximations to the scalar dissipation rate using direct numerical simulations of plane jet flames," *Proc. Combust. Inst.* **32**, 1455-1463(2009).
- W.D. Kulatilaka, J.H. Frank, T.B. Settersten, "Interference-free two-photon LIF imaging of atomic hydrogen in flames using picosecond excitation," *Proc. Combust. Inst.* **32**, 955-962 (2009).
- S.A. Kaiser and J.H. Frank, "Spatial scales of extinction and dissipation in the near field of non-premixed turbulent jet flames," *Proc. Combust. Inst.* **32**, 1639-1646 (2009).
- W. D. Kulatilaka, J. H. Frank, B. D. Patterson, and T. B. Settersten, "Analysis of 205-nm photolytic production of atomic hydrogen in methane flames," *Appl. Phys. B*, DOI: 10.1007/s00340-009-3474-3 (2009).
- J.H. Frank and R. S. Barlow, "Nonpremixed turbulent combustion," in *Combustion Phenomena: Selected Mechanisms of Flame Formation, Propagation, and Extinction*, J. Jarosinski and B. Veyssiere, Eds., CRC Press, 2009, pp. 153-162.
- U.D. Lee, C.S. Yoo, J.H. Chen, J.H. Frank, "Effect of NO on extinction and re-ignition of vortex-perturbed hydrogen flames," *Combust. Flame*, submitted (2009).

MECHANISM AND DETAILED MODELING OF SOOT FORMATION

Principal Investigator: Michael Frenklach

Department of Mechanical Engineering

The University of California

Berkeley, CA 94720-1740

Phone: (510) 643-1676; E-mail: myf@me.berkeley.edu

Project Scope: Soot formation is one of the key environmental problems associated with operation of practical combustion devices. Mechanistic understanding of the phenomenon has advanced significantly in recent years, shifting the focus of discussion from conceptual possibilities to specifics of reaction kinetics. However, along with the success of initial models comes the realization of their shortcomings. This project focuses on fundamental aspects of physical and chemical phenomena critical to the development of predictive models of soot formation in the combustion of hydrocarbon fuels, as well as on computational techniques for the development of predictive reaction models and their economical application to CFD simulations. The work includes theoretical and numerical studies of gas-phase chemistry of gaseous soot particle precursors, soot particle surface processes, particle aggregation into fractal objects, and development of economical numerical approaches to reaction kinetics.

Recent Progress:

A New Graphene Edge Surface Kinetics Model (with R. Whitesides)

Graphene, large polycyclic aromatic hydrocarbon (PAH), has become an important surrogate for theoretical studies of soot particle surface. Recently, graphene has also gained interest in the areas of condensed physics, materials science, and physical chemistry for its interesting physical and chemical properties. We have investigated graphene-edge chemistry in high temperature environments with the goal of developing predictive reaction models for soot growth in combustion. The gained knowledge may also help in manufacturing graphene in such environments.

In the previous years, in collaboration with William Lester's group, we performed theoretical analysis of elementary reactions occurring on zigzag graphene edges. We have identified several new reaction classes, among them migration of lone five-member rings along the zigzag edge, their transformations into six-member rings, and, most recently, migration of five-member rings embedded into six-member-ring layers (for references, see the List of Publications).

The migration of lone five-member rings was examined in kinetic Monte-Carlo (KMC) simulations [M. Frenklach, C.A. Schuetz, J. Ping, *Proc. Combust. Inst.* 30:1389 (2005)]. During the past year, we developed a new, detailed KMC (DKMC) model for growth of zigzag edges of graphene. The new model extends the previous KMC model in several important aspects.

The first alteration to the previous model is inclusion of more individually-resolved surface species. The steady-state assumption used for intermediate elementary reactions of "single step" transformation in the kinetic mechanism was found to be inadequate in some cases due to long lived intermediates. Removal of these assumptions has necessitated a more fine-grained description of surface species, and hence the new model can be qualified as *detailed*.

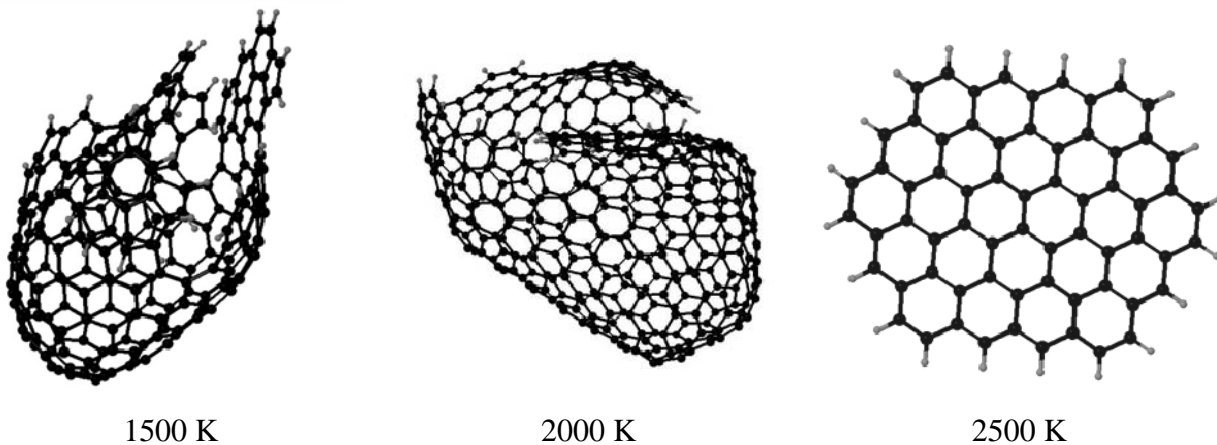
The second improvement to the previous model is the inclusion of many more reaction steps. A total of 41 surface transformations are included in the new model. Reactions forming five- and six-member ring complexes and those describing embedded five-member rings are of particular

interest. Rate coefficients for the reactions have been taken from experimental data, quantum chemical calculations, or assigned based on analogy to other reactions when data were not available.

Finally, because of the incorporation of five-member rings, substrates become curved and substrate geometry cannot be described by a two-dimensional lattice as it was previously. Instead, the new KMC model has been linked to the TINKER molecular mechanics package which provides geometry optimization routine with the MM3 potential. This approach properly accounts for substrate curvature while maintaining physically accurate bonding and geometric configuration of the growing substrates.

Five different initial molecular substrates were used in the simulations: pyrene, coronene, pentacene, decacene, isosacene. Pyrene and coronene were allowed to grow on all sides and thus were used to simulate the initial stages of soot-precursor growth. The linear species, pentacene, decacene, and isosacene, were used as models for surface growth and hence the lower row of carbon atoms was not allowed to react. The simulations were run isothermally, at temperatures 1500, 2000, and 2500 K. As in our prior simulations, the nominal gas phase composition was $x_{C_2H_2} = x_{H_2} = 0.1$ and $x_H = 0.01$. The environment was held constant over the entire simulation. Simulations were typically run for 5 ms. In some cases simulations were halted early, due to inconsistency developed between the bonding described by the kinetic simulation and the geometry optimization.

Representative examples of structures resulting from pyrene growth at the three temperatures are shown in the figure below.



Visual inspection of these structures indicates that five-member-ring incorporation is most frequent at the lower temperature and less so as temperature increases.

The analysis of all DKMC results indicated that the growing layers become significantly curved regardless of temperature or initial substrate, although lower temperatures lead to higher degree of curvature caused by higher inclusion of five-member rings. Calculated growth rates lie mainly in the range of 10^4 to 10^5 C-atom/s, in agreement with the previous KMC model and with experimental data. Quantitative analysis of growth rates and the degree of five-member-ring incorporation into growing substrates indicated that substrates become kinetically similar as they grow, irrespective of their initial configuration. The convergence of the growth rates to their respective limiting behaviors happened more quickly at 1500 and 2000 K than it did at 2500 K.

At 1500 K, the growth rates for all substrates decreased with time. This decrease was caused by formation of unreactive regions through inclusion of five-member rings. No such decline in

reactivity was seen at higher temperatures. It is possible that these computational results reproduce one of the features of the experimentally observed phenomenon referred to as soot aging.

Local Electronic Structure and Stability of Pentacene Oxyradicals (with D. Yu. Zubarev, N. Robertson, D. Domin, J. McClean, J. Wang, W. A. Lester, Jr., R. Whitesides, and X. You)

During the past year, we turned our attention to soot oxidation. As the first step in this direction, we started, in collaboration with William Lester's group, examination of the thermodynamic stability of critical oxygenated intermediates. The initial analysis revealed a somewhat unexpectedly pronounced, yet systematic, trend in the relative stability of graphene-edge oxyradicals. A series of pentacene oxyradicals were selected for a detailed theoretical study. The results revealed that the relative stability of the oxyradical species can be rationalized on the basis of the concept of local aromaticity. Qualitative and quantitative measures of delocalized bonding showed that formation of the π -aromatic fragments associated with different prototypical π -aromatic systems explains the relative energies and thermodynamic stabilities of one-dimensional graphene-edge oxyradicals.

Molecular Dynamics Simulations of PAH Dimerization: Dimerization of Aliphatically-linked and Oxygenated PAH (with N. Robertson, R. Whitesides, and D. Wong)

In pursuit of mechanistic understanding of soot nucleation, collisions between aromatic molecules were investigated using molecular dynamics (MD) simulations with on-the-fly quantum forces. Simulations were conducted at a temperature of 1600 K, with vibrationally and rotationally equilibrated colliders, investigating the formation of dimers for a series of aromatic hydrocarbons. Our previous studies explored the phenomena of PAH dimerization by performing the MD simulations for a wide range of peri-condensed PAHs (PCAH), from pyrene up to coronene, as well as for aromatic molecules linked by aliphatic chains (AALH). The results demonstrated the feasibility of dimerization of these aromatic hydrocarbons at flame conditions. The dynamics of the dimerization process consist of the absorption and trapping of the energy from the intermolecular modes into the rotational and vibrational modes of the molecules. The dominant trend observed in the MD simulations was an increase in the dimer lifetime with an increase in molecular mass (Publication 13).

During the past year, we performed additional MD simulations examining collisions between PCAH and AALH. The results appeared to be close to those obtained in collisions among PCAHs and those among AALH and to follow the same trend with the molecular mass as PCAH and AALH. Likewise, new results obtained with a series of oxygen-containing PAH essentially fell together with those of PCAHs (the results are reported in Publication 16).

Future Plans

Graphene Layer Growth and Oxidation Chemistry: We will continue exploration of reactions on graphene edges. This work will be performed in collaboration with William Lester's group, performing DFT analysis of the reaction systems and then QMC analysis on most critical reaction steps identified in the prior DFT studies. For every reaction system, a complete set of rate coefficients will be established in master-equation solutions.

Graphene Layer Evolution: We will continue exploration of the evolution of graphene sheets through our newly-developed detailed KMC approach, by inclusion of additional reaction steps as they become available and by extending the simulation conditions and constraints.

Developing Models for Representing Combustion Chemistry at Varying Levels of Complexity to Use with Models for Laminar and Turbulent Flow Fields to Describe Combustion Processes: The collaboration with the Sandia group of Habib Najm has continued on the combination of the CSP-slow-manifold projection method and PRISM to construct an adaptive reduced-order model for stiff dynamical systems.

DOE-BES Supported Publications (2007-2009)

1. "A CSP and Tabulation Based Adaptive Chemistry Model," J. C. Lee, H. N. Najm, S. Lefantzi, J. Ray, M. Frenklach, M. Valorani, and D. A. Goussis, *Combust. Theory Model.* **11**, 73 (2007).
2. "Transforming Data into Knowledge Process Informatics for Combustion Chemistry," M. Frenklach, *Proc. Combust. Inst.* **31**, 125 (2007).
3. "Graphene layer growth: Collision of migrating five-member rings," R. Whitesides, A. C. Kollias, D. Domin, W.A. Letser, Jr., and M. Frenklach, *Proc. Combust. Inst.* **31**, 539 (2007).
4. "Numerical Simulations of Soot Aggregation in Premixed Laminar Flames," N. Morgan, M. Kraft, D. Wong, M. Frenklach, P. Mitchell, *Proc. Combust. Inst.* **31**, 693 (2007).
5. "Efficient Slow Manifold Identification for Tabulation Based Adaptive Chemistry," *Proceedings of the 5th U.S. National Combustion Meeting*, San Diego, CA, March 25-28, 2007, Paper No. C31.
6. "Graphene Layer Growth Chemistry: Five-Six-Ring Flip Reaction," R. Whitesides, D. Domin, W. A. Lester, Jr., and M. Frenklach, *Proceedings of the 5th U.S. National Combustion Meeting*, San Diego, CA, March 25-28, 2007, Paper No. D31.
7. "Molecular Dynamics Simulations of PAH Dimerization," D. Wong, C. A. Schuetz, and M. Frenklach, *Proceedings of the 5th U.S. National Combustion Meeting*, San Diego, CA, March 25-28, 2007, Paper No. F21.
8. "Optimization of Reaction Models with Solution Mapping," M. Frenklach, A. Packard, and R. Feeley, in *Modeling of Chemical Reactions* (R. W. Carr, Ed.), Elsevier: Amsterdam 2007, (Elsevier series Comprehensive Chemical Kinetics, Vol. 42), pp. 243-291.
9. "Efficient Slow Manifold Identification for Tabulation Based Adaptive Chemistry," J. M. Ortega, H. N. Najm, M. Valorani, D. A. Goussis, and M. Y. Frenklach, 21st International Colloquium on the Dynamics of Explosions and Reactive Systems, Poitiers, France, July 22-27, 2007, Paper 231.
10. "Isomer Energy Differences for the C₄H₃ and C₄H₅ Isomers Using Diffusion Monte Carlo," D. Domin, W. A. Lester Jr., R. Whitesides, and M. Frenklach, *J. Phys. Chem.* **112**, 2065 (2008).
11. "Graphene Layer Growth Chemistry: Five- and Six-Member Ring Flip Reaction," R. Whitesides, D. Domin, R. Salomón-Ferrer, W. A. Lester Jr., and M. Frenklach, *J. Phys. Chem.* **112**, 2125 (2008).
12. "Embedded-Ring Migration on Graphene Zigzag Edge," R. Whitesides, D. Domin, W. A. Lester Jr., and M. Frenklach, *Proc. Combust. Inst.* **32**, 577 (2009).
13. "Molecular Dynamics Simulations of PAH Dimerization," D. Wong, R. Whitesides, C. A. Schuetz and M. Frenklach, in *Proceedings of the International Workshop on Combustion Generated Fine Carbon Particles* (H. Bockhorn, A. D'Anna, A. F. Sarofim, H. Wang, Eds.), Karlsruhe University Press, Karlsruhe, Germany, 2009, p. 245.
14. "Modeling Particle Dynamics with MOMIC," M. Frenklach, in *Modeling and Computation of Nanoparticles in Fluid Flows*, Lecture Series of van Karman Institute for Fluid Mechanics, in press.
15. "Modeling Particle Aggregation," M. Frenklach, in *Modeling and Computation of Nanoparticles in Fluid Flows*, Lecture Series of van Karman Institute for Fluid Mechanics, in press.
16. "Modeling Nanoparticle Formation," M. Frenklach and R. Whitesides, in *Modeling and Computation of Nanoparticles in Fluid Flows*, Lecture Series of van Karman Institute for Fluid Mechanics, in press.
17. "A New Graphene Edge Surface Kinetics Model," R. Whitesides and M. Frenklach, *Proceedings of the 6th U.S. National Combustion Meeting*, Ann Arbor, MI, May 17-19, 2009.

Computer-Aided Construction of Chemical Kinetic Models

William H. Green, MIT Department of Chemical Engineering,
77 Massachusetts Ave., Cambridge, MA 02139. email: whgreen@mit.edu

Project Scope

The combustion chemistry of even simple fuels can be extremely complex, involving hundreds or thousands of kinetically significant species. The most reasonable way to deal with this complexity is to use a computer not only to numerically solve the kinetic model, but also to construct the kinetic model in the first place. Our research spans a wide range from quantum chemical calculations on individual molecules and elementary-step reactions, through the development of improved rate/thermo estimation procedures, the creation of algorithms and software for constructing and solving the simulations, the invention of methods for model-reduction while maintaining error control, through comparisons with experiment. We are developing methods needed to make computer-construction of accurate combustion models practical, as well as tools to make it feasible to handle and solve the resulting large kinetic models, even in multidimensional reacting flows. Many of the parameters in the models are derived from quantum chemistry, and the models are compared with experimental data measured in our lab or in collaboration with other researchers.

Recent Progress

The main focus of our research continues to be the development of methodology for constructing, reducing, and solving combustion simulations (including computing the rate coefficients and thermochemistry) [1-6,8-13], supplemented by experimental measurements [2,3,7,8,11,12,14]. With funding from NSF, we are integrating our extensible open-source reaction-mechanism-generation software RMG (<http://rmg.sourceforge.net>) with the PrIMe database (<http://primekinetics.org>). We recently released RMG v.3.0, which builds kinetic models valid over the user-specified range of pressure and temperature, and which automatically identifies and computes the rates of chemically-activated reactions; this software has already been downloaded by dozens of users. We continue to make progress in automated mechanism reduction, to facilitate the use of detailed chemistry in reacting flow simulations[1,9,13], with a special focus on controlling the error associated with approximating the chemistry with a reduced model.[1,9] We directly measured the rate coefficients of several reactions of the vinyl radical using laser flash photolysis.[4,11,12,14]

Future Plans

Curiously, our measured rate coefficients for addition of vinyl radical to different alkenes do not follow the trend expected from Evans-Polanyi relations or the Hammond postulate. Similar findings were previously reported based on quantum chemistry for other addition reactions by Radom and by Marin. However, most existing large combustion chemistry models use Evans-Polanyi or similar relations to estimate the rates of addition reactions and their reverse beta-scission reactions. We have performed high-level quantum calculations to understand this in detail, and have recently submitted our explanation of this phenomena and a practical rate-estimation procedure for this case to *J.*

Phys. Chem.. Reactions through the adduct compete with direct H-abstraction reactions yielding resonantly-stabilized radicals; to quantitatively understand this competition we plan to measure the branching ratio to allyl radical resulting from vinyl + propene.

We have computed the rates of many intramolecular reactions of ROO and HOOQOO species. From these calculations we are currently developing more accurate rate-estimation rules, which will allow us to build more accurate models for ignition and cool flame chemistry. We are also collaborating with other research groups building large kinetic models to develop a unified compendium of rate-estimation rules, and to identify discrepancies.

We are incorporating a solution technique for the master equation based on an approximation suggested by NJB Green into the next RMG update, this should allow more accurate computations of $k(T,P)$ at reasonable computational cost. The latest version of RMG is using the Modified-Strong-Collision approximation, which is very efficient, but which introduces errors up to about a factor of 3 in $k(T,P)$ in unfavorable cases.

Using the software we developed for fast multi-cycle HCCI engine simulations [6], we have identified the mechanisms by which fuel composition affects the range of operability of HCCI engines. We previously published papers explaining the fuel-dependence of the low-load-limit, and will soon submit manuscripts explaining fuel-dependent phenomena observed in HCCI engines near the high-load limit.

We have modeled McEnally & Pfefferle's measurements on aromatic formation in methane diffusion flames doped by various isomers of butanol and hexadiene. The chemistry is fairly complicated, for example the hexadienes form cyclic C₅ species, and to compute several of the important reactions of these species, high-level quantum chemistry and variational transition state theory is required. We have submitted a manuscript on the reaction $C_5H_5 + CH_3$, which ultimately leads to benzene, and have also computed rates for C_5H_5 and C_5H_6 plus several C₃ species (leading to styrene) which we presented at the US Combustion meeting in mid-May. We expect to submit manuscripts on the full flame simulations soon.

Acknowledgements

Several of our recent flash photolysis experiments have been done in collaboration with Craig Taatjes, and we are also grateful to him for lending us a laser needed for our radical recombination experiments. The kinetic experiments at MIT were made possible by Bob Field lending us lasers and other equipment. The probe laser system was paid for in part by an NSF equipment grant to the Harrison Spectroscopy Laboratory. The HCCI engine research at MIT was supported in large part through funding by Ford and BP, and was done in collaboration with Wai Cheng. Our work on the formation of titania clusters and nanotubes in combustion systems was done in collaboration with Markus Kraft. Our work on numerical methods and model reduction has benefited significantly from ongoing interactions with Paul Barton.

Publications Resulting from DOE Sponsorship (Since 2007)

1. O.O. Oluwole, P.I. Barton, & W.H. Green, "Obtaining Accurate Solutions using Reduced Chemical Kinetic Models: A new Model Reduction method for models rigorously validated over ranges", *Combust. Theory Model.* **11**(1), 127-146 (2007).
2. William H. Green, "Predictive Kinetics: A New Approach for the 21st Century", *Advances in Chemical Engineering* **32**, 1-50 (2007).
3. S.V. Petway, H. Ismail, W.H. Green, E.G. Estupiñán, L.E. Jusinski, and C.A. Taatjes, "Measurements and Automated Mechanism Generation Modeling of OH Production in Photolytically-Initiated Oxidation of the Neopentyl Radical", *Journal of Physical Chemistry A* **111**, 3891-3900 (2007).
4. Huzeifa Ismail, C. Franklin Goldsmith, Paul R. Abel, Pui-Teng Howe, Askar Fahr, Joshua B. Halpern, Leonard E. Jusinski, Yuri Georgievskii, Craig A. Taatjes and William H. Green, "Pressure and Temperature Dependence of Reaction of Vinyl Radical (C₂H₃) with Ethylene", *J. Phys. Chem. A* **111**, 6843-6851 (2007).
5. William H. Green, "Building and Solving Accurate Combustion Chemistry Simulations", *Journal of the Combustion Society of Japan* **50**, 19-28 (2008).
6. John P. Angelos, Marcel Puignou, Morgan M. Andreae, Wai K. Cheng, William H. Green & Michael A. Singer, "Detailed Chemical Kinetic Simulations of HCCI Engine Transients", *International Journal of Engine Research*, **9**, 149-164 (2008).
7. John Z. Wen, Henning Richter, William H. Green, Jack B. Howard, Meri Treska, Paula M. Jardim and John B. Vander Sande, "Experimental study of catalyst nanoparticle and single walled carbon nanotube formation in a controlled premixed combustion", *J. Materials Chem.*, **18**, 1561-1569 (2008)
8. Jason Ploeger, William H. Green, and Jefferson W. Tester, "Co-oxidation of ammonia and ethanol in supercritical water, part 2: Modeling demonstrates the importance of H₂NNO_x", *Int. J. Chem. Kinet.* **40**, 653-662 (2008).
9. Alexander Mitsos, Geoffrey M. Oxberry, Paul I. Barton, and William H. Green, "Optimal Automatic Reaction and Species Elimination in Kinetic Mechanisms", *Combustion & Flame* **155**, 118-132 (2008).
10. Robert W. Ashcraft and William H. Green, "Thermochemical Properties and Group Values for Nitrogen-Containing Molecules", *J. Phys. Chem. A.* **112**, 9144 (2008).
11. Sandeep Sharma, C. Franklin Goldsmith, Teppei Ogura, Michael R. Harper, Gregory R. Magoon, Huzeifa Ismail, John P. Angelos, and William H. Green, "Pulling it all Together: Fuel chemistry modeling across the scales from individual molecules to engine simulations", *Prepr. ACS Div. of Fuel Chemistry* (2008). [received ACS Glenn Award for best paper presented in Fuel Chemistry].
12. C. Franklin Goldsmith, Huzeifa Ismail, Paul R. Abel, and William H. Green, "Pressure and Temperature Dependence of the Reaction of Vinyl Radical with Alkenes II: Measured Rates and Predicted Product Distributions for Vinyl + Propene", *Proceedings of the Combustion Institute* **32**, 139-148 (2009).
13. M.A. Singer and W.H. Green, "Using adaptive proper orthogonal decomposition to solve the reaction-diffusion equation", *Appl. Num. Math.* **59**, 272 (2009).
14. H. Ismail, P.R. Abel, W.H. Green, A. Fahr, L. Jusinski, A. Knepp, J. Zador, G. Meloni, T. Selby, D. Osborn, and C.A. Taatjes, "Temperature-Dependent Kinetics of the Vinyl Radical (C₂H₃) Self-Reaction", *J. Phys. Chem. A* (2009, accepted).

Quantum Dynamics of Elementary Combustion Reactions

Hua Guo

Department of Chemistry and Chemical Biology, University of New Mexico

ABSTRACT

Many combustion reactions are of complex-forming nature, in which the reaction path is dominated by a deep potential well. One such example is the $\text{H} + \text{O}_2 \rightarrow \text{HO} + \text{O}$ reaction, which forms the bottleneck in combustion of hydrogen and hydrocarbon fuels.¹ We have recently focused on the elucidation of the reaction dynamics of this important combustion reaction using quantum mechanical approaches. The codes developed in our group are based on the highly accurate and efficient Chebyshev propagator,² and are capable of calculating both initial state-resolved and state-to-state scattering attributes including differential cross sections.³

Quantum mechanical characterization of such seemingly simple reactions is very challenging. A large basis is often needed because of the deep well and the long-range interactions in the product channel. In the wave packet approach, long propagation is also expected because of the long-lived intermediate complex. The difficulties are compounded by the floppy nature of the reaction intermediate, which renders many commonly used dynamical approximations (e.g., the centrifugal sudden approximation) inadequate. In addition, the barrierless reaction pathway requires a large number of partial waves.

Very recently, we have (in collaboration with D. Xie at Nanjing, D. H. Zhang at DICP, and G. Lendvay at Hungarian Academy of Sciences) reported state-to-state differential cross sections and product state distributions (Fig. 1) for the $\text{H} + \text{O}_2 \rightarrow \text{HO} + \text{O}$ reaction,⁴ using an improved global potential energy surface based on high level *ab initio* calculations.⁵ An interesting finding of this study is that the reaction deviates significantly from the statistical limit, and the deviation increases with the collision energy. These observations are consistent with experimental findings,^{6,7} and in support of the earlier quasi-classical trajectory (QCT) work of Miller, who found significant non-statistical behaviors on several less-accurate potential energy surfaces.^{8,9} It is now

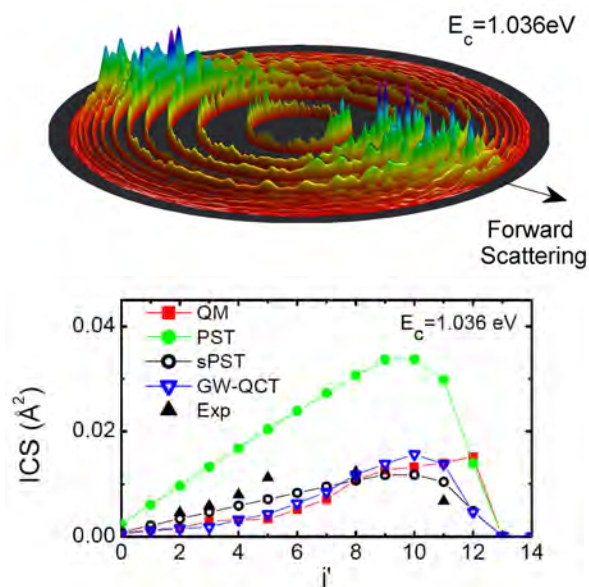


Fig. 1 Upper panel: polar plot of the differential cross section for the $\text{H} + \text{O}_2(\nu=0, j=1)$ reaction at 1.036 eV of collision energy. Lower panel: Comparison of the QM rotational state distribution of OH (\blacksquare) with the PST results (\bullet), GW-QCT results (\blacktriangledown), and available experimental data (\blacktriangle). The PST result normalized to the QM distribution

well established, based on both our quantum and earlier QCT studies on several potential energy surfaces, that this important combustion reaction has an intrinsic non-statistical character.

Another unresolved problem associated with the $\text{H} + \text{O}_2$ reaction is the discrepancy between the measured and calculated rate constants.¹⁰ In a recent work (in collaboration with G. Lendvay), we have examined the effect of reactant rotational excitation on the rate constant.¹¹ Evidence is presented to show that the O_2 rotational excitation can significantly enhance the reactivity. Detailed analysis has also been presented for the origin of the enhancement.

We have also been interested in the reverse reaction $\text{OH} + \text{O} \rightarrow \text{H} + \text{O}_2$. In collaboration with P. Honvault at Franche-Comte, we have reported QCT calculations of the rate constant for this reaction,¹² which is in good agreement with the earlier quantum results except at very low temperatures. In another collaborative project with E. Herbst at Ohio State, we have shown that the attenuated reactivity at very low temperatures could be responsible for the low oxygen abundance in interstellar media.¹³

We have recently expanded our quantum scattering codes to non-adiabatic systems. To this end, we investigated the quantum dynamics of the $\text{O}(^1D) + \text{H}_2 \rightarrow \text{OH}(X) + \text{H}$ reaction, which is also dominated by a complex-forming pathway. In this system, there are three electronic states that are involved in the reaction. The ground $1^1A'$ state has a deep well (H_2O) and is non-adiabatically coupled in the reactant channel with the excited $2^1A'$ state. In addition, there is an excited $1^1A''$ state that adiabatically correlates the reactants with the products. We have recently finished an elaborate quantum mechanical study of the reaction at the state-to-state level on a single¹⁴ and multiple potential energy surfaces.¹⁵ Because of a small barrier in the excited state potential energy surface, the reaction is dominated at low energies by the ground state adiabatic pathway. As expected, the differential cross section is largely symmetrical in the forward and backward directions.¹⁴ However, the participation of the $1^1A''$ state at higher energies results in a backward bias, as shown in Fig. 2, due apparently to the

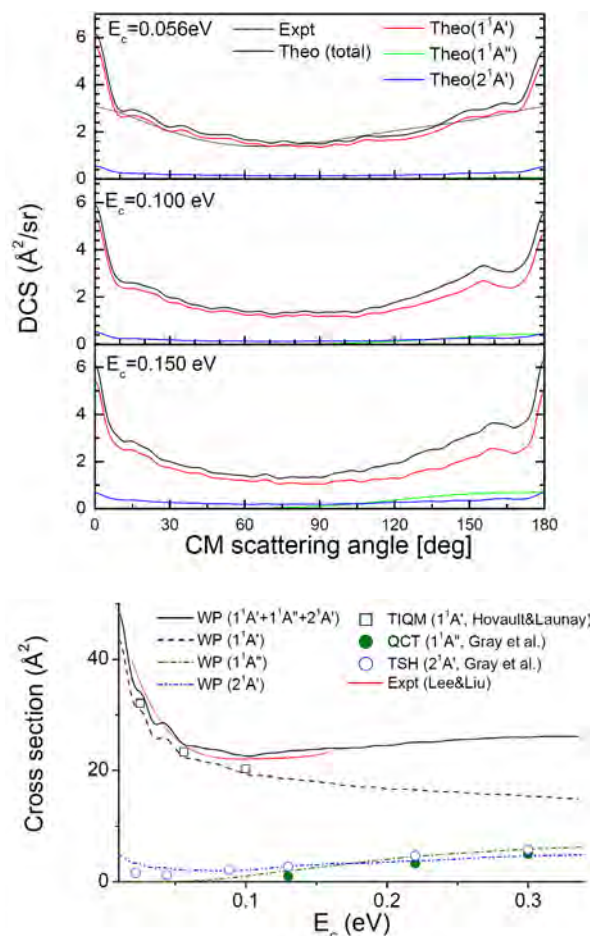


Fig. 2 Comparison of the differential (upper panel) and integral cross sections (lower panel) for the $\text{O}(^1D) + \text{H}_2$ reaction obtained from our quantum wave packet (WP) calculations with previous theoretical and experimental results.

abstraction pathway on its potential energy surface. In addition, the total integral cross section (Fig. 2) has an unusual shape, decreasing first and then increasing. Our results are in good agreement with experimental data,^{16,17} which represent a significant improvement over the earlier surface hopping trajectory results.¹⁸ Significant differences between the quantum and QCT results have also been found for adiabatic dynamics, due apparently to tunneling effects. It is shown that the rate constant obtained by considering quantum dynamics in all three lowest-lying states is in near perfect agreement with experiment.

In addition to the aforementioned reaction dynamics studies, we have also carried out a full-dimensional quantum study of the ammonia photodissociation dynamics.¹⁹ This system is considered to be a prototype for understanding mode specificity in chemical reactions. Several theoretical studies of molecular spectroscopy have also been reported by our group.²⁰⁻²²

In the near future, we would like to expand the capacity of our state-to-state quantum scattering codes to other non-adiabatic systems. One such system is the $N(^2D) + H_2$ reaction, which is affected by the Renner-Teller coupling in linearity. We have already constructed a highly accurate potential energy surface for the ground state of NH_2 ,²³ and are working to develop the excited state potential energy surface with the same accuracy. The other system is the NH_3 photodissociation, which undergoes non-adiabatic transitions near a conical intersection. Our recent work has computed the absorption spectrum¹⁹ and we are now working on the product state distributions. These studies will shed light on the dramatic mode selectivity observed by the Crim group.²⁴

References (* indicates DOE funded work in the past year):

- 1 J. A. Miller, R. J. Kee, and C. K. Westbrook, *Annu. Rev. Phys. Chem.* **41**, 345 (1990).
- 2 H. Guo, *Rev. Comput. Chem.* **25**, 285 (2007).
- 3 S. Y. Lin and H. Guo, *Phys. Rev. A* **74**, 022703 (2006).
- *4 Z. Sun, D. H. Zhang, C. Xu, S. Zhou, D. Xie, G. Lendvay, S.-Y. Lee, S. Y. Lin, and H. Guo, *J. Am. Chem. Soc.* **130**, 14962 (2008).
- 5 C. Xu, D. Xie, D. H. Zhang, S. Y. Lin, and H. Guo, *J. Chem. Phys.* **122**, 244305 (2005).
- 6 K. Kleinermanns, E. Linnebach, and M. Pohl, *J. Chem. Phys.* **91**, 2181 (1989).
- 7 R. Fei, X. S. Zheng, and G. E. Hall, *J. Phys. Chem. A* **101**, 2541 (1997).
- 8 J. A. Miller, *J. Chem. Phys.* **84**, 6170 (1986).
- 9 J. A. Miller and B. C. Garrett, *Inter. J. Chem. Kinet.* **29**, 275 (1997).
- *10 S. Y. Lin, Z. Sun, H. Guo, D. H. Zhang, P. Honvault, D. Xie, and S.-Y. Lee, *J. Phys. Chem. A* **112**, 602 (2008).
- *11 S. Y. Lin, H. Guo, G. Lendvay, and D. Xie, *Phys. Chem. Chem. Phys.* in press.
- *12 M. Jorfi, P. Honvault, P. Halvick, S. Y. Lin, and H. Guo, *Chem. Phys. Lett.* **462**, 53 (2008).
- *13 D. Quan, E. Herbst, T. Millar, S. Y. Lin, H. Guo, P. Honvault, and D. Xie, *Astrophys. J.* (2008).
- *14 S. Y. Lin and H. Guo, *J. Chem. Phys.* **129**, 124311 (2008).

- *15 S. Y. Lin and H. Guo, *J. Phys. Chem. A*, in press.
- 16 Y. T. Hsu, J. H. Wang, and K. Liu, *J. Chem. Phys.* **107**, 2351 (1997).
- 17 S.-H. Lee and K. Liu, *J. Chem. Phys.* **111**, 4351 (1999).
- 18 S. K. Gray, G. G. Balint-Kurti, G. C. Schatz, J. J. Lin, X. Liu, S. Harich, and X. Yang, *J. Chem. Phys.* **113**, 7330 (2000).
- *19 W. Lai, S. Y. Lin, D. Xie, and H. Guo, *J. Chem. Phys.* **129**, 154311 (2008).
- *20 S. Lin, D. Xie, and H. Guo, *J. Chem. Phys.* **129**, 154313 (2008).
- *21 Z. Li, L. Wang, H. Ran, D. Xie, N. Blinov, P.-N. Roy, and H. Guo, *J. Chem. Phys.* **128**, 224513 (2008).
- *22 L. Pei, J. Zhang, W. Kong, D. Xu, and H. Guo, *Chem. Phys. Lett.* **462**, 173 (2008).
- *23 S. Zhou, D. Xie, S. Y. Lin, and H. Guo, *J. Chem. Phys.* **128**, 224316 (2008).
- 24 M. L. Hause, Y. H. Yoon, and F. F. Crim, *J. Chem. Phys.* **125**, 174309 (2006).

Gas-Phase Molecular Dynamics: High Resolution Spectroscopy and Collision Dynamics of Transient Species

Gregory E. Hall and Trevor J. Sears
Department of Chemistry, Brookhaven National Laboratory
Upton, NY 11973-5000
gehall@bnl.gov; sears@bnl.gov

Program Scope

This research is carried out as part of the Gas-Phase Molecular Dynamics program in the Chemistry Department at Brookhaven National Laboratory. High-resolution spectroscopy, augmented by theoretical and computational methods, is used to investigate the structure and collision dynamics of chemical intermediates in the elementary gas-phase reactions involved in combustion chemistry. Applications and methods development are equally important experimental components of this work.

I. Recent Progress

A. Sub-Doppler spectroscopy of radicals

We have completed a series of experiments to measure spectral lines of the CN radical at sub-Doppler resolution. These measurements provide insights into the radical's hyperfine structure and provide preliminary experience for us on the path to future ultra-precise measurements using frequency-comb-stabilized lasers. Several alternate experimental configurations have been explored, leading to a sensitive and very high-resolution measurement using a strong, amplitude-modulated bleach beam and a weak, counterpropagating, frequency-modulated probe beam derived from a single Ti:sapphire ring laser. Fully resolved hyperfine lines are observed with MHz precision in the red A-X band of CN, as illustrated in the figure to the right. Accurate hyperfine splittings have been observed in a sufficient set of rotational lines to determine all the hyperfine parameters of the A state and the nuclear quadrupole parameters at the ^{14}N nucleus. Many ground state hyperfine measurements have been previously performed by microwave spectroscopy, but it is rare to be able to characterize an excited state this fully. Sufficient sensitivity has even been attained to record the hyperfine splittings due to the ^{13}C nuclear spin interaction with the unpaired electron, using natural abundance $^{13}\text{C}^{14}\text{N}$ photoproducts from the 193 nm photodissociation of unlabeled C_2N_2 in a room-temperature bulb experiment.

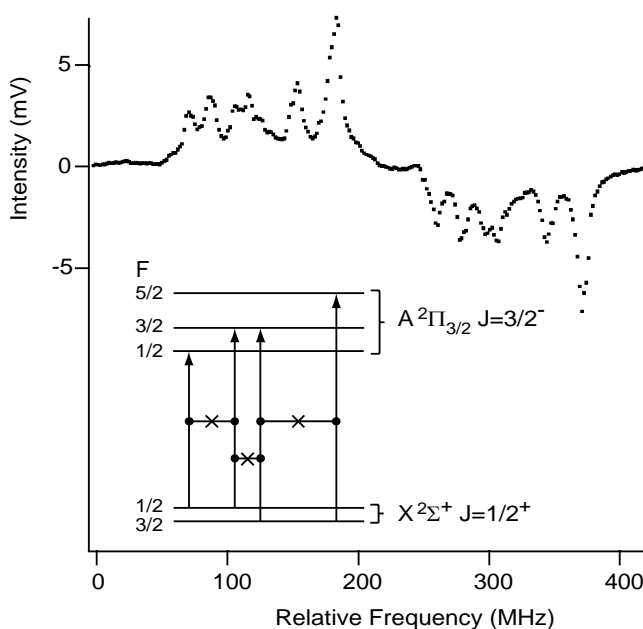


Figure 1. Sub-Doppler spectrum of CN showing hyperfine resolution of a single rotational line $R_1(1/2)$ in the A-X (1-0) band near 919 nm. Vertical arrows in the energy level diagram inset are aligned with the corresponding transition frequencies; crossover resonances are observed at the frequencies marked by X symbols, midway between transitions sharing a common level.

B. Stark and Zeeman effects in radical transients

Molecular dipole moments and g-factors give direct information on electronic wavefunctions that is difficult to obtain otherwise. Experimental measurements of these quantities have traditionally been restricted to ground electronic states because spectroscopic experiments of resolution sufficient to measure Stark and Zeeman level shifts are mostly limited to the microwave region. We have observed that the Doppler-free, hyperfine-resolved transitions in CN A-X show measurable changes with transverse electric fields as low as a few hundred V/cm. The Stark effect most easily observed at relatively low field is the mixing of nearly degenerate parity levels, which causes an increasing intensity for transitions forbidden by parity selection rules in zero field, even before substantial broadening or shifting is observed. We expect to be able to extract an excited state dipole moment from the field-dependent spectra. We have also observed changes in the sub-Doppler spectra as a function of longitudinal magnetic fields up to 50 Gauss, although the precision of our present Zeeman measurements is insufficient to provide any new information about the CN A state.

C. Double resonance studies of collision dynamics in CH₂

Rotational energy transfer within the \tilde{a} state of CH₂ is studied by saturation recovery and saturation transfer double resonance kinetic spectroscopy. The return to a thermal rotational distribution following pulsed laser depletion of selected rotational states is monitored by transient FM spectroscopy. The hole in a Boltzmann rotational distribution induced by pulsed excitation broadens and spreads to other rotational states with a time-dependence that depends on details of the state-to-state matrix of energy transfer rates. Levels strongly coupled to the depleted level show larger and faster growth of depletion than weakly and indirectly coupled levels, although all will eventually be depleted by the same fraction once the hole is thermalized. Polarization effects provide still further information on the energy transfer process: a polarized saturation laser creates an aligned hole, which depolarizes at a rate distinguishable from the population recovery. More challenging experimentally, but containing richer information about reorientation during state-to-state rotationally inelastic collisions, is the transfer of alignment in the saturation transfer experiments. These extended studies of rotational energy transfer and depolarization have been undertaken because of the deep connection between rotational energy transfer and collision-induced intersystem crossing mechanisms in systems like CH₂, where a few special singlet-triplet mixed states are suspected of mediating the intersystem crossing. The cross sections for elastic depolarization (*M*-changing, *JK*-conserving collisions)

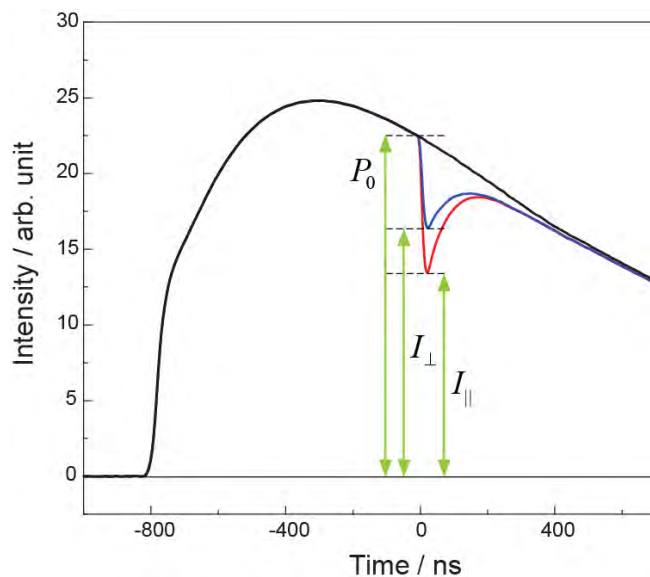


Figure 2. Polarized saturation recovery measurements on singlet methylene. Black solid waveform illustrates formation, thermalization and decay of 4_{14} rotational state in a bulb sample of 5% ketene in Ar. Depletion and recovery signals are shown for parallel and perpendicular polarizations of a pulsed bleach laser at $t=0$, tuned to the same rotational transition of a different band. Transient population and alignment are independently and directly extracted from the measured waveforms.

are found to have magnitudes generally comparable to those for rotationally inelastic collisions with Ar or He. Unusual details of the observations are an even-odd J alternation in the total rotationally inelastic cross sections for $K_a=1$ states of *ortho* nuclear spin symmetry, and a tendency for those levels with the most rapid relaxation to also show the slowest depolarization. The transfer of depletion to other rotational states is readily observed, although the concomitant alignment transfer is inefficient. Only in the case of mixed-state saturation and probing the partner mixed state have we observed large collisional transfer of alignment, an observation consistent with a long-range dephasing mechanism of interconverting the mixed eigenstates. The measured rotationally inelastic and depolarizing collisions of singlet CH₂ with He will be compared to quantum scattering calculations on a van der Waals potential computed by our co-worker, Hua-Gen Yu.

D. New spectroscopy of singlet CH₂

New Doppler-limited FM absorption spectra of the CH₂ \tilde{a} state have been recorded in the 760-795 nm region by summer visitors in our laboratory. With partial support from a NSF Faculty and Student Team award and with participation of a DOE supported SULI student, seven new sub-bands terminating in vibronic levels of the \tilde{a} and \tilde{b} states have been characterized. Thousands of new transition frequencies have been measured in this spectral region, and hundreds assigned. Optical-optical double resonance (OODR) techniques similar to those described below were used to confirm some initial spectroscopic assignments of these mostly irregular transitions, then many more were made by an automated combination difference program, all guided by the high level calculations of Jensen and co-workers.

Transitions in the $\tilde{b} - \tilde{a}$ origin band of CH₂ near 1200 nm have been detected for the first time, using OODR spectroscopy. In collaboration with Professor Bor-Chen Chang from National Central University, Taiwan, these origin band transitions have been observed and unambiguously assigned using pulsed infrared light from a scanning OPO laser system to induce transient depletion signals similar to those illustrated in Figure 2 above.

Other OODR techniques combining light from high resolution cw sources (diode and Ti:sapphire lasers) with near ultraviolet ns pulsed lasers were used to map out predissociating rotational levels lying within several hundred cm⁻¹ of the best estimate for the singlet dissociation energy of methylene. The OODR technique permits quantum number labels to be attached to the dissociating levels, which have lifetimes of 1-3 ps as judged from the observed spectroscopic linewidths. The data open up routes for future dynamics measurements of CH₂ dissociation. The newly identified predissociating levels offer a route to a measurement of the bond dissociation energy of singlet CH₂. In collaborative experiments with Prof. Arthur Suits (Wayne State University) we will attempt to measure the velocity of the hydrogen atom product using resonant ionization followed by velocity map imaging. If successful, this should provide a good measurement of the maximum energy in the atomic product and hence the dissociation energy when combined with the precisely known energy in the dissociating level.

Other Future Work

A. Sub-Doppler spectroscopy of radicals

A time-domain version of sub-Doppler saturation spectroscopy allows us to observe the transient absorption response following rapid change in the saturation intensity. A combination of 20 ns switching times and MHz spectral resolution provides data into the Fourier boundary of spectral resolution and time response. The recovery of sub-Doppler bleached absorption signals after the saturating light is abruptly extinguished follows pressure-dependent rates, dominated by velocity-changing collisions, a time-domain

characterization of pressure-broadening mechanisms. Preliminary indications suggest that the alignment of the sub-Doppler saturation holes remains constant as the saturation recovery proceeds, a confirmation that elastic depolarization is not significant without a change in laboratory velocity (Doppler shift). The growth kinetics of the saturation signals following a rapid switching on of the saturating light show both intensity and pressure dependence in a regime where the resonant Rabi frequency is comparable to the switching rate of the strong field. Measurements such as these probe the details of the collision processes that mediate pressure broadening, and can be contrasted with the Doppler-broadened double resonance kinetic data measured with ns laser bleaching and cw laser probing of rotational energy and alignment transfer with the same collision partners. In addition to fundamental studies in collision dynamics, the results have direct application to the interpretation of astronomical spectra of CN and for modeling collisional broadening in terrestrial samples.

Work is continuing on implementing frequency comb measurements of the laser frequencies so that sub-Doppler line positions in our spectra can be measured precisely. Currently, our measurement precision is limited by a combination of laser source instability over the time required to acquire data and the limitations of our high resolution wavemeters. Locking the laser to a component of a stabilized frequency comb will eliminate both these issues and spectroscopic line positions in the visible and near-IR region will be able to be measured to 3×10^{-10} fractional accuracy. This will have an immediate effect on the quality of our sub-Doppler measurements. In the longer term, we plan to make high resolution measurements of the A-X origin band of PbF, in collaboration with Prof Neil Shafer-Ray (University of Oklahoma). This DOE EPSCoR funded project is directed toward investigating parity violation effects in small molecules containing a heavy atom.

B. Low energy photoelectron spectroscopy of aromatic species

In collaboration with Prof. Philip Johnson (Stony Brook University) we have recently completed building a new photoelectron spectrometer based on an imaging detector. This permits very sensitive detection of low energy photoelectrons, unlike conventional time-of-flight or dispersive instruments where the low energy electrons are the most difficult to detect. It also gives an image of the spatial distribution of the photoelectron energies and therefore angular information on the ejected photoelectrons as well as their energies, thereby providing information on the symmetry of the molecular electronic states involved in the spectroscopic transitions. This is potentially very useful for identifying the symmetries and structure of excited electronic states of larger molecules, an area where modern electronic structure theory still has some problems. We have a large amount of new data on phenylacetylene and fluorene where initial excitation is via the neutral S_1 and (possibly) S_2 states, and the technique appears to be generally useful. Analysis of the data is presently in progress.

Publications supported by this project since 2007

Coherent and incoherent orientation and alignment of ICN photoproducts, M. L. Costen and G. E. Hall, *Phys. Chem. Chem. Phys.* **9**, 272-287 (2007).

State mixing and predissociation in the $\tilde{c} - \tilde{a}$ band system of singlet methylene studied by optical-optical double resonance, Z. Wang, Y. Kim, G. E. Hall and T. J. Sears, *J. Phys. Chem. A*, **112**, 9248-9254 (2008)

The fate of excited states in jet-cooled aromatic molecules: Bifurcating pathways and very long-lived species from the S_1 excitation of phenylacetylene and benzonitrile, J. Hofstein, H. Xu, T. J. Sears, and P. M. Johnson, *J. Phys. Chem. A*, **112**, 1195-1201 (2008).

Sub-Doppler laser absorption spectroscopy of the $A^2\Pi_i - X^2\Sigma^+$ (1,0) band of CN. Measurement of the ^{14}N hyperfine parameters in $A^2\Pi_i$ CN. M. L. Hause, G. E. Hall, and T. J. Sears, *J. Mol. Spectr.* **253** 122-128 (2008)

The Zeeman effect on lines in the (1,0) band of the $F^4\Delta - X^4$ transition of the FeH radical. J. J. Harrison, J. M. Brown, J. Chen. T. Steimle and T. J. Sears. *Astrophys. J.* **679**, 854-861 (2008).

Flame Chemistry and Diagnostics

Nils Hansen

Combustion Research Facility, Sandia National Laboratories, Livermore, CA 94551-0969

Email: nhansen@sandia.gov

SCOPE OF THE PROGRAM

The goal of this program is to provide a rigorous basis for the elucidation of chemical mechanisms of combustion, combining experimental measurements employing state of the art combustion diagnostics with detailed kinetic modeling. The experimental program concentrates on the development and application of combustion diagnostics for measurements of key chemical species concentrations. These measurements are carried out in low-pressure, one-dimensional laminar flames and are designed to serve as benchmarks for the validation of combustion chemistry models. Comparison of experimental data to models employing detailed chemical kinetics is critical to determining important chemical pathways in combustion and in pollutant formation in combustion systems. As turbulent combustion models become increasingly sophisticated, accurate chemical mechanisms will play a larger role in computations of realistic combustion systems. Verification of detailed chemistry models against a range of precise measurements under thoroughly characterized steady conditions is necessary before such flame models can be applied with confidence in turbulent combustion calculations.

PROGRESS REPORT

Molecular Beam Mass Spectrometry at the Advanced Light Source

In collaboration with T. A. Cool of Cornell University, K. Kohse-Höinghaus of Bielefeld University, and P. R. Westmoreland of the University of Massachusetts, great progress has been made measuring low-pressure flames using molecular-beam mass spectrometry (MBMS) with synchrotron photoionization at the Advanced Light Source (ALS) of the Lawrence Berkeley National Laboratory. In the past year, different flames fueled by larger hydrocarbons and oxygenated species have been characterized over a wide range of stoichiometries. The data is currently being processed for comparison to detailed kinetic flame models.

Combustion Chemistry in Flames fueled by Oxygenates and Hydrocarbon

Fuel-consumption and initial steps of aromatic ring formation were studied in fuel-rich flames of allene, propyne, 1,3-butadiene, cyclohexane, 1-hexene, and tetrahydrofuran. These experimental studies provide a broad database for flame modeling.

Stoichiometric Allene and Propyne Flames: In close collaboration with J. A. Miller (Sandia), combined experimental and modeling studies were performed to elucidate the isomer-specific combustion

chemistry in fuel-rich and stoichiometric allene(propyne)/O₂/Ar flames. Quantitative mole fraction profiles of various combustion intermediates were compared to highlight isomer-specific differences between the stoichiometric allene and propyne flames. The observed differences between allene and propyne flames can be largely explained by the ability to form allyl or to dissociate into acetylene and methyl through H-atom addition to allene or propyne, respectively, and by the greater thermodynamic stability of propyne. These small differences in the early fuel-consumption processes subsequently resulted in larger concentrations of for example propene and ethenol in the allene flame and of methyl, acetylene, ethane, and acetaldehyde in the propyne flame. The larger concentration of ketene in the allene flame resulted from a direct reaction between allene and OH. Also, more propyne was formed in the allene flame than allene was formed in the propyne flame.

Smaller peak mole fractions for C₃H₃ and C₃H₅ were observed in the propyne flame. Again, the smaller concentration of C₃H₃ in the propyne flame can be understood in light of the demethylation reaction which competes with the H-atom abstraction reaction and thus makes the latter less important. In the allene flame there is substantially more allyl present, mainly because H atoms can diffuse forward into the cooler regions of the flame and add to allene. Larger concentrations of propargyl and allyl radicals subsequently lead to larger concentrations of benzene and fulvene in the allene flame. The modeling results clearly showed that in the flames considered in this study, benzene was formed almost exclusively from the C₃H₃ + C₃H₃ reaction, either directly or indirectly through fulvene followed by H-assisted isomerization to benzene.

Fuel-rich 1,3-Butadiene Flame: Remaining uncertainties about the significance of different cyclization steps in 1,3-butadiene flames motivated another collaborative effort with J. A. Miller (Sandia). Some earlier experimental and theoretical studies of the combustion chemistry of 1,3-butadiene indicated that besides the propargyl + propargyl and the propargyl + allyl reactions other benzene formation pathways are likely to be significant: vinyl addition to 1,3-butadiene or vinylacetylene and C₄H₅ addition to acetylene.

In a combined experimental and theoretical effort we studied the formation of benzene and its precursors in premixed 1,3-butadiene flames. We compared Miller's detailed kinetic modeling results, which used the latest theoretical rate constants of the *i*- and *n*-C₄H₅ + C₂H₂ reactions, against flame-sampled molecular-beam mass spectrometry data obtained in a fuel-rich 1,3-butadiene/O₂/Ar flame ($\phi = 1.8$) flame. The results clearly indicated that the C₃H₃ recombination reaction alone is not sufficient to produce the observed benzene levels. Instead, contributions of the *i*-C₄H₅ + C₂H₂ reaction needed to be included. Indeed, the C₃H₃ + C₃H₃ and *i*-C₄H₅ + C₂H₂ reactions were found to be roughly of equal importance. Minor contributions of the order of 10 % result from the C₃H₃ + C₃H₅ reaction.

FUTURE DIRECTIONS

One key immediate task is the analysis of the large body of ALS data accumulated in the past years, which may compel further or confirmatory measurements during subsequent beam cycles. We will continue to explore isomer specific pathways of fuel-consumption and aromatic ring formation in flames fueled by C₅-C₇ species. In particular the emphasis will be on the determination of the absolute molar composition of flames fueled by isomeric C₆H₁₂ species. However, more work on a cyclopentene flame is also needed with respect to the development of a more detailed model and to the characterization of the growth mechanism of aromatic species beyond the first ring, that is the formation, for example, of indene and naphthalene. The following C₆H₁₂ isomers are thought to be of the highest interest as fuels because of the variety of chemical structures: 1-hexene, cyclohexane, methylcyclopentane, and 3,3-dimethyl-1-butene. These isomers represent the classes of long-chain alkenes, fully saturated and methyl-substituted cycloalkanes, and branches alkenes. The combustion chemistry of these species will be investigated in unprecedented detail using otherwise identical flame conditions and important fuel destruction and benzene formation pathways will be elucidated. In this context, the flame chemistry of the methyl-substituted derivative of cyclohexane, methylcyclohexane, will also be studied.

Studies of formation of aromatic species employing synchrotron generated VUV photoionization will be complemented by resonance-enhanced multiphoton ionization (REMPI) experiments in the laser laboratory. REMPI is an ionization technique, where the ionization energy is transferred to the molecule with two or more photons. It can be used for flame studies for the detection of aromatic species like benzene, substituted benzenes, and polycyclic aromatic hydrocarbons (PAH's). It is known that a single wavelength near 269 nm can be used to efficiently ionize polyaromatics up to about C₂₀-PAH's, while for larger species a wavelength of 208 nm will be profitable.

In recent years, tightened regulations for emissions from internal combustion engines have stimulated a pronounced interest in non-conventional oxygenated fuels. The initiated studies of oxygenated fuel chemistry will continue with experimental and modeling investigations of flames fueled by cyclic ethers which, as contents in biomass derived fuels, are of considerable interest. Well suited as model fuels to learn more about the characteristic combustion chemistry of cyclic ethers are tetrahydrofuran (THF) and tetrahydropyran (THP).

The kinetic modeling efforts require experimental flame temperature measurements. The temperatures of all flat flames investigated will be measured either by OH or NO laser induced fluorescence after excitation near 308 or 226 nm, respectively. To avoid probe disturbances in the molecular-beam mass spectrometer, a second flame-chamber will be used, which has been built solely for the purpose of in-situ laser-diagnostics.

PUBLICATIONS ACKNOWLEDGING BES SUPPORT 2007-PRESENT

1. T. A. Cool, J. Wang, N. Hansen, P. R. Westmoreland, F. L. Dryer, Z. Zhao, A. Kazakov, T. Kasper, K. Kohse-Höinghaus, "Photoionization Mass Spectrometry and Modeling Studies of the Chemistry of fuel-rich Dimethyl Ether Flames", *Proc. Combust. Inst.*, **31**, 285-293 (2007).
2. M. E. Law, P. R. Westmoreland, T. A. Cool, J. Wang, N. Hansen, C. A. Taatjes, T. Kasper, "Benzene Precursors and Formation Routes in a Stoichiometric Cyclohexane Flame", *Proc. Combust. Inst.*, **31**, 565-573 (2007).
3. K. Kohse-Höinghaus, P. Oßwald, U. Struckmeier, T. Kasper, N. Hansen, C. A. Taatjes, J. Wang, T. A. Cool, S. Gon, P. R. Westmoreland, "The Influence of Ethanol Addition on a premixed fuel-rich Propene-Oxygen-Argon Flame", *Proc. Combust. Inst.*, **31**, 1119-1127 (2007).
4. N. Hansen, J. A. Miller, C. A. Taatjes, J. Wang, T. A. Cool, M. E. Law, P. R. Westmoreland, "Photoionization Mass Spectrometric Studies and Modeling of Fuel-Rich Allene and Propyne Flames", *Proc. Combust. Inst.*, **31**, 1157-1164 (2007).
5. N. Hansen, T. Kasper, S. J. Klippenstein, P. R. Westmoreland, M. E. Law, C. A. Taatjes, K. Kohse-Höinghaus, J. Wang, T. A. Cool, "Initial Steps of Aromatic Ring Formation in a Laminar Premixed Fuel-Rich Cyclopentene Flame", *J. Phys. Chem. A*, **111**, 4081-4092 (2007).
6. P. Oßwald, U. Struckmeier, T. Kasper, K. Kohse-Höinghaus, J. Wang, T. A. Cool, N. Hansen, P. R. Westmoreland, "Isomer-Specific Fuel Destruction Pathways in Rich Flames of Methyl Acetate and Ethyl Formate and Consequences for the Combustion Chemistry of Esters", *J. Phys. Chem. A*, **111**, 4093-4101 (2007).
7. C. A. Taatjes, N. Hansen, D. L. Osborn, K. Kohse-Höinghaus, T. A. Cool, P. R. Westmoreland, "Imaging' Combustion Chemistry via Multiplexed Synchrotron-Photoionization Mass Spectrometry", *Phys. Chem. Chem. Phys.*, **10**, 20-34 (2008).
8. N. Hansen, S. J. Klippenstein, P. R. Westmoreland, T. Kasper, K. Kohse-Höinghaus, J. Wang, T. A. Cool, "A Combined *ab-initio* and Photoionization Mass Spectrometric Study of Polyynes in Fuel-Rich Flames", *Phys. Chem. Chem. Phys.*, **10**, 366-374 (2008).
9. J. Wang, B. Yang, T. A. Cool, N. Hansen, T. Kasper, "Near-threshold Absolute Photoionization Cross Sections of some Reaction Intermediates in Combustion", *Int. J. Mass Spectrom.*, **269**, 210-220 (2008).
10. J. D. Cardoza, F. M. Rudakov, N. Hansen, P. M. Weber, "Identification of Isomeric Hydrocarbons by Rydberg Photoelectron Spectroscopy", *J. Electron Spectrosc.*, **165**, 5-10 (2008).
11. J. Wang, U. Struckmeier, B. Yang, T. A. Cool, P. Oßwald, K. Kohse-Höinghaus, T. Kasper, N. Hansen, P. R. Westmoreland, "Isomer-Specific Influences on the Composition of Reaction Intermediates in Dimethyl Ether/Propene and Ethanol/Propene Flames", *J. Phys. Chem. A*, **112**, 9255-9265 (2008).
12. N. Hansen, J. A. Miller, T. Kasper, K. Kohse-Höinghaus, P. R. Westmoreland, J. Wang, T. A. Cool, "Benzene Formation in Premixed Fuel-Rich 1,3-Butadiene Flames", *Proc. Combust. Inst.*, **32**, 623-630 (2009).
13. A. Lucassen, P. Oßwald, U. Struckmeier, K. Kohse-Höinghaus, T. Kasper, N. Hansen, T. A. Cool, P. R. Westmoreland, "Species identification in a laminar premixed low-pressure flame of morpholine as a model substance for oxygenated nitrogen-containing fuels", *Proc. Combust. Inst.*, **32**, 1269-1276 (2009).
14. C. K. Westbrook, W. J. Pitz, P. R. Westmoreland, F. L. Dryer, M. Chaos, P. Oßwald, K. Kohse-Höinghaus, T. A. Cool, J. Wang, B. Yang, N. Hansen, T. Kasper, "A Detailed Chemical Kinetic Mechanism for Oxidation of Four Small Alkyl Esters in Laminar Premixed Flames", *Proc. Combust. Inst.*, **32**, 221-228 (2009).
15. N. Hansen, T. A. Cool, P. R. Westmoreland, K. Kohse-Höinghaus, "Recent Contributions of Flame-Sampling Molecular-Beam Mass Spectrometry to a Fundamental Understanding of Combustion Chemistry", *Prog. Energy Combust. Sci.*, **35**, 168-191 (2009).
16. J. Wang, M. Chaos, B. Yang, T. A. Cool, F. L. Dryer, T. Kasper, N. Hansen, P. Oßwald, K. Kohse-Höinghaus, P. R. Westmoreland, "Composition of Reaction Intermediates for Stoichiometric and Fuel-Rich Dimethyl Ether flames: Flame-Sampling Mass Spectrometry and Modeling Studies", *Phys Chem. Chem. Phys.*, **11**, 1328-1339 (2009).
17. N. Hansen, J. A. Miller, P. R. Westmoreland, T. Kasper, K. Kohse-Höinghaus, J. Wang, T. A. Cool, "Isomer-Specific Combustion Chemistry in Allene and Propyne Flames", *Combust. Flame*, submitted

SPECTROSCOPY AND KINETICS OF COMBUSTION GASES AT HIGH TEMPERATURES

Ronald K. Hanson and Craig T. Bowman
Department of Mechanical Engineering
Stanford University, Stanford, CA 94305-3032
rkhanon@stanford.edu, ctbowman@stanford.edu

Program Scope

This program involves two complementary activities: (1) development and application of cw laser absorption methods for the measurement of concentration time-histories and fundamental spectroscopic parameters for species of interest in combustion; and (2) shock tube studies of reaction kinetics relevant to combustion. Species currently being investigated in the spectroscopic portion of the research include OH (at 306 nm) and several species with strong deep UV absorption features including methyl (CH₃) propargyl (C₃H₃), alkyl radicals (C₂H₅, C₃H₇), peroxy radical and hydrogen peroxide (HO₂ and H₂O₂).

Recent reaction kinetics work has advanced on several fronts. We have investigated and resolved reasons for the discrepancy between the predictions of current hydrogen and propane mechanisms and shock tube ignition delay time measurements of these fuels at low temperatures. We have also measured elementary reaction rates for decomposition and oxidation of dimethyl ether, and surveyed the ignition delay time behavior of several simple oxygenates. Finally we have made good progress in implementing new methods for reducing non-ideal facility effects in shock tubes and for modeling reactive gasdynamics behind reflected shock waves in shock tubes.

Recent Progress:

Oxygenates: The first high-temperature rate measurements of two dimethyl ether (DME) reactions, (1) DME + Ar → CH₃O + CH₃ + Ar and (2) DME + OH → CH₃OCH₂ + H₂O, were measured in a shock tube by monitoring OH radicals. OH was measured with a narrow-linewidth laser absorption diagnostic using the well-known R₁(5) line of the A-X(0,0) transition at 306.7 nm. The rate k₁ was measured at several pressures from 0.6 – 11.5 atm, and temperatures from 1349 – 1790 K. OH radicals were formed by shock-heating mixtures of DME and O₂ in Ar. These mixtures take advantage of the rapid decomposition of the product CH₃O, forming H-atoms, which react with O₂ to form OH. In carefully chosen mixtures, OH concentration is primarily sensitive to k₁ and the well-known rate of H + O₂ → OH + O. Uncertainty in the new k₁ measurements was conservatively estimated to be ±35%. The rate measurements were then modeled using RRKM theory. Both the rate measurements and RRKM model were fit from 1000 to 1800 K using the Troe falloff form: $k_{1,\infty}(T) = 4.38 \cdot 10^{21} T^{-1.57} \exp(-42220K/T)$ 1/s, $k_{1,0} = 7.52 \cdot 10^{15} \exp(-21537K/T)$ cm³/mol/s, and $F_{\text{cent}} = 0.454 \exp(-T/2510K)$. The rate of k₂ was measured at pressures near 1.6 atm and temperatures from 923 – 1423 K. OH radicals were generated by the thermal decomposition of the OH precursor tert-butyl hydroperoxide, and k₂ was inferred from the observed decay of OH with an estimated uncertainty of ±40%. The rate evaluation by Curran et al. of $k_2 = 6.32 \times 10^6 * T^2 * \exp(328K/T)$ cm³/mol/s was found to be an excellent fit to both the previous low-temperature measurements and this work; see Fig. 1.

Ignition delay time data for oxygen-carrying species are required for the development of oxygenate fuel mechanisms. To fill this need, a survey of ignition delay times was performed using pressure and OH* emission diagnostics behind reflected shock waves for several simple oxygenates. Reflected shock conditions covered temperatures of 1150-1550 K and pressures of

1-4 atm. Fuel mixtures tested include four oxygenates: acetone, n-butanal, methyl butanoate, and 3-pentanone; see Fig. 2. All fuels were tested in O₂/argon mixtures with equivalence ratios of 0.5 to 2.0. The Dooley et al. (2009) mechanism for methyl butanoate was extended to enable modeling of both n-butanal and methyl butanoate data.

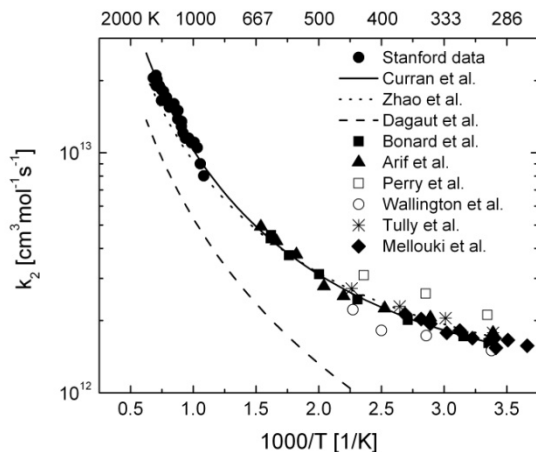


Figure 1. Comparison of measured high-temperature k_2 rate to rates used in DME mechanisms (lines) and low-temperature measurements (LIF, solid symbols; fluorescence, open symbols).

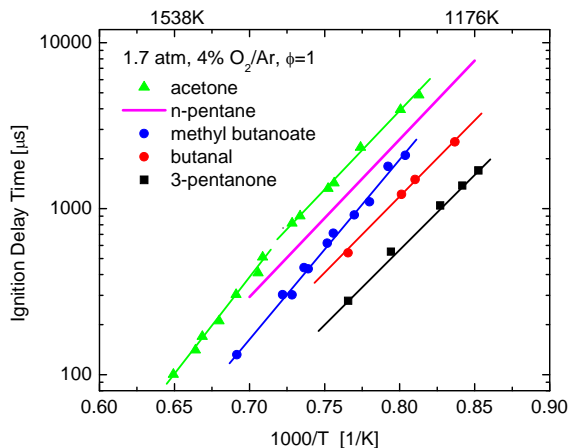


Figure 2. Arrhenius plot of selected oxygenate species ignition delay times: $\phi = 1.0$. N-Pentane data at similar conditions are included for comparison.

Hydrogen/Oxygen and Propane/Oxygen Ignition: Validation of detailed reaction mechanisms to describe combustion processes relies on a direct comparison of mechanism simulations with reliable experimental measurements. However, even for two of the simplest hydrocarbon-related combustion systems, hydrogen and propane oxidation, large uncertainties still exist in the abilities of current detailed mechanisms and gas dynamic models to accurately simulate ignition time and species time-histories in shock tube experiments conducted at lower temperatures. These uncertainties are linked to uncertainties in the detailed reaction mechanism at low temperatures (below 1000 K) where hydroperoxyl reactions are believed to be important, and to uncertainties introduced by, or associated with, facility-related non-ideal effects. These facility effects become important only at long test times (typically greater than 1 ms).

We have extended our low-temperature ignition delay time database (which included our previous work on hydrogen-oxygen) to include similar measurements in propane; see Figs. 3 and 4. Shock tube ignition delay time data were taken behind reflected shock waves for 0.8% propane, 8% oxygen in argon near 6 atm for temperatures from 1420 to 980 K. Small gradual changes in the pressures and temperatures of these experiments {e.g. $(dP_5/dt)/P_5 = \sim 2\%/ms$ } at long time due to facility effects have a measurable effect on the ignition delay times. Through the use of driver inserts and tailored driver gas mixtures, these changes can be reduced effectively to zero. A direct comparison with normal idealized constant volume (V) and constant internal energy (E) simulations can then be performed. However, we have shown that non-ideal effects associated with facility performance and energy release can be included in the modeling (using a new model CHEMSHOCK which couples the experimental pressure trace with the constant V, E assumptions), and the simulations can be properly extended to experiments in which facility-related pressure increases occur.

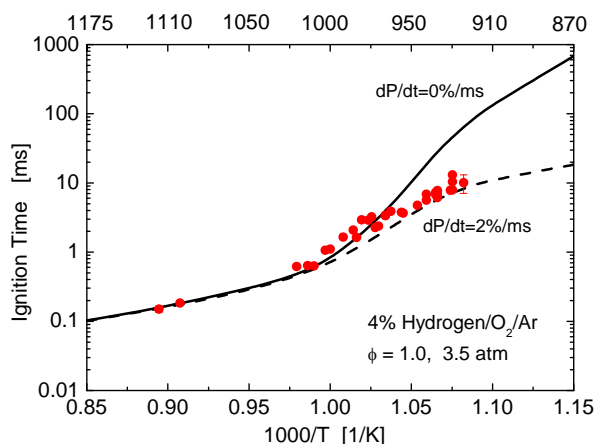


Figure 3. Simulations of H_2/O_2 ignition delay time measurements using CHEMSHOCK for two values of dP/dt : 0%/ms and 2%/ms.

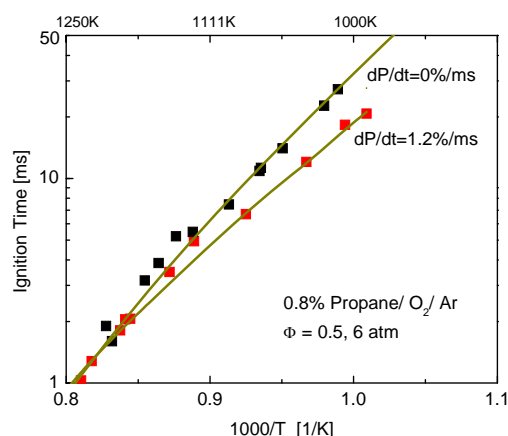


Figure 4. Simulations of propane/ O_2 ignition delay time measurements using CHEMSHOCK for two values of dP/dt : 0%/ms and 1.2%/ms.

Advances in Shock Tube/Laser Diagnostics Methods: Non-ideal shock tube facility effects, such as incident shock wave attenuation, can cause variations in the pressure time-histories recorded in reflected shock wave experiments. These variations can be reduced, and in some cases eliminated, by the use of driver inserts. Driver inserts, when designed appropriately, act as sources for expansion waves which can counteract or compensate for gradual increases in reflected shock pressure profiles. An algorithm for the design of these inserts has been generated, and example pressure measurements recorded that demonstrate the success of this approach. When these driver inserts are employed, near-ideal, constant-volume performance in reflected shock wave experiments can be achieved, even at long test times. This near-ideal behavior simplifies the interpretation of shock tube chemical kinetics experiments, particularly in experiments which are highly sensitive to temperature and pressure changes, such as measurements of ignition delay time of exothermic reactions.

Recent work is shown in Fig. 5. Here the modification of the shock tube driver section (by the addition of inserts) fully compensates for the small facility effects seen in the reflected shock tube test conditions. The temperature behind the reflected shock can also now be measured very accurately using a new IR tunable DFB diode laser CO_2 absorption diagnostic at 2.7 microns, and measurements indicate that measured and predicted reflected temperatures are within 5 K of each other as shown in Fig. 6.

Deep UV Spectroscopy: We are in the process of taking possession of a new Coherent™ MIRA laser system capable of accessing wavelengths from the shorter wavelength limit of b-BBO frequency-doubling (near 205 nm) to the longer wavelength limit of a Ti-Sapphire laser (near 1000 nm). This system will be used in conjunction with our existing IR diode and gas laser systems (capable of accessing wavelengths to 11 microns) to detect combustion species.

Future Plans

We plan to finalize our investigations of facility-related and mechanistic reasons for the discrepancies between the predictions of detailed mechanisms and shock tube measurements for the hydrogen and propane oxidative systems. In a new thrust, we plan to measure the reaction rate of selected alkenes + OH using OH laser absorption. We also plan to investigate reaction

kinetics of selected oxygenate fuels, such as the methyl esters, e.g., methyl butanoate. Lastly, we plan to advance development of our deep-UV frequency-doubled laser capabilities and use this new diagnostic to measure several important radical species including: methyl (CH_3) propargyl (C_3H_3), alkyl radicals (C_2H_5 , C_3H_7), peroxy radical and hydrogen peroxide (HO_2 and H_2O_2). Alkanes (CH_4 , C_3H_8) and alkenes (C_2H_4 , C_3H_6) will be monitored with new IR absorption measurements.

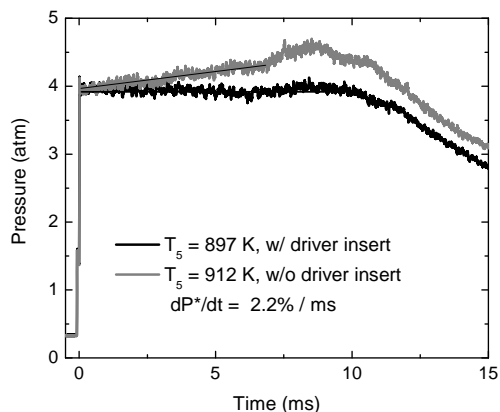


Figure 5. End section pressure profile for identical pure argon shock wave experiments using a 50/50 He/N₂ tailored driver gas mixture with and without a driver insert. The nominal initial reflected shock conditions were 900K, 4 atm.

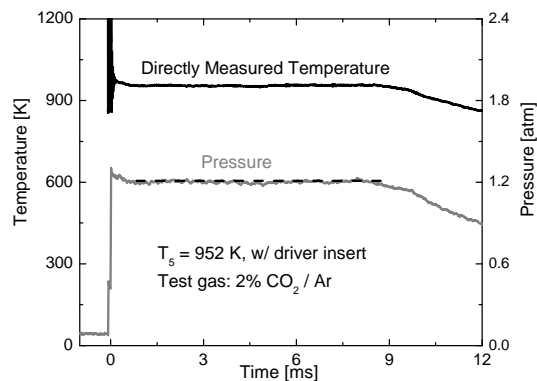


Figure 6. Highly uniform temperature profile obtained when pressure is precisely maintained constant using a driver insert. Tailored driver gas mixture is 60/40 helium/nitrogen; test gas is argon seeded with 2% CO₂. Reflected shock conditions: 952 K, 1.2 atm.

List of Recent Publications

D. F. Davidson, R. K. Hanson, "Fundamental Kinetics Database Utilizing Shock Tube Measurements, Volume 3: Reaction Rate Measurements," January 2009, available at <http://hanson.stanford.edu>.

Z. Hong, G. A. Pang, S. S. Vasu, D. F. Davidson, R. K. Hanson, "The Use of Driver Inserts to Reduce Non-Ideal Pressure Variations behind Shock Waves," accepted for publication Journal of Shock Waves, February 2009.

G. A. Pang, D. F. Davidson, R. K. Hanson, "Experimental Study and Modeling of Shock Tube Ignition Delay Times for Hydrogen-Oxygen-Argon Mixtures at Low Temperatures," Proceedings of the Combustion Institute 32 (2009) 181-188.

D. F. Davidson, R. K. Hanson, "Recent Advances in Shock Tube/Laser Diagnostic Methods for Improved Chemical Kinetics Measurements," submitted to Journal of Shock Waves, December 2008.

D. F. Davidson, S. C. Ranganath, K.-Y. Lam, M. Liaw, Z. Hong, R. K. Hanson, "Ignition Delay Time Measurements of Normal Alkanes and Oxygenates," submitted to the Journal of Propulsion and Power, February 2009.

V. Vasudevan, R. D. Cook, R. K. Hanson, C. T. Bowman, D. M. Golden, "High Temperature Shock Tube Study of the Reactions of $\text{CH}_3+\text{OH}=\text{Products}$ and $\text{CH}_3\text{OH}+\text{Ar}=\text{Products}$," Int. J. Chem. Kinet. 40 (2008) 488-495.

R. D. Cook, D. F. Davidson, R. K. Hanson, "Rate Measurements of DME Decomposition and DME+OH at Elevated Temperatures," to be presented at the U. S. Combustion Meeting, Ann Arbor MI, May 2009.

R. D. Cook, D. F. Davidson, R. K. Hanson, "High-Temperature Shock Tube Measurements of Dimethyl Ether Decomposition and the Reaction of Dimethyl Ether with OH," submitted to Journal of Physical Chemistry A: February 2009.

R. D. Cook, D. F. Davidson, R. K. Hanson, "Shock Tube Measurements of Ignition Delay Times and OH Time-Histories in Dimethyl Ether Oxidation," Proceedings of the Combustion Institute 32 (2009) 189-196.

Theoretical Studies of Potential Energy Surfaces*

Lawrence B. Harding
Chemistry Sciences and Engineering Division
Argonne National Laboratory, Argonne, IL 60439
harding@anl.gov

Program Scope

The goal of this program is to calculate accurate potential energy surfaces for both reactive and non-reactive systems. Our approach is to use state-of-the-art electronic structure methods (CASPT2, MR-CI, CCSD(T), etc.) to characterize multi-dimensional potential energy surfaces. Depending on the nature of the problem, the calculations may focus on local regions of a potential surface (for example, the vicinity of a minimum or transition state), or may cover the surface globally. A second aspect of this program is the development of techniques to fit multi-dimensional potential surfaces to convenient, global, analytic functions that can then be used in dynamics calculations.

Recent Progress

OH+NH: The reactions of OH with NH have been cited as the most important reactions of NH in flames, yet there have been no direct measurements of the rates of these reactions. We have

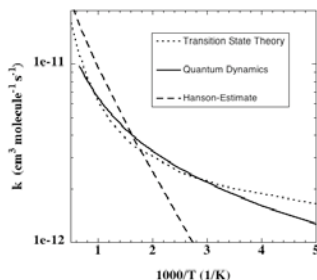


Figure 1.

begun a detailed theoretical study of these reactions. Last year we located the relevant stationary points using the CCSD(T)/aug-cc-pvqz // CCSD(T)/aug-cc-pvtz level of theory and made transition state theory estimates of the rates on the doublet and quartet surfaces. This year we fit a global, analytic, 6D surface for the quartet. In collaboration with Stephen Gray we have now used this surface in a fully-dimensional, quantum dynamics treatment of the abstraction reaction on the quartet surface. The results are shown in Figure 1 where they are compared to our transition state theory rate and an earlier estimate by Hanson¹. We find the transition state theory and quantum dynamics results are in excellent agreement with each other and both are in good agreement with Hanson's earlier estimate for temperatures greater than 500 K.

Roaming Radical Mechanisms: In an attempt to better understand roaming radical mechanisms we have fit several reduced-dimensional potential surfaces using a straight-forward modification of Bowman's approach (direct product, multinomial in Morse variables). To date we have fit 3D surfaces for H+HCO, H+C₂H₃, and H+C₂H₅, a 5D surface for CH₃O+OH and a 6D surface for CH₃+HCO. In each case the internal degrees of freedom of the radical fragments are kept fixed. As an example, in Figure 2 we show a plot of a two dimensional slice through the six dimensional CH₃+HCO interaction potential. In collaboration with Klippenstein we have run rigid fragment trajectory calculations to predict the branching between roaming and simple bond cleavage. Preliminary results suggest that in most cases roaming is a relatively minor channel (<20%).

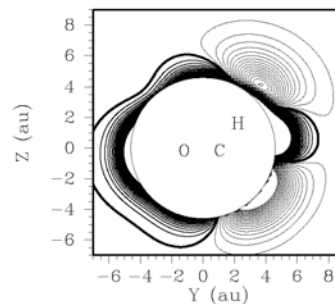


Figure 2

CH₃+CH₃: To aid in the interpretation of recent high temperature measurements by Tranter we

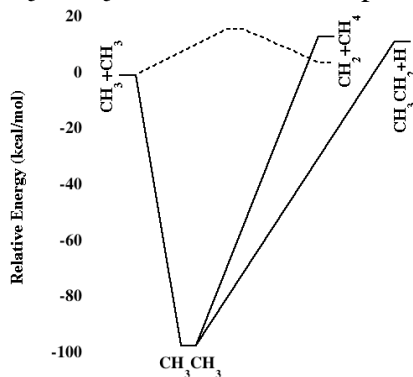


Figure 3. CCSD(T)/aug-cc-pvqz energies. The solid lines refer to the singlet, dashed to the triplet. Further calculations to quantify the temperature and pressure dependence of the branching ratios are in progress.

have examined possible secondary pathways for the reaction of CH₃+CH₃. The primary process is the addition to form C₂H₆. At high pressures the C₂H₆ can be stabilized. At lower pressures it can dissociate either back to reactants, or at higher temperatures to C₂H₅+H. The question we are addressing is the possible importance of pathways leading to abstraction products, CH₄+CH₂. On the triplet surface we find a transition state for abstraction with a barrier of 16 kcal/mol with CCSD(T)/aug-cc-pvqz. On the singlet surface we find a barrierless path for insertion ¹CH₂+CH₄→C₂H₆. Since singlet methylene plus methane is endothermic relative to CH₃+CH₃ by just 13 kcal/mol this implies the lowest “abstraction” pathway leads to ¹CH₂ via an addition/reverse insertion mechanism.

Recently a question was raised in the literature² concerning the method we developed several years ago for calculating rates of radical-radical association reactions³. Our approach employs inexpensive CASPT2/cc-pvdz calculations together with a one-dimensional basis set correction designed to give aug-cc-pvtz “quality” results. The question concerns the adequacy of the one dimensional basis set correction. It was stated², “Since the variational transition states at high temperature are located at short distances the potential energy surface is more anisotropic than at low temperature. The one dimensional orientation independent correction of previous work is therefore questionable whereas our M06 and M06-L calculations sample potential energy directly without any corrections.” To address this issue we have repeated our calculations for the CH₃+CH₃ association reaction using CASPT2/aug-cc-pvtz energies

The results are shown in Figure 4. The solid line is the new, large basis set, result. The dotted line is the uncorrected CASPT2/cc-pvdz result and the dash-dot line is our original prediction obtained with the one-dimensional correction to the cc-pvdz energies. We find excellent agreement between our previous calculations and the new large basis set results, especially at higher temperatures where the two are within a few percent. This demonstrates that the CASPT2/cc-pvdz energies accurately describe the anisotropy of the potential. Also shown in Figure 4 are the M06-L (a parameterized DFT method) results from reference 2. The rate obtained using M06-L energies is almost a factor of three too low at the higher temperatures. We also note that, for this particular reaction, the DFT calculations are more than a factor of ten slower than the CASPT2/cc-pvdz calculations.

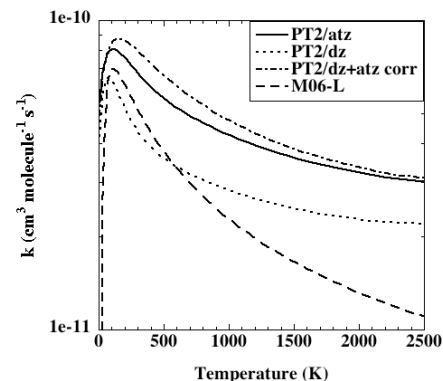


Figure 4

Future Plans

One of the reactions we plan to focus on in the near future is $\text{OH} + \text{HO}_2 \rightarrow \text{H}_2\text{O} + \text{O}_2$. Combustion mechanisms have shown a high sensitivity to this reaction but there is considerable uncertainty in the rate of this reaction. There is also some evidence for a highly non-Arrhenius temperature dependence. We also plan to continue our development of techniques for fitting reduced dimensional potential surfaces.

Acknowledgement: This work was performed under the auspices of the Office of Basic Energy Sciences, Division of Chemical Sciences, Geosciences and Biosciences, U.S. Department of Energy, under Contract DE-AC02-06CH11357.

References:

- (1) R. K. Hanson and S. Salimian, in *Combustion Chemistry* (W. C. Gardiner Jr., Ed.) Springer-Verlag, New York, P.361, (1984).
- (2) J. Zheng, S. Zhang, D. G. Truhlar, *J. Phys. Chem. A* **112**, 11509 (2008)
- (3) S. J. Klippenstein, Y. Georgievskii and L. B. Harding, *Phys. Chem. Chem. Phys.* **8**, 1133 (2006)

PUBLICATIONS (2007 - Present):

On the Formation and Decomposition of C_7H_8

S.J. Klippenstein, L.B. Harding and Y. Georgievskii, *Proc. Combust. Inst.* **31**, 221-229 (2007)

Direct Measurement and Theoretical Calculation of the Rate Coefficient for $\text{Cl} + \text{CH}_3$ from $T=202\text{-}298\text{ K}$

J. K. Parker, W. A. Payne, R. J. Cody, F.L. Nesbitt, L.J. Stief, S.J. Klippenstein, and L.B. Harding *J. Phys. Chem. A* **111**, 1015-1023 (2007)

Experimental and Theoretical Rate Constants for $\text{CH}_4 + \text{O}_2 \rightarrow \text{CH}_3 + \text{HO}_2$

N. K. Srinivasan, J. V. Michael, L. B. Harding and S. J. Klippenstein
Combustion and Flame **149**, 104-111 (2007)

Interpolated Moving Least-Squares Methods for Fitting Potential Energy Surfaces: Application to the H_2CN Unimolecular Reaction

Y. Gao, L. B. Harding, A. F. Wagner, M. Minkoff and D. L. Thompson
J. Chem. Phys. **126**, 104105 (2007)

On the Combination Reactions of Hydrogen Atoms with Resonance Stabilized Hydrocarbon Radicals

L.B. Harding, S.J. Klippenstein and Y. Georgievskii, *J. Phys. Chem. A* **111**, 3789-3801 (2007)

Kinetics of Methyl Radical-Hydroxyl Radical collisions and Methanol Decomposition

A. W. Jasper, S. J. Klippenstein, L. B. Harding, and B. Ruscic
J. Phys. Chem. A **111**, 3932-3950 (2007)

Reflected Shock Tube and Theoretical Studies of High-Temperature Rate Constants for $\text{OH} + \text{CF}_3\text{H} \leftrightarrow \text{CF}_3 + \text{H}_2\text{O}$ and $\text{CF}_3 + \text{OH} \rightarrow \text{Products}$

N. K. Srinivasan, M.-C. Su, J. V. Michael, S. J. Klippenstein and L. B. Harding
J. Phys. Chem. A **111**, 6822-6831 (2007)

Ab Initio Methods for Reactive Potential Surfaces

L. B. Harding, S. J. Klippenstein, and A. W. Jasper
Phys. Chem. Chem. Phys. **9**, 4055-4070 (2007)

Dissociative Ionization of Hot C_3H_5 Radicals

H. Fan, L. B. Harding, and S. T. Pratt, Mol. Phys. **105**, 1517-1534 (2007)

Secondary Kinetics of Methanol Decomposition: Theoretical Rate Coefficients for $^3\text{CH}_2 + \text{OH}$, $^3\text{CH}_2 + ^3\text{CH}_2$ and $^3\text{CH}_2 + \text{CH}_3$

A. W. Jasper, S. J. Klippenstein, L. B. Harding, J. Phys. Chem. A **111**, 8699-8707 (2007)

Performance of the Spin-Flip and Multi-reference methods for Bond-Breaking in Hydrocarbons: A Benchmark Study

A. A. Golubeva, A. V. Nemukhin, S. J. Klippenstein, L. B. Harding and A. Krylov
J. Phys. Chem. A **111**, 13264-13271 (2007)

The Thermal Decomposition of CF_3 and the Reaction of $\text{CF}_2 + \text{OH} \rightarrow \text{CF}_2\text{O} + \text{H}$

N. K. Srinivasan, M.-C. Su, J. V. Michael, A. W. Jasper, S. J. Klippenstein and L. B. Harding, J. Phys. Chem. A **112**, 31-37 (2008)

The Kinetics of $\text{CH} + \text{N}_2$ Revisited with Multi-Reference Methods

L. B. Harding, S. J. Klippenstein and J. A. Miller, J. Phys. Chem. A **112**, 522-532 (2008)

Quantum States of the Endohedral Fullerene $\text{Li}@\text{C}_{60}$

M. Zhang, L. B. Harding, S. K. Gray, S. A. Rice, J. Phys. Chem. A **112**, 5478-5485 (2008)

Kinetics and Product Branching Ratios of the Reaction of $^1\text{CH}_2$ with H_2 and D_2

K. L. Gannon, M. A. Blitz, M. J. Pilling, P. W. Seakins, S. J. Klippenstein and L. B. Harding
J. Phys. Chem. A. **112**, 9575-9583 (2008)

Kinetics of the $\text{H} + \text{NCO}$ Reaction

S. J. Klippenstein and L. B. Harding, 32nd Symposium (International) on Combustion (in press)

Theoretical rate coefficients for the reaction of methyl radical with hydroperoxyl radical and for methylhydroperoxide decomposition

A. W. Jasper, S. J. Klippenstein and L. B. Harding
32nd Symposium (International) on Combustion (in press)

CHEMICAL ACCURACY FROM AB INITIO MOLECULAR ORBITAL CALCULATIONS

Martin Head-Gordon

Department of Chemistry, University of California, Berkeley, and,
Chemical Sciences Division, Lawrence Berkeley National Laboratory,
Berkeley, CA 94720.
mhg@cchem.berkeley.edu

1. Scope of Project.

Short-lived reactive radicals and intermediate reaction complexes are believed to play central roles in combustion, interstellar and atmospheric chemistry. Due to their transient nature, such molecules are challenging to study experimentally, and our knowledge of their structure, properties and reactivity is consequently quite limited. To expand this knowledge, we develop new theoretical methods for reliable computer-based prediction of the properties of such species [18]. We apply our methods, as well as existing theoretical approaches, to study prototype radical reactions, often in collaboration with experimental efforts. These studies help to deepen understanding of the role of reactive intermediates in diverse areas of chemistry. They also sometimes reveal frontiers where new theoretical developments are needed in order to permit better calculations in the future.

2. Summary of Recent Major Accomplishments.

2.1 *Improved density functionals for ground and excited states.*

One of the principal problems with present-day density functional theory (DFT) methods is self-interaction error, which causes problems ranging from reaction energy barriers being too low, to radical electrons being overly delocalized to the gross failure of charge-transfer excited states. We have recently completed the systematic optimization of a new density functional called ω B97 that includes 100% exact exchange at long range, thereby eliminating long-range self-interaction error [13]. Tests show that ω B97, and an additional functional, ω B97X [13], which includes a fraction of short-range exact exchange also, out-perform widely used density functionals such as B3LYP and B97 for thermochemical properties, reaction barriers, and intermolecular interactions, while eliminating the worst pathologies for charge transfer excited states and the treatment of radical electrons [13]. Results for intermolecular interactions can be greatly improved by inclusion of atom-atom dispersion corrections, yielding the ω B97X-D functional, which is fully reoptimized to avoid double-counting correlation effects [25]. The success of these functionals for thermochemistry stems from their treatment of exchange which is non-local on the order of a bond-length [27].

2.2 *Excited states of large molecules without self-interaction errors.*

The density functionals described above are one way to overcome some of the difficulties of present-day DFT. Another approach is to use wavefunction-based methods, and modify relatively simple treatments of electron correlation effects to improve accuracy

and at the same time enable applications to large molecules. For excited states, we recently proposed the scaled opposite spin (SOS) doubles correction to single excitation CI for this purpose. SOS-CIS(D) [6], and its extension to a quasi-degenerate theory [19] has a number of desirable properties. The cost scales only 4th order with molecular size, versus 5th order for conventional perturbation methods such as CIS(D). And, because the method is wavefunction-based, there is no self-interaction error, and charge-transfer excited states are correctly described. Since there is a single empirical parameter describing excited state correlations and one describing ground state correlations, it is possible to also achieve accuracy for excitation energies that exceeds the conventional CIS(D) method by nearly a factor of two. This approach appears promising for valence excited states of large organic molecules.

2.3 *Spin contamination and low-order perturbation theory.*

One of the reasons that the SOS-CIS(D) method described above cannot be recommended for excited states of radicals is that it is the excited state counterpart of the ground state second order Moller-Plesset (MP2) method, which can perform very poorly for radicals because of spin-contamination in the Hartree-Fock (HF) reference. For instance, if one takes a large conjugated radical such as phenalenyl (C₁₃H₉), the HF determinant exhibits $\langle S^2 \rangle > 2.0$ rather than 0.75 as desired. We have explored a modification of MP2 that is designed to overcome this problem by optimizing the orbitals in the presence of electron correlation [5]. We include only opposite spin correlations (as above) and scale them by a single empirical factor (chosen as 1.2). The resulting optimized second order method (termed the O2 method) dramatically reduces spin contamination in calculations on large radicals, and therefore is a promising inexpensive approach to studying such systems. Returning to the C₁₃H₉ example, the O2 reference determinant has $\langle S^2 \rangle = 0.76$, which is virtually free of spin-contamination.

2.4 *Pairing methods for strong electron correlations.*

To treat large molecules that have strong electron correlations (e.g. singlet biradicaloids), we have been developing generalized valence bond coupled cluster methods, which systematically approximate CASSCF. Perfect pairing is the starting point: exact for one pair, and extensive. The next well-defined level is the perfect quadruples model [29], which is exact for two pairs and extensive. Methods which correlate only pairs of pairs suffer from symmetry-breaking problems for molecules with multiple resonance structures – benzene for example prefers a D_{3h} symmetry structure to D_{6h}. We have explored methods that reduce this symmetry-breaking by at least an order of magnitude by including correlations that couple three electron pairs by perturbation theory [10,26].

2.5 *Valence bond methods for strong electron correlations.*

Instead of approximating the CASSCF limit for treating strong correlations, another, relatively unexplored possibility is to approximate the spin-coupled valence bond limit (also exponentially expensive). We have made exciting recent progress on this problem, yielding a new approximate valence bond method that can break any number of chemical bonds with only a quadratic number of spin-coupling variables, maintaining extensivity, and spin-purity [30]. While we only have a pilot program at the moment, there is tremendous incentive to further explore this technique, as this appears to be a

tremendously economical and natural way to treat delicate electron correlation effects that are very difficult to handle otherwise.

2.6 Fundamental studies of chemical bonding.

We have used the ground and excited state methods discussed above in a variety of chemical applications for which they are appropriate. The coupling of the cation of a polycyclic aromatic hydrocarbon (PAH) radical and a neutral PAH molecule is one interesting example that may have relevance to the mechanism of condensation of charged PAH clusters [1]. Separately we have recently examined the changes in chemical bonding as a function of oxidation state in 4-membered CuPCuP heterocycles [16], the coordination of alkanes to transition metal centers [4], and collaboratively explored the photophysics of cobalt-nitrosyl complexes [24].

3. Summary of Research Plans.

- Testing the new density functionals for excited states (including charge-transfer)
- Development and testing of pairing methods for radicals
- New studies of the properties of reactive radicals and radical reactions.

4. Publications from DOE Sponsored Work, 2007-present.

- [1] "Charged polycyclic aromatic hydrocarbon clusters and the galactic extended red emission", Y.M. Rhee, T.J. Lee, M.S. Gudipati, L.J. Allamandola, and M. Head-Gordon, Proc. Nat. Acad. USA 104, 5274-5278 (2007).
- [2] "Quartic scaling analytical gradient of scaled opposite spin second order Møller-Plesset Perturbation theory", R.C. Lochan, Y. Shao, and M. Head-Gordon, J. Chem. Theory Comput. 3, 988-1003 (2007).
- [3] "Fast evaluation of scaled opposite spin second order Møller-Plesset correlation energies using auxiliary basis expansions and exploiting sparsity", Y. Jung, Y. Shao, and M. Head-Gordon, J. Comput. Chem. 28, 1953-1964 (2007).
- [4] "Theoretical study of the rhenium-alkane interaction in transition metal-alkane sigma-complexes", Erika A. Cobar, Rustam Z. Khaliullin, Robert G. Bergman, and Martin Head-Gordon, Proc. Nat. Acad. USA 104, 6963-6968 (2007).
- [5] "Orbital-optimized opposite-spin second order correlation: an economical method to improve the description of open-shell molecules", R.C. Lochan and M. Head-Gordon, J. Chem. Phys. 126, 164101 (2007)
- [6] "Scaled second order perturbation corrections to configuration interaction singles: efficient and reliable excitation energy methods", Y.M. Rhee and M. Head-Gordon, J. Phys. Chem. A 111, 5314-5326 (2007).
- [7] "A correction to constrained CCSD models based on the 2nd order coupled cluster moment", D.W. Small, and M. Head-Gordon, J. Chem. Phys. 127, 064102 (2007).
- [8] "Theoretical study of solvent effects on the thermodynamics of Iron(III) [Tetrakis(pentafluorophenyl)]porphyrin Chloride Dissociation", R.Z. Khaliullin, M. Head-Gordon, and A.T. Bell, J. Phys. Chem. B. 111, 10992-10998 (2007)
- [9] "Localized orbital theory and ammonia triborane", J.E. Subotnik, A. Sodt and M. Head-Gordon, Phys. Chem. Chem. Phys. 9, 5522-5530 (2007).
- [10] "Symmetry-breaking in benzene and larger aromatic molecules within generalized valence bond coupled cluster methods", K.V. Lawler, G.J.O. Beran, and M. Head-Gordon, J. Chem. Phys. 128, 024107 (2008) (13 pages).

- [11] “The limits of local correlation theory: electronic delocalization and chemically smooth potential energy surfaces”, J.E. Subotnik, A. Sodt and M. Head-Gordon, *J. Chem. Phys.* 128, 034103 (2008) (12 pages).
- [12] “Central moments in quantum chemistry”, D.W. Small and M. Head-Gordon, *Int. J. Quantum Chem.* 108, 1220-1231 (2008)
- [13] “Systematic optimization of long-range corrected hybrid density functionals”, Jeng-Da Chai and M. Head-Gordon, *J. Chem. Phys.* 128, 084106 (2008).
- [14] “A two-parameter Coulomb attenuator with a cutoff radius for two-electron repulsion integrals: the effect of attenuation on correlation energies”, A.D. Dutoi and M. Head-Gordon, *J. Phys. Chem A* 112, 2110-2119 (2008).
- [15] “Hartree-Fock exchange computed using the atomic resolution of the identity approximation”, A. Sodt and M. Head-Gordon. *J. Chem. Phys.* 128, 104106 (2008).
- [16] “A Delicate Electronic Balance between Metal and Ligand in [Cu-P-Cu-P] Diamondoids: Oxidation State Dependent Plasticity and the Formation of a Singlet Diradical”, Y.M. Rhee and M. Head-Gordon, *J. Am. Chem. Soc.* 130, 3878-3887 (2008)
- [17] “Semiempirical double-hybrid density functional with improved description of long-range correlation”, T. Benighaus, R.A. Distasio Jr., R.C. Lochan, J.D. Chai and M. Head-Gordon, *J. Phys. Chem. A*, 112, 2702-2712 (2008).
- [18] “Chemistry at the Computer”, M. Head-Gordon and E. Artacho, *Physics Today*, 61 (4), 58-63 (2008).
- [19] “Quasidegenerate scaled opposite spin second order perturbation corrections to single excitation configuration interaction”, D. Casanova, Y.M. Rhee and M. Head-Gordon, *J. Chem. Phys.* 128, 164106 (2008).
- [20] “Near infrared spectroscopy of nitrogenated polycyclic aromatic hydrocarbon cations from 0.7 to 2.5 micrometers”, A.L. Mattioda, L. Rutter, J. Parkhill, M. Head-Gordon, T.J. Lee, and L.J. Allamandola, *Astrophys. J.* 680, 1243-1255 (2008).
- [21] “Exploring the accuracy of relative molecular energies in local correlation theory”, J.E. Subotnik and M. Head-Gordon, *J. Phys.: Condens. Matter* 20 (2008) 294211.
- [22] “Effects of ligands and spin-polarization on the preferred conformation of distannynes” W. Kurlancheek, Y. Jung and M. Head-Gordon, *Dalton Trans.* 33, 4428-4435 (2008).
- [23] “The spin-flip extended single excitation configuration interaction method”, D. Casanova and M. Head-Gordon, *J. Chem. Phys.* 129, 064104 (2008).
- [24] “Direct observation of photoinduced bent nitrosyl excited state complexes”, K.R. Sawyer, R.P. Steele, E.A. Glascoe, J.F. Cahoon, J.P. Schlegel, M. Head-Gordon and C.B. Harris, *J. Phys. Chem. A*, 112, 8505-8514 (2008).
- [25] “Long-range corrected hybrid density functionals with damped atom-atom dispersion corrections”, J.-D. Chai and M. Head-Gordon, *Phys. Chem. Chem. Phys.* 44, 6615-6620 (2008).
- [26] “Penalty functions for combining coupled cluster and perturbation amplitudes in local correlation methods with optimized orbitals”, K.V. Lawler, J.A. Parkhill and M. Head-Gordon, *Mol. Phys.* 106, 2309-2324 (2008).
- [27] “Optimal operators for Hartree-Fock exchange from long-range corrected hybrid density functionals”, J.D. Chai and M. Head-Gordon, *Chem. Phys. Lett.* 467, 176-178 (2008).
- [28] “Double spin-flip approach within equation-of-motion coupled cluster and configuration interaction formalisms: Theory, implementation and examples” D. Casanova, L.V. Slipchenko, A.I. Krylov, and M. Head-Gordon, *J. Chem. Phys.* 130, 044103 (2009).
- [29] “The perfect quadruples model for electron correlation in a valence active space”, J.A. Parkhill, K.V. Lawler, and M. Head-Gordon, *J. Chem. Phys.* 130, 084101 (2009)
- [30] “Tractable spin-pure methods for bond-breaking: Local many-electron spin-vector sets and an approximate valence bond model”, D.W. Small and M. Head-Gordon, *J. Chem. Phys.* 130, 084103 (2009).

Laser Studies of Combustion Chemistry

John F. Hershberger

Department of Chemistry and Molecular Biology
North Dakota State University
NDSU Dept. 2735, PO Box 6050
Fargo, ND 58108-6050
john.hershberger@ndsu.edu

Time-resolved infrared diode laser absorption and laser-induced fluorescence spectroscopy are used in our laboratory to study the kinetics and product channel dynamics of chemical reactions of importance in the gas-phase combustion chemistry of nitrogen-containing radicals. This program is aimed at improving the kinetic database of reactions crucial to the modeling of NO_x control strategies such as Thermal de-NO_x, RAPRENO_x, and NO-reburning. The emphasis in our study is the quantitative measurement of both total rate constants and product branching ratios.

HCNO Kinetics

Previous to recent studies in our laboratory, there have been no literature data available on the kinetics of HCNO, the fulminic acid molecule. Recent modeling studies have suggested the importance of this molecule in NO-reburning mechanisms.¹ In combustion, HCNO is primarily formed via acetylene oxidation:



Recent experimental and computational work in several laboratories, including ours, has identified (2a) as a major product channel.²⁻⁵

Earlier reports have summarized our results for the OH+HCNO, CN+HCNO, and NCO+HCNO reactions. We report here results on the O+HCNO reaction, which has many possible channels (we only show three here):

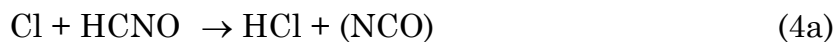


Because we do not have oxygen atom detection capabilities in our laboratory, we measured the total rate constant of this reaction using a relative rate technique, by detecting OCS created from the O+CS₂ reaction in competition with the title reaction.

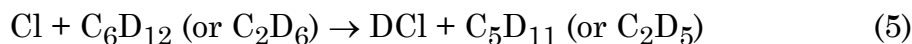
Analysis of our data gives $k_3 = (9.84 \pm 3.52) \times 10^{-12} \exp[(-195 \pm 120)/T]$ (cm³ molecule⁻¹ s⁻¹) over the temperature range 298 - 375 K, with a value of $k_3 = (5.32 \pm 0.40) \times 10^{-12}$ cm³ molec⁻¹s⁻¹ at 298 K. Detection and quantification of products indicates that CO forming channels dominate the reaction, with ϕ_{3c} (CO + NO + H) >0.74.

We have also performed ab initio calculations on this system. Using B3LYP/6-311++G(d,p) optimizations followed by single point energy CCSD(T)/6-311++G(d,p) calculations, we find that O+HCNO readily forms an HC(O)NO intermediate, which may then dissociate to HCO+NO and again to H+CO+NO. Initial calculations indicated that the initial intermediate is formed without any barrier. Further calculations, however, using optimizations at the CCSD(T)/6-31G(d,p) level have revealed a small barrier of ~3.6 kcal/mole to HC(O)NO formation, which is at least qualitatively consistent with the rather low rate constants determined experimentally.

We have also begun experiments on the Cl+HCNO reaction:



We will measure the total rate constant by a relative rate technique, using deuterated hydrocarbons as competing reactants:



We have detected DCl under these conditions, and expect measurement of [DCl] vs. [C₆D₁₂] to yield the rate constant.

HCCN + NO_x Reactions

The HCCN + NO reaction was studied earlier by Curl et al.⁶ They found a fast rate constant at 296 K, and detected but did not quantify products:





We have recently acquired a laser diode in the 3300 cm^{-1} region which for the first time allows us to detect and quantify HCN products. Using HBr_2CCN photolysis followed by detection of HCN, N_2O , CO, and CO_2 products, we have concluded that $\text{HCN} + \text{NCO}$ is the dominant product channel. (N_2O , CO, and CO_2 come from the $\text{NCO} + \text{NO}$ reaction). We did not detect any HNCO (or its less stable isomer, HCNO). Future work includes product detection in the $\text{HCCN} + \text{NO}_2$ reaction.

CN + O₂ Reaction

The total rate constant of the $\text{CN} + \text{O}_2$ reaction has been previously investigated by many workers over an extremely large temperature range of 13-3800 K. Two product channels are possible:



Previous estimates of the branching ratio into channel (7b) have ranged from 0.06 to 0.29. A major difficulty in these studies is the possible contribution of secondary chemistry, especially the reaction



All previous work involving detection of channel (7b) have been bulb experiments; a recent molecular beam study only detected channel (7a).⁷

Previous work in our laboratory⁸ attempted to distinguish CO formation from channel (7b) from the secondary reaction (8) by using SiH_4 to quench NCO, suppressing formation of CO from the secondary reaction. Unfortunately, SiH_4 also reacts with CN. Using literature rate constants available at the time, we showed using kinetic modeling that the dependence of CO yield on reagent SiH_4 concentration was consistent with direct CO formation from channel (7b). Subsequent measurements by Macdonald et al, however, showed $k_8 = 2.1 \times 10^{-10} \text{ cm}^3 \text{ molecule}^{-1} \text{ s}^{-1}$, about a factor of three greater than previous values.⁹ This substantially complicates the modeling, and reduces our confidence in our previous work, forcing us to consider an alternate approach.

The essential difficulty of the above approach is that SiH_4 reacts with both CN and NCO. Ideally, one would like to add a reagent that removes NCO, quenching the secondary reaction, but does not react with CN. In fact, NO is a nearly ideal choice:



Of course, this approach will not work if we are detecting CO formation, because NCO+NO produces CO. We can, however, use labeled $^{15}\text{N}^{18}\text{O}$ to remove NCO, and then, without spectroscopic interference, probe unlabeled NO formation from reaction (7b). By using this approach combined with kinetic modeling, we have conclusively shown that channel (7b) is in fact real, with only minor contributions from the secondary reaction. We estimate $\phi_{7b} = 0.20 \pm 0.02$ over the temperature range 296-475 K.

References

1. J.A. Miller, S.J. Klippenstein, and P. Glarborg, *Comb. Flame* **135**, 357 (2003).
2. J.P. Meyer and J.F. Hershberger, *J. Phys. Chem B* **109**, 8363 (2005).
3. I.V. Tokmakov, L.V. Moskaleva, D.V. Paschenko, and M.C. Lin, *J. Phys. Chem. A* **107**, 1066 (2003).
4. L. Vereecken, R. Sumathy, S.A. Carl, and J. Peeters, *Chem. Phys. Lett.* **344**, 400 (2001).
5. U. Eickhoff and T. Temps, *Phys. Chem. Chem. Phys.* **1**, 243 (1999).
6. J.D. Adamson, J.D. DeSain, R.F. Curl, and G.P. Glass, *J. Phys. Chem. A* **101**, 874 (1997).
7. M.F. Witinski, M. Ortiz-Suarez, and H.F. Davis, *J. Chem. Phys.* **124**, 94307 (2006).
8. K.T. Rim, J.F. Hershberger, *J. Phys. Chem. A*, **103**, 3721 (1999).
9. Y. Gao, R.G. Macdonald, *J. Phys. Chem. A*, **107** 4625 (2003).

Publications acknowledging DOE support (2006-present)

1. "Ab Initio Study of the HCCO+NO₂ Reaction", J.P. Meyer and J.F. Hershberger, *Chem. Phys.* **325**, 545 (2006).
2. "Kinetics of the OH+HCNO Reaction", W. Feng, J.P. Meyer, and J.F. Hershberger, *J. Phys. Chem. A* **110**, 4458 (2006).
3. "Kinetics of the CN+HCNO Reaction", W. Feng and J.F. Hershberger, *J. Phys. Chem. A* **110**, 12184 (2006).
4. "Kinetics of the NCO+HCNO Reaction", W. Feng and J.F. Hershberger, *J. Phys. Chem. A* **111**, 3831 (2007).
5. "Kinetics of the O+HCNO Reaction", W. Feng and J.F. Hershberger, *J. Phys. Chem. A* **111**, 10654 (2007).
6. "Theoretical Study of the Reaction of O(³P) with HCNO", W. Feng and J.F. Hershberger, *Chem. Phys. Lett.* **457**, 307 (2008).
7. "Kinetics of Reactions of CN with chlorinated Methanes", V. Samant and J.F. Hershberger, *Chem. Phys. Lett.* **460**, 64 (2008).
8. "A Re-investigation of the Branching Ratio of the CN + O₂ Reaction", W. Feng and J.F. Hershberger, *J. Phys. Chem. A*, accepted.

Breakthrough Design and Implementation of Electronic and Vibrational Many-Body Theories

So Hirata (principal investigator: DE-FG02-04ER15621)

Quantum Theory Project and The Center for Macromolecular Science and Engineering,
Departments of Chemistry and Physics, University of Florida, Gainesville, FL 32611

hirata@qtp.ufl.edu

Program Scope

Predictive chemical computing requires hierarchical many-body methods of increasing accuracy for both electronic and vibrational problems. Such hierarchies are established, at least conceptually, as configuration-interaction (CI), many-body perturbation (PT), and coupled-cluster (CC) methods for electrons and for vibrations, which all converge at the exact limit with increasing rank of a hierarchical series. These methods can generate results of which the convergence with respect to various parameters of calculations can be demonstrated and which can be predictive in the absence of experimental information.

The progress in these methods and their wide use are, however, hindered by (1) the immense complexity and cost of designing and implementing some of the high-rank members of the hierarchical methods and by (2) the extremely slow convergence of electronic energies and wave functions with respect to one-electron basis set sizes, which is compounded with the high-rank polynomial or even factorial molecular size dependence of the computational cost of these methods.

The overarching goal of our research is to address both difficulties for electrons and vibrations. We will eradicate the first difficulty for electrons by developing a computerized symbolic algebra system that completely automates the mathematical derivations of electron-correlation methods and their implementation. For vibrations, the vibrational SCF (VSCF) and CI (VCI) codes will be developed in the general-order algorithm that is applicable to polyatomic molecules and allows us to include anharmonicity and vibrational mode-mode couplings to any desired extent. We address the second difficulty by radically departing from the conventional Gaussian basis set and introduce a new hierarchy of converging electron-correlation methods with completely flexible but rational (e.g., satisfying asymptotic decay and cusp conditions) basis functions such as numerical basis functions on interlocking multicenter quadrature grids and explicit r_{12} (inter-electronic distance) dependent basis functions. They, when combined with high-rank electron-correlation methods, can in fact achieve the exact solutions of the Schrödinger equation.

Recent Progress

Significant progress has been made in the last year. Capitalizing upon the developments made in the previous year,^{9,12} we have implemented⁶ complete explicitly correlated coupled-cluster methods including up to connected quadruple excitation operator, namely, F12-CCSDT and F12-CCSDTQ for the first time. Together with the F12-CCSD method reported by us,⁹ these methods form a hierarchy of systematic approximations that are most rapidly converging toward the exact solutions of the Schrödinger equations of general polyatomic molecules. In Ref. 6, we have demonstrated that a combination of these methods can predict the exact eigenvalue solutions of the Schrödinger equation of small polyatomic molecules such as hydrogen fluoride and water within a few kcal/mol without invoking statistical treatments or empirical extrapolations. While one is rarely interested in total energies, our ability to compute them with such high accuracy will have a great impact on all areas of chemistry and on some of biology and physics in which predictive chemical computing is essential.

We have also extended electronic and vibrational many-body methods to solids. In Ref. 5, we applied rigorous electron-correlation treatments such as second-order Møller–Plesset (MP2) and CC singles and doubles (CCSD) as well as perturbative triples [CCSD(T)] to energies, structures, and phonon dispersions as well as phonon densities of solid hydrogen fluoride. Our linear-scaling, localized-basis scheme underlying this application is only loosely coupled with the periodic boundary conditions and can obtain the frequencies of the phonons that lift the periodic symmetry. Furthermore, not only harmonic frequen-

cies but also anharmonic frequencies of infrared- and/or Raman-active phonons have been obtained by *vibrational* MP2 in the two-mode coupling and the Γ approximations (see below) to provide accurate predictions. We have also introduced⁴ a new approximation that brings about one to two orders of magnitude speedup in the MP2 crystalline orbital (CO) method for energies and quasi-particle energy bands.

We have performed chemical applications of vibrational many-body methods on 7 key species of hydrocarbon combustion, interstellar, and/or atmospheric chemistry³ as well as on the guanine-cytosine base pair.¹ The latter application has shed light on the nature of vibrational energy dissipation in base pairs (and hydrogen-bonded complexes in general) as a DNA photoprotection mechanism.

Since the 2008 DOE Research Meeting (CPIMS), six (6) papers²⁻⁷ have been published and one more¹ is under review for publication. In total, twenty-eight (28) publications²⁻²⁹ have resulted from this grant in 2006–09. In 2008–09, the PI has been an invited speaker at fifteen (15) conferences and universities. The PI has also been selected to receive National Science Foundation’s CAREER Award and his students working on the DOE project have won two best poster awards, a best contributed lecture award, a Japan Society for Promotion of Science fellowship, a dissertation award, and an alumni fellowship. The PI has also been invited to contribute reviews or perspectives to *Annual Reports of Computational Chemistry*, *Physical Chemistry Chemical Physics*, and two books.

Higher-order explicitly correlated CC methods.^{2,6} Efficient computer codes for the explicitly correlated CC (R12- or F12-CC) methods with up to triple (F12-CCSDT) and quadruple excitations (F12-CCSDTQ), which take account of the spin, Abelian point-group, and index-permutation symmetries and are based on complete diagrammatic equations,¹² have been implemented with the aid of the computerized symbolic algebra SMITH. Together with the explicitly correlated CCSD (F12-CCSD) method reported earlier,⁹ they form a hierarchy of systematic approximations (F12-CCSD, F12-CCSDT, F12-CCSDTQ) that converge very rapidly toward the exact solutions of the polyatomic Schrödinger equations with respect to both the highest excitation rank and basis-set size. Using the Slater-type function $1 - \exp(-\eta r_{12})$ as a correlation function, a F12-CC method can provide the aug-cc-pV5Z-quality results of the conventional CC method of the same excitation rank using only the aug-cc-pVTZ basis set. Combining these F12-CC methods with the grid-based, numerical Hartree-Fock equation solver,¹⁵ the exact solutions (eigenvalues) of the Schrödinger equations of neon, boron hydride, hydrogen fluoride, and water at their equilibrium geometries have been obtained as -128.9377 ± 0.0004 , -25.2892 ± 0.0002 , -100.459 ± 0.001 , and $-76.437 \pm 0.003 E_h$, respectively, without resorting to complete-basis-set extrapolations. These absolute total energies or the corresponding correlation energies agree within the quoted uncertainty with the accurate, nonrelativistic, Born-Oppenheimer values derived experimentally and/or computationally.

This and the previous related work^{9,12} have been the focus of our review on explicitly correlated CC methods that is to be published in *Annual Reports of Computational Chemistry*.²

CC and MP2 study of energies, structures, and phonons of solid hydrogen fluoride.⁵ With the binary-interaction method,⁷ we have optimized the geometry and obtained the phonon dispersion curves of solid hydrogen fluoride at the CCSD/aug-cc-pVDZ and BSSE-corrected MP2/aug-cc-pVTZ levels. The predicted geometries have been in quantitative agreement with the diffraction data. The calculated frequencies of the infrared- and/or Raman-active phonons do not agree with the observed, with the largest errors exceeding a few hundred cm^{-1} (Fig. 1). The errors are not due to the electronic

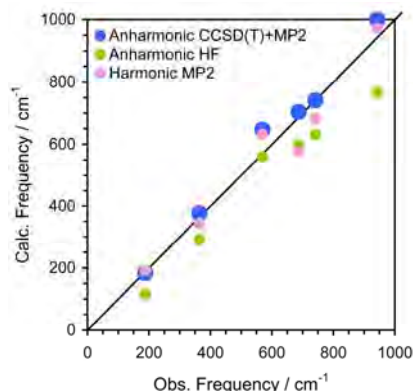


Fig.1 Calculated and observed phonon frequencies of solid hydrogen fluoride.

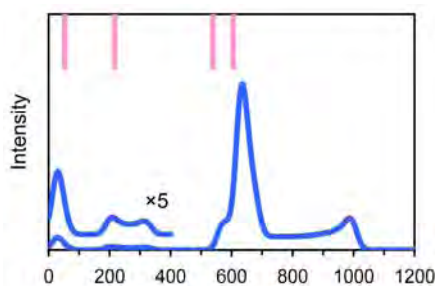


Fig. 2 Calculated hydrogen-amplitude-weighted density of states (blue) and observed peak positions (red) of inelastic neutron scattering from solid hydrogen fluoride

structure treatment, but are caused by strong anharmonicity in the potential energy surfaces of this hydrogen-bonded solid. When we perform a vibrational MP2 calculation in the Γ approximation using the potential energy surface scanned by the binary-interaction method, vastly improved agreement is achieved between the first-principles theory and experiments (**Fig. 1**). The bands in the observed inelastic neutron scattering from solid hydrogen fluoride have also been straightforwardly assignable to the peaks in the hydrogen-amplitude-weighted phonon density of states (harmonic) (**Fig. 2**).

Efficient Brillouin-zone integrations in MP2 calculations for extended systems of one-dimensional periodicity.⁴ The validity and accuracy of various ways of drastically reducing the number of k -points in the Brillouin zone integrations occurring in MP2 calculations of one-dimensional solids has been investigated. The most promising approximation can recover correlation energies of polyethylene and polyacetylene within 1% of converged values at less than a tenth of usual computational cost. The quasi-particle energy bands have also been reproduced quantitatively with the same approximation (**Fig. 3**). In the most drastic approximation, in which only one zone-center k -point (Γ point) in the BZ is sampled (the Γ approximation), the correlation energies are recovered within 10% of the converged values with a speedup by a factor of 80–100.

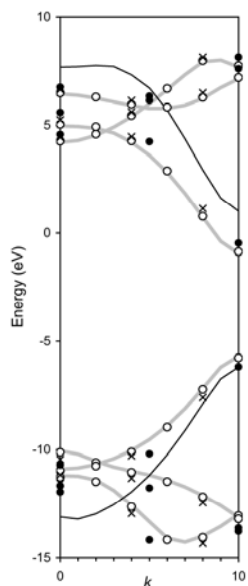


Fig. 3 The MP2/6-31G* quasi-particle energy bands of polyacetylene. The grey curves: exact; the open circles, the crosses, the filled circles: approximations. The thin dark curves are the HF/6-31G* conduction and valence bands.

Anharmonic vibrational frequencies and vibrationally averaged structures of key species in hydrocarbon combustion.³ A general scheme to predict anharmonic vibrational frequencies and vibrationally averaged structures and rotational constants of molecules is proposed with applications to HCO^+ , HCO , HNO , HOO , HOO^- , CH_3^+ , and CH_3 . A combination of CCSD, CCSD with a second-order perturbation correction in the space of triples and in the space of triples and quadruples, and a correlation-consistent basis set series has been employed to achieve the complete-correlation, complete-basis-set limits of the potential energy surfaces of these species near equilibrium geometries. A new representation of potential energy surfaces that combines two existing representations, namely, a fourth-order Taylor expansion and numerical values on a rectilinear grid, has been proposed and shown to yield accurate frequencies, when combined with vibrational general-order configuration-interaction method. The mean absolute deviation in the predicted frequencies is 11 cm^{-1} .

First-principles quantum anharmonic dynamics simulations on the guanine-cytosine base pair.¹ The origin of extremely broad features in the $2800\text{--}3800\text{-cm}^{-1}$ region of the infrared spectrum of the guanine-cytosine (GC) base pair remains a mystery. Unraveling this is crucial in understanding the ultrafast relaxation (< 100 femtoseconds) of the NH stretching vibrational energy that is believed to help protect DNA against a UV damage. We have carried out a full 81 dimensional quantum anharmonic vibrational calculations

combined with *ab initio* potential energy surface to study the spectrum and dynamics of the GC base pair. A strong vibrational resonance among fundamental tones of intermolecular NH stretching modes (red-shifted by hydrogen bonds) and various overtones and combination tones of fingerprint modes is shown to play a vital role in the manifestation of the observed phenomena.

Future Plans

Important extensions of the F12-CC methods include combined F12-CC and perturbation theories, relativistic F12-CC, the introduction of an explicit three-particle function or F123-CC methods, and the treatment of ionization and electron-attachment energies. The combinations of the F12-CC methods with the vibrational many-body methods as well as the binary-interaction method for molecular clusters and crystals are being examined. The latter methods are being extended to covalently bonded macromolecules. The k -point downsampling will be applied to CCSD for polymers. The validity of the Born–Oppenheimer approximation between low- and high-frequency vibrations is being tested along with the accuracy of its diagonal corrections.

Submitted Publications of DOE Sponsored Research

1. K. Yagi, H. Karasawa, S. Hirata, and K. Hirao, *ChemPhysChem* (submitted, 2009), "First-principles quantum vibrational simulations of the guanine-cytosine base pair."

References to Publications of DOE Sponsored Research (2006–Present)

2. **Invited review:** T. Shiozaki, E. F. Valeev, and S. Hirata, *Annual Reports of Computational Chemistry* (in press, 2009), "Explicitly correlated coupled-cluster methods."
3. M. Keçeli, T. Shiozaki, K. Yagi, and S. Hirata, *Molecular Physics* [Schaefer Special Issue] (in press, 2009), "Anharmonic vibrational frequencies and vibrationally-averaged structures of key species in hydrocarbon combustion: HCO⁺, HCO, HNO, HOO, HOO⁻, CH₃⁺, and CH₃."
4. T. Shimazaki and S. Hirata, *International Journal of Quantum Chemistry* [Harris Special Issue] (in press, 2009), "On the Brillouin-zone integrations in second-order many-body perturbation calculations for extended systems of one-dimensional periodicity"
5. O. Sode, M. Keçeli, S. Hirata, and K. Yagi, *International Journal of Quantum Chemistry* [Hirao Special Issue] (in press, 2009), "Coupled-cluster and many-body perturbation study of energies, structures, and phonon dispersions of solid hydrogen fluoride."
6. T. Shiozaki, M. Kamiya, S. Hirata, and E. F. Valeev, *The Journal of Chemical Physics* **130**, 054101 (2009) (10 pages), "Higher-order explicitly correlated coupled-cluster methods."
7. S. Hirata, *The Journal of Chemical Physics* **129**, 204104 (2008) (11 pages), "Fast electron-correlation methods for molecular crystals: An application to the α , β_1 , and β_2 modifications of solid formic acid."
8. **Invited article:** S. Hirata and K. Yagi, *Chemical Physics Letters* **464**, 123–134 (2008) [a Frontiers article], "Predictive electronic and vibrational many-body methods for molecules and macromolecules."
9. T. Shiozaki, M. Kamiya, S. Hirata and E. F. Valeev, *The Journal Chemical Physics (Communications)* **129**, 071101 (2008) (4 pages), "Explicitly correlated coupled-cluster singles and doubles method based on complete diagrammatic equations."
10. **Invited book chapter:** S. Hirata, P.-D. Fan, T. Shiozaki, and Y. Shigeta, *Radiation Induced Molecular Phenomena in Nucleic Acid: A Comprehensive Theoretical and Experimental Analysis* edited by Jerzy Leszczynski and Manoj Shukla (Springer, 2008), "Single-reference methods for excited states in molecules and polymers."
11. S. Hirata, K. Yagi, S. A. Perera, S. Yamazaki, and K. Hirao, *The Journal of Chemical Physics* **128**, 214305 (2008) (9 pages), "Anharmonic vibrational frequencies and vibrationally averaged structures and nuclear magnetic resonance parameters of FHF⁺."
12. **Invited article:** T. Shiozaki, M. Kamiya, S. Hirata, and E. F. Valeev, *Physical Chemistry Chemical Physics* **10**, 3358–3370 (2008) [in the issue on "Explicit-R12 correlation methods and local correlation methods"], "Equations of explicitly-correlated coupled-cluster methods."
13. K. Yagi, S. Hirata, and K. Hirao, *Physical Chemistry Chemical Physics* **10**, 1781–1788 (2008), "Vibrational quasi-degenerate perturbation theory: Application to Fermi resonances in CO₂, H₂CO, and C₆H₆."
14. M. Kamiya, S. Hirata, and M. Valeev, *The Journal of Chemical Physics* **128**, 074103 (2008) (11 pages), "Fast electron correlation methods for molecular clusters without basis set superposition errors."
15. T. Shiozaki and S. Hirata, *Physical Review A (Rapid Communications)* **76**, 040503(R) (2007) (4 pages), "Grid-based numerical Hartree–Fock solutions of polyatomic molecules."
16. K. Yagi, S. Hirata, and K. Hirao, *The Journal of Chemical Physics* **127**, 034111 (2007) (7 pages), "Efficient configuration selection scheme for vibrational second-order perturbation theory."
17. T. Shiozaki, K. Hirao, and S. Hirata, *The Journal of Chemical Physics* **126**, 244106 (2007) (11 pages), "Second- and third-order triples and quadruples corrections to coupled-cluster singles and doubles in the ground and excited states."
18. M. Kamiya and S. Hirata, *The Journal of Chemical Physics* **126**, 134112 (2007) (10 pages), "Higher-order equation-of-motion coupled-cluster methods for electron attachment."
19. P.-D. Fan, M. Kamiya, and S. Hirata, *The Journal of Chemical Theory and Computation* **3**, 1036–1046 (2007), "Active-space equation-of-motion coupled-cluster methods through quadruple excitations for excited, ionized, and electron-attached states."
20. V. Rodriguez-Garcia, S. Hirata, K. Yagi, K. Hirao, T. Taketsugu, I. Schweigert, and M. Tasumi, *The Journal of Chemical Physics* **126**, 124303 (2007) (6 pages), "Fermi resonance in CO₂: A combined electronic coupled-cluster and vibrational configuration-interaction prediction."
21. K. Yagi, S. Hirata, and K. Hirao, *Theoretical Chemistry Accounts* **118**, 681–691 (2007) [Fraga special issue], "Multiresolution potential energy surfaces for vibrational state calculations."
22. S. Hirata, T. Yanai, R. J. Harrison, M. Kamiya, and P.-D. Fan, *The Journal of Chemical Physics* **126**, 024104 (2007), "High-order electron-correlation methods with scalar relativistic and spin-orbit corrections."
23. **Invited article:** S. Hirata, *Journal of Physics: Conference Series* **46**, 249–253 (2006), "Automated symbolic algebra for quantum chemistry."
24. M. Kamiya and S. Hirata, *The Journal of Chemical Physics* **125**, 074111 (2006), "Higher-order equation-of-motion coupled-cluster methods for ionization processes."
25. **Invited article:** S. Hirata, *Theoretical Chemistry Accounts* **116**, 2–17 (2006) [a part of the special issue "New Perspective in Theoretical Chemistry"], "Symbolic algebra in quantum chemistry."
26. V. Rodriguez-Garcia, K. Yagi, K. Hirao, S. Iwata, and S. Hirata, *The Journal of Chemical Physics* **125**, 014109 (2006) [selected as an article in *Virtual Journal of Biological Physics Research*, July 15 (2006)], "Franck–Condon factors based on anharmonic vibrational wave functions of polyatomic molecules."
27. **Invited article:** Y. Shao, *et al. Physical Chemistry Chemical Physics* **8**, 3172–3191 (2006), "Advances in methods and algorithms in a modern quantum chemistry package."
28. P.-D. Fan and S. Hirata, *The Journal of Chemical Physics* **124**, 104108 (2006), "Active-space coupled-cluster methods through connected quadruple excitations."
29. Y. Shigeta, K. Hirao, and S. Hirata, *Physical Review A (Rapid Communications)* **73**, 010502(R) (2006), "Exact-exchange time-dependent density-functional theory with the frequency-dependent kernel."
30. **Invited article:** P. Piecuch, S. Hirata, K. Kowalski, P.-D. Fan, and T. L. Windus, *International Journal of Quantum Chemistry* **106**, 79–97 (2006), "Automated derivation and parallel computer implementation of renormalized and active-space coupled-cluster methods."

Non-Born–Oppenheimer Molecular Dynamics and Theoretical Kinetics

Ahren W. Jasper

Combustion Research Facility, Sandia National Laboratories

Livermore, CA 94551-0969

ajasper@sandia.gov

I. Program Scope

Excited electronic states play an important role in a wide variety of chemical processes, including intersystem crossing, photodissociation, internal conversion, charge transfer, etc. The term “non-Born–Oppenheimer” (NBO) may be generally applied to these systems to emphasize the idea that the Born–Oppenheimer separation of the nuclear and electronic time scales breaks down and that electronic surfaces other than the ground adiabatic surface play a key role in the dynamics. The focus of this program is the development and validation of theoretical methods for making quantitative predictions of the dynamics of NBO processes using molecular dynamics (MD) simulations, transition state theory (TST), and quantum chemical calculations.

Molecular dynamics. In NBO MD simulations, classical mechanics is used to describe the nuclear motion, and electronic transitions between the various electronic states are modeled via potential energy surface switches. Surface hopping (SH) methods model these electronic transitions as instantaneous hops, whereas in decay of mixing (DM) methods the surface switches occur over some finite time. Several variants of the SH and DM methods have been proposed, and these methods differ from one another in the details of how they treat electronic state coherence, electronic-nuclear energy transfer, and electronic state tunneling. We have recently summarized our previous systematic tests of several NBO MD methods against accurate quantum mechanical calculations for a series of triatomic two-state systems.ⁱ The best NBO MD methods predict branching ratios and product rovibrational energy distributions for these model systems with errors of only ~25%. The computational cost of the NBO MD methods is similar to that of single surface MD, and these validated methods may be readily applied to polyatomic systems.

A major goal of this project is the development, application, and validation of NBO MD for polyatomic systems. We are also developing strategies for using direct molecular dynamics simulations to compute energy transfer parameters for use in master equation calculations.

Transition state theory. Another major goal of this project is the characterization of the kinetics of elementary reactions relevant to combustion systems. In these studies, accurate rate coefficients are obtained using a combination of variable reaction coordinate TST for barrierless reactions, variational rigid rotor–harmonic oscillator TST for finite barrier reactions, master equation calculations, and high level ab initio calculations.

Quantum chemistry. MD and TST calculations require efficient methods for generating a potential energy surface (and its gradient for MD) for each electronic state over a wide range of nuclear configurations. One strategy is to generate these surfaces “on-the-fly” by making direct calls to electronic structure programs. Direct NBO MD and TST calculations for small and moderate-sized systems are being carried out, and methods for improving the efficiency of these calculations are being developed. The large number of potential energy surface evaluations required often limits the accuracy of the electronic structure method that may be used in direct dynamics calculations. Another strategy is to use a semiautomated surface fitting algorithm. Several such methods have been proposed.ⁱⁱ In general, these methods use the results of previous nearby electronic structure calculations to make interpolated surface fits and require significantly fewer electronic structure calculations than full direct dynamics. A major goal of this project is the development of semiautomated surface fitting strategies for NBO MD and TST applications.

II. Recent Progress

A. Non-Born–Oppenheimer Molecular Dynamics Simulations

Several improvements to the SH and DM methods have been made via systematic comparisons with accurate quantum mechanical results. In one such study, the accuracy of NBO MD methods for simulating deep quantum systems (i.e., systems with large electronic state energy gaps) was reevaluated in light of new quantum mechanical calculationsⁱⁱⁱ of the photodissociation of the Na^+FH van der Waals complex. Previously, it was suggested that the accuracy of the NBO MD methods would degrade for systems with large energy gaps. In our work and in contrast to the conclusion arrived at in an earlier study,^{iv} the semiclassical trajectory methods were shown to be qualitatively accurate for the Na^+FH system, thus validating their use for deep quantum systems. In the course of this study, a stochastic decoherence (SD) model was introduced into the SH method and shown to improve the quantitative agreement of the NBO MD and quantum mechanical calculations.

In other work and in collaboration with D. G. Truhlar and R. Valero, the nonadiabatic photodissociation of HBr was modeled using several semiclassical trajectory methods. The calculated branching fractions for the $\text{H} + \text{Br}(^2\text{P}_{3/2})$ and $\text{H} + \text{Br}(^2\text{P}_{1/2})$ products were found to be in good agreement with experimental measurements and with the results of more complete theoretical treatments over a wide range of photon energies. The photodissociation of NH_3 was also studied, and the results of the NBO MD calculations were compared with the experimental results of Crim and co-workers.^v The NBO MD calculations adequately reproduced several of the experimental trends, but a discrepancy remains in the predicted and measured dynamics of NH_3 photoexcited into a vibrationally and electronically excited state with one quantum in the antisymmetric stretch.

B. Theoretical Chemical Kinetics

In collaboration with S. J. Klippenstein and L. B. Harding, several detailed kinetics studies of elementary reactions have been made. Rate coefficients for the $\text{CH}_3 + \text{OH}$ bimolecular reaction and for the decomposition of methanol were obtained over a wide range of temperatures and pressures. Of particular importance in this study was the use of variable reaction coordinate TST to describe the kinetics of the barrierless bimolecular channels, the use of a two transition state model for the important product channel $^1\text{CH}_2 + \text{H}_2\text{O}$, and the use of accurate experimental thermochemistry obtained from the Active Thermochemical Tables of B. Ruscic and co-workers. Comparisons were made with available experimental and previous theoretical results, including a companion set of shock tube studies carried out by N. K. Srinivasan and J. V. Michael.^{vi} The predicted results were found to be in excellent agreement with the experimental results. The major products of the bimolecular reaction at 1 atm are CH_3OH (for $T < 1200$ K) and $\text{CH}_2 + \text{H}_2\text{O}$ (for $T > 1200$ K). The $\text{H} + \text{CH}_2\text{OH}$ product channel is also important at high temperatures. The major product channels for CH_3OH decomposition are $\text{CH}_3 + \text{OH}$ and $\text{CH}_2 + \text{H}_2\text{O}$, formed in a ratio of 4:1.

In the course of the methanol study, we computed several rate coefficients useful for describing the secondary chemistry of methanol decomposition. Rates for the $^3\text{CH}_2 + \text{OH}$, $^3\text{CH}_2 + ^3\text{CH}_2$, and $^3\text{CH}_2 + \text{CH}_3$ barrierless association reactions were obtained; these reactions were previously not well characterized. The use of the theoretical rate coefficients for these reactions qualitatively improved the accuracy of the reaction mechanism used to model the long-time behavior of the OH absorption profiles measured in the shock tube experiments of N. K. Srinivasan and J. V. Michael.^{vi}

A theoretical study of the kinetics of the $\text{CH}_3 + \text{HO}_2$ bimolecular reaction was performed at temperatures and pressures relevant to combustion. The predicted product branching ratio of 4:1 for the $\text{CH}_3\text{O} + \text{OH}$ and $\text{CH}_4 + \text{O}_2$ products was found to be in close agreement with revised values recently obtained in two modeling studies. Earlier theoretical and modeling studies predicted significantly more formation of $\text{CH}_3\text{O} + \text{OH}$. This result has important consequences for understanding ignition in hydrocarbon combustion at high pressures. Rate coefficients for the $\text{CH}_3\text{O} + \text{OH}$ reaction and for CH_3OOH decomposition were also presented.

Direct molecular dynamics calculations were carried out to compute energy transfer parameters for use in master equation calculations for the $\text{CH}_4 \rightleftharpoons \text{CH}_3 + \text{H}$ reaction in Helium. A computationally efficient strategy (requiring only several hundreds of trajectories) was developed and employed, and the resulting values of the exponential-down-model energy transfer parameters ($\alpha = 110 (T/300 \text{ K})^{0.81} \text{ cm}^{-1}$) are in good agreement with previous empirically adjusted values. The results of master equation calculations using the calculated values for α , along with previous ab initio calculations of the properties of the reactants and the barrierless kinetics, are in good agreement with experimental results.^{vii} This work provides a complete first-principles characterization of the temperature and pressure dependent kinetics for this simple single-well system.

III. Future Work

A. Non-Born–Oppenheimer Molecular Dynamics Simulations

A major component of future work will involve the application of the improved NBO MD methods discussed above to polyatomic systems. Trajectory studies of the photodissociation of the series of vinyl halides will be used to interpret the experimental results of D. L. Osborn and co-workers^{vi} and others. The doublet-quartet crossing of C_{2v} HCN_2 has been implicated as an important dynamical bottleneck in the $\text{CH} + \text{N}_2$ reaction, and, while this process has been studied previously using quantum chemistry and TST calculations,^{vii} future NBO MD trajectory studies will further characterize the dynamics at this crossing. We will also study intersystem crossing in the spin-orbit coupled systems formed from the addition of oxygen atoms to hydrocarbons.

Direct NBO MD simulations of the photodissociation of HNCN and the $\text{H} + \text{NCO}$ reaction will also be performed. Upon photoexcitation to the S_1 state, HNCN may decay by one of several pathways: adiabatically to form $^1\text{NH} + \text{CO}$, nonadiabatically to $^3\text{NH} + \text{CO}$ via a spin-forbidden transition to the T_1 state, or nonadiabatically via a transition to the S_0 state to form either $\text{H} + \text{NCO}$ or $^1\text{NH} + \text{CO}$. This system has been well characterized experimentally^{viii} and provides an excellent test case for the validation and development of the NBO MD methods.

B. Theoretical Chemical Kinetics

We will continue to use established theoretical kinetics techniques to make quantitative predictions for important elementary combustion reactions. Several applications are underway in collaboration with theorists and experimentalists T. Selby and D. L. Osborn (phenyl + propargyl), J. Zádor and C. A. Taatjes (propene + OH), and R. S. Tranter (dioxane decomposition and diacetyl decomposition). The close collaboration of theoretical calculations and experimental measurements drives the development of new and more accurate theoretical models as well as extends and clarifies the experimental results.

We will also study the applicability of TST to systems that are currently not well described by statistical theories. One such class of systems features spin-orbit split electronic states. We will study the effect of spin-orbit splitting on the kinetics of barrierless reactions by considering the reactions of halogen atoms with several hydrocarbon radicals. Barrierless abstraction reactions are also challenging to treat using TST. For these reactions, variable reaction coordinate TST is appropriate for characterizing the kinetics at low temperatures, but the assumptions involved in this approach are not suitable at higher temperatures where the reacting fragments are significantly distorted from their isolated geometries at the important dynamical bottlenecks. A two transition state approach will be applied to study these systems.

C. Quantum Chemistry

An important practical bottleneck for performing NBO MD simulations is the need for inexpensive and accurate potential energy surfaces and their couplings. Two strategies will be pursued

for obtaining potential energy surfaces in the NBO MD simulations. Direct dynamics methods will be developed based on single reference methods (DFT, MP2, etc) for spin-orbit coupled systems and multireference methods (CASPT2, etc) for valence coupled systems. Semiautomated surface fitting strategies will also be implemented. Schemes for modeling the coupling between the electronic surfaces will also be developed.

IV. References

- i. A. W. Jasper, S. Nangia, C. Zhu, and D. G. Truhlar, *Acc. Chem. Res.* **39**, 101 (2006).
- ii. See, e.g., O. Godsi, C. R. Evenhuis, and M. A. Collins, *J. Chem. Phys.* **125**, 104105 (2006). O. Tishchenko and D. G. Truhlar, *J. Chem. Theory Comput.* **3**, 938–948 (2007). R. Dawes, D. L. Thompson, Y. Guo, A. F. Wagner, and M. Minkoff, *J. Chem. Phys.* **126**, 184108 (2007).
- iii. S. Garashchuk and V. A. Rassolov, *Chem. Phys. Lett.* **446**, 395 (2007).
- iv. Y. Zeiri, G. Katz, R. Kosloff, M. S. Topaler, D. G. Truhlar, and J. C. Polanyi, *Chem. Phys. Lett.* **300**, 523 (1999).
- v. A. Bach, J. M. Hutchison, R. J. Holiday, and F. F. Crim, *J. Phys. Chem. A* **107**, 10490 (2003).
- vi. N. K. Srinivasan, M.-C. Su, and J. V. Michael, *J. Phys. Chem. A* **111**, 3951 (2007).
- vii. M. Brouard, M. T. Macpherson, and M. J. Pilling, *J. Phys. Chem.* **93**, 4047 (1989).
- viii. P. Zou, K. E. Strecker, J. Ramirez-Serrano, L. E. Jusinski, C. A. Taatjes, and D. L. Osborn, *Phys. Chem. Chem. Phys.* **10**, 713 (2008).
- ix. Q. Cui, K. Morokuma, J. M. Bowman, and S. J. Klippenstein, *J. Chem. Phys.* **110**, 9469 (1999).
- x. T. Droz-Georget, M. Zyrianov, H. Reisler, and D. W. Chandler, *Chem. Phys. Lett.* **276**, 316 (1997). H. L. Berghout, S. Hsieh, and F. F. Crim, *J. Chem. Phys.* **114**, 10835 (2001).

V. Publications and submitted journal articles supported by this project 2007-2009

1. A. W. Jasper, S. J. Klippenstein, L. B. Harding, and B. Ruscic, "Kinetics of the reaction of methyl radical with hydroxyl radical and methanol decomposition," *J. Phys. Chem. A* **111**, 3932 (2007). (James A. Miller Festschrift)
2. L. B. Harding, S. J. Klippenstein, and A. W. Jasper "Ab initio methods for reactive potential energy surfaces," *Phys. Chem. Chem. Phys.* **9**, 4055 (2007).
3. A. W. Jasper, S. J. Klippenstein, and L. B. Harding, "Secondary kinetics of methanol decomposition," *J. Phys. Chem. A* **111**, 8699 (2007).
4. A. W. Jasper and D. G. Truhlar, "Non-Born–Oppenheimer molecular dynamics study of the photodissociation of Na⁺FH," *J. Chem. Phys.* **127**, 194306 (2007).
5. N. K. Srinivasan, M.-C. Su, J. V. Michael, A. W. Jasper, S. J. Klippenstein, and L. B. Harding, "The thermal decomposition of CF₃ and the reaction of CF₂ + OH → CF₂O + H," *J. Chem. Phys. A* **112**, 31 (2008).
6. R. Valero, D. G. Truhlar, and A. W. Jasper, "Photodissociation of HBr: Semiclassical trajectory study using adiabatic states derived from a spin-coupled diabatic transformation," *J. Phys. Chem. A* **112**, 5756 (2008).
7. A. W. Jasper, S. J. Klippenstein, and L. B. Harding, "Theoretical rate coefficients for the reaction of methyl radical with hydroperoxyl radical and for methylhydroperoxide decomposition," *Proc. Combust. Inst.* **32**, 279 (2009).
8. D. Bonhommeau, R. Valero, D. G. Truhlar, and A. W. Jasper, "Coupled-surface investigation of the photodissociation of NH₃(A): Effect of exciting the symmetric and antisymmetric stretching modes," *J. Chem. Phys.*, submitted.
9. A. W. Jasper and J. A. Miller, "Collisional energy transfer in unimolecular reactions: Direct classical trajectories for CH₄ ⇌ CH₃ + H in Helium," *J. Phys. Chem. A*, submitted.

Probing the Reaction Dynamics of Hydrogen-Deficient Hydrocarbon Molecules and Radical Intermediates via Crossed Molecular Beams

Ralf I. Kaiser

Department of Chemistry, University of Hawai'i at Manoa, Honolulu, HI 96822

ralfk@hawaii.edu

1. Program Scope

The major goals of this project are to explore experimentally in crossed molecular beams experiments the reaction dynamics and potential energy surfaces (PESs) of hydrocarbon molecules and their corresponding radical species which are relevant to combustion processes. The reactions are initiated under single collision conditions by crossing two supersonic reactant beams containing radicals and/or closed shell species under a well-defined collision energy and intersection angle. By recording angular resolved time of flight (TOF) spectra, we obtain information on the reaction products, intermediates involved, on branching ratios for competing reaction channels, on the energetics of the reaction(s), and on the underlying reaction mechanisms. These data are of crucial importance to understand the formation of carbonaceous nanostructures as well as of polycyclic aromatic hydrocarbons and their hydrogen deficient precursors in combustion flames. Chemical reaction networks modeling the formation of polycyclic aromatic hydrocarbons (PAHs) in combustion flames imply that the phenyl radical, C_6H_5 , presents one of the most important transient species involved in the formation of PAHs. The crucial steps of these reaction models are believed to be hydrogen abstraction – unsaturated hydrocarbon addition sequences. All chemical networks concur that reactions of the phenyl radical with acetylene, for instance, initiates the PAH synthesis via an addition of phenyl to the carbon-carbon triple bond. Due to the central role of the phenyl – unsaturated hydrocarbon reactions, the kinetics of these systems have been well-established up to temperatures of a couple of thousand Kelvin. Theoretical studies of these benchmark systems predicted the initial formation of adducts which either decomposed back to the reactants or fragmented to the reactant molecules such as phenylacetylene and styrene, for instance. Nevertheless, despite the central role of the phenyl – unsaturated hydrocarbon reactions as the trigger to PAH formation, the theoretical investigations have never been verified experimentally under single collision conditions and, consequently, the nature of the true reaction products of these elementary reactions have remained elusive so far. Therefore, we carry out a systematic research program to investigate the reaction dynamics of phenyl radicals with unsaturated hydrocarbons.

2. Recent Progress

First, we have expanded our studies of phenyl radical reactions from the *acetylene*, *ethylene*, *methylacetylene*, *allene*, *benzene*, *propylene*, and *molecular oxygen* systems and conducted crossed beams experiments of phenyl radicals with four C_4H_6 isomers: *1,3-butadiene*, *1,2-butadiene*, 1-butyne, and 2-butyne together with (partially) deuterated molecules. These investigations explore the important $C_{10}H_{11}$ and $C_{10}H_{10}$ potential energy surfaces- among them dihydronaphthalene; theoretical investigations of these surfaces are conducted in collaboration with Prof. Alexander Mebel (FIU); those systems indicated in italics have been published, are in press, or have been submitted for publication; the data analysis of the 1-butyne and 2-butyne is in progress and will be released in one single paper. Upcoming reactions of phenyl radicals with diacetylene and vinylacetylene conclude the study of phenyl radical reactions with unsaturated hydrocarbons at *high collision energies* from 80 to 185 kJmol^{-1} . Second, in collaboration with Dr. Musa Ahmed

(ALS, Berkeley), we conducted experiments at the Chemical Dynamics Beamline to extract the ionization potential and thermodynamics properties of important hydrogen-deficient combustion intermediates. These are resonantly stabilized free radicals (C_nH_3 ; $n=4-6$), highly unsaturated, unstable hydrocarbon intermediates (C_nH_4 ; $n=4-6$), and oxygen- as well as nitrogen terminated carbon clusters (C_nO and C_nN ; $n = 2-11$). These data are currently being analyzed.

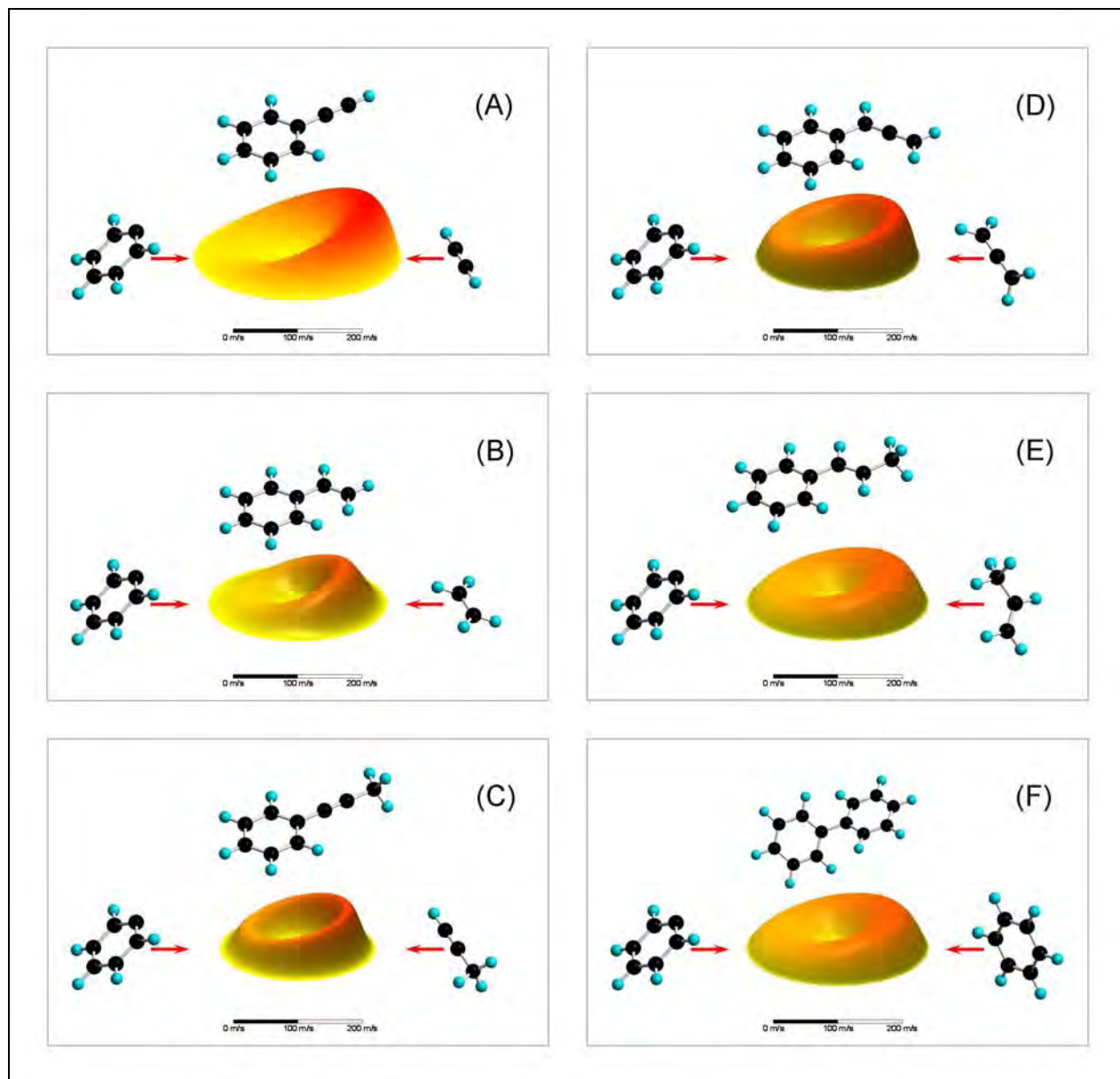


Figure 1: Selected center-of-mass velocity contour flux maps for the reaction of phenyl radicals (left; 0°) with acetylene (A), ethylene (B), methylacetylene (C), allene (D), propylene (E), and D6-benzene (F) to form phenylacetylene (A), styrene (B), 1-phenylmethylacetylene (C), phenylallene (D), 1,- and 3-phenylpropylene (E), and diphenyl (F) (right; 180°). The colors connect data points with an identical flux and range from red (highest flux) to yellow (lowest flux). The units of axis are given in ms^{-1} .

3. Future Plans

We aim to explore the energetics, chemical dynamics, potential energy surfaces (PESs), and reactions of key representatives of resonantly stabilized free radicals (RSFRs) and of aromatic radicals (ARs) under single collision conditions: the propargyl (C_3H_3 ; X^2B_1) and the phenyl radical (C_6H_5 ; X^2A_1), respectively. Our studies will focus on three key systems. Firstly, we explore the hitherto poorly understood stability (unimolecular decomposition) of one of the key RSFRs: the propargyl radical (C_3H_3 ; X^2B_1). This is achieved by accessing various regions of the C_3H_3 surface through the bimolecular radical–neutral reaction of methylidyne (CH ; $X^2\Pi$) with acetylene (C_2H_2 ; $X^1\Sigma_g^+$) and the atom–radical reaction of ground state carbon atoms ($C(^3P_j)$) with vinyl radicals (C_2H_3 ; X^2A'). Secondly, we attempt elucidating the collision energy-dependent dynamics of the reaction of the resonantly stabilized propargyl radical with another propargyl radical leading via chemically activated C_6H_6 intermediates to C_6H_5 isomers like the phenyl radical and/or acyclic isomers. So far, this reaction has never been studied under true single collision conditions, and the detection of the phenyl radical as an aromatic ring product of the propargyl radical self reaction under collision-less conditions has remained elusive so far. Thirdly, we investigate the chemical dynamics of the phenyl radical (C_6H_5 ; X^2A_1) under single collision conditions with selected hydrocarbons at *lower* collision energies to form individual PAHs with indene and naphthalene cores and their acyclic isomers utilizing a low velocity (photolytic) phenyl radical source. These studies access the important C_9H_x ($x=8,10$) and $C_{10}H_x$ ($x=6,8,10$) PESs, among them crucial combustion intermediates with indene and naphthalene cores. As of to date, no experiment has been conducted in which an individual PAH(like) species is formed via a *bimolecular gas phase reaction* under single collision conditions in crossed beams experiments.

4. Acknowledgements

This work was supported by US Department of Energy (Basic Energy Sciences; DE-FG02-03-ER15411).

5. Publications Acknowledging DE-FG02-03-ER15411 (2007-2009)

X. Gu, Y. Guo, F. Zhang, A. M. Mebel, R.I. Kaiser, *A Crossed Molecular Beams Study of the Reaction of Dicarbon Molecules with Benzene*, Chem. Phys. Lett 436, 7-14 (2007).

X. Gu, Y. Guo, R.I. Kaiser, *Mass Spectra of the 2,4-Pentadiynylidyne (C_5H ; $X^2\Pi$) and the 2,4-Pentadiynyl-1 Radicals ($n-C_5H_3$; X^2B_1)*. Int. J. Mass Spectrometry 261, 100-107 (2007).

Y. Guo, X. Gu, F. Zhang, A.M. Mebel, R.I. Kaiser, *A Crossed Molecular Beams Study on the Formation of Hexenediynyl Radicals ($H_2CCCCCCH$; C_6H_3 (X^2A')) via Reactions of Tricarbon Molecules, $C_3(X^1\Sigma_g^+)$, with Allene (H_2CCCH_2 ; X^1A_1) and Methylacetylene (CH_3CCH ; X^1A_1)*. PCCP 9, 1972 – 1979 (2007).

X. Gu, Y. Guo, F. Zhang, A.M. Mebel, R.I. Kaiser, *A Crossed Molecular Beams Study on the Formation and Energetics of the Resonantly Stabilized *i*- C_4H_3 radical, $H_2CCCH(X^2A')$, together with its Isotopomers*. Chemical Physics 335, 95-108 (2007).

A.M. Mebel, G.S. Kim, V.V. Kislov, R.I. Kaiser, *The Reaction of Tricarbon with Acetylene: An Ab Initio/RRKM Study of the Potential Energy Surface and Product Branching Ratios*. JPCA 111, 6704-6712 (2007).

- X. Gu, Y. Guo, F. Zhang, A.M. Mebel, R.I. Kaiser, *Unimolecular Decomposition of Chemically Activated Singlet and Triplet D3-Methyldiacetylene*. Chem. Phys. Lett. 444, 220-225 (2007).
- X. Gu, F. Zhang, Y. Guo, R.I. Kaiser, *A Crossed Molecular Beam Study on the Formation of Phenylacetylene from Phenyl Radicals and Acetylene*. Angew. Chemie Int. Edition 46, 6866-6869 (2007).
- F. Zhang, X. Gu, Y. Guo, R. I. Kaiser, *Reaction Dynamics on the Formation of Styrene (C₆H₅C₂H₃) - A Crossed Molecular Beam Study of the Reaction of Phenyl Radicals (C₆H₅) with Ethylene (C₂H₄)*, J. Organic Chem. 72, 7597-7604 (2007).
- X. Gu, F. Zhang, R.I. Kaiser, *A Crossed Beam Reaction of the Phenyl Radical, (C₆H₅, X²A₁) with Molecular Oxygen (O₂, X³Σ_g⁻): Observation of the Phenoxy Radical, (C₆H₅O, X²A')*. Chem. Phys. Lett. 448, 7-10 (2007).
- X. Gu, F. Zhang, Y. Guo, R. I. Kaiser, *Reaction Dynamics of Phenyl Radicals (C₆H₅, X²A₁) with Methylacetylene (CH₃CCH(X¹A₁)), Allene (H₂CCCH₂(X¹A₁)), and Their D4-Isotopomers*. J. Phys. Chem. A 111, 11450-11459 (2007).
- A. M. Mebel, V. V. Kislov, R. I. Kaiser, *Theoretical Studies of Potential Energy Surfaces and Product Branching Ratios for the Reactions of C₂ with Small Unsaturated Hydrocarbons (Acetylene, Ethylene, Methylacetylene, and Allene)*. in: Gas Phase Molecular Reaction and Photodissociation Dynamics, Editors: K.C. Lin and P.D. Kleiber, Transworld Research Network 2007, pp. 113-159
- X. Gu, Y. Guo, A.M. Mebel, R.I. Kaiser, *A Crossed Beams Investigation of the Reactions of Tricarbon Molecules, C₃(X¹Σ_g⁺), with Acetylene, C₂H₂(X¹Σ_g⁺), Ethylene, C₂H₄(X¹A_g), and Benzene C₆H₆(X¹A_{1g})*. Chem. Phys. Lett. 449, 44-52 (2007).
- X. Gu, R.I. Kaiser, A.M. Mebel, *Chemistry of Energetically Activated Cumulenes - From Allene (H₂CCCH₂) to Hexapentaene (H₂CCCCCCH₂)*. Invited Review. Chem. Phys. Chem. 9, 350-369 (2008).
- F. Zhang, X. Gu, R.I. Kaiser, *Formation of the Diphenyl Molecule in the Crossed Beam Reaction of Phenyl Radicals with Benzene*. JCP 128, 084315/1-5(2008).
- F. Zhang, X. Gu, Y. Guo, R.I. Kaiser, *Reaction Dynamics of Phenyl Radicals (C₆H₅) with Propylene (CH₃CHCH₂) and Its Deuterated Isotopologues*. JPCA 112, 3284-3290 (2008).
- X. Gu, F. Zhang, R.I. Kaiser, *A Crossed Molecular Beam Study of the Phenyl Radical Reaction with 1,3-Butadiene and its Deuterated Isotopomers*. JPCA 113, 998-1006 (2009).
- X. Gu, R.I. Kaiser, *Reaction Dynamics of Phenyl Radicals in Extreme Environments - A Crossed Molecular Beam Study*. Invited Account. Acc. Chem. Res. 42, 290-302 (2009).
- R.I. Kaiser, *Reaction Dynamics of Carbon-Centered Radicals in Extreme Environments Studied by the Crossed Molecular Beams Technique*. in: Carbon-Centered Radicals: Structure, Dynamics and Reactivity. Malcolm D. E. Forbes, Editor, Wiley (in press 2009)
- X. Gu, F. Zhang, A.M. Mebel, R.I. Kaiser, *Probing the C₁₀H₁₁ and C₁₀H₁₀ potential energy surfaces under single collisions - A crossed beams reaction of phenyl radicals with 1,2-butadiene*. JPCA (submitted 2009).

DYNAMICAL ANALYSIS OF HIGHLY EXCITED MOLECULAR SPECTRA

Michael E. Kellman

Department of Chemistry, University of Oregon, Eugene, OR 97403

kellman@uoregon.edu

PROGRAM SCOPE:

Highly excited vibrational dynamics of small molecular species are crucial to understanding fundamental processes important for combustion systems. The goal of our program is to develop theoretical tools to understand spectra and dynamics of highly excited systems. It is clear that anharmonic effects lead to profound changes in the vibrational dynamics of molecules when nonlinearities can no longer be treated as perturbative effects. The standard picture of anharmonic normal modes breaks down. We emphasize particularly the role of bifurcations and the “birth of new modes in bifurcations from the low energy normal modes”. References to numerous examples can be found in a recent review [1]. We use bifurcation analysis of semiclassical versions of the effective Hamiltonians used by spectroscopists to fit complex experimental spectra. Observable phenomena associated with bifurcations such as changes in spectral patterns have been predicted and observed. A future long-range focus is systems approaching and undergoing chemical reactivity, including intramolecular (isomerization) reactions.

RECENT PROGRESS: The progress described in the next two headings is in collaboration with postdoctoral associates Aniruddha Chakraborty and Vivian Tyng, respectively.

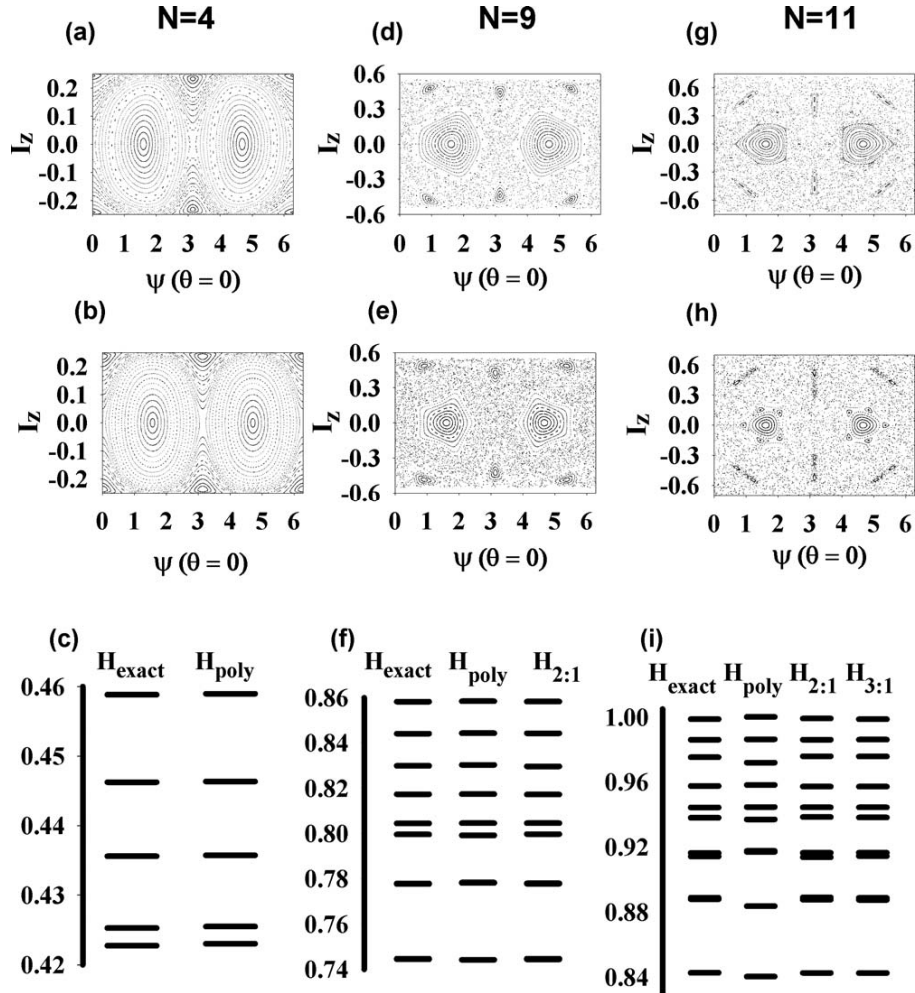
Spectroscopic Hamiltonians for polyad breaking spectra. Spectroscopic fitting Hamiltonians are enormously useful as a tool to analyze molecular spectra. The fitting Hamiltonian is an effective quantum matrix Hamiltonian. Virtually all spectroscopic fitting Hamiltonians to date invoke the “polyad approximation” of a conserved total vibrational quantum number. However, at sufficiently high energy, the polyad approximation must fail. Spectra of systems that break the polyad action, time-dependent transport in these systems, and the representation of these phenomena with a generalized effective fitting Hamiltonian are mostly unexplored areas. Recently we have been working to construct an effective spectroscopic Hamiltonian to encompass the polyad breakdown.

We are testing a simple generalized effective Hamiltonian capable of encompassing the major dynamical and spectral effects of the polyad breakdown, using a model system of two coupled anharmonic oscillators as test “data”. Our first results have been published as a Communication to the Journal of Chemical Physics [3]. We demonstrate that a generalized effective Hamiltonian successfully describes the polyad breaking by successively adding a very small number of additional resonance couplings. Each additional resonance coupling induces bifurcations to give new low-order periodic orbits,

incompatible with the original polyad number, that reorganize the surrounding phase space structure into large-scale resonance zones. In a quantum system, the spectrum shows clear signatures of these new structures that should be observable in experiments.

It is noteworthy that these fits have been obtained using Hamiltonians constructed with shift operators defined to have the simple action of harmonic raising and lowering operators, even up to dissociation energy $E = 1.0$. This extends the practice of spectroscopic fitting at low energy – it has not been necessary to use operators adapted to the special characteristics of the anharmonic oscillator system, here coupled Morse oscillators. In this sense we have performed a “fair” test of the effective Hamiltonian, even though we knew the nature of the exact model system. The success of ordinary harmonic raising and lowering operators bodes well for fitting real systems without the need for too much prior knowledge.

FIG. 1. Surfaces of section and spectra of H_{exact} and various effective Hamiltonians indicated in the figure. Top row: surfaces of section of exact system; middle row: of effective Hamiltonian; bottom row: spectra of exact Hamiltonian and of fits. Axes of surface of section are $I_z = n_1 - n_2$ and conjugate angle $\psi = 1/2(\phi_1 - \phi_2)$ at fixed $\theta = 1/2(\phi_1 + \phi_2) = 0$. The columns are labeled by polyad numbers of the polyad effective Hamiltonian H_{polyad} . For the middle and right columns, the polyad number is not actually a good approximate constant.

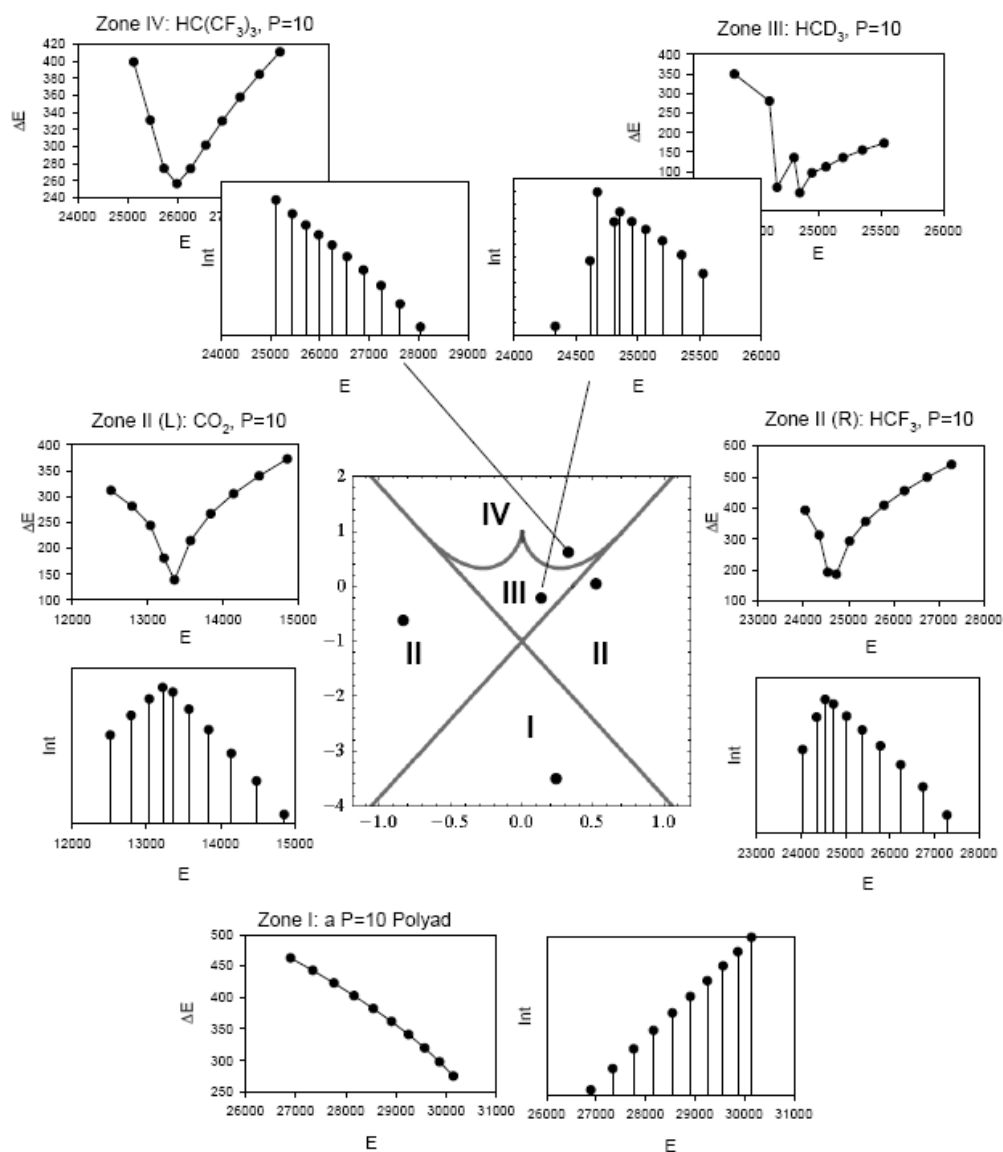


Spectral intensity patterns. It is well established that nonlinear effects of anharmonicity and coupling of normal modes have a profound effect on molecular vibrational dynamics. Perhaps the first outstanding example was the normal to local mode transition in the stretch modes of molecules with light atoms, notably O-H and C-H bonds in molecules such as H₂O and benzene. An extended line of theoretical development from our group employs ideas of classical phase space structure and bifurcations. Experimental access to these nonlinear effects has been achieved, relying mostly on energy level patterns, with use of effective spectroscopic fitting Hamiltonians to make the link between experiment and dynamics. In contrast, there has been far less systematic use of intensity patterns as a probe of phase space bifurcations. We are making an effort to begin to fill this gap. We have been using a simple model of intensities to investigate patterns in the spectra of systems with an anharmonic resonance, specifically the standard 2:1 Fermi resonance, relying on earlier systematic investigations in our group of phase space structure in resonant systems.

Resonances lead to bifurcations in phase space in which new modes are born in phase space out of normal modes or even erupt "out of nothing" (in saddle-node bifurcations). The phase space structure of the polyads for a given form of the resonance Hamiltonian can be mapped onto the catastrophe map, a kind of phase diagram. Each zone of the map corresponds to a distinct polyad phase space structure. Distinct energy level patterns are found for each zone. The patterns consist of well-marked indicators of phase space separatrix structure when differences in energy levels of adjacent levels in phase space are plotted.

Our strategy for extending this to intensity patterns is the following. In the 2:1 Fermi resonance system, the catastrophe map has 4 zones, corresponding to four types of phase space structure. In an earlier paper (J. Svitak, Z. Li, J. Rose, and M.E. Kellman, *J. Chem. Phys.* 102, 4340-54 (1995)) we examined energy patterns of molecules with a 2:1 Fermi resonance between the local stretch and bend of a C-H stretch. One molecule we examined was (CF₃)₃CH with polyads in all 4 zones. We also looked at energy patterns for different molecular exemplars for each of the 4 zones, using an example for each zone that brings out the pattern for that zone most clearly.

We follow a parallel path, now comparing intensity patterns to energy patterns. The four zones differ basically in the phase space structure at and surrounding the zero order C-H local mode stretch overtone. Our "minimal" intensity model is based on the not unreasonable supposition that dipole strength is carried by the C-H local mode stretch overtone. Intensity is then spread among the eigenstates because of mixing of zero order states by the Fermi resonance coupling. The expectation is that the different phase space structure surrounding the C-H stretch will be reflected in the intensity pattern. This is confirmed by explicit calculation, as seen in the diagram below.



Recent publications (in print, in press 2007-2009) related to DOE supported research:

1. M.E. Kellman and V. Tyng, "The Dance of Molecules: New Dynamical Perspectives on Highly Excited Molecular Vibrations", *Accounts of Chemical Research* 40, 243-250 (2007).
2. V. Tyng and M.E. Kellman, "Spectral Anomaly, Moment of Inertia Backbending, and Bifurcations", *J. Chem. Phys.* 041101, 1-4 (2007).
3. A. Chakraborty and M.E. Kellman, "Effective Hamiltonian for Chaotic Coupled Oscillators", *J. Chem. Phys.* 129, 171104 (2008).
4. V. Tyng and M.E. Kellman, "Catastrophe Map and the Role of Individual Resonances in C_2H_2 Bending Dynamics", in press, *J. Chem. Phys.*
5. V. Tyng and M.E. Kellman "Critical Points Bifurcation Analysis of High- ℓ Bending Dynamics in Acetylene", to be submitted, *J. Chem. Phys.*

Theory and Modeling of Small Scale Processes in Turbulent Flow

Alan R. Kerstein
Combustion Research Facility
Sandia National Laboratories
Livermore, CA 94551-0969
Email: arkerst@sandia.gov

PROJECT SCOPE

The need for a computational model of turbulent reacting flow that encompasses a wide range of length scales and associated phenomena is gaining increasing recognition with the DOE Office of Science as well as in the broader scientific community. Specifically, a multi-scale modeling paradigm is needed that is distinctly different from the usual sub-grid parameterization of phenomena not resolved on the computational mesh. To achieve the fidelity required to address current scientific, technological, and societal needs in an affordable computation, some reduced yet physically sound representation of diverse nonlinear processes and their unsteady interactions over the relevant range of scales is required. Meeting this requirement is recognized as one of the premier grand challenges of combustion science.

The primary focus of this project is development and demonstration of a computational modeling approach that is responsive to this challenge, and use of the methodology for scientific discovery and fundamental explanation of turbulent combustion phenomena. The strategy that is adopted for time-accurate advancement of unsteady interactions while affordably spanning the needed range of scales is to employ a novel mesh geometry and associated physical modeling.

The mesh geometry is analogous to the ‘pencil’ algorithm long used for 3D Cartesian domain decomposition. View the flow domain as a collection of pencils, i.e., 1D stacks of cubic control volumes (CVs). Advancement involves a sub-step within each stack, followed by a stack-coupling sub-step. The length scale associated with stack coupling is the CV edge length M . The new idea is spatial refinement of each stack along its axis so that its spatial resolution scale W is much smaller than M , and the intra-stack advancement time step is commensurately smaller.

If W is the resolution needed to capture small scale processes, then applying this refinement in one direction rather than all three requires order $(W/M)^2$ fewer mesh cells than full 3D refinement, where M is now the scale at which 3D motions are resolved. This offers the possibility of orders of magnitude cost reduction relative to 3D direct numerical simulation (DNS), thereby significantly broadening the scope of applicability of high-fidelity numerical prediction of turbulent combustion.

The trade-off is that the scale range from W to M is resolved in only one direction (1D) on any given stack. (The method involves interpenetrating stacks in all coordinate directions, but no 3D coupling below scale M .) A longstanding focus of this project has been the development of a physically based mathematical approach for capturing turbulent motions in 1D. A solution to this problem that captures the relevant phenomenology while obeying applicable conservation laws has been found within the framework of map-based advection. The familiar (in other contexts) numerical technique of conservative Lagrangian displacement of an entire flow field, i.e., a map of the entire flow onto itself, has been recast into a map-based method that emulates turbulent motions in 1D (and also has uses in higher-dimensional simulation).

During this project, two map-based 1D formulations have been developed, the Linear-Eddy

Model (LEM), which predicts mixing under prescribed flow conditions but does not predict the flow *per se*, and One-Dimensional Turbulence (ODT), that is a predictive model of turbulence and turbulent combustion in its own right and is also well suited for use as the 1D flow representation with the 3D framework described above. In fact, ODT is a complete enough flow representation so that the coupled array of ODT instantiations can in principle simulate the complete flow with no higher-level advancement operation. Development and demonstration of a novel flow simulation strategy, Autonomous Microscale Evolution (AME), based on this concept is a major goal of planned future efforts.

RECENT PROGRESS

One focus of recent efforts has been the development of algorithmic and physical modeling capabilities that are of immediate use as well as contributing to the anticipated future completion of a full-featured AME formulation. Recent and ongoing algorithm efforts, some of which are subsequently elaborated, include: 1. Domain decomposition within individual LEM and ODT objects. 2. The recently demonstrated [5] coupling of an array of ODT objects to simulate 3D constant-property flow, albeit in this instance requiring a higher-level advancement operation, hence differing from the AME concept. 3. The coupling of a complementary array of LEM objects that evolve reactive scalars based on turbulent motions prescribed by the ODT array or by a conventional flow solver implemented at scale M (coarse mesh). 4. Implementation of all of the above on an adaptive mesh, enabling efficient pseudo-compressible coupling of ODT objects (which eliminates the need for higher-level advancement) and extension to non-Cartesian meshes.

AME is an inherently scalable approach for simulation on leadership-class platforms because the time step for coupling of 1D objects at the coarse scale M is much larger than the time step for fine-grained (scale W) processes. Distribution of the 1D objects among processors is straightforward and communication requirements are manageable. However, there could be a need for a further degree of partitioning. ODT is a complete enough flow model so that the needed fidelity might be achieved using coarser 3D (scale M) resolution than is typically needed in large-eddy simulations with less complete small-scale treatments. Therefore thousands of ODT objects could suffice for many applications, but future computers will have orders of magnitude more processors. Accordingly, a spatial decomposition algorithm applicable to the individual 1D objects has been formulated. A preliminary numerical implementation targeted on LEM (because it is a simpler model) demonstrated the feasibility of the approach [A]. In fact, it provides a substantial speedup even for serial implementation because the map-based model is a nonlocal formulation that imposes a global (domain-size-dependent) constraint on the time step for advancement of small-scale processes. Domain decomposition eases this constraint.

A coupled array of uniform-mesh LEM objects has been developed for constant-property flow and its extension to variable-property flow has begun [B]. Adaptive-mesh implementation will begin later this year. For some applications, the needed flow information will be provided by Reynolds-average Navier-Stokes (RANS) steady-state flow solvers, where the LEM advancement will introduce the unsteadiness and spatial resolution needed for physically sound mixing simulation.

Nuclear-driven astrophysical flames and detonations present unique challenges because they occur at turbulence intensities that would extinguish terrestrial flames. No experiment or simulation had probed the relevant conditions until a recent LEM study [7]. A regime transition was found that required five decades of scale resolution to identify, presently achievable for turbulent combustion only with LEM. Patches of homogeneous mixture occurred sporadically between more variable regions. Post-processing of LEM mixture states using a compressible

solver showed that these conditions can induce a natural analog of multi-stage detonation (igniter, primer, main charge). The astrophysical implication is that the ‘delayed detonation’ scenario for type-1A supernova explosion, which is dictated by observational data (Doppler measurements of explosion speed and spectral measurements of composition), can now be reconciled with a detailed physical picture of the deflagration-to-detonation transition. The newly identified deflagration regime implies a delayed detonation scenario is quantitatively consistent with observational constraints, unlike previous analyses based on terrestrially accessible deflagration phenomenology. Obtaining the first plausible physical picture consistent with observational constraints is an important step, yet calls for further investigation to verify the correctness of LEM predictions (see Future Work).

A key feature of ODT relative to LEM is the representation of important physical phenomena such as buoyant as well as shear forcing, radiative as well as conductive heat transfer, and immiscible fluids with interfacial surface tension. An obvious target for an efficient numerical simulation with these capabilities is geophysical flow. As a prelude to planned ODT simulations of stratiform clouds, an effort to simulate a laboratory analog of these clouds has begun. The experiment involved an opaque fluid layer atop a transparent layer, initially stable gravitationally but destabilized by radiant heating from below. The rate of the resulting mixing was dependent on whether the initial stabilization was imposed thermally or compositionally. Preliminary ODT results capture this heretofore unexplained dependence and demonstrate that the difference between thermal and solutal diffusivities is the underlying cause. This shows that ODT captures molecular transport sensitivities in this context, which is important because it enables benchmarking to this aqueous experiment as a basis for future application to clouds.

FUTURE WORK

As noted above, the overarching goal of planned efforts is the development of a full-featured high-fidelity AME formulation with the capability to simulate affordably a wider range of scientifically and technologically relevant combustion regimes than are accessible using DNS. Ongoing algorithm and code development addressing this as well as map-based 1D formulations that are narrower in scope is described in Recent Results. In addition, introduction of 1D gas dynamics into ODT will be undertaken to enable pseudo-compressible coupling of ODT objects. This coupling will rely on thermodynamic information provided by the complementary LEM reactive-scalar objects, which rely for their coupling on flow information provided by the ODT objects. Care is required to maintain consistency because LEM uses zero-Mach-number (uniform-pressure) thermodynamics while ODT is pseudo-compressible. (Greater thermodynamic generality is possible but the planned approach is best for initial proof of principle.)

A planned scientific focus is mixing and related phenomenology of turbulent flows with large density variations. A recent DNS study [C] reported an asymmetry of the mixing of heavy and light fluids, seemingly specific to the particular case (Rayleigh-Taylor flow, which is buoyancy driven), but in fact previously observed in an ODT study of shear-driven flow [D]. ODT of the Rayleigh-Taylor flow will be run to test, within the ODT framework, the generality of the asymmetric behavior and to investigate the strong-turbulence limits of some transitional behaviors observed in the DNS (which cannot affordably explore the limiting behaviors). This study will validate the ODT representation of flows with large density variations, which will support a planned ODT application to primary breakup of turbulent liquid jets. For this application, immiscible fluid phases with interfacial surface tension will be incorporated into ODT. This application is challenging due to the wide range of droplet sizes that are generated. An experimental study of primary breakup [E] yielded results consistent with the interpretation

that breakup ceases when the flow residence time exceeds the time scale for formation of a droplet as large as the jet width. This interpretation seems counterintuitive; ODT will be used to check the validity of this versus other possible interpretations.

Several turbulent combustion studies involving comparisons between LEM and DNS results are planned, both to validate and benchmark LEM and to use LEM to explore a wider parameter space than is accessible using DNS. Regimes to be investigated in this manner include premixed hydrogen flames, n-heptane combustion under compression-ignition conditions, and soot-radiation-turbulence interactions in an ethylene-air jet. DNS of the latter could not fully resolve thin soot layers. ODT will be used to test the sensitivity of results to spatial resolution of these layers.

The supernova study (see Recent Progress) indicated the importance of homogeneous patches predicted by the LEM simulations. There is indirect support for the realism of this intermittency property predicted by LEM, but this requires further attention. In particular, it is surprising that a model as simple as LEM would capture this subtle effect. The possibility that this implies an unexpectedly simple explanation of the effect will be investigated.

REFERENCES

- A. D. Murer, M.S. Thesis, ETH (2009).
- B. S. Sannan, A. Kerstein, and T. Weydahl, to appear in *Proc. Eur. Combust. Mtg.* (2009).
- C. D. Livescu and J. R. Ristorcelli, *J. Fluid Mech.* **605**, 145 (2008).
- D. Wm. T. Ashurst and A. R. Kerstein, *Phys. Fluids* **17**, 025105 (2005).
- E. P.-K. Wu and G. M. Faeth, *Phys. Fluids* **7**, 2915 (1995).

PUBLICATIONS SINCE 2007

1. J. R. Mayo and A. R. Kerstein, "Scaling of Huygens-Front Speedup in Weakly Random Media," *Phys. Lett. A* **372**, 5 (2007).
2. J. R. Mayo and A. R. Kerstein, "Fronts in Randomly Advected and Heterogeneous Media and Nonuniversality of Burgers Turbulence: Theory and Numerics," *Phys. Rev. E* **78**, 056307 (2008).
3. M. Oevermann, H. Schmidt, and A. R. Kerstein, "Investigation of Autoignition under Thermal Stratification using Linear-Eddy Modeling," *Combust. Flame* **155**, 370 (2008).
4. A. R. Kerstein, "ODT: Stochastic Simulation of Multi-Scale Dynamics," in *Interdisciplinary Aspects of Turbulence*, Springer Lecture Notes in Physics, eds. W. Hillebrandt and F. Kupka (Springer-Verlag, New York, 2009).
5. R. C. Schmidt, A. R. Kerstein, and R. J. McDermott, "ODTLES: A Multi-Scale Model for 3D Turbulent Flow Based on One-Dimensional Turbulence Modeling," *Comput. Methods Appl. Mech. Engrg.* (in press).
6. A. J. Ricks, J. C. Hewson, A. R. Kerstein, J. P. Gore, S. R. Tieszen, and Wm. T. Ashurst, "A Spatially Developing One-Dimensional Turbulence (ODT) Study of Soot and Enthalpy Evolution in Meter-Scale Buoyant Turbulent Flames," *Combust. Sci. Tech.* (submitted).
7. S. E. Woosley, A. R. Kerstein, V. Sankaran, and F. Roepke, "Type Ia Supernova: Calculations of Turbulent Flames Using the Linear Eddy Model," *Astrophys. J.* (submitted).
8. J. R. Schmidt, J. O. L. Wendt, and A. R. Kerstein, "Non-equilibrium Wall Deposition of Inertial Particles in Turbulent Flow," *J. Stat. Phys.* (submitted).

KINETICS OF COMBUSTION-RELATED PROCESSES AT HIGH TEMPERATURES

J. H. Kiefer

Department of Chemical Engineering

University of Illinois at Chicago
Chicago, IL 60607
(kiefer@uic.edu)

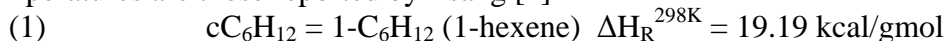
Program Scope

This program again involves the use of the shock tube with laser-schlieren (LS) and time-of-flight mass spectrometry (TOF), as diagnostics for the exploration of reaction rates and energy relaxation processes over a range of temperatures and pressures of particular interest in combustion. We are particularly interested in energy transfer and falloff in unimolecular reactions. This work includes considerable collaboration with R. S. Tranter, L.B. Harding and S J. Klippenstein at Argonne Nat'l Lab.

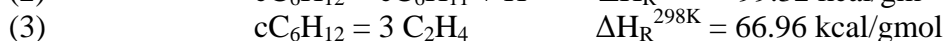
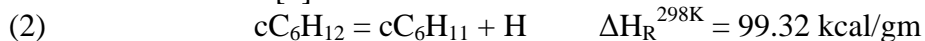
Cyclohexane and 1-Hexene Decomposition

The decomposition of cyclohexane (cC_6H_{12}) was examined using laser schlieren (LS) in 1500-2100 K and 50 to 200 torr using mixtures of 2, 4 and 10% cyclohexane in Kr.. The dissociation of 1-hexene, apparently the only product of cyclohexane dissociation [1], was also studied over 1200-1700 K for 50 torr and 200 torr using 2 and 3% 1-hexene in Kr.

The decomposition of cyclohexane has been extensively studied in the past and various decomposition channels have been proposed [2]. The most likely channels for the present high temperatures are those reported by Tsang [1]

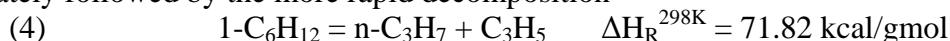


and by Braun-Unkhoff et al [3]



Channel (1), isomerization of cyclohexane to 1-hexene, was proposed by Tsang based on a GC product analysis of single pulse shock tube experiments and trends seen in other cycloalkanes [1]. Channel (2) and (3) were proposed by Braun-Unkhoff [3] to explain the production of H atoms in shock-tube H-atom ARAS studies and the large amounts of C_2H_4 found in GC analysis of single pulse shock tube experiments.

The LS Cyclohexane dissociation experiments were characterized by a large and sustained positive density gradient which is a clear indication of strongly endothermic secondary chemistry following initial cyclohexane dissociation. Cyclohexyl radical generated in (2) could dissociate further [4], but our theoretical [5] k_∞ for (2) is so much lower than the rate constant reported in ref. [3] that no contribution is expected from channel (2). Channel (3) is also ruled out since the channel is not expected theoretically; and no stable product like C_2H_4 can generate a sustained following density gradient. Channel (1) is thus decisively favored both by theory and experiment. This channel is immediately followed by the more rapid decomposition



This reaction and its accompanying chain processes now produce a density gradient of the required magnitude and duration. The theoretical basis of all this is illustrated in Fig. 1.

In support of the above, we have successfully modeled an H-atom ARAS profile reported in [3] using channels (1) and (4) with no contribution from (2) or (3).

1-Hexene dissociation (4) was also observed, and the derived rate constants were fit using RRKM theory using a restricted rotor Gorin model treatment for the bond-fission transition state. The optimum high pressure limit rate constant is a factor > 2 higher than the rate constant reported by Tsang [2]. This disagreement also is seen in the cyclohexane rates of Figs. 3,4, and is again probably a consequence of residual falloff and some temperature errors in Tsang's analysis.

A complete dissociation mechanism for 1-hexene was obtained by modeling and this mechanism was included in the cyclohexane decomposition mechanism. In cyclohexane only the initial rate of (1) was varied to accurately model all the density gradients. The model performs very well for all the higher pressure data (>100 torr), producing the curved profiles resulting from fast 1-hexene dissociation (see Fig. 2).

It is also possible, as is evident in Fig. 1, that cyclohexane can dissociate via a 'direct' reaction through unstabilized 1-C₆H₁₂



Channel (5) yields the same result as (1) and (4) combined but it changes the characteristics of the density gradient profile; the upward curvature exemplified in Fig. 2 is missing. Our latest experiments at extremely low pressures (~25 Torr) are somewhat better fit by (5) than the combination of (1) and (4), but this is not conclusive, mainly because the modeling is complicated by the likelihood of an unobservable incubation time. An RRKM model that fits the cyclohexane rates, Fig. 3, is constructed and its optimum k_∞ is found to be very close to a convincing theoretical calculation [2], as seen in Fig.4..

Dissociation of s-triazine

The three-body dissociation of 1,3,5-triazine (s-C₃H₃N₃ → 3HCN) has been observed in incident shock waves with the laser-schlieren technique. The experiments use 5% triazine/Kr and cover 1630-2350K, for 100-600 torr. These experiments show dissociation rates with strong falloff and a slight but fully expected pressure dependence. The dissociation is without secondary reaction save for a possible, but rather unlikely, contribution from the isomerization HCN → HNC. Electronic structure calculations of the transition-state properties (G3B3, HL1, E_o = 84.6kcal/mol) are used to construct an RRKM model whose fit to the rate measurements that suggests a < E>_{down} of 1200cm⁻¹. However, a seemingly better fit is achieved using the barrier of 81kcal/mol proposed by Dyakov, et al. (J. Phys. Chem. A **2007**, 9591). With this barrier k_∞ (s⁻¹) = 5.3x10¹⁶exp-86.6(kcal/mol)/RT, and the fit now accepts the more routine < E>_{down} = 126(T/298)^{0.9}. It seems the dissociation most probably occurs by the direct, one-step "triple" dissociation to 3 HCN. Vibrational relaxation of the triazine was also examined in 5 and 20% mixtures with Kr and over 770-1500K for pressures between 6 and 14 torr. Relaxation is very fast, with an inverse temperature dependence and P_{relax} rising from 100 to 200 nsec-atm over the full temperature range. Integrated gradients are in good accord with calculated total changes in density indicating an accurately single exponential relaxation.

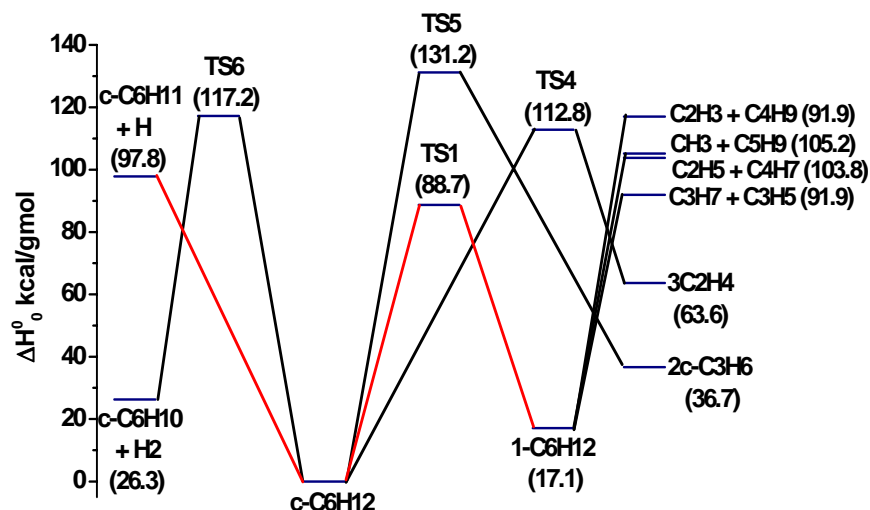
A separate investigation of relaxation in the related molecule pyrazine (500-1300 K, in 1 and 5% in Kr, between 13 and 66 torr) is included. Again relaxation is rapid, but here the temperature dependence seems more normal, the relaxation times decreasing with temperature.

References

- [1] W. Tsang. *Int. J. Chem. Kinet.* **10** (1978) 1119-1138.
- [2] B. Sirjean, P. A. Glaude, M. F. Ruiz-Lopez, R. Fournet. *J. Phys. Chem. A* **110** (2006) 12693-12704.
- [3] M. Braun-Unkhoff, C. Naumann, P. Frank, *Abstracts Papers Am. Chem. Soc.* **227** (2004) U1096.
- [4] I. Iwan, W. S. McGivern, J. A. Manion, W. Tsang. *Proc. 5th US Combust. Meeting, San Diego, CA* (2007).
- [5] L. B. Harding, Y. Georgievskii, S. J. Klippenstein, *J. Phys. Chem. A* **109** (2005) 4646-4656.
- [6] Y. A. Dyakov, A. M. Mebel, S. H. Lin, Y. T. Lee, C.-K. Ni, *J. Phys. Chem. A* (2007), **111** 9591.

Publications (two years)

- 1) "Decomposition of Acetaldehyde: Experiment and Theory", K. S. Gupte, J. H. Kiefer, R.S. Tranter, S. J. Klippenstein, and L.B. Harding, *Proc. Combust. Inst.* **31**, 167 (2007).
- 2) "Relaxation, Incubation, and Dissociation in CO₂", S. Saxena, J. H. Kiefer, and R. S. Tranter, *J. Phys. Chem. A*, **111**,3884-3890 (2007).
- 3) "Shock tube Study of Dissociation and Relaxation in 1,1-difluoroethane and Vinyl fluoride", H. Xu, J. H. Kiefer, R. Sivaramakrishnan, B. R. Giri and R. S. Tranter, *Phys. Chem. Chem. Phys.* **9**, 4164-4176 (2007).
- 4) "A Shock tube and Theory Study of the Dissociation of Acetone and Subsequent Recombination of Methyl Radicals", S. C. Saxena, J. H. Kiefer and S. J. Klippenstein, *Proc. Comb. Inst.* **32** 123-139 (2009),.
- 5) "Shock Tube Study of Relaxation in HCN" N. K. Srinivasan, K. S. Gupte and J. H. Kiefer, *J. Chem. Phys.* **129**, 074309 (2008).
- 6) "An Experimental and Theoretical High Temperature Kinetic Study of the Thermal Unimolecular Dissociation of Fluoroethane", R.S. Tranter, B. R. Giri, S. J. Klippenstein and J. H. Kiefer, *Phys. Chem. Chem. Phys.* **10**, 6266 - 6273., (2008),



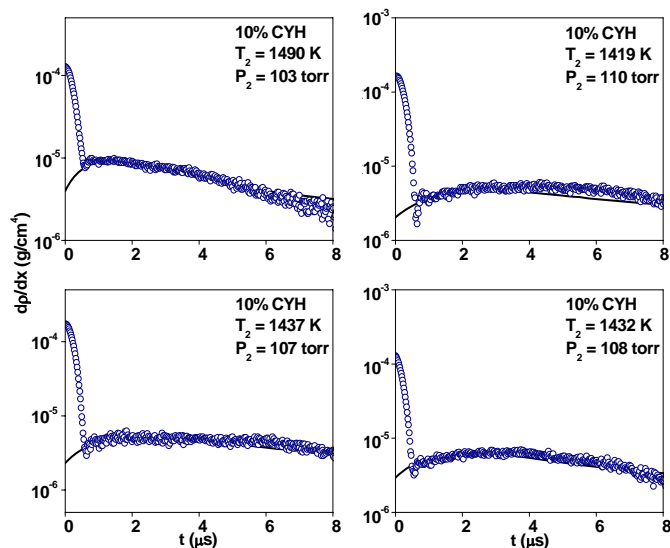


Figure 2: Semilog plots of curved density gradient profiles produced by pyrolysis of cyclohexane/Kr mixtures at the indicated temperatures and pressures. The open circles [○] are the measurements and the solid lines in these figures are simulations generated by the ‘two-step’ process of (1) and (2).

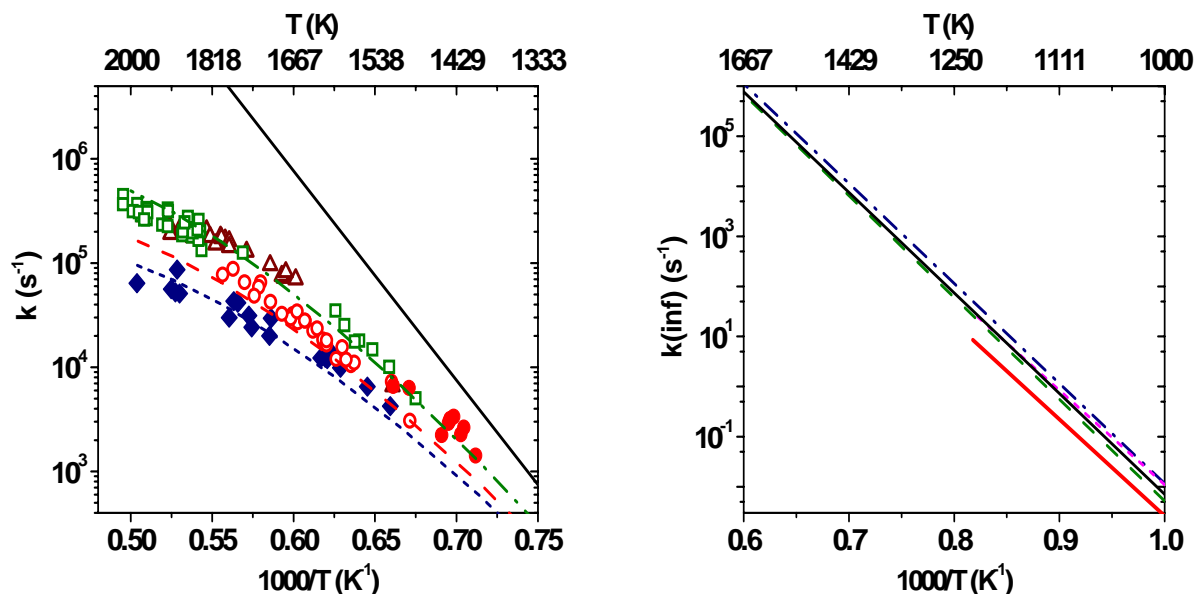


Figure 3: Arrhenius plot of rate constants for cyclohexane dissociation (1). The 25 [◆], 50 [○], 100 [●], 150 [△] and 200 [□] Torr groups contain experiments in the following ranges P=25: (16-35 Torr), P=50: (38-67 Torr), P=100: (97-123 Torr), P=150: (144-162 Torr), P=200: (185-233 Torr). The RRKM fall-off curves for 25 [---], 50 [---], 200 Torr [---] and, the high pressure limit [—] are also shown. Figure 4: Comparison with the literature high pressure limit rate constants for cyclohexane dissociation. [—]: Present work (RRKM); [—]: Tsang¹; [---]: T. C. Brown; K. D. King; T. T. Nguyen, *J. Phys. Chem.* **1986**, 90, (3), 419-24.; [---]: Sirjean, et al. Scheme 7 [2], [---]: Sirjean, et al. Scheme 8 [2].

THEORETICAL CHEMICAL KINETICS

Stephen J. Klippenstein
Chemical Sciences and Engineering Division
Argonne National Laboratory
Argonne, IL, 60439
sjk@anl.gov

Program Scope

The focus of this program is the theoretical estimation of the kinetics of elementary reactions of importance in combustion chemistry. The research involves a combination of *ab initio* quantum chemistry, variational transition state theory (TST), classical trajectories, and master equation simulations. The emphasis of our current applications is on (i) reactions of importance in soot formation, (ii) radical oxidation reactions, and (iii) NO_x chemistry. We are also interested in a detailed understanding of the limits of validity of and, where feasible, improvements in the accuracy of specific implementations of transition state theory. Detailed comparisons with experiment and with other theoretical methods are used to explore and improve the predictive properties of the transition state theory models. Dynamics simulations are performed as a means for testing the statistical assumptions, for exploring reaction mechanisms, and for generating theoretical estimates where statistical predictions are clearly inadequate. Master equation simulations are used to study the pressure dependence of the kinetics and to obtain phenomenological rate coefficients for use in kinetic modeling.

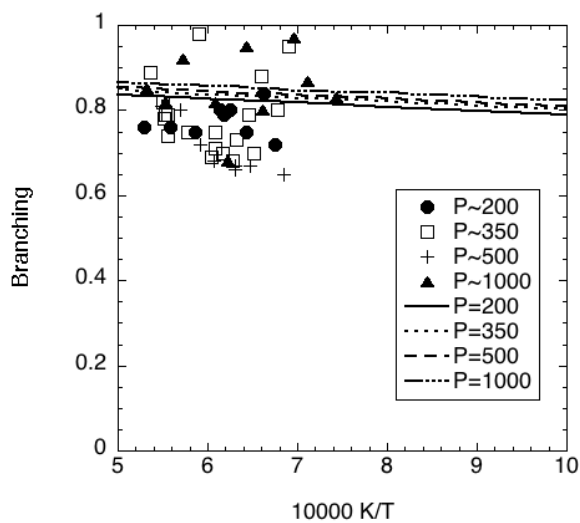
Recent Progress

Roaming Radical Reactions

In collaboration with Harding and Georgievskii we have been studying the dynamics and kinetics of roaming radical reactions. Simple bond fission in a closed shell molecule generally leads to two radicals. In some instances one of these radicals can abstract an atom or group from the other as they are departing. This roaming radical mechanism yields two closed shell molecules instead of two radicals.

We have developed an approach for determining the branching between the radical and molecular channels via rigid body trajectory simulations. We have applied this approach to the dissociations of H₂CO, CH₃CHO, and C₂H₄ employing analytic potentials developed by Harding. For H₂CO our predictions are in good agreement with photodissociation measurements of Suits and coworkers. Interestingly, these calculations predict quantized steps in the branching, which correlate with the vibrational frequencies of HCO in the roaming region.

There is some indication of such steps in the experimental data. For CH₃CHO, Michael has



recently made the first measurements of the branching to radicals versus molecules in a thermal dissociation. As illustrated in the Figure, our a priori predictions (lines) quantitatively reproduce these observations (symbols). These predictions are based on an analytical fit to a CASPT2/aug-cc-pvdz potential energy data combined with one-dimensional corrections for basis set extrapolation, geometry relaxation, and vibrational frequency changes along the minimum energy path. Our predictions for the roaming versus tight channel are also in agreement with the photodissociation measurements of Osborn and coworkers. We are in the process of applying these methods to a series of other dissociations including CH₃OOH and C₂H₆.

Finally, we have developed a TST based approach to estimating this branching. Calculations with this approach are in good agreement with trajectory simulations, thereby refuting the claim that the roaming dynamics is non-statistical in nature.

Soot Formation

In collaboration with Tranter and Kiefer we have studied the reaction of two phenyl radicals. Interestingly, the rate for the abstraction to form C₆H₄ + C₆H₆ is comparable to that for the addition to form biphenyl. This abstraction does not appear to have been considered in prior studies of this reaction. There is also some contribution from radical addition across the pi-bond of the ring. The recombination rate is predicted with direct variable reaction coordinate transition state theory employing CASPT2/cc-pvdz interaction energies. The properties of the abstraction and pi-addition saddle points are also studied at the CASPT2/cc-pvdz level. Basis set corrections are obtained on the basis of extrapolation of energies obtained with the cc-pvdz and cc-pvtz bases. The predicted rate coefficients are in reasonably satisfactory agreement with experiment.

Hydrocarbon Oxidation

In a collaborative study with Michael we have studied the thermal decomposition of C₂H₅OH. We have used ab initio transition state theory based master equation simulations to predict the rate coefficients for the three primary channels: (1) C₂H₅OH → C₂H₄ + H₂O, (2) → CH₃ + CH₂OH, and (3) → C₂H₅ + OH. The predicted rate coefficients, which differ in various significant ways from related prior calculations, are in quantitative agreement with the experimental data over a wide range of temperature. The predictions for channels (2) and (3) are based on our direct variable reaction coordinate transition state theory approach.

NO_x Chemistry

In another collaborative study with Michael we have studied the thermal decomposition of NH₂OH. Michael has observed the OH and O time profiles in the shock induced decomposition of the reactants. The OH profiles are primarily sensitive to the initial decomposition to NH₂ + OH. However, secondary sensitivities arise from subsequent reactions of these primary products. To aid in the interpretation and modeling of these profiles we have obtained *ab initio* transition state theory estimates of the rate constants for a number of reactions in this system, including NH₂OH ↔ NH₂ + OH decomposition, NH₂ + OH ↔ NH₃ + O, NH₂ + OH ↔ NH + H₂O, NH₂OH + OH → NH₂O + H₂O, NH₂OH + OH → NHOH + H₂O, NH₂OH + NH₂ → NH₂O + NH₃, NH₂OH + NH₂ → NHOH + NH₃, NH + OH → N + H₂O, NH + OH → H + HNO, NH + NH → HNNH, NH + NH → N + NH₂, NH + NH₂ → HNNH + H, and NH + NH₂ → N + NH₃.

Future Directions

We will continue our studies of aromatic ring formation, hydrocarbon oxidation, and NO_x chemistry. In collaboration with Wang (USC) we have begun an analysis of the reactions of ortho-benzyne with alkynes and alkenes. The reaction with C_4H_2 may provide a significant pathway to naphthalene. We will consider the reaction of CH_2 with various alkenes, which may be of importance to hydrocarbon growth processes. We are studying the branching between different bond fission channels in the decomposition of n-heptane, since this branching affects the ignition properties in this simple fuel surrogate. Our oxidation studies will now consider the decompositions of 1-butanol, as a model alcohol. In collaboration with Goldsmith we are considering the kinetics of O_2 reacting with $\text{C}_3\text{H}_6\text{OOH}$ species. This reaction serves as a prototype for the second oxygen addition, which is a key step in low temperature combustion.

DOE Supported Publications, 2007-Present

1. **Decomposition of Acetaldehyde: Experiment and Detailed Theory**, K. S. Gupte, J. H. Kiefer, R. S. Tranter, S. J. Klippenstein, and L. B. Harding, *Proc. Comb. Inst.*, **31**, 167-174 (2007).
2. **Oxidation Pathways in the Reaction of Diacetylene with OH Radicals**, Juan P. Senosiain, Stephen J. Klippenstein, and James A. Miller, *Proc. Comb. Inst.*, **31**, 185-192 (2007).
3. **On the Formation and Decomposition of C_7H_8** , Stephen J. Klippenstein, Lawrence B. Harding, and Yuri Georgievskii, *Proc. Comb. Inst.*, **31**, 221-229 (2007).
4. **Experimental and Theoretical Rate Constants for $\text{CH}_4 + \text{O}_2 \rightarrow \text{CH}_3 + \text{HO}_2$** , N. K. Srinivasan, J. V. Michael, L. B. Harding, and S. J. Klippenstein, *Comb. Flame*, **149**, 104-111 (2007).
5. **Direct Measurement and Theoretical Calculation of the Rate Coefficient for $\text{Cl} + \text{CH}_3$ from $T = 202 - 298 \text{ K}$** , James K. Parker, Walter A. Payne, Regina J. Cody, Fred L. Nesbitt, Louis J. Stief, Stephen J. Klippenstein, and Lawrence B. Harding, *J. Phys. Chem. A*, **111**, 1015-1023 (2007).
6. **On the Combination Reactions of Hydrogen Atoms with Resonance Stabilized Hydrocarbon Radicals**, Lawrence B. Harding, Stephen J. Klippenstein, and Yuri Georgievskii, *J. Phys. Chem. A*, **111**, 3789-3801 (2007). [Miller Festschrift issue]
7. **Strange Kinetics of the $\text{CN} + \text{C}_2\text{H}_6$ Reaction Explained**, Yuri Georgievskii and Stephen J. Klippenstein, *J. Phys. Chem. A*, **111**, 3802-3811 (2007). [Miller Festschrift issue]
8. **Kinetics of the Reaction of Methyl Radical with Hydroxyl Radical and Methanol Decomposition**, Ahren W. Jasper, Stephen J. Klippenstein, Lawrence B. Harding, and Branko Ruscic, *J. Phys. Chem. A*, **111**, 3932-3950 (2007). [Miller Festschrift issue]
9. **Measurements and Modeling of DO_2 Formation in the Reactions of C_2D_5 and C_3D_7 Radicals with O_2** , Edgar G. Estupinan, Jared D. Smith, Atsumu Tezaki, Stephen J. Klippenstein, and Craig A. Taatjes, *J. Phys. Chem. A*, **111**, 4015-4030 (2007). [Miller Festschrift issue]
10. **Reaction Kinetics of $\text{CO} + \text{HO}_2 \rightarrow \text{Products}$: Ab Initio Transition State Theory Study with Master Equation Modeling**, Xiaoqing You, Hai Wang, Elke Goos, C.-J. Sung, Stephen J. Klippenstein, *J. Phys. Chem. A*, **111**, 4031-4042 (2007). [Miller Festschrift issue]
11. **Initial Steps of Aromatic Formation in a Laminar Premixed Fuel-Rich Cyclopentene Flame**, N. Hansen, T. Kasper, S. J. Klippenstein, P. R. Westmoreland, M. E. Law, C. A. Taatjes, K. Kohse-Hoinghaus, J. Wang, and T. A. Cool, *J. Phys. Chem. A*, **111**, 4081-4092 (2007). [Miller Festschrift issue]
12. **A Two Transition State Model for Radical-Molecule Reactions: Applications to Isomeric Branching in the OH-Isoprene Reaction**, Erin E. Greenwald, Simon W. North, Yuri Georgievskii, and Stephen J. Klippenstein, *J. Phys. Chem. A*, **111**, 5582-5592 (2007).
13. **Reflected Shock Tube and Theoretical Studies of High-Temperature Rate Constants for $\text{OH} + \text{CF}_3\text{H} \rightleftharpoons \text{CF}_3 + \text{H}_2\text{O}$ and $\text{CF}_3 + \text{OH} \rightarrow \text{Products}$** , N. K. Srinivasan, M.-C. Su, J. V. Michael, S. J. Klippenstein, and L. B. Harding, *J. Phys. Chem. A*, **111**, 6822-6831 (2007). [Lin Festschrift issue]

14. **Ab Initio Methods for Reactive Potential Energy Surfaces**, Lawrence B. Harding, Stephen J. Klippenstein, and Ahren W. Jasper, *Phys. Chem. Chem. Phys.*, **9**, 4055-4070 (2007). [Invited; Theory/Experiment Synergy Special Issue]
15. **Association Rate Constants for Reactions between Resonance Stabilized Radicals: $C_3H_3 + C_3H_3$, $C_3H_3 + C_3H_5$, and $C_3H_5 + C_3H_5$** , Yuri Georgievskii, Stephen J. Klippenstein, and James A. Miller, *Phys. Chem. Chem. Phys.*, **9**, 4259-4268 (2007). [Theory/Experiment Synergy Special Issue]
16. **Theory, Measurements, and Modeling of OH and HO₂ Formation in the Reaction of Cyclohexyl Radicals with O₂**, Adam M. Knepp, Giovanni Meloni, Leonard E. Jusinski, Craig A. Taatjes, Carlo Cavallotti, and Stephen J. Klippenstein, *Phys. Chem. Chem. Phys.*, **9**, 4315-4331 (2007). [Theory/Experiment Synergy Special Issue; hot article]
17. **Understanding Reactivity at Very Low Temperatures: The Reactions of Oxygen Atoms with Alkenes**, Hassan Sabbah, Ludovic Biennier, Ian R. Sims, Yuri Georgievskii, Stephen J. Klippenstein, and Ian W. M. Smith, *Science*, **317**, 102-105 (2007).
18. **Secondary Kinetics of Methanol Decomposition: Theoretical Rate Coefficients for $^3CH_2 + OH$, $^3CH_2 + ^3CH_2$, and $^3CH_2 + CH_3$** , Ahren W. Jasper, Stephen J. Klippenstein, and Lawrence B. Harding, *J. Phys. Chem. A*, **111**, 8699-8707 (2007).
19. **Performance of the Spin-Flip and Multi-Reference Methods for Bond-Breaking in Hydrocarbons: A Benchmark Study**, Anna A. Golubeva, Alexandr V. Nemukhin, Stephen J. Klippenstein, Lawrence B. Harding, and Anna I. Krylov, *J. Phys. Chem. A*, **111**, 13264-13271 (2007).
20. **Thermal Decomposition of CF₃ and the Reaction of CF₂ + OH → CF₂O + H**, N. K. Srinivasan, M.-C. Su, J. V. Michael, A. W. Jasper, S. J. Klippenstein, and L. B. Harding, *J. Phys. Chem. A*, **112**, 31-37 (2008).
21. **A Combined Ab Initio and Photoionization Mass Spectrometric Study of Polyynes in Fuel-Rich Flames**, N. Hansen, S. J. Klippenstein, P. R. Westmoreland, T. Kasper, K. Kohse-Hoinghaus, J. Wang, and T. A. Cool, *Phys. Chem. Chem. Phys.*, **10**, 366-374 (2008).
22. **Kinetics of CH + N₂ Revisited with Multireference Methods**, Lawrence B. Harding, Stephen J. Klippenstein, and James A. Miller, *J. Phys. Chem. A*, **112**, 522-532 (2008).
23. **Theory of Low Temperature Gas-Phase Reactions**, Stephen J. Klippenstein and Yuri Georgievskii, in "Low Temperatures and Cold Molecules", edited by I. W. M. Smith, (Imperial College, London, 2008), p. 175-231.
24. **Reactions over Multiple, Interconnected Potential Wells: Unimolecular and Bimolecular Reactions on a C₃H₅ Potential**, James A. Miller, Juan P. Senosiain, Stephen J. Klippenstein, and Yuri Georgievskii, *J. Phys. Chem. A*, **112**, 9429-9438 (2008).
25. **Kinetics and Product Branching Ratios of the Reaction of 1CH_2 with H₂ and D₂**, K. L. Gannon, M. A. Blitz, M. J. Pilling, P. W. Seakins, S. J. Klippenstein, L. B. Harding, *J. Phys. Chem. A*, **112**, 9575-9583 (2008).
26. **An Experimental and Theoretical High Temperature Kinetic Study of the Thermal Unimolecular Dissociation of Fluoroethane**, Binod R. Giri, John H. Kiefer, Hui Xu, Stephen J. Klippenstein, and Robert S. Tranter, *Phys. Chem. Chem. Phys.*, **10**, 6266-6273 (2008).
27. **A Shock Tube and Theory Study of the Dissociation of Acetone and Subsequent Recombination of Methyl Radicals**, Saumitra Saxena, John H. Kiefer, and Stephen J. Klippenstein, *Proc. Comb. Inst.*, **32**, 123-130 (2009).
28. **Kinetics of the H + NCO Reaction**, Stephen J. Klippenstein and Lawrence B. Harding, *Proc. Comb. Inst.*, **32**, 149-155 (2009).
29. **Theoretical Rate Coefficients for the Reaction of Methyl Radical with Hydroperoxyl Radical and for Methylhydroperoxide Decomposition**, Ahren W. Jasper, Stephen J. Klippenstein, and Lawrence B. Harding, *Proc. Comb. Inst.*, **32**, 279-286 (2009).
30. **Detailed Balance in Multiple-Well Chemical Reactions**, James A. Miller, Stephen J. Klippenstein, Struan H. Robertson, Michael J. Pilling, and Nicholas J. B. Green, *Phys. Chem. Chem. Phys.*, **11**, 1128-1137 (2009). [Perspectives Article]

Theoretical modeling of spin-forbidden channels in combustion reactions

Anna I. Krylov

Department of Chemistry, University of Southern California,
Los Angeles, CA 90089-0482

krylov@usc.edu

1 Scope of the project

The goal of our research is to develop predictive theoretical methods, which can provide crucial quantitative data (e.g., rate constants, branching ratios, heats of formation), identify new channels and refine reaction mechanisms. Specifically, we are developing tools for computational studies of spin-forbidden and non-adiabatic pathways of reactions relevant to combustion, and applying these tools to study electronic structure and reactions of open-shell and electronically excited species involved in these processes.

2 Summary of recent major accomplishments

During the past year, we conducted several computational studies of open-shell and electronically excited species. The common theme in these studies is interactions between states of different character and intersections between the corresponding potential energy surfaces (PESs). The DOE support is acknowledged in four publications[1, 2, 3, 4]. Motivated by the experiments conducted in Prof. Hanna Reisler group, we investigated the origin of the dramatic difference (about 1 eV) between the ionization energies (IEs) of the hydroxymethyl (CH_2OH) and hydroxyethyl (CH_3CHOH) radicals. Based on electronic structure calculations, we explained the observed large decrease in IE in terms of hyperconjugative interactions between the σ_{CH} orbitals of the methyl group in CH_3CHOH , the singly occupied p orbital of C, and the lone pair p orbital of O. In collaboration with Prof. Hanna Reisler, we investigated electronically excited states of diazirine[4]. Our calculations of excitation energies and transition probabilities identified the initial electronic state in Reisler experiments to be a valence 1^1A_2 ($\pi^* \leftarrow \sigma_{NN}$) state, which is reached via the intermediate 1^1B_2 ($\pi^* \leftarrow n$) state in a two-photon process. Using our code for minimal minimum energy crossing points (MECP) within EOM-CC, we located and characterized the singlet-triplet MECP in formaldehyde, and investigated[3] mechanistic consequences on formaldehyde photodissociation in collaboration with Prof. Joel Bowman (Emory). The DOE support is also acknowledged in a review on “*Interacting Rydberg and valence states in radicals and molecules: Experimental and theoretical studies*” by H. Reisler and A.I. Krylov, which has

been submitted for publication in *Int. Rev. Phys. Chem.* Some of the recent results are highlighted below.

2.1 Vibrational spectra of the hydroxycarbene isomers

In collaboration with J. Bowman and B. Braams (Emory), we computed accurate infrared spectra of the two hydroxycarbene isomers[2]. The vibrational levels were computed by diagonalizing the Watson Hamiltonian including up to four modes couplings using full dimensional potential energy and dipole moment surfaces calculated at the CCSD(T)/cc-pVTZ (frozen core) and CCSD/6-311G** (all electrons correlated) levels, respectively. We found that anharmonic corrections are very important for these elusive higher-energy isomers of formaldehyde. Both the energy levels and intensities of stretching fundamentals and all overtone transitions are strongly affected by anharmonic couplings between the modes. The results for trans-HCOH/HCOD are in excellent agreement with the recently reported IR spectra [Schreiner; *et al.*, *Nature* **453**, 862 (2008)) validating our predictions for the cis-isomer, which has not yet been characterized spectroscopically.

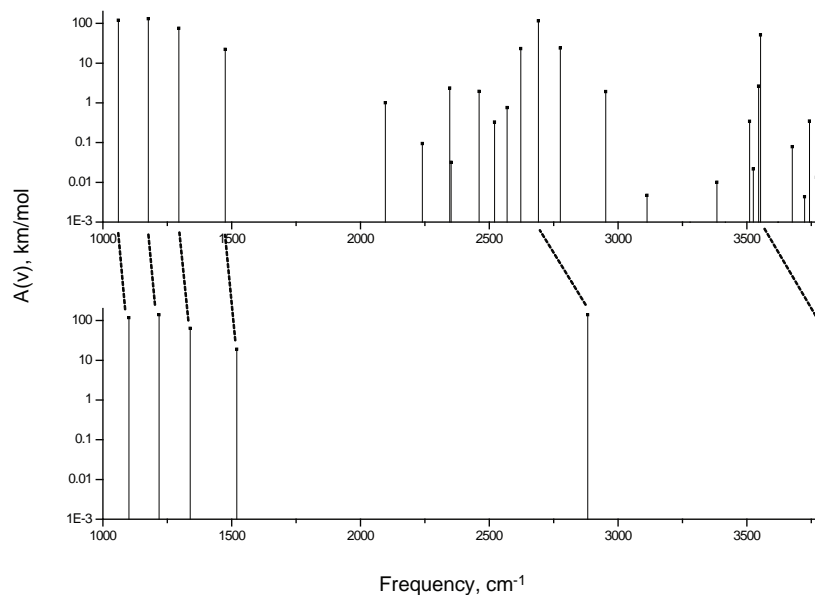


Figure 1: VCI (top) and harmonic (bottom) IR spectrum for trans-HCOH.

2.2 Photodissociation dynamics of formaldehyde initiated at the T_1/S_0 minimum energy crossing configurations

The photodissociation dynamics of H_2CO is known to involve electronic states S_1 , T_1 and S_0 , as depicted in Fig. 2. Recent quasiclassical trajectory (QCT) calculations, in conjunction with experiment, have identified a roaming H-atom pathway to the molecular products, H_2+CO [Townsend; *et al.*, *Science* **306**, 1158 (2004)]. These calculations were initiated at

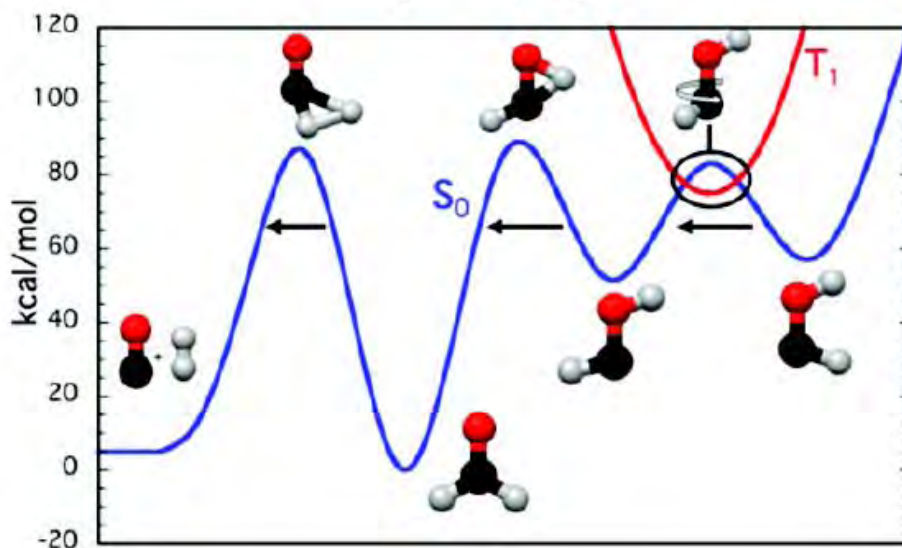


Figure 2: Schematic of H_2CO T_1/S_0 reaction profile. The T_1/S_0 MECP corresponds to a highly-distorted geometry.

the global minimum (GM) of S_0 , which is where the initial wave function is located. The roaming mechanism is not seen if trajectories are initiated from the molecular transition state saddle point (SP). In collaboration with J. Bowman and K. Morokuma, we identified the minimum energy-crossing configurations and energy of the T_1/S_0 potentials as a step toward studying the multisurface nature of the photodissociation (see Fig. 3). QCT calculations were initiated at these configurations on a revised potential energy surface and the results were compared to those initiated, as previously, from the S_0 GM, as well as the S_0 SP. The product state distributions of $\text{H}_2 + \text{CO}$ from trajectories initiated at the T_1/S_0 crossing are in excellent agreement with those initiated at the S_0 GM.

2.3 Hyperconjugation at play

Analyses of the vertical and adiabatic IEs and hyperconjugation energies in CH_2OH and CH_3CHOH computed by NBO suggested that the decrease is due to the destabilization of the singly occupied molecular orbital in CH_3CHOH radical, as well as due to geometrical relaxation of the cation, which maximizes hyperconjugation. The stabilization is achieved through the shortening of the CO and CC bonds, whereas changes in torsional angles have a small effect on the total hyperconjugation energies and, therefore, on the IEs. An interesting feature of these radicals is that the hyperconjugation involves *three* interacting orbitals, i.e., carbon's p-orbital hosting the unpaired electron, the lone pair on oxygen, and σ_{CH} .

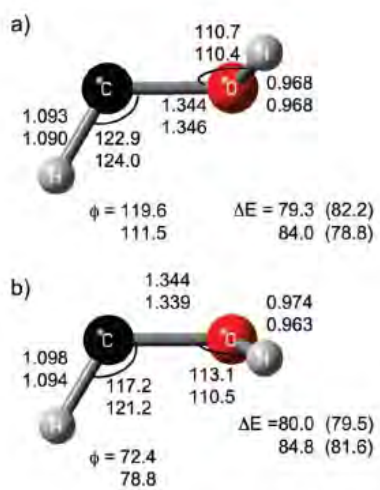


Figure 3: Structures and energies relative to the H_2CO global minimum (kcal/mol) for the minimum energy crossing points of the T_1 and S_0 surfaces. The trans crossing point is given in upper panel (a) and the cis crossing point in lower panel (b). The upper numbers for the structures were computed at the MRCI+Q/aug-cc-pVTZ level of theory and the lower numbers at the EOM-CCSD(dT)/cc-pVTZ level of theory. The upper energy was computed with MRCI+Q/aug-cc-pV5Z, and the lower with EOM-CCSD(dT)/cc-pVTZ. The numbers in parenthesis are the energies from the fitted PES for the corresponding structure.

3 Current developments and future plans

Currently, we are pursuing modeling of photoelectron spectra of cis- and trans-hydroxycarbenes, as well as their isomerisation dynamics (in collaboration with Prof. Joel Bowman). We are also finalizing for publication the results for EOM-CC MECP calculations for characterization of singlet-triplet crossings in several prototypical hydrocarbon diradicals.

References

- [1] B. Karpichev, H. Reisler, A.I. Krylov, and K. Dirí, Effect of hyperconjugation on ionization energies of hydroxyalkyl radicals, *J. Phys. Chem. A* **112**, 9965 (2008).
- [2] L. Koziol, Y. Wang, B.J. Braams, J.M. Bowman, and A.I. Krylov, The theoretical prediction of infrared spectra of trans- and cis- hydroxycarbene calculated using full dimensional ab initio potential energy and dipole moment surfaces, *J. Chem. Phys.* **128**, 204310 (2008).
- [3] B.C. Shepler, E. Epifanovsky, P. Zhang, J.M. Bowman, A.I. Krylov, and K. Morokuma, Photodissociation dynamics of formaldehyde initiated at the T_1/S_0 minimum energy crossing configuration, *J. Phys. Chem. A* **112**, 13267 (2008).
- [4] I. Fedorov, L. Koziol, A.K. Mollner, A.I. Krylov, and H. Reisler, Multiphoton ionization and dissociation of diazirine: A theoretical and experimental study, *J. Phys. Chem. A* (2009), in press.

SYNCHROTRON STUDIES OF COMBUSTION RADICAL REACTIONS AND AEROSOL CHEMISTRY

*Stephen R. Leone, Fabien Goulay, Jared Smith, Kevin Wilson, Daphne Che,
Chen-Lin Liu, Adam Trevitt, and Musahid Ahmed*

*Departments of Chemistry and Physics and Lawrence Berkeley National Laboratory
University of California
Berkeley, California 94720
(510) 643-5467 srl@berkeley.edu*

Scope of the Project

Combustion is a complex process involving short-lived radical species, highly excited states, kinetics, transport processes, heterogeneous chemistry on aerosols such as organic liquid nanoparticles and soot, fluid dynamics, and energy transfer. Detailed measurements of microscopic reaction pathways, rate coefficients, product state distributions, and thermochemistry result in considerable information to aid in the understanding of combustion processes. Vacuum ultraviolet (VUV) light from the Chemical Dynamics Beamline of the Advanced Light Source (ALS) provides a powerful tool to study photoionization properties of small molecules and radicals, to selectively detect reaction products of carbon-based species (e.g. C_2H , CH) with unsaturated hydrocarbons, and to measure the energetics and photoionization spectroscopy of important combustion species. A kinetics apparatus at the ALS was jointly constructed with David Osborn and Craig Taatjes of the Sandia Combustion Research Facility. Products from key combustion reactions can now be detected and branching ratios estimated. A new theme has also been initiated to study aerosol heterogeneous chemistry. This endeavor is exploring aerosol species, their reactivity from fuel sprays and their production in combustion, and the resulting particulate species chemistries.

C_2H + propyne, allene

Reactions of ethynyl radical (C_2H) with propyne and allene are studied by 193 nm photolysis of CF_3CCH to produce C_2H followed by single photon ionization mass spectrometry detection of the products using synchrotron radiation for ionization. By tuning the wavelength of the synchrotron, photoionization efficiency curves are obtained to determine isomer-specific analysis of the products. For example, the C_5H_4 products of the reaction of C_2H with allene (CH_2CCH_2) are analyzed at room temperature. Using a suitable model for the cross sections for ionization of the isomer species, the isomer distribution is obtained to be: 35-45% ethynylallene, 20-25% methylacetylene, and 45-30% 1,4-pentadiyne. The other possible product, diacetylene (C_4H_2) is not observed for this reaction (<30%), whereas for C_2H with propyne (CH_3CCH) the diacetylene product is 50-70%. Isomer results are also obtained for C_2H reaction with propyne. The results provide a new window onto the formation of polyynes, which furthers the goal of understanding the building up of molecules that eventually may produce PAHs.

CH + ethylene: Cyclic C_3H_2

A comprehensive study of the reactions of the methylidyne radical (CH) with ethylene, acetylene, allene, and methylacetylene (propyne) has been performed at room temperature using the tunable synchrotron for analysis. The reactions proceed by either CH insertion or addition followed by H atom elimination from the intermediate adduct. For the $CH + C_2H_4$ reaction, the C_3H_3 intermediate decays by H atom loss to form 70±8% allene, 30±8% methylacetylene (propyne), and <10% cyclopropene. In the $CH + C_2H_2$ reaction, the cyclic C_3H_2 product is primarily observed, in contradiction to previous calculations that suggested linear triplet propargylene ($HCCCH$) accounts for 90% of the product formation. New calculations indicate that a somewhat higher production of the cyclic product (27%) should be expected, however, from these calculations together with D atom isotope studies in the laboratory measurements, it is shown that H -atom assisted isomerization of the triplet propargylene is likely to be responsible for the additional large conversion to the observed $c-C_3H_2$. Cyclic isomers are also observed for the reactions of CH with methylacetylene. The reaction of CH with allene produces 23±5% 1,2,3-butatriene and 77±5% vinylacetylene, and no cyclic isomers are detectable. This study has revised the understanding of the CH

reaction systems and the formation of cyclic isomers. It demonstrates the power of isomer specific detection, and it also validates the computational methods through the good agreement with experiment.

CN + C₂H₄ and C₃H₆

Radical attack by CN (from ICN photolysis) on C₃H₆ can occur at either the CH₂ terminal group or the central CH group, producing a secondary and primary radical intermediate complex, respectively. From the CN terminal intermediate there are three plausible exit channels; H + CH₃(CH)₂CN, CH₃ + CH₂CHCN and addition/elimination forming HCN + CH₂CHCH₂. If the reaction proceeds via CN attack on the central CH group then the sole likely exit pathway is H + CH₃CCH₂CN. A thorough experimental investigation of the product branching ratios of the CN + C₃H₆ reaction is needed to quantitatively obtain the exit channels, to understand the mechanisms leading to the products and to test the theoretical treatments that have been developed for this and similar systems. Results show that both the CN + C₂H₄ and CN + C₃H₆ reactions proceed predominantly via CN addition to the π -orbital of the olefin. For CN + ethylene, cyanoethylene (C₂H₃CN) is detected as the sole product in agreement with recent other studies of this reaction. Multiple products are identified for the CN + propene reaction. Of the detected products, cyanoethylene (from a CH₃ elimination channel) is formed in a ratio of 3:1 compared to the H elimination channel, C₄H₅. The C₄H₅N mass channel consists of 57% 1-cyanopropene, 43% 2-cyanopropene and <15% 3-cyanopropene isomers. No evidence for the direct H abstraction and formation of HCN was detected.

Aerosol Chemistry – reactions of squalane with OH and Cl in the presence of oxygen

New experiments are being developed to investigate the oxidation of fuel droplet sprays, such as biodiesel nanodroplet surfaces, using the aerosol apparatus. Studies will address the reactions from the fuel perspective as well as subsequent chemistry relating to the atmosphere. Ambient aerosols are known to play a significant role in a variety of atmospheric processes such as direct and indirect effects on radiative forcing. Chemical composition can be an important factor in determining the magnitude of these effects (optical density, hygroscopicity, etc.). However, a major fraction (80 – 90%) of organic aerosols cannot be resolved at the molecular level. Recent identification of high mass oligomeric species as a major component in laboratory and ambient organic aerosols has received attention due to the possibility that these species may account for much of the unknown organic mass in ambient aerosols. Although, a few mechanisms have been proposed, the origin and formation processes of these compounds remain largely unknown. Using VUV photoionization aerosol mass spectrometry we find strong evidence for a sequential oxidation mechanism of organic aerosols. We observe the rapid condensed phase formation of high molecular weight species (oligomers), via OH radical initiated oxidation of organic aerosols. Rapid volatilization, followed by oligomerization, is also important for specific reaction systems (i.e. n-alkane particles) and can lead to the loss of a large fraction (> 60%) of a particle. Such rapid processing (oxidation, oligomerization and volatilization) can be driven by radical chain reactions that propagate throughout the particle when initiated by the surface OH reaction.

The reactive uptake coefficient is a conventional parameter used to quantitatively represent all the physical effects governing the rate of heterogeneous reaction between gas phase and condensed phase species. It may be defined as the fraction of OH-squalane molecule collisions in the particle that leads to reaction. The average value of γ in a lower pressure stirred tank reactor at low OH concentrations is found to be 0.59 ± 0.13 upon the exposure of squalane particle to OH concentrations of $1-7 \times 10^8$ molec cm⁻³ in 1-3 hour reaction time. The reactive uptake calculated by this method agrees well with the uptake range, $\gamma = 0.2$ to 1, found in other experiments. However, other work in our laboratory also measured the reactive uptake coefficient of OH on squalane particles in a flow tube system at higher OH concentrations and found a value of $\gamma = 0.3 \pm 0.7$ [OH = 10^{10} molec cm⁻³]. The discrepancy between the results indicates the occurrence of secondary chemistry, which plays an important role depending on the OH concentration. To investigate secondary chemistry further, a series of experiments are investigating the heterogeneous oxidation of squalane particles initiated by Cl radicals in the presence of O₂. Squalane radical (R·) generated from reaction between squalane and Cl radical can react with Cl₂ that has diffused

into the particle or is arriving at the surface of the particle to generate *particle-phase* Cl radicals (which are termed Cl' to differentiate these radicals from gas-phase Cl radical). This Cl' readily reacts with squalane, creating a chain reaction loop in the mechanism. Furthermore, when O₂ is present in the system, squalane radical (R·) can also react with O₂. Therefore, there are two reaction channels competing with each other depending on the Cl₂, O₂ and Cl concentrations in both the gas phase and the particle phase systems; the latter depend on Henry's law constants. Experiments are in progress to delineate and separate the particle phase and gas-liquid phase chemistries.

Future Plans

New studies will explore radical-molecule and radical-radical reactions using VUV-ionization. Using the kinetics machine developed in conjunction with Sandia National Laboratory, we will investigate coupled carbon-nitrogen chemistry by studying the products of CH radical reactions with pyridine and CCN radical reactions, to determine the carbyne like reactive behavior with saturated and unsaturated hydrocarbons (e.g. insertion mechanisms). Important experiments will be performed concerning the reaction of hydrocarbon radicals on biodiesel and oil shale related chemical species in nanodroplets using VUV ionization to probe volatile and nonvolatile components of the heterogeneous reactions and secondary chemistry. Major studies will exploit the aerosol generation and detection instrumentation discussed above. Finally, radical reaction/heterogeneous chemistry on carbonaceous soot particles has yet to be explored at the level of detail that is now possible by using aerosol introduction instruments, flow tube reactors, and mass spectrometric detection tools. By preparing fresh soot particles in a flame and immediately introducing them into a flow tube system, we will study their reactivity and products with radicals, such as Cl atoms or C₂H.

Recent Publications Citing DOE Support (2007-2009):

J. D. Smith, J. H. Kroll, C. D. Cappa, D. L. Che, M. Ahmed, S. R. Leone, D. R. Worsnop, and K. R. Wilson, "The heterogeneous reaction of hydroxyl radicals with sub-micron squalane particles: A model system for understanding the oxidative aging of ambient aerosols," *Atmos. Chem. and Phys. Disc.* (in press) (2009).

F. Goulay, A. J. Trevitt, G. Meloni, T. M. Selby, D. L. Osborn, C. A. Taatjes, L. Vereeken, and S. R. Leone, "Cyclic versus linear isomers produced by reaction of the methylidyne radical (CH) with small unsaturated hydrocarbons," *J. Am. Chem. Soc.* **131**, 993 (2009).

A. J. Trevitt, F. Goulay, G. Meloni, D. L. Osborn, C. A. Taatjes, and S. R. Leone, "Isomer-specific product detection of CN radical reactions with ethene and propene by tunable VUV photoionization mass spectrometry," *Int. J. Mass. Spectrom.* **280**, 113 (2009).

T. M. Selby, G. Meloni, F. Goulay, S. R. Leone, C. A. Taatjes, A. Fahr, and D. L. Osborn, "Synchrotron photoionization mass spectrometry measurements of kinetics and product formation in the allyl radical H₂CCHCH₂ self-reaction," *J. Phys. Chem. A* **112**, 9366 (2008).

D. L. Osborn, P. Zou, H. Johnsen, C. C. Hayden, C. A. Taatjes, V. D. Knyazev, S. W. North, D. S. Peterka, M. Ahmed, and S. R. Leone, "The multiplexed chemical kinetic photoionization mass spectrometer: a new approach to isomer-resolved chemical kinetics," *Rev. Sci. Instrum.* **79**, 104 (2008).

G. Meloni, T. M. Selby, F. Goulay, S. R. Leone, D. L. Osborn, and C. A. Taatjes, "Photoionization of 1-alkenylperoxy and alkylperoxy radicals and a general rule for the stability of their cations," *J. Am. Chem. Soc.* **129**, 14019, (2007).

L. Belau, S. E. Wheeler, B. W. Ticknor, M. Ahmed, S. R. Leone, W. D. Allen, H. F. Schaefer III, and M. A. Duncan, "Ionization thresholds of small carbon clusters: tunable VUV experiments and theory," *J. Am. Chem. Soc.* **129**, 10229 (2007).

L. Belau, K. R. Wilson, S. R. Leone, and M. Ahmed, "Vacuum Ultraviolet (VUV) photoionization of small water clusters," *J. Phys. Chem. A* **111**, 10075 (2007).

K. R. Wilson, S. Zou, J. Shu, E. Rühl, S. R. Leone, G. C. Schatz, and M. Ahmed, "Size-dependent angular distributions of low energy photoelectrons emitted from NaCl nanoparticles," *Nano Lett.* **7**, 2014 (2007).

R. I. Kaiser, L. Belau, S. R. Leone, M. Ahmed, Y. Wang, B. J. Braams, and J. M. Bowman, "A combined experimental and computational study on the ionization energies of the cyclic and linear C₃H isomers," *Chem. Phys. Chem.* **8**, 1236 (2007).

C. Howle, A. N. Arrowsmith, V. Chikan, and S. R. Leone, "State-resolved dynamics of the CN(B₂Σ⁺) and CH(A²Δ) excited products resulting from the VUV photodissociation of CH₃CN," *J. Phys. Chem. A* **111**, 6637 (2007).

L. Belau, K. R. Wilson, S. R. Leone, and M. Ahmed, "Vacuum-ultraviolet photoionization studies of the microhydration of DNA bases (Guanine, Cytosine, Adenine, and Thymine)," *J. Phys. Chem. A* **111**, 7562 (2007).

F. Goulay, D. L. Osborn, C. A. Taatjes, P. Zou, G. Meloni, and S. R. Leone, "Direct detection of polyynes formation from the reaction of ethynyl radical (C₂H) with propyne (CH₃CCH) and allene (CH₂=C=CH₂)," *Phys. Chem. Chem. Phys.* **9**, 4291 (2007).

Intermolecular Interactions of Hydroxyl Radicals on Reactive Potential Energy Surfaces

Marsha I. Lester

Department of Chemistry, University of Pennsylvania
Philadelphia, PA 19103-6323
milester@sas.upenn.edu

I. Program Scope

Hydroxyl radicals are important in combustion and atmospheric environments, where they are often detected by laser-induced fluorescence (LIF) on the $A^2\Sigma^+ - X^2\Pi$ band system. However, collision partners known to quench electronically excited OH $A^2\Sigma^+$ radicals are ubiquitous in these environments. Thus, great effort has been made to quantify the rates and/or cross sections for collisional quenching, so that its effects on LIF signals may be taken into account to allow an accurate determination of OH concentrations.^{1,2} Despite extensive kinetic measurements, fundamental questions remain regarding the fate of the collisionally quenched molecules and the mechanism by which these nonadiabatic processes occur. The experimental work carried out under DOE funding in this laboratory is aimed at understanding the fundamental chemical dynamics governing quenching of OH $A^2\Sigma^+$ by molecular partners (M) of significance in combustion environments.

II. Recent Progress

Collisional quenching of electronically excited OH $A^2\Sigma^+$ can occur by two types of processes: nonreactive quenching that returns OH $A^2\Sigma^+$ to its ground $X^2\Pi$ electronic state



and reaction. For H_2 , reactive quenching leads to the formation of highly vibrationally excited water and hydrogen atoms³⁻⁵



This group has also carried out extensive experimental studies of the nonreactive quenching channel for OH $A^2\Sigma^+$ with H_2 and D_2 partners.⁶⁻⁹ High level theoretical studies of quenching are available for OH $A^2\Sigma^+$ with only a few partners, including H_2 and N_2 .^{2,7,10} For quenching of OH $A^2\Sigma^+$ by N_2 , an energetically accessible conical intersection leading to nonreactive quenching ($\Delta E = -4.02 \text{ eV}$) has been located theoretically.² In addition, a reactive channel producing $\text{H} + \text{N}_2\text{O}$ products ($\Delta E = -1.03 \text{ eV}$) is potentially open, but has not been observed in experimental or theoretical studies.^{11,12}

Most recently, we have focused on the outcomes of collisional quenching for OH $A^2\Sigma^+$ by N_2 , O_2 , and CO_2 . These experiments characterize the nonreactive pathway by examining the OH $X^2\Pi$ product state distribution as well as the branching fraction for OH $X^2\Pi$ products. The experiments are performed using a pump-probe technique in the collisional region of a pulsed supersonic expansion. OH radicals are generated photolytically, pumped to the OH $A^2\Sigma^+$ ($v'=0, N'=0$) state, and probed after a short delay on various OH $A^2\Sigma^+ - X^2\Pi$ transitions to characterize the OH $X^2\Pi$ products with rovibrational and fine-structure resolution.

The nascent quantum state distribution of the OH $X^2\Pi$ products arising from quenching of OH $A^2\Sigma^+$ by N_2 under single collision conditions is shown in Fig. 1 (blue).¹² The OH $X^2\Pi$ products from the nonreactive quenching are released principally in $v''=0$ with far less in $v''=1$. The OH $X^2\Pi$ products are generated with a remarkable degree of rotational excitation, peaking around $N''=18$ and extending to at least $N''=27$ in the dominant $v''=0$ vibrational state. These OH ($v''=0$) products are released with $6540 \pm 390 \text{ cm}^{-1}$ of rotational energy on average. A similar rotational distribution is observed for $v''=1$. A

moderate propensity for $p\pi$ orbital alignment of the OH products is observed as evidenced by a preference for the $\Pi(A')$ Λ -doublet. The F_1 and F_2 manifolds are equally populated. The branching fraction for OH $X^2\Pi$ products, summed over rovibrational and fine structure states, shows that more than 88% of quenching events result in nonreactive quenching. The remaining 12% is not observed, but is likely produced in yet higher rotational levels that cannot be probed by LIF on the OH A-X (0,0) transition.

Quenching of OH $A^2\Sigma^+$ by H_2 provides an interesting point of comparison with quenching by N_2 . Therefore, we also show the OH $X^2\Pi$ ($v''=0$) products of the nonreactive quenching channel following quenching by H_2 in Fig. 1 (red). These OH $X^2\Pi$ products have significant rotational excitation, peaking at $N''=15$ with an average rotational energy of $3680 \pm 160 \text{ cm}^{-1}$,⁹ but notably less rotational excitation than observed with N_2 as the quencher. In addition, the OH $X^2\Pi$ ($v''=0$) distribution is clearly broader for N_2 as a collision partner as compared to H_2 . However, the branching between reactive and nonreactive pathways is drastically different, as quenching of OH $A^2\Sigma^+$ by N_2 occurs overwhelmingly through the nonreactive channel, while this is the minor channel for quenching by H_2 .⁸

To better understand these results, the measurements have been complemented by a theoretical study of the conical intersection (CI) region in the OH- N_2 system, in particular, the \mathbf{g} - \mathbf{h} branching plane.¹² The energy difference gradient \mathbf{g} vector drives the OH and N_2 moieties toward or away from one another at the CI. The interstate coupling \mathbf{h} vector puts a large torque on the OH radical, giving rise to the significant rotational excitation of the OH $X^2\Pi$ products. Interestingly, the \mathbf{h} vector is found to be substantially larger in magnitude for OH with N_2 as compared to H_2 , consistent with the more extensive rotational excitation of the OH products upon quenching by N_2 .

The branching fraction between reactive and nonreactive quenching pathways is perhaps the most striking difference between the two systems. The topography of the CI, especially the tilt of the cone, is predicted to play a large role in determining the branching between pathways.¹⁰ Indeed, the present calculations indicate a significant tilt of the cone for OH- N_2 by comparison with a vertical cone for OH- H_2 as depicted in Fig. 2. The $-\mathbf{g}$ direction drives the OH + N_2 (or H_2) moieties apart, leading to nonreactive quenching. On the other hand, the $+\mathbf{g}$ direction can result in reactive quenching. For OH- H_2 , the forces in the vicinity of the CI will lead to both reactive and nonreactive outcomes. For OH- N_2 , there is principally a strong gradient in the $-\mathbf{g}$ direction causing the OH + N_2 partners to separate. Thus, we conclude that the

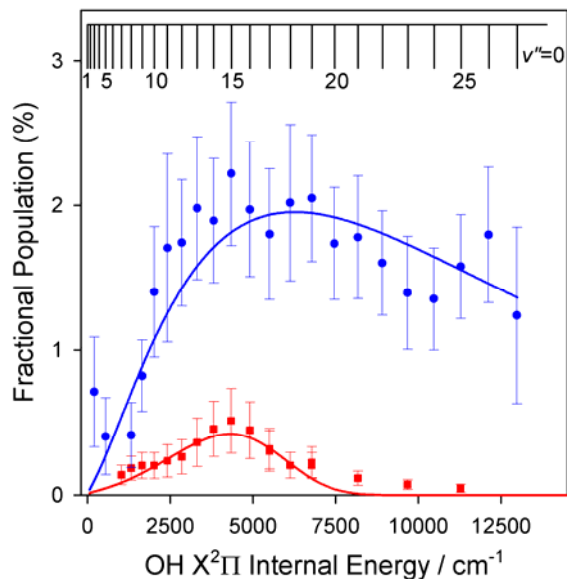


Fig. 1 Comparison of quantum state distributions for OH $X^2\Pi$ ($v''=0$) products arising from quenching of OH $A^2\Sigma^+$ ($v'=0, N'=0$) by N_2 and H_2 under single-collision conditions. Fractional population is shown for quenching by N_2 (blue) and H_2 (red). Only population for the $\Pi(A')$ Λ -doublet of the F_1 manifold are shown for clarity.

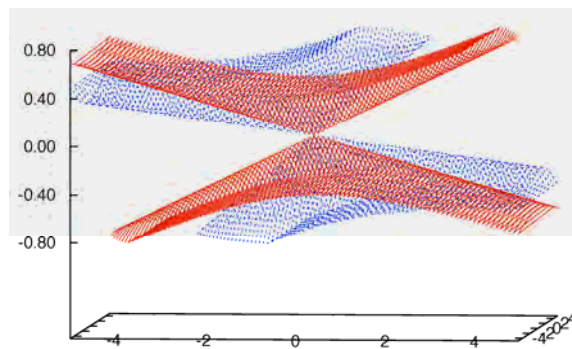


Fig. 2 Upper $2^2A'$ (OH $A^2\Sigma^+ + H_2/N_2$) and lower $1^2A'$ (OH $X^2\Pi + H_2/N_2$) potentials are connected by conical intersections when O-side of OH points toward H_2 (red) and N_2 (blue). The topography of the cone of intersection is illustrated schematically with energy (vertical axis) relative to \mathbf{g} - \mathbf{h} plane (\mathbf{g} on horizontal axis) in atomic units.

product quantum state distribution and branching between reactive and nonreactive products are dynamical signatures of passage through the CI, reflecting the topography of the potential surfaces in this region.

Comprehensive quantum state distributions have also been obtained for the OH $X^2\Pi$ products from quenching OH $A^2\Sigma^+$ ($v'=0, N'=0$) by O_2 and CO_2 .¹³ For both collision partners, OH products are formed predominantly in $v''=0$ with less population in $v''=1$ and none detected in $v''=2$. With O_2 as the collision partner, the ground-state OH $X^2\Pi$ products are generated with a significant degree of rotational excitation, peaking at $N'' \sim 17$ with $\sim 4800 \text{ cm}^{-1}$ of rotational energy on average. Branching fraction measurements reveal that 40(1)% of the products are OH $X^2\Pi$ ($v''=0, 1$). With CO_2 as the collision partner, OH $X^2\Pi$ radicals are produced with a more moderate degree of rotational excitation, peaking at $N'' \sim 5$ with an average rotational energy of $\sim 1800 \text{ cm}^{-1}$. In the case of quenching by CO_2 , 64(5)% of the products are identified as OH $X^2\Pi$ ($v''=0, 1$). Thus, nonreactive quenching is found to be a significant decay pathway for both systems. The balance may be found in higher OH $X^2\Pi$ vibrational levels $v'' \geq 2$ or reactive quenching channels.

III. Ongoing Work

Hydroxyl radicals are predicted to form strong hydrogen bonds with water, making complexes of OH with water important in a variety of environments from the atmosphere to heterogeneous interfaces of water. This system also provides a framework for understanding solvation of radicals in water. Spectroscopic studies of binary OH-water complexes using microwave¹⁴⁻¹⁶ and infrared methods are expected to shed new light on the intermolecular interaction between the OH radical and water molecule.¹⁷ We have predicted,¹⁸ and recently observed, the rotational band structure associated with infrared transitions of the OH-water complex as an initial step to our infrared spectroscopic studies of this complex and OH embedded in small water clusters. In our initial experimental study, the binary OH- H_2O complex is produced by association of photolytically generated OH radicals with H_2O from dilute nitric acid. Infrared action spectroscopy is used to identify the fundamental OH radical stretch of the complex, which displays a frequency shift of nearly 80 cm^{-1} , consistent with theoretical predictions. Following infrared excitation of OH- H_2O , the OH products of vibrational predissociation are detected by laser-induced fluorescence. By utilizing information from the OH product state distribution, we estimate a binding energy for the complex of $D_0 \leq 5.1 \text{ kcal mol}^{-1}$. Work is continuing in other spectral regions using an improved dual nozzle design for introducing water vapor into the carrier gas.

IV. References

- ¹ D. R. Crosley, *J. Phys. Chem.* **93**, 6273 (1989).
- ² M. I. Lester, R. A. Loomis, R. L. Schwartz, and S. P. Walch, *J. Phys. Chem. A* **101**, 9195 (1997).
- ³ D. T. Anderson, M. W. Todd, and M. I. Lester, *J. Chem. Phys.* **110**, 11117 (1999).
- ⁴ M. W. Todd, D. T. Anderson, and M. I. Lester, *J. Phys. Chem. A* **105**, 10031 (2001).
- ⁵ M. Ortiz-Suárez, M. F. Witinski, and H. F. Davis, *J. Chem. Phys.* **124**, 201106 (2006).
- ⁶ I. B. Pollack, Y. X. Lei, T. A. Stephenson, and M. I. Lester, *Chem. Phys. Lett.* **421**, 324 (2006).
- ⁷ P. A. Cleary, L. P. Dempsey, C. Murray, M. I. Lester, J. Kłos, and M. H. Alexander, *J. Chem. Phys.* **126**, 204316 (2007).
- ⁸ L. P. Dempsey, C. Murray, and M. I. Lester, *J. Chem. Phys.* **127**, 151101 (2007).
- ⁹ L. P. Dempsey, C. Murray, P. A. Cleary, and M. I. Lester, *Phys. Chem. Chem. Phys.* **10**, 1424 (2008).
- ¹⁰ B. C. Hoffman and D. R. Yarkony, *J. Chem. Phys.* **113**, 10091 (2000).
- ¹¹ E. G. Estupinan, R. E. Stickel, and P. H. Wine, *Chem. Phys. Lett.* **336**, 109 (2001).
- ¹² L. P. Dempsey, T. D. Sechler, C. Murray, M. I. Lester, and S. Matsika, *J. Chem. Phys.* **130**, 104307 (2009).
- ¹³ L. P. Dempsey, T. D. Sechler, C. Murray, and M. I. Lester, *J. Phys. Chem. A*, submitted (2009).

- 14 Y. Ohshima, K. Sato, Y. Sumiyoshi, and Y. Endo, *J. Am. Chem. Soc.* **127**, 1108 (2005).
15 C. S. Brauer, G. Sedo, E. M. Grumstrup, K. R. Leopold, M. D. Marshall, and H. O. Leung, *Chem.*
16 *Phys. Lett.* **401**, 420 (2005).
16 C. S. Brauer, G. Sedo, E. Dahlke, S. Wu, E. M. Grumstrup, K. R. Leopold, M. D. Marshall, H. O.
17 Leung, and D. G. Truhlar, *J. Chem. Phys.* **129**, 104304 (2008).
17 S. Du, J. S. Francisco, G. K. Schenter, T. D. Iordanov, B. C. Garrett, M. Dupuis, and J. Li, *J.*
18 *Chem. Phys.* **124**, 224318 (2006).
18 M. D. Marshall and M. I. Lester, *J. Phys. Chem. B* **109**, 8400 (2005).

V. Publications supported by this project 2007-2009

1. P. A. Cleary, L. P. Dempsey, C. Murray, M. I. Lester, J. Klos and M. H. Alexander, "Electronic Quenching of OH A $^2\Sigma^+$ Radicals in Single Collision Events with Molecular Hydrogen: Quantum State Distribution of the OH X $^2\Pi$ Products", *J. Chem. Phys.* **126**, 204316 (2007).
2. L. P. Dempsey, C. Murray, and M. I. Lester, "Product Branching between Reactive and Nonreactive Pathways in the Collisional Quenching of OH A $^2\Sigma^+$ Radicals by H₂", *J. Chem. Phys.* [Communication] **127**, 151101 (2007).
3. L. P. Dempsey, C. Murray, P. A. Cleary, and M. I. Lester, "Electronic Quenching of OH A $^2\Sigma^+$ Radicals in Single Collision Events with H₂ and D₂: A Comprehensive Quantum State Distribution of the OH X $^2\Pi$ Products", *Phys. Chem. Chem. Phys.* **10**, 1424-1432 (2008).
4. L. P. Dempsey, T. D. Sechler, C. Murray, and M. I. Lester, "State-resolved distribution of OH X $^2\Pi$ products arising from electronic quenching of OH A $^2\Sigma^+$ by N₂", *J. Chem. Phys.* **130**, 104307 (2009).

Theoretical Studies of Molecular Systems

William A. Lester, Jr.
Chemical Sciences Division,
Ernest Orlando Lawrence Berkeley National Laboratory and
Kenneth S. Pitzer Center for Theoretical Chemistry
Department of Chemistry, University of California, Berkeley
Berkeley, California 94720-1460
walester@lbl.gov

Program Scope

This research program is directed at extending fundamental knowledge of atoms and molecules. The approach combines the use of ab initio basis set methods and the quantum Monte Carlo (QMC) method to describe the electronic structure and energetics of systems of primarily combustion interest.

Recent Progress

The continuing quest for better diffusion MC (DMC) trial functions led us to investigate trans-correlated variational Monte Carlo (TC-VMC) trial functions for DMC. The TC-VMC method has generated very good VMC energies. TC-VMC trial functions were constructed for the first-row atoms Li to Ne. The resulting DMC energies were compared with those obtained using Hartree-Fock and DFT trial functions. Despite major VMC energy improvement with TC-VMC trial functions with simple Jastrow functions, no improvement in DMC energies was observed for the first-row atoms studied. A next step is to carry out a similar comparison using more sophisticated Jastrow functions, a direction that is planned as a collaborative effort with Naoto Umezawa of the National Institute for Materials Science, Tsukuba, Japan.

In collaboration with Michael Frenklach, reaction pathways were determined for hydrogen-mediated isomerization of a zigzag graphene edge containing a five-member carbon ring surrounded by six-member rings. A new reaction sequence in which this embedded five-member ring moves, or migrates, through the edge was identified. The elementary steps of the pathways were analyzed using DFT. The Frenklach group determined rate coefficients using classical transition state theory and the DFT energies, frequencies, and geometries. The results indicate that this new reaction sequence is competitive with other important zigzag edge reactions allowing embedded five-member rings to move freely within a zigzag edge. The embedded rings have slight thermodynamic preference for the interior of the edge over the corner for large substrates.

More recently, in collaboration with the Frenklach group, we initiated a study of soot oxidation. As the first step in this direction, we began the study of the thermodynamic stability of critical oxygenated intermediates. The initial analysis revealed a somewhat unexpected but systematic

trend in the relative stability of graphene-edge oxyradicals. A series of pentacene oxyradicals were selected for a detailed theoretical study. The results revealed that the relative stability of the oxyradical species can be rationalized on the basis of the concept of local aromaticity. Qualitative and quantitative measures of delocalized bonding showed that formation of the π -aromatic fragments associated with different prototypical π -aromatic systems explains the trends in relative energies and thermodynamic stabilities of one-dimensional graphene-edge oxyradicals.

In research laboratories, academic institutions produce some of the most advanced software for scientific applications. However, this software is usually developed only for local application or for method development. In spite of having the latest advances in the particular field of science and engineering, such software often lacks adequate documentation and therefore is difficult to use by anyone other than the code developers. Typically, as such codes become more complex, so do the input files and command statements necessary to operate them. Many programs offer the flexibility of performing calculations based on different methods that have their own set of variables and options to be specified. Moreover, situations can arise in which certain options are incompatible with each other. For this reason, users outside the development group can be unaware of how the program runs in detail. The opportunity can be lost to make the software readily available outside of the laboratory of origin. This is a long-standing problem in scientific programming. Rappture, Rapid Application Infrastructure is a new GUI (graphical user interface) development kit that enables a developer to build an I/O interface for a specific application. We have used the Rappture toolkit to generate a GUI for our Zori QMC computer code.

Future Plans

During the past year following research with the Frenklach group to determine the energetics and kinetics of a series on newly discovered reactions of graphene layer growth, we jointly turned our attention to soot oxidation. We have initiated the investigation of the thermodynamics of oxygenated edges of graphene emulated by polycyclic aromatic hydrocarbons (PAH). We performed quantum chemical calculations on a series of 5-ring PAH substrates. The quantum chemical calculations were carried out at both the PM3 semi-empirical and B3LYP/3-21G DFT levels of theory. The initial set of studies explored modes of attack of oxygen on a zigzag edge of a polyaromatic substrate.

Upon completion of these studies, our focus will shift to DMC computations in order to accurately assess the energetics indicated in these system. From the computed energetics, a series of thermodynamic equilibrium calculations will be carried out to compare the relative stabilities of the oxidized 5-ring species. The results indicate that oxygen bonded on interior rings is more stable than oxygen bonded on exterior rings. Further calculations and analysis are in progress.

Recent photodissociation studies of propargyl, propynl, and phenyl by the Neumark group provide an excellent opportunity to test further the benchmark capability of the DMC method and to contribute to understanding fundamental chemical physical processes. The plan is to characterize fully the energetics of the pathways to dissociation of these systems. Although theoretical/computational studies have been carried out on these systems, there is considerable uncertainty concerning the nature of the excited states accessed in both radicals.

Investigation of approaches for the computation of forces in the DMC formalism will be continued in collaboration with Dr. Roland Assaraf [Chargé de Recherches in the Laboratoire de Chimie Théorique at the Université Pierre et Marie Curie (Paris VI)]. The goal is to develop and test improved force estimators in which the statistical error is independent of molecular size. Obtaining such estimators is highly desirable, since statistical fluctuations in the total energy grow as the size of the molecule increases. The primarily local nature of chemical bonds promises that the statistical fluctuations in the force should be independent of system size. Preliminary computations appear to indicate that DMC bond dissociation energies based on valence bond trial wave functions are accurate for hydrocarbons, and therefore it is promising that this research will yield accurate forces for hydrocarbons. DMC calculations will be performed on closed and open-shell hydrocarbons and the accuracy and statistical error of the energies and forces will be studied as a function of molecule size

DoE Supported Publications (2007-2009)

1. R. Whitesides, A. C. Kollias, D. Domin, W. A. Lester, Jr., and M. Frenklach, "Graphene Layer Growth: Collision of Migrating Five-Member Rings," *Proc. Comb. Inst.* **31**, 539 (2007).
2. R. Whitesides, A. C. Kollias, D. Domin, W. A. Lester, Jr., and M. Frenklach, "Graphene Layer Growth: Five-Six-Ring Flip Reaction," Proceedings of the 5th U.S. National Combustion Meeting, San Diego, CA, March 25-28, 2007, Paper No. D31,
3. B. Austin, A. Aspuru-Guzik, R. Salomon-Ferrer, and W. A. Lester, Jr., "Linear α -Scaling Evaluation of the Local Energy in Quantum Monte Carlo," in Proceedings of the Pacificchem Symposium on Advances in Quantum Monte Carlo, J. B. Anderson and S. M. Rothstein, eds., ACS Symposium Series **953**, 55 (2007).
4. R. Prasad, N. Umezawa, D. Domin, R. Salomon-Ferrer, and W. A. Lester, Jr., "Quantum Monte Carlo Study of First-Row Atoms using Transcorrelated Variational Monte Carlo Trial Functions," *J. Chem. Phys.* **126**, 164109 (2007).
5. C. Amador-Bedolla, R. Salomon-Ferrer, J. A. Vazquez-Martinez, and W. A. Lester, Jr., "Reagents for Electrophilic Amination: A Quantum Monte Carlo Study," *J. Chem. Phys.* **126**, 204308 (2007).
6. A. Aspuru-Guzik, B. Austin, D. Domin, P. T. A. Galek, N. Handy, R. Prasad, R. Salomon-Ferrer, N. Umezawa, and W. A. Lester, Jr., "Recent Developments in Quantum Monte Carlo: Methods and Applications," in *Computation in Modern Science and Engineering*, **2**, Part A, T. E. Simos and G. Maroulis, eds., AIP Conference Proceedings, 963 (2007), p. 210.
8. D. Domin, W. A. Lester, Jr., R. Whitesides, and M. Frenklach, "Isomer Energy Differences for the C₄H₃ and C₄H₅ Isomers Using Diffusion Monte Carlo," *J. Phys. Chem. A*, **112**, 2065 (2008).
9. M. T. Nguyen, M. H. Matus, W. A. Lester, Jr., and D. A. Dixon, "Heats of Formation of Triplet Ethylene, Ethylidene, and Acetylene," *J. Phys. Chem. A*, **112**, 2082 (2008).
10. R. Whitesides, D. Domin, R. Salomon-Ferrer, W. A. Lester, Jr., and M. Frenklach, "Graphene Layer Growth Chemistry: Five-Six-Ring Flip Reaction," *J. Phys. Chem. A*, **112**, 2125 (2008).
11. W. A. Lester, Jr. and D. Domin, "Some Recent Developments of Quantum Monte Carlo to Molecular Systems," in *Nuclei and Mesoscopic Physics*, P. Danielowicz, P. Piecuch, and V. Zelevinsky, eds., AIP Conference Proceedings 995, (2008), p. 72.
12. D. Domin, B. Braida, and W. A. Lester, Jr., "The Breathing Orbital Valence Bond Method in Diffusion Monte Carlo: C-H Bond Dissociation of Acetylene," *J. Phys. Chem. A*, **112**, 8964 (2008).

13. R. Olivares-Amaya, R. Salomón-Ferrer, W. A. Lester Jr., and C. Amador-Bedolla, "Creation of a GUI for Zori, a Quantum Monte Carlo program, using Rappture," *Computing in Science and Engineering*, January/February 2009, Vol. 11, No.1, p. 41.
14. R. Whitesides, D. Domin, R. Salomon-Ferrer, W.A. Lester, Jr., and M. Frenklach, "Embedded-Ring Migration on Graphene Zigzag Edge," *Proc. Int. Symp. Combustion*, **32**, 577 (2009).

Advanced Nonlinear Optical Methods for Quantitative Measurements in Flames

Robert P. Lucht

School of Mechanical Engineering, Purdue University

West Lafayette, IN 47907-2088

Lucht@purdue.edu

I. Program Scope

Nonlinear optical techniques such as laser-induced polarization spectroscopy (PS), resonant wave mixing (RWM), and electronic-resonance-enhanced (ERE) coherent anti-Stokes Raman scattering (CARS) are techniques that show great promise for sensitive measurements of transient gas-phase species, and diagnostic applications of these techniques are being pursued actively at laboratories throughout the world. We have continued our fundamental theoretical and experimental investigations of these techniques. We have also initiated both theoretical and experimental efforts to investigate the potential of femtosecond (fs) laser systems for sensitive and accurate measurements in gas-phase media. Our initial efforts have focused on fs CARS.

The objective of this research program is to develop and test strategies for quantitative concentration and temperature measurements using nonlinear optical techniques in flames and plasmas. We are investigating the physics of these processes by direct numerical integration (DNI) of the time-dependent density matrix equations for the resonant interaction. Significantly fewer restrictive assumptions are required using this DNI approach compared with the assumptions required to obtain analytical solutions. Inclusion of the Zeeman state structure of degenerate levels has enabled us to investigate the physics of PS and of polarization effects in DFWM and ERE CARS. We are concentrating on the accurate simulation of two-photon processes, including Raman transitions, where numerous intermediate electronic levels contribute to the two-photon transition strength. The DNI numerical methods can be extended to the calculation of the interaction of laser pulses as short as 50 fs simply by decreasing the integration time step (for pulses shorter than this the rotating wave approximation will no longer be valid and the density matrix equations will need to include terms that are negligible for longer pulses).

During the last year we continued our numerical simulations of high-resolution two-photon-induced laser-induced fluorescence (LIF) spectroscopy and ERE CARS spectroscopy of nitric oxide (NO). We have incorporated an effective intermediate electronic level in our calculations to account for the effects of the numerous intermediate electronic levels for the $A^2\Sigma^+ - X^2\Pi$ two-photon resonances. During the last year we made significant progress in developed a unified intermediate electronic level model for both two-photon absorption and Raman transitions in the nitric oxide molecule based on the results of pure rotational CARS measurements of NO. We also continued a detailed investigation of ERE CARS spectroscopy of nitric oxide, concentrating on a DNI analysis of saturation effects in the ERE CARS process, and we have developed a DNI model for broadband Stokes, single-pulse ERE CARS measurements. We have modified significantly our numerical code for calculations of H-atom PS and resonant six-wave mixing (6WM). We have continued a detailed DNI analysis of the fs CARS process for gas-phase N_2 . We have demonstrated the acquisition of single-shot fs CARS signals from flames using a chirped pulse probe pulse following excitation of the Raman coherence using nearly Fourier-transform-limited pump and Stokes pulses. We are presently concentrating on the development of analytical techniques and numerical codes for the accurate determination of temperature from chirped-pulse probe fs CARS signals. We have also continued our development and application of injection-seeded optical parametric sources for high-resolution spectroscopy. In particular, we have demonstrated the use of an optical parametric oscillator (OPO) system with pulsed dye amplification (PDA) for the generation of pulsed, tunable, single-axial-mode laser radiation. This system was used for dual-pump CARS spectroscopy.

II. Recent Progress

A. Electronic-Resonance-Enhanced CARS Spectroscopy of Nitric Oxide

We continue to investigate the physics and explore the diagnostic potential of ERE CARS for measurements of NO [P2,P3,P4,P7,P10,P11]. The primary motivation for the work is to determine whether ERE CARS can be used to measure NO in high-pressure environments, where LIF measurements are very difficult because of interfering LIF signals from species such as O₂, H₂O, and CO₂. ERE CARS is inherently more selective because of the requirement for both electronic and Raman resonance for signal generation. We have developed a method of performing single-shot NO ERE CARS measurements using a broadband Stokes laser, and we applied this during the last year to measurements in counterflow diffusion flames. We have completed a detailed investigation of saturation effects in narrowband, scanning NO ERE CARS spectroscopy. The coupling of saturation effects for the Raman transition and the ultraviolet probe transition is quite complex and was investigated in detail, and we have obtained excellent agreement between experimental and calculated ERE CARS spectra. As was discussed above in terms of two-photon NO LIF, an effective intermediate level is used in the DNI calculations to allow us to account for the numerous intermediate levels that contribute to the two-photon Raman cross section. We have also recently developed a DNI model for single-shot, broadband Stokes ERE CARS. The broadband Stokes laser is simulated using a multimode laser model with random phases for the modes and Gaussian-distributed mode amplitudes. The temporal dependence of the resulting ERE CARS signal is calculated using DNI methods, and the signal is then Fourier transformed to generate the ERE CARS spectrum for comparison with experiment. The theoretical spectra are in good qualitative agreement with experimental single-shot spectra.

B. Femtosecond CARS Calculations

Fs CARS offers several major potential advantages compared with nanosecond (ns) CARS; i.e., CARS as usually performed with nanosecond pump and Stokes lasers. These potential advantages include an elimination of collisional effects in the generation of the signal and the capability of performing real-time temperature and species measurements at data rates of 1 kHz or greater as compared to 10-50 Hz for ns CARS. Single-laser-shot temperature measurements at a data rate of 1 kHz were performed in a room-pressure cell at temperatures of 300 K, 500K, 700K, and 900K. The measurements were performed using a laser system at Wright-Patterson Air Force base in collaboration with Drs. Sukesh Roy and James R. Gord; a schematic diagram of the experiment is shown in Fig. 1. The single-laser-shot measurements were performed by using a chirped probe pulse to map the time-dependent frequency-spread decay of the Raman coherence into the spectrum of the CARS signal pulse. Temperature was determined from the spectral shape of the chirped-probe-pulse (CPP) fs CARS signal for probe delays of approximately 2 ps with respect to the impulsive pump-Stokes excitation of the Raman coherence. Measured and calculate CPP fs CARS spectra are shown in Fig. 2, and comparison of experiment and theory is excellent.

The physics of the CPP fs CARS process was analyzed using a time-dependent density matrix analysis [P5]. The time-dependent density matrix equations for the fs CARS process were formulated and manipulated into a form suitable for solution by direct numerical integration (DNI). The temporal shapes of the pump, Stokes, and probe laser pulses are specified as an input to the DNI calculations. Based on these numerical results, a much faster fitting code was developed to generate synthetic CPP fs CARS spectra. The parameters in the fitting code were varied to obtain the best fit theoretical spectrum for a given experimental spectrum, and temperature was determined as one of the best-fit parameters. A histogram of 1000 single-laser-shot measurements, recorded in 1 second) for the 900 K case is shown in Fig. 3. The temperature histogram has a width that is comparable to that typical of single-shot ns CARS experiments at 900 K.

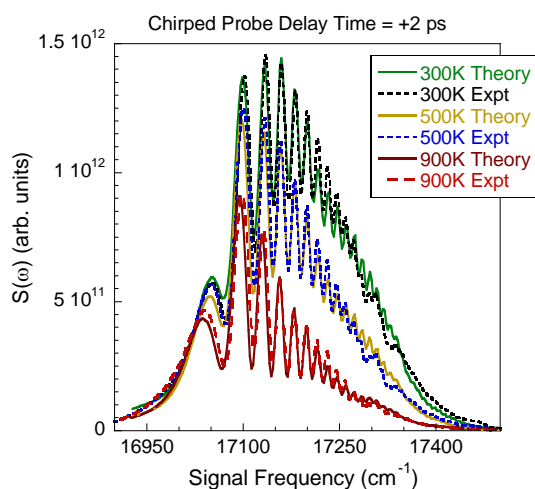
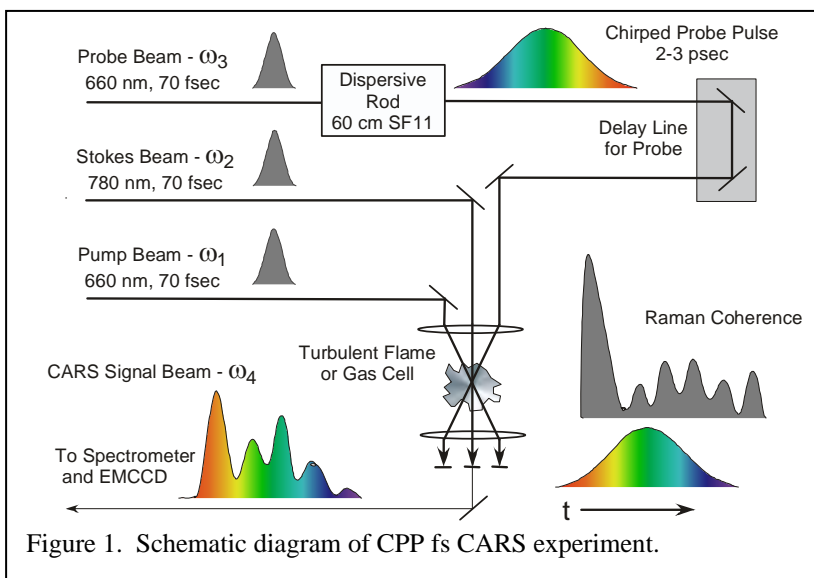


Figure 2. Comparison of experimental and theoretical spectra for CPP fs CARS.

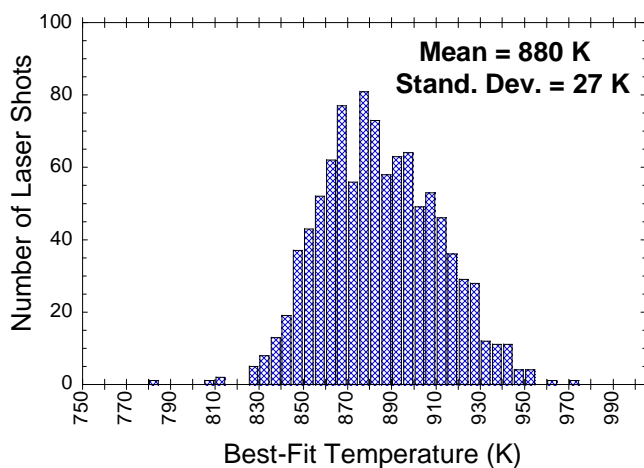


Figure 3. Histogram of single-shot temperatures determined from 900k, 1 bar gas cell using CPP fs CARS.

C. Modeling of Two-Photon Resonances and Six-Wave Mixing Processes

We are continuing our collaborative efforts with Dr. Thomas B. Settersten at Sandia's Combustion Research facility on six-wave mixing (6WM) spectroscopy and polarization spectroscopy of atomic hydrogen. In the last year further experiments were performed using the picosecond laser facilities in Tom Settersten's laboratory. The dependence of the signals on the power and polarization of the pump and probe beams was investigated,

and spectra were recorded by scanning the pump beam across the two-photon 1s-2s resonance and the probe beam across the single-photon 2s-3p resonance. The DNI computer code for the calculation of 6WM and PS signals from atomic hydrogen was significantly modified to incorporate all of the different possible photon mixing processes that can potentially contribute to both the 6WM and PS signals. The modeling of collisional processes in atomic hydrogen has also been modified to account for coherence transfer as well as population transfer.

D. Further Development of Optical Parametric Sources Coupled with Pulse Dye Amplifiers

We have continued to develop optical parametric systems coupled with pulsed dye amplifiers. We are currently operating OPO/PDA systems to produce high-resolution laser radiation at 452 nm and 560 nm. The 452-nm laser radiation is frequency-doubled to generate 226-nm laser radiation for high-spectral-resolution PLIF imaging of NO in high-speed flows. The 560-nm laser radiation is used as the second pump beam in dual-pump CARS. The use of single-mode laser radiation for both pump beams in dual-pump CARS increases the precision and reduces the potential for

systematic errors in temperature and concentration measurements.

III. Future Work

We plan to pursue further theoretical and experimental investigations of the ERE CARS process for NO, CH, and C₂H₂, especially at higher pressures where collisional narrowing may result in significant improvement in the detection limits. The DNI code for single-pulse, broadband Stokes ERE CARS has been developed and will be used to explore the physics of the single-pulse ERE CARS process. Further theoretical investigations of the interaction of fs laser radiation with gas-phase resonances will be performed, and the computer code to extract temperature from single-shot, chirped-probe fs CARS signals will be optimized. Our investigation of the physics of two-photon, two-color PS and 6WM for H-atom measurements will continue in collaboration with Tom Settersten at Sandia. We will continue to explore the physics of these processes using our DNI code. We plan to develop the capability for simultaneous operation of injection-seeded OPG/PDA and OPO/PDA systems. We will use the systems for two-color PS and 6WM measurements of atomic hydrogen and atomic oxygen.

IV. Publications and submitted journal articles supported by this project 2007-2009

1. W. D. Kulatilaka, R. P. Lucht, S. Roy, J. R. Gord, and T. B. Settersten, "Detection of Atomic Hydrogen in Flames Using Two-Color Two-Photon-Resonant Six-Wave-Mixing Spectroscopy," *Appl. Opt.* **46**, 3921-3927 (2007).
2. N. Chai, W. D. Kulatilaka, S. V. Naik, N. M. Laurendeau, R. P. Lucht, J. P. Kuehner, S. Roy, and J. R. Gord, "Nitric Oxide Concentration Measurements in Atmospheric Pressure Flames using Electronic-Resonance-Enhanced Coherent Anti-Stokes Raman Scattering" *Appl. Phys. B* **88**, 141-150 (2007).
3. W. D. Kulatilaka, N. Chai, S. V. Naik, S. Roy, N. M. Laurendeau, R. P. Lucht, J. P. Kuehner, and J. R. Gord, "Effects of Pressure Variations on Electronic-Resonance-Enhanced Coherent Anti-Stokes Raman Scattering of Nitric Oxide," *Opt. Commun.* **274**, 441-446 (2007).
4. N. Chai, W. D. Kulatilaka, S. V. Naik, N. M. Laurendeau, R. P. Lucht, S. Roy, and J. R. Gord, "Detection of Acetylene by Electronic-Resonance-Enhanced Coherent Anti-Stokes Raman Scattering" *Appl. Phys. B* **87**, 731-737 (2007).
5. R. P. Lucht, P. J. Kinnius, S. Roy, and J. R. Gord, "Theory of Femtosecond Coherent Anti-Stokes Raman Scattering for Gas-Phase Transitions," *J. Chem. Phys.* **127**, 044316 (2007).
6. S. V. Naik, J. Hwang, R. P. Lucht, and N. M. Laurendeau, "Measurement and Calculation of the Q-Branch Spectrum of Nitrogen Using Inverse Raman Spectroscopy and cw Raman-Induced Polarization Spectroscopy," *J. Raman Spectrosc.* **39**, 68-78 (2008).
7. J. P. Kuehner, W. D. Kulatilaka, N. Chai, S. V. Naik, N. M. Laurendeau, R. P. Lucht, A. Patnaik, M. O. Scully, S. Roy, and J. R. Gord, "Perturbative Theory and Modeling of Electronic-Resonance-Enhanced Coherent Anti-Stokes Raman Scattering Spectroscopy of Nitric Oxide," *J. Chem. Phys.* **128**, Art. No. 174308 (2008).
8. A. H. Bhuiyan, D. R. Richardson, S. V. Naik, and R. P. Lucht, "Development of an Injection-Seeded Optical Parametric Generator/Pulsed Dye Amplifier System for High-Resolution Spectroscopy," *Appl. Phys. B* **94**, 559-567 (2009).
9. S. Roy, D. R. Richardson, P. J. Kinnius, R. P. Lucht, and J. R. Gord, "Effects of N₂-CO Polarization Beating on Femtosecond Coherent Anti-Stokes Raman Scattering (CARS) Spectroscopy of N₂," *Appl. Phys. Lett.*, accepted for publication (2009).
10. A. K. Patnaik, S. Roy, R. P. Lucht, and J. R. Gord, "Collisional Effects on Molecular Dynamics in Electronic-Resonance-Enhanced CARS," *J. Mod. Opt.* **55**, 3263-3272 (2008).
11. A. K. Patnaik, S. Roy, R. P. Lucht, J. R. Gord and T. B. Settersten, "Effects of Collisions on Electronic-Resonance-Enhanced Coherent Anti-Stokes Raman Scattering of Nitric oxide," *J. Chem. Phys.*, accepted for publication (2009).

Time-Resolved Infrared Absorption Studies of Radical Reactions

R. G. Macdonald
Chemistry Division
Argonne National Laboratory
Argonne, IL 60439
Email: rgmacdonald@anl.gov

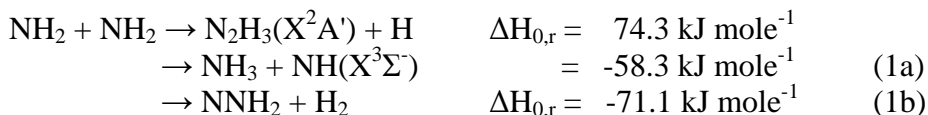
Background

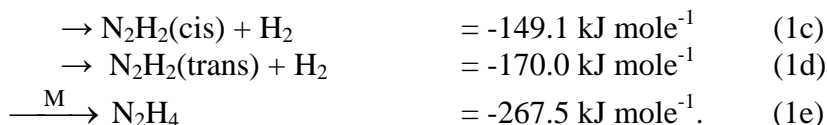
Information about the dynamics of radical-radical reactions is sparse. However, these processes are important in combustion being either chain propagating or terminating steps as well as potentially producing new molecular species. For almost all radical-radical reactions, multiple product channels are possible, and the determination of product channels will be a central focus of this experimental effort. In the current experiments, both transient species are produced by excimer laser photolysis of suitable photolytes, and if possible, two species are detected simultaneously using different continuous-wave laser sources operating in the red, near infrared and infrared spectral regions. This approach allows for the direct determination of the second-order rate constant under any concentration conditions if the appropriate absorption cross sections have been measured. The time dependence of individual ro-vibrational states of the reactants and/or products is followed by frequency- and time-resolved absorption spectroscopy. The simultaneous detection of multiple species ensures that species concentration profiles can be normalized to a common set of reaction conditions. In order to determine branching ratios and second-order rate constants, it is necessary to measure state-specific absorption coefficients and transition moments of radicals. These measurements play an important role in this experimental study.

Recent Results

$\text{NH}_2(\text{X}^2\text{B}_1) + \text{NH}_2(\text{X}^2\text{B}_1)$. The NH_2 radical is an important intermediate in both the production of NO_x in combustion processes and the removal of NO_x from combustion exhaust gases. The removal processes are based on the addition of NH_3 , $(\text{HOCN})_3$ or $(\text{NH}_2)_2\text{CO}$ to the gas stream, resulting in the Thermal De NO_x , RAPRENO $_x$ and NO_x OUT treatment processes, respectively. A key reaction in these processes is the $\text{NH}_2 + \text{NO}$ reaction. The NH_2 radical also plays a key role in the pyrolysis of NH_3 and other environments where nitrogen chemistry is important. However, in spite of its importance, the chemistry of the NH_2 radical, especially in reactions with other transient species, has not been widely studied. As the first step in investigating the chemistry of NH_2 with other radicals, and in particular the reaction with OH, a study of the self-reaction of NH_2 at low pressure and a temperature of 293K was undertaken and completed. Previously, this laboratory has investigated the self-reaction of the OH radical at low pressure near room temperature.

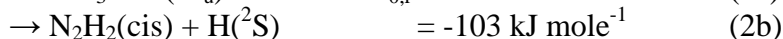
There is only a singlet and triplet spin manifold but still many product channels:





In the present investigation, the NH_2 radical was created by the 193 nm photolysis of NH_3 dilute in CF_4 . Temporal concentration profiles of both NH_3 and NH_2 were recorded simultaneously using time- and frequency-resolved absorption spectroscopy. At the low pressures of the present experiments k_{1e} is close to the pure three-body limit and the total removal rate constant of NH_2 is given by $k_1 = k_0 + k_{1e}[\text{M}]$, where k_0 is the sum of the two-body disproportionation channels and k_{1e} is the recombination rate constant. The results of the present experiments are significantly different from previous measurements. The value of k_{1e} was found to be $(8.0 \pm 0.5) \times 10^{-29} \text{ cm}^6 \text{ molecules}^{-2} \text{ s}^{-1}$ a factor of ten larger than previous determinations (K. Fagerstrom, J. T. Jodkowski, A. Lund and E. Ratajczak, Chem. Phys. Lett. **236**, 103 (1995)).

$\text{NH}_2(\text{X}^2\text{B}_1) + \text{NH}(\text{X}^3\Sigma^-)$ and $\text{NH}_2(\text{X}^2\text{B}_1) + \text{H}(^2\text{S})$. The 193 nm photolysis of NH_3 is known to produce small quantities of the NH radical by a variety of one or two photon processes (A. Kaes and F. Stuhl, J. Chem. Phys. **97**, 7362 (1992)). This allowed for the direct determination of the $\text{NH}_2 + \text{NH}$ rate constant. Two spin manifolds, corresponding to doublet and quartet spin states, correlate to the $\text{NH}_2 + \text{NH}$ asymptote with four possible product channels:



The reverse of reaction 2a is assumed to have a large activation barrier. The rate constant for reaction 2 was found independent of pressure (3-10 Torr), and the most likely reaction products are channels 2b and 2c, $\text{N}_2\text{H}_2 + \text{H}$. Both NH_2 and NH were monitored simultaneously, NH_2 in the red spectral region, at 14800.59 cm^{-1} and NH in the infrared, at 3242.890 cm^{-1} . The modeling of the system required a source of the NH radical as the reaction proceeded. The mostly likely source of the NH radical is the $\text{NH}_2 + \text{H} \rightarrow \text{NH} + \text{H}_2$ reaction, and the data analysis provided a measurement of the rate constant for this process. Although the initial concentration of NH_2 was several hundred of times larger than the initial NH concentration, the NH concentration profiles were not described by a single exponential decay. The rate constant for the $\text{NH}_2 + \text{NH} \rightarrow \text{N}_2\text{H}_2 + \text{H}$ reaction was $(9.6 \pm 3.2) \times 10^{-11} \text{ cm}^3 \text{ molecules}^{-1} \text{ s}^{-1}$ in good agreement with the only previous measurement of $(1.3 \pm 0.5) \times 10^{-11}$ (P. Dransfeld, H. Hack, H. Kurzke, F. Temps, and H. G. Wagner, 20th Sym. (Int.) Comb. 655 (1984)). The rate constant for the $\text{NH}_2 + \text{H}$ reaction was found to be $(7.7 \pm 14) \times 10^{-15} \text{ cm}^3 \text{ molecules}^{-1} \text{ s}^{-1}$. There are no previous measurements near 300 K.

$\text{NH}_2(\text{X}^2\text{B}_1) + \text{OH}(\text{X}^2\Pi)$. Preliminary experiments have begun on the $\text{NH}_2 + \text{OH}$ reaction system. The OH radical possess electronic angular momentum so that the singlet and triplet spin manifolds now have A' and A'' electronic symmetry in planar C_s geometry. There are several possible product channels:





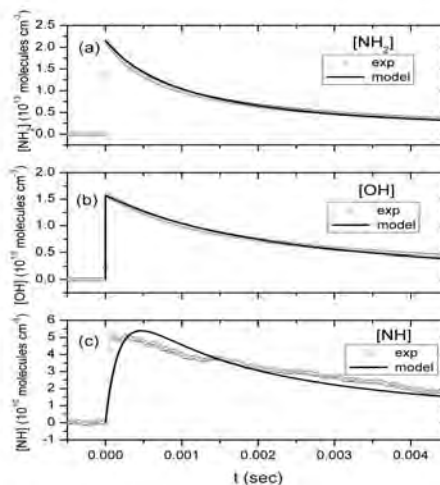
NH_2 and either OH or NH were detected simultaneously on each photolysis laser pulse. The chemical model describing this system is more complicated than the sum of the individual self-reaction mechanisms because of the large number of cross-reactions between the two systems. Under the

conditions of the experiment, reactions 3b and 3d are expected to dominate with the recombination channel the major channel.

Over 3 to 9 Torr pressure range, the value of k_{3b} was found to be $(6.4 \pm 4.2) \times 10^{-13} \text{ cm}^3 \text{ molecules}^{-1} \text{ s}^{-1}$ and accounted for about 6% of the total reaction rate. Typical concentration profiles are shown in the figure for a total pressure of 4.79 Torr.

The open symbols are the experimental data shown every 10 data point and the solid curves are the model predictions optimizing k_{1e} , with H_2O as third body, k_{3b} , k_{3d} , and $k_{\text{NH}+\text{OH}}$.

The NH concentration profile was fit by varying the $\text{NH} + \text{OH}$ rate constant, and $k_{\text{NH}+\text{OH}}$ was estimated to be $1.3 \pm 0.7 \times 10^{-10} \text{ cm}^3 \text{ molecules}^{-1} \text{ s}^{-1}$. Further work requires the determination of pressure broadening parameters on the OH spectroscopic transition and the direct measurement of the NH_2OH product from channel 3d.



Publications 2007-present.

Determination of the rate constant for the $\text{NCO}(X^2\Pi) + \text{CH}_3(X^2A_2'')$ reaction at 293 K and an estimate of possible product channels.

-Y. Gao and R. G. Macdonald
J. Phys. Chem. A **110**, 977-989 (2006).

Determination of the rate constant for the $\text{OH}(X^2\Pi) + \text{OH}(X^2\Pi) \rightarrow \text{O}(^3P) + \text{H}_2\text{O}$ reaction over the temperature range 293-373 K.

-Mi-Kyung Bahng and R. G. Macdonald
J. Phys. Chem. A **111**, 3850-3861 (2007).

Determination of the rate constant for the $\text{NH}_2(X^2B_1) + \text{NH}_2(X^2B_1)$ reaction at low pressure and 293 K.

-Mi-Kyung Bahng and R. G. Macdonald
J. Phys. Chem. A **112**, 13432-13443 (2008).

Determination of the rate constants for the radical-radical reactions $\text{NH}_2(X^2B_1) + \text{NH}(^3\Sigma)$ and $\text{NH}_2(X^2B_1) + \text{H}(^2S)$ at 293 K.

-Mi-Kyung Bahng and R. G. Macdonald
J. Phys. Chem. A **113**, 2415-2423 (2009).

Theoretical studies of chemical reactions related to the formation and growth of polycyclic aromatic hydrocarbons and molecular properties of their key intermediates

Alexander M. Mebel

Department of Chemistry and Biochemistry, Florida International University
Miami, Florida 33199. E-mail: mebela@fiu.edu

Program Scope

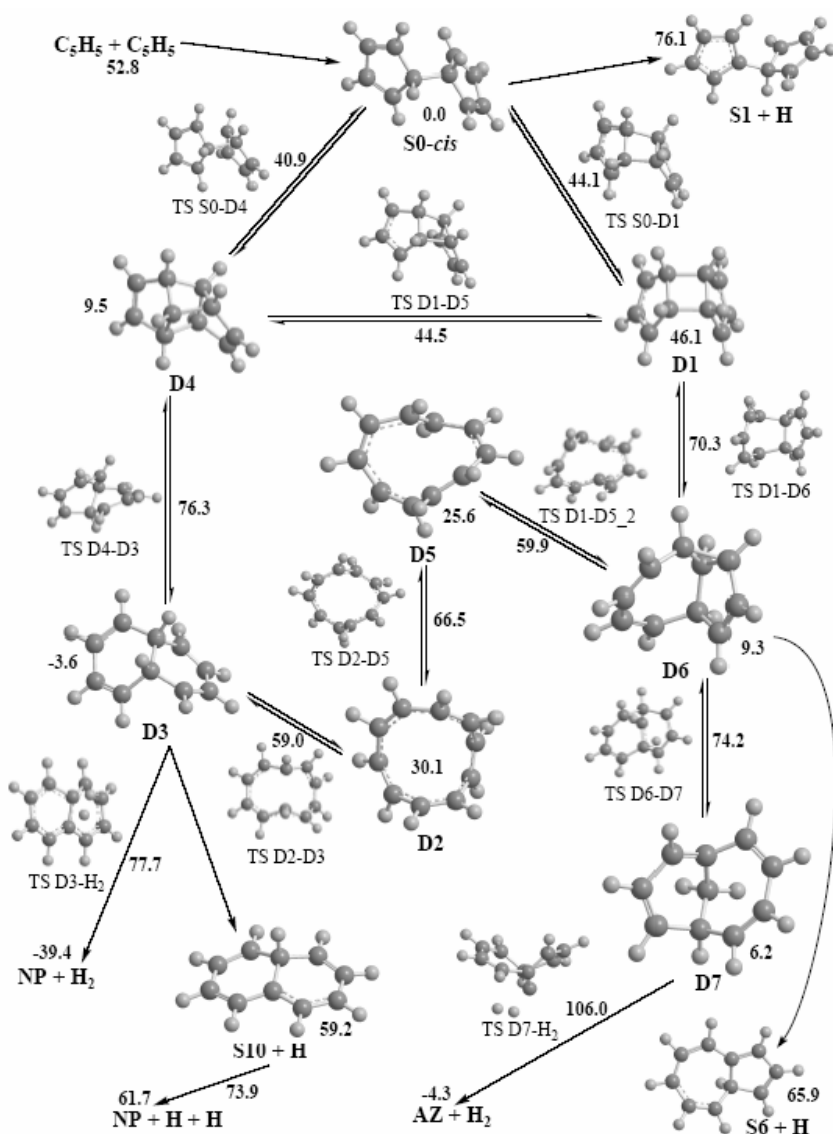
We perform theoretical studies of the reactions of PAH formation and growth using *ab initio* molecular orbital and density functional calculations of potential energy surfaces (PES) and statistical (RRKM and TST) computations of absolute rate constants and relative product yields. In particular, we address the reactions of cyclopentadienyl radicals and cyclopentadiene involving the C₁₀H₁₁, C₁₀H₁₀, and C₁₀H₉ PES and producing naphthalene, azulene, fulvalene, and indene, and investigate the formation mechanisms of naphthalene and indene from smaller hydrocarbons, alternative to the HACA sequences. Our studies also include related chemical reactions under single-collision conditions, such as crossed molecular beam reactions of singlet and triplet C₂ with C₄H₆ isomers and C₆H₆ accessing previously unexplored regions of the C₆H₆ (benzene) and C₈H₆ (phenylacetylene) surfaces and the reactions of phenyl radical with C₃H₄, C₃H₆, and C₄H₆ occurring on the C₉H₉, C₉H₁₁, and C₁₀H₁₁ PES and directly linked to the indene, naphthalene, and azulene formation routes. The objective of these studies is to untangle elementary reaction mechanisms for these complex reactions and to predict their rate constants and product yields in a broad range of reaction conditions. In addition, we investigate molecular properties, potential energy surfaces, and dissociation mechanisms of hydrocarbon cations, which are relevant to the photoionization spectroscopy and mass spectrometry diagnostics of various products of elementary combustion reactions.

Recent Progress

Variational calculations of thermal rate constants for the C₆H₅ + O₂ association reaction using density functional and ab initio potentials. Variational calculations of thermal rate constants for the C₆H₅ + O₂ → C₆H₅OO barrierless association reaction have been carried out using canonical variational transition state (CVTST) and variable reaction coordinate transition state (VRC-TST) theories with minimal energy reaction path (MEP) potentials computed employing the *ab initio* multireference CASPT2(19,14)//CASSCF(9,9)/aug-cc-pVDZ, CASPT2(9,9)//CASSCF(9,9)/aug-cc-pVDZ, and density functional B3LYP/6-311++G** methods. The best agreement of the calculated rate constants, within a factor of 2 from the available experimental data in the low-temperature 297-473 K range, is achieved when the most accurate CASPT2(19,14)//CASSCF(9,9)/aug-cc-pVDZ MEP potential is utilized in conjunction with CVTST. The CVTST approach with the CASPT2(9,9)//CASSCF(9,9)/aug-cc-pVDZ potential gives very similar results despite the fact that the CASPT2(9,9) method greatly overestimates the energy of the forming C-O bond. The results demonstrate that the behavior of the potential energy at large separation between the C₆H₅ and O₂ fragments is most critical for accurate description of the rate constant. The CCSD(T)/aug-cc-pVDZ long-range potential exhibits an artificial barrier for the reaction and therefore is not suitable for rate constant calculations. The CVTST B3LYP/6-311++G** approach gives qualitatively similar thermal rate constants but overestimate the experimental values by factors 3-5. The rate expression obtained

by fitting our best CVTST CASPT2(19,14) calculated rate constants, $k(T) = 4.54 \times 10^{15} T^{-1.056} \exp(910.3/RT)$ for $T = 298-3000$ K, qualitatively reproduces the observed experimental temperature dependence both in the 297-473 K (negative) and 418-815 K (positive) temperature ranges and generally underestimates the experimental rate constants by a factor of 2.

Potential energy surface of $C_{10}H_{10}$ related to the recombination of two cyclopentadienyl radicals and the production of $C_{10}H_8$ (naphthalene and its isomers) + $2H$ and $C_{10}H_8 + H_2$.



According to multi-reference CASPT2/CASSCF calculations, if 9,10-dihydrofulvalene **S0** formed by the recombination of two C_5H_5 radicals does not lose an H atom immediately, it can eventually rearrange to 9,10-dihydronaphthalene **D3**, with the latter producing naphthalene either by four-center 9,10- H_2 loss or via two consecutive H eliminations. The mechanism of the **S0-D3** isomerization involves the formation of a tricyclic intermediate **D1**, which then ring-opens to a ten-member cyclic structure **D2** rearranging in turn to 9,10-dihydronaphthalene. RRKM calculations of rate constants and product branching ratios are currently underway to compare relative importance of the $C_{10}H_9 + H$ and $C_{10}H_8 + H_2$ product channels depending on the reaction conditions, such as temperature and pressure.

Theoretical study of unimolecular decomposition of allene and propyne cations. Ab initio CCSD(T) and CASPT2 calculations with geometry optimization at the density functional B3LYP or multireference CASSCF levels have been carried out to compute ionization energies and to unravel the dissociation mechanism of allene and propyne cations, $C_3H_4^{n+}$ ($n = 1-3$). The results indicate that the dominant decomposition channel of the monocation is $c-C_3H_3^+ + H$, endothermic by 37.9 kcal/mol and occurring via a barrier of 43.1 kcal/mol, with possible minor contributions from $H_2CCCH^+ + H$ and $HCCCH^+ + H_2$. For the dication, the competing reaction channels are

predicted to be $c\text{-C}_3\text{H}_3^+ + \text{H}^+$, $\text{H}_2\text{CCCH}^+ + \text{H}^+$, and $\text{CCCH}^+ + \text{H}_3^+$, with dissociation energies of -20.5, 8.5, and 3.0 kcal/mol, respectively. The calculations reveal an H_2 -roaming mechanism for the H_3^+ loss, where a neutral H_2 fragment is formed first, then roams around and abstracts a proton from the remaining molecular fragment before leaving the dication. According to RRKM calculations of energy-dependent rate constants for individual reaction steps, relative product yields vary with the available internal energy, with $c\text{-C}_3\text{H}_3^+ + \text{H}^+$ being the major product just above the dissociation threshold of 69.6 kcal/mol, in the energy range of 70-75 kcal/mol, and $\text{CCCH}^+ + \text{H}_3^+$ taking over at higher energies. The $\text{C}_3\text{H}_4^{3+}$ trication is found to be not very stable and to decompose with thresholds of 18.5 and 3.7 kcal/mol for allene and propyne, respectively, producing $\text{H}_2\text{CCCH}^{2+} + \text{H}^+$, $\text{CHCHCH}^{2+} + \text{H}^+$, $\text{C}_2\text{H}_2^{2+} + \text{CH}_2^+$, and $\text{CCH}_2^{2+} + \text{CH}_2^+$ with high exothermicity of 98-185 kcal/mol. The tetracation of C_3H_4 is concluded to be unstable and therefore no more than 3 electrons can be removed from this molecule before it falls apart.

Future Plans

We will continue theoretical calculations of rate constants for the recombination reaction of two cyclopentadienyl radicals and further rearrangement and decomposition routes on the $\text{C}_{10}\text{H}_{10}$ PES. The emphasis will be on predicting a reliable rate expression for the $\text{C}_5\text{H}_5 + \text{C}_5\text{H}_5$ association step using CVTST and VRC-TST approaches and determining relative yields of the $\text{C}_{10}\text{H}_9 + \text{H}$ and $\text{C}_{10}\text{H}_8 + \text{H}_2$ product channels at various temperatures and pressures. Next, we will map out the PES for naphthyl radical oxidation, $\text{C}_{10}\text{H}_7 + \text{O}_2$, carry out RRKM calculations of the reaction rate constants and product branching ratios (including variational calculations for the initial reaction step), and will compare the naphthyl + O_2 and phenyl + O_2 reactions. We will also continue our systematic survey of chemical reactions potentially leading to the formation of indene and/or naphthalene in combustion flames, including C_7/C_2 (toluene + C_2H_2), C_6/C_3 (benzene, fulvene, or phenyl + C_3H_3 , and phenyl + allene C_3H_4), C_5/C_2 (cyclopentadienyl + $2\text{C}_2\text{H}_2$), C_5/C_4 (cyclopentadienyl + vinylacetylene), and C_6/C_4 (phenyl + C_4H_6 isomers, benzene + C_4H_5). In relation to cross molecular beams experiments carried out by Dr. Kaiser's group within the DOE/GPCP program, we will complete our ab initio/statistical theory studies of the reactions of phenyl radical with C_4H_6 isomers, including 1,2-butadiene, 1- and 2-butyne, and will investigate mechanisms of the $\text{C}_2 + \text{C}_4\text{H}_6$ reactions in singlet and triplet electronic states potentially leading to the formation of the first aromatic ring (phenyl radical).

DOE/BES sponsored publications (2007-2009)

1. X. Gu, Y. Guo, F. Zhang, A. M. Mebel, R. I. Kaiser, "A crossed molecular beam study of the reaction of dicarbon molecules with benzene – identification of the phenylethynyl radical ($\text{C}_6\text{H}_5\text{CC}; X^2A'$)", *Chem. Phys. Lett.*, 436, 7 (2007).
2. V. V. Kislov, A. M. Mebel, "An ab initio G3-type / statistical theory study of the formation of indene in combustion flames. I. The pathways involving benzene and phenyl radical", *J. Phys. Chem. A*, 111, 3922-3931 (2007).
3. Y. Guo, X. Gu, F. Zhang, A. M. Mebel, R. I. Kaiser, "A crossed molecular beam study on the formation of hexenediynyl radical ($\text{H}_2\text{CCCCCCH}; \text{C}_6\text{H}_3 (X^2A')$) via reactions of tricarbon molecules, $\text{C}_3(X^1\Sigma_g^+)$ with allene ($\text{H}_2\text{CCCH}_2; X^1A_1$) and methylacetylene ($\text{CH}_3\text{CCH}; X^1A_1$)", *Phys. Chem. Chem. Phys.*, 16, 1972-1979 (2007).
4. A. M. Mebel, G.-S. Kim, V. V. Kislov, R.I. Kaiser, "The reaction of tricarbon with acetylene: An ab initio/RRKM study of the potential energy surface and product branching ratios, *J. Phys. Chem. A*, 111, 6704-6712 (2007).

5. A. M. Mebel, V. V. Kislov, R. I. Kaiser, "Theoretical studies of potential energy surfaces and product branching ratios for the reactions of C_2 with small unsaturated hydrocarbons (acetylene, ethylene, methylacetylene, and allene)", in *Modern Gas Phase Molecular Dynamics*, K. C. Lin, P. D. Kleiber, Eds., Transworld Research Network, Kerala, India, 113-159 (2007).
6. X. Gu, Y. Guo, F. Zhang, A. M. Mebel, R. I. Kaiser, "A crossed molecular beams study on the formation and energetics of the resonantly stabilized free $i-C_4H_3(X^2A')$ radical and its isotopomers, *Chem. Phys.*, 335, 95-108 (2007).
7. L. Yao, A. M. Mebel, H. F. Lu, H. J. Nausser, S. H. Lin, "Anharmonic effect on unimolecular reactions with application to the photodissociation of ethylene", *J. Phys. Chem. A*, 111, 6722-6729 (2007).
8. Y. Guo, A. M. Mebel, F. Zhang, X. Gu, R. I. Kaiser, "Crossed molecular beam studies of the reactions of allyl radicals, $C_3H_5(X^2A_1)$, with methylacetylene ($CH_3CCH(X^1A_1)$), allene ($H_2CCCH_2(X^1A_1)$), and their isotopomers", *J. Phys. Chem. A*, 111, 4914-4921 (2007).
9. A. M. Mebel, V. V. Kislov, M. Hayashi, "Prediction of product branching ratios in the $C(^3P) + C_2H_2 \rightarrow l-C_3H + H/c-C_3H + H/C_3 + H_2$ reaction using ab initio coupled clusters/complete basis set calculations combined with RRKM and radiationless transition theories", *J. Chem. Phys.*, 126, 204310, 11 pp. (2007).
10. X. Gu, Y. Guo, F. Zhang, A. M. Mebel, R. I. Kaiser, "Unimolecular decomposition of chemically activated singlet and triplet D3-methyldiacetylene molecules", *Chem. Phys. Lett.*, 444, 220-225 (2007).
11. V. V. Kislov, Mebel A.M., "The formation of naphthalene, azulene, and fulvalene from the recombination product of two cyclopentadienyl radicals: An ab initio/RRKM study of rearrangements of the $C_5H_5-C_5H_4$ (9-H-fulvalenyl) radical", *J. Phys. Chem. A*, 111, 9532-9543 (2007).
12. Y. A. Dyakov, A. M. Mebel, S. H. Lin, Y. T. Lee, C.-K. Ni, "Photodissociation of 1,3,5-triazine: An ab initio and RRKM study", *J. Phys. Chem. A*, 111, 9591-9599 (2007).
13. X. Gu, Y. Guo, A. M. Mebel, R. I. Kaiser, "A crossed beam investigation of the reactions of tricarbon molecules, $C_3(X^1\Sigma_g^+)$, with acetylene, $C_2H_2(X^1\Sigma_g^+)$, ethylene, $C_2H_4(X^1A_g)$, and benzene, $C_6H_6(X^1A_{1g})$ ", *Chem. Phys. Lett.*, 449, 44-52 (2007).
14. Kislov V.V., Mebel A.M., "An ab initio G3-type / statistical theory study of the formation of indene in combustion flames. II. The pathways originated from reactions of cyclic C_5 species - cyclopentadiene and cyclopentadienyl Radical", *J. Phys. Chem. A*, 112, 700-716 (2008).
15. Gu X., Kaiser R.I., Mebel A.M., "Chemistry of energetically activated cumulenes – from allene (H_2CCCH_2) to hexapentaene ($H_2CCCCCCH_2$)", *ChemPhysChem*, 9, 350-369 (2008).
16. Wang Q., Wu D., Jin M., Liu F., Hu F., Cheng X., Liu H., Hu Z., Ding D., Mineo H., Dyakov Y.A., Mebel A.M., Chao S.D., Lin S.H., "Experimental and theoretical investigation of ionization / dissociation of cyclopentanone molecule in a femtosecond laser field", *J. Chem. Phys.*, 129, 204302 (2008).
17. Mebel A.M., Bandrauk A.D., "Theoretical study of unimolecular decomposition of allene cations", *J. Chem. Phys.*, 129, 224311 (2008).
18. Kislov V.V., Xu Z.F., Mebel A.M., Lin M.C., "Variational calculations of thermal rate constants for the $C_6H_5 + O_2$ reaction using density functional and ab initio potentials", *Phys. Chem. Chem. Phys.*, submitted (2009).
19. Gu X., Zhang F., Kaiser R.I., Kislov V.V., Mebel A.M., "Reaction dynamics of the phenyl radical with 1,2-butadiene", *Chem. Phys. Lett.*, submitted (2009).

FLASH PHOTOLYSIS-SHOCK TUBE STUDIES

Joe V. Michael

Gas Phase Chemical Dynamics Group, Chemistry Division
Argonne National Laboratory, Argonne, IL 60439
E-mail: jmichael@anl.gov

The scope of the program is to measure high-temperature thermal rate constants for use in high-temperature combustion with the reflected shock tube technique. As described earlier, we have used a multi-pass optical system for detecting OH-radicals¹⁻⁴ and Atomic Resonance Absorption Spectrometry (ARAS) for detecting H- and/or D-atoms.⁵⁻⁷

During the past year, the reflected shock tube technique using OH-radical absorption at 308 nm has been used to study two thermal decompositions and twelve bimolecular reactions at path lengths ranging from 1.75 to 7.00 m with $[\text{OH}]_t$ being determined from measured absorbance through an earlier determination¹ of the absorption cross-section at 308 nm ($\sigma_{\text{OH}} = (4.516 - 1.18 \times 10^{-3} T) \times 10^{-17} \text{ cm}^2 \text{ molecule}^{-1}$). The present optical configuration gives an S/N ratio of one at $\sim 1.0 \times 10^{12}$ radicals cm^{-3} .

Alkanes + OH

High temperature rate constant experiments on OH with five large (C_5 - C_8) saturated hydrocarbons (n-heptane, neo-octane, n-pentane, n-hexane, and 2,3 dimethylbutane) were performed with the reflected shock tube technique over the T-range, 789-1308 K, using multi-pass absorption spectrometric detection of OH radicals at 308 nm. The experimental data and the evaluations obtained for these five larger alkanes in the present work have been used along with prior data/evaluations obtained in this laboratory for H abstractions by OH from a series of smaller alkanes (C_3 - C_5) to derive rate rules for abstractions from various types of primary, secondary, and tertiary H atoms. Specifically, the current group scheme has been applied with good success to H abstractions by OH from a series of n-alkanes (n-octane through n-cetane) and serves to reduce the uncertainties in rate constants for this class of reactions. The results can be expressed in Arrhenius form (in units, $\text{cm}^3 \text{ molecule}^{-1} \text{ s}^{-1}$) as:

$$k_{\text{OH}+\text{n-heptane}} = (2.48 \pm 0.17) \times 10^{-10} \exp(-1927 \pm 69 \text{ K}/T) \quad (838\text{-}1287 \text{ K}) \quad (1)$$

$$k_{\text{OH}+2,2,3,3\text{-TMB}} = (8.26 \pm 0.89) \times 10^{-11} \exp(-1337 \pm 94 \text{ K}/T) \quad (789\text{-}1061 \text{ K}) \quad (2)$$

$$k_{\text{OH}+\text{n-pentane}} = (1.60 \pm 0.25) \times 10^{-10} \exp(-1903 \pm 146 \text{ K}/T) \quad (823\text{-}1308 \text{ K}) \quad (3)$$

$$k_{\text{OH}+\text{n-hexane}} = (2.79 \pm 0.39) \times 10^{-10} \exp(-2301 \pm 134 \text{ K}/T) \quad (798\text{-}1299 \text{ K}) \quad (4)$$

$$k_{\text{OH}+2,3\text{-DMB}} = (1.27 \pm 0.16) \times 10^{-10} \exp(-1617 \pm 118 \text{ K}/T) \quad (843\text{-}1292 \text{ K}) \quad (5)$$

Using the next nearest neighbor (NNN) group method of Cohen,⁸ earlier experimental results for smaller n-alkanes, and experimental evaluations including low-T data,⁹ rate constants per H atom were derived for primary and two secondary abstraction groups in n-alkanes. In addition we have identified a third type of secondary abstraction for n-alkanes C_7 and larger, and the use of the derived groups allows accurate rate constants for H abstraction by OH from any large n-alkane (e.g., n-cetane) to be determined.

NH_2OH Thermal Decomposition

We have studied, for the first time, the thermal decomposition of hydroxylamine, NH_2OH . The motivation and goal of the study is to demonstrate the possibility of using

this molecule as an additional OH-radical source for bimolecular reaction studies at somewhat lower-T than is possible with CH₃OH, thereby bridging the temperature gap between CH₃OH and tert-butyl peroxide (tBH) sources. The utility of this new OH source was demonstrated in our recent study of the reactions of OH with acetylene and ethylene.¹⁰ The present analysis of the NH₂OH decomposition employs a combination of theory and experiment to explore the products and rate constants. High level *ab initio* calculations suggest two possible product channels, NH₂ + OH and NH₃ + O. Experimental observations of the OH and O time profiles demonstrate that only the NH₂ + OH channel is significant.

The experimentally observed OH profiles arising from the NH₂OH decomposition are found to have secondary sensitivity to two additional reactions, namely, OH + NH₂OH → products and, OH + NH₂ → NH + H₂O. Figure 1 shows a typical example of an experiment at 1535 K. In this experiment, we identified three processes



that, in different time regimes, determine the shape of the profile over the entire time range of 1.4 ms. Hence, estimates for these sensitive reactions could be determined. The results for k_6 can be described in Arrhenius form between 1355 and 1880 K by

$$\log[k_6/(\text{cm}^3 \text{ molecule}^{-1} \text{ s}^{-1})] = (-10.12 \pm 0.20) + (-6793 \pm 317 \text{ K}/T) \quad (9)$$

A first principles theoretical description with $\langle \Delta E_d \rangle = 500 \text{ cm}^{-1}$ provides a good fit to the experimental data for reaction (6). In the intermediate time regime, reaction (7) becomes important, and, from profile fits, the rate constant for (7) is obtained as:

$$\log[k_7/(\text{cm}^3 \text{ molecule}^{-1} \text{ s}^{-1})] = (-9.75 \pm 0.08) + (-1248 \pm 123 \text{ K}/T) \quad (11)$$

From long time fits, k_8 can be obtained as:

$$\log[k_8/(\text{cm}^3 \text{ molecule}^{-1} \text{ s}^{-1})] = (-10.00 \pm 0.06) + (-879 \pm 101 \text{ K}/T) \quad (12)$$

For reactions (7) and (8), rate constants were also theoretically determined and moderate agreement with experiment is obtained in both cases. Also, there is little known about the rate coefficients for the subsequent reactions of NH. A number of these reactions, specifically, NH + OH, NH + NH and NH + NH₂ might be expected to have a significant impact on the OH profiles. Thus, for these reactions *a priori* theoretical predictions of their rate constants were obtained and incorporated in the modeling of the OH time profiles. Finally, during the course of the theoretical analysis we derived rate constant predictions for the NH₂ + OH → NH₃ + O reaction. These various reactions in the NH₂OH decomposition system are also important in the thermal de-NO_x mechanism¹¹ and the present rate constant estimates should prove useful for modeling studies of NO_x formation during combustion.

Ethanol Dissociation

Dissociation rate constants for ethanol have been measured at high-T in reflected shock waves using OH optical absorption at 308 nm with a multi-pass optical White cell and H-atom ARAS. Three dissociation processes are dominant at high-T are (1) $C_2H_5OH \rightarrow C_2H_4 + H_2O$, (2) $\rightarrow CH_3 + CH_2OH$, and/or (3) $\rightarrow C_2H_5 + OH$. Reaction (3) could be measured directly. In order to measure the other channels, high sensitivity H-atom ARAS detection was used to measure the sum of (2) and (3) since H-atoms are instantaneously formed from CH_2OH and C_2H_5 . By difference, rate constants for (1) were obtained. A potential low-T complication is the scavenging of OH by unreacted ethanol in the OH experiments, and therefore rate constants for $OH + C_2H_5OH \rightarrow$ products were measured. The experimental results are compared to earlier work and are rationalized in terms of modern unimolecular reaction rate theory. The experimental branching ratios and the theoretical predictions are shown in Fig. 2.

We also have completed work on the bimolecular reactions of D with ethanol and acetaldehyde, and on the thermal decompositions of CH_3CHO and C_3H_8 . Additional atom and radical with molecule reaction studies (e. g. Cl + hydrocarbons) are in the planning stage. We are also planning thermal decomposition studies using H/D-atom ARAS on C_2H_4 , toluene and benzyl.

This work was supported by the U. S. Department of Energy, Office of Basic Energy Sciences, Division of Chemical Sciences, Geosciences, and Biosciences, under Contract No. DE-AC02-06CH11357.

References

1. Srinivasan, N. K.; Su, M.-C.; Sutherland, J. W.; Michael, J. V. *J. Phys. Chem. A* **2005**, *109*, 1857.
2. Su, M.-C.; Kumaran, S. S.; Lim, K. P.; Michael, J. V. *Rev. Sci. Instr.* **1995**, *66*, 4649.
3. Su, M.-C.; Kumaran, S. S.; Lim, K. P.; Michael, J. V.; Wagner, A. F.; Dixon, D. A.; Kiefer, J. H.; DiFelice, J. *J. Phys. Chem.* **1996**, *100*, 15827.
4. Su, M.-C.; Kumaran, S. S.; Lim, K. P.; Michael, J. V.; Wagner, A. F.; Harding, L. B.; Fang, D.-C. *J. Phys. Chem. A* **2002**, *106*, 8261.
5. S. L. Mielke, K. A. Peterson, D. W. Schwenke, B. C. Garrett, D. G. Truhlar, J. V. Michael, M.-C. Su, and J. W. Sutherland, *Phys. Rev. Lett.* **2003**, *91*, 063201.
6. J. V. Michael, M.-C. Su, and J. W. Sutherland, *J. Phys. Chem. A* **2004**, *108*, 432.
7. J. V. Michael, M.-C. Su, J. W. Sutherland, L. B. Harding, and A. F. Wagner, *Proc. Combust. Inst.* **2004**, *30*, 965.
8. N. Cohen, *Int. J. Chem. Kin.* **1991**, *23*, 397.
9. R. Sivaramakrishnan and J. V. Michael, *J. Phys. Chem. A*, in press.
10. N. K. Srinivasan, M.-C. Su, and J. V. Michael, *Phys. Chem. Chem. Phys.* **2007**, *9*, 4155.
11. (a) R. K. Lyon, *Int. J. Chem. Kinet.* **1976**, *8*, 315. (b) J. A. Miller and P. Glarborg, in *Gas Phase Chemical Reaction Systems, Experiments and Models 100 Years after Max Bodenstein*, Springer Series in Chemical Physics 61, Springer-Verlag Berlin Heidelberg, pp. 318-333, 1996.
12. J. Li, A. Kazakov, F. L. Dryer, *J. Phys. Chem. A* **2004**, *108*, 7671.
13. J. Park, R. S. Zhu, M. C. Lin, *J. Chem. Phys.* **2002**, *117*, 3224.

PUBLICATIONS FROM DOE SPONSORED WORK FROM 2007-2009

- *Experimental and Theoretical Rate Constants for $CH_4 + O_2 \rightarrow CH_3 + HO_2$* , N. K. Srinivasan, J. V. Michael, L. B. Harding, and S. J. Klippenstein, *Combust. Flame*, **149**, 104-111 (2007).
- *High-Temperature Rate Constants for $CH_3OH + Kr \rightarrow$ Products, $OH + CH_3OH \rightarrow$ Products, $OH + (CH_3)_2CO \rightarrow CH_2COCH_3 + H_2O$, and $OH + CH_3 \rightarrow CH_2 + H_2O$* ,

- N. K. Srinivasan, M.-C. Su, and J. V. Michael, *J. Phys. Chem. A* **111**, 3951 (2007).
- *Experimental and Theoretical Studies of High-Temperature Rate Constants for OH + CF₃H ⇌ CF₃ + H₂O and CF₃ + OH → Products*, N. K. Srinivasan, M.-C. Su, J. V. Michael, S. J. Klippenstein, and L. B. Harding, *J. Phys. Chem. A* **111**, 6822 (2007).
 - *CH₃ + O₂ → H₂CO + OH Revisited*, N. K. Srinivasan, M.-C. Su, J. V. Michael, *J. Phys. Chem. A* **111**, 11589 (2007).
 - *Reflected Shock Tube Studies of High-Temperature Rate Constants for OH + C₂H₂ and OH + C₂H₄*, N. K. Srinivasan, M.-C. Su, and J. V. Michael, *Phys. Chem. Chem. Phys.* **9**, 4155 (2007).
 - *Thermal Decomposition of CF₃ and the Reaction of CF₂ + OH → CF₂ + H*, N. K. Srinivasan, M.-C. Su, J. V. Michael, S. J. Klippenstein, and L. B. Harding, *J. Phys. Chem. A* **112**, 31 (2008).
 - *High Temperature Rate Constants for OH + Alkanes*, R. Sivaramakrishnan, N. K. Srinivasan, M.-C. Su, and J. V. Michael, *Proc. Combust. Inst.* **32**, 107 (2009).
 - *Shock Tube Measurements of High Temperature Rate Constants for OH with Cyclo-alkanes and Methyl-cycloalkanes*, R. Sivaramakrishnan and J. V. Michael, *Combust. and Flame*, In Press, doi:10.1016/J.COMBUSTFLAME.2008.10.010.
 - *Shock Tube Measurements of High Temperature Rate Constants for OH with Selected Alkanes*, R. Sivaramakrishnan and J. V. Michael, *J. Phys. Chem. A*, in press.
 - *Reflected Shock Tube and Theoretical Studies on the Thermal Decomposition of C₂H₅OH AND OH + C₂H₅OH → PRODUCTS*, R. Sivaramakrishnan, M.-C. Su, J. V. Michael, S. J. Klippenstein, and L. B. Harding, *J. Phys. Chem. A*, submitted.
 - *The Thermal Decomposition of NH₂OH: Reflected Shock Tube Experiments and Ab Initio Transition State Theory*, S. J. Klippenstein, L. B. Harding, N. K. Srinivasan, R. Sivaramakrishnan, M.-C. Su, and J. V. Michael, *J. Phys. Chem. A*, submitted.

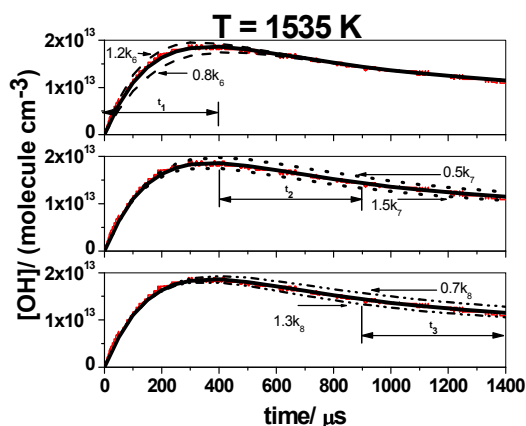


Fig. 1: [OH] profile at 1535 K. The experimental conditions are $P_1 = 5.97$ Torr, $M_s = 2.471$, $\rho_s = 1.129 \times 10^{18}$ molecules cm^{-3} , $[\text{NH}_2\text{OH}]_0 = 2.944 \times 10^{13}$ molecules cm^{-3} , and $[\text{H}_2\text{O}]_0 = 4.235 \times 10^{14}$ molecules cm^{-3} . The bold solid lines in all 3 panels are simulations using a full reaction mechanism scheme and the final fitted values for k_6 , k_7 , and k_8 . Dashed lines in the upper panel: Simulation using the same reaction mechanism scheme as the solid line and changing only k_6 by $\pm 20\%$. Dotted lines in middle panel: Simulation using the same reaction mechanism as the solid line and changing only k_7 by $\pm 50\%$. Dash-Dot-Dot lines in the lower panel: Simulation using the same reaction mechanism as the solid line and changing only k_8 by $\pm 30\%$.

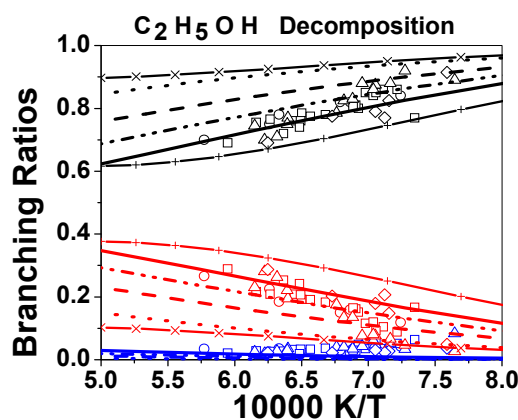


Fig. 2: Branching ratios for the three ethanol dissociation channels. $[\circ]$ – 0.20-0.28 atm expt. present work, $[\square]$ – 0.36-0.50 atm expt. present work, $[\Delta]$ – 0.49-0.69 atm expt. present work, $[\diamond]$ – 0.95-1.28 atm expt. present work. Dotted lines – 0.1 atm theory present work, Dashed Lines – 0.26 atm theory present work, Dash-Dot-Dot lines – 0.53 atm theory, Solid line – 1 atm theory present work. x-x-x – 1 atm theory Li et al.¹², +--+ – 1 atm theory Park et al.¹³ Black symbols and lines represent $\text{BR}_1 = k_1/(k_1+k_2+k_3)$, Red symbols and lines represent $\text{BR}_2 = k_2/(k_1+k_2+k_3)$, Blue symbols and lines represent $\text{BR}_3 = k_3/(k_1+k_2+k_3)$.

Multiphase Combustion Diagnostics Development

H. A. Michelsen

Sandia National Labs, MS 9055, P. O. Box 969, Livermore, CA 94551

hamiche@sandia.gov

1. Program Scope

Combustion in practical combustors, such as internal combustion engines, frequently evolves through multiple phases. Liquid fuels injected into such combustors are generally vaporized and mixed with a gas-phase oxidizer. Combustion processes often produce solid carbon particles, i.e., soot. These particles may be oxidized to form gas-phase species or released into the exhaust stream, where they can be coated with liquid coatings. These coatings can be comprised of any of a number of components, including unburned fuel, lube oil, sulfuric acid, water, and other combustion by-products.^{1,2} The research program described here focuses on the development of optical diagnostics for soot particles in combustion environments and combustion exhaust plumes. The goal of this work is *in situ* measurements of volume fraction, size, composition, and morphology of combustion-generated particles with fast time response and high sensitivity. Future work will expand the scope of this program to include optical diagnostics development for studies of the structure and evolution of liquid-jet sprays.

2. Recent Progress

Our work has focused on developing a detailed understanding of the chemical and physical mechanisms that influence the applicability of laser-induced incandescence (LII) for soot detection under a wide range of conditions. In our recent work we have spectrally and temporally resolved the emission from laser-heated soot irradiated at either 532 or 1064 nm over a wide fluence range. We have used these spectra to infer soot temperatures as a function of time relative to the laser pulse. In addition to broad quasi-blackbody emission, at moderate to high laser fluences our spectra demonstrate discrete features from electronically excited carbon clusters C_2 and C_3 and several unidentified features. Along with the corresponding time resolved LII signals, these data comprise a dataset for use in developing and validating models of LII signal generation and evolution.

2.1. Temperatures inferred from spectrally resolved emission from laser-irradiated soot.

Soot is composed of branched-chain aggregates of small (15-50 nm diameter) carbon spheroids called primary particles. LII is used extensively as a sensitive optical technique for measurements of soot volume fraction and primary particle size.^{3,4} This technique involves heating the particles with a high-power pulsed laser to temperatures of 2500-4000 K and measuring the radiative emission from the hot particles. The magnitude of the signal is correlated with the soot volume fraction. The signal decay rate depends on particle size, and recent efforts have focused on developing LII for particle size measurements. Broadband emission is observed for laser wavelengths from 213 to 1064 nm,⁵⁻⁷ and LII is typically measured at wavelengths between 400 and 800 nm.

We have used the 532- or 1064-nm output from a Nd:YAG laser to heat soot generated in an atmospheric laminar diffusion flame and a gated spectrograph (~2-ns gate) to spectrally and temporally resolve the emission. Spectra were recorded over a wide range of fluences. Figure 1 presents spectra recorded at different times relative to the laser pulse and the Planck-function fits to these spectra to derive particle temperatures. The sharp features are predominantly due to excited carbon cluster (C_2 and C_3) emission and are more prevalent with 532-nm excitation. Figure 2 shows peak particle temperatures recorded during the laser pulse as a function of laser fluence and the corresponding normalized peak LII signal measured at 682 nm. Inferred temperatures do not exceed the sublimation point of graphite (~4100 K) at fluences below 1 J/cm². At higher fluences interferences from C_2 and C_3 emission increase the error bars of the measured temperatures.

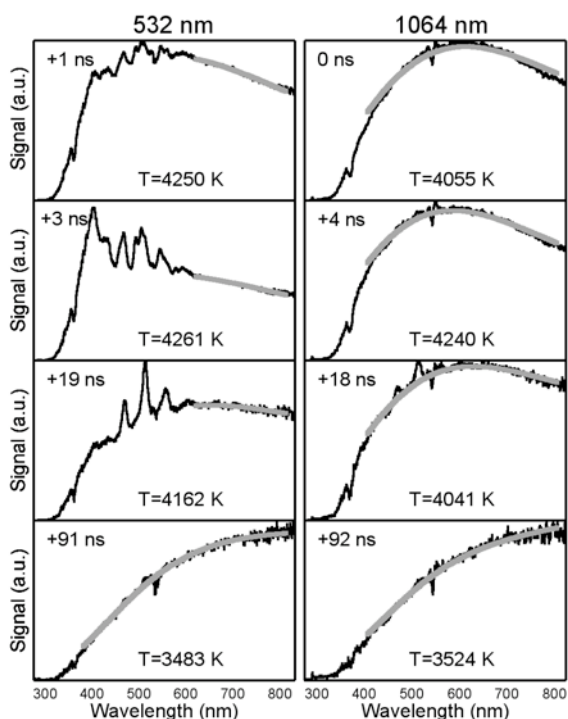


Fig. 1. Spectrally resolved emission from laser-heated soot. Spectra were recorded at the indicated delay times after the peak of the 532-nm (left) or 1064-nm (right) laser pulse. The fluence was 0.8 J/cm^2 . Spectra were fit using the Planck function (thick gray lines), and the resulting temperatures are given in the figure.

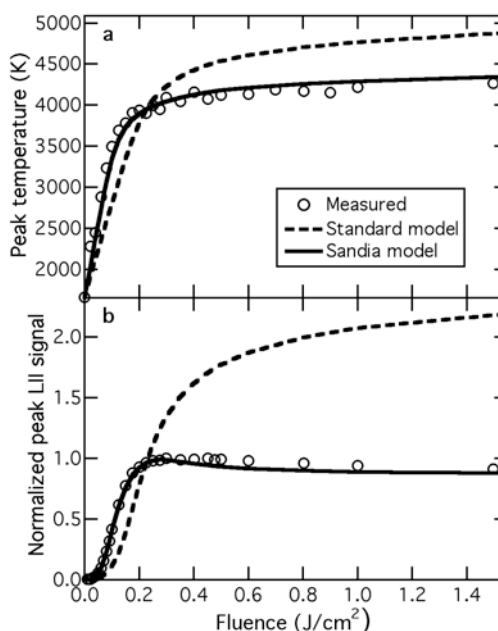


Fig. 2. Peak particle temperatures (a) and peak LII signals (b) are plotted as a function of laser fluence. Soot was irradiated at 1064 nm. (a) Temperatures were inferred from spectrally and temporally resolved LII. (b) Time resolved LII signals were collected at 682 nm, and the peak values were normalized to unity at 0.2 J/cm^2 .

2.2. Modeling laser-induced incandescence of soot.

Large uncertainties plague quantitative applications of LII for soot detection. These uncertainties can likely be narrowed with a deeper understanding of the physical mechanisms that control LII signal generation. One approach to developing such an understanding involves modeling LII signal behavior under a wide range of conditions. A large number of models have been developed for analyzing LII signals, but the results vary widely,^{4,8} and few have been validated against data sets collected under controlled conditions.^{9,10} None of these LII models has been able to reproduce experimental results demonstrating that temperatures of laser-heated soot do not exceed graphite sublimation temperatures except at very high laser fluences.^{7,11,12}

We have developed a model that is capable of reproducing measured soot temperatures and LII signals during and after laser heating. The model solves the heat- and mass-balance equations as a set of coupled differential equations to account for particle heating by laser absorption and oxidation and cooling by conduction to the surrounding atmosphere, radiative emission, sublimation, non-thermal photodesorption of molecular carbon clusters, and thermionic emission in which electrons are thermally ejected from the particle. Particle-size reduction during sublimation, photodesorption, and oxidation is also calculated. Models typically used for analysis of LII data do not include photodesorption, oxidation, or thermionic emission.⁸ Our model additionally accounts for other factors not typically taken into account in LII models, including (1) temperature-dependent thermodynamic parameters for sublimation, conduction, and internal energy storage by the particle; (2) wavelength-dependent optical parameters for absorption and emission of radiation; (3) a particle- and gas-temperature dependent thermal accommodation coefficient for conductive cooling; (4) a conductive cooling mechanism assuming free molecular flow at low pressure and a transition regime at high pressure; and (5) a work function for thermionic emission that depends on the particle size and charge; and (6) an effective reduction in active surface area that accounts for the shielding effects of aggregation on conductive cooling, oxidation, sublimation, and photodesorption rates.

Representative results of this model for 1064-nm excitation are compared with measured LII temporal profiles in Fig. 3a for low fluences and in Fig. 4 for higher fluences. Corresponding results from a typical model⁸ used for LII data analysis are shown in Figs. 3b and 4. Figure 2 shows examples of the fluence dependence of the peak temperature and LII signal for both models.

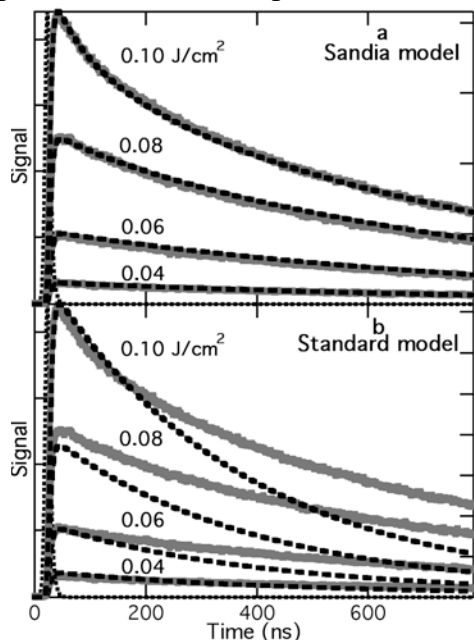


Fig. 3. Modeled and measured low-fluence LII temporal profiles. (a) Sandia-model and (b) standard-model predictions (dashed black lines) are compared with low-fluence LII temporal profiles measured with 1064-nm excitation at 682 nm (gray lines). The peak of the highest fluence curve is scaled to the top of the graph. The dotted curve represents the laser temporal profile.

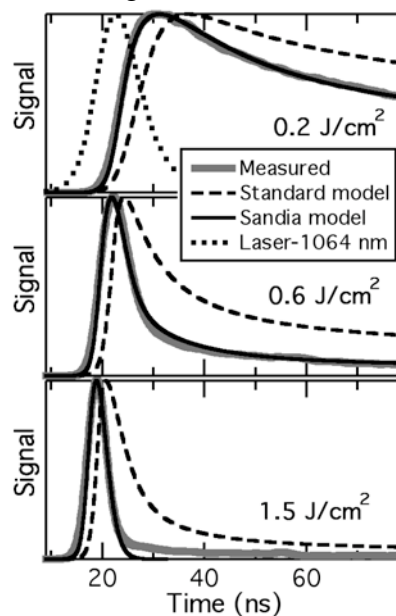


Fig. 4. Modeled and measured high-fluence LII temporal profiles. Sandia-model (solid black lines) and standard-model (dashed black lines) predictions are compared with high-fluence LII temporal profiles measured with 1064-nm excitation at 682 nm (gray lines). The peak of each curve is scaled to the top of the graph. The dotted curve in the top panel represents the laser temporal profile.

Our results demonstrate excellent agreement with measured temporal profiles of LII signal and particle temperature over the entire fluence range of 0.02-3.5 J/cm² for both 532- and 1064-nm excitation. These results represent a major advance over previous modeling studies. Our model is the only model capable of reproducing LII temporal profiles and particle temperatures throughout the entire heating and cooling process, particularly at high fluence and during the laser pulse. Even models targeted at low fluences are unable to reproduce the signal and temperature evolution during and just after the laser pulse.

3. Future plans

Current work builds on these results and extends it to combustion-generated particles with inorganic and organic coatings representative of particles found in exhaust plumes. In order to simulate exhaust-plume particulates, we have modified our flow-tube system to allow controlled deposition of a coating with low volatility on flame-generated soot. The thickness of the coating can be varied and the particles collected for analysis by TEM and NEXAFS. Coatings investigated to date have been selected for diagnostic development for diesel exhaust and include sulfuric acid, heptamethylnonane, and oleic acid. These experiments are currently limited by our inability to determine the mass loading of particle coatings. Developing an understanding of the cause and magnitude of the effects of coatings will require characterization of the particle coatings. Coating the particles increases the mean aggregate size as measured by the SMPS, but measurements of electric mobility diameter provided by the SMPS do not provide a quantitative measure of the volatile coating fraction either by volume or by mass. In order to measure the volatile fraction, we will build a chamber that includes a temperature-controlled oscillating crystal microbalance for differential mass measurements on coated and evaporatively dried particles.

4. References

- (1) Kittelson, D. B. *J. Aerosol Sci.* **1998**, *29*, 575.
- (2) Lighty, J. S.; Veranth, J. M.; Sarofim, A. F. *J. Air Waste Manage. Assoc.* **2000**, *50*, 1565.
- (3) Santoro, R. J.; Shaddix, C. R. Laser-Induced Incandescence. In *Applied Combustion Diagnostics*; Kohse-Höinghaus, K., Jeffries, J. B., Eds.; Taylor & Francis: New York, NY, 2002.
- (4) Schulz, C.; Kock, B. F.; Hofmann, M.; Michelsen, H. A.; Will, S.; Bougie, B.; Suntz, R.; Smallwood, G. J. *Appl. Phys. B* **2006**, *83*, 333.
- (5) Rohlfiing, E. A. *J. Chem. Phys.* **1988**, *89*, 6103.
- (6) Vander Wal, R. L.; Weiland, K. J. *Appl. Phys. B* **1994**, *59*, 445.
- (7) Schraml, S.; Dankers, S.; Bader, K.; Will, S.; Leipertz, A. *Combust. Flame* **2000**, *120*, 439.
- (8) Michelsen, H. A.; Liu, F.; Kock, B.; Bladh, H.; Boiarciuc, A.; Charwath, M.; Dreier, T.; Hadeif, R.; Hofmann, M.; Reimann, J.; Will, S.; Bengtsson, P.-E.; Bockhorn, H.; Foucher, F.; Geigle, K. P.; Mounaïm-Rousselle, C.; Schulz, C.; Stirn, R.; Tribalet, B.; Suntz, R. *Appl. Phys. B* **2007**, *87*, 503.
- (9) Michelsen, H. A. *J. Chem. Phys.* **2003**, *118*, 7012.
- (10) Snelling, D. R.; Liu, F.; Smallwood, G. J.; Gülder, Ö. L. *Combust. Flame* **2004**, *136*, 180.
- (11) De Iuliis, S.; Cignoli, F.; Zizak, G. *Appl. Opt.* **2005**, *44*, 7414.
- (12) Goulay, F.; Schrader, P. E.; Michelsen, H. A. *Appl. Phys. B* **2009**, submitted.

5. Recent BES-supported, peer-reviewed publications

H. A. Michelsen, "Derivation of a temperature-dependent accommodation coefficient for use in modeling laser-induced incandescence of soot", *Appl. Phys. B* **94**, 103-117 (2009).

F. Goulay, P. E. Schrader, and H. A. Michelsen, "The effects of pulsed laser injection seeding and triggering on the temporal behavior and magnitude of laser-induced incandescence from soot", *Appl. Phys. B.*, in press (2009).

F. Goulay, P. E. Schrader, and H. A. Michelsen, "A dataset for validation of models of laser-induced incandescence from soot: Temporal profiles of LII signal and particle temperature", *Appl. Phys. B.*, submitted (2009).

F. Goulay, P. E. Schrader, L. Nemes, M. A. Dansson, and H. A. Michelsen, "Photochemical interferences for laser-induced incandescence of flame-generated soot", *Proc. Comb. Inst.* **32**, 963-970 (2009).

H. A. Michelsen, M. A. Linne, B. F. Kock, M. Hofmann, B. Tribalet, and C. Schulz, "Modeling laser-induced incandescence of soot: Enthalpy changes during sublimation, conduction, and oxidation", *Appl. Phys. B* **93**, 645-656 (2008).

M. A. Dansson, M. Boisselle, M. A. Linne, and H. A. Michelsen, "Complications to optical measurements using a laser with an unstable resonator: A case study on laser-induced incandescence of soot", *Appl. Opt.* **46**, 8095-8103 (2007).

H. A. Michelsen et al., "Modeling laser-induced incandescence of soot: A summary and comparison of LII models", *Appl. Phys. B* **87**, 503-521 (2007).

L. Nemes, A. M. Keszler, C. G. Parigger, J. O. Hornkohl, H. A. Michelsen, and V. Stakhursky, "On spontaneous emission from the C₃ radical in carbon plasma", *Appl. Opt.* **46**, 4032-4040 (2007).

H. A. Michelsen, A. V. Tivanski, M. K. Gilles, L. H. van Poppel, M. A. Dansson, and P. R. Buseck, "Particle formation from pulsed laser irradiation of soot aggregates studied with a scanning mobility particle sizer, a transmission electron microscope, and a scanning transmission x-ray microscope", *Appl. Opt.* **46**, 959-977 (2007).

Chemical Kinetics and Combustion Modeling

James A. Miller

**Combustion Research Facility, Sandia National Laboratories
MS 9055, Livermore, CA, 94551-0969
email: jamille@sandia.gov**

Program Scope

The goal of this project is to gain qualitative insight into how pollutants are formed in combustion systems and to develop quantitative mathematical models to predict their formation and destruction rates. The approach is an integrated one, combining theory, modeling, and collaboration with experimentalists to gain as clear a picture as possible of the processes in question. My efforts and those of my collaborators are focused on problems involved with the nitrogen chemistry of combustion systems and the formation of soot and PAH in flames, as well as on general problems in hydrocarbon combustion. Current emphasis is on determining phenomenological rate coefficients from the time-dependent, multiple-well master equation for reactions involved in the pre-cyclization and cyclization chemistry of flames burning aliphatic fuels.

Recent Results (all in collaboration with Judit Zádor)

Engine technology is going through a dual change. On one hand, the composition of the fuels is changing and moving toward biofuels as well as heavier streams of oil. On the other hand, compression ignition (CI) technologies promise higher efficiency and lower emissions. The co-emergence of the new technology and the new fuels has put ignition chemistry at the center of interest, because CI relies almost exclusively on homogeneous gas-phase kinetics to time the ignition. Special emphasis is being placed on oxygenated compounds (alcohols, ethers, esters) and cyclic alkenes, because these are new components in the new fuels. The critical chemical steps during low-temperature ignition are the formation, isomerization, and dissociation of the peroxy radicals (RO_2).

The α - and β -hydroxyethyl + O_2 reaction

We studied the oxidation of the α - and β -hydroxyethyl radicals,¹ CH_3CHOH and $\text{CH}_2\text{CH}_2\text{OH}$, which are the primary radicals formed during the ignition of ethanol. We have characterized the $\text{CH}_3\text{CHOH} + \text{O}_2$ and $\text{CH}_2\text{CH}_2\text{OH} + \text{O}_2$ potential energy surfaces using RQCISD(T)/cc-pV ∞ Z//B3LYP/6-311++G(d,p) level of theory, calculating frequencies and hindered rotors at the B3LYP/6-311++G(d,p) level of theory. The entrance channels for both reactions are barrierless, and consequently they were treated in the framework of the direct variable-reaction-coordinate transition-state theory. Using the master equation we calculated the pressure and temperature dependence of the rate coefficients, which are in good agreement with the few available experimental data in the literature. The α -hydroxyethyl + O_2 reaction shows very little pressure dependence, while the

collisionless and the high-pressure limit rate coefficients for the β -hydroxyethyl radical differ by two orders of magnitude at 1000 K. We have also determined the products of the reactions using multiplexed photoionization mass spectrometry in the Advanced Light Source in Berkeley. We have, for the first time, shown both experimentally and theoretically that the β -hydroxyethyl + O₂ reaction leads to the formation of vinyl alcohol,² although the predicted and observed branching fractions disagree somewhat.

The propene + OH reaction

The combustion of alcohols is closely related to alkene oxidation, since the general β -hydroxyalkyl radicals can easily fall apart at elevated pressures to form an alkene and an OH radical. The reaction of alkenes can also result in the formation of enols, or in potential soot precursors. The ethene + OH reaction was already studied in this program,³ and we carried on by exploring the PES of the propene + OH reaction using high-level ab initio methods. The PES is surprisingly rich in intermediates and products, including vinyl alcohol, acetaldehyde, allyl radical, acetone, ethene, propanal, propenol and formaldehyde. The reactants first go through a barrierless transition state to form a van der Waals complex, which is followed by submerged saddle points leading to the terminal or central addition of OH. OH can also abstract a hydrogen from propene; this channel becomes important at high temperatures. The results of our multiwell master-equation model were tested against the experimental data available in the literature and good agreement was found, showing the predictive strength of our model.

The cyclohexyl + O₂ reaction at high pressures

In a previous, low-pressure study at the Combustion Research Facility the chlorine-initiated oxidation of cyclohexane oxidation was studied.⁴ It was shown that a detailed description of the underlying C₆H₁₁ + O₂ potential energy surface (PES) coupled to master equation (ME) is absolutely necessary in order to model the experiments successfully. It was also shown that the phenomenological rate coefficients belonging to both sequential and direct formation of the OH and HO₂ products are essential.

Using the same methodology we (with our experimental collaborators) carried out experiments at in-cylinder pressures (6.5–20.3 bar) at 586–828 K and measured the concentration of OH radicals via laser induced fluorescence in a newly built high-pressure cell.⁵ We found that direct, well-skipping pathways are still important in order to model the temperature- and time-dependent features of our concentration profiles. This further emphasizes the importance of the consistent ME treatment of chemical reactions. We found, however, a significant discrepancy between the magnitude of the measured and calculated OH concentrations. We showed that the existence of fast chain-branching steps (“second O₂ addition”) is very likely, and adding this reaction to our model reconciles all experimental data.

References

- [1] J. Zádor, R.X. Fernandes, Y. Georgievskii, G. Meloni, C.A. Taatjes, J.A. Miller, *Proc. Combust. Inst.* 32 (2009) 271-277.
- [2] C.A. Taatjes, N. Hansen, A. McIlroy, J.A. Miller, J.P. Senosiain, S.J. Klippenstein, F. Qi, L. Sheng, Y. Zhang, T.A. Cool, J. Wang, P.R. Westmoreland, M.E. Law, T. Kasper, K. Kohse-Höinghaus, *Science* 308 (2005) 1887-1889.
- [3] J.P. Senosiain, S.J. Klippenstein, J.A. Miller, *J. Phys. Chem. A* 110 (2006) 6960-6970.
- [4] A.M. Knepp, G. Meloni, L.E. Jusinski, C.A. Taatjes, C. Cavallotti, S.J. Klippenstein, *Phys. Chem. Chem. Phys.* 9 (2007) 4315-4331.
- [5] R.X. Fernandes, J. Zador, L.E. Jusinski, C.A. Taatjes, J.A. Miller, *Phys. Chem. Chem. Phys.* 11 (2009) 1320-1327.

Future Directions

We shall resume our work on the chemical kinetics of rich flames of aliphatic fuels, particularly that concerned with the formation of the first aromatics containing one or two rings. In the next year we expect to finish our work on the reactions of allyl and OH with propargyl. The work on allyl + propargyl is being pursued in collaboration with Wesley Allen and co-workers at the University of Georgia. We shall continue to develop our chemical kinetic model, particularly in conjunction with the flame experiments at the Advanced Light Source. We expect in the next year to begin to investigate the possibility of using the rate-controlled, constrained-equilibrium formalism to predict the concentrations of aromatic compounds with more than 2 rings. We shall also continue to maintain our interest in the nitrogen chemistry of combustion, particularly that concerned with NO_x control technologies such as reburning, Thermal De-NO_x, and RAPRENO_x.

Publications of James A. Miller 2007-2009

- J. A. Miller, S.J. Klippenstein, S. H. Robertson, M. J. Pilling, and N. J. B. Green, "Detailed Balance in Multiple-Well Chemical Reactions," "Perspective" for *Phys. Chem. Chem. Phys.* 11, 1128-1137 (2009)
- A. W. Jasper and J. A. Miller, "Collisional Energy Transfer in Unimolecular Reactions: Direct Classical Trajectories for CH₄ ⇌ CH₃+H in Helium, *J. Phys. Chem. A* in press (2009)
- J. A. Miller, J. P. Senosiain, S. J. Klippenstein, and Y. Georgievskii, "Reactions Over Multiple, Interconnected Potential Wells: Unimolecular and Bimolecular Reactions on a C₃H₅ Potential", *J. Phys. Chem. A* 112, 9429-9438 (2008)
- S. R. Sellevåg, Y. Georgievskii, and J. A. Miller, "Kinetics of the Gas-Phase Recombination Reaction of Hydroxyl Radicals to form Hydrogen Peroxide," *J. Phys. Chem. A*, in press (2009)
- N. Hansen, J. A. Miller, P. R. Westmoreland, T. Kasper, K. Kohse-Höinghaus, J. Wang, and T. A. Cool, "Isomer-Specific Combustion Chemistry in Allene and Propyne Flames," *Combustion and Flame*, submitted (2009)

- R. X. Fernandes, J. Zádor, L. E. Jusinski, J. A. Miller, and C. A. Taatjes, “Formally Direct Pathways and Low-Temperature Chain Branching in Hydrocarbon Autoignition: The Cyclohexyl + O₂ Reaction at High Pressure,” *Phys. Chem. Chem. Phys.* **11**, 1320-1327(2009)
- N. Hansen, J. A. Miller, T. Kasper, K. Kohse-Höinghaus, P. R. Westmoreland, J. Wang, and T. A. Cool, “Benzene Formation in Premixed Fuel-Rich 1,3 Butadiene Flames,” *Proc. Combust. Inst.* **32**, 623-630 (2009)
- S. R. Sellevåg, Y. Georgievskii, and J. A. Miller, “The Temperature and Pressure Dependence of the Reactions $H+O_2(+M)\rightleftharpoons HO_2(+M)$ and $H+OH(+M)\rightleftharpoons H_2O(+M)$,” *J. Phys. Chem. A* **112**, 5085-5095 (2008)
- J. Zádor, R. X. Fernandes, Y. Georgievskii, G. Meloni, C. A. Taatjes, and J. A. Miller, “The Reaction of Hydroxyethyl Radicals with O₂: A Theoretical Analysis and Experimental Product Study,” *Proc. Combust. Inst.* **32**, 271-277(2009)
- L. B. Harding, S. J. Klippenstein, and J. A. Miller, “The Kinetics of CH+N₂ Revisited with Multi-Reference Methods,” *J. Phys. Chem. A* **112**, 522-532(2008)
- Y. Georgievskii, S. J. Klippenstein, and J. A. Miller, “Association Rate Constants for Reactions between Resonance Stabilized Radicals: C₃H₃+C₃H₃, C₃H₃+C₃H₅, and C₃H₅+C₃H₅,” *Phys. Chem. Chem. Phys.* **9**, 4259-4268 (2007)
- H. Fan, S. T. Pratt, and J. A. Miller, “Secondary Decomposition of C₃H₅ Radicals Formed by the Photodissociation of 2-Bromopropene,” *J. Chem. Phys.* **127**, 144301 (2007)
- J.P. Senosiain and J.A. Miller, “The Reaction of n- and i-C₄H₅ Radicals with Acetylene,” *J. Phys. Chem. A* **111**, 3740-3747(2007)
- J.P. Senosiain, S.J. Klippenstein, and J.A. Miller, “Oxidation Pathways in the Reaction of Diacetylene with OH Radicals”, *Proc. Combust. Inst.* **31**, 185-192 (2007)
- N. Hansen, J. A. Miller, C. A. Taatjes, J. Wang, T. A. Cool, M.E. Law, and P. R. Westmoreland, “Photoionization Mass Spectrometric Studies and Modeling of Fuel-Rich Allene and Propyne Flames,” *Proc. Combust. Inst.* **31**, 1157-1164 (2007)

Detection and Characterization of Free Radicals Relevant to Combustion Processes

Terry A. Miller

Laser Spectroscopy Facility, Department of Chemistry

The Ohio State University, Columbus OH 43210, email: tamiller@chemistry.ohio-state.edu

1 Program Scope

Combustion processes have been studied for many years, but the chemistry is very complex and yet to be fully understood. Modern computer codes for its modelling typically employ hundreds of reaction steps with a comparable number of chemical intermediates. The predictions of such models are obviously limited by the fundamental dynamical and mechanistic data that is input. Spectroscopic identifications and diagnostics for the chemical intermediates in the reaction mechanisms constitute an important experimental benchmark for the models, as well as providing molecular parameters that are experimental “gold standards” against which quantum chemistry computations of molecular properties may be judged. Our work has emphasized the spectroscopy of reactive organic peroxy radical intermediates, that are known to be of key importance in combustion processes.

2 Recent Progress

Our recent work has focussed on two distinct but strongly coupled areas. The first area builds on our previous investigations, using cavity ringdown spectroscopy (CRDS), of the $\tilde{A} - \tilde{X}$ electronic transition of the open-chain alkyl peroxy radicals that are key intermediates in the combustion of alkanes, which dominate traditional petroleum-based fuels. Since cyclic hydrocarbons and other organic species are also present in petroleum-based fuels and are often more abundant in alternate fuel sources, e.g., bio-derived fuels, extracts from tar sands, etc. we have begun an experimental program to observe corresponding peroxy radical spectra derived from such species. Our first results are described below for the cycloalkyl peroxy radicals.

Our second focus has been on maximizing the usefulness of the observed $\tilde{A} - \tilde{X}$ spectra. For some diagnostic work the presence or absence of the spectrum of a reactive intermediate suffices. However in other situations, measuring the concentration of the species is critical. In principle, absorption spectroscopy, including CRDS of the $\tilde{A} - \tilde{X}$ transition characteristic of all organic peroxy radicals, should provide an excellent means for concentration measurements. However such results require knowledge of absolute absorption cross-sections, quantities that are notoriously difficult to obtain for reactive species. Below we describe our initial results with a new apparatus designed to measure cross-sections for peroxy radicals and other reactive intermediates.

2.1 Cycloalkyl Peroxy Radicals

We began our efforts to obtain ambient temperature cycloalkyl peroxy CRDS $\tilde{A} - \tilde{X}$ spectra with the cyclohexyl peroxy ($c\text{-C}_6\text{H}_{11}\text{O}_2$) and cyclopentyl peroxy ($c\text{-C}_5\text{H}_9\text{O}_2$) radicals. In Fig. 1, we show the observed CRDS spectra of $c\text{-C}_6\text{H}_{11}\text{O}_2$ and $c\text{-C}_5\text{H}_9\text{O}_2$, and the perdeutero isotopologue of the latter. To generate the peroxy radicals, we first produced the cycloalkyl radical by ArF excimer laser photolysis of the corresponding bromide derivative. However due to the relatively low vapor pressure of the bromide, we found that one could obtain significantly more peroxy radicals ($\text{RO}_2\cdot$) by producing the alkyl radicals ($\text{R}\cdot$) via H extraction

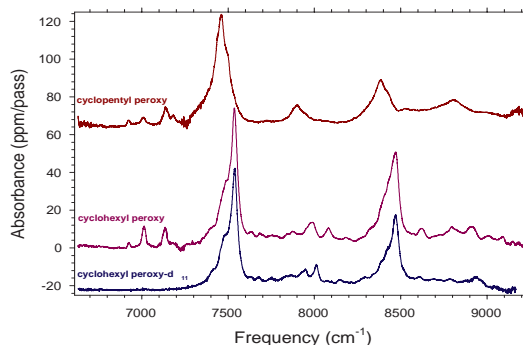


Figure 1: Survey spectra of the $\tilde{A} - \tilde{X}$ electronic transitions of cyclopentyl, cyclohexyl, and cyclohexyl- d_{11} peroxy radicals. The absence of the bands below 7300 cm^{-1} in the perdeutero spectrum indicates that they are unlikely part of the $\tilde{A} - \tilde{X}$ electronic transitions of the proteo analogues.

from the cycloalkane (RH) with Cl atoms produced by photolyzing oxalyl chloride, $(\text{COCl})_2$, according to the reaction mechanism,



Fig. 1 shows that while the spectra of $c\text{-C}_5\text{H}_9\text{O}_2$ and $c\text{-C}_6\text{H}_{11}\text{O}_2$ are similar they are clearly sufficiently different to distinguish clearly between the two species. The lowest frequency, strong line of the spectrum of $c\text{-C}_5\text{H}_9\text{O}_2$, which we identify as the origin transition, is at 7461 cm^{-1} . This value is distinctly different from the origin bands of 1-pentyl, 2-pentyl and *t*-pentyl peroxy which occur, respectively, at 7351 , 7567 , and 7761 cm^{-1} , clearly providing a means of identifying uniquely each of the pentyl peroxy structural isomers.

Our procedures for analyzing and assigning the other bands in the spectra of $c\text{-C}_5\text{H}_9\text{O}_2$ and $c\text{-C}_6\text{H}_{11}\text{O}_2$ are based on the previously observed characteristics of the open-chain alkyl peroxy radical spectra and electronic structure calculations for the \tilde{A} and \tilde{X} states of the cyclic radicals. For brevity we will concentrate our discussion on the $c\text{-C}_6\text{H}_{11}\text{O}_2$ spectrum, but similar considerations apply for $c\text{-C}_5\text{H}_9\text{O}_2$. In addition to the $\tilde{A} - \tilde{X}$ electronic origin band of $c\text{-C}_6\text{H}_{11}\text{O}_2$, we expect significant Franck-Condon factors for transitions to the fundamental “O-O stretching” and “C-O-O bending” vibrations in the \tilde{A} state. Experimentally observed frequencies for these bands in the acyclic alkyl peroxies are in the range of $870\text{-}1000\text{ cm}^{-1}$ and $350\text{-}600\text{ cm}^{-1}$, respectively. The “O-O stretch” band is typically moderately strong, with an intensity roughly one-third that of the electronic origin, while the “C-O-O bend” is typically about a factor of 3 weaker, but with considerable variability. Additionally, low frequency ($< 200\text{ cm}^{-1}$) O-O-C-H torsional vibrations can have several quanta populated at room temperature, contributing to sequence band structure.

The other consideration in interpreting the observed spectra is the possible presence of multiple conformers of a given peroxy radical isomer. For open-chain alkyl peroxy radicals it is known that the number of possible conformers increases rapidly with chain length, already reaching approximately 170 by pentyl peroxy. In the case of cycloalkyl peroxies with comparable numbers of carbon atoms, the situation simplifies considerably. The $c\text{-C}_6\text{H}_{11}\text{O}_2$ should exist in chair and twist-boat forms, but the latter is predicted to lie $> 2000\text{ cm}^{-1}$ above the chair and has a negligible Boltzmann population at ambient temperatures. The chair form itself may be substituted in axial (a) and equatorial (e) positions; in each case the O_2 moiety may be *cis* (C) or *gauche* (G) with respect to the ring, giving a total of four expected conformers, aC, aG, eC, and eG. (See Fig. 2.)

The use of electronic structure calculations which are summarized in Table 1 allow us to make quantitative predictions for bands in the spectrum of $c\text{-C}_6\text{H}_{11}\text{O}_2$, thereby significantly aiding the spectral assignments. Fig. 3 shows a comparison between the observed spectrum and the predictions based on electronic structure calculations. Referring to the Boltzmann weights in Table 1 we conclude that the aC conformer should make a negligible contribution to the spectrum. The relative contribution from each of the other 3 conformers is indicated in Fig. 3 by the overall intensity of its trace. The origin frequencies in the simulated spectra are based upon G2 predictions of T_{00} of the $\tilde{A} - \tilde{X}$ transition and the vibrational intervals are determined from scaled B3LYP frequencies. The relative intensities of the bands are from predictions using a multi-dimensional Franck-Condon program with input parameters from the B3LYP electronic structure

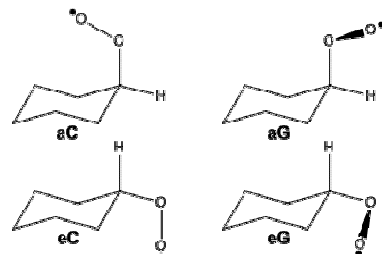


Figure 2: Conformers of $c\text{-C}_6\text{H}_{11}\text{O}_2$. Each G conformer exists as mirror image pairs.

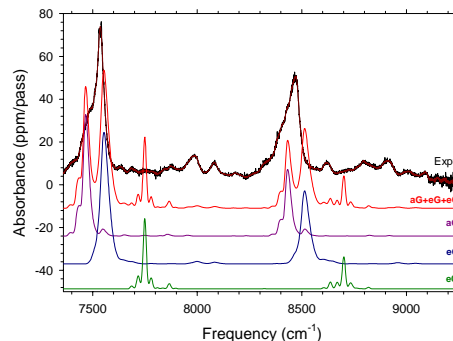


Figure 3: Comparison of experimental and predicted $\tilde{A} - \tilde{X}$ spectrum of $c\text{-C}_6\text{H}_{11}\text{O}_2$. The contributions of the various conformers are shown individually in the lowest 3 traces.

Table 1: Calculated \tilde{A} and \tilde{X} state energies (cm^{-1}) and origin frequencies (T_{00}) for conformers of the cyclohexyl peroxy radical. Energies have been zero-point corrected and Boltzmann weights are given in parentheses.

Conformer	\tilde{X}	\tilde{A}	T_{00}	Conformer	\tilde{X}	\tilde{A}	T_{00}
eC (1.00)	0	7751	7751	eG (3.30)	-104	7443	7547
aC (0.01)	915	8186	7271	aG (2.31)	-30	7428	7458

calculations.

Fig. 3 shows the aG and eG conformers make the strongest, and comparable, contributions to the spectrum. We therefore assign the main origin peak to the eG conformer and its lower frequency shoulder to the aG conformer. Corresponding assignments can be made in the “O-O stretch” region below 8500 cm^{-1} . Indeed the correlation between the predicted and observed spectra for these strongest bands is remarkable.

However the weaker bands are not nearly so well predicted and their assignment is a bit of an enigma. The next strongest bands, a pair near 8000 cm^{-1} (and comparable structure above the “O-O stretch” band), may well be assigned to multiple bands of the two G conformers sharing the “C-O-O bend” intensity. Indeed the eG simulation clearly shows two such bands very close to the experimentally observed positions, but the bands are all predicted to be considerably weaker than the observed ones. Nonetheless the “C-O-O bend” intensities are known to vary considerably among peroxy radicals and it is not particularly surprising that the simulation would not accurately depict the intensities of these relatively weak transitions.

On the other hand, the simulation clearly predicts observable intensity for the eC conformer origin (with comparable “O-O stretch” structure between 8700 and 8800 cm^{-1}). There are weak bands in this region of the observed spectrum, but they are largely consistent with weak torsional sequences expected in the aG and eG conformers. One is therefore forced to conclude that either the eC conformer is higher in energy and therefore weaker in intensity than predicted, or its $\tilde{A} - \tilde{X}$ origin frequency is shifted so that the band falls under either the origin or coincides with the “C-O-O bend” bands of the G conformers. Either result is rather unexpected for the normally reliable G2 calculations. Further analyses and experiments are being pursued to resolve these discrepancies.

2.2 Absorption Cross-sections

Accurate measurement of the absorption cross-section of a molecule using CRDS, or other absorption techniques, requires knowledge of the fractional light absorption, the absorption path length, and the concentration of the species. While the first two quantities are typically readily available experimentally, the latter is usually not for a short-lived reactive intermediate. We have proposed that the absolute concentration of such intermediates can be determined by simultaneous monitoring of the absorption of a non-reactive co-product whose spectroscopic properties, including absorption cross-section, are well established and whose concentration can therefore be derived from its observed spectrum.

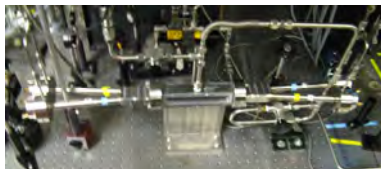


Figure 5: Photo of reaction chamber and ringdown cavity of the DCRDS apparatus.

As Fig. 4 shows the axes of the individual arms define nearly coinciding optical paths for two IR interrogating beams that intersect at $\lesssim 8$ degrees at the center. To demonstrate experimentally the equivalence of the two optical paths, the spectrum of the “O-O stretch plus methyl torsion” combination band ($7_0^{12}1_1^{12}$) of methyl

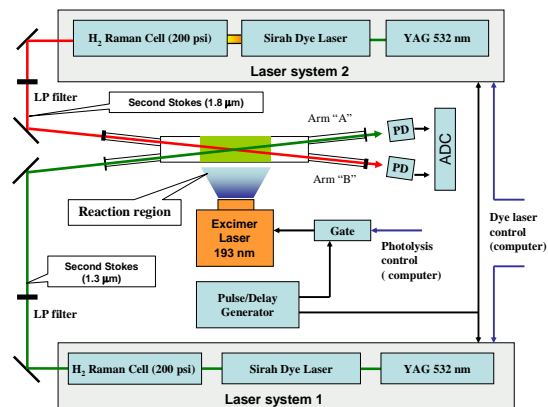


Figure 4: Block diagram of DCRDS apparatus. The radiation sources indicated are chosen to monitor simultaneously transitions in $\text{C}_2\text{H}_5\text{O}_2$ and HCl.

While the approach is potentially quite general, a particularly apropos example is provided by the reaction scheme of Eqs. 1-3, producing peroxy radicals via the photolysis of oxalyl chloride. CRDS measurements of the relatively non-reactive HCl molecule establish its concentration (using its known cross-section) which is stoichiometrically equivalent to that of RO_2 , for the times ($\lesssim 100 \mu\text{sec}$) involved in the measurement.

To implement this approach we have designed and constructed the dual wavelength cavity ringdown spectrometer (DCRDS), whose block-diagram is shown in Fig. 4 with a photo of the reaction chamber in Fig. 5.

peroxy, CH_3O_2 has been recorded. (This transition is not optimal as it is a factor of ≈ 3 -4 weaker than the origin band. It has, however, been chosen because of the fact that we currently possess *two* pairs of high reflectivity ringdown mirrors for this wavelength region.) For this experiment, the output of a single laser was split into two beams which were coupled to arms “A” and “B” of the apparatus. The resulting spectra are shown in Fig. 6, which clearly demonstrates equivalent absorption along the two paths within the experimental uncertainty set by the signal/noise ratio.

For the initial experiments monitoring the absorption of two different species, the ethyl peroxy radical, $\text{C}_2\text{H}_5\text{O}_2$, and its co-product, HCl, were chosen. With the available laser sources and ringdown mirrors, we can scan simultaneously the origin region of the G conformer of $\text{C}_2\text{H}_5\text{O}_2$ near 7600 cm^{-1} and the P-branch region of the first vibrational overtone of H^{35}Cl and H^{37}Cl . We measure the H^{35}Cl (natural abundance 76%) absorption on the P(3) and P(4) transitions near 5600 cm^{-1} . These spectra have been recorded and are now being analyzed to obtain an initial value for the absorption cross-section and to identify possible sources, if any, of systematic error. We will then compare the resulting cross-sections with ones previously obtained by less direct radical concentration measurements based either upon absorption of the photolysis beam by precursor molecules or the rate of disappearance of ethyl peroxy.

3 Future Directions

With respect to the cycloalkyl peroxy radicals, we expect to complete shortly the analysis of the $\tilde{A} - \tilde{X}$ spectra of cyclohexyl and cyclopentyl peroxy. We will then pursue the corresponding spectra of cyclobutyl and cyclopropyl peroxy. These latter spectra are of particular importance as theoretical benchmarks. Furthermore the combination of spectra from all the cycloalkyl peroxy radicals with 3 to 6 carbon atoms will provide an excellent basis for comparison between the cyclic and acyclic alkyl peroxy radicals.

We plan to complete our analysis of the DCRDS results to obtain the absolute absorption cross-section for $\text{C}_2\text{H}_5\text{O}_2$. We hope to explore an independent cross-section measurement using the photolysis of $\text{C}_2\text{H}_5\text{Br}$ to produce ethyl radicals which are quantitatively converted to $\text{C}_2\text{H}_5\text{O}_2$ by reaction 3. In this case the co-product Br atom concentration can be determined from the CRDS absorption on its fine-structure transition at 3685 cm^{-1} , utilizing its magnetic-dipole-transition cross-section. Additionally we will extend our cross-section measurements to other reactive species.

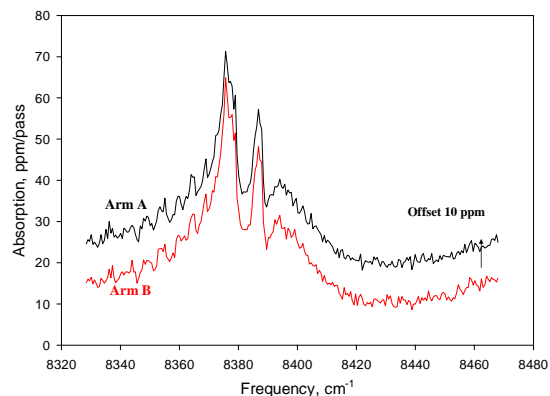


Figure 6: The spectra of the $7_0^1 12_1^1$ combination band of CH_3O_2 obtained from the two arms of the DCRDS apparatus. The black trace from arm “A” is vertically offset by +10 ppm for clarity.

Publications Supported by DOE (2007-2009)

- [1] “Investigation of Ethyl Peroxy Radical Conformers Via Cavity Ringdown Spectroscopy of the $\tilde{A} - \tilde{X}$ Electronic Transition,” P. Rupper, E. N. Sharp, G. Tarczay, and T. A. Miller, *J. Phys. Chem. A* **111**, 832 (2007).
- [2] “Rovibronic Bands of the $\tilde{A} \leftarrow \tilde{X}$ Transition of CH_3OO and CD_3OO Detected with Cavity Ringdown Absorption Near 1.2 - $1.4\ \mu\text{M}$,” C.-Y. Chung, C.-W. Cheng, Y.-P. Lee, H.-Y. Liao, E. N. Sharp, P. Rupper, and T. A. Miller, *J. Chem. Phys.* **127**, 044311 (2007).
- [3] “Observation of the $\tilde{A} - \tilde{X}$ Electronic Transition of the Isomers and Conformers of Pentyl Peroxy Radical Using Cavity Ringdown Spectroscopy,” E. N. Sharp, P. Rupper, and T. A. Miller, *J. Phys. Chem. A* **112**, 1445 (2008).
- [4] “The Structure and Spectra of Organic Peroxy Radicals,” E. N. Sharp, P. Rupper, and T. A. Miller, *Phys. Chem. Chem. Phys.* **10**, 3955 (2008).

Reaction Dynamics in Polyatomic Molecular Systems

William H. Miller

Department of Chemistry, University of California, and
Chemical Sciences Division, Lawrence Berkeley National Laboratory
Berkeley, California 94720-1460
millerwh@berkeley.edu

Program Scope or Definition

The goal of this program is the development of theoretical methods and models for describing the dynamics of chemical reactions, with specific interest for application to polyatomic molecular systems of special interest and relevance. There is interest in developing the most rigorous possible theoretical approaches and also in more approximate treatments that are more readily applicable to complex systems.

Recent Progress

Research efforts are being focused on the problem of how to add quantum mechanical effects to the classical molecular dynamics (MD) simulations that are now so ubiquitously applied to all types of dynamical processes in complex molecular systems. Semiclassical (SC) theory—since it is based on the classical trajectories of the molecular system—is a natural way to approach the problem, and one knows from much work¹ in the early 1970's that SC theory describes all quantum effects in molecular dynamics at least qualitatively, and typically quite quantitatively; the primary challenge is thus to develop methods for implementing it for large molecular systems. In this regard, the 'initial value representation'² (IVR) of SC theory has emerged as the most useful starting point since it replaces the non-linear boundary value problem of earlier SC approaches by a Monte Carlo average over the initial conditions of classical trajectories, a procedure more amenable to systems with many degrees of freedom.³

A particular kind of 'linearized' approximation of the SC-IVR (denoted LSC-IVR) leads to an especially simple (and thus attractive) approach that can fairly routinely be applied to large molecular systems; though it cannot describe true quantum coherence phenomena, the LSC-IVR does describe some quantum features (e.g., zero point energy effects, and tunneling corrections to thermal rate constants) quite well. Figure 1, for example, shows force-force correlation functions⁴ for liquid *para*-H₂ (that are related to vibrational relaxation in this solvent) at several temperatures as given by the LSC-IVR approach, compared to the corresponding classical results. At the higher temperature (14K) the two are very similar, i.e., quantum effects are negligible, while at the lower temperature one sees that the classical results show an oscillatory behavior indicative of incipient freezing of these clusters. The SC results, though, show only the faintest hint of this behavior, because zero point energy prevents the system from freezing; quantum effects are thus very prominent in this regime.

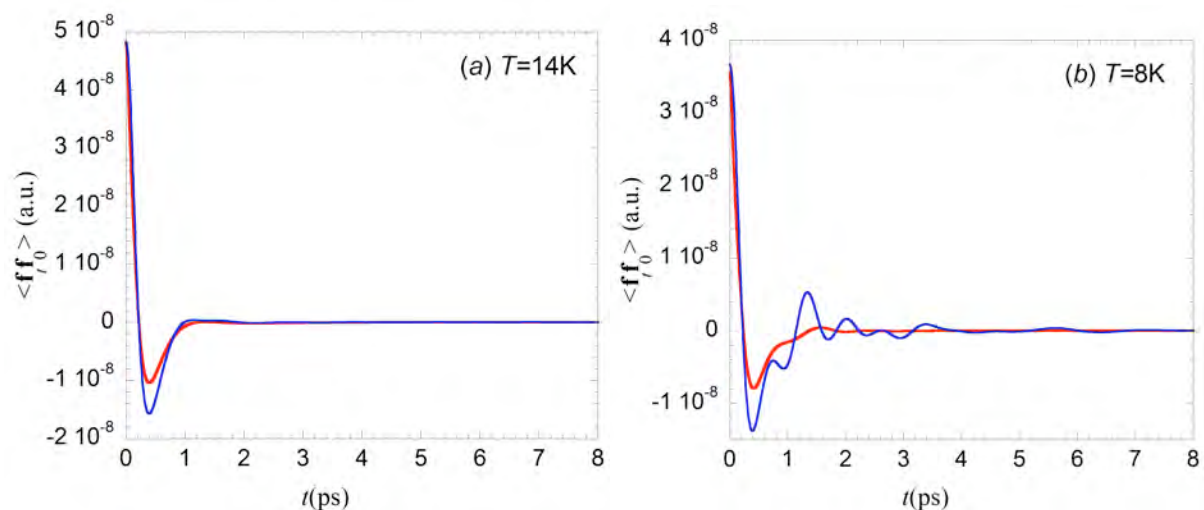


Figure 1. Force-force autocorrelation function of liquid *para*-H₂, at various temperatures; blue curves are the result of a purely classical MD calculation, and the red curves that of the linearized version of the SC-IVR.

An illustration of how the LSC-IVR describes tunneling in thermal rate constants is shown in Figure 2, an Arrhenius plot of the rate constant for a standard model problem for H atom transfer reactions (the 1d Eckart barrier). The tunneling correction factor is given to within ~10% for temperatures down to ~250K, at which the correction factor is greater than a factor of 10², and is correct to a factor of ~2 at 150K where the correction factor is > 10⁶.

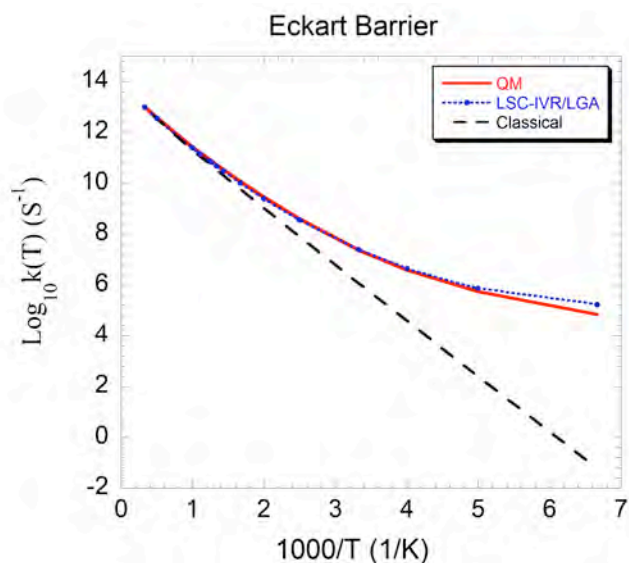


Figure 2. Arrhenius plot of the thermal rate constant for a 1d Eckart barrier corresponding to a standard H atom transfer reaction. Broken curve is the classical result, red curve the exact quantum result, and blue curve the result given by the LSC-IVR.

It should be noted, too, that the results shown in Figure 2 utilize a new, *modified* ‘local harmonic approximation’⁵ (mLHA) for evaluating the Wigner function involving the Boltzmann operator, which is the only non-trivial aspect of a LSC-IVR calculation. The LHA itself it not able to handle regions of a potential energy surface with significant negative curvature (where the local frequencies are imaginary), i.e., regions dominated by potential barriers that are most important for chemical reactions; e.g., for the results shown in Figure 2, the LHA itself (not shown in Fig. 2) diverges for T < 700K, making it essentially useless. The mLHA, on the other hand, is seen to be usefully accurate to below 200K. The mLHA thus solves the last remaining ‘bottleneck’ to making the ‘linearized’ SC-IVR approach a completely general dynamical approach, applicable to any system for which classical MD simulations are possible.

As noted, though, when coherence effects are important one must go beyond the linearized approximation, and the forward-backward⁶ (FB) IVR is the simplest treatment that is able to describe true coherence effects. Figure 3 shows an example such a calculation⁷ where coherence effects are significant: the quantity shown is the radial distribution function of the I₂ molecule (in its excited electronic state) in an Argon cluster, 352 fsec after excitation from the ground state. One sees some distribution at large r , corresponding to dissociation, and for smaller r , corresponding to bounded I₂, coherence effects are quite prominent even in this cluster environment.

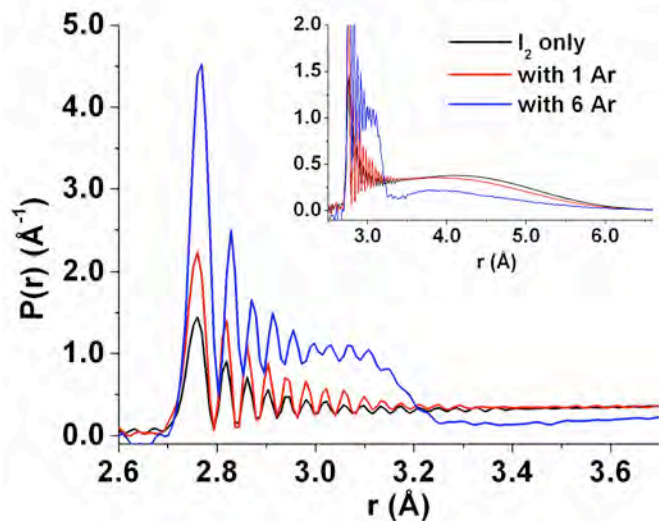


Figure 3. Solvent effect on quantum coherence of vibrational motion of iodine molecule. Shown are probability distribution functions of iodine molecule at $t = 352$ fs. All results are calculated by FB-IVR in three dimensional space. The probability distribution of a free iodine molecule is shown in black. The red line is for a system consisting of iodine molecule and one argon solvent. The blue line is the result for a cluster of iodine molecule and 6 argon atoms. The inset shows the same results for a longer range where dissociation exists.

Future Plans

The ‘linearized’ approximation to the general SC-IVR is now generally applicable to essentially any molecular system for which classical MD calculations are feasible. To describe true quantum coherence effects, however, requires a more accurate version of the SC-IVR, and the ‘forward-backward’ IVR is the simplest step up on the ‘ladder of rigor’ that is able to do so. Further effort will thus be devoted to developing the FB-IVR also into a generally applicable methodology. It is more difficult to apply than the ‘linearized’ version, but considerable progress has been made. A particularly interesting application to the FB-IVR is to electronically non-adiabatic dynamics, where quantum coherence is an important aspect of such processes.^{8,9}

References

1. For reviews, see W. H. Miller, *Adv. Chem. Phys.* **25**, 69 (1974); **30**, 77 (1975).
2. W. H. Miller, *J. Chem. Phys.* **53**, 1949 (1970).
3. For reviews, see (a) W. H. Miller, *J. Phys. Chem. A* **105**, 2942-2955 (2001); (b) W. H. Miller, *Proceedings of the National Academy of Sciences*, **102**, 6660-6664 (2005); (c) W. H. Miller, *J. Chem. Phys.* **125**, 132305.1-8 (2006).
4. J. Liu and W. H. Miller, *J. Chem. Phys.* **127**, 114506.1-10 (2007).
5. J. Liu and W. H. Miller, work in progress.
6. W. H. Miller, *Faraday Disc. Chem. Soc.* **110**, 1-21 (1998).

7. G. Tao and W. H. Miller, Semiclassical description of vibrational quantum coherence in a 3d I_2Ar_n ($n \leq 6$) cluster: A forward-backward initial value implementation, J. Chem. Phys. (submitted).
8. N. Ananth, C. Venkataraman and W. H. Miller, J. Chem. Phys. **127**, 084114.1-9 (2007).
9. W. H. Miller, J. Phys. Chem. **113**, 1405-1415 (2009).

2007 - 2009 (to date) DOE Publications

1. C. Venkataraman and W. H. Miller, "Chemical reaction rates using the semiclassical Van-Vleck initial value representation," J. Chem. Phys. **126**, 094104.1-8 (2007). LBNL-62085.
2. T. F. Miller and C. Predescu, "Sampling diffusive transitions paths," J. Chem. Phys. **126**, 144102.1-11 (2007). LBNL-62178.
3. J. Liu and W. H. Miller, "Real time correlation function in a single phase space integral — Beyond the linearized semiclassical initial value representation," J. Chem. Phys. **126**, 234110.1-11 (2007). LBNL-63117.
4. J. Vanicek and W. H. Miller, "Efficient estimators for quantum instanton evaluation of the kinetic isotope effects: Application to the intramolecular hydrogen transfer in pentadiene," J. Chem. Phys. **127**, 114309.1-9 (2007). LBNL-63540.
5. N. Ananth, C. Venkataraman and W. H. Miller, "Semiclassical (SC) description of electronically non-adiabatic dynamics via the initial value representation (IVR)," J. Chem. Phys. **127**, 084114.1-9 (2007). LBNL-63541.
6. J. Liu and W. H. Miller, "Linearized semiclassical initial value time correlation functions using the thermal gaussian approximation: Applications to condensed phase systems," J. Chem. Phys. **127**, 114506.1-10 (2007). LBNL-63535.
7. W. H. Miller, "The initial value representation of semiclassical theory: A practical way for adding quantum effects to classical molecular dynamics simulations of complex molecular systems," in Physical Biology – From Atoms to Medicine, ed. A. Zewail, Imperial College Press, London, UK, pp. 505-525 (2008). LBNL-1583E.
8. J. Liu and W. H. Miller, "Test of the consistency of various linearized semiclassical initial value time correlation functions in application to inelastic neutron scattering from liquid *para*-hydrogen," J. Chem. Phys. **128**, 144511.1-15 (2008). LBNL-191E.
9. J. Liu and W. H. Miller, "Linearized semiclassical initial value time correlation functions with maximum entropy analytic continuation," J. Chem. Phys. **129**, 124111.1-17 (2008). LBNL-901E.
10. W. H. Miller, "Electronically non-adiabatic dynamics via semiclassical initial value methods," J. Phys. Chem. **113**, 1405-1415 (2009). LBNL-1582E.
11. G. Tao and W. H. Miller, "Semiclassical description of vibrational quantum coherence in a 3d I_2Ar_n ($n \leq 6$) cluster: A forward-backward initial value implementation," J. Chem. Phys. (submitted). LBNL-(to be assigned).

GAS-PHASE MOLECULAR DYNAMICS: THEORETICAL STUDIES IN SPECTROSCOPY AND CHEMICAL DYNAMICS

James T. Muckerman (muckerma@bnl.gov) and Hua-Gen Yu (hgy@bnl.gov)
Chemistry Department, Brookhaven National Laboratory, Upton, NY 11973-5000

Program Scope

The goal of this program is the development and application of computational methods for studying chemical reaction dynamics and molecular spectroscopy in the gas phase. We are interested in developing rigorous quantum dynamics algorithms for small polyatomic systems and in implementing approximate approaches for complex ones. Particular focus is on the dynamics and kinetics of chemical reactions and on the rovibrational spectra of species involved in combustion processes. This research also explores the potential energy surfaces of these systems of interest using state-of-the-art quantum chemistry methods.

Recent Progress

Kinetics and dynamics study of the reaction of HOCO radical with H, HO₂ and Cl radicals

The important combustion reactions H/HO₂ + HOCO have been characterized by high level *ab initio* methods (QCISD(T) and CCSD(T)). Their dynamics have been investigated using the *ab initio* molecular dynamics approach based on CASSCF or SAC/CCSD energies and forces. Results show that both reactions are very fast. At room temperature, for the HO₂ + HOCO reaction, the calculated thermal rate coefficient is $(6.52 \pm 0.44) \times 10^{-11} \text{ cm}^3 \text{ molec}^{-1} \text{ s}^{-1}$ with the product branching fractions: 0.77 (CO₂ + H₂O₂), 0.15 (HOC(O)O + OH), 0.056 (CO₃ + H₂O), 0.019 (O₂(a ¹Δ) + HOC(O)H), and 0.01 (O₂(X ³Σ) + HOC(O)H). For the H + HOCO reaction, the rate coefficient is predicted to be $1.07 \times 10^{-10} \text{ cm}^3 \text{ molec}^{-1} \text{ s}^{-1}$ with a negligible activation energy of $E_a = 0.06 \text{ kcal/mol}$, and the branching fractions are estimated to be 0.87 for H₂ + CO₂, and 0.13 for H₂O + CO. In addition, a combined *ab initio* and direct dynamics study was also carried for the Cl + HOCO reaction. The thermal rate coefficients in the range 200-600 K were calculated. At room temperature, the thermal rate coefficient is predicted to be $3.0 \times 10^{-11} \text{ cm}^3 \text{ molec}^{-1} \text{ s}^{-1}$ with an activation energy of -0.2 kcal/mol . Only the HCl + CO₂ products are obtained. Interestingly, trajectories demonstrated that the reaction occurs via a dual-path complex-formation mechanism that is characterized by very short- and moderately long-lived complexes, both involving the addition of Cl to HOCO. The lifetimes of the HOC(O)Cl intermediates are predicted to be 310 fs and 1.9 ps for the short- and longer-lived intermediates. The coexistence of both mechanisms results from the poor vibration-vibration energy transfer in the newly formed HOC(O)Cl complex. This work was carried out in collaboration with J. Francisco (Purdue).

A spherical electron cloud hopping (SECH) model for dissociative recombination

A spherical electron cloud hopping (SECH) model has been developed for studying the product branching ratios of dissociative recombination (DR) of polyatomic systems. In this model, the fast electron-capture process is treated as an instantaneous hopping of a cloud of uniform spherical fractional point charges onto a target M^{+q} ion (or molecule). The sum of point charges (-1) simulates the incident electron. The sphere radius is

determined by a critical distance (R_{eM}^c) between the incoming electron (e^-) and the target, at which the potential energy of the e^-M^{+q} system is equal to that of the electron-captured molecule M^{+q-1} in a symmetry-allowed electronic state with the same structure as M^{+q} . During the hopping procedure, the excess energy of the electron association reaction is distributed over the kinetic energies of M^{+q-1} atoms to conserve total energy. The kinetic energies are adjusted by adding atomic momenta in the direction of driving forces induced by the scattering electron. The nuclear dynamics of the resultant M^{+q-1} molecule are studied using a direct ab initio dynamics method on the adiabatic potential energy surface of M^{+q-1} , or together with extra adiabatic surfaces of M^{+q-1} . For the latter case, the “fewest switches” surface hopping algorithm of Tully was adapted to deal with the nonadiabaticity in trajectory propagations. The SECH model has been applied to study the DR of both CH^+ and $H_3O^+(H_2O)_2$. The theoretical results are consistent with the experiment. It was found that water molecules play an important role in determining the product branching ratios of the molecular cluster ion.

Rovibrational spectroscopy of large amplitude molecule HO_3

An analytic potential energy surface has been constructed by fitting about 28 thousand energy points for the electronic ground-state (X^2A'') of HO_3 . The energy points are calculated using a hybrid density functional HCTH and a large basis set aug-cc-pVTZ, i.e., a HCTH/aug-cc-pVTZ density functional theory (DFT) method. The DFT calculations show that the trans- HO_3 isomer is the global minimum with a potential well depth of 9.94 kcal/mol with respect to the $OH + O_2$ asymptote. The minimum-energy geometry of the cis- HO_3 conformer is located 1.08 kcal/mol above that of trans- HO_3 with an isomerization barrier of 2.41 kcal/mol from trans- to cis- HO_3 . Using this surface, a rigorous quantum dynamics (QD) computation has been carried out to determine the rovibrational energy levels of HO_3 . The calculated results predict a dissociation energy of 6.15 kcal/mol, which is in excellent agreement with the experimental value of Lester et al. [J. Phys. Chem. A **111**, 4727 (2007).].

Vibronic spectra of boron nitride nanotubes

Radiative transitions of boron nitride nanotubes (BNNTs) in the energy range 1-6 eV have been studied using both experimental and theoretical approaches (in collaboration with W.-Q. Han, BNL CFN). In addition to the direct band-gap transition at 5.38 eV, diffuse structures near 4.09 eV were observed in the cathodoluminescence (CL) spectra for BNNTs. Our calculations suggested that these diffuse spectra could arise from a phonon-electron coupling mechanism via defects or impurities in the nanotubes. That is, they are typical vibronic spectra analogous to molecular electronic spectra. For the ^{10}B N nanotubes, the phonon frequency was determined as 0.1752 eV (or 1413 cm^{-1}), and this mode produces a progression of up to five phonon replicas which gives equally spaced peaks starting at 4.09 eV toward lower energies. The calculated frequency is in excellent agreement with the Raman value of 1390 cm^{-1} . It is assigned to a B-N bond stretching deformation mode. In addition, the DFT calculations with an oxygen-atom-substituted BN(5,5) nanotube indicate that BN_xO_{1-x} tubes are stable, which could substantially enhance the intensities of the vibronic spectra of BNNTs, together with excitons.

Future Plans

Kinetics and dynamics study of radical-radical reactions

We will continue to study some important combustion reactions using our direct *ab initio* molecular dynamics program. Of particular interest are fast radical-radical reactions. Two ongoing examples are the $\text{CH}_3/\text{ClO} + \text{HOCO}$ reactions, which are being carried out in collaboration with J. Francisco (Purdue). Here we will address the energies, geometries, and vibrational frequencies of the stationary points on the singlet ground-state surfaces, and the reaction mechanism. The dynamics will be carried out using CASSCF methods, together with variational RRKM theory. Our preliminary electronic structure calculations show that the reaction can occur *via* two reaction pathways. One is a direct abstraction reaction. The other occurs *via* an intermediate complex. However, the two pathways lead to different products. The aim of this research is to determine the product branching ratios as well as rate coefficients.

Our study of a series of reactions involving the HOCO radical will conclude with the disproportionation of the HOCO radical. Here we will address the energies, geometries, and vibrational frequencies of the stationary points on the singlet ground-state surface, and the reaction mechanism. If one HOCO radical abstracts the hydrogen atom from the other, the products would be HC(O)OH and CO_2 . If the two HOCO radicals form an intermediate oxalic acid, HOC(O)C(O)OH , complex, the products could be H_2O , CO and CO_2 , or two CO_2 and H_2 . The dynamics will be carried out using dual level *ab initio* methods. The aim of this research is to determine the mechanism and product branching ratio as well as rate coefficients.

Vibronic spectrum calculations of CH_2

In the GPMD group at BNL, Sears and Hall have successfully detected the predissociation spectra of CH_2 radicals. In order to approach a full understanding of the rich and complicated rovibronic levels of CH_2 near the $\text{C} + \text{H}_2$ and $\text{CH} + \text{H}$ dissociation limits, we have calculated five low-lying electronic potential energy surfaces of CH_2 using a multireference CI (MRCI) method. The adiabatic surfaces have been transformed into a set of diabatic ones using the quasi-adiabatic approximation of Koppel et al. Based on the surfaces, full dimensional quantum dynamics will be performed. The energy levels and non-adiabatic coupling effects will be explored, together with a detailed comparison with experimental observations.

Molecular dynamics studies of molecular ion reactions

Molecular ions such as C_3H_7^+ and H_3O^+ are important species in jet exhausts and interstellar media. It is very interesting to study their reactions and the product branching ratios. The results of such studies would be helpful for understanding the properties and evolutions of neutral molecular species in those environments. In this proposal, we will continue to develop and extend our direct *ab initio* molecular dynamics program, DualOrthGT, to study the reactivity of polyatomic molecular ions. Two example reactions are the dissociation recombination of H_3O^+ with slow electrons, and the $\text{H}_3^+ + \text{CO}$ reaction. For both reactions, we will focus on the product branching ratios of the reactions. For the latter, the H isotopic effect may also be investigated. Eventually, we hope to explore the properties and dynamics of combustion-related neutral radicals with the help of these similar reactions of corresponding cations.

Publications supported by this project since 2007

- H.-G. Yu, J. T. Muckerman and J.S. Francisco, *Quantum force molecular dynamics study of the O atoms with HOCO reaction*, J. Chem. Phys. **127**, 094302 (2007).
- H.-G. Yu, *Ab initio molecular dynamics simulation of photodetachment reaction of cyclopentoxide*, Chem. Phys. Lett, **441**, 20 (2007).
- H.-G. Yu and J.S. Francisco, *Energetics and kinetics of the reaction of HOCO with hydrogen atoms*, J. Chem. Phys. **128**, 244315 (2008).
- H.-G. Yu, J.S. Francisco and J. T. Muckerman, *Ab initio and direct dynamics study of the reaction of Cl atoms with HOCO*, J. Chem. Phys. **129**, 064301 (2008).
- H.-G. Yu, G. Poggi, J.S. Francisco and J. T. Muckerman, *Energetics and molecular dynamics of the reaction of HOCO with HO₂ radicals*, J. Chem. Phys. **129**, 214307 (2008).
- H.-G. Yu, *A spherical electron cloud hopping model for studying product branching ratios of dissociative recombination*, J. Chem. Phys. **128**, 194106 (2008).
- B. J. Braams and H.-G. Yu, *Potential energy surface and quantum dynamics study of rovibrational states of HO₃(X²A'')*, Phys. Chem. Chem. Phys. **10**, 3150 (2008).
- W.-Q. Han, H.-G. Yu, C. Zhi, J. Wang, Z. Liu, T. Sekiguchi and Y. Bando, *Isotope effect on band gap and radiative transitions properties of boron nitride nanotubes*, Nano Lett. **10**, 491 (2008).
- H.-G. Yu and J.S. Francisco, *A theoretical study of the reaction of CH₃ with HOCO radicals*, J. Phys. Chem. A (ASAP # 10.1021, 2009).

Selected related publications by PIs of this project since 2007

- A. D. Wilson, R. K. Shoemaker, A. Miedaner, J. T. Muckerman, D. L. DuBois, M. R. DuBois, *Nature of hydrogen interactions with Ni(II) complexes containing cyclic phosphine ligands with pendant nitrogen bases*, PNAS **104**, 6951-6956 (2007).
- J. T. Muckerman, E. Fujita, C. D. Hoff, G. J. Kubas, *Theoretical Investigation of the Binding of Small Molecules and the Intramolecular Agostic Interaction at Tungsten Centers with Carbonyl and Phosphine Ligands*, J. Phys. Chem. B **111**, 6815-6821 (2007).
- D. Polyansky, Cabelli, D.; Muckerman, J. T.; Fujita, E.; Koizumi, T.-a.; Fukushima, T.; Wada, T.; Tanaka, K., *Photochemical and Radiolytic Production of Organic Hydride Donor with Ru(II) Complex Containing an NAD⁺ Model Ligand*, Angew. Chem. Int. Ed. **46**, 4169-4172 (2007).
- D. E. Polyansky, D. Cabelli, J. T. Muckerman, T. Fukushima, K. Tanaka, E. Fujita, *Mechanism of Hydride Donor Generation using a Ru(II) Complex Containing an NAD⁺ Model Ligand: Pulse and Steady-State Radiolysis Studies*, Inorg. Chem. **47**, 3958-3968 (2008).
- L. Jensen, J. T. Muckerman, M. D. Newton, *First-Principles Studies of the Structural and Electronic Properties of the (Ga_{1-x}Zn_x)(N_{1-x}O_x) Solid Solution Photocatalyst*, J. Phys. Chem. C, **112**, 3439-3446 (2008).
- J. T. Muckerman, D. E. Polyansky, T. Wada, K. Tanaka, E. Fujita, *Water Oxidation by a Ruthenium Complex with Non-Innocent Quinone Ligands: Possible Formation of an O–O Bond at a Low Oxidation State of the Metal*, Forum on 'Making Oxygen,' Inorg. Chem., **47**, 1787-1802 (2008).
- H.-W. Tseng, R. Zong, J. T. Muckerman, R. Thummel, *Mononuclear Ru(II) Complexes That Catalyze Water Oxidation*, Inorg. Chem., **47**, 11763-11773 (2008).

Dynamics of Activated Molecules

Amy S. Mullin

Department of Chemistry and Biochemistry, University of Maryland

College Park, MD 20742

mullin@umd.edu

I. Program Scope

The focus of my research program is to investigate collisional energy transfer of molecules with large amounts of internal energy. Collisional energy transfer is ubiquitous in gas-phase chemistry and can have important effects on overall reaction rates and branching ratios. However there are substantial challenges to making detailed experimental measurements of energy transfer at energies that are relevant to chemistry under combustion conditions. High energy molecules contain extremely large densities of states, are of transient nature and have poorly understood interactions with other molecules. Currently, there are no first-principle theories of collisional energy transfer and the lack of fundamental knowledge often results in cursory and insufficient treatments in reactive models. A goal of my research is to gain new insights into the microscopic details of relatively large complex molecules at high energy as they undergo quenching collisions.

We use state-resolved transient IR absorption to characterize the energy transfer pathways that are responsible for the collisional cooling of high energy molecules. To overcome the inherent difficulties in developing a molecular level understanding of collisions involving high energy molecules, we use high-resolution IR probing to measure population changes in small collision partners that undergo collisions with high energy molecules. Using this technique, we have performed in-depth spectroscopic studies that provide a greater understanding of high energy molecules and their collisional energy transfer.

II. Recent Progress

A. State-resolved probes of low- ΔE energy transfer: Energy gain via “weak” collisions

We have continued using transient IR absorption probing to monitor the simultaneous appearance and depletion of population in low energy rotational states of bath molecules that are involved in the collisional quenching of high energy molecules. This approach gives us access to measure the energy partitioning and rates for the full distribution of bath molecules that scatter from collisions. Our measurements so far have focused on the nascent products generated from single collisions, but could be applied to mapping out the evolution of energy distributions under higher pressure and multi-collision conditions.

Until recently, high-resolution probing of collisional energy transfer of high energy molecules has been limited to measuring large ΔE collisions that scattered bath molecules into previously unpopulated states. By measuring the dynamics associated with low energy rotational states we measure the outcome of small ΔE collisions are associated with so-called “weak” collisions. The terms “weak” and “strong” are qualitative descriptors that refer to collisions leading to small- ΔE and large- ΔE energy transfer, based historically on Hirschfelder’s strong collision assumption.

Collisions that induce small exchanges of energy make up the vast majority of energy transfer events but they are difficult to distinguish from the ambient background population in low- J states at 300 K. Parallel energy transfer processes that excite bath vibrational states (V-to-V energy transfer) interfere with high-resolution absorption measurements by moving population into upper states of the IR probe transitions. If this is the case, it is impossible to sort out how distinct processes contribute to the overall absorption signals. We overcome this problem by judiciously choosing probe transitions that have negligible cross sections for V-to-V energy transfer. For CO_2 probing, we use $00^0_0 \rightarrow 10^0_1$ transitions near $\lambda=2.7 \mu\text{m}$. For HOD and DCl probing, we do not observe collisional transfer to the stretching modes and single quantum probe transitions are used at $\lambda=2.7 \mu\text{m}$ and $4.5 \mu\text{m}$, respectively.

To measure the transient populations associated with weak collisions, we collect transient Doppler-broadened IR line profiles for individual states of bath molecules immediately following single collisions

with highly excited molecules. For low- J states of the bath molecule, signals are dominated by negative-going depletion of the initial population at the center frequency of the probe transition. In the Doppler-broadened wings, positive-going appearance signals correspond to the products of collisional energy transfer. The data are fit using a double Gaussian function that distinguishes contributions of the appearance and depletion signals. Appearance line widths directly yield the distribution of recoil velocities in the scattered molecules. The integrated area of the appearance component corresponds to the nascent population of bath molecules that are scattered into a final rotational state. In this way, we measure nascent rotational and translational energy distributions for the full range of rotational states of the scattered bath molecules.

B. Energy Dependence of Recoil Energies and Product Rotational State Distributions

We have measured the nascent appearance of individual rotational states of CO_2 ($v=00^0$, $J=2-80$) following single collisions with pyrazine(E) at two initial donor energies, $E=32700\text{ cm}^{-1}$ and 37900 cm^{-1} . The center-of-mass recoil energies of the scattered bath molecules are plotted in Fig. 1 as a function of bath rotational state. For both donor energies, the low- J states of CO_2 are scattered with modest recoil energies. The recoil energy increases nonlinearly above a threshold bath state J_{th} . For CO_2 the threshold is near $J_{\text{th}} \sim 60$ which has a rotational energy of $E_{\text{rot}} \sim 1450\text{ cm}^{-1}$. Pyrazine has a number of vibrational modes in this region: C–H bending modes are at 1230 and 1350 cm^{-1} and C–H stretching modes are 1410 to 1580 cm^{-1} . The recoil velocities associated with a given CO_2 product state approximately double for a 16% increase in pyrazine’s vibrational energy.

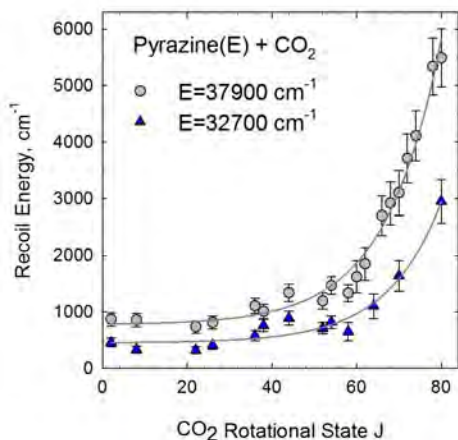


Fig. 1. Nascent center-of-mass recoil energies due to collisions of pyrazine(E) with CO_2 at two different vibrational energies, $E=32700$ and 37900 cm^{-1} shown as a function of CO_2 rotational state. The product translational energies double for a 16% increase in pyrazine energy.

The nascent rotational states of scattered CO_2 molecules have bimodal distributions for both pyrazine energies, as shown in Fig. 2. The low- J states ($J=2-54$) fit to temperatures of $T_{\text{rot}}=420\text{ K}$ and 451 K while the high- J states ($J=56-80$) have temperatures of $T_{\text{rot}} = 930$ and 1145 K . This observation indicates that there are two subpopulations of CO_2 molecules that are generated through collisions. It is worth noting that in related energy gain measurements for pyrazine quenching with DCI and HOD , the bath molecules are scattered with single rotational distributions. Furthermore, the V-to-RT data in Figure 2 account for more than 95% of all collisions and include the outcome of both elastic and inelastic collisions. V-to-V energy transfer accounts for the remaining 5% of collisions. The total V-to-RT energy transfer rate is very close to the Lennard-Jones collision rate.

The low- J states arise from weak collisions that involve small changes in angular momentum and recoil velocity. The high- J states result from strong collisions involving larger changes in both angular momentum and recoil velocity. The high- J product states are much more sensitive than the low- J states to changes in pyrazine’s internal energy.

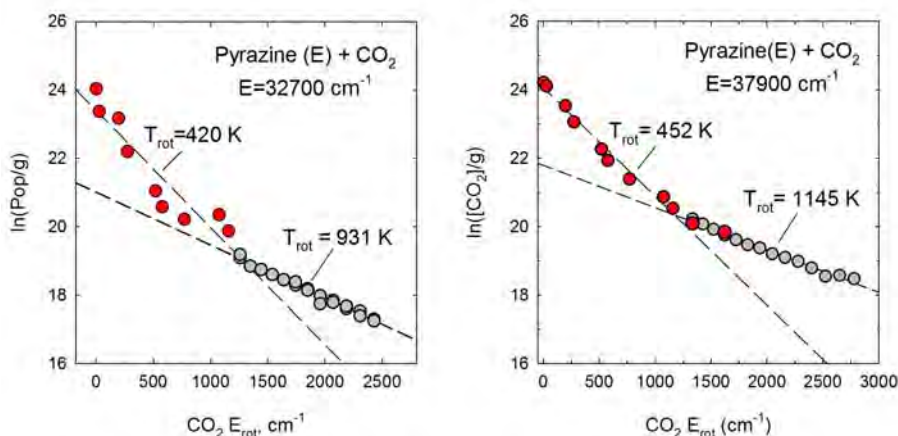


Fig. 2. Nascent distributions of CO_2 (00^0 , $J=2-80$) following collisions with highly excited pyrazine at two different vibrational energies, $E=32700$ and 37900 cm^{-1} . Low- J data (red circles) were collected on a newly constructed spectrometer. High- J data (grey circles) have been published previously.

Based on the data in Fig. 2, we have developed a two-component model to characterize the two subpopulations of scattered molecules. The strong collision component is characterized using the high- J T_{rot} values shown in Fig. 2. We subtract this subpopulation from the observed bimodal distribution to obtain the weak-collision subpopulation. Interestingly, the weak collision subpopulations at both donor energies have rotational temperatures near the ambient cell temperature. The weak collision component predominates at both donor energies. The fraction of strong collisions nearly doubles for a 16% increase in pyrazine energy. The hot distribution makes up 13% of the total scattered population for the lower energy donor and 25% for the higher energy donor.

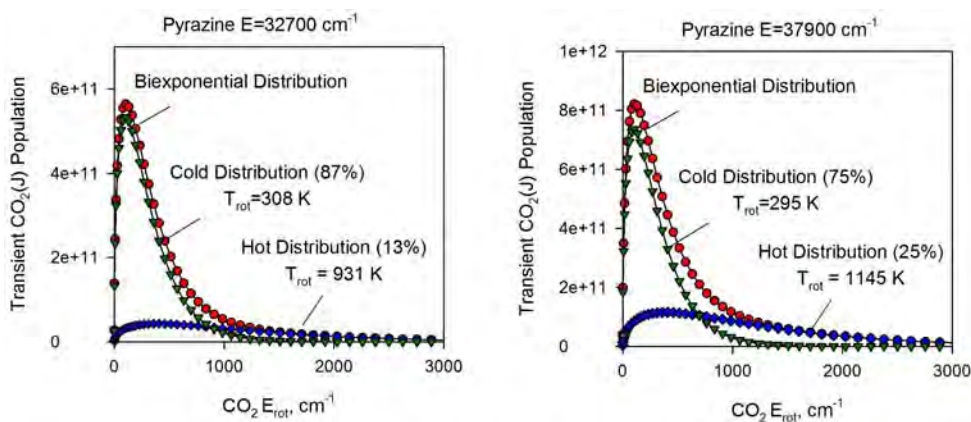


Fig. 3. Subpopulations of scattered CO_2 molecules from collisions with pyrazine(E), where $E=32700$ and 37900 cm^{-1} . The weak collision components have rotational temperatures near the ambient experimental temperature of 298 K. The fraction of strong collisions nearly doubles for a 16% increase in pyrazine internal energy.

C. Collisions in the presence of hydrogen bonding: dynamics and collision rates

We have also performed a number of studies that investigate the collisional quenching of highly excited donor molecules with H_2O and HOD to learn what role, if any, hydrogen bonding has on energy transfer dynamics. These results of these studies have already been published and details can be found in the corresponding papers listed below. We find that energy gain profiles, particularly for bath rotation, are sensitive to details of the hydrogen bonding interactions. The data suggest that the dynamics are affected by the number of hydrogen bonding sites between the highly excited donor and water and by the structure of the local energy minima. We also learn from these studies that collision rates for H_2O and HOD can be as much as 3 times larger than Lennard-Jones collision rates. This is distinct from collisions involving DCI and CO_2 with highly excited aromatic donors that have experimental collision rates that are very close to Lennard-Jones rates.

III. Future Work

We are planning to measure energy transfer dynamics of highly excited molecules in collisions with HCl. The results of the HCl studies will be compared with earlier work on DCI collisional energy gain. These experiments will provide a benchmark for testing how rotational and translational energy partitioning scales with angular momentum constraints for the same intermolecular potential energy surface. We are also setting up to investigate collision dynamics of HOD with highly excited molecules that have structurally distinct hydrogen bonding sites.

IV. Recent Publications

“Relaxation dynamics of highly vibrationally excited picoline isomers ($E_{\text{vib}}=38300\text{ cm}^{-1}$) with CO_2 : The role of state density in impulsive collisions,” E. M. Miller, L. Murat, N. Bennette, M. Hayes, and A. S. Mullin, *J. Phys. Chem. A* **110**, 3266-3272 (2006).

“Direct determination of collision rates beyond the Lennard-Jones model through state-resolved measurements of strong and weak collisions,” D. K. Havey, Q. Liu, Z. Li, M. S. Elioff, M. Fang, J. Neudel and A. S. Mullin, *J. Phys. Chem. A* **111**, 2458-2460 (2007).

“Strong Collisions of Highly Vibrationally Excited Alkylated Pyridines ($E_{\text{vib}}\sim 38800\text{ cm}^{-1}$) with CO_2 ” by Q. Liu, J. Du, D. K. Havey, Z. Li, E. M. Miller and A. S. Mullin, *J. Phys. Chem. A* **111**, 4073-4080 (2007).

“Collisions of highly vibrationally excited pyrazine with HOD: State-resolved probing of strong and weak collisions,” D. K. Havey, Q. Liu, Z. Li, M. S. Elioff, and A. S. Mullin, *J. Phys. Chem. A* **111**, 13321-13329 (2007).

“State resolved strong collisions of vibrationally excited azulene ($E_{\text{vib}}=20,100$ and $38,500\text{ cm}^{-1}$) with CO_2 ,” L. Yuan, J. Du and A. S. Mullin, *J. Chem. Phys.* **129**, 014303/1-11 (2008).

“Energy transfer dynamics of weak and strong collisions between vibrationally excited pyrazine($E_{\text{vib}}=37900\text{ cm}^{-1}$) + DCI,” J. Du, L. Yuan, S. Hsieh, F. Lin and A. S. Mullin, *J. Phys. Chem. A* **112**, 9396-9404 (2008).

“Energy transfer dynamics in the presence of preferential hydrogen bonding: Collisions of highly vibrationally excited pyridine- h_5 , - d_5 , and - f_5 with water,” D. K. Havey, Q. Liu and A. S. Mullin, *J. Phys. Chem. A* **112**, 9509-9515 (2008).

“Effects of alkylation on deviations from Lennard-Jones collision rates for highly excited aromatic molecules: Collisions of methylated pyridines with HOD” Q. Liu, D. K. H., Z. Li and A. S. Mullin, *J. Phys. Chem. A*, in press (2009).

Reacting Flow Modeling with Detailed Chemical Kinetics

Habib N. Najm

Sandia National Laboratories
P.O. Box 969, MS 9051, Livermore, CA 94551
hnnajm@sandia.gov

1 Program Scope

The goal of this research program is to improve our fundamental understanding of reacting flow, thereby advancing the state of the art in predictive modeling of combustion. The work involves: (1) Using computations to investigate the structure and dynamics of flames using detailed chemical kinetics; (2) Developing techniques for analysis of multidimensional reacting flow; (3) Developing numerical methods for the efficient solution of reacting flow systems of equations with detailed kinetics and transport; (4) Developing massively parallel codes for computing large scale reacting flow with detailed kinetics; and (5) Developing numerical methods for uncertainty quantification in reacting flow computations, including methods for the construction of uncertain chemical models from experimental data.

2 Recent Progress

2.1 Reacting Flow Computations, Analysis, and Model Reduction

We have continued our study of methane-air edge flame structure using computational singular perturbation (CSP) analysis. The goal of this study is to examine the internal structure of this flame, identify the chemical processes that comprise its various layers, evaluate the transport/chemical processes most important to the local structure, and arrive at simplified chemical models. Examining the chemical (forward/backward) and transport processes determining the fastest chemical time scale, we highlighted a range of fuel breakup reactions that are dominant in this context in the premixed preheat zone around the rim of the edge flame. These include



On the other hand, throughout the region *inside* the edge flame, a single reaction $\text{NNH} \Leftrightarrow \text{N}_2 + \text{H}$ was found to be largely responsible for the fastest chemical time scale. The CSP radicals associated with the fastest chemical time scale, being the species whose fast consumption processes dominate the equilibrium of the exhausted fastest mode, were found to be NNH in the internal edge flame region, $\text{CH}_2(\text{S})$ in the preheat region, and CH in the cold reactants outside of the edge flame. We also identified, in a similar manner, the corresponding processes relevant to the active time scale and mode. This information, identifying the key reactions/species determining specific aspects of the dynamical behavior of the flame, is important both from a computational perspective, and, more importantly, for purposes of model reduction.

In the computational development context, we demonstrated our recently developed massively parallel low Mach number flame code, employing large-scale runs, on the latest NERSC hardware, Franklin. These demonstrations employed full nHeptane chemistry, with 560 species and 2538 reactions, on 512×512 two-dimensional domains. The particular structure of this machine necessitated code modifications to achieve acceptable performance with the nHeptane chemistry. Note that the same code setup with a $10 \times$ smaller chemical model, e.g. GRImech3.0 with 53 species and 325 reactions, performed well without code enhancements. The key challenge on this machine, as with other modern massively parallel hardware, is memory handling, which becomes much more significant in the larger nHeptane case. Our starting code incurred a $3 \times$ performance hit for nHeptane resulting from the 4-core structure of the processors. We improved the code in various ways to remove this performance hit. Of primary importance was using more modern linear algebra in the stiff integration algorithm, employing LAPACK instead of the older LINPACK library. The mixed structure of the code, employing a mixed distributed-shared memory model was also helpful in terms of performance, where we run in shared memory among the cores on each processor, while employing the distributed memory model with a message passing paradigm outside the

chip. The result has been an optimal code structure, with demonstrated strong scalability, *i.e.* with a fixed problem size, up to 8000 cores. We observe a slow decay rate of the parallel efficiency at large numbers of cores, with 56% efficiency observed for 4000 cores, decaying to 51% for 8000 cores, compared to a base-case with 16 cores.

We studied the structure of an nHeptane-air edge flame using two CSP-simplified nHeptane mechanisms, one with 66 species (M66) and the other with 139 species (M139). Overall the M66 flame structure was similar to the M139 flame, although differences of species mass fractions by up to 30% were observed for HCO, HO₂, O, OH, HCCO, CH, and H₂O₂ in different parts of the flame. Comparison with the detailed 560-species nHeptane model will be done next, after the completion of the relevant massively parallel runs presently in progress at NERSC.

We have also started analysis of ignition of iso-octane/air mixtures using the LLNL 857-species model. We are analysing the ignition results using CSP, focusing on the dynamics of OH, HO₂, and temperature, to identify important reactions that determine the timing and temperature rise of the second (main) ignition event.

2.2 Uncertainty Quantification in Chemical Systems

We conducted a detailed uncertainty quantification (UQ) study in constant pressure ignition of a preheated methane-air mixture, using a single-step global methane kinetic model, employing multi-resolution analysis with local polynomial chaos (PC) constructions on block-decomposed stochastic domains. Uncertainties were postulated in the pre-exponential rate constant A and activation energy E . The joint PDF for (A, E) was constructed using Bayesian inference, starting with GRI_{mech}3.0-simulated “data” of species concentration with presumed experimental noise, and was found to exhibit strong correlation. This empirical correlation was then built into the PC representation of these two uncertain parameters, and propagated through the ignition process. We conducted a detailed examination of the role of correlation between the uncertain parameters in the resulting uncertainty in model predictions. Results exhibited strong dependence of the output uncertainties on the presumed correlation between the parameters. For one particular slope of this correlation, there was, in fact, zero uncertainty in the predictions. While increasing/decreasing the slope away from this critical value lead to significant rise in the resulting uncertainty. This observation is explained by the dependence of the rate expression, and therefore the ignition time, on A and E . Specifically, the ignition time is found to vary inversely with A , but directly with E . Depending on the particular slope of correlation between the two parameters, one or the other trend wins. Moreover, there is a “critical” slope for which the two trends cancel, resulting in no uncertainty in the results. These observations highlight the crucial need for properly characterized correlations between uncertain parameters, informed by *data*, in order to properly estimate the effective resulting uncertainty in model predictions. The fact that these correlations are rarely known, let alone available in the literature, is a serious challenge to relevant application of UQ in chemical systems, irrespective of the particular methodology.

2.3 High-Order Structured Adaptive Mesh Refinement

We have continued development of parallel high-order structured adaptive mesh refinement (SAMR) algorithms and code components for the solution of the low Mach number reacting flow equations. We have demonstrated fourth-order spatial accuracy and second-order time accuracy for the full solver with detailed chemical kinetics. The scheme incorporates a coupled construction including (1) a SAMR solution of the species and energy equations, and (2) a uniform mesh solution of the momentum equations. This construction is motivated by the observation that mesh adaptivity is primarily needed for the radical profiles, and not so much the velocity field. The order of accuracy was observed on all fields, including species, temperature, velocity and pressure; in a one-dimensional flame problem. Demonstrations in two-dimensions are in progress.

We have also continued working on finalizing our transition to the CHOMBO SAMR library, as our mesh component. The aim of this effort has been a componentization of CHOMBO in a manner that respected the AMR mesh interfaces that we have already developed. This involves the design and implementation of a “translation” layer that provides the functionality of the mesh interface, using the data structures provided by CHOMBO, particularly their data storage, parallel computing and box calculus capabilities. This translation-layer has been largely implemented and has been undergoing testing. We have successfully tested it for the invocation/application of boundary conditions and various parallel functionalities. The primary outstanding testing issues involve prolongations and restrictions using high-order interpolations, in multi-level grid hierarchies. While components that perform these operations exist, the code to “translate” CHOMBO structures/operations into a form accepted by the existing components remains to be written. This is expected to be an exercise in box-calculus. Thereafter, we expect the CHOMBO component to be put through its paces using canonical problems to gauge correctness.

2.4 CSP Tabulation and Adaptive Chemistry

We have continued development of adaptive methods for tabulating low-dimensional chemical manifolds in high-dimensional spaces, identified via Computational Singular Perturbation (CSP) analysis. We have put together a non-parametric construction, employing *kd*-trees to facilitate high-dimensional space representations. This structure allows for local parametric representations employing response surfaces, where sufficient data is available for their construction. We have demonstrated the basic *kd*-tree implementation for the tabulation of CSP quantities pertaining to the low-dimensional manifold structure in a hydrogen-oxygen ignition context, based on a 9-species $\text{H}_2\text{-O}_2$ kinetic model. We demonstrated both the construction of the table, and its use for time integration of the ODE system using an explicit time integrator utilizing CSP projection operations to filter-out fast time scales. The algorithm uses the tabulated information for the low-dimensional manifold at each stage during the ignition process time integration, from the preheat phase, through the fast ignition transient, and towards equilibrium. Quantitative performance comparisons with the stiff time integration of the full system are in progress.

3 Future Plans

3.1 Reacting Flow Computations, Analysis, and Model Reduction

Having completed the development of our massively parallel MPI-OpenMP flame code, and given our present in-progress computations of a detailed nHeptane-air edge flame on NERSC, our next effort in the immediate time frame will be focused on analysis of the associated results with respect to the predictions of the same flame using simplified mechanisms. We will also explore parametric studies of the nHeptane-air edge flame system, analyzing the effect of different degrees of premixing in the fuel stream on the flame structure. We will also continue our ignition study of the iso-octane/air system, over a range of stoichiometry. Using CSP for analysis of the results, we will strive to advance the state of understanding of the ignition process in this system. We will highlight reactions of key importance in specific observables, providing useful information to mechanism developers. Finally, with the MPI-OpenMP code in routine use, our next code development effort towards a fourth-order axisymmetric construction, which has been in progress in the background, will be ramped up. This development will allow targeted investigation of laboratory scale axisymmetric jet flames, with associated comparisons to ongoing experiments.

3.2 Uncertainty Quantification in Chemical Systems

In the intrusive polynomial chaos (PC) uncertainty quantification (UQ) context, challenges have existed in terms of stability as well as computational performance. In the stability context, it is now clear that relatively slow decay rate of spectral energy in the PC expansions leads to positive eigenvalues in the resulting PC ODE system jacobian, resulting in instabilities in the implicit time integration. This highlights the need for spectral filtering strategies, which we will explore with a view to understanding how to design these optimally. In the computational performance context, block refinement/coarsening strategies as well as asynchronous time integration strategies are needed. We anticipate access to an efficient refinement/coarsening multiwavelet code, that we intend to apply to uncertain 1D premixed flame computations. At the same time, there is a clear need for efficient unstructured mesh tessellation for high dimensional stochastic spaces. In this regard, we will examine the extension of PC spectral Galerkin constructions to unstructured triangular meshes. These will be relevant both in the intrusive and non-intrusive PC UQ contexts. Finally, we will study the structure of uncertain stiff chemical systems, from the point of view of model reduction under uncertainty. Particularly, it is interesting to consider the structure of low dimensional manifolds, both in the original deterministic problem, and in the Galerkin-reformulated PC UQ system. We will explore the consequences of uncertainty in both fast and slow directions, on the uncertain reduced model structure.

3.3 High-Order Structured Adaptive Mesh Refinement

Having empirically demonstrated the theoretical order of convergence of the construction in 1D, we plan to demonstrate this convergence soon in 2D. Following this, our next target is to pursue detailed flame structure comparisons to known solutions. These will be relevant for verifying the overall code. Further, we will study computational speedup as a function of mesh refinement parameters, and load partitioning/balancing strategies. We will also evaluate the computational performance of our implementation of the CHOMBO mesh component and examine

the scalability of the overall construction with large numbers of processors. In this context we will also examine the possibility of decoupling the mesh component from the partitioning algorithm to further increase the flexibility of the code. We will use the resulting toolkit for studying canonical flames in vortical reacting flow involving complex fuels in laboratory scale geometry. As we plan to extend our tests to 3D flame configurations we will explore efficient approaches for fine-coarse grid interpolations, e.g. the Smolyak algorithm, as well as wavelet decomposition methods for grid adaptation and refinement.

3.4 CSP Tabulation and Adaptive Chemistry

We will extend the present demonstrations with hydrogen-oxygen ignition in various ways. We will conduct a detailed performance study, evaluating the costs of table construction and lookup, and examining the performance of the CSP integrator with tabulation in comparison to stiff time integration of the original system. We will also develop the tabulation algorithms towards *in situ* adaptive table construction. Moreover, we will pursue a hybrid parametric/non-parametric structure, where local response surfaces are built over hypercubes in the state space in dense subsets of the *kd*-tree. The demonstrations in the hydrogen system will be followed by others involving more complex hydrocarbon fuels, including methane, propane, and nHeptane.

4 BES-Supported Published/In-Press Publications [2007-2009]

- [1] Najm, H.N., Debusschere, B.J., Marzouk, Y.M., Widmer, S., and Le Maître, O.P., Uncertainty Quantification in Chemical Systems, *Int. J. Num. Meth. Eng.* (2009) in press.
- [2] Marzouk, Y. M., and Najm, H. N., Dimensionality reduction and polynomial chaos acceleration of Bayesian inference in inverse problems, *Journal of Computational Physics* (2009) in press.
- [3] Valorani, M., and Paolucci, S., The *G-Scheme*: A Framework for Multi-Scale Adaptive Model Reduction, *Journal of Computational Physics* (2009) in press.
- [4] Najm, H.N., Uncertainty Quantification and Polynomial Chaos Techniques in Computational Fluid Dynamics, *Annual Review of Fluid Mechanics*, 41(1):35–52 (2009).
- [5] Prager, J., Najm, H., Valorani, M., and Goussis, D., Skeletal Mechanism Generation with CSP and Validation for Premixed n-Heptane Flames, *Proc. Comb. Inst.*, 32(1):509–517 (2008).
- [6] Najm, H.N., Ponganis, D., and Prager, J., Analysis of NO Structure in a Methane-Air Edge Flame, *Proc. Comb. Inst.*, 32(1):1117–1124 (2008).
- [7] Najm, H.N., Ray, J., Safta, C., Marzouk, Y., Valorani, M., and Goussis, D.A., High-order AMR computations of reacting flow with adaptive reduction of chemical stiffness, *Journal of Physics: Conference Series* (2008).
- [8] Valorani, M., Creta, F., Li Brizzi, A., Najm, H.N., and Goussis, D.A., Surrogate Fuel Analysis and Reduction using Computational Singular Perturbation, *AIAA-2008-1009* (2008) AIAA 46th AIAA Aerospace Sciences Meeting and Exhibit, Reno, NV.
- [9] Marzouk, Y. M., Najm, H. N., and Rahn, L. A., Stochastic spectral methods for efficient Bayesian solution of inverse problems, *Journal of Computational Physics*, 224(2):560–586 (2007).
- [10] Le Maître, O.P., Najm, H.N., Pébay, P.P., Ghanem, R.G., and Knio, O.M., Multi-resolution-analysis scheme for uncertainty quantification in chemical systems, *SIAM J. Sci. Comput.*, 29(2):864–889 (2007).
- [11] Ray, J., Kennedy, C.A., Lefantzi, S., and Najm, H.N., Using High-Order Methods on Adaptively Refined Block-Structured Meshes, *SIAM J. Sci. Comp.*, 29(1):139–181 (2007).
- [12] Lee, J.C., Najm, H.N., Lefantzi, S., Ray, J., Frenklach, M., Valorani, M., and Goussis, D., A CSP and Tabulation Based Adaptive Chemistry Model, *Combustion Theory and Modeling*, 11(1):73–102 (2007).
- [13] Ortega, J.M., Najm, H.N., Ray, J., Valorani, M., Goussis, D.A., and Frenklach, M., Adaptive Chemistry Computations of Reacting Flow, *Journal of Physics: Conference Series*, 78:012054 (2007).
- [14] Valorani, M., Creta, F., Donato, F., Najm, H.N., and Goussis, D.A., Skeletal Mechanism Generation and Analysis for n-heptane with CSP, *Proc. Comb. Inst.*, 31:483–490 (2007).

Spectroscopy, Kinetics and Dynamics of Combustion Radicals

David J. Nesbitt

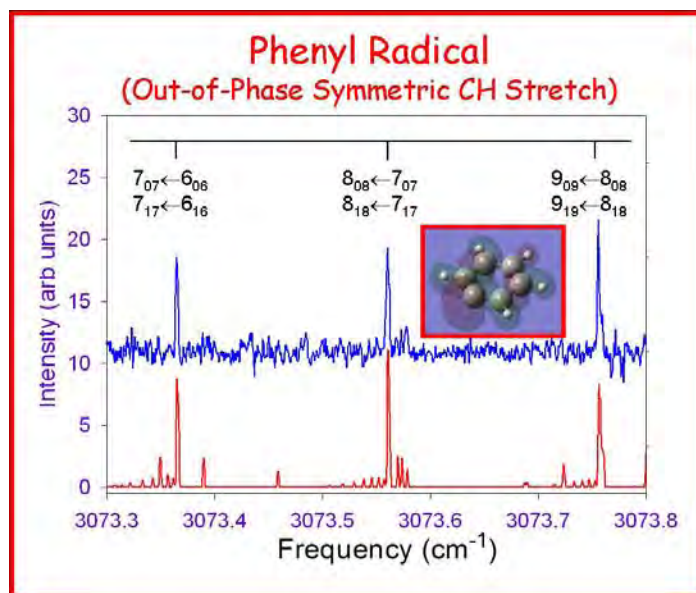
*JILA, University of Colorado and National Institute of Standards and Technology, and
Department of Chemistry and Biochemistry, University of Colorado, Boulder, Colorado
29th Annual Combustion Research Conference, May 26-29, 2009*

High resolution IR spectroscopy, kinetics and dynamics of jet cooled hydrocarbon transient radicals relevant to the DOE combustion mission have been explored, exploiting i) slit discharge sources of jet cooled radicals, and ii) high sensitivity detection with direct IR laser absorption methods at the quantum shot noise limit. The key advantage is that high concentrations of radicals can be formed under high pressure combustion conditions with the resulting species rapidly cooled ($T \approx 10\text{-}20\text{K}$) in the slit supersonic expansion. In conjunction with IR laser absorption methods, this combination offers prospects for first time spectral detection and study of many critical combustion radicals. Highlights from work over the last year are summarized below.

I. High Resolution IR Spectroscopy of Jet-cooled Phenyl (C_6H_5) Radical

Phenyl radical (C_6H_5) is a highly reactive 6-membered organic hydrocarbon ring intermediate formed from homolytic cleavage of a CH bond in benzene.¹⁻³ By virtue of its overall reactivity, this radical plays a central role in combustion, specifically for fossil fuels which are typically rich in aromatics.^{4,5} Indeed, it is one of the simplest prototypes of an open shell aromatic species, achieving partial stabilization of the radical due to resonance structures arising from electron delocalization around the ring. This radical stabilization also makes it a prime target intermediate for ring formation in complex combustion processes, which highlights phenyl as a crucial species in mediating the early stages of soot formation.⁶⁻⁹

We have recently been successful in obtaining first gas phase infrared CH stretch spectra of jet cooled phenyl radical, via high resolution direct laser absorption methods. This work represents the only IR spectroscopy of phenyl in the gas phase with rovibrational resolution, which has been used to monitor fundamental excitation of the out-of-phase symmetric CH stretching mode (ν_{19}) of b_2 symmetry. Rigorous assignment of rotational structure in the gas phase spectra is obtained from precision 2-line ground state combination differences from radio frequency spectroscopy.² The analysis yields rotational constants and vibrational energies for the excited state, the latter of which proves to be in remarkably good agreement with matrix isolation studies by Ellison and coworkers,¹ and indicates only a surprisingly small shift ($\approx 0.1 \pm 1 \text{ cm}^{-1}$) between the gas and Ar matrix phase environment. The ability to obtain rovibrationally resolved spectra for such a prototypical aromatic species represents an

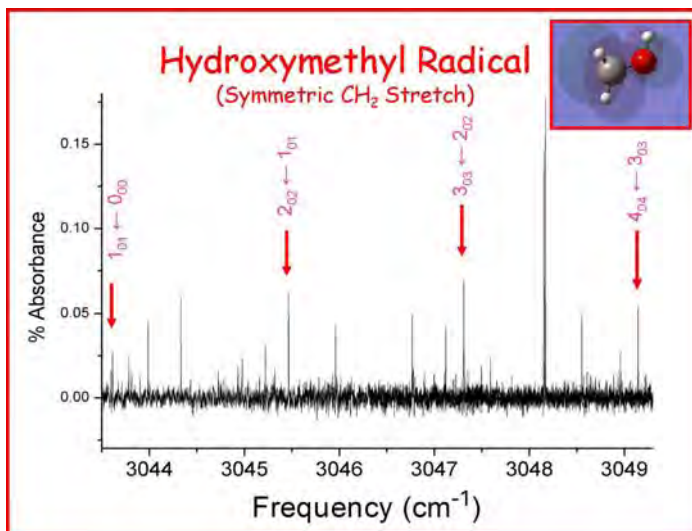


important milestone for highly reactive combustion intermediates, and bodes well for spectroscopic detection and analysis of other complex aromatic radicals in the gas phase.

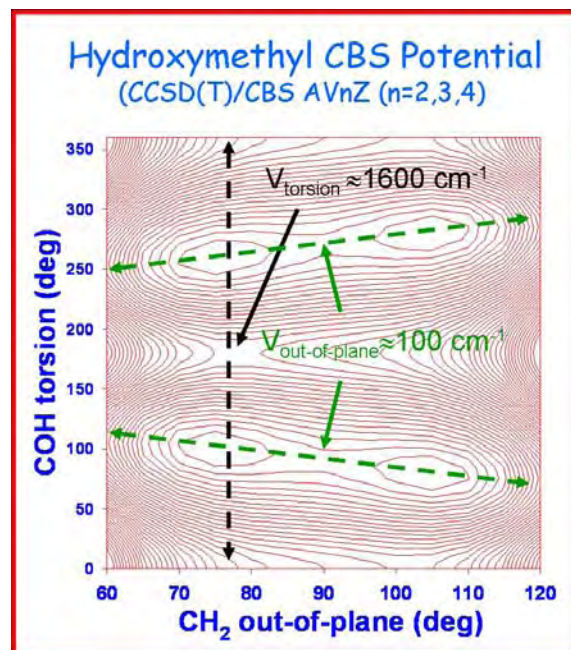
II. High Resolution Spectroscopy of Jet Cooled Hydroxymethyl (CH_2OH) Radical

Encouraged by these results in phenyl radicals, we have begun to tackle oxygenated species such as hydroxyalkyl radicals (ROH), which represent crucial intermediates in combustion models. The simplest of these, hydroxymethyl (CH_2OH), is predicted to have a slightly non-planar equilibrium structure with a low barrier across a C_s transition state due to OH torsion. This work builds on the vibrationally tagged double resonance ion depletion studies of Reisler and coworkers^{10,11} for CH_2OH , which yielded structured spectra in the CH and OH stretch regions limited by linewidth of their pulsed laser ($\approx 0.4 \text{ cm}^{-1}$). We have recently obtained much higher resolution ($\approx 0.002 \text{ cm}^{-1}$) spectra in a methanol doped discharge of CH_2OH in the symmetric CH_2 stretch region. At sub-Doppler resolution, CH_2OH reveals a surprisingly intense spectrum, with typical S/N of 20:1. We have made A-type rotational assignments in the $K_a=0\leftarrow 0$ and $1\leftarrow 1$ manifolds, providing first precision gas phase molecular constants for this oxyradical species, with fitted values in reasonable agreement with predictions from previous work.¹¹ A pure A-type band would be consistent with expectations for the CH_2 symmetric stretch, whose transition dipole moment lies essentially parallel to the A inertial axis. At high resolution the band is indeed pure A-type, as opposed to a mixed A/B type band inferred from modeling rotational contours at lower resolution. Interestingly, we see evidence for significant coupling between CH_2 symmetric stretching and the inertial framework by virtue of significant changes in the A rotational constant upon vibrational excitation. This coupling signals the presence of large amplitude motion on the ground state potential surface, which we are pursuing in parallel theoretically.

Of particular dynamical interest, there is strong evidence for extreme amplitude motion due to coupling between the CH_2 flip and COH torsional coordinate, which makes the spectra potentially much more informative regarding large amplitude dynamics. From a freshman chemistry perspective, this coupling can be rationalized as arising from valence electron repulsion of radical and lone pair orbitals, amplified by a “soft” barrier between sp^2 and sp^3 hybridization of the C radical center. We have performed 2D potential surface calculations at the CCSD(T) level as a function of torsion and flip coordinates, systematically progressing from AVDZ to AVTZ to AVQZ basis sets, and thereby permitting extrapolation to the “complete basis limit” (CBS).¹² This potential surface builds on and substantially extends the early *ab initio* work of Hudgens et al.,¹³ who developed a potential calculated at the MP2/6-311G(2df,2p) level. The data elucidate the presence of an exceptionally low barrier “valley” ($\approx 100 \text{ cm}^{-1}$) between



$(\theta_{\text{CH}_2}, \theta_{\text{COH}}) \approx (76.4^\circ, 98.4^\circ)$ and $\approx (103.6^\circ, 81.6^\circ)$ as well as a higher barrier ($\approx 1600 \text{ cm}^{-1}$) “ridge” for large amplitude torsional motion between $\phi_{\text{COH}} \approx 90^\circ - 270^\circ$. This higher barrier ridge is comparable to the barrier height for α -CH tunneling in vinyl radical, for which the splittings are resolved at our resolution.^{14,15} Thus, it is likely that tunneling is sufficiently rapid in CH_2OH to be evident in the spectrum and should help further elucidate torsional barrier dynamics. Analysis of the spectra will require 2D quantum treatment of both large amplitude coordinates, which should provide unprecedented insight into radical isomerization dynamics in such a benchmark oxyhydrocarbon radical species.



III. Future Direction: Apparatus Modification

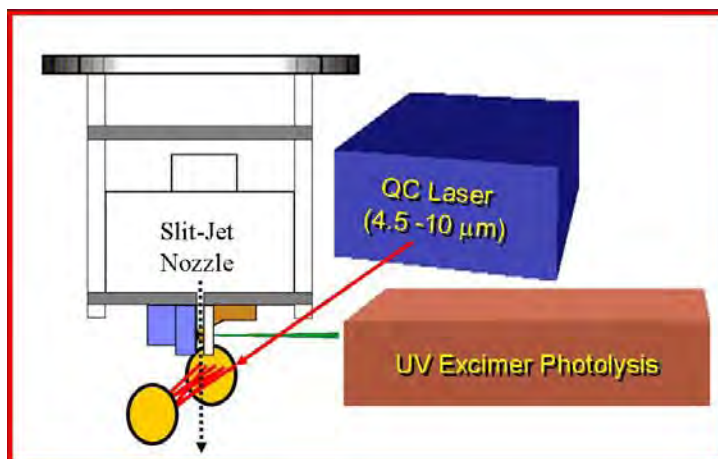
Interest in extending these studies in several new directions is requiring modifications to the current apparatus. The first incorporates UV laser photolysis of radical precursors in the throat of the slit supersonic expansion.^{16,17} This permits clean photolytic generation of radicals in the absence of the plasma and avoids precursor influence on discharge stability, which becomes challenging for species with larger fractional hydrocarbon content (e.g., cyclopentyl halides) as well as CC bond unsaturation (e.g. vinyl or phenyl halides). The output of a compact UV excimer laser is focused with cylindrical optics at the slit orifice to generate desired radicals, either by direct photolysis or secondary chemistry, which then supersonically expands into the IR laser detection region. For strong UV absorbers such as alkyl halides, HNO_3 , CCl_4 , H_2S , etc, a 10 mJ UV excitation pulse at 193 nm yields initial radical densities in the slit of $\approx 10^{15} - 10^{16}$ radicals/ cm^3 for 1-10% precursor concentrations at 400 Torr stagnation pressures.¹⁸ This translates into a $\approx 20 \mu\text{s}$ pulse at the IR probe region due to velocity spread in the jet, which dilutes radical density and duty cycle with respect to the 500 μs pulse. The initial photolysis densities are sufficiently high, however, that this translates into “equivalent” densities of $10^{13} - 10^{14}$ radicals/ cm^3 averaged over the 500 μs discharge pulse length. Indeed, photolysis via UV excitation at the slit orifice offers a critical alternative method for achieving sufficiently high densities for spectroscopic and kinetic access to many hydrocarbon radical systems of interest.¹⁹

A second modification involves extending the range of tunable IR wavelengths, which with difference frequency generation methods is limited to $\approx 2 - 4 \mu\text{m}$. Though ideal for the OH, CH, NH stretching regions, these sources miss the invaluable “fingerprint” region from 4.5-11 μm , of key importance for access to intense O-O, C-C, C-O stretches ($\approx 9 - 11 \mu\text{m}$) in oxyhydrocarbon intermediates, and the equally intense CH bending (6.7 μm) and wagging (10.5 μm) vibrations. This region has been traditionally accessed by Pb-salt diode lasers, which have been less attractive to implement due to low single mode powers ($< 1 \mu\text{W}$) and discontinuous tuning. However, the past several years have witnessed enormous technological advances in the field of quantum cascade lasers (QCL), which now can provide access throughout the “fingerprint” region of the spectrum with $> 10 \text{ mW}$ cw

powers, excellent beam quality, continuous mode hop free tuning $> 100 \text{ cm}^{-1}$, shot noise limited stability and narrow linewidths ($< 10 \text{ MHz}$).^{20,21} To avoid optical saturation, we typically need to work at $< 100 \mu\text{W}$ over a 1 mm^2 beam area.

However, this already translates into a additional 5-10-fold increase in shot noise limited absorbance sensitivities over the 1-2 μW from our difference frequency system, as well as provides

access to a crucial wavelength window of the mid IR spectrum for combustion intermediates. We have initiated a collaboration with the primary company commercializing this technology (Daylight Solutions) to test their QCL prototypes for frequency tuning and stability, which should permit us to have early access to these novel IR laser sources.



References

- 1 A. V. Friderichsen, J. G. Radziszewski, M. R. Nimlos, P. R. Winter, D. C. Dayton, D. E. David, and G. B. Ellison, *J. Am. Chem. Soc.* **123**, 1977 (2001).
- 2 R. J. McMahon, M. C. McCarthy, C. A. Gottlieb, J. B. Dudek, J. F. Stanton, and P. Thaddeus, *Astrophys. J.* **590**, L61 (2003).
- 3 J. G. Radziszewski, M. R. Nimlos, P. R. Winter, and G. B. Ellison, *J. Am. Chem. Soc.* **118**, 7400 (1996).
- 4 J. Y. Niu and J. Y. Hu, *Marine And Petroleum Geology* **16**, 85 (1999).
- 5 O. P. Strausz, T. W. Mojelsky, J. D. Payzant, G. A. Olah, and G. K. S. Prakash, *Energy & Fuels* **13**, 558 (1999).
- 6 G. L. Agafonov, I. Naydenova, P. A. Vlasov, and J. Warnatz, *Proc. Combust. Inst.* **31**, 575 (2007).
- 7 J. A. Miller and C. F. Melius, *Combust. Flame* **91**, 21 (1992).
- 8 N. M. Marinov, W. J. Pitz, C. K. Westbrook, M. J. Castaldi, and S. M. Senkan, *Combust. Sci. Technol.* **116**, 211 (1996).
- 9 H. Wang and M. Frenklach, *J. Phys. Chem.* **98**, 11465 (1994).
- 10 J. Wei, B. Karpichev, and H. Reisler, *J. Chem. Phys.* **125**, 034303 (2006).
- 11 L. Feng, J. Wei, and H. Reisler, *J. Phys. Chem. A* **108**, 7903 (2004).
- 12 K. A. Peterson, R. A. Kendall, and T. H. Dunning, *J. Chem. Phys.* **99**, 1930 (1993).
- 13 R. D. Johnson and J. W. Hudgens, *J. Phys. Chem.* **100**, 19874 (1996).
- 14 K. Tanaka, M. Toshimitsu, K. Harada, and T. Tanaka, *J. Chem. Phys.* **120**, 3604 (2004).
- 15 F. Dong, M. Roberts, and D. J. Nesbitt, *J. Chem. Phys.* **128**, 044305 (2008).
- 16 D. T. Anderson, R. L. Schwartz, M. W. Todd, and M. I. Lester, *J. Chem. Phys.* **109**, 3461 (1998).
- 17 R. A. Loomis, R. L. Schwartz, and M. I. Lester, *J. Chem. Phys.* **104**, 6984 (1996).
- 18 H. Okabe, *Photochemistry of Small Molecules*. (John Wiley and Sons, New York, 1978).
- 19 S. H. Wu, P. Dupre, and T. A. Miller, *Phys. Chem. Chem. Phys.* **8**, 1682 (2006).
- 20 M. J. Weida, D. Arnone, and T. Day, *Laser Focus World* **42**, 109 (2006).
- 21 J. Faist, F. Capasso, C. Sirtori, D. L. Sivco, J. N. Baillargeon, A. L. Hutchinson, S. N. G. Chu, and A. Y. Cho, *App. Phys. Lett.* **68**, 3680 (1996).

Radical Photochemistry and Photophysics

Daniel M. Neumark
Chemical Sciences Division
Lawrence Berkeley National Laboratory
Berkeley, CA 94720

Our research program is focused on fundamental aspects of radical photochemistry and photophysics, with particular emphasis on radicals that play an important role in the combustion of hydrocarbons. Radicals are generated from neutral or anionic precursors and photodissociated in the ultraviolet. We then determine which fragmentation channels occur and measure the photofragment translational energy and angular distributions for each channel. These measurements address the following central issues. First, they yield the primary photochemistry for a particular radical as a function of excitation energy. While many photodissociation experiments provide extremely sensitive probes of particular products (i.e. Rydberg tagging to detect H atoms), our experiments incorporate more universal detection schemes that are sensitive to all or most photofragmentation channels. Secondly, measurements of the product translational energy distributions provide considerable insight into the dissociation mechanism following photoexcitation and how this mechanism might vary with excitation energy. For example, very different translational energy distributions are expected if dissociation occurs on an excited state surface as opposed to internal conversion (IC) to the ground state followed by statistical decay. The relative importance of these two limiting mechanisms is a sensitive probe of the conical intersections that govern the dynamics of electronically excited polyatomic molecules. Moreover, results for radicals that decay from the ground state can be directly compared to experiments in which the thermal decomposition rates and products of radicals are determined, since in both cases internal energy tends to be randomized prior to dissociation. Finally, photodissociation experiments can provide direct measures of bond dissociation energies in free radicals, information that is critical in developing kinetic mechanisms for complex combustion processes in which radicals serve as key intermediates.

Recent experimental efforts have focused on the ultraviolet photodissociation of free radicals and the three-body decay dynamics following electronic excitation of clusters. The radicals investigated include propargyl, propynyl, and phenyl, all of which play a key role in combustion chemistry. Three-body decay experiments were carried out on I_2^- (Ar).

The radical photodissociation experiments were carried out on two instruments with complementary capabilities: a fast beam photofragment translational spectroscopy apparatus, and a molecular beam photodissociation instrument. In the fast beam experiment, radicals are generated by laser photodetachment of a fast (8–10 keV) beam of mass-selected negative ions. The radicals are then photodissociated by a second laser, and the photofragments are collected with high efficiency. We can measure the total dissociation signal as a function of excitation wavelength, thereby mapping out the photofragment yield spectrum of the radical. In addition, at fixed wavelengths, photofragment coincidence imaging yields the position and arrival times for all photofragments from each photodissociation event, from which the photofragment translational energy and angular distribution are obtained for each mass channel. In the molecular beam experiments, radicals are generated by either photolysis or pyrolysis of a stable

precursor and then photodissociated at either 248 or 193 nm. Photofragments are detected and analyzed using a rotating mass spectrometer with electron impact ionization. The choice of experiment for a particular radical depends on whether it can be generated more easily by photodetachment or by photolysis/pyrolysis. Also, compared to the fast beam experiment, the molecular beam instrument is more suitable for radicals that dissociate via loss of H atoms.

The propargyl radical is the most stable isomer on the C_3H_3 potential energy surface and is a key intermediate in combustion and interstellar chemistry. The bimolecular reaction of two propargyl radicals produces an aromatic ring which may serve as a precursor to formation of polyaromatic hydrocarbons and soot. We investigated the photodissociation of propargyl radical, C_3H_3 , and its perdeuterated isotopolog using molecular beam photofragment translational spectroscopy. Propargyl radicals were produced by 193 nm photolysis of allene entrained in a molecular beam expansion, and then photodissociated at 248 nm. Photofragment time-of-flight spectra were measured at a series of laboratory angles using electron impact ionization coupled to a mass spectrometer. Data for ion masses corresponding to $C_3H_2^+$, C_3H^+ , C_3^+ , and the analogous deuterated species show that both H and H_2 loss occur; our results represent the first observation of H_2 loss from the primary photodissociation of propargyl. The translational energy distributions for H and H_2 loss are characterized by $\langle E_T \rangle = 5.7$ and 15.9 kcal/mol, respectively, and are consistent with dissociation on the ground state following internal conversion, with no exit barrier for H loss but a tight transition state for H_2 loss. Our translational energy distribution for H atom loss is similar to that in previous work on propargyl in which the H atom, rather than the heavy fragment, was detected. The branching ratio for H loss/ H_2 loss was determined to be $97.6/2.4 \pm 1.2$, in good agreement with RRKM results.

This study was complemented by an investigation of the photodissociation of perdeuterated propargyl (D_2CCCD) and propynyl (D_3CCC) radicals on the fast beam instrument. These radicals were selectively produced from their respective anions by photodetachment at 540 nm and 450 nm, below and above the electron affinity of propynyl, making use of the overall anion and neutral energetics shown in Fig. 1. The radicals were then photodissociated by 248 nm or 193 nm light. The recoiling photofragments were detected in coincidence with a time- and position-sensitive detector. Three channels were observed: D_2 loss, $CD + C_2D_2$, and $CD_3 + C_2$. Observation of the D loss channel was incompatible with this experiment and was not attempted. Our translational energy distributions for D_2 loss peaked at nonzero translational energy, consistent with ground state dissociation over small (<1 eV) exit barriers with respect to separated products. Translational energy distributions for the two heavy channels peaked near zero kinetic energy, indicating dissociation on the ground state in the absence of exit barriers. Considerably more CD_3

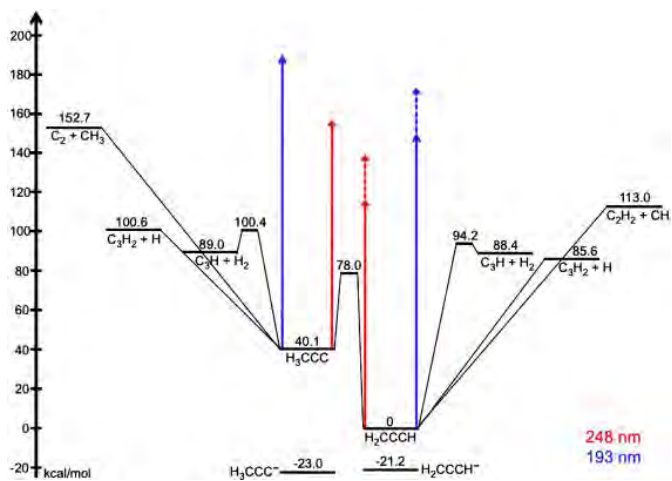


Figure 1. Anion and neutral energetics for propargyl and propynyl radicals.

+ C₂ production was seen from propynyl than from propargyl. These experiments represent the first study of propynyl dissociation. This radical is very difficult to generate from photolysis or pyrolysis of a neutral precursor, because it readily isomerizes to the lower energy propargyl isomer, but it can be generated by photodetachment of the D₃CCC⁻ anion.

We have recently investigated the photodissociation of phenyl in our molecular beam instrument. The radicals were produced by flash pyrolysis of nitrosobenzene and photodissociated at 248 nm. Two channels were observed, H + C₆H₄ and C₂H₂ + C₄H₃, but the latter channel was seen only under conditions that most likely produced internally hot radicals. The lowest energy channel is H + benzyne, occurring via C-H bond fission, and the H + C₆H₄ channel, which peaks at very low translational energy, presumably corresponds to this channel, which is the only channel seen in the thermal decomposition of phenyl. The higher energy C₂H₂ + C₄H₃ channel can be produced only if ring-opening occurs prior to dissociation. The translational energy distribution for this channel peaks well away from zero, consistent with a sizeable exit barrier with respect to separated products. Our results suggest that subsequent to 248 nm excitation, internal conversion to the ground state occurs prior to either dissociation channel.

Experiments on I₂⁻Ar were motivated by extensive previous work on I₂·Ar as a model system for competing energy transfer pathways in a simple van der Waals cluster. In particular, upon excitation of I₂ chromophore to the B(³Π_{0_u⁺) state, the complex undergoes vibrational predissociation (VP) to I₂(B) + Ar, a process detected via fluorescence from the excited I₂ fragment. However, the VP yield oscillates with the initial B state level prepared in the complex. One possible explanation for this phenomenon is a “dark” channel such as three-body decay to I + I + Ar. In order to probe whether this channel was present, we performed systematic dissociative photodetachment (DPD) studies of the I₂⁻ and I₂⁻·Ar anions in the region 4.24-4.78 eV.³⁰ The resulting neutral fragments were detected by time-and position-sensitive (TPS) coincident imaging. For the I₂·Ar complex, channels resulting from two-body dissociation leading to I₂ + Ar photoproducts were observed at all photon energies employed. We also reported the first direct observation of the previously-inferred three-body dissociation channel leading to I+I+Ar photoproducts. The relative intensities of each decay channel were investigated in relation to the electronic state being accessed. Translational energy distributions of the I₂·Ar complex provided further insight into the decay mechanism for each channel.}

In the near future, we will examine the photodissociation of a series of hydrocarbon radicals, including C₆H₅, C₃H₇, and C₃H₂, at 248, 193, and 157 nm in order to map out their primary photochemistry and dissociation dynamics, and to gain a better understanding of competing channels that involve loose and tight transition states through our ability to observe channels other than loss of an H atom. We will also investigate the photodissociation of alkyl-peroxy radicals, such as CH₃O₂ and C₂H₃O₂, that play a key role in combustion chemistry, and the CH₃OCO radical, an important intermediate in the thermal decomposition of methyl esters that serve as model compounds for the fatty esters that make up biodiesels. In radicals such as the C_nN series, which can readily be generated by anion photodetachment, we can vary the photodetachment wavelength to prepare radicals only in their ground electronic states or with a significant population in low-lying excited electronic states, and thereby map out the dissociation dynamics in two different electronic manifolds.

Publications:

A. E. Faulhaber, J. R. Gascooke, A. A. Hoops, and D. M. Neumark, "Photodissociation Dynamics of the HCNN Radical," *J. Chem. Phys.* 124, 204303 (2006).

J. H. Kim, D. S. Peterka, C. C. Wang, and D. M. Neumark. "Photoionization of Helium Nanodroplets Doped with Rare Gas Atoms," *J. Chem. Phys.* 124, 214301 (2006).

D. S. Peterka, J. Hyun Kim, C. C. Wang, and D. M. Neumark. "Photoionization and Photofragmentation of SF₆ in Helium Droplets," *J. Phys. Chem. B.* 110, 19945-19955 (2006).

D. E. Szpunar, K. E. Kautzman, A. E. Faulhaber, and D. M. Neumark, "Photofragment Coincidence Imaging of Small I(H₂O)_n Clusters Excited to the Charge-transfer-to-solvent State," *J. Chem. Phys.* 124, 054318 (2006).

D. M. Neumark, "Probing Chemical Dynamics with Negative Ions," *J. Chem. Phys.* 125, 132303 (2006).

N. E. Sveum, S. J. Goncher, and D. M. Neumark, "Determination of Absolute Photoionization Cross Sections of the Phenyl Radical," *Phys. Chem. Chem. Phys.* 8, 592 (2006).

D. S. Peterka, J. H. Kim, C. C. Wang, L. Poisson, and D. M. Neumark. "Photoionization Dynamics in Pure Helium Droplets," *J. Phys. Chem. A* 111, 7449 (2007).

D. Szpunar, A. E. Faulhaber, K. E. Kautzman, P. E. Crider, and D. M. Neumark, "D Atom Loss in the Photodissociation of the DNCN Radical: Implications for Prompt NO Formation," *J. Chem. Phys.* 126, 114311 (2007).

K. E. Kautzman, P. E. Crider, D. E. Szpunar, and D. M. Neumark, "Dissociative Photodetachment Studies of I₂⁻·Ar: Coincident Imaging of Two and Three-body Product Channels," *J. Phys. Chem. A.* 111, 12795 (2007).

C. C. Wang, O. Kornilov, O. Gessner, J. H. Kim, D. Peterka, and D. M. Neumark. "Photoelectron Imaging of Helium Droplets Doped with Xe and Kr Atoms," *J. Phys. Chem A.* 112, 9356 (2008).

S. J. Goncher, D. T. Moore, N. E. Sveum, and D. M. Neumark, "Photofragment Translational Spectroscopy of Propargyl Radicals at 248nm," *J. Chem Phys.* 128, 114303 (2008).

P. E. Crider, L. Castiglioni, K. K. Kautzman, and D. M. Neumark, "Photodissociation of the Propargyl and Propynyl (C₃D₃) Radicals at 248 nm and 193 nm," *J. Chem Phys.* 130, 044310 (2009).

Determination of Accurate Energetic Database for Combustion Chemistry by High-Resolution Photoionization and Photoelectron Methods

C. Y. Ng

Department of Chemistry, University of California, Davis, California 95616

E-mail Address: cyng@chem.ucdavis.edu

I. Program Scope:

The main goal of this research program is to obtain accurate thermochemical data, such as ionization energies (IEs), 0 K dissociative photoionization thresholds or appearance energies (AEs), 0 K bond dissociation energies (D_0 's), and 0 K heats of formation ($\Delta H_{f,0}^{\circ}$'s) for small and medium sizes molecular species and their ions of relevance to combustion chemistry. Accurate thermochemical data determined by high-resolution photoionization and photoelectron studies for selected polyatomic neutrals and their ions are also useful for benchmarking the next generation of *ab initio* quantum computational procedures.

II. Recent Progress:

1. Y. Hou *et al.*, "Vacuum ultraviolet pulsed field ionization-photoelectron and infrared-photoinduced Rydberg ionization study of 1,3-butadiene", *J. Chem. Phys.* **129**, 114305 (2008).

The vacuum ultraviolet (VUV) laser pulsed field ionization-photoelectron (PFI-PE) spectrum of *trans*-1, 3-butadiene (*trans*-CH₂=CHCH=CH₂) has been measured in the region of 0-1700 cm⁻¹ above its IE to probe the vibrational modes ν_i^+ (i = 1-18) of *trans*-CH₂=CHCH=CH₂⁺. The high-frequency vibrational modes ν_i^+ (i = 19, 22, and 23) of *trans*-CH₂=CHCH=CH₂⁺ have also been probed by the VUV-infrared-photo-induced Rydberg ionization (VUV-IR-PIRI) measurement. On the basis of the semi-empirical simulation of the origin VUV-PFI-PE band, the IE(*trans*-CH₂=CHCH=CH₂) is determined to be 73150.1±1.5 cm⁻¹ (9.06946±0.00019 eV). This value has been used to benchmark the state-of-the-art theoretical IE prediction based on the CCSD(T,Full)/CBS procedures, the calculation of which is reported in the present study. The vibrational bands observed in the VUV-PFI-PE and VUV-IR-PIRI spectra were assigned based on *ab initio* anharmonic vibrational frequencies and Franck-Condon factor calculations for the photoionization transitions. Combining the VUV-PFI-PE and VUV-IR-PIRI measurements, 17 fundamental vibrational frequencies of *trans*-CH₂=CHCH=CH₂⁺ have been determined, including $\nu_1^+ = 182\pm 3$, $\nu_2^+ = 300\pm 3$, $\nu_3^+ = 428\pm 3$, $\nu_4^+ = 514\pm 3$, $\nu_5^+ = 554\pm 5$, $\nu_6^+ = 901\pm 3$, $\nu_7^+ = 928\pm 5$, $\nu_8^+ = 994\pm 3$, $\nu_9^+ = 1008\pm 5$, $\nu_{10}^+ = 1094\pm 5$, $\nu_{13}^+ = 1258\pm 3$, $\nu_{14}^+ = 1293\pm 3$, $\nu_{16}^+ = 1479\pm 3$, $\nu_{18}^+ = 1620\pm 3$, $\nu_{19}^+ = 2985\pm 10$, $\nu_{22}^+ = 3030\pm 10$, and $\nu_{23}^+ = 3105\pm 10$ cm⁻¹.

2. J. Zhou *et al.*, "A vacuum ultraviolet laser photoionization and pulsed field ionization study of nascent S(³P_{2,1,0}; ¹D₂) formed in the 193.3 nm photodissociation of CS₂", *J. Chem. Phys.* **128**, 014305 (2008).

The photoionization efficiency (PIE) and PFI-PI spectra for sulfur atoms S(³P_{2,1,0}) and S(¹D₂) resulting from the 193.3 nm photodissociation of CS₂ have been measured using tunable VUV laser radiation in the frequency range of 82,750-83,570 cm⁻¹. The PIE spectrum of S(³P_{2,1,0}) near their ionization threshold exhibits steplike structures. On the basis of the velocity-mapped ion-imaging measurements, four strong autoionizing peaks observed in the PIE measurement in this frequency range have been identified to originate from VUV excitation of S(¹D₂). The PFI-PI measurement reveals over 120 previously unidentified new Rydberg lines. They have been assigned as Rydberg states [$3p^3$ (⁴S^o) nd ³D^o ($n = 17-64$)] converging to the ground ionic state S⁺(⁴S^o) formed by VUV excitations of S(³P_{2,1,0}). The converging limits of these Rydberg series have provided more accurate values, 82,985.43±0.05, 83,162.94±0.05, and 83,559.04±0.05 cm⁻¹ for the respective ionization energies of S(³P₀), S(³P₁), and S(³P₂) to form S⁺(⁴S^o). The relative intensities of the PFI-PI bands for S(³P₀), S(³P₁), and S(³P₂) have been used to determine the branching ratios for these fine structure states, S(³P₀) : S(³P₁) : S(³P₂) = 1.00 : 1.54 : 3.55, produced by photodissociation of CS₂ at 193.3 nm.

3. X. Yang *et al.*, "Single-photon vacuum ultraviolet excitation spectroscopy of autoionizing Rydberg states of atomic sulfur", *J. Chem. Phys.* **128**, 084303 (2008).

The PIE spectra of S atoms in the metastable $S(^1D)$ and $S(^1S)$ states in the wavelength range of 73,350-84,950 cm^{-1} have been recorded using tunable VUV laser radiation. The $S(^1D)$ and $S(^1S)$ atoms are produced by the 193 nm photodissociation of CS_2 . The PIE spectra of $S(^1D)$ and $S(^1S)$ observed shows 35 autoionizing resonances with little contribution from direct photoionization into the $S(^4S_{3/2}) + e^-$ ionization continuum. Velocity-mapped ion image of S^+ measured at individual autoionizing Rydberg resonances are used to identify the origins from $S(^1D)$ or $S(^1S)$. The analysis and assignment of these Rydberg peaks revealed 23 new Rydberg states, which have not been characterized in previous studies. The profiles of these well-resolved autoionizing resonances are fitted using the Fano line shape formula, yielding values for the line shape parameters, level energies, and line widths of the autoionizing Rydberg states. The autoionization lifetimes (τ) of the Rydberg states that were determined using the line widths are found to deviate from the scaling law of $\tau(n^*) \propto n^{*3}$, where n^* is the effective quantum number of the Rydberg state. This observation can be ascribed to perturbations by nearby Rydberg states, leading to shortening of autoionization lifetimes of the Rydberg levels.

4. Xi Xing *et al.*, “Rovibrationally selected and resolved pulsed field ionization photoelectron study of propyne: Ionization energy and spin-orbit interaction in the propyne cation”, *J. Chem. Phys.* **128**, 094311 (2008).

By using a high-resolution IR laser to prepare propyne (C_3H_4) in selected rotational levels of the excited ν_1 (acetylenic C-H stretching) vibration mode prior to VUV laser PFI-PE measurements, we have obtained rotationally resolved VUV-PFI-PE spectra for the $\text{C}_3\text{H}_4^+(\text{X}^2\text{E}_{3/2,1/2}; \nu_1^+=1)$ band. The analysis of these PFI-PE spectra leads to the determination of the spin-orbit constant of $A=-13.0\pm 0.2 \text{ cm}^{-1}$ for the $\text{C}_3\text{H}_4^+(\text{X}^2\text{E}_{3/2,1/2}; \nu_1^+=1)$ state. Using this A constant and the relative rotationally selected and resolved state-to-state photoionization cross sections thus measured, we have obtained an excellent simulation for the VUV-PFI-PE origin band of $\text{C}_3\text{H}_4^+(\text{X}^2\text{E}_{3/2,1/2})$, yielding a value of $83,619.0\pm 1.0 \text{ cm}^{-1}$ ($10.36744\pm 0.00025 \text{ eV}$) for the adiabatic ionization energy of C_3H_4 [$\text{IE}(\text{C}_3\text{H}_4)$]. The present two-color IR-VUV-PFI-PE study has also made possible the determination of the C-H stretching frequencies, $\nu_1^+ = 3,217.1\pm 0.2 \text{ cm}^{-1}$ for $\text{C}_3\text{H}_4^+(\text{X}^2\text{E}_{3/2,1/2})$. The spectral assignment and simulation were guided by high-level *ab initio* calculations on the $\text{IE}(\text{C}_3\text{H}_4)$, Franck-Condon factors for photoionization transitions, and rotational constants and vibrational frequencies for C_3H_4^+ .

5. J. Wang *et al.*, “Interstellar Enols Are Formed in Plasma Discharge of Alcohols”, *Astrophys. J.* **676**, 416-419 (2008).

Laboratory low-pressure cold plasma discharges of alcohols have been investigated by employing single-photon VUV photoionization mass spectrometry. Enols with two to four carbon atoms were detected in plasma discharges of alcohols. This observation, together with the detection of ethenol towards Sgr B2, suggests that larger enols, such as propenols and butenols, should be in the search list of potential molecular species to be identified in the interstellar space. The laboratory experiment presented here shows that VUV photoionization sampling of plasma discharges is a valuable method for guiding the search for new interstellar molecules and helping to understand the transformation mechanism of molecular species of astrochemical significance.

6. M. Oku *et al.*, “3s Rydberg and cationic states of pyrazine studied by photoelectron spectroscopy”, *J. Phys. Chem. A* **112**, 2293-2310 (2008).

We have studied $3s(n^{-1})$ and π^{-1} Rydberg states and $\text{D}_0(n^{-1})$ and $\text{D}_1(\pi^{-1})$ cationic states of pyrazine [1,4-diazabenzene] by picosecond (2+1) resonance-enhanced multiphoton ionization (REMPI), (2+1) REMPI photoelectron imaging, He(I) ultraviolet photoelectron spectroscopy, and VUV-PFI-PE. The new He(I) photoelectron spectrum of pyrazine in a supersonic jet revealed considerably finer vibrational structure than a previous photoelectron spectrum of pyrazine vapor. We performed Franck-Condon analysis on the observed photoelectron and REMPI spectra in combination with *ab initio* density functional theory and molecular orbital calculations to determine the equilibrium geometries in the D_0 and $3s(n^{-1})$ states. The equilibrium geometries were found to differ slightly between the D_0 and $3s$ states, indicating the influence of a Rydberg electron on the molecular structure. The locations of the D_1 - D_0 and $3s(\pi^{-1})$ - $3s(n^{-1})$ conical intersections were estimated. From the linewidth in the $\text{D}_1 \leftarrow \text{S}_0$ spectrum, we estimated the lifetime of D_1 to be 12 fs for pyrazine and 15 fs for fully-deuterated pyrazine. Similar lifetime was estimated for the $3s(\pi^{-1})$ state of pyrazine by REMPI spectroscopy. The vibrational feature of D_1 observed in the VUV-PFI-PE measurement differed

dramatically from that in the UPS spectrum, which suggests that the high- n Rydberg (ZEKE) states converging to the D_1 vibronic state are short-lived due to electronic autoionization to the D_0 continuum.

7. B. Jones *et al.*, “High-resolution Rydberg tagging time-of-flight measurements of atomic photofragments by single-photon vacuum ultraviolet Laser Excitation”, *Rev. Sci. Instrum.* **79**, 123106 (2008).

By coupling a comprehensive tunable VUV laser system to a velocity-mapped ion imaging apparatus, we show that high-resolution high- n Rydberg tagging TOF measurements of nascent atomic photofragments formed by laser photodissociation can be made using single-photon VUV laser photoexcitation. To illustrate this method, we present the results of the VUV laser high- n Rydberg tagging TOF measurements of $O(^3P_2)$ and $S(^3P_2)$ formed in the photodissociation of SO_2 and CS_2 at 193.3 and 202.3 nm, respectively. These results are compared to those obtained by employing the VUV laser photoionization time-sliced velocity-mapped ion imaging technique. The fact that the kinetic energy resolutions achieved in the VUV laser high- n Rydberg tagging TOF measurements of O and S atoms are found to be higher than those observed in the VUV laser photoionization time-sliced velocity-mapped ion-imaging studies shows that the single-photon VUV laser high- n Rydberg tagging TOF method is useful and complementary to state-of-the-art time-sliced velocity-mapped ion imaging measurements of heavier atomic photofragments, such as O and S atoms.

8. C. Y. Ng, “Spectroscopy and Dynamics of Neutrals and Ions by high-resolution infrared-vacuum ultraviolet photoionization and photoelectron methods”, in “*Frontiers of Molecular Spectroscopy*”, edited by Jaan Laane (Elsevier, 2009) Chap. 19, page 659-691.

By using a broadly tunable IR optical parametric oscillator laser and a comprehensive tunable VUV laser, together with the supersonic molecular beam and PFI detection techniques, we have demonstrate an array of novel two-color IR-VUV and VUV-IR photoion-photoelectron methods. The isomeric and conformation sensitivity of IR excitation and detection sensitivity of VUV photoionization detection, together with the long lifetimes of IR excited rovibrational states and VUV excited high- n Rydberg states, make the combination of IR and VUV excitations ideal for two-color spectroscopic and photoionization dynamics probes of polyatomic species and their ions. Selected experiments are presented to illustrate the principles, information contents, and unique capabilities of these IR-VUV and VUV-IR photoionization methods.

III. Ongoing experiments and Future Plans:

We are making excellent progress in PIE and PFI-PE measurements of small radicals using the VUV laser PFI apparatuses established in our laboratory. In collaboration with Xu Zhang (Jet propulsion Laboratory, NASA), Barney Eillison (Univ. of Colorado, Boulder), Ralf Kaiser (Univ. of Hawaii, Manoa) and Branko Ruscic (Argonne National Laboratory), progress is being made in the study of the IR spectroscopy and photoionization-photoelectron spectroscopy of hydrocarbon radicals of relevance to combustion chemistry using the single-photon VUV-PFI-PE and PIE, and two-color IR-VUV PI, and IR-VUV-PFI-PE methods, which have recently developed in our laboratory. We have also initiated high-resolution VUV threshold photoelectron imaging measurements on selected radicals, such as propargyl (C_3H_3), allyl (C_3H_5), and phenyl C_6H_5 radicals, which is expected to provide excited states information for the cations of these radicals.

IV. Publications of DOE sponsored research (2007-present)

1. S. Stimson, M. Evans, C.-W. Hsu, and C. Y. Ng, “Rotationally Resolved Vacuum Ultraviolet Pulsed Field Ionization-Photoelectron Bands for $HD^+(X^2\Sigma_g^+, v^+=0-20)$ ”, *J. Chem. Phys.* **126**, 164303 (2007).
2. X. Xing, B. Reed, K.-C. Lau, C. Y. Ng, X. Zhang, G. B. Ellison, “Vacuum ultraviolet laser pulsed field ionization-photoelectron study of allyl radical $CH_2CHCH_2^+$ ”, *J. Chem. Phys.* (communication), **126**, 171101 (2007).
3. J. Li, J. Yang, Y. Mo, K.-C. Lau, and C. Y. Ng, “A combined vacuum ultraviolet laser and synchrotron pulsed field ionization study of CH_2BrCl^+ ”, *J. Chem. Phys.* **126**, 184304 (2007). Selected for the May 28, 2007 issue of Virtual Journal of Nanoscale Science & Technology.
4. X. N. Tang, H. F. Xu, C. Houchins, C. Y. Ng, Y. Chiu, R. A. Dressler, and D. J. Levandier. “An experimental and quasi-classical trajectory study of the rovibrationally state-selected reactions: $HD^+(v=0-15, j=1) + He \rightarrow HeH^+ (HeD^+) + H$ ”, *J. Chem. Phys.* **126**, 234305 (2007).

5. X. Xing, B. Reed, K.-C. Lau, S.-J. Baek, M.-K. Bahng, and C. Y. Ng, "Assignment of rovibrational transitions of propyne in the region of 2934-2952 cm^{-1} measured by the two-color IR-VUV laser Photoion and Photoelectron methods", *J. Chem. Phys.* **127**, 044313 (2007).
6. C. Chang, C. Y. Ng, S. Stimson, M. Evans, and C.-W. Hsu, "Rotationally Resolved Pulsed Field Ionization-Photoelectron Bands of $\text{H}_2^+(X^2\Sigma_g^+, v^+=0-18)$ ", *Chinese J. Chem. Phys.* (invited article), **20**, 352 (2007).
7. X. N. Tang, C. Houchins, Kai-Chung Lau, C. Y. Ng, R. A. Dressler, Y.-H. Chiu, T.-Sh. Chu, and K.-L. Han, "A time-dependent wave packet quantum scattering study of the reaction $\text{HD}^+(v=0-3; j=1) + \text{He} \rightarrow \text{HeH}^+(\text{HeD}^+) + \text{D}(\text{H})$ ", *J. Chem. Phys.* **127**, 164318 (2007).
8. J. Zhou, B. Jones, X. Yang, W. M. Jackson, and C. Y. Ng, "A vacuum ultraviolet laser photoionization and pulsed field ionization study of nascent $\text{S}(^3P_{2,1,0}; ^1D_2)$ formed in the 193.3 nm photodissociation of CS_2 ", *J. Chem. Phys.* **128**, 014305 (2008). Selected for the February 2008 issue of Virtual Journal of Ultrafast Science.
9. X. Yang, J. Zhou, B. Jones, C. Y. Ng, and W. M. Jackson, "Single-photon vacuum ultraviolet excitation spectroscopy of autoionizing Rydberg states of atomic sulfur", *J. Chem. Phys.* **128**, 084303 (2008).
10. X. Xing, M.-K. Bahng, B. Reed, C. S. Lam, K.-C. Lau, and C. Y. Ng, "Rovibrationally selected and resolved pulsed field ionization photoelectron study of propyne: Ionization energy and spin-orbit interaction in the propyne cation", *J. Chem. Phys.* **128**, 094311 (2008).
11. X. Xing, B. Reed, M.-K. Bahng, S. J. Baek, P. Wang, and C. Y. Ng, "Infrared-vacuum ultraviolet pulsed field ionization-photoelectron study of CH_3I^+ using a high-resolution infrared laser", *J. Chem. Phys.* **128**, 104306 (2008).
12. J. Wang, Y. Li, T. Zhang, Z. Tian, B. Yang, K. Zhang, F. Qi, A. Zhu, Z. Cui, and C. Y. Ng, "Interstellar Enols Are Formed in Plasma Discharge of Alcohols", *Astrophys. J.* **676**, 416-419 (2008).
13. X. Xing, B. Reed, M.-K. Bahng, and C. Y. Ng, "Infrared-vacuum ultraviolet pulsed field ionization-photoelectron study of C_2H_4^+ using a high-resolution infrared laser", *J. Phys. Chem. A* **112**, 2572-2578 (2008).
14. M. Oku, Y. Hou, X. Xing, B. Reed, H. Xu, C. Y. Ng, K. Nishizawa, K. Ohshimo, and T. Suzuki, "3s Rydberg and cationic states of pyrazine studied by photoelectron spectroscopy", *J. Phys. Chem. A* **112**, 2293-2310 (2008).
15. X. Xing, P. Wang, H.-K. Woo, M.-K. Bahng, S.-J. Baek, and C. Y. Ng, "Rotationally resolved infrared-vacuum ultraviolet pulsed field ionization-photoelectron depletion method for infrared spectroscopic studies of neutral molecules", *Chem. Phys. Lett.* **455**, 321 (2008).
16. X. Xing, B. Reed, M.-K. Bahng, P. Wang, H.-K. Woo, S.-J. Baek, C. S. Lam, and C. Y. Ng, "High-resolution infrared-vacuum ultraviolet photoion and pulsed field ionization-photoelectron methods for spectroscopic studies of neutrals and cations", *Chinese J. Chem. Phys.* **21**, 193 (2008).
17. C. Chang, Q.-Z. Yin, and C. Y. Ng, "Testing of self-shielding model for early solar nebula with laboratory experiment", *Geochimica et Cosmochimica Acta* **72**, A148, Suppl. 1 (2008).
18. Xi Xing, Peng Wang, Beth Reed, S. J. Baek, and C. Y. Ng, "Infrared-vacuum ultraviolet pulsed field ionization-photoelectron study of CH_3Br^+ ", *J. Phys. Chem. A*, **112**, 9277 (2008).
19. Y. Hou, H.-K. Woo, P. Wang, X. Xing, C. Y. Ng, and K.-C. Lau, "Vacuum ultraviolet pulsed field ionization-photoelectron and infrared-photoinduced Rydberg ionization study of 1,3-butadiene", *J. Chem. Phys.* **129**, 114305 (2008).
20. B. Jones, J. Zhou, L. Yang, and C. Y. Ng, "High-resolution Rydberg tagging time-of-flight measurements of atomic photofragments by single-photon vacuum ultraviolet Laser Excitation", *Rev. Sci. Instrum.* **79**, 123106 (2008).
21. C. Y. Ng, "Spectroscopy and Dynamics of Neutrals and Ions by high-resolution infrared-vacuum ultraviolet photoionization and photoelectron methods", in "*Frontiers of Molecular Spectroscopy*", edited by Jaan Laane (Elsevier Science and Technology, 2009) Chap. 19, page 659-691.
22. B. Reed, C.-S. Lam, Y.-C. Chang, X. Xing, and C. Y. Ng, "A high-resolution photoionization study of ^{56}Fe using vacuum ultraviolet laser", *Astrophys. J.*, accepted.
23. Y.-C. Chang, C.-S. Lam, B. Reed, K.-C. Lau, H. T. Liou, and C. Y. Ng, "Rovibronically selected and resolved two-color laser photoionization and photoelectron study of the iron carbide cation", *J. Phys. Chem. A*, accepted.

Large Eddy Simulation of Turbulence-Chemistry Interactions in Reacting Multiphase Flows

Joseph C. Oefelein

Combustion Research Facility, Sandia National Laboratories
Livermore, CA 94551-9051 (oefelei@sandia.gov)

Program Scope

Application of the Large Eddy Simulation (LES) technique within the Diagnostics and Reacting Flows program at the CRF was initiated with two primary objectives. The first is to establish a set of high-fidelity computational benchmarks that identically match the geometry (i.e., experimental test section and burner) and operating conditions of selected experimental target flames. The second is to establish a scientific foundation for advanced model development. The goal is to provide a direct one-to-one correspondence between measured and modeled results at conditions unattainable using the Direct Numerical Simulation (DNS) technique by performing a series of detailed simulations that progressively incorporate the fully coupled dynamic behavior of reacting flows with detailed chemistry and realistic levels of turbulence. Our focal point is the series of flames that have been studied as part of the Experimental Reacting Flow Research program in collaboration with Rob Barlow and Jonathan Frank (see related abstracts). This represents a direct extension of joint activities being pursued as part of the International Workshop on Measurement and Computation of Turbulent Nonpremixed Flames organized by Barlow *et al.* (www.ca.sandia.gov/TNF).

Recent Progress

Over the past year our research has been focused in two areas. First, we continue to optimize our LES flow solver for use on DOE “capability-class” computers. Second, we continue to address issues related to model development using the DLR CH₄/H₂/N₂ jet flames as a baseline. Figure 1 shows the reference condition associated with the DLR-A flame along with representative results. To the left is a photograph of the flame in the experimental test section. At center is the corresponding solution from LES. To the right are representative comparisons between experimentally measured (symbols) and modeled (lines) results showing acceptable agreement with the 1D Raman/Rayleigh/CO-LIF line images acquired by Barlow *et al.*

Our LES flow solver (RAPTOR) is a massively parallel code designed specifically for application of LES to turbulent, chemically reacting, multiphase flows. It solves the fully coupled conservation equations of mass, momentum, total-energy, and species (gas or liquid) in complex geometries. It also accounts for detailed chemistry, thermodynamics, and transport processes at the molecular level and uses detailed chemical mechanisms. The code is sophisticated in its ability to handle complex geometries and a generalized subgrid-scale (SGS) model framework. It is capable of treating spray combustion processes using a Lagrangian-Eulerian formulation. The numerical formulation treats the compressible form of the conservation equations, but can be evaluated in the incompressible limit. The theoretical framework handles both multi-component and mixture-averaged systems. The baseline formulation employs a general treatment of the equation of state, thermodynamics, and transport properties that accommodates real gas or liquids with detailed chemistry. The temporal integration scheme employs an all Mach number formulation using the dual-time stepping technique with generalized preconditioning. The spatial scheme is designed using non-dissipative, discretely-conservative, staggered, finite-volume differencing. The discretization is formulated

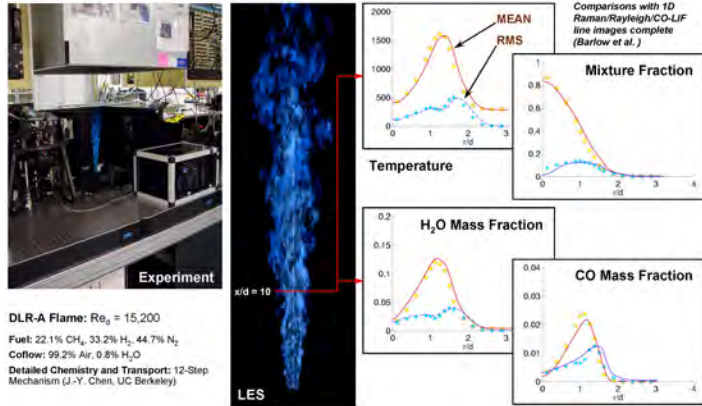


Figure 1: To the left is a photograph of the DLR-A flame in the experimental test section. At center is the corresponding solution from LES. To the right are representative comparisons between experimentally measured (symbols) and modeled (lines) results showing acceptable agreement.

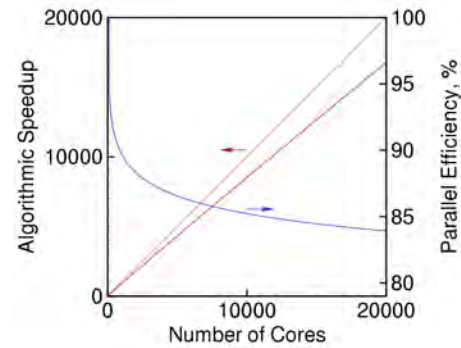


Figure 2: Strong (fine-grain) scaling attributes exhibited by RAPTOR on the ORNL NCCS CRAY-XT system (Jaguar) using DLR-A as a baseline.

in generalized curvilinear (i.e., body-fitted) coordinates and employs a general R-refinement adaptive mesh (AMR) capability. This allows us to account for the inherent effects of geometry on turbulence over the full range of relevant scales while significantly reducing the total number of grid cells required in the computational domain. The staggered grid formulation fulfills two key accuracy requirements. First, it is spatially non-dissipative, which eliminates numerical contamination of the SGS models due to artificial dissipation. Second, the stencils provide discrete conservation of mass, momentum, total energy and species, which is an imperative requirement for LES. This eliminates the artificial build up of energy at the high wavenumbers, which causes both accuracy problems and numerical instabilities in turbulent flow calculations.

The code framework is massively-parallel and has been optimized to provide excellent parallel scalability attributes using a distributed multiblock domain decomposition with generalized connectivity. Figure 2 shows an example of the fine-grain scaling attributes recently exhibited by RAPTOR on the NCCS CRAY-XT systems at Oak Ridge National Laboratory (see www.nccs.gov) using the DLR-A case as a baseline (Fig. 1). The total grid size was 10,285,056 computational cells. Results were obtained by holding the total grid size fixed and successively increasing the number of processors used to perform the calculation. Note that this particular case produces an extremely fine-grain test where the fraction of communicated grid cells per processor was approaching 40 percent of the total. Maintaining the level of performance indicated for such a fine-grain decomposition can be attributed to the explicit nature of the solver. More recently, we have initiated a series of weak scaling studies on up to 100,000 cores as part of the DOE Joule Code Metric exercise. Achieving this level of performance has facilitated implementation of joint investigations of the DLR flames with emphasis placed on the dynamics of scalar dissipation.

Results shown in Fig. 1 were obtained using a new class of reconstruction models for the combustion closure that combine the approximate deconvolution procedure with physical information from an assumed scalar spectrum. A surrogate to the exact scalar field is used to approximate the SGS variances, which are precisely the input required to generate a correlated set of fluctuations stochastically using a Cholesky decomposition. The combined methodology provides an approximation of SGS velocity and scalar fluctuations with the correct time history and spatial distribution. The modeled instantaneous field (i.e., $\phi_i = \tilde{\phi}_i + \phi_i''$, where $\tilde{\phi}_i$ represents the resolved-scale contribution of a scalar and ϕ_i'' the fluctuation) is used to evaluate the filtered chemical source terms directly. Here we use the 12-step mechanism for methane-air developed by J.-Y. Chen (U.C. Berkeley). While results to date have been promising, there are still several questions that need to be answered regarding the merits of such a model and the related resolution requirements. To aid in answering these questions and investigate the more fundamental issues related to scalar-mixing, we

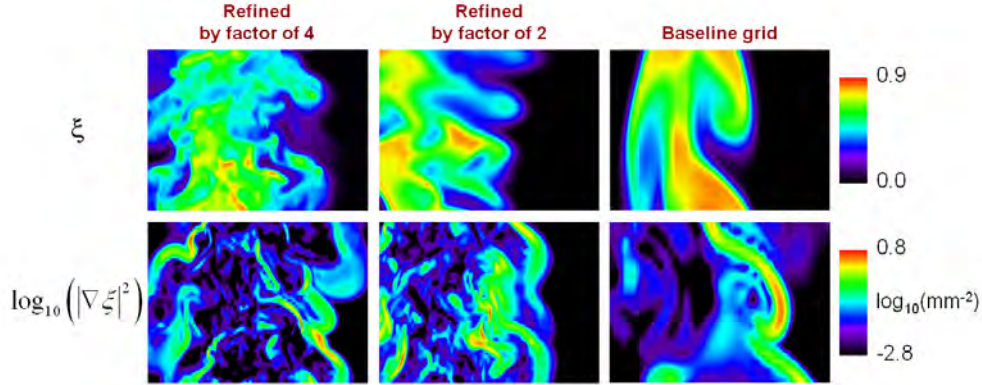


Figure 3: Instantaneous mixture fraction (top) and scalar dissipation (bottom) fields from respective LES calculations at $x/d = 10$. Results correspond to the companion figure shown in the abstract by Frank *et al.*.

have begun to develop a systematic approach for comparing laser-based imaging measurements of scalar dissipation to simulations using data from both the DLR flames and a companion set nonreacting jets.

Recent images of the thermal and scalar dissipation fields acquired by Frank *et al.* have revealed the convoluted inhomogenous structure of the fine-scale scalar mixing processes. Using these data, we are developing a systematic approach for comparing laser-based imaging measurements and LES with emphasis on 1) understanding the relationship between typical grid spacing and the measured turbulence length scales, and 2) the grid resolution required for LES to accurately represent scalar mixing processes. Details related to the approach are given in the abstract by Frank. A novel feature was to design the LES grids using the measured dissipation spectrum cutoff length scales. We constructed an initial grid such that the local spacing was on the same order of magnitude as the measured dissipation cutoff wavelengths. We then coarsened this grid by factors of 2 in each coordinate direction to produce a set of 3 successive configurations with 1,285,632 (the baseline), 10,285,056 and 82,280,448 total cells, respectively. Note that the baseline grid provides the level of resolution typically used in state of the art calculations. Details related to the grid spacing and measured turbulence scales along with a cross-section of the 3-D grid topology are given by Frank. Using the set of three grids we performed a series of LES calculations at conditions that identically matched the experiments. The calculations were carried out initially using the baseline grid and a time-step of approximately $1 \mu s$. Calculations performed with the two successively refined grids were integrated using time-steps of 0.5 and $0.25 \mu s$, respectively, in a manner consistent with the spatial refinement.

One of the challenges of using instantaneous measurements is that the LES simulations track the evolution of resolved-scale fields, which can lead to the development of very different turbulence structures. To demonstrate this point, we spatially filtered single-shot Rayleigh images such that the effective spatial resolution matched the resolved-scale of the LES calculations (see Frank's abstract). Several interesting observations arise as a consequence. First, for all of the grids the dissipation structures span multiple LES cells in the longitudinal direction and are of the same order of magnitude as the grid spacing in the transverse direction. This implies that LES must account for the overlap of dissipation structures in both the subgrid and resolved-scales. Additionally, the assumption of isotropy in the subgrid for treatment of scalar mixing must be examined. Second, transporting filtered quantities in time introduces artificial damping and dispersion errors that can produce a markedly different result compared to the spatially filtered Rayleigh images. To illustrate this we have plotted in Fig. 3 results from LES that are analogous to the filtered measurements (see companion figure in Frank's abstract). Comparing the two figures, it is clear that the effects of temporal damping and dispersion can be significant. On the coarsest mesh, there is no correlation at all between the measured and computed fields. As the resolution is increased, however, we begin to see an increasing

correspondence with the actual fields. The mixture fraction field begins to resemble the measured field, but the scalar dissipation is still quite different. The effects of artificial coalescence and dispersion errors is apparent with all of the grids. The impact of these errors must be investigated further.

Future Plans

Imaging of scalar dissipation and a companion set of LES calculations have provided insights into requirements for accurate LES calculations. In both non-reacting jets and jet flames, the measurements revealed a dissipation field that consisted of elongated and convoluted filaments of high dissipation. The morphology of these dissipation structures suggests that LES must account for the overlap of dissipation structures in both the subgrid and resolved-scales. The limited quantity of dissipation structures in each LES grid cell also suggests that widely used assumptions regarding the sampling of statistically significant quantities of turbulence structures within each grid cell must be carefully examined. These results represent a first step in the development of a systematic approach for using imaging diagnostics to evaluate needs regarding LES model development. We will continue to explore these issues as part of our future research.

DOE Sponsored Publications (2007–2009)

- R. C. Knaus, C. Pantano, and J. C. Oefelein. Statistical analysis and modeling of scalar dissipation and its relation to the filtered mixture fraction. *Physics of Fluids*, 2009. Submitted.
- J. C. Oefelein and R. Sankaran. Large eddy simulation of turbulence-chemistry interactions in reacting flows: Experiences on the ORNL NCCS Cray-XT platforms (Jaguar). *Proceedings of the 21st International Conference on Parallel Computational Fluid Dynamics*, May 18-22 2009. Moffett Field, California.
- L. Lu, P. M. Najt, T.-W. Kuo, V. Sankaran, and J. C. Oefelein. A fully integrated linear eddy model and chemistry agglomeration model with detailed chemical kinetics for studying the effect of stratification on HCCI combustion. *Proceedings of the 6th Joint Meeting of the US Sections of the Combustion Institute, Paper 13C2*, May 17-20 2009. Ann Arbor, Michigan.
- J. H. Frank, S. A. Kaiser, and J. C. Oefelein. Coupling imaging measurements and LES of dissipation structures in turbulent nonreacting jets and nonpremixed jet flames. *Proceedings of the 6th Joint Meeting of the US Sections of the Combustion Institute, Paper 32D1*, May 17-20 2009a. Ann Arbor, Michigan.
- J. H. Frank, S. A. Kaiser, and J. C. Oefelein. Coupling imaging diagnostics and large eddy simulation in turbulent nonreacting jets and nonpremixed jet flames. *Proceedings of the 4th European Combustion Meeting*, April 14-17 2009b. Vienna, Austria.
- V. Sankaran, T. G. Drozda, and J. C. Oefelein. A tabulated closure for turbulent nonpremixed combustion based on the linear eddy model. *Proceedings of the Combustion Institute*, 32:In Press, 2009.
- J. C. Oefelein. Toward high-fidelity simulations for clean and efficient combustion of alternative fuels. *IFP Workshop on Large Eddy Simulation for Internal Combustion Flows*, December 1-2 2008b. Ruell-Malmaison, France.
- T. G. Drozda, G.-H. Wang, V. Sankaran, J. R. Mayo, J. C. Oefelein, and R. S. Barlow. Scalar filtered mass density functions in non-premixed turbulent jet flames. *Combustion and Flame*, 155:54–69, 2008.
- J. H. Chen, C. S. Yoo, R. Sankaran, and J. C. Oefelein. High-fidelity simulations for clean and efficient combustion of alternative fuels. *Journal of Physics*, 125:1–6, 2008. DOI 10.1088/1742-6596/125/1/012028.
- T. G. Drozda and J. C. Oefelein. Large eddy simulation of direct injection processes for hydrogen and LTC engine applications. *SAE World Congress, Paper 2008-01-0939*, April 14-17 2008. Detroit, Michigan.
- V. Sankaran, T. G. Drozda, J. R. Mayo, J. C. Oefelein, and A. R. Kerstein. A tabulated closure for turbulent nonpremixed combustion. *Proceedings of the 2007 Fall Meeting of the Western States Section of the Combustion Institute*, October 16-17 2007. Livermore, California.
- R. R. Steeper, V. Sankaran, J. C. Oefelein, and R. P. Hessel. Simulation of the effect of spatial fuel distribution using a linear eddy model. *SAE Powertrain and Fluid Systems Conference, Paper 2007-01-4131*, April 14-17 2007. Detroit, Michigan.
- T. G. Drozda, G.-H. Wang, V. Sankaran, J. C. Oefelein, and R. S. Barlow. Scalar filtered mass density functions in non-premixed turbulent jet flames. *Proceedings of the 5th Joint Meeting of the US Sections of the Combustion Institute, Paper B02*, March 25-28 2007. San Diego, California.
- T. C. Williams, R. W. Schefer, J. C. Oefelein, and C. R. Shaddix. Idealized gas turbine combustor for performance research and validation of large eddy simulations. *Review of Scientific Instruments*, 78(3):035114–1–9, 2007.
- V. Sankaran and J. C. Oefelein. Advanced preconditioning strategies for chemically reacting flows. *45th AIAA Aerospace Sciences Meeting and Exhibit, Paper 2007-1432*, January 8-11 2007. Reno, Nevada.
- J. C. Oefelein, V. Sankaran, and T. G. Drozda. Large eddy simulation of swirling particle-laden flow in a model axisymmetric combustor. *Proceedings of the Combustion Institute*, 31:2291–2299, 2007.

KINETICS AND DYNAMICS OF COMBUSTION CHEMISTRY

David L. Osborn

Combustion Research Facility, Mail Stop 9055

Sandia National Laboratories

Livermore, CA 94551-0969

Telephone: (925) 294-4622

Email: UUDlosbor@sandia.gov

PROGRAM SCOPE

The goal of this program is to elucidate mechanisms of elementary combustion reactions through the use of multiplexed optical spectroscopy and mass spectrometry. We employ time-resolved Fourier transform spectroscopy (TR-FTS) to probe multiple reactants and products with broad spectral coverage ($> 1000 \text{ cm}^{-1}$), moderate spectral resolution (0.1 cm^{-1}), and a wide range of temporal resolution (ns – ms). The inherently multiplexed nature of TR-FTS makes it possible to simultaneously measure product branching ratios, internal energy distributions, energy transfer, and spectroscopy of radical intermediates. Together with total rate coefficients, this additional information provides further constraints upon and insights into the potential energy surfaces that control chemical reactivity. Because of its broadband nature, the TR-FTS technique provides a global view of chemical reactions and energy transfer processes that would be difficult to achieve with narrow-band, laser-based detection techniques.

Over the last three years, time-resolved photoionization mass spectrometry (PIMS) has become a much larger part of this program, and is used to sensitively and selectively probe unimolecular and bimolecular reactions. This work is in collaboration with Craig Taatjes and many scientists from other institutions. The Sandia-designed Multiplexed Chemical Kinetics Photoionization Mass Spectrometer utilizes tunable vacuum ultraviolet light from the Advanced Light Source synchrotron at Lawrence Berkeley National Laboratory for sensitive, isomer-specific ionization of reactant and product molecules in chemical reactions.

RECENT PROGRESS

Isomer-resolved mass spectrometry

The multiplexed chemical kinetics photoionization mass spectrometer operates both at Sandia National Laboratories (using a discharge lamp to create VUV radiation), and at the Chemical Dynamics Beamline of the Advanced Light Source (ALS) synchrotron of LBNL. The chemical reactor is based on the Gutman design,¹ which allows the study of photodissociation and bimolecular reactions at pressures of 1 – 10 Torr and temperatures of 300 – 1000 K.

While the study of chemical kinetics using PIMS is well-established, this apparatus has two unique features that make it especially powerful for chemical kinetics. First, the widely tunable, intense VUV radiation from the ALS enables isomer-specific ionization of product species. As an example, we have recently studied the isomer-resolved products of the CH + acetylene, ethylene, propyne, and allene reactions, measuring the branching ratios for the different product isomers.

The second unusual feature of this experiment is the mass spectrometer. We employ a small magnetic sector instrument coupled to a time- and position-sensitive single-ion counting detector. This approach creates a mass spectrometer with 100% duty cycle (like a quadrupole instrument) and the multiplex advantage of measuring a broad range of masses simultaneously (as in time-of-flight spectrometry). This detector also measures the time dependence of each observed reactant and product molecule, which provides kinetic information on the reaction.

The $C_3H_5 + C_3H_5 \rightarrow C_6H_{10}$ reaction

The reactions of resonance-stabilized radicals are key players in molecular weight growth chemistry leading to polycyclic aromatic hydrocarbons and eventually soot formation. As part of an ongoing study of such systems, we have recently completed work on the self reaction of allyl radicals (H_2CCHCH_2). All previous measurements of the kinetics of this reaction have been made with optical absorption spectroscopy of the allyl radical, and hence rely on the accuracy of the allyl radical absorption cross section. Our measurements by PIMS are independent of this value. Our derived rate coefficient $(2.7 \pm 0.7) \times 10^{-11} \text{ cm}^3 \text{ molecule}^{-1} \text{ s}^{-1}$ is in agreement with those of Tulloch *et al.*² and Jenkin *et al.*,³ providing indirect support of the accepted absorption cross section of allyl radical at $\lambda = 223 \text{ nm}$.

We also analyzed the isomeric distribution of the C_6H_{10} product. The initial 1,5-hexadiene adduct, which intuitively should form upon reaction of two allyl radicals, is the only C_6H_{10} isomer observed at pressures of 1 – 6 Torr and temperatures from 300 – 600 K. Disproportionation to form $C_3H_4 + C_3H_6$ is a minor process, with an upper limit of 3%. Other acyclic and cyclic isomers are up to 20 kcal mol⁻¹ more stable than 1,5-hexadiene. Their absence implies that the barriers to these deeper wells on the potential energy surface are substantially higher than similar barriers in the $C_3H_3 + C_3H_3 \rightarrow C_6H_6$ reaction, in which isomerization is facile at these pressures and temperatures. With only two π bonds in acyclic C_6H_{10} versus four in acyclic C_6H_6 , there are fewer opportunities to facilitate isomerization via uncoupling and recoupling of π bonds.

The $C_3H_3 + C_6H_5 \rightarrow C_9H_8$ reaction

The most important reaction in the formation of the first aromatic ring in combustion appears to be the propargyl (C_3H_3) self reaction. Propargyl radicals are resonance stabilized, leading to slow reactivity with closed-shell species, and can therefore attain concentrations much higher than most free radicals. By analogy, it seems probable that the next steps in soot formation, beyond the first aromatic ring, might involve reactions of propargyl with resonance-stabilized aromatic radicals, such as phenyl (C_6H_5).

We have nearly completed a combined experimental and theoretical study on the isomer distributions of the C_9H_8 product from this reaction from 1 – 10 Torr and from 300 – 1000 K. At low temperature (300 K) the only C_9H_8 products formed are the expected initial adducts of the barrierless association of propargyl with phenyl, namely, phenyl allene and 3-phenyl propyne. As temperature increases to 600 K, a clear signature of an additional isomer is present, which is

most easily explained by including 1-phenyl propyne in the fits to the data. At the highest temperature investigated, 1000K, we observe strong evidence for isomerization forming indene, a resonance-stabilized compound consisting of a 6-member ring fused to a 5-member ring. This structural motif leads to polycyclic aromatic hydrocarbons that are non-planar.

To aid in interpretation of these results, we have investigated several isomerization pathways using high level electronic structure calculations. In collaboration with Ahren Jasper we are conducting multiple well master equation calculations to predict the branching ratios of different isomers in this system as a function of temperature and pressure.

Future Directions

Using TR-FTS, we will continue to investigate photodissociation reactions that show evidence for roaming dynamics. Following on the recent work of Suits and coworkers⁴ on acetone photodissociation, we plan to study production of C₂H₆ in this system.

A significant improvement to the multiplexed photoionization mass spectrometer is also planned in the coming year. Leveraging designs from the analytical chemistry community, we will implement an orthogonal acceleration time-of-flight mass spectrometer (OA-TOF) to replace the magnetic sector instrument currently in use. Although the OA-TOF approach does not have a 100% duty cycle, the duty cycle is as high as possible for a time-of-flight system. In return, the design simulations promise mass resolution in excess of 3000 using a simple linear (i.e., not reflectron) approach. This mass resolution will be sufficient to resolve O from CH₄ (both nominally mass 16) and such substitutions in larger hydrocarbons (e.g., acetone vs. butane), providing another method for increased selectivity in hydrocarbon oxidation experiments.

One interesting problem to explore using the multiplexed chemical kinetics mass spectrometer apparatus instrument is the reaction C₃H₃ + C₂H₂. Previous work by Knyazev and Slagle⁵ has shown that the initial product (C₅H₅) can react with excess acetylene to form C₇H₇. This process continues to form C₉H₈ and perhaps larger species. Measuring the isomeric forms of these products will provide information critical to the reaction mechanism for this molecular weight growth process. We have preliminary data on this system, and will soon attempt to start the reaction with acetylene at the C₅H₅ or C₇H₇ points with isomerically-pure radical samples for comparison with the C₃H₃ + C₂H₂ data.

References

- ¹ I. R. Slagle and D. Gutman, *J. Am. Chem. Soc.* **107**, 5342 (1985).
- ² Tulloch, J. M.; Macpherron, M. T.; Morgan, C. A.; Pilling, M. J. *J. Phys. Chem.* **1982**, *86*, 3812.
- ³ Jenkin, M. E.; Murrells, T. P.; Shalliker, S. J.; Hayman, G. D. *J. Chem. Soc. Faraday Trans.* **1993**, *89*, 433.
- ⁴ V. Goncharov, N. Herath, and A. G. Suits, *J. Phys. Chem. A* **112**, 9423 (2008).
- ⁵ V. D. Knyazev and I. R. Slagle, *J. Phys. Chem. A* **106**, 5613 (2002).

BES-sponsored publications, 2007 - present

- 1) "Cyclic versus linear isomers produced by reaction of the methylidyne radical (CH) with small unsaturated hydrocarbons" F. Goulay, A. J. Trevitt, G. Meloni, T. M. Selby, D. L. Osborn, C. A. Taatjes, L. Vereecken, and S. R. Leone, *Journal of the American Chemical Society* **131**, 993 (2009).
- 2) "Temperature-Dependent Kinetics of the Vinyl Radical (C₂H₃) Self-Reaction," H. Ismail, P. Abel, W. Green, A. Fahr, L. Jusinski, A. Knepp, J. Zádor, G. Meloni, T. M. Selby, D. L. Osborn, C. A. Taatjes, *Journal of Physical Chemistry A* **113**, 1278 (2009).
- 3) "Isomer-specific product detection of CN radical reactions with ethene and propene by tunable VUV photoionization mass spectrometry," A. J. Trevitt, F. Goulay, G. Meloni, D. L. Osborn, C. A. Taatjes, and S. R. Leone, *International Journal of Mass Spectrometry* **208**, 113 (2009).
- 4) "Enol Formation and Ring-Opening in OH-Initiated Oxidation of Cycloalkenes," G. Meloni, T. M. Selby, and D. L. Osborn, and C. A. Taatjes, *Journal of Physical Chemistry A* **112**, 13444 (2008).
- 5) "The multiplexed chemical kinetic photoionization mass spectrometer: a new approach to isomer-resolved chemical kinetics," D. L. Osborn, P. Zou, H. Johnsen, C. C. Hayden, C. A. Taatjes, V. D. Knyazev, S. W. North, D. S. Peterka, M. Ahmed, and S. R. Leone, *Review of Scientific Instruments* **79**, 104103 (2008).
- 6) "Synchrotron photoionization mass spectrometry measurements of kinetics and product formation in the allyl radical (H₂CCHCH₂) self-reaction," T. M. Selby, G. Meloni, F. Goulay, S. R. Leone, A. Fahr, C. A. Taatjes, and D. L. Osborn, *Journal of Physical Chemistry A* **112**, 9366 (2008).
- 7) "Absolute photoionization cross-section of the methyl radical," C. A. Taatjes, D. L. Osborn, T. M. Selby, G. Meloni, H. Fan, and S. T. Pratt, *Journal of Physical Chemistry A* **112**, 9336 (2008).
- 8) "Roaming is the dominant mechanism for molecular products in acetaldehyde photodissociation" B.R. Heazlewood, M.J.T. Jordan, S.H. Kable, T.M. Selby, D.L. Osborn, B. C. Shepler, B.J. Braams, and J.M. Bowman, *Proceedings of the National Academy of Sciences* **105**, 12719 (2008).
- 9) "Direct Observation of the Gas-Phase Criegee Intermediate (CH₂OO)" C. A. Taatjes, G. Meloni, T. M. Selby, A. J. Trevitt, D. L. Osborn, C. J. Percival, and D. E. Shallcross, *Journal of the American Chemical Society* **130**, 11883 (2008).
- 10) "Ultraviolet photodissociation of vinyl iodide: understanding the halogen dependence of photodissociation mechanisms in vinyl halides" P. Zou, K. E. Strecker, J. Ramirez-Serrano, L. E. Jusinski, C. A. Taatjes, D. L. Osborn, *Physical Chemistry Chemical Physics* **10**, 713 (2008).
- 11) "Imaging combustion chemistry via multiplexed synchrotron-photoionization mass spectrometry" C. A. Taatjes, N. Hansen, D. L. Osborn, K. Koehse-Hoinghaus, T. A. Cool, P. R. Westmoreland, *Physical Chemistry Chemical Physics* **10**, 20 (2008).
- 12) "Exploring multiple reaction paths to a single product channel" D. L. Osborn, *Advances in Chemical Physics* **138**, 213 (2008).
- 13) "Photoionization of 1-alkenylperoxy and Alkylperoxy radicals and a general rule for the stability of their cations" G. Meloni, T. M. Selby, F. Goulay, S. R. Leone, D. L. Osborn, and C. A. Taatjes, *Journal of the American Chemical Society* **129**, 14019 (2007).
- 14) "Direct detection of polyynes formation from the reaction of ethynyl radical (C₂H) with propyne (CH₃-C≡CH) and allene (CH₂=C=CH₂)" F. Goulay, D. L. Osborn, C. A. Taatjes, P. Zou, G. Meloni, and S. R. Leone, *Physical Chemistry Chemical Physics* **9**, 4291 (2007).

The Dynamics of Large-Amplitude Motion in Energized Molecules

David S. Perry, Principal Investigator
Department of Chemistry, The University of Akron
Akron OH 44325-3601
DPerry@UAkron.edu

I. Program Scope

Most theories of reaction rely, either explicitly or implicitly, on a separation of the large-amplitude degrees of freedom from the other nuclear motions. For example, transition state theory (including its unimolecular variant RRKM theory) identifies a reaction coordinate and assumes thermal equilibrium among the other degrees of freedom. The transition state is a dividing hypersurface between reactants and products located at some point along the reaction coordinate so as to minimize recrossing. At high energies, particularly just below the threshold for a new fragmentation channel, there may be “roaming” trajectories, which may favor particular product channels and which clearly involve more than one large-amplitude degree of freedom. An alternative to transition state theory is the adiabatic channel model in which the excitation in one of more of the orthogonal degrees of freedom is assumed to be conserved as the system moves along the reaction coordinate. At the other end of the spectrum from statistical theories, close-coupled quantum scattering calculations are limited by practical considerations to a few degrees of freedom. Thus in systems larger than 3 or 4 atoms, one must define the active degrees of freedom and separate them in some way from the other degrees of freedom.

In this research, we test the limits of the adiabatic separation of different nuclear degrees of freedom, in particular, the separation of the large amplitude nuclear degrees of freedom (LADF) from the small amplitude vibrations (SAV). We will call this *vibrational adiabaticity* to distinguish it from *electronic adiabaticity*, that is, from the Born-Oppenheimer approximation. Nonadiabatic coupling terms scale as $(m/M)^{1/4}$ where m is the reduced mass for the fast degree of freedom and M is that for the slow degree of freedom. In the Born-Oppenheimer approximation, $m \ll M$, but in the vibrational case, often $m \approx M$. Therefore, the vibrational adiabatic approximation is on much more tenuous ground. The limits of its usefulness and the consequences of its failure are examined in this project.

While scattering systems are of primary interest in reactive chemistry, the collision complexes are relatively short lived and can rarely be probed directly. For this reason, we choose bound molecules, including methanol, nitromethane and methylamine, as our laboratory for studying adiabatic separations and consequent nonadiabatic effects. Bound systems are by definition long-lived, which means that we are able to use high-resolution spectroscopy to probe the interactions with a high level of precision and detail. In addition to cavity ringdown experiments and calculations at the university of Akron, experimental work on this project involves a collaboration with Brooks Pate’s group at the University of Virginia (CD-FTMW-IR).

II. Recent Progress

A. Torsion-Vibration Dynamics and the Adiabatic Approximation

The work on methanol and nitromethane under this project, when taken together with work by other authors on these molecules (i, ii) and on hydrogen peroxide (iii), points to a number of conclusions that may have some generality [6]:

- The coupling of the torsion to the stretching vibrations of adjacent hydrogens is strong, typically 40 to 80 cm^{-1} per quantum of XH stretch. The peak-to-peak values reach 270, 500, 265, 460 cm^{-1} by $v_{\text{XH}}=6$ in the methanol OH, CH, nitromethane CH, and hydrogen peroxide OH manifolds respectively. It is noteworthy that the magnitude of the torsion-vibration coupling is generally similar even though the ground state torsional potentials are very different.

- The form of the leading torsion-vibration coupling term is determined by the symmetry of the rotor at the opposite end of the torsional bond from the excited stretching vibration. The couplings with the lowest Fourier term ($\cos\alpha$ for methanol CH and hydrogen peroxide OH) are almost a factor of two larger than the higher Fourier couplings ($\cos3\alpha$ for methanol OH and $\cos2\alpha$ for nitromethane CH).
- The adiabatic treatment of torsional motion as occurring in an effective potential determined by the high frequency vibrations is a useful tool for analyzing torsion-vibration spectra. The OH overtones in CH_3OH and HOOH are well treated in this way as well as are the methyl CH stretch fundamentals in CH_3OH and CH_3NO_2 . The adiabatic approximation incorporating geometric phase appears to offer a general means of predicting the occurrence of inverted torsional tunneling but does not account for the pattern of CH stretch-torsion levels in CH_3OH at high torsional excitation [1].
- In the high CH overtone region of CH_3OH and CH_3NO_2 ($v_{\text{CH}} \geq 4$), there is a transition from adiabatic to diabatic behavior [3]. In the adiabatic limit, the CH stretch vibrational amplitude moves from one methyl hydrogen to the next as the torsional angle changes. In the diabatic limit, the several quanta of CH stretch reside on one CH bond and stay there through the full range of torsional angles. The diabatic effective torsional potential curves cross in several places, whereas the adiabatic curves do not. The adiabatic-to-diabatic transition is a consequence of the transition from normal mode CH vibrations to local modes as the CH stretch excitation is increased.
- In CH_3OH , we found that neither the adiabatic nor the diabatic approximation is quantitatively accurate relative to fully coupled calculations, even within its respective domain of applicability [3]. The torsion-vibration coupling results in “nonadiabatic” IVR coupling matrix elements, which we investigated at the $v_{\text{CH}}=1$ level. The result is energy exchange between the torsion and the CH vibrations. The scaling properties of the IVR coupling, which derive from the nature of the 1-dimensional torsional motion, indicate a role for direct high-order coupling [1].

B. Two-Dimensional Large-Amplitude Motion

The two-dimensional torsion-inversion potential energy surfaces of methylamine, protonated methanol, and ethyl radical have been investigated with partially optimized *ab initio* calculations [5]. All three molecules belong to the G_{12} molecular symmetry group and each has six equivalent minima. CH_3NH_2 has a high barrier to inversion ($\sim 1960 \text{ cm}^{-1}$), whereas in CH_3OH_2^+ the barrier is lower ($\sim 880 \text{ cm}^{-1}$). In $\text{CH}_3\text{CH}_2\cdot$, there is no barrier to inversion. The torsional barriers in these systems are about 714, 404, and 144 cm^{-1} respectively. The computed torsion-inversion surfaces were fit to a function of the form (Fig. 1),

$$V(\alpha, \tau) = \sum_{n=0}^4 \sum_{m=0}^{12} V_{m,3n} \tau^m \cos(3n\alpha),$$

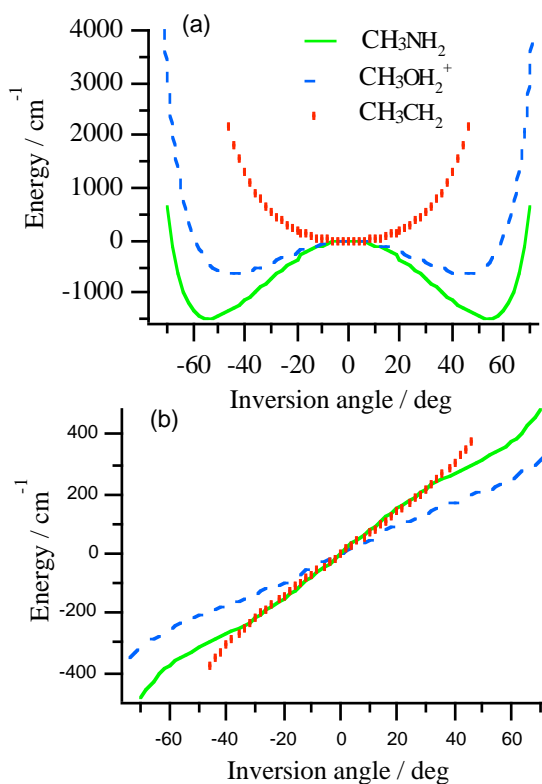


Fig. 1. *Ab initio* results at the CCSD(T)/6-311++G(3df,2p)//MP2/6-311++G(3df,2p) level on three CH_3XH_2 molecules. (a) The torsionally invariant part ($V_{m,0}$ terms) of the fitted potentials. (b) The $\cos 3\alpha$ part of the torsion-inversion coupling ($V_{m,3}$ terms).

where α , is the torsional angle, τ is the inversion angle, and $m+n = \text{even}$. Even though the three surfaces are quite different (Fig. 1(a)), we find that the torsion-inversion coupling is similar in strength (Fig. 1(b)). The dominant torsion-inversion coupling term in all three cases has the form, $V_{1,3}\tau\cos 3\alpha$, with $V_{1,3}$ in the range 280 to 450 cm^{-1} .

The synthesis these results with those of section A. above indicates that the coupling terms, whether torsion-vibration or torsion-inversion, have typical values that vary by less than a factor of two in a range of systems where the barriers to torsion or inversion vary by orders of magnitude.

C. Multistage Torsion-Vibration Coupling in the ν_3 CH Stretch Region of Methanol

The methanol ν_3 symmetric CH stretch is found to be coupled to most of the available combination vibrations (Fig. 2). A new experimental technique for rotationally selected infrared spectra is used to obtain assignments for 12 interacting bends in the ν_3 region [4]. The technique, developed at the University of Virginia, is coherence-detected Fourier transform microwave – infrared spectroscopy (CD-FTMW-IR).

Population transfer induced by a pulsed IR laser is detected by FTMW spectroscopy using a sequence two microwave pulses. The first pulse converts the thermal population difference to a coherence using an approximate “ $\pi/2$ ” pulse. Then, an IR laser pulse interacts with the polarized sample. Finally, second microwave pulse with a 180° phase shift is applied to perform a “ $-\pi/2$ ” excitation. The sequence of two microwave pulses produces a null signal in the absence of the IR pulse and hence a flat baseline upon which the state-detected infrared transitions are observed. Spectra have been recorded over the whole range 2750 – 3000 cm^{-1} for both CH_3OH and CH_3OD and for several rotational states of the E-species of each. The band origins and intensities for CH_3OH are shown in Fig. 2(b).

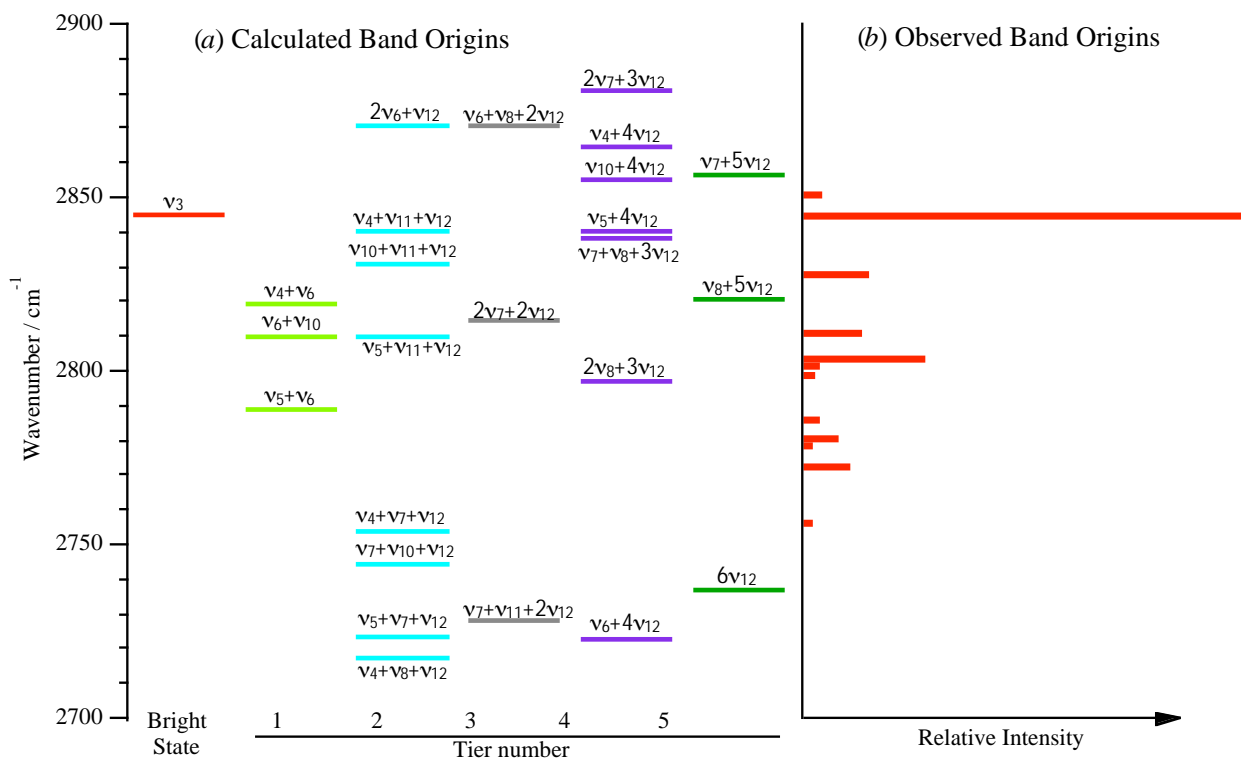


Fig. 2. The ν_3 symmetric CH stretch region of CH_3OH . (a) The calculated zeroth-order band positions based on the fundamental frequencies. The bands are sorted into tiers according to coupling order relative to ν_3 . (b) Vibrational band origins from the analysis of CD-FTMW-IR spectra.

The zeroth-order vibrational state energies are arranged into tiers in Fig. 2 according to the coupling order relative to the ν_3 bright state. Tier 1 represents a third-order coupling; tier 2 fourth order coupling etc. The pattern of the spectrum suggests the following coupling pathway:

- ν_3 CH stretch \Rightarrow HCH bend + COH band (tier 1)
- \Rightarrow HCH bend + methyl rock + torsion (tier 2)
- \Rightarrow combination states with additional quanta of torsion (tier 3 and higher)

We were able to test this mechanism with CH_3OD spectra, for which the first tier states are shifted from resonance. In CH_3OD , none of the coupled vibrations represented in Fig. 2(b) is observed, which confirms the sequential coupling through the first tier.

III. Future Work

The development of the continuous-wave cavity ringdown (CW-CRDS) and CD-FTMW-IR techniques will continue, targeting experiments on the CH manifolds in methylamine and methanol. Extension of the CD-FTMW-IR technique to the 48 GHz range will allow improved sensitivity and access to the methanol A species. The calculations on the CH_3XH_2 systems will be extended to include the coupling of the two large amplitude motions to CH stretch vibrations.

IV. Cited References

- (i) B. Fehrensen, D. Luckhaus, M. Quack, M. Willeke, and T. R. Rizzo, *J. Chem. Phys.* **119**, 5534 (2003).
- (ii) D. Cavagnat, L. Lespade, *J. Chem. Phys.* 106 (1997) 7946-7957.
- (iii) H. R. Dübal, F. F. Crim, *J. Chem. Phys.* 83 (1985) 3863-72; B. Kuhn, T. R. Rizzo, D. Luckhaus, M. Quack, M. A. Suhm, *J. Chem. Phys.* 111 (1999) 2565-2587.

V. Publications from this Project, 2006-2009

- [1] Trocia N Clasp and David S Perry, Torsion-vibration coupling in methanol: The adiabatic approximation and IVR scaling, *J. Chem. Phys.*, **125**, 104313 (2006). (9 pages) <http://link.aip.org/link/?JCPSA6/125/104313/>
- [2] Pavel Maksyutenko, Oleg V. Boyarkin, Thomas R. Rizzo and David S. Perry, Conformational dependence of intramolecular vibrational redistribution in methanol, *J. Chem. Phys.*, **126**, 044311 (2007). (6 pages) <http://link.aip.org/link/?JCPSA6/126/044311/1>
- [3] David S. Perry, Torsion-vibration coupling in methanol: Diabatic behavior in the CH overtone region, *J. Phys. Chem. A* 112, 215-223 (2008). <http://dx.doi.org/10.1021/jp077269q>.
- [4] Sylvestre Twagirayezu, David S. Perry, Justin L. Neill, Matt T. Muckle, Brooks H. Pate, Vibrational coupling pathways in the ν_3 CH stretch fundamental region of methanol as revealed by coherence-detected FTMW-IR spectroscopy, *Bull. Am. Phys. Soc.* 54(1), V37.00007 (2009). http://absimage.aps.org/image/MWS_MAR09-2008-001026.pdf
- [5] Ram S. Bhatta and David S. Perry, *Ab initio* torsion-wag surface for the ethyl radical, *Bull. Am. Phys. Soc.* 54(1), V37.00008 (2009). http://absimage.aps.org/image/MWS_MAR09-2008-002174.pdf
- [6] David S. Perry, The adiabatic approximation as a diagnostic tool for torsion-vibration dynamics, *J. Mol. Spectrosc.*, submitted for publication.

New Single- and Multi-Reference Coupled-Cluster Methods for High Accuracy Calculations of Ground and Excited States

Piotr Piecuch

Department of Chemistry, Michigan State University
East Lansing, MI 48824
piecuch@chemistry.msu.edu

I. Program Scope

This research program focuses on the development and applications of new generations of *ab initio* electronic structure methods and computer codes, exploiting coupled-cluster (CC) wave function ansatz, which can provide an accurate description of chemical reactions pathways, radicals, biradicals, potential energy surfaces (PESs), properties other than energy, and electronic excitations in molecules. The goal is to design and apply affordable computational methods that enable precise modeling of molecular processes and properties relevant to combustion, catalysis, and photochemistry. Among the most promising methods developed in this program are (i) the renormalized CC and equation-of-motion CC (EOMCC) approaches, and the linear scaling, local correlation extensions of the conventional and renormalized CC methods to larger systems involving hundreds of correlated electrons, (ii) the active-space CC and EOMCC methods, and (iii) the genuine multi-reference CC (MRCC) theories. The renormalized CC methods and their open-shell, local correlation, and excited-state extensions extend the standard single-reference theories to multi-reference situations created by radicals, biradicals, bond breaking, and two-electron excitations with an ease of a black-box calculation that can be performed by non-experts. The active-space CC and EOMCC approaches, and their open-shell generalizations via the electron attached (EA) and ionized (IP) theories as well as the genuine MRCC methods have the flexibility that enables accurate *ab initio* calculations for all kinds of closed- and open-shell electronic states with manageable computer costs. All methods pursued in this program can effectively utilize modern multi-node computer architectures and are well suited for pursuing novel coding strategies, such as the automated computer implementation. They address two important challenges of electronic structure theory, which are (i) the development of practical computational schemes that can provide a balanced and accurate description of closed- and open-shell systems, and the rapidly changing electron correlation effects along reaction coordinates, and (ii) the development of algorithms that can reduce prohibitive costs of traditional high-accuracy *ab initio* calculations by attacking the scaling laws that define the dependence of computer costs on the system size. The most promising methods developed in this program are shared with the community by incorporating them in the GAMESS package.

II. Recent Progress (2007-2009)

We have extended the left-eigenstate, completely renormalized (CR) CC method with singles, doubles, and non-iterative triples, termed CR-CC(2,3), and its excited-state CR-EOMCC(2,3) analog to open shell systems [6,14,in preparation]. We have integrated the CR-CC(2,3) code using the restricted open-shell Hartree-Fock (ROHF) reference in GAMESS, so that both the closed-shell and the open-shell CR-CC(2,3) methods are standard GAMESS options now [6]. Test calculations, including bond breaking in OH and F_2^+ , singlet-triplet gaps in the CH_2 and $H_2Si_2O_2$ biradicals and a few magnetic systems, and the activation energies of the $C_2H_4+H \rightarrow C_2H_5$ forward and reverse reactions indicate that the ROHF-based CR-CC(2,3) approach is more accurate and robust than other non-iterative triples CC methods proposed to date, without making the calculations substantially more expensive [6,14]. The open-shell CR-EOMCC(2,3) approach utilizing the ROHF reference provides great improvements in the EOMCCSD results for doublet and quartet states of radicals, particularly for the excited states dominated by two-electron processes where errors in the excitation energies obtained with EOMCCSD often exceed 1 eV, as shown by examining the excited states of CH, CNC, C_2N , N_3 , and NCO (in preparation). We have provided the alternative derivation of the biorthogonal method of moments of CC equations, on which CR-CC(2,3) is based, which explains why CR-CC(2,3) is more accurate than the earlier CR-CCSD(T) approach [14]. We have developed the CR-CC(2,4) and CR-EOMCC(2,4) codes

that correct the CR-CC(2,3) and CR-EOMCC(2,3) energies for quadruples effects [4,18] and completed work on the non-iterative CC methods using multi-reference perturbation theory wave functions [16].

We have developed the local correlation CCSD, CCSD(T), and CR-CC(2,3) approaches [21,25,26]. The resulting CIM-CCSD, CIM-CCSD(T), and CIM-CR-CC(2,3) methods use localized orthonormal orbitals and enable high accuracy calculations for systems with hundreds of correlated electrons and thousands of basis functions. Our local correlation CIM-CC algorithms are characterized by the linear scaling of the CPU time with the system size, trivial parallelism, and the non-iterative character of triples corrections to CCSD energies. By comparing the canonical and CIM-CC results for alkanes and water clusters, we have demonstrated that CIM-CCSD, CIM-CCSD(T), and CIM-CR-CC(2,3) recover the corresponding CC correlation energies to within 0.1 % or so, while offering huge savings in the computer effort. By examining bond breaking reactions in alkanes and low-energy structures of the $(\text{H}_2\text{O})_n$ clusters, we have shown that the CIM-CC methods accurately reproduce the relative energetics of the corresponding canonical CC calculations. Although the focus of our initial work [21,25,26] has been on benchmarking the CIM vs. canonical CCSD, CCSD(T), and CR-CC(2,3) approaches, we have explored water clusters as large as $(\text{H}_2\text{O})_{22}$ and normal alkanes as large as $\text{C}_{32}\text{H}_{66}$.

We have continued applying the CR-CC methods, including CR-CCSD(T), CR-CCSD(TQ), CR-CC(2,3), CR-CC(2,4), and CR-CC(2,3)+Q [1-3,8-15,18-20,24]. Benchmark calculations for the diverse set of reaction barrier heights included in the DBH24 database of Truhlar et al. have shown that CR-CC(2,3) provides high accuracy results for thermochemical kinetics [10] that can compete with those obtained with CCSD(T), while eliminating failures of CCSD(T) in the bond breaking region [1-3,6,8,9,13]. We have shown that CR-CC(2,3) offers an excellent description of bond breaking reactions of several closed- and open-shell species consisting of C, H, Si, and Cl, relevant to the gas-phase chemistry of the silicon carbide chemical vapor deposition [8,19]. In particular, we have shown that the PESs obtained with the ROHF-based CR-CC(2,3) have smaller non-parallelity errors than those obtained with the UHF-based CCSD(T), while reducing the reaction energy errors resulting from multi-reference MP2 calculations [19]. We have proposed an efficient computational strategy to estimate the CR-CC(2,3)/cc-pVTZ PESs, in which the most expensive steps are defined by MP2/cc-pVTZ and CR-CC(2,3)/cc-pVDZ calculations [19]. We have demonstrated that the CR-CC(2,3)+Q approach, in which one corrects the CR-CC(2,3) energy in a relatively inexpensive fashion for the effect of connected quadruples, describes the PESs of H_2O and H_2S , all the way up to the dissociation of H_2O into $2\text{H}+\text{O}$ and H_2S into $2\text{H}+\text{S}$ [including the $\text{Y}(2p^4\ ^1\text{D})+\text{H}_2(\text{X}^1\Sigma_g^+) \rightarrow \text{YH}(\text{X}^2\Pi)+\text{H}(1s^2\text{S})$, $\text{Y}=\text{O},\text{S}$, processes, of significance in combustion and atmospheric chemistry], in the accurate and computationally efficient manner, comparable to the best multi-reference configuration interaction (MRCI) data [1,9,13]. Our CR-CC(2,3)+Q results [1,9,13] suggest new ways of improving the existing global PESs of water and H_2S . The CR-CC(2,3)+Q method has been useful in making the new best estimates of the stationary point energetics for the cycloadditions of ozone to ethyne and ethane [24].

We have examined the low-lying states of the CNC, C_2N , N_3 , and NCO species [20,in preparation] and the singlet-triplet gaps in the BN and C_2 molecules [18]. We have shown that the black-box CR-CC(2,4) approach provides excellent values of the small singlet-triplet gaps in BN and C_2 that agree with the expert, reduced MRCC (RMRCC) calculations, termed RMRCCSD(T), and with experiment [18]. We have continued our work on the copper-dioxygen systems, of significance in catalysis and activation of oxygen by metalloenzymes [11]. By comparing the CR-CC(2,3), CASPT2, and DFT results, we have explained why the relative energies and singlet-triplet gaps of the various CuO_2 motifs are sensitive to the nature of the supporting ligands, and how and why these characteristics depend upon the geometric arrangement of ligands relative to the O_2 binding site [11]. We have also provided new insights into the performance of various DFT methods in such calculations [11].

We have developed the extrapolation procedure which predicts the smooth molecular PES corresponding to a larger basis set or to the complete basis set (CBS) limit from a series of inexpensive calculations using smaller basis sets by scaling the electron correlation energies [12,15]. By examining the isomerization pathways of bicyclobutane to butadiene and by comparing the extrapolated CR-CC(2,3) results with the explicit CR-CC(2,3) calculations using the cc-pVQZ basis set, we have shown

that the CR-CC(2,3)/cc-pVQZ PESs obtained by the extrapolation from the smaller basis set calculations are identical, to within fractions of a millihartree, to the true CR-CC(2,3)/cc-pVQZ PESs [12,15]. The same applies to the CR-CC and MRCI calculations for other PESs. We have shown that the above extrapolation procedure predicts the CBS limits of the calculated PESs from the results of smaller basis set calculations at a tiny fraction of the effort required by point-wise CBS extrapolations [12,15].

We have continued our work on extending the active-space CC and EOMCC theories to radicals and other valence systems by combining the active-space formalism with the EA- and IP-EOMCC. As illustrated by the calculations for the ground- and excited-state PESs of CH and OH, the resulting EA-EOMCCSDt and IP-EOMCCSDt approaches and their higher-order analogs in which one uses a small subset of active orbitals to select the 4p-3h/4h-3p excitations, in addition to the 3p-2h/3h-2p excitations already selected in the EA/IP EOMCCSDt approaches, provide an accurate description of the electronic spectra of radicals, including excited states displaying a manifestly multi-determinantal nature, with the low costs comparable to the standard (and failing) EOMCCSD, EA-EOMCCSD(2p-1h), and IP-EOMCCSD(2h-1p) methods [5]. We have demonstrated a superb performance, both in terms of accuracy and computational efficiency, of the active-space EA-EOMCCSD(3p-2h)=EA-EOMCCSDt and IP-EOMCCSD(3h-2p)=IP-EOMCCSDt approaches in calculations of the excitation energies in CNC, C₂N, N₃, and NCO, where the low-lying excited states have a significant multi-reference character, causing problems to EOMCCSD, EA-EOMCCSD(2p-1h), and IP-EOMCCSD(2h-1p) [20]. We have shown that the active-space EA/IP EOMCC schemes reproduce the results of their parent methods, while requiring much less computational effort [5,20]. We have also applied the method of moments of CC equations to the generalized MRCC formalism representing the transition between the Brillouin-Wigner-type and Rayleigh-Schrödinger-type theories based on the Jeziorski-Monkhorst ansatz and derived the novel formula for the non-iterative corrections to the corresponding MRCC energies that recover the exact energies in the general model space case [22]. We have extended the previously established relationship between the moments of the state-universal MRCC (SUMRCC) equations within the Jeziorski-Monkhorst-Paldus-Piecuch and Kucharski-Bartlett formulations of SUMRCC to the general model space case and established conditions under which both formulations are equivalent [22].

As in the past, we have shown that the CC methods developed in the quantum chemistry context enable accurate calculations for medium size nuclei, such as ¹⁶O, ⁵⁵Ni, ⁵⁶Ni, and ⁵⁷Ni [4,7,17,23].

III. Immediate Future Plans

- Migration of the standalone full and active-space EA-EOMCCSD(3p-2h) and IP-EOMCCSD(3h-2p) codes to GAMESS and extension of such methods to multiply attached/ionized schemes.
- Extension of the linear scaling, local correlation CIM-CC methodology to open-shell species.
- Development of the improved PES extrapolation procedure where one determines the correlation energy scaling factor using one of the low-order *ab initio* approaches instead of the target *ab initio* method used to determine the PES (e.g., MP4-SDQ in the PES calculations using CR-CC(2,3)).
- New studies of radical and biradical reactions and radical excitation spectra.

IV. Publications and submitted journal articles supported by this project (2007-2009)

1. P. Piecuch, M. Włoch, and A.J.C. Varandas, "Renormalized Coupled-Cluster Methods: Theoretical Foundations and Application to Potential Function of Water," in: *Progress in Theoretical Chemistry and Physics*, Vol. 16, S. Lahmar, J. Maruani, S. Wilson, and G. Delgado-Barrio, Eds. (Springer, 2007), pp.63-121.
2. A. Kinal and P. Piecuch, "Computational Investigation of the Conrotatory and Disrotatory Isomerization Channels of Bicyclo[1.1.0]butane to Buta-1,3-diene: A Completely Renormalized Coupled-Cluster Study," *J. Phys. Chem. A* **111**, 734-742 (2007).
3. P. Piecuch, I.S.O. Pimienta, P.-D. Fan, and K. Kowalski, "New Alternatives for Accurate Electronic Structure Calculations of Potential Energy Surfaces Involving Bond Breaking," in: *Electron Correlation Methodology*, ACS Symposium Series, Vol. 958, edited by A.K. Wilson and K.A. Peterson (ACS, 2007), pp. 37-73.
4. M. Horoi, J.R. Gour, M. Włoch, M.D. Lodriguito, B.A. Brown, and P. Piecuch, "Coupled-Cluster and Configuration-Interaction Calculations for Heavy Nuclei," *Phys. Rev. Lett.* **98**, 112501-1 - 112501-4 (2007).
5. Y. Ohtsuka, P. Piecuch, J.R. Gour, M. Ehara, and H. Nakatsuji, "Active-Space Symmetry-Adapted-Cluster Configuration-Interaction and Equation-of-Motion Coupled-Cluster Methods for High Accuracy Calculations of Potential Energy Surfaces of Radicals," *J. Chem. Phys.* **126**, 164111-1 - 164111-28 (2007).

6. M. Włoch, J.R. Gour, and P. Piecuch, "Extension of the Renormalized Coupled-Cluster Methods Exploiting Left Eigenstates of the Similarity-Transformed Hamiltonian to Open-Shell Systems: A Benchmark Study," *J. Phys. Chem. A* **111**, 11359-11382 (2007).
7. G. Hagen, T. Papenbrock, D.J. Dean, A. Schwenk, A. Nogga, M. Włoch, and P. Piecuch, "Coupled-Cluster Theory for Three-Body Hamiltonians," *Phys. Rev. C* **76**, 034302-1 - 034302-11 (2007).
8. Y. Ge, M.S. Gordon, and P. Piecuch, "Breaking Bonds with the Left Eigenstate Completely Renormalized Coupled-Cluster Method," *J. Chem. Phys.* **127**, 174106-1 - 174106-6 (2007).
9. P. Piecuch, M. Włoch, and A.J.C. Varandas, "Application of Renormalized Coupled-Cluster Methods to Potential Function of Water," *Theor. Chem. Acc.* **120**, 59-78 (2008).
10. J. Zheng, J.R. Gour, J.J. Lutz, M. Włoch, P. Piecuch, and D.G. Truhlar, "A Comparative Assessment of the Perturbative and Renormalized Coupled Cluster Theories with a Non-iterative Treatment of Triple Excitations for Thermochemical Kinetics, Including a Study of Basis Set and Core Correlation Effects," *J. Chem. Phys.* **128**, 044108-1 - 044108-7 (2008).
11. C.J. Cramer, J.R. Gour, A. Kinal, M. Włoch, P. Piecuch, A.R.M. Shahi, and L. Gagliardi, "Stereochemical Effects on Molecular Geometries and State-Energy Splittings of Ligated Monocopper Dioxide Complexes," *J. Phys. Chem. A* **112**, 3754-3767 (2008).
12. J.J. Lutz and P. Piecuch, "Extrapolating Potential Energy Surfaces by Scaling Electron Correlation: Isomerization of Bicyclobutane to Butadiene," *J. Chem. Phys.* **128**, 154116-1 - 154116-12 (2008).
13. Y.Z. Song, A. Kinal, P.J.S.B. Caridade, A.J.C. Varandas, and P. Piecuch, "A Comparison of Single-Reference Coupled-Cluster and Multi-Reference Configuration Interaction Methods for Representative Cuts of the H₂S(¹A₁) Potential Energy Surface," *J. Mol. Struct.: THEOCHEM* **859**, 22-29 (2008).
14. P. Piecuch, J.R. Gour, and M. Włoch, "Biorthogonal Method of Moments of Coupled-Cluster Equations: Alternative Derivation, Further Considerations, and Application to a Model Magnetic System," *Int. J. Quantum Chem.* **108**, 2128-2149 (2008).
15. J.J. Lutz and P. Piecuch, "Extrapolating Potential Energy Surfaces by Scaling Electron Correlation: Isomerization of Bicyclobutane to Butadiene," in: *Nuclei and Mesoscopic Physics, Workshop on Nuclei and Mesoscopic Physics, WNMP 2007*, AIP Conference Proceedings, Vol. 995, P. Danielewicz, P. Piecuch, and V. Zelevinsky, Eds. (APS, 2008), pp. 62-71.
16. M.D. Lodriguito and P. Piecuch, "Method of Moments of Coupled Cluster Equations Employing Multi-Reference Perturbation Theory Wavefunctions: General Formalism, Diagrammatic Formulation, Implementation, and Benchmark Studies," in: *Progress in Theoretical Chemistry and Physics*, Vol. 18, S. Wilson, P. Grout, J. Maruani, G. Delgado-Barrio, and P. Piecuch, Eds. (Springer, 2008), pp. 67-174.
17. J.R. Gour, M. Horoi, P. Piecuch, and B.A. Brown, "Coupled-Cluster and Configuration-Interaction Calculations for Odd-A Heavy Nuclei," *Phys. Rev. Lett.* **101**, 052501-1 - 052501-4 (2008).
18. X. Li, J.R. Gour, J. Paldus, and P. Piecuch, "On the Significance of Quadruply Excited Clusters in Coupled-Cluster Calculations for the Low-Lying States of BN and C₂," *Chem. Phys. Lett.* **461**, 321-326 (2008).
19. Y. Ge, M.S. Gordon, P. Piecuch, M. Włoch, and J.R. Gour, "Breaking Bonds of Open-Shell Species with the Restricted Open-Shell Size Extensive Left Eigenstate Completely Renormalized Coupled-Cluster Method," *J. Phys. Chem. A* **112**, 11873-11884 (2008).
20. M. Ehara, J.R. Gour, and P. Piecuch, "Low-Lying Valence Excited States of CNC, C₂N, N₃, and NCO Studied Using the Electron-Attached and Ionized Symmetry-Adapted-Cluster Configuration-Interaction and Equation-of-Motion Coupled-Cluster Methodologies," *Mol. Phys.*, in press; published on-line on 16 February, 2009.
21. W. Li, P. Piecuch, and J.R. Gour, "Local Correlation Calculations Using Standard and Renormalized Coupled-Cluster Methods," in: *Theory and Applications of Computational Chemistry - 2008*, AIP Conference Proceedings, Vol. 1102, D.-Q. Wei and X.-J. Wang, Eds. (APS, 2009), pp. 68-113.
22. J. Pittner and P. Piecuch, "Method of Moments for the Continuous Transition Between the Brillouin-Wigner-Type and Rayleigh-Schrödinger-Type Multireference Coupled Cluster Theories," *Mol. Phys.*, in press (2009).
23. R. Roth, J.R. Gour, and P. Piecuch, "Ab Initio Coupled-Cluster and Configuration Interaction Calculations for ¹⁶O Using V_{UCOM}," *Phys. Rev. C*, submitted, revised, re-submitted.
24. Y. Zhao, O. Tishchenko, J.R. Gour, W. Li, J.J. Lutz, P. Piecuch, and D.G. Truhlar, "Thermochemical Kinetics for Multireference Systems: Addition Reactions of Ozone," *J. Phys. Chem. A*, in press (2009).
25. W. Li, J.R. Gour, P. Piecuch, and S. Li, "Local Correlation Calculations Using Standard and Renormalized Coupled-Cluster Approaches," *J. Chem. Phys.*, submitted, in revision.
26. W. Li, P. Piecuch, and J.R. Gour, "Linear Scaling Local Correlation Extensions of the Standard and Renormalized Coupled-Cluster Methods," in: *Progress in Theoretical Chemistry and Physics*, Vol. 19, P. Piecuch, J. Maruani, G. Delgado-Barrio, and S. Wilson, Eds. (Springer, 2009), in press.

Chemical Kinetic Modeling of Combustion Chemistry

William J. Pitz and Charles K. Westbrook
Lawrence Livermore National Laboratory
Livermore, CA 94551
pitz1@llnl.gov

I. Program Scope

Our research project focuses on developing detailed chemical kinetic reaction mechanisms for the combustion of a wide variety of hydrocarbon and alternative fuels. These reaction mechanisms are designed to be applicable over extended ranges of operating conditions, including temperature, pressure, and fuel/oxidizer ratio, making them so-called “comprehensive” reaction mechanisms. They can then be systematically reduced in size and complexity as needed for specific types of modeling applications. We also use these detailed kinetic mechanisms to carry out modeling studies of practical combustion systems, and we contribute to basic information on thermochemistry and chemical kinetics.

II. Recent Progress

During the past year, we have developed detailed kinetic mechanisms and carried out kinetic modeling studies in several areas including large iso-alkanes, and components and mixtures relevant to gasoline fuels.

A. Large iso-alkanes

Although models have been developed for smaller branched alkanes such as iso-octane, additional efforts are required to properly capture the kinetics of larger branched alkanes. Recently, we have developed a chemical kinetic model that can be used to represent 2,2,4,4,6,8,8-heptamethylnonane (HMN), a large iso-alkane and a primary reference fuel for diesel. The same reaction rate rules used in our previous iso-octane mechanism were incorporated in the HMN mechanism. Both high and low temperature chemistry were included so that the chemical kinetic model would be applicable to advanced internal combustion engines using low temperature combustion strategies. The chemical kinetic model consists of 1114 species and 4468 reactions.

Currently, there are no experimental data available on neat HMN in the literature to validate the predictions of the chemical kinetic model. Instead, the results of the HMN chemical kinetic model were compared to other alkane model predictions and experimental measurements. In Fig. 1, the autoignition properties of HMN are compared to n-alkanes and to an iso-alkane, iso-octane. It is seen that the ignition delay times of HMN lie between large n-alkanes and iso-octane at low temperatures and are nearly the same as the other fuels at high temperatures. This low temperature ignition behavior can be explained in terms of the alkylperoxy (RO_2) isomerization reactions that control the overall, low-temperature reaction rate. The RO_2 isomerization reactions with the highest rate constants have six membered transition states and generally occur between CH_2 groups. This type of RO_2 isomerization reaction also leads to a subsequent addition of O_2 followed by another isomerization and finally chain branching with the production of two OH radicals. It is this chain branching that contributes greatly to low temperature reactivity. The CH_2 groups in HMN interact through six-membered ring RO_2 isomerization reactions that lead to a greater extent of chain-branching than seen for iso-octane which has only one CH_2 group.

Our previously developed chemical kinetic model for n-hexadecane and the newly developed one for HMN represent a significant advance in modeling of fuels for diesel engines because they are the primary reference fuels used to determine the cetane number used to rate ignition properties of diesel fuels. Also, these two components are the ones recommended by Farrell et al.¹ as components in a four component surrogate mixture to represent diesel fuel.

B. Components and mixtures relevant to gasoline fuels

During the last year, we extensively reviewed our detailed kinetic mechanisms for n-heptane, iso-octane and toluene which are important component models need to simulate gasoline fuels. We also

compared predictions of the mechanisms to experimental data in the literature. The main goal is the definition of a comprehensive and reliable database of mechanisms that can be merged together to simulate the behavior of complex fuel surrogates used to represent real fuels.

An important improvement to the mechanism involved the isomerization rate constants of the alkyl-peroxy radicals which were slightly increased in magnitude compared to previous values. We accomplished this increase by lowering the values of the activation energies by 400 kcal/mole. This relatively small change led to a stronger dependence of the system on pressure. This is because the now faster isomerization steps, whose rates are linear with pressure, are no longer as important as rate-controlling steps compared to bimolecular $R+O_2$ addition steps, whose rate are quadratic with pressure. The increased reactivity from the isomerization steps has been compensated for with an increase in the rate constants of direct elimination, $ROO \Rightarrow \text{alkene} + HO_2$, which slow the reactivity.

The toluene mechanism was recently updated by Sakai et al.² including new reaction pathways proposed by recent studies. Further revisions were carried out in the past months in collaboration with Milano's combustion chemistry group.

The n-heptane, iso-octane and toluene mechanisms were then merged into a detailed kinetic model for the simulation of surrogates including about 1550 species and 8000 reactions. The interaction among the oxidation pathways of the different components of the mixture are accounted for by the reactions of smaller radicals contained in the core mechanism and by a specific block of reactions involving the alkyl and peroxy radicals of the different fuels.

Figure 2 shows the comparison between model predictions and experiments over a wide range of conditions for n-heptane. The recent modifications improved the agreement over a wide range of pressure moving from 3 up to nearly 50 atm covering both the high and the low temperature reaction domain. In particular this new version of the model is a solid step in the direction of mimicking the strong dependence of ignition delay times on pressure evidenced by many experimental evidences for this class of fuel³⁻⁵.

The toluene model has been also validated over a wide range of operating conditions. Figure 2 shows a few comparisons of modeling results with shock tube and rapid compression machine data^{6,7}. It's interesting to notice how the slope of these sets changes depending on the experimental device used to measure them. As a matter of fact, rapid compression machine (RCM) experiments are affected by a conspicuous amount of heat losses that effectively delay the ignition timing at lower temperature. These experimental results, supported also by chemical kinetic simulations, evidence the role of heat transfer and prove it to be a fundamental aspect to include when simulating these experiments.

During the last year, we compared simulations of a number of different binary mixtures and a ternary mixture with experiments on their ignition delay times in a rapid compression machine⁸. The following mixtures were considered: 50/50% mole toluene/n-heptane, 35/65% mole toluene/isooctane, 18/82% mole 1-hexene/iso-octane, 30/70% mole 1-hexene/toluene and 47/35/18% iso-octane/toluene/1-hexene gasoline surrogate. We obtained good agreement between the predictions of the chemical kinetic model for the mixtures and the experiments for all cases considered. The ternary mixture results are shown in Fig. 3. This mixture can be thought of a surrogate for gasoline where iso-octane and toluene components represent iso-alkanes and aromatics present in gasoline. The 1-hexene component represents both n-alkane and alkene groups in gasoline, because it has a relatively long alkyl chain which can be effectively undergo the low temperature branching mechanism typical of n-alkanes.

The model does a good job in reproducing all the main aspects of ignition behavior (Fig. 3). The most reactive component (in this case 1-hexene) triggers the low temperature reactivity. This blend shows long delays between the cool flame and the high temperature ignition, a feature mostly due to the presence of toluene.

III. Summary

A detailed chemical kinetic mechanism for heptamethylnonane has been developed. Together with a previously developed n-hexadecane mechanism, they comprise the primary reference fuel mechanisms for diesel fuel.

We have made considerable progress in developing reliable mechanisms to represent components and mixtures relevant to gasoline. These components include n-heptane and iso-octane, primary reference fuels for gasoline. We have also included 1-hexene and toluene to represent alkene and aromatic chemical classes in gasoline.

IV. Future Work

We plan on developing chemical kinetic mechanisms of C3 and C4 alcohols and comparing simulations with molecular beam sampling measurements taken in low pressure flames, experimental work supported by Basic Energy Sciences.

This work was performed under the auspices of the U.S. Department of Energy by Lawrence Livermore National Laboratory under Contract DE-AC52-07NA27344.

V. References

1. J. T. Farrell *et al.*, SAE Paper 2007-01-0201, 2007.
2. Y. Sakai; A. Miyoshi; M. Koshi; W. J. Pitz, *Proc. Combustion Institute* **2009**, 32, 411-418.
3. R. Minetti; M. Carlier; M. Ribaucour; E. Therssen; L. Sochet, *Comb. Flame* **1995**, 102, (3), 298-309.
4. H. K. Ciezki; G. Adomeit, *Combustion and Flame* **1993**, 93, 421-433.
5. B. M. Gauthier; D. F. Davidson; R. K. Hanson, *Combustion and Flame* **2004**, 139, (4), 300-311.
6. G. Mittal; C.-J. Sung, *Combustion and Flame* **2007**, 150, (4), 355-368.
7. H.-P. S. Shen; J. Vanderover; M. A. Oehlschlaeger, *Proceed. Combust. Instit.* **2009**, 32, (1), 165-172.
8. G. Vanhove; G. Petit; R. Minetti, *Combustion and Flame* **2006**, 145, (3), 521-532.
9. K. Fieweger; R. Blumenthal; G. Adomeit, *Combustion and Flame* **1997**, 109, (4), 599-619.
10. U. Pfahl; K. Fieweger; G. Adomeit, *Proc. Combust. Inst.* **1996**, 26, 781-789.

VI. Publications and submitted journal articles supported by this project 2008-2009

1. Westbrook, C. K., Pitz, W. J., Westmoreland, P. R., Dryer, F. L., Chaos, M., Osswald, P., Kohse-Hoinghaus, K., Cool, T. A., Wang, J., Yang, B., Hansen, N. and Kasper, T., "A Detailed Chemical Kinetic Reaction Mechanism for Oxidation of Four Small Alkyl Esters in Laminar Premixed Flames," *Proceedings of the Combustion Institute*, 32 (2009) 221-228.
2. M. A. Oehlschlaeger, J. Steinberg, C. K. Westbrook and W. J. Pitz, "The Autoignition of iso-Cetane: Shock Tube Experiments and Kinetic Modeling," *Combustion and Flame*, submitted (2009).
3. Westbrook, C. K., Pitz, W. J., Herbinet, O., Curran, H. J. and Silke, E. J., "A Detailed Chemical Kinetic Reaction Mechanism for n-Alkane Hydrocarbons from n-Octane to n-Hexadecane," *Combustion and Flame* 156 (1) (2009) 181-199.
4. Mehl, M., Vanhove, G., Pitz, W. J. and Ranzi, E., "Oxidation and Combustion of the n-Hexene Isomers: A Wide Range Kinetic Modeling Study," *Combustion and Flame* 155 (2008) 756-772.
5. Herbinet, O., Pitz, W. J. and Westbrook, C. K., "Detailed Chemical Kinetic Oxidation Mechanism for a Biodiesel Surrogate," *Combustion and Flame* 154 (2008) 507-528.
6. Seshadri, K., Lu, T., Herbinet, O., Humer, S., Niemann, U., Pitz, W. J. and Law, C. K., "Ignition of Methyl Decanoate in Laminar Nonpremixed Flows," *Proceedings of the Combustion Institute* 32 (2009) 1067-1074.
7. Sakai, Y., Miyoshi, A., Koshi, M. and Pitz, W. J., "A Kinetic Modeling Study on the Oxidation of Primary Reference Fuel-Toluene Mixtures Including Cross Reactions between Aromatics and Aliphatics," *Proceedings of the Combustion Institute*, 32 (2009) 411-418.
8. Westbrook, C. K., Pitz, W. J., Curran, H. J. and Mehl, M., "The Role of Comprehensive Detailed Chemical Kinetic Reaction Mechanisms in Combustion Research" in: M. Dente, (Eds), *Chemical Engineering Greetings to Prof. Eliseo Ranzi on Occasion of His 65th Birthday*, AIDIC (Italian Association of Chemical Engineering) with the cultural partnership of Reed Business Information, 2008.

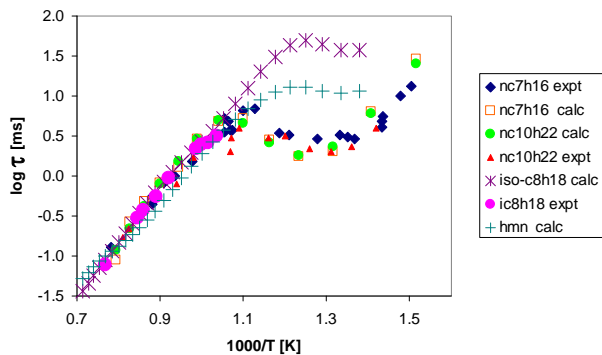


Figure 1. Autoignition of n-heptane, n-decane, iso-octane and 2,2,4,4,6,8,8-heptamethylnonane at 13 bar with stoichiometric, fuel/air mixtures. Computations: n-heptane (nc7h16), iso-octane (ic8h18), n-decane (nc10h22), heptamethylnonane (hmn). Experiments: n-heptane⁴, iso-octane⁹, n-decane¹⁰.

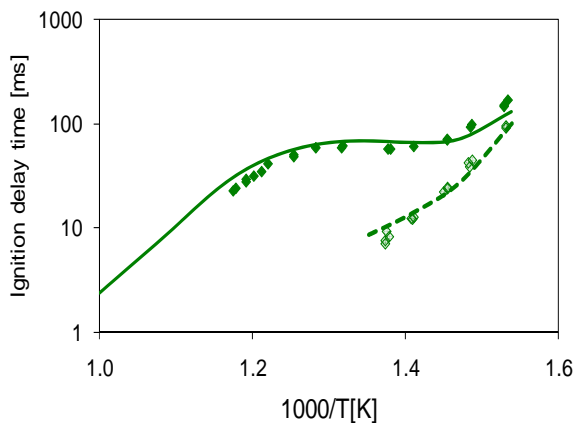


Figure 3. Total ignition delay times (solid) and first stage ignition delay times (dotted) of a gasoline surrogate mixture of 47/35/18% iso-octane/toluene/1-hexene in a RCM over a range of compression temperatures. Mixture is stoichiometric in $O_2/Ar/CO_2/N_2$. Curves: model, symbols: experiment⁸.

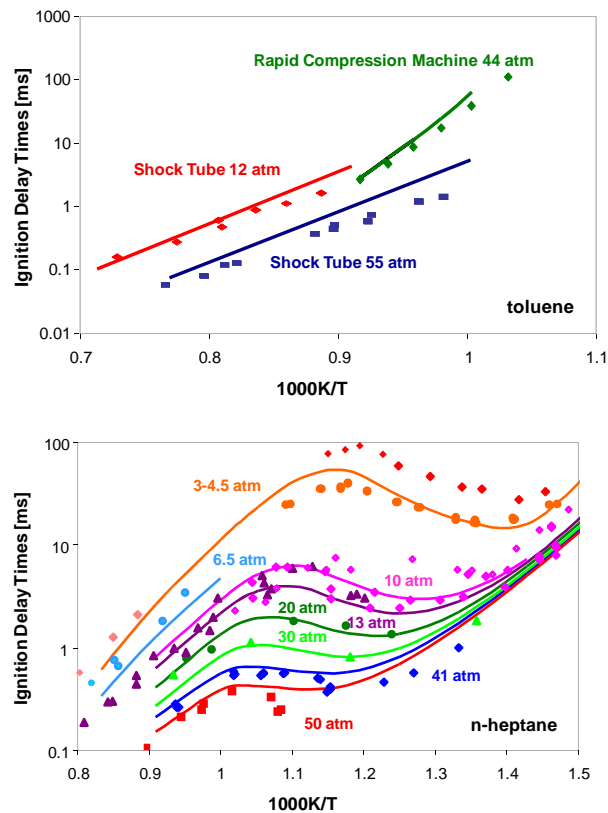


Figure 2. Experimental and calculated ignition delay times of toluene^{6,7} and n-heptane,³⁻⁵ over a wide range of operating conditions. Data collected in shock tubes and rapid compression machines.

INVESTIGATION OF NON-PREMIXED TURBULENT COMBUSTION

Grant: DE-FG02-90ER14128

Stephen B. Pope
Sibley School of Mechanical & Aerospace Engineering
Cornell University
Ithaca, NY 14853
s.b.pope@cornell.edu

1 Scope of the Research Program

The focus of the current work is on the development of computational approaches which allow our detailed knowledge of the chemical kinetics of combustion to be applied to the modeling and simulation of combustion devices. In the past year, the work has been focused in two general areas. The first area is the evaluation of different approaches to model mixing in turbulent reacting flows, and their numerical implementation in large-eddy simulations (LES) using the filtered density function (FDF) approach for turbulence chemistry interactions. The second area of research, which is described in the next section, is the combination of dimension-reduction and tabulation strategies for the computationally-efficient implementation of combustion chemistry in LES/FDF and other modeling approaches.

2 Recent Progress

The principal research results from this program are described in the publications listed in Section 4. Progress in the computationally-efficient implementation of combustion chemistry is described in the following subsection.

2.1 Dimension Reduction and Tabulation of Combustion Chemistry using ICE-PIC and ISAT

Dimension reduction is essential to the use of detailed chemical kinetics in computations of combustion and many other reactive flows. Modern chemical mechanisms for hydrocarbon fuel may contain of order 1,000 species [1], and it is clearly impracticable to use this detailed information directly in multi-dimensional computational fluid dynamics (CFD) calculations. A combination of three approaches that enables the use of detailed chemical information consists of: (1) reduction to a skeletal mechanism [2, 3, 4] involving of order 100 species; (2) dimension reduction (DR) to reduce the number of degrees of freedom to of order ten; and (3) tabulation to significantly reduce the cost of expensive evaluations, e.g., the integration of ordinary differential equations (ODEs).

In this work we develop a general, combined dimension reduction/tabulation methodology by considering the integration of two successful techniques, namely, the invariant constrained-equilibrium edge pre-image curve (ICE-PIC) method for dimension reduction [5, 6, 7], and *in situ* adaptive tabulation (ISAT) [8, 9]. An example of the application of this type of methodology is as follows. A detailed mechanism with n_s species is provided. In the reduced description given by ICE-PIC/ISAT, the reactive flow calculation is performed in terms of a small number of n_r reduced

variables, and chemical reaction is separated from other processes into a reaction fractional step, by using a splitting scheme. Given the reduced variables at time t , the task in this reaction fractional step is to determine the corresponding reduced variables after (adiabatic, isobaric) reaction has occurred for the time-step interval. The ISAT algorithm, a storage/retrieval technique, tabulates the reduced variable information before and after reaction, so that, given the reduced variables before the reaction substep, the corresponding values after reaction can be retrieved from the table. Only when needed, ISAT adds new entries to the table by invoking the ICE-PIC dimension reduction procedure together with the detailed mechanisms. In other words, the reduction/tabulation methodology determines and tabulates (*in situ*) the necessary information about the n_r -dimensional reduced system based on the n_s -species detailed mechanism.

The ICE-PIC dimension reduction method is based on constrained equilibrium theory [10, 11, 12], trajectory-generated manifolds [13] and the pre-image curve method [14]. More details can be found in [5, 6, 7].

2.2 Test case: premixed methane combustion

The test case considered is a partially-stirred reactor (PaSR) involving premixed combustion of a methane/air mixture. The PaSR was used previously to investigate ISAT performance [8, 9, 12].

In this study, the GRI-Mech 1.2 mechanism involving 31 species is used to describe the methane combustion. The species involved are

$$\begin{aligned} & \{H_2, H, O_2, OH, H_2O, CH_3, CH_4, CO, CO_2, \\ & CH_2O, C_2H_4, O, HO_2, H_2O_2, C, CH, CH_2, CH_2(S), \\ & HCO, CH_2OH, CH_3O, CH_3OH, C_2H, C_2H_2, C_2H_3, \\ & C_2H_5, C_2H_6, HCCO, CH_2CO, HCCOH, N_2\} \end{aligned} \quad (1)$$

The pressure is atmospheric throughout. The specified time scales are $\tau_{res} = 10ms$, $\tau_{mix} = 1ms$, $\tau_{pair} = 1ms$, and the time step is constant with $\Delta t = 0.1ms$. There are two inflowing streams: one premixed stream of air and methane at 600 K and a pilot stream consisting of the adiabatic equilibrium products of a stoichiometric fuel/air mixture at 2375 K (corresponding to an unburnt gas temperature of 600 K). The mass flow rates of the two streams are in the ratio 0.95:0.05. Initially ($t = 0$), all particle compositions are set to be the pilot-stream composition. The number of particles in the reactor, N , is 100. All the calculations performed result in about 1×10^6 queries.

In the following, we present the results obtained with dimension reduction using ICE-PIC, and compare them with the full chemistry (FC) results involving all the species without dimension reduction. Specifically, we present preliminary results on the dimension reduction error incurred by ICE-PIC.

2.2.1 Dimension reduction error

We define error, ϵ_{DR} , in a property, ϕ , due to dimension reduction as

$$\epsilon_{DR} = \frac{\|\phi_{DR} - \phi_{FC}\|_2}{\max\{|\phi_{FC}|\}}, \quad (2)$$

where ϕ_{DR} and ϕ_{FC} are the predictions from the reduced description and the full description, respectively (with the ISAT error tolerance $\epsilon_{tol} = 10^{-5}$). The dimension reduction error is calculated by tracking and comparing all the particles for all time.

Figure 1 shows the dimension reduction error percentages in the represented species concentrations using the ICE-PIC method. For each reduced description with n_{rs} , the set of first n_{rs} number of species in Eq. 1 are used as the represented species. The errors are computed for the represented

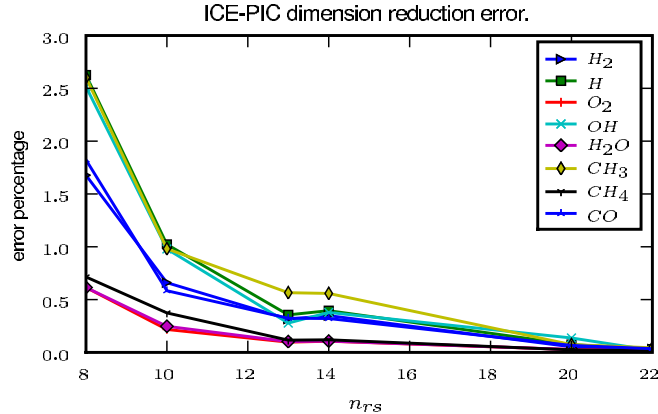


Figure 1: Plot of the ICE_PIC dimension reduction error in the concentration of the represented species vs. the number of represented species for the methane premixed combustion.

species used at the lowest dimension $n_{rs} = 8$, i.e the first 8 species in Eq. 1 (which are also present in all the higher dimensions). It should be noted that the current approach of choosing the first n_{rs} species as the represented species is not the optimal, and is used only for the convenience of explaining the procedure of dimension reduction error calculation. In future work of ICE-PIC, the best possible set of represented species which give the minimum error would be chosen for a given dimension.

It is readily seen from Fig. 1 that the errors incurred by ICE-PIC in the species concentrations are small. For all the cases considered, the maximum dimension reduction error incurred by ICE-PIC is about 2.5%. As expected, as the number of represented species increases, the dimension reduction error incurred by ICE-PIC decreases.

2.3 Conclusions

The combination of ICE-PIC and ISAT offers accurate dimension reduction and efficient tabulation. Advances have been made both in the theory (e.g., in the accurate and efficient evaluation of the tangent vectors) and in the computational implementation.

The study shows that the dimension reduction errors in species concentration and thermodynamic properties incurred by ICE-PIC are well controlled and decrease as the number of represented species increases. In the PaSR test case of premixed methane combustion involving 31 species, with 8 represented species, the maximum dimension reduction error incurred by ICE-PIC is only about 2.5%.

3 Future Plans

The focus of current and future work is on the development of a computationally-efficient implementation of “local” turbulent mixing models, and combustion chemistry. Later this year we expect to publish a paper based on studies of mixing models in the context of LES/FDF modeling. The work on combining ICE-PIC and ISAT continues. In future work, a more robust and efficient implementation of ICE-PIC/ISAT will be developed as well as a methodology to choose the optimal represented species, and the application of this combined method in practical combustion calculations is expected.

4 Publications from DOE Research 2005-2007

1. R.R. Cao, H. Wang and S.B. Pope (2007) “The effect of mixing models in PDF calculations of piloted jet flames,” Proceedings of the Combustion Institute, **31**, 1543–1550.
2. Z. Ren and S.B. Pope (2007) “Sensitivity calculations in PDF particle methods,” Combustion and Flame, **153**, 202–215.
3. Z. Ren and S.B. Pope (2008) “Sensitivity calculations in PDF modelling of turbulent flames,” Proceedings of the Combustion Institute, **32**, 1629–1637.
4. S. Viswanathan and S.B. Pope (2008) “Turbulent dispersion behind line sources in grid turbulence,” Physics of Fluids, **20**, 101514.
5. H. Wang and S.B. Pope (2008) “Lagrangian investigation of local extinction, re-ignition and auto-ignition in turbulent flames,” Combustion Theory and Modelling, **12**, 857-882.

References

- [1] C.K. Law, Proc. Combust. Inst. 31 (2007) 1-29.
- [2] T. Lu, C.K. Law, Proc. Combust. Inst. 30 (2005) 1333-1341.
- [3] P. Pepiot, H. Pitsch, Combust. Flame 154 (2008) 61-81.
- [4] T. Nagy, T. Turányi, Combust. Flame 156 (2009) 417-428.
- [5] Z. Ren, S.B. Pope, A. Vladimirov, J.M. Guckenheimer, J. Chem. Phys. 124 (2006) 114111.
- [6] Z. Ren, S.B. Pope, A. Vladimirov, J.M. Guckenheimer, Proc. Combust. Inst. 31 (2007) 473-481.
- [7] Z. Ren, S.B. Pope, J. Phys. Chem. A 111(34) (2007) 8464-8474.
- [8] S.B. Pope, Combust. Theory Modelling 1 (1997) 41-63.
- [9] L. Lu, S.B. Pope, J. Comput. Phys. 228 (2009) 361-386.
- [10] J.C. Keck, D. Gillespie, Combust. Flame 17 (1971) 237-241.
- [11] J.C. Keck, Prog. Energy Combust. Sci. 16 (1990) 125-154.
- [12] Q. Tang, S.B. Pope, Proc. Combust. Inst. 29 (2002) 1411-1417.
- [13] S.B. Pope, U. Maas, “Simplifying chemical kinetics: trajectory-generated low-dimensional manifolds”, Cornell Report FDA 93-11, 1993.
- [14] Z. Ren, S.B. Pope, Proc. Combust. Inst. 30 (2005) 1293-1300.
- [15] M. Caracotsios, W.E. Stewart, Comput. Chem. Eng. 9(4) (1985) 359-365.
- [16] S.B. Pope, Combust. Flame 139 (2004) 222-226.

OPTICAL PROBES OF ATOMIC AND MOLECULAR DECAY PROCESSES

S.T. Pratt
Building 200, B-125
Argonne National Laboratory
9700 South Cass Avenue
Argonne, Illinois 60439
E-mail: spratt@anl.gov

PROJECT SCOPE

Molecular photoionization and photodissociation dynamics can provide considerable insight into how energy and angular momentum flow among the electronic, vibrational, and rotational degrees of freedom in isolated, highly energized molecules. This project involves the study of these dynamics in small polyatomic molecules, with an emphasis on understanding the mechanisms of intramolecular energy flow and determining how these mechanisms influence decay rates and product branching ratios. It is also aimed at understanding how internal energy can influence photoionization cross sections and dissociative ionization processes. The experimental approach combines double-resonance laser techniques, which are used to prepare selected highly excited species, with mass spectrometry, ion-imaging, and high-resolution photoelectron spectroscopy, which are used to characterize the decay of the selected species.

RECENT PROGRESS

We have continued to focus on using a combination of ion imaging, vuv single-photon ionization, and resonant multiphoton ionization to probe the photodissociation dynamics of halogenated hydrocarbons, as well as any secondary decomposition of the resulting hydrocarbon radicals. As part of a joint project with Laurie Butler, we have investigated the photodissociation of 2-iodoethanol within the A ($\sigma^* \leftarrow n$) absorption band, and used velocity map ion imaging to determine the velocity distributions and angular distributions of the photofragments. In this system, the two dominant dissociation channels correspond to the production of the 2-hydroxyethyl radical, C_2H_4OH , and I ($^2P_{3/2}$) and I* ($^2P_{1/2}$). The branching fraction for the I* channel at 266 nm was determined to be 0.71 by using a combination of (1) the translational energy distributions for the separate I and I* channels determined by two-photon resonant, three-photon ionization; (2) the distributions for the combined I + I* channels determined by single-photon ionization at 118 nm; and (3) the relative photoionization cross sections of I and I* at 118 nm. We were particularly interested in potential secondary dissociation of the C_2H_4OH fragment, because this species is an intermediate in the reaction of $OH + C_2H_4$. However, as has been discussed previously by Sapers and Hess, very little secondary dissociation is observed because most of the excess energy lies in the rotation of the radical. Instead, we find evidence for dissociative ionization of a significant fraction of the C_2H_4OH .

We have also recently completed a systematic study of the photodissociation of isopropyl iodide in the A absorption band. The translational energy distributions and translational-energy dependence of the angular distributions of the I $^2P_{3/2}$ and $^2P_{1/2}$ photofragments were recorded as a function of the photodissociation wavelength, and these distributions were used to decompose the $i-C_3H_7 + I^2P_{3/2}$ channel into contributions from two processes, corresponding to direct dissociation on a single surface, and indirect dissociation by crossing from the initially excited

surface to the second surface. The contributions for the direct process were most significant only in the red tail of the absorption band, which is consistent with earlier studies of CH₃I.

This past year I made considerable progress in my collaboration with Christian Jungen (Laboratoire Aimé Cotton) to develop simple models for vibrational autoionization in polyatomic molecules. As mentioned last year, we have adapted the three-state model of the Renner-Teller interaction developed by Gauyacq and Jungen to the framework of multichannel quantum defect theory, and we have used it to predict vibrational autoionization widths in Rydberg states of molecules such as NO₂ and HCO. This approach has also allowed us to make some general predictions about the relative vibrational autoionization rates for different normal modes of these molecules. One advantage of this approach is that we have developed an analytic formula that only requires information about the vibrational frequencies of the ionic state of interest and the Renner-Teller interaction parameters on low-lying Rydberg states. In the case of NO₂ and HCO, this information was available from a number of sources, most notably from the work of Ed Grant and coworkers. In a somewhat surprising development, by using these expressions for the autoionization width for the electron capture widths by the corresponding ions, and by assuming that electron capture was the rate limiting step for dissociative recombination, we could calculate rates for the process $\text{HCO}^+ + e^- \rightarrow \text{HCO}^* \rightarrow \text{H} + \text{CO}$ for low energy collisions ($< \sim 0.4$ eV). The observed rates were in good agreement with the results of state-of-the-art ab initio calculations, and with existing experimental data from ion-storage rings.

Based on this success, Christian Jungen and I also developed a related formalism for vibrational autoionization mediated by the Jahn-Teller interaction in symmetric triatomic molecules. The goal of this work was to see if we could develop a simple analytic formula for the dissociative recombination of H₃⁺. This process is of considerable importance in models of astrochemistry because H₃⁺ is a key species for building larger molecules in interstellar environments, and because dissociative recombination is the key destruction mechanism of H₃⁺. We were able to derive a formula that again made use of only the vibrational frequencies of the H₃⁺ ion and the Jahn-Teller interaction parameters determined for low-lying Rydberg states of H₃. The results of this calculation were in excellent agreement with the best existing experimental data, as well as with large-scale ab initio calculations. Furthermore, we were able to predict the corresponding dissociative recombination rates for the isotopomers D₃⁺, H₂D⁺, and D₂H⁺, and these were also in remarkably good agreement with experiment. While such simple calculations are not meant to replace high level calculations (which provide significantly more detail), they provide an independent validation of the proposed mechanism, and provide the means to extrapolate to much larger systems than are currently feasible by the brute force approach.

Finally, in collaboration with the group of Murnane and Kapteyn at JILA, I was involved in an experimental study of the vuv photoionization of laser-aligned CO₂ and N₂. This study showed how the use of laser alignment can provide insight into the parallel or perpendicular character of the photoionization matrix elements. This work is directly relevant to future work proposed for the Linac Coherent Light Source (LCLS) at Stanford. In this context, I am a member of a team that has been granted beamtime in the initial experimental runs at the LCLS this coming fall.

FUTURE PLANS

We plan on continuing our studies of the photodissociation and photoionization of combustion-relevant radicals by using ion-imaging techniques, vacuum-ultraviolet single-photon ionization, and resonant multiphoton ionization techniques. For example, we have initiated a study on the photodissociation of formic acid as a means of producing a number of interesting combustion radicals including OH, HCO, HOCO, and HCOO. This study is expected not only to provide insight into the dissociation dynamics of formic acid, but also to allow studies on the radicals directly. In particular, by using a variety of deuterated compounds, we believe it will be possible to examine the HOCO and HCOO species separately, to study their photoionization dynamics, and ultimately to determine their photoionization cross sections. The latter may require a study of the photodissociation dynamics of acetaldehyde (CH_3CHO , which can dissociate to CH_3 and HCO) to determine the photoionization cross section of HCO relative to CH_3 . Because our approach for determining absolute photoionization cross sections of radicals is relatively simple, these measurements can be performed simultaneously with other imaging studies, and we plan to perform such measurements to a number of other systems, such as CF_3 , C_2H_5 , the different isomers of C_3H_5 and C_3H_7 , and $\text{C}_2\text{H}_4\text{OH}$. Construction of a new imaging apparatus is nearing completion, and we hope to begin studies on the photodissociation of cold radicals prepared by using a jet-cooled photolysis or pyrolysis source to produce cold radicals. We also plan on using photoelectron imaging to provide insight on the photoionization dynamics of both stable and reactive species. The ability to record photoelectron angular distributions directly is expected to have significant utility in the identification and understanding of ionization mechanisms. I will also continue to collaborate with Dr. Valerie Blanchet (CNRS, Toulouse) on femtosecond photoelectron spectroscopy following the photodissociation of CH_3Br . This work complements my imaging experiments on photodissociation processes with nanosecond lasers.

I will continue to collaborate with Christian Jungen on theoretical models of vibrational autoionization and dissociative recombination in polyatomic molecules. We will attempt to understand the puzzling observation that experimental dissociative recombination spectra show very little resonance structure compared to that observed in high level theoretical calculations. We will also explore the implications of our model for the dissociative recombination in more complex species. Similarly, we will also examine the implications of our work Renner-Teller induced autoionization and dissociative recombination. In general, it appears that the propensity rule for vibrational autoionization will have significant implications for the dissociative recombination of many species.

This work was supported by the U.S. Department of Energy, Office of Science, Office of Basic Energy Sciences, Division of Chemical Sciences, Geosciences, and Biological Sciences under contract No. DE-AC02-06CH11357.

DOE-SPONSORED PUBLICATIONS SINCE 2007

1. Haiyan Fan and S. T. Pratt
DETERMINATION OF SPIN-ORBIT BRANCHING FRACTIONS IN THE
PHOTODISSOCIATION OF HALOGENATED HYDROCARBONS
J. Phys. Chem. A, **111**, 3901-3906 (2007).
2. H. Fan, L. B. Harding, and S. T. Pratt

- DISSOCIATIVE IONIZATION OF HOT C₃H₅ RADICALS
Mol. Phys., **105**, 1517-1534 (2007).
3. H. Fan, S. T. Pratt, and J. A. Miller
SECONDARY DECOMPOSITION OF C₃H₅ RADICALS FORMED BY THE
PHOTODISSOCIATION OF 2-BROMOPROPENE
J. Chem. Phys., **127**, 144301 (2007).
 4. E. R. Peterson, C. Buth, D. A. Arms, R. W. Dunford, E. P. Kanter, B. Krässig, E. C.
Landahl, S. T. Pratt, R. Santra, S. H. Southworth, and L. Young
X-RAY ABSORPTION BY LASER-ALIGNED MOLECULES
Appl. Phys. Lett. **92**, 094106 (2008).
 5. C. A. Taatjes, D. L. Osborn, T. Selby, G. Meloni, H. Fan, and S. T. Pratt
ABSOLUTE PHOTOIONIZATION CROSS SECTION OF THE METHYL RADICAL.
Phys. Chem. A **112**, 9336-9343 (2008).
 6. I. Thomann, R. Lock, V. Sharma, E. Gagnon, S. T. Pratt, H. C. Kapteyn, M. M. Murnane,
and W. Li
DIRECT MEASUREMENT OF THE ANGULAR DEPENDENCE OF THE SINGLE-
PHOTON IONIZATION OF ALIGNED N₂ AND CO₂
J. Phys. Chem. A **112**, 9382-9386 (2008).
 7. Ch. Jungen and S. T. Pratt
RENNER-TELLER INTERACTIONS IN THE VIBRATIONAL AUTOIONIZATION OF
POLYATOMIC MOLECULES
J. Chem. Phys. **129**, 164310 (2008).
 8. Ch. Jungen and S. T. Pratt
RENNER-TELLER INTERACTIONS IN THE DISSOCIATIVE RECOMBINATION OF
HCO⁺
J. Chem. Phys. **129**, 164311 (2008).
 9. Ch. Jungen and S. T. Pratt
JAHN-TELLER INTERACTIONS IN THE DISSOCIATIVE RECOMBINATION OF H₃⁺
Phys. Rev. Lett. **102**, 023201 (2009).
 10. S. T. Pratt
HIGH-RESOLUTION VALENCE-SHELL PHOTOIONIZATION
in *Handbook of High-Resolution Spectroscopies*, edited by M. Quack and F. Merkt (Wiley,
New York, XXXX). (in press).
 11. V. A. Shubert, M. Rednic, and S. T. Pratt
PHOTODISSOCIATION OF I-C₃H₇I WITHIN THE A BAND AND ANISOTROPY-
BASED DECOMPOSITION OF THE TRANSLATIONAL ENERGY DISTRIBUTIONS
J. Chem. Phys. (in press).

Photoinitiated Reactions of Radicals and Diradicals in Molecular Beams

Hanna Reisler

Department of Chemistry, University of Southern California

Los Angeles, CA 90089-0482

reisler@usc.edu

Program Scope

Open shell species such as radicals and diradicals are central to reactive processes in combustion and environmental chemistry. Our program is concerned with photoinitiated reactions of hydroxyalkyl radicals and carbenes. The goal is to investigate the detailed dynamics of dissociation of free radicals and diradicals for which multiple pathways including molecular rearrangements compete, and compare them with high level calculations. Studies include unimolecular reactions on the ground state of CH_2OH initiated by overtone excitation to above the barriers to dissociation and isomerization. The photochemistry of the 2-hydroxyethyl radical, a primary intermediate in the $\text{OH} + \text{C}_2\text{H}_4$ reaction, will be elucidated with special emphasis on the vinyl alcohol (enol) channel. The photodissociation of triplet methylene, the prototypical carbene, exhibits conical intersections and experiments will be compared with high-level electronic structure calculations.

Recent Progress

Ionization energies of the hydroxymethyl and 1-hydroxyethyl radicals

One of the notable characteristics of hydroxyalkyl radicals, as compared for example to the corresponding alcohols or the isomeric alkoxy radicals, is their low ionization energies (IEs). The adiabatic IEs of the hydroxymethyl and hydroxyethyl radicals are 7.56 and 6.64 eV, respectively, whereas the corresponding values for methanol, ethanol, methoxy, and ethoxy radicals are 10.85, 10.41, 10.72, and 9.11 eV, respectively. What is striking is not only the large reduction in ionization energy in going from the closed- to the open-shell compounds but also the large decrease (about 0.9 eV) in going from hydroxymethyl to the hydroxyethyl radical, which is much larger than the 0.4 eV difference between the corresponding alcohols.

In a joint study with the group of Anna Krylov we proposed a physical explanation for the decrease in IE by using high-level electronic structure calculations and in particular by comparing the highest occupied, singly occupied, and lowest unoccupied molecular orbitals (HOMO, SOMO, and LUMO, respectively) of the radicals and the cations. Specifically, our analysis highlights the role of hyperconjugation in stabilizing the hydroxyethyl cation and destabilizing the radical, compared to hydroxymethyl.

Hyperconjugation is a concept used often in physical organic chemistry to describe conjugation effects that involve σ -bonds in addition to π -bonds. Both conjugation between double or triple bonds and hyperconjugation involve delocalization of charge density over several atoms or groups of atoms.

Because of the presence of the OH group, hyperconjugation in the 1-hydroxyethyl radical involves three interacting molecular orbitals (MO's). The participating orbitals are two p-like orbitals on C and O and one σ_{CH} MO of the methyl group that has favorable overlap with the p-like orbitals. In molecular orbital language, these orbitals, which have the same symmetry, can interact, creating a new set of three allyl-like delocalized orbitals. The bonding and antibonding

character of these delocalized MOs and the extent to which they are filled are responsible for the low IE of the 1-hydroxyethyl radical and the stabilization/destabilization of the neutral and cation species relative to the case of no hyperconjugation interaction. NBO analysis confirms this qualitative picture, and the computed hyperconjugation energies are in qualitative agreement with estimates derived from a simple Hückel-like model. Our main conclusion is that hyperconjugation destabilizes the neutral hydroxyethyl radical due to the antibonding character of the SOMO, while stabilizing the cation by lowering the energies of the HOMO and HOMO-1 relative to hydroxymethyl. Additional stabilization is achieved owing to the more extensive charge delocalization in hydroxyethyl. At the radical geometry, the change in IE due to SOMO destabilization is estimated to be 0.53 eV, which is in excellent agreement with the hyperconjugation energy of the hydroxyethyl cation computed by NBO.

Upon geometry relaxation following ionization, the hyperconjugation energy increases by about 0.1 eV, which explains the larger difference between the vertical and adiabatic IEs in hydroxyethyl relative to hydroxymethyl. Thus, we can interpret the large observed change between the adiabatic and vertical IE's in CH_3CHOH as the cumulative effects of the bonding interactions between the carbon's unpaired electron, the lone pair of oxygen, and hyperconjugation interaction with σ_{CH} . The energy relaxation upon ionization is due to more efficient hyperconjugation at shorter CC and CO bond lengths, whereas energy changes due to the CH_3 torsion are minor.

The low IE of CH_3CHOH also explains why its Rydberg states lie so low in energy and rationalizes the observation that its electronic absorption spectrum extends down to the visible region. The results should be relevant to other 1-hydroxyalkyl radicals.

Two photon dissociation of diazirine

In our quest for a clean and convenient source of methylene radicals in the ground triplet state, we have explored the pyrolysis of diazirine, which more stable than its structural isomer diazomethane (studied by us before). We can prepare diazirine cleanly and safely, supersonically expand it in a He carrier gas, and following pyrolysis in the nozzle observe the formation of $^3\text{CH}_2$ by REMPI. The radical is formed at a rotational temperature of 50-200 K, which is typical of pyrolysis sources. Figure 1 presents a 2+1 REMPI spectrum of $^3\text{CH}_2$ obtained via the 3p Rydberg manifold in a Chen-type molecular beam source.

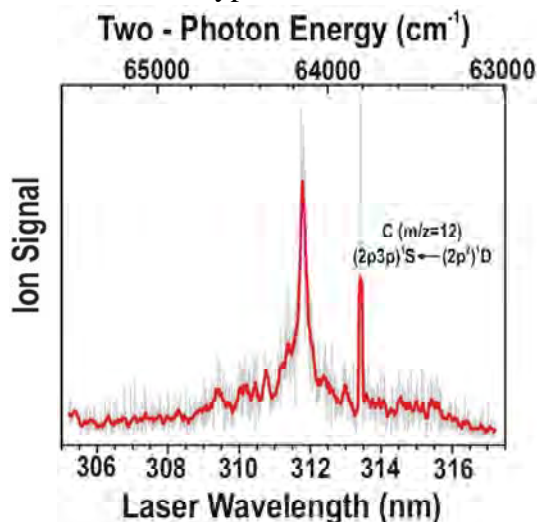


Fig. 1: 2+1 REMPI spectrum of $^3\text{CH}_2$ obtained via excitation to the 3p Rydberg manifold. Pyrolysis of diazirine is carried out in He, at a backing pressure that converts the nascent $^1\text{CH}_2$ to $^3\text{CH}_2$ before it exits the heated SiC tube.

We have also studied the two-photon ionization and dissociation dynamics of diazirine, and in particular the formation of CH products. Diazirine (*c*-CH₂N₂) belongs to the family of isoelectronic molecules known as "16-electron molecules", which have attracted considerable attention for decades because of the inherent complexity of their photodissociation dynamics and certain similarities in their properties. In addition, HNCO, H₂CNN and H₂CCO, all members of this family, are known to have structural isomers. Our studies of the multiphoton ionization and photochemistry of diazirine were aided by high-level electronic structure calculations.

The lowest lying UV absorption bands of diazirine belong to the structured $1^1B_2 \leftarrow 1^1A_1 (\pi^* \leftarrow n)$ system with a band origin at 31,187 cm⁻¹ (320.65 nm). Its VUV absorption spectrum shows an intense, structureless band centered at 145-185 nm as well as diffuse structures at ~ 120-143 nm. The vertical (adiabatic) ionization energy (IE) of diazirine was determined experimentally at 10.75 eV (10.3 eV).

We have studied the multiphoton ionization and dissociation of diazirine experimentally by using 304-325 nm two-photon absorption and theoretically, in collaboration with Anna Krylov's group, by using the EOM-CCSD and B3LYP methods. The electronic structure calculations identified two excited valence states and four Rydberg states in the region 4.0-8.5 eV. In one-photon excitation, the strongest absorption is to the $2^1A_1(3p_x \leftarrow n)$ Rydberg state, whereas in two-photon absorption at comparable energies the first photon excites the low-lying $1^1B_2 (\pi^* \leftarrow n)$ valence state, from which the strongest absorption is to the dissociative valence $1^1A_2 (\pi^* \leftarrow \sigma_{NN})$ state. The diazirine ion is calculated to be rather unstable, with a binding energy of only 0.73 eV and a geometry that resembles a weakly bound CH₂⁺...N₂ complex. In the experimental studies, REMPI experiments show no ions at the parent diazirine mass but only CH₂⁺ ions from dissociative photoionization. We propose that weak one-photon absorption to the 1^1B_2 state is immediately followed by more efficient absorption of another photon to reach the 1^1A_2 state from which competition between a third photon absorption to achieve ionization and fast dissociation takes place.

Strong signals of CH⁺ ions were detected in the experiment and assigned to 2+1 REMPI via the $D^2\Pi (v'=2) \leftarrow X^2\Pi (v''=0)$ two-photon transition of CH fragments (see Fig. 2). Velocity map CH⁺ images obtained by dc slice velocity map imaging show that CH(X, v''=0, N'') fragments are born with substantial translational energy corresponding to absorption of two photons in diazirine (see Fig. 3).

We argue that two photon processes via the 1^1B_2 intermediate state are very efficient in this wavelength range, leading predominantly to dissociation of diazirine from the 1^1A_2 excited valence state. The most likely route to CH(X) formation is isomerization to isodiazirine (*c*-HCNNH) followed by dissociation to CH + HN₂. This mechanism agrees well with the measured maximum in the c.m. translational energy, and is similar to the mechanism proposed for formation of CH(X) in two-photon dissociation of the isoelectronic ketene. Comparison between one- and two-photon dissociation at 150-170 nm would be enlightening.

In closing, and in agreement with previous theoretical papers, we propose a revision of the heats of formation of diazirine and diazomethane to 77 ± 3 and 67 ± 3 kcal/mol, respectively.

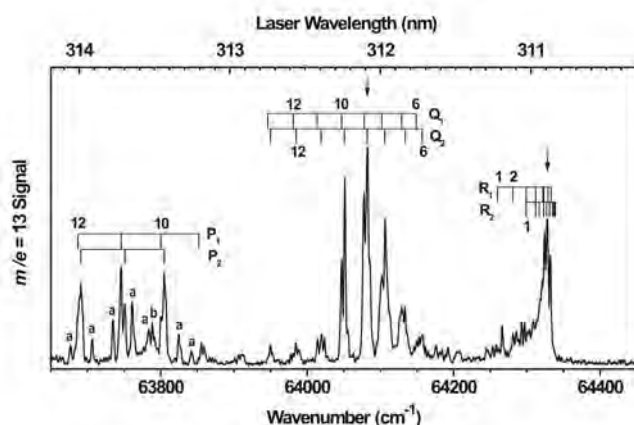


Fig. 2: CH 2+1 REMPI spectrum obtained via the $D^2\Pi \leftarrow \leftarrow X^2\Pi$ transition

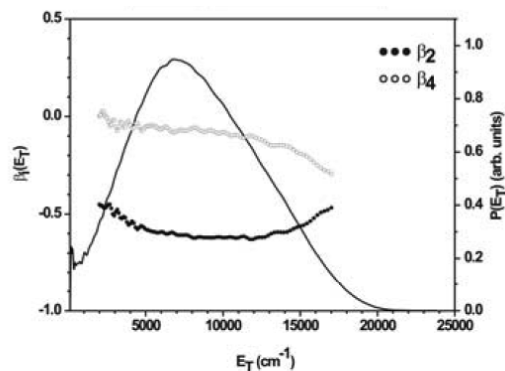


Fig. 3: c.m. translational energy distribution and recoil anisotropy parameters of CH(X) in $v''=0, N''=9$.

Future Work

Studies in progress on the photodissociation of the 2-hydroxyethyl radical, $\text{CH}_2\text{CH}_2\text{OD}$ reveal the formation of D atoms in addition to OD fragments. The $\text{CH}_2\text{CH}_2\text{OH}$ isomer of the $\text{C}_2\text{H}_5\text{O}$ group does not belong to the homologous series of hydroxymethyl radical and is more similar to a substituted ethyl radical. Very little is currently known about its photoionization and photochemistry and we plan to elucidate its dissociation dynamics from low-lying electronic states, and high vibrational levels of the ground state. In addition, we plan to study the photodissociation of $^3\text{CH}_2$ produced by pyrolysis of diazirine.

Publications 2007-2009

1. Fedorov, I., Koziol, L., Li, G. S., Reisler, H., and Krylov, A. I. "Vibronic structure and ion core interactions in Rydberg states of diazomethane: An experimental and theoretical investigation," *J. Phys. Chem. A* **111** (2007): 13347-13357.
2. Fedorov, I., Koziol, L., Li, G. S., Parr, J. A., Krylov, A. I., and Reisler, H. "Theoretical and experimental investigations of the electronic rydberg states of diazomethane: Assignments and state interactions," *J. Phys. Chem. A* **111** (2007): 4557-4566.
3. Karpichev, B., Reisler, H., Krylov, A. I., and Diri, K. "Effect of hyperconjugation on ionization energies of hydroxyalkyl radicals," *J. Phys. Chem. A* **112** (2008): 9965-9969.
4. Karpichev, B., Edwards, L. W., Wei, J., and Reisler, H. "Electronic spectroscopy and photodissociation dynamics of the 1-hydroxyethyl radical CH_3CHOH ," *J. Phys. Chem. A* **112** (2008): 412-418.
5. Fedorov, I., Koziol, L., Mollner A. K., Krylov, A. I., and Reisler H, "Multiphoton ionization and dissociation of diazirine: A theoretical and experimental study" *J. Phys. Chem. A* (in press).

Accurate Calculations and Analyses of Electronic Structure, Molecular Bonding and Potential Energy Surfaces

Klaus Ruedenberg

Ames Laboratory USDOE, Iowa State University, Ames, Iowa, 50011
ruedenberg@iastate.edu

Scope

Theoretical treatments of molecular reactions and their kinetics require accurate potential energy surfaces in non-equilibrium regions of the internal coordinate space. A major obstacle is the sufficiently accurate description of the non-relativistic electron correlations in the presence of a *multiconfigurational* dominant zeroth-order component in the electronic wavefunction, as is the case along most reaction paths. In this context, the correlation energy extrapolation by intrinsic scaling (CEEIS) method, recently developed by this group, has been a significant advance.

Recent Work

The method made it possible for us to calculate the first full potential energy curve of any 18-electron system, namely the $^1\Sigma_g^+$ ground state of the F_2 molecule with an accuracy of 0.1 kcal/mole (Figure 1). From this curve, the experimentally known vibrational spectrum of 22 levels was calculated with a mean absolute deviation of less than 5 cm^{-1} and the rotational constants within 10^{-3} cm^{-1} . The equilibrium distance and the dissociation energy were recovered within 0.001 \AA and 30 cm^{-1} respectively.

The method made it furthermore possible for us to calculate the first high-accuracy potential energy curve for the $^3\Sigma_g^-$ ground state of the O_2 molecule (Figure 2). Its equilibrium distance and dissociation energy were recovered within 0.0001 \AA and 10 cm^{-1} respectively. The 31 experimentally known vibrational levels (out of a total of 41) were obtained with a mean absolute deviation of about 14 cm^{-1} .

The unprecedented accuracy of these curves led us to focus on a problem that has never been concretely elucidated, it seems, namely the real shape of the potential energy curve of a covalently bonded molecule between the covalent and the van der Waals regions and in the non-asymptotic long range region. For F_2 , we resolved these questions by expressing the potential energy curve as $V(R) = V(\text{uncorrelated}) + V(\text{correlation})$, where the total $V(R)$ as well as $V(\text{uncorrelated})$ are calculated while $V(\text{correlation})$ is *deduced as the difference*. We showed that, at long range, (i) $V(\text{uncorrelated})$ becomes exactly the interaction between the *quadrupoles* of the F atoms and is *repulsive* for the $^1\Sigma_g^+$ state (Figure 3) and (ii) the *difference* $V(\text{correlation})$ becomes exactly the *dispersion attraction* and is in fact very similar to the potential between two neon atoms (Figure 4). In the long range competition between the two, the former (decaying as R^{-5}) prevails over the latter (decaying as R^{-6}), which leads to a slight barrier in the intermediate region before covalent bonding takes over (Figure 5). At about twice the equilibrium distance, a sudden drastic regime change occurs in the gradient of $V(R)$. In about the same region, several Π states cross the $^1\Sigma_g^+$ state because, for Π symmetries, the (mutually perpendicular) atomic quadrupoles attract each other (Figure 5).

Future Work

Using localized orbitals, the CEEIS method will be extended to reactions in polyatomic, notably combustion and atmospheric systems. The method will be adapted to the treatment of core correlations. The method will be adapted to excited states.

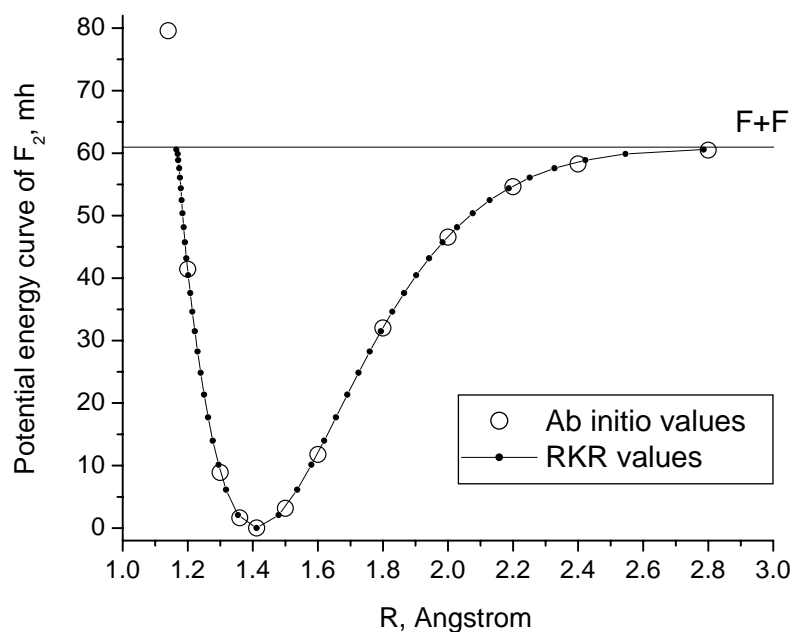


Figure 1. Theoretical and experimental $^1\Sigma_g^+$ ground state curve of fluorine

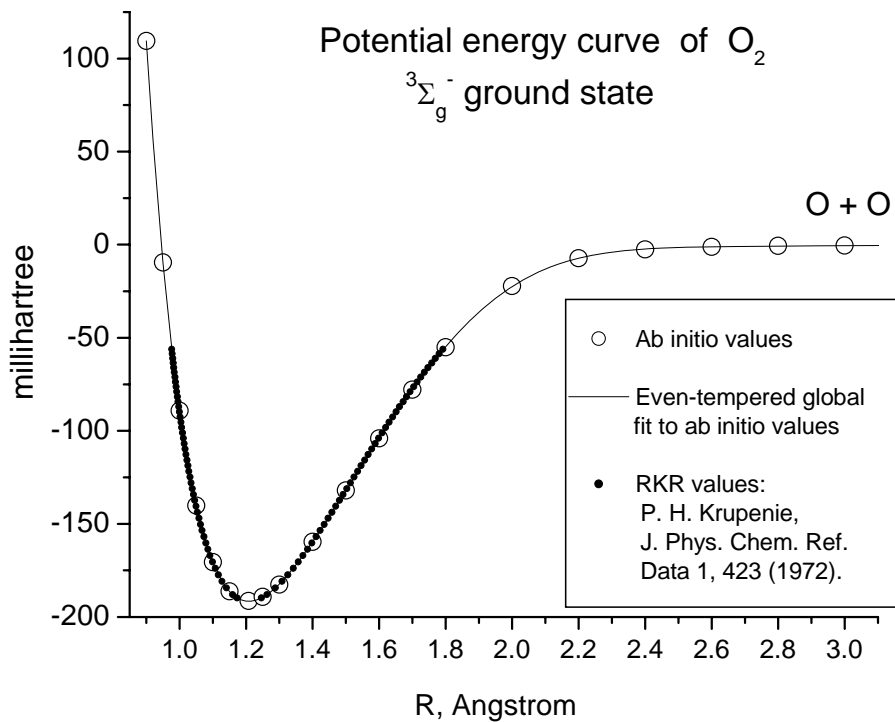


Figure 2. Theoretical and experimental potential energy curve of oxygen

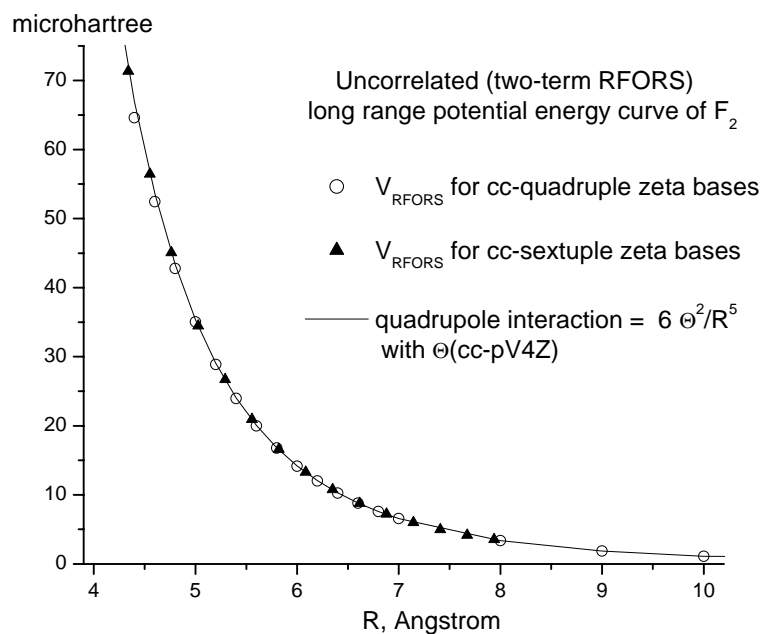


Figure 3. Long range $V(\text{uncorrelated})$ curve of F_2 becomes $+6\Theta^2/R^5 \equiv$ quadrupole repulsion of $2F$

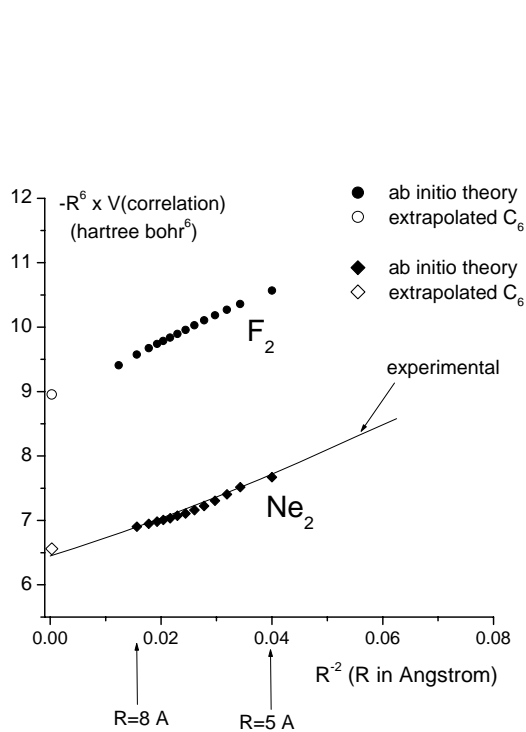


Figure 4. Long range $-R^6 \times V(\text{correlation})$ of F_2 becomes $C_6 + C_8(R^{-2}) \equiv$ dispersion

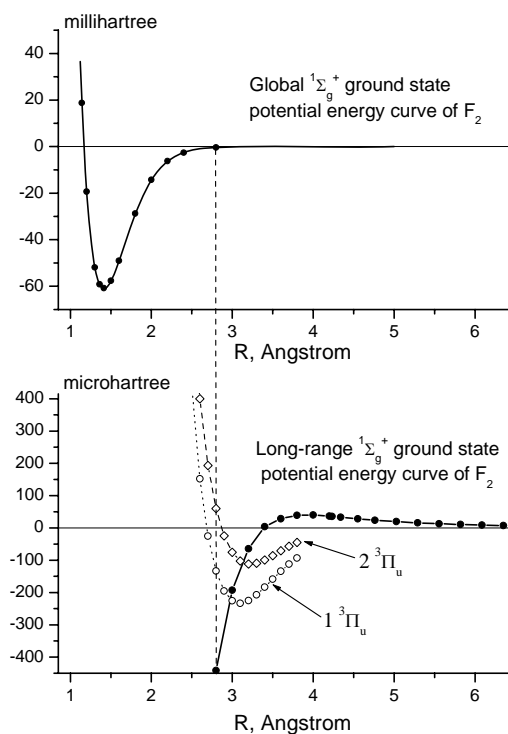


Figure 5. Global PEC of F_2 at short, intermediate and long range

Publications in 2007, 2008, 2009

Why Does Electron Sharing Lead to Covalent Bonding? A Variational Analysis.

Klaus Ruedenberg and Michael W. Schmidt, *J. Comp. Chem.*, **28**, 391-410 (2007).

Toward a Physical Understanding of Electron-Sharing in Two-Center Bonds. I.

T. Bitter, K. Ruedenberg, W.H.E. Schwarz, *J. Comp. Chem.*, **28**, 411-422 (2007).

Economical Description of Electron Correlation,

L. Bytautas and K. Ruedenberg, *Advances in Electron Correlation Methodology* (A. K. Wilson and K. A. Peterson Edtrs), ACS Symposium Series Volume **958**, p. 103-124 (2007).

Accurate Ab Initio Potential Energy Curve of F₂. I. Non-Relativistic Full Valence CI Energies by the CEEIS Method.

L. Bytautas, T. Nagata, M. S. Gordon, K. Ruedenberg, *J. Chem. Phys.* **127**, 164317, 1-20 (2007).

Accurate Ab Initio Potential Energy Curve of F₂. II. Core-Valence Correlations, Relativistic Contributions and Long-Range Interactions.

L. Bytautas, N. Matsunaga, T. Nagata, M. S. Gordon, K. Ruedenberg, *J. Chem. Phys.* **127**, 204301, 1-12 (2007).

Accurate Ab Initio Potential Energy Curve of F₂. III. The Vibration Rotation Spectrum.

L. Bytautas, N. Matsunaga, T. Nagata, M. S. Gordon, K. Ruedenberg, *J. Chem. Phys.* **127**, 204313 1-19 (2007)

Intrinsic Local Constituents of Molecular Electronic Wave Functions. I. Exact Representation of the Density Matrix through Chemically Deformed and Oriented Atomic Minimal Basis Orbitals.

J. Ivanic, G. J. Atchity and K. Ruedenberg, *Theor. Chem. Acc.* **120**, 281-294 (2008).

Intrinsic Local Constituents of Molecular Electronic Wave Functions. II. Electronic Structure Analyses in terms of Intrinsic Oriented Quasi-Atomic Molecular Orbitals for the Molecules FOOH, H₂BH₂BH₂, H₂CO and the Isomerization HNO → NOH.

J. Ivanic and K. Ruedenberg, *Theor. Chem. Acc.* **120**, 295-305 (2008).

Correlation Energy and Dispersion Interaction in the Ab Initio Potential Energy Curve of the Neon Dimer.

Laimutis Bytautas and Klaus Ruedenberg, *J. Chem. Phys.*, **128**, 214308, 1-12 (2008).

A-Priori Identification of Configurational Deadwood.

Laimutis Bytautas and Klaus Ruedenberg, *Chem. Phys.*, **356**, 64-75 (2009)

Physical Understanding through Variational Reasoning: Electron Sharing and Covalent Bonding.

K. Ruedenberg and M.W. Schmidt, *J. Phys. Chem.*, **113**, 1954-1968 (2009)

Ab Initio Potential Energy Curve of F₂. IV. Transition from the Covalent to the van der Waals Regime. Competition between Multipolar and Correlation Forces.

L. Bytautas and K. Ruedenberg, *J. Chem. Phys.*, submitted

Active Thermochemical Tables – Progress Report

Branko Ruscic
Chemical Sciences and Engineering Division, Argonne National Laboratory,
9700 South Cass Avenue, Argonne, IL 60439
ruscic@anl.gov

Program Scope

The *spiritus movens* of this program is the need to provide the scientific community with accurate and reliable thermochemical, spectroscopic, and structural information on chemical species that are relevant in combustion, or play prominent roles in related post-combustion environmental chemistry, thus contributing to the comprehension of the underlying chemical reactions and/or providing reliable benchmark values for development and testing of state-of-the-art theoretical approaches. In particular, thermochemistry is one of the essential underpinning scientific blocks that is enabling DOE to understand and successfully model energy-producing chemical reactions and thus fulfill its mission, and is, as such, a long-term component of the DOE BES research program. The current focal point of this program is to bring substantial innovations to the field of thermochemistry through the development of new tools and methodologies, and utilize these new approaches to systematically advance the quality and quantity of available thermochemical data relevant in energy-producing processes. In order to accomplish the stated goal, this program has recently developed a novel approach centered on the idea of optimally extracting the knowledge content from thermochemically relevant measurements, and hence producing not only *the best currently possible* thermochemical parameters for the target chemical species, but also providing *critical tests of new experimental or theoretical data*, developing *pointers to future determinations that will most efficiently improve the thermochemical knowledge base*, and allowing efficient updates with new knowledge, instantly propagating its consequences through all affected chemical species. The effort of this program is synergistically coordinated with related experimental and theoretical efforts within the Argonne Chemical Dynamics Group to provide a broad perspective of this area of science.

Recent Progress

Development of Active Thermochemical Tables and the Core (Argonne) Thermochemical Network

Active Thermochemical Tables (ATcT) are a new paradigm of how to derive accurate, reliable, and internally consistent thermochemical values for stable, reactive, and transient chemical species. Availability of high-quality thermochemical values for a broad range of species, accompanied by properly quantified uncertainties, is central to chemistry, and critical in such areas as experimental and computational chemical kinetics and dynamics, development of credible chemical reaction mechanisms, and formulation of realistic models for complex chemical environments such as flames, internal combustion engines, or the atmosphere. In addition, the availability of accurate and reliable thermochemical benchmarks has been historically the strongest *spiritus movens* for the advancement of sophisticated electronic structure theories.

The success of ATcT is rooted in its Thermochemical Network (TN) approach.^{1,2,3} The legacy approach to thermochemistry, which uses a stepwise sequential path (A begets B which begets C etc.), has serious limitations in how the underlying thermochemical data can be utilized and how it treats the interdependencies between species. As opposed to traditional thermochemistry, ATcT produces consistent and accurate thermochemistry by simultaneously analyzing the entire knowledge content of the TN. The TN Graph is constructed by incorporating all available thermochemically-relevant experimental determinations. These are typically prescreened by an *a priori* critical analysis. The available data is further complemented both by existing and new (largely driven by the discovery of “weak links” in the TN) high-quality theoretical results and experiments. The TN Graph explicitly exposes the maze of

inherent thermochemical interdependencies between various chemical species, and allows, *inter alia*, a thorough statistical evaluation of the individual real (experimental) and virtual (theoretical) measurements. The goal of the latter scrutiny is to isolate “optimistic” uncertainties that invariably occur with some of the original determinations (both real and virtual), and which, if left unchecked, would adversely affect the quality of the resulting knowledge. The ATcT analysis in turn flags determinations that may require an additional critical analysis and, when necessary and possible, a reinterpretation. The end result of this iterative cycle is the extraction of *best possible thermochemical values* for all chemical species described by the TN, based on optimal use of *all the available knowledge*, hence making conventional tabulations of thermochemical values obsolete.

The central TN, which is the essential source of all new ATcT thermochemical values, is the Core (Argonne) TN, C(A)TN. The Network is under continuous development, and currently encompasses ~900 chemical species of C/H/O/N/Hal composition, intertwined by >10,000 thermochemically-relevant determinations. As opposed to a *localized* TN (which we sometimes use for preliminary testing and development), C(A)TN is an *ab ovo* TN, i.e. it does not contain any species that are constrained to an externally selected or imposed value of enthalpy of formation (other than the definitions of the reference state for each element). The fact that C(A)TN is devoid of non-transparent external dependences allows ATcT to coerce the knowledge contained in the TN toward full self-consistency.

The current C(A)TN contains a significant number of sections that are nearly mature, spanning a substantial number of “key” chemical species. An important part of our developmental effort is presently focused on bringing the thermochemistry of a number of these ‘nearly mature’ sections to a ‘release’ status. The first candidate for release is the O/H group of species. Some time ago^{4,5} we have shown by traditional (non-ATcT) methods that the accepted enthalpy of formation of OH (Gurvich et al.,⁶ 9.41 ± 0.05 kcal mol⁻¹ at 298.15 K) must be wrong, and proposed a significant revision to $\Delta_f H^\circ_{298}(\text{OH}) = 8.91 \pm 0.07$ kcal mol⁻¹. With the advent of ATcT it became possible to utilize all of the relevant information (such as, for example, the related value for the bond dissociation energy of H₂O₂) much more completely and without involving tenuous and potentially inconsistent external dependencies (such as a dependence on an external value for the enthalpy of formation of H₂O₂). ATcT not only fully corroborates the revised OH value, but it further increases its accuracy. Thus we have recently⁷ reported an interim ATcT value of 8.93 ± 0.03 kcal mol⁻¹ (298 K). While we expect to still add a few concluding touches (which may slightly change the final value), the current⁸ ATcT value appears to be settling at $\Delta_f H^\circ_{298}(\text{OH}) = 8.96 \pm 0.01$ kcal mol⁻¹. It should be, however, noted that as of this time there is no direct measurement of D₀(OH) with sufficient accuracy (± 2 cm⁻¹ or better would help), and thus the enthalpy of formation of OH is implicitly dependent on some fundamental non-gas phase thermochemistry, such as calorimetric determinations of the enthalpy of formation of H₂O, the enthalpy of vaporization of liquid water to ideal-gas water, etc. The latter, for example, depends on the proper characterization of the real vs. ideal properties of gas-phase water, which in turn depend on the correct knowledge of the role of water dimers (and potentially of higher water clusters as well). In general, the problem encountered with some of the “core” thermochemical measurements is that they have not been ever repeated with competitive accuracy, and, at the same time, the topology of the surrounding TN does not always offer effective ways to close independent alternative thermochemical cycles. We are thus currently trying to utilize the recently developed scientific formulation of the equation of state of water (IAPWS-95, Wagner and Pruss⁹) to extract a corroborative value for $\Delta_{\text{vap}} H^\circ(\text{H}_2\text{O})$, as well as to determine independently the thermochemical properties of water dimer. This exploration of vaporization processes should also give us some valuable general insights on the potential importance (or lack thereof) of effects ranging from cluster formation to outright condensation (as well as other non-ideal behavior) in high-pressure combustion processes.

Early ATcT results for another important reactive species, HO₂, have been already published¹⁰, and the most recent^{8,11} (and further improved) value is $\Delta_f H^\circ_{298}(\text{HO}_2) = 2.92 \pm 0.04$ kcal mol⁻¹. In conjunction with the finalization of the O/H species we have not only determined the enthalpies of formation of a number of stable and ephemeral species of this group, but we have also determined¹¹ highly accurate values for a

number of other important properties, such as proton affinities and gas-phase basicities, viz. $PA(O_2) = 100.87 \pm 0.03 \text{ kcal mol}^{-1}$, $GB(O_2) = 95.06 \pm 0.03 \text{ kcal mol}^{-1}$, $PA(H_2) = 101.18 \pm 0.01 \text{ kcal mol}^{-1}$, $GB(H_2) = 94.64 \pm 0.01 \text{ kcal mol}^{-1}$ (which determine very accurately the endothermicity and exergonicity of the important proton-exchange reaction $H_3^+ + O_2 \rightarrow H_2 + HO_2^+$), $PA(O) = 116.17 \pm 0.01 \text{ kcal mol}^{-1}$, etc.

Of all the O/H species that we have so far incorporated in C(A)TN, the one that continuously keeps eluding us is HOOO. For this species it is, in fact, presently even unclear which conformer (*cis* or *trans*) is more stable, yet alone what would be a reliable value for its enthalpy of formation. The experimental data are very scarce and inconsistent, and computational studies even at relatively high level of accuracy appear to be equally inconsistent. (One can make analogous statement about the related cation, HOOO⁺.) With respect to this potentially quite relevant intermediate, matters are unlikely to get settled until there appear several (hopefully mutually consistent) state-of-the-art experimental and theoretical studies.

Building upon our recent progress in improving essential NO_x species^{8,10} (which in turn builds upon the improvements on the thermochemistry of the ‘key’ N atom that were based on a recent collaborative experimental determination¹² involving C.-Y. Ng, UC Davis), we have now made significant progress toward improving the thermochemistry of a number of NO_y species. This effort also resulted in significantly improving the thermochemistry NH_n species. The latter results, together with some of the new results on the NO_y species, are currently being used in a collaborative effort that includes the theorists (S. J. Klippenstein, L. B. Harding) and kineticists (J. V. Michael) in the Argonne group.

In parallel, we have expanded our prior effort on the thermochemistry of the CH_n species, which depend critically not only on species from the H/O manifold, but also on the value for C atom. The latter thermochemical quantity is not only a pivoting peg influencing the TN interdependencies toward more complex carbon-containing species, but it directly affects the results of state-of-the-art electronic structure theories (which, in order to convert computed electronic energies into thermochemical quantities depend either directly on its value, or, alternatively, on experimental values of *several* more complex carbon-containing species). The thermochemistry of C atom crucially depends on the correct value for the bond dissociation energy of CO, which we have previously found – via elaborate ATcT analyses – to be off. We believe that we are now on the path of completely resolving this problem by utilizing new experimental data (again in collaboration with C.-Y. Ng). This has allowed us to start addressing the thermochemistry of more complex carbon-containing species, such as radicals and stable species resulting from successive bond-dissociation processes of methanol and ethanol (both of which are extremely important as alternative fuels). Thus, we now believe that we have nearly completed the thermochemistry of the most prominent CH_nO species, and have made considerable progress toward establishing accurate thermochemistry of several C₂H_nO species.

Future Plans

Future plans of this program pivot around further developments and expansive use of Active Thermochemical Tables, providing accurate thermochemistry, and driving targeted theoretical and laboratory experimental investigation of radicals and transient species that are intimately related to combustion processes. The most pressing task for the forthcoming period is to continue the effort toward disseminating the ATcT results. One prerequisite is to have the related thermochemistry converge to a stable, “release quality” value, and we intend to continue expanding the number of species that belong to this category. Another prerequisite is the continuation of the current effort on designing and producing an entirely computer-generated ATcT web site that will be populated by “release quality” results automatically by a suitable post-processing step in ATcT. An essential feature of such web site is that it needs to be produced without physically retyping any values (which would be a sure recipe for disaster) and that it should contain sufficient background information to provide an extensive pedigree tree for any recommended value. Another design desideratum of the web site is to automatically and permanently archive (with full access) all previously published versions of web-exposed ATcT results.

This work is supported by the U.S. Department of Energy, Office of Basic Energy Sciences, Division of Chemical Sciences, Geosciences, and Biosciences, under Contract No. DE-AC02-06CH11357.

References

- ¹ B. Ruscic, R. E. Pinzon, M. L. Morton, G. von Laszewski, S. Bittner, S. G. Nijsure, K. A. Amin, M. Minkoff, and A. F. Wagner, *J. Phys. Chem. A* **108**, 9979 (2004)
- ² B. Ruscic, R. E. Pinzon, G. von Laszewski, D. Kodeboyina, A. Burcat, D. Leahy, D. Montoya, and A. F. Wagner, *J. Phys. Conf. Ser.* **16**, 561 (2005)
- ³ B. Ruscic, "Active Thermochemical Tables", in *2005 Yearbook of the McGraw-Hill Encyclopedia of Science and Technology*, pp. 3–7, McGraw-Hill, New York (2004)
- ⁴ B. Ruscic, A. F. Wagner, L. B. Harding, R. L. Asher, D. Feller, D. A. Dixon, K. A. Peterson, Y. Song, X. Qian, C.-Y. Ng, J. Liu, W. Chen, and D. W. Schwenke, *J. Phys. Chem. A* **106**, 2727 (2002)
- ⁵ B. Ruscic, D. Feller, D. A. Dixon, K. A. Peterson, L. B. Harding, R. L. Asher, and A. F. Wagner, *J. Phys. Chem. A* **105**, 1 (2001)
- ⁶ L. V. Gurvich, I. V. Veyts, and C. B. Alcock, "Thermodynamic Properties of Individual Substances", Vol. 1, Parts 1 and 2, Hemisphere, New York, 1989
- ⁷ B. Ruscic, R. E. Pinzon, M. L. Morton, N. K. Srinivasan, M.-C. Su, J. W. Sutherland, and J. V. Michael, *J. Phys. Chem. A* **110**, 6592 (2006)
- ⁸ B. Ruscic, unpublished result using ATcT (Ref. 1), based on C(A)TN ver. 1.074.
- ⁹ W. Wagner and A. Pruss, *J. Phys. Chem. Ref. Data* **31**, 387 (2002)
- ¹⁰ B. Ruscic, R. E. Pinzon, M. L. Morton, N. K. Srinivasan, M.-C. Su, J. W. Sutherland, and J. V. Michael, *J. Phys. Chem. A* **110**, 6592 (2006)
- ¹¹ S. L. Widicus Weaver, D. E. Woon, B. Ruscic, and B. J. McCall, *Astrophys. J.*, in press (2009)
- ¹² X. Tang, Y. Hou, C. Y. Ng, and B. Ruscic, *J. Chem. Phys.* **123**, 074330/1-7 (2005)

Publications resulting from DOE sponsored research (2007 - present)

- *Unimolecular Thermal Fragmentation of ortho-Benzyne*, X. Zhang, A. T. Maccarone, M. R. Nimlos, S. Kato, V. M. Bierbaum, B. K. Carpenter, G. B. Ellison, B. Ruscic, A. C. Simmonett, W. D. Allen, and H. F. Schaefer III, *J. Chem. Phys.* **126**, 044312/1-20 (2007).
- *Benchmark Atomization Energy of Ethane: Importance of Accurate Zero-point Vibrational Energies and Diagonal Born-Oppenheimer Corrections for a 'Simple' Organic Molecule*, A. Karton, B. Ruscic, and J. M. L. Martin, *J. Mol. Struct. (Theochem)* **811**, 345-353 (2007).
- *Kinetics of the Reaction of Methyl Radical with Hydroxyl Radical and Methanol Decomposition*, A. W. Jasper, S. J. Klippenstein, L. B. Harding, and B. Ruscic, *J. Phys. Chem. A* **111**, 3932-3950 (2007).
- *Portal-based Knowledge Environment for Collaborative Science*, K. Schuchardt, C. Pancerella, L. A. Rahn, B. Didier, D. Kodeboyina, D. Leahy, J. D. Myers, O. O. Oluwole, W. Pitz, B. Ruscic, J. Song, G. von Laszewski, and C. Yang, *Concurrency Computat.: Pract. Exper.* **19**, 1703-1716 (2007).
- *HEAT: High Accuracy Extrapolated ab initio Thermochemistry. III. Additional Improvements and Overview*, M. E. Harding, J. Vazquez, B. Ruscic, A. K. Wilson, J. Gauss, and J. F. Stanton, *J. Chem. Phys.* **128**, 114111/1-15 (2008).
- *Accurate ab initio Computation of Thermochemical Data for C₃H_x (x = 0,...,4) Species*, J. Aguilera-Iparraguirre, A. D. Boese, W. Klopper, and B. Ruscic, *Chem. Phys.* **346**, 56-68 (2008).
- *Atomization Energies from Coupled-Cluster Calculations Augmented with Explicitly-Correlated Perturbation Theory*, W. Klopper, B. Ruscic, D. P. Tew, F. A. Bischoff, and S. Wolfsegger, *Chem. Phys.* **356**, 14-24 (2009).
- *Is HO₂⁺ a Detectable Interstellar Molecule?*, S. L. Widicus Weaver, D. E. Woon, B. Ruscic, and B. J. McCall, *Astrophys. J.*, in press (2009).

Theoretical Studies of Elementary Hydrocarbon Species and Their Reactions

Henry F. Schaefer III and Wesley D. Allen
Center for Computational Chemistry
University of Georgia, Athens, GA 30602-2525
E-mail: hfs@uga.edu and wdallen@uga.edu; Phone: (706) 542-2067

Explicitly Correlated R12 Methods for Radicals

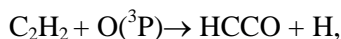
Quantum mechanical wavefunction methods ideally seek the correlation energy in a complete basis set (CBS). Unfortunately, conventional correlation methods using orbital basis sets converge slowly. In standard extrapolation schemes the residual error only decays as n^{-3} , where n is the cardinal number of a Dunning-type cc-pVnZ basis set. Beginning with a cc-pVDZ basis set, decreasing the error one order of magnitude typically requires a cc-pV5Z basis. For second-order perturbation theory (MP2), which scales as $N_{\text{occ}}N^4$ in the number of occupied (N_{occ}) and total (N) orbitals, the computational time would be more than six hundred fold larger! In general, the correlation energy error only decays as $t^{1/4}$ in the total computational time, clearly demonstrating a need for methods that accelerate basis set convergence. The slow convergence of correlated methods is now understood as the inability of one-particle basis sets to treat the coalescence region between two electrons. Because of the Coulomb singularity in the Hamiltonian, the exact wavefunction must have a cusp and corresponding depletion of electron density (Coulomb hole) near $r_{12}=0$.

Two-particle basis functions that depend explicitly on the interelectronic distance, r_{12} , can effectively describe the cusp region without large orbital basis sets. Numerous explicitly correlated methods that incorporate r_{12} -dependent terms have therefore been developed, especially the R12 methods originally introduced by Kutzelnigg and Klopper. Unfortunately, inclusion of r_{12} dependent terms in the basis set results in a large number of difficult 3-electron and 4-electron integrals that restrict computations to small molecules if no additional approximations are introduced. In R12 methods, these difficult integrals are avoided through a resolution of the identity (RI) approximation. The numerous, many-electron integrals are evaluated as sums over products of two-electron integrals computed in an RI basis, greatly reducing the number and complexity of the integrals that must be computed.

We have recently completed the development of an explicitly correlated ZAPT2 theory for high-spin open-shell states and have implemented it within the freely available Massively Parallel Quantum Chemistry (MPQC) package. In contrast to other open-shell perturbation theories, the ZAPT2 equations can be solved non-iteratively with only a single integral transformation. In extending the method to coupled-cluster, the symmetry of the ZAPT amplitudes should provide even greater speedups. Even with modest aug-cc-pVTZ basis sets, the ZAPT2-R12 results outperform conventional methods with the aug-cc-pV6Z basis. In the O₂, N₂, and NO₂ examples, ZAPT2-R12/aug-cc-pVTZ obtains atomization energies within 1 kJ mol⁻¹ of the complete basis set (CBS) limit of the second-order correlation energy; in contrast, the corresponding conventional computations never come within 2.5 kJ mol⁻¹ of the CBS limit even with the massive aug-cc-pV6Z basis set. If basis sets larger than aug-cc-pVDZ are to be used, we have also presented a reduced RI approach for approximation C of explicit correlation methods, which greatly reduces the cost of the integral transformation. In the context of high accuracy thermochemistry, the R12 results are generally competitive with conventional complete basis set extrapolations. For dissociation reactions, the basis imbalance between reactants and products leads to basis set superposition errors. Counterpoise corrections may therefore be useful in accelerating basis set convergence. The intended application of the ZAPT2-R12 method is to high-spin, open-shell radicals. In particular, computing accurate thermochemistry for the numerous radicals occurring in hydrocarbon combustion would benefit from methods that minimize basis set errors as efficiently as possible. For the R12 corrections to be most useful in this regard, however, it must be more accurate than conventional extrapolation techniques. With the development of R12 basis sets, however, R12 extrapolations should provide accuracy competitive with the "gold standard" cc-pV5Z/cc-pV6Z extrapolation at a fraction of the cost.

The Ketenyl Radical HCCO

The ketenyl (HCCO) radical was long ago recognized as a prevalent component of hydrocarbon flames and is thought to have astrophysical significance as well. Thus, it has been the subject of numerous kinetic, spectroscopic, and theoretical investigations. The HCCO radical is produced as an intermediate during acetylene combustion in flames by the reaction



which has been studied extensively. The emission of NO_x species from combustion systems is recognized as a contributing factor to acid rain and smog formation, and much research has been dedicated to reducing these emissions. One such strategy is reburning, in which the reduction of HCCO by nitric oxide features prominently. In research just submitted for publication, the geometry and barrier to linearity for the HCCO radical have been determined by high level *ab initio* quantum chemical methods. A full quartic force field has also been computed to determine HCCO fundamental frequencies that agree satisfactorily with the three fundamentals available from experiment; the reported force field can be used to predict myriad spectroscopic properties accurately and will be of utility in the experimental characterization of HCCO isotopologues.

The Problematic $\text{C}_2\text{H}_4 + \text{F}_2$ Reaction Barrier

The reaction of F_2 with the simplest alkene (C_2H_4) is an archetype for the fluorination of organic compounds. Very recent crossed molecular beam studies of this reaction show that the fluoroethyl radical and fluorine atom are the exclusive products for collision energies up to at least 11 kcal mol⁻¹. Prompted by these experiments, we have investigated the $\text{C}_2\text{H}_4 + \text{F}_2$ reaction by state-of-the-art *ab initio* computations. Laborious geometry optimizations and complete harmonic vibrational analyses were executed at the CCSD(T)/aug-cc-pVQZ level for the reactants, products, and intervening transition state. The reaction energy and barrier height were then subjected to computationally intensive focal point analyses in order to converge toward the *ab initio* limits. The largest explicit computations involved the coupled-cluster CCSD(T)/aug-cc-pV5Z and CCSDT(Q)/cc-pVDZ techniques, the latter method pushing the envelope of current capabilities by explicitly treating connected quadruple excitations. To ensure a comprehensive theoretical treatment, auxiliary core correlation, DBOC, and relativistic corrections were also included. As a byproduct of our work, a new $\Delta_f H_{298}^\circ(\text{CH}_2\text{CH}_2\text{F}) = -13.4 \pm 0.2$ kcal mol⁻¹ was determined, which has much greater precision than previous values.

We have established that the transition state for the $\text{C}_2\text{H}_4 + \text{F}_2$ reaction has a C_s rather than a C_{2v} structure. The geometry of the C_2H_4 group in the TS is rather close to that of free ethylene. The final 0 K reaction barrier and enthalpy from our focal point analyses are 7.98 kcal mol⁻¹ and -7.39 kcal mol⁻¹, respectively. Adopting our new $\Delta_f H_{298}^\circ(\text{CH}_2\text{CH}_2\text{F})$ and literature values for C_2H_4 and F as reference enthalpies, our reaction energy is confirmed to be accurate to 0.2-0.3 kcal mol⁻¹. In contrast, our final theoretical barrier is 2.5 kcal mol⁻¹ higher than the barrier (5.5 ± 0.5 kcal mol⁻¹) deduced from the crossed molecular beam experiments.

The perplexing disparity between the state-of-the-art theoretical and experimental barriers for the $\text{C}_2\text{H}_4 + \text{F}_2$ reaction elevates this system as an important testing ground for chemical physics. In research just released, the reaction of F_2 with propene has also been investigated in crossed molecular beam experiments. As in the ethylene case, the measured threshold (2.4 ± 0.3 kcal mol⁻¹) for the production of $\text{C}_3\text{H}_6\text{F} + \text{F}$ is 2-3 kcal mol⁻¹ lower in energy than the barrier height predicted by CCSD(T) theory. Thus, the barriers for alkene + F_2 reactions may pose a general problem to be resolved between theory and experiment.

The issues for theory in predicting these barriers are apparent from our study. The focal point analyses show that there are large oscillations in the electron correlation series for the $\text{C}_2\text{H}_4 + \text{F}_2$ reaction barrier, despite the lack of much multireference character in the transition state. While improving the correlation treatment from CCSD to CCSD(T) lowers the barrier by 12.0 kcal mol⁻¹, further extension to

the CCSDT(Q) level produces a change of only 0.2 mol^{-1} . The latter observation indicates good convergence of the final result, although due caution is warranted. Full CCSDTQ and CCSDTQ(P) computations are currently not feasible for $\text{C}_2\text{H}_4 + \text{F}_2$ if a reasonable basis set is used. Moreover, the oscillatory pattern of the correlation series suggests that a full CCSDTQ computation would actually increase the reaction barrier above $8.0 \text{ kcal mol}^{-1}$. In brief, if the actual barrier for the $\text{C}_2\text{H}_4 + \text{F}_2$ reaction is indeed near the experimental threshold, surprising aspects of the coupled cluster series remain to be discovered. The interplay between theory and experiment witnessed in the classic $\text{F} + \text{H}_2$ problem could well be repeated in a next generation of chemical complexity.

Hydroxymethylene: A Tunneling Phenomenon

Our research on the identification of HCOH was published in the journal *Nature* (Vol. **453**, p. 906-909). In essentially perfect agreement with experiment, HCOH is predicted to have a half life of ca. 2 hours. Under the same conditions, the predicted lifetime of HCOD is greater than 1200 years! The discovery of the tunneling mechanism of hydroxymethylene was met with acclaim in several prestigious scientific publications. *Nature* (Vol. **453**, p. 862) highlighted the work in a viewpoint article entitled "Cool it, Baby". In *Chemistry World* (July 2008, p. 23), the news publication of the Royal Society of Chemistry, the research was described in a piece entitled: "Houdini Molecule Escapes Energy Trap. Molecule Hunters Capture Elusive Hydroxymethylene - Only to see it Get Away". In *Angewandte Chemie* (Vol. **47**, p. 2), the most respected chemistry journal in Europe, a Highlight was published with another eye-catching slant: "Hydroxycarbene: Watching a Molecular Mole at Work". Our hydroxymethylene research was also described in a Highlight published in *ChemPhysChem* **9**, 1829 (2008), with the theme of "Tamed Tigers". Finally, the work was hailed in the *Chemical & Engineering News* publication (June 16, 2008) of the American Chemical Society and even the *Frankfurter Allgemeine Zeitung* (the *New York Times* of Germany).

Publications Supported by the U. S. Department of Energy 2006-2009

A total of 25 publications resulted from DOE funding during the current grant period:

1. B. N. Papas and H. F. Schaefer, "Concerning the Precision of Standard Density Functional Programs: GAUSSIAN, MOLPRO, NWCHEM, QCHEM, and GAMESS," *J. Mol. Struct.* **768**, 175-181 (2006).
2. X. Zhang, Q. Li, J. B. Ingels, A. C. Simmonett, S. E. Wheeler, Y. Xie, R. B. King, H. F. Schaefer, and F. A. Cotton, "Remarkable Electron Accepting Properties of the Simplest Benzenoid Cyanocarbons: Hexacyanobenzene, Octacyanonaphthalene, and Decacyanoanthracene," *J. Chem. Soc. (London) Chem. Comm.* 758-760 (2006).
3. N. C. Handy, S. Carter, Y. Yamaguchi, S. Li, and H. F. Schaefer, "Rovibrational Energy Levels for the Electronic Ground State of AlOH," *Chem. Phys. Lett.* **427**, 14-17 (2006).
4. D. Moran, A. C. Simmonett, F. E. Leach, W. D. Allen, P. v. R. Schleyer, and H. F. Schaefer, "Popular Theoretical Methods Predict Benzene and Arenes to be Nonplanar," *J. Am. Chem. Soc.* **128**, 9342-9343 (2006), communication. See highlight in Editor's Choice, *Science* **313**, 149 (July 14, 2006 issue).
5. V. Kasalová, W. D. Allen, H. F. Schaefer, E. D. Pillai, and M. A. Duncan, "Model Systems for Probing Metal Cation Hydration," Roger E. Miller Memorial Issue, *J. Phys. Chem. A* **111**, 7599-7610 (2007).
6. X. Zhang, A. T. Maccarone, M. R. Nimlos, S. Kato, V. M. Bierbaum, G. B. Ellison, B. Ruscic, A. C. Simmonett, W. D. Allen, and H. F. Schaefer, "Unimolecular Thermal Fragmentation of *Ortho*-Benzene," *J. Chem. Phys.* **126**, 044312: 1-20 (2007).
7. S. E. Wheeler, K. A. Robertson, W. D. Allen, H. F. Schaefer, Y. J. Bomble, and J. F. Stanton, "Thermochemistry of Key Soot Formation Intermediates: C_3H_3 Isomers," *Jim Miller Festschrift, J. Phys. Chem. A* **111**, 3819-3830 (2007).

8. P. Bera, Y. Yamaguchi, and H. F. Schaefer, "The Low-Lying Quartet Electronic States of Nitrogen Dioxide," *J. Chem. Phys.* **127**, 174303: 1-12 (2007).
9. A. C. Simmonett, F. A. Evangelista, W. D. Allen, and H. F. Schaefer, "In Search of Definitive Signatures of the Elusive NCCO Radical," *J. Chem. Phys.* **127**, 014306: 1-9 (2007).
10. L. Belau, S. E. Wheeler, B. W. Ticknor, M. Ahmed, S. R. Leone, W. D. Allen, H. F. Schaefer, and M. A. Duncan, "Ionization Thresholds of Small Carbon Clusters: Tunable VUV Experiments and Theory," *J. Am. Chem. Soc.* **129**, 10229-10243 (2007).
11. S. E. Wheeler, W. D. Allen, and H. F. Schaefer, "On the Convergence of Z-Averaged Perturbation Theory (ZAPT)," *J. Chem. Phys.* **128**, 074107: 1-11 (2008).
12. J. J. Wilke, W. D. Allen, and H. F. Schaefer, "Establishment of the $C_2H_5 + O_2$ Reaction Mechanism: A Combustion Archetype," *J. Chem. Phys.* **128**, 074308: 1-9 (2008).
13. P. P. Bera, Y. Yamaguchi, H. F. Schaefer, and T. D. Crawford, "Born-Oppenheimer Symmetry Breaking in the \tilde{C}^{∞} State of NO_2 : Importance of Static and Dynamic Correlation Effects," *J. Phys. Chem. A* **112**, 2669-2676 (2008).
14. R. K. Sreeruttun, P. Ramasami, C. S. Wannere, A. C. Simmonett, and H. F. Schaefer, " π - and σ -Phenylethynyl Radicals and their Isomers *o*-, *m*-, and *p*-Ethynylphenyl: Structures, Energetics, and Electron Affinities," *J. Phys. Chem. A* **112**, 2838-2845 (2008).
15. S. Carter, N. C. Handy, Y. Yamaguchi, J. M. Turney, and H. F. Schaefer, "Vibrational Energy Levels for the Electronic Ground State of the Diazocarbene (CNN) Molecule," Raphael D. Levine Special Issue, *Molecular Physics* **106**, 357-366 (2008).
16. L. D. Speakman, J. M. Turney, and H. F. Schaefer, "Toward the Experimental Observation of Quartet States of the Ozone Radical Cation: Insights from Coupled Cluster Theory," *J. Chem. Phys.* **128**, 214302: 1-12 (2008).
17. P. R. Schreiner, H. P. Reisenauer, F. C. Pickard, A. C. Simmonett, W. D. Allen, E. Mátyus, and A. G. Császár, "Capture of Hydroxymethylene and Its Fast Disappearance through Tunnelling," *Nature*, **453**, 906-909 (2008). See commentaries and news articles on this work in *Nature* (Vol. 453, p. 862), *Chemistry World* (July 2008, p. 23), and *Angewandte Chemie* (Vol. 47, p. 2).
18. A. C. Simmonett, H. F. Schaefer, and W. D. Allen, "The Enthalpy of Formation and Anharmonic Force Field of Diacetylene," *J. Chem. Phys.* **130**, 044301: 1-10 (2009).
19. A. U. Sokolov, N. J. Stibrich, and H. F. Schaefer, "BO₃ Molecular Structures: Examples of the Importance of Electron Correlation", accepted, Rudolf Zahradnik Special Issue, *Collect. Czech Chem. Commun.* **73**, 1495-1508 (2008).
20. S. E. Wheeler, K. N. Houk, P. v. R. Schleyer, and W. D. Allen, "A Hierarchy of Homodesmotic Reactions," *J. Am. Chem. Soc.* **131**, 2547-2560 (2009).
21. Y. Yamaguchi and H. F. Schaefer, "Analytic Derivative Methods in Molecular Electronic Structure Theory and its Applications to Spectroscopy," in press, *Handbook of High Resolution Spectroscopy*, Editors M. Quack and F. Merkt (Wiley, Chichester, 2009).
22. N. J. Stibrich, A. C. Simmonett, B. N. Papas, H. F. Schaefer, and W. D. Allen, "Barrier to Linearity and Anharmonic Force Field of the Ketenyl Radical," *J. Phys. Chem. A*, submitted (2009).
23. H. Feng and W. D. Allen, "The Problematic $F_2 + C_2H_4$ Reaction Barrier," *J. Chem. Phys.*, submitted (2009).
24. J. J. Wilke, H. F. Schaefer, and W. D. Allen, "The Subtleties of ROHF References in R12 Methods: The Complete Basis Correlation Energy of Radicals with Explicitly Correlated Z-Averaged Perturbation Theory", *J. Chem. Phys.*, submitted (2009).
25. S. E. Wheeler and H. F. Schaefer, "Thermochemistry of the HOSO Radical, a Key Intermediate in Fossil Fuel Combustion", *J. Chem. Phys.*, submitted (2009).

Picosecond Nonlinear Optical Diagnostics

Thomas B. Settersten
Combustion Research Facility, Sandia National Laboratories
P.O. Box 969, MS 9055
Livermore, CA 94551-0969
tbsette@sandia.gov

Program Scope

This program focuses on the development of innovative laser-based detection strategies for important combustion radicals and the investigation of the fundamental physical and chemical processes that directly affect quantitative application of these techniques. These investigations include the study of fundamental spectroscopy, energy transfer, and photochemical processes. This aspect of the research is essential for the correct interpretation of diagnostic signals, enabling reliable comparisons of experimental data and detailed combustion models. Many of these investigations use custom-built tunable picosecond (ps) lasers, which enable efficient nonlinear excitation, provide high temporal resolution for pump/probe studies of collisional processes, and are amenable to detailed physical models of laser-molecule interactions. Although our work has been limited previously to systems at atmospheric or lower pressure, recent construction of high-pressure cells provides part of the necessary infrastructure for future development of spectroscopic approaches for high pressure.

Recent Progress

Multiplexed time-resolved picosecond CARS. Coherent Anti-Stokes Raman Spectroscopy (CARS) is a well developed technique for concentration and temperature measurement. By using broadband excitation of rovibrational Raman coherences and probing with a narrowband probe, the entire vibrational CARS spectrum can be recorded on a single shot. A similar “multiplexed” measurement of the pure-rotational spectrum is possible through Raman excitation via a single broadband laser. Unfortunately collisional line-mixing, non-resonant four-wave mixing, and resonant interference can restrict the utility of CARS at high pressures. Pure-rotational CARS is significantly less affected by line mixing than vibrational CARS. Non-resonant background, which only occurs when the pump, Stokes, and probe laser pulses are coincident, can be eliminated by delaying the probe pulse after the Raman coherence is generated by the pump and Stokes pulses.¹ Although this approach eliminates the unwanted coherent interference, it is still sensitive to collisions that occur during the probe delay. Not only do the collisions dephase the Raman coherences, thus reducing overall signal levels, but they reshape the signal spectrum. We collaborated with S. Roy (Wright Patterson AFB) to investigate collisional effects on vibrational CARS in flames and in heated gases at pressures of up to 10 bar. The results demonstrate clearly that J -dependent RET preferentially dephases the low- J coherences, causing delayed spectra to appear hotter. Furthermore, we also observe that high-temperature spectra are less sensitive to delay because of the weaker rotational-level dependence of RET at high J . In an ongoing collaboration with T. Seeger (Erlangen), we are studying collisional effects in pure-rotational CARS. Initial experiments investigated pressures of up to 6 bar. Results successfully demonstrate that the time-resolved approach can eliminate the resonant background from fuel molecules that prevents the use of this technique in many systems. An example of the interference posed by C_2H_4 and its elimination and recovery of a clean N_2 CARS spectrum via a time-delayed probe is presented in Fig. 1a. Coherence dephasing times were measured for N_2 , O_2 , CO_2 , CO , C_2H_2 , C_2H_4 , and C_3H_8 (Fig. 1b).

Photolytic generation of atomic hydrogen in flames. Atomic hydrogen plays a key role

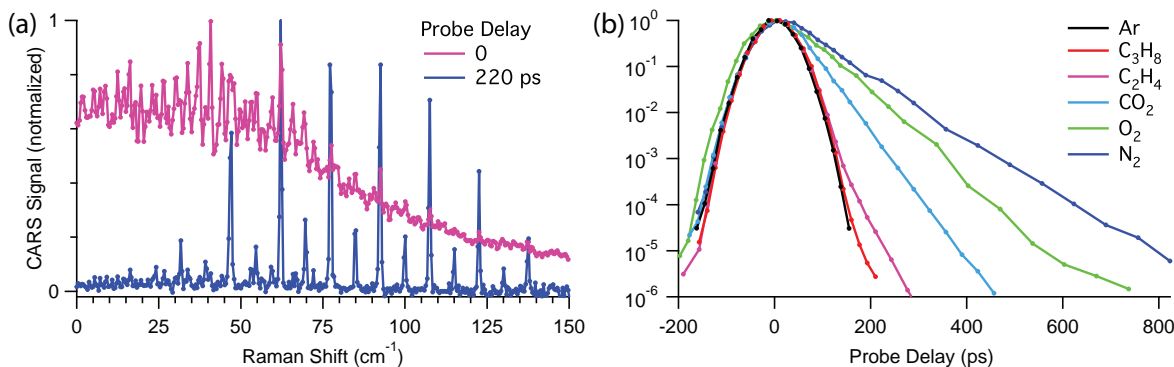


Figure 1: (a) Dual-broadband pure-rotational CARS spectra from a mixture of C_2H_4 and N_2 . The zero-delay spectrum contains a significant resonant contribution from C_2H_4 , which overwhelms the N_2 contribution and precludes an accurate spectral evaluation. The resonant fuel contribution and the non-resonant contribution to χ^3 are negligible for the 220-ps delay, and a clean N_2 spectrum is recovered. (b) Time-dependent signals (integrated spectra) for gases at 750 Torr and 294 K indicate that the dephasing of Raman coherences in fuel molecules is greater than three times more rapid than dephasing of Raman coherences N_2 molecules.

in ignition, flame propagation, and heat release in hydrocarbon combustion because of its high reactivity and diffusivity. Multi-photon laser-induced fluorescence (LIF) can be used for sensitive, spatially resolved detection of H in flames. The simplest approach employs two photons at 205 nm to excite $3s \ ^2\text{S}, 3d \ ^2\text{D} \leftarrow \leftarrow 1s \ ^2\text{S}$ transitions, which produces fluorescence at 656 nm ($n=3 \rightarrow n=2$). Prior work, however, demonstrates that this approach is prone to photolytic interference because two-photon-resonant excitation requires high-intensity UV laser pulses, which can readily photodissociate flame constituents with H as a product.² In collaboration with J.H. Frank (see abstract in this book), we studied this process via pump-probe experiments in a series of methane flames. A detuned, ns-duration, laser pulse photolytically produced atomic hydrogen under different flame conditions, and the photoproduct was probed using a weak, nonperturbing ps pulse and directly compared to nascent H in each flame. Analysis revealed two “classes” of photolytic precursors that pose significant interference in conventional two-photon-resonant laser-induced fluorescence imaging of atomic hydrogen in flames. Product precursors include water vapor and the hydroxyl radical. Transient precursors include methyl radical and acetylene. A photolytic interference model was developed and demonstrated excellent agreement with experimental results.³

Electronic-resonance-enhanced CARS. In collaboration with A. Patnaik, S. Roy, and J.R. Gord (Wright Patterson AFB) and R.P. Lucht (Purdue), we developed a non-perturbative density-matrix-based model for ERE-CARS that incorporates collisional effects of RET, electronic quenching, and electronic dephasing.⁴ Steady-state signal expressions predict that the integrated signal intensity scales as $\gamma_r^{-2}\gamma_{el}^{-2}$, where γ_r and γ_{el} are the dephasing rates for the Raman and electronic coherences, respectively. For nitric oxide, the Raman dephasing rate is primarily a result of inelastic RET collisions, whereas the electronic dephasing is primarily determined by elastic dephasing collisions. Although the ERE-CARS signal is very sensitive to the absolute collision rate (and, thus, to the pressure), we expect that the sensitivity to the chemical composition of the bath gas is weak because the available (limited) data generally indicate that both rates are only weakly dependent on collision partner. This behavior is in stark contrast to LIF, for example, where the signal scales inversely with the electronic quenching rate, which can vary dramatically with different collision partners. Numerical solutions demonstrate a significant reduction in the collision-rate dependence with saturation, but also reveal an additional probe-intensity-dependent dephasing of the Raman coherence. The significance of the latter effect is a direct result electronic-resonance enhancement of the probe interaction. The potentially strong dependence on RET and electronic dephasing rates

emphasizes the need for accurate data and models of the species and temperature dependencies of these processes for combustion-relevant conditions.

Six-wave mixing and Stark effects in atomic hydrogen. In a continuing collaboration with R.P. Lucht (Purdue), we have extended the density matrix theory for SWM from our previous model⁵ to include all relevant 6-photon pathways as well as the effects of hyperfine coherence. Line shapes for the H_α and the two-photon L_α transitions have been measured in flames. Results demonstrate dramatic effects of Stark broadening and shifting at practical experimental conditions. The numerical code should be completed and running on the CRF clusters by Summer 2009.

Collision-induced resonance in wave-mixing spectroscopy. In collaboration with A.P. Kouzov (St. Petersburg State University, Russia), we have developed a generalized quantum-mechanical treatment of collision-induced resonances in two-color resonant four-wave mixing spectroscopy.⁶ This formalism incorporates the relaxation (super)operator, which describes complete state-to-state transfer within a vibrational manifold in terms of the first three moments of the angular momentum distribution. A perturbation analysis yields a simplified picture that enables determination of the the relaxation matrix elements from time-resolved four-wave-mixing signals.⁷

Future Plans

Picosecond time-resolved CARS. Based on the success of our recent experiments, we will use ps time-resolved CARS to measure temperatures in sooting flames (see H.A. Michelsen's abstract in this book). In addition, we will characterize time-dependent spectra for a range of collisional environments in heated pressure cells. Currently, we have fielded a 30-bar, room-temperature cell and expect to implement a 15-bar, 1000-K cell in Summer 2009. These experiments will be used to develop a time-dependent CARS model that will enable reliable and accurate extraction of temperature from time-delayed spectra. Initial experiments that will focus on N_2 will test collision models for common collision partners. To further develop the collision models, we have proposed a multiplexed RET diagnostic, which will enable direct measurement of state-to-state RET rates for an entire rotational manifold. This approach relies on our independently tunable, transform-limited, picosecond lasers to excite individual rotational coherences on a time scale that is short compared to dephasing. A third delayed laser pulse will simultaneously probe the directly excited coherence as well as all collisionally coupled coherences. Because the signals from all Raman coherences are simultaneously recorded in a single spectrum, their relative calibration is automatic. By collecting time-dependent spectra, we will map-out total relaxation rates as well as state-to-state rates for the entire manifold.

Photofragment-LIF detection of H_2O_2 . We will continue experiments aimed at developing an imaging diagnostic for H_2O_2 at elevated pressures. We will directly compare single-step and two-step approaches for pressures up to 10 bar. Immediate work will quantify OH(A) yields using multi-photon excitation at 266 and 355 nm. Because excitation at 355 nm will simultaneously excite H_2O_2 photofragment LIF and LIF from CH_2O , we will investigate the possibility of a two-detector, single-laser, imaging diagnostic for these two species, which are important in low- and intermediate-temperature combustion chemistry. Subsequent experiments will investigate the two-step process, in which a second laser probes the OH(X) photoproduct via PLIF. Because ps photodissociation of H_2O_2 results in vibrationless products in a rotationally hot distribution, we will evaluate the efficacy of probing the prompt rotationally hot product distribution with a ps laser to discriminate against background (thermalized) OH in the sample. A further refinement of the technique uses a dual-image camera and two OH lasers to measure both the nascent OH before the photodissociation pulse and the nascent-plus-photoproduct OH following the photodissociation pulse.

Ignition Experiments using ps H-atom LIF. Based on the success of our ps two-photon LIF imaging of H, we plan to continue collaboration with J. H. Frank to apply this technique to study preferential diffusion in edge flames during extinction and re-ignition in pulsed counterflows. Studies of H-atom preferential diffusion in flames with different Lewis numbers are also envisioned.

CO imaging. We will investigate a two-photon scheme proposed by V. Sick to image CO in high-pressure systems. The approach relies on excitation to the *A* state, which permits red-shifting the excitation wavelength from 230 nm. The temperature- and species-dependent quenching cross sections of the fluorescing states will be characterized at Sandia using time-resolved ps LIF. This work will involve an extended visit by Sick and a graduate student.

References

- [1] S. Roy, T. R. Meyer, J. R. Gord, *Appl. Phys. Lett.* **87**, 264103 (2005).
- [2] W. D. Kulatilaka, B. D. Patterson, J. H. Frank, T. B. Settersten, *Appl. Opt.* **47**(26), 4672 (2008).
- [3] W. D. Kulatilaka, J. H. Frank, B. D. Patterson, T. B. Settersten, "Analysis of 205-nm photolytic production of atomic hydrogen in methane flames," *Appl. Phys. B.*, in press (2009).
- [4] A. Patnaik, S. Roy, R. Lucht, J. Gord, T.B. Settersten, "Effects of collisions on electronic-resonance-enhanced coherent anti-Stokes Raman scattering of nitric oxide," *J. Chem. Phys.*, in press (2009).
- [5] W. D. Kulatilaka, R. P. Lucht, S. Roy, J. R. Gord, T. B. Settersten, *Appl. Opt.* **46**(19), 3921 (2007).
- [6] X. Chen, T. B. Settersten, A. P. Kouzov, "State- and time-resolved rotational relaxation signatures in two-color resonant four-wave mixing spectra," *J. Raman. Spectrosc.*, DOI: 10.1002/jrs.2229 (2009).
- [7] X. Chen, T. B. Settersten, *Appl. Opt.* **46**(19), 3911 (2007).

BES-Supported Publications (2007-present)

- A. K. Patnaik, S. Roy, R. P. Lucht, J. R. Gord, T. B. Settersten, "Effects of collisions on electronic-resonance-enhanced coherent anti-Stokes Raman scattering of nitric oxide," *J. Chem. Phys.*, in press (2009).
- T. B. Settersten, B. D. Patterson, C. Carter, "Collisional quenching of NO $A^2\Sigma^+(v'=0)$ between 125 and 300 K," *J. Chem. Phys.*, submitted (2009).
- W. D. Kulatilaka, J. H. Frank, B. D. Patterson, T. B. Settersten, "Analysis of 205-nm photolytic production of atomic hydrogen in methane flames," *Appl. Phys. B*, DOI: 10.1007/s00340-009-3474-3 (2009).
- X. Chen, T. B. Settersten, A. P. Kouzov, "State- and time-resolved rotational relaxation signatures in two-color resonant four-wave mixing spectra," *J. Raman Spectrosc.*, DOI: 10.1002/jrs.2229 (2009).
- R. W. Schefer, W. D. Kulatilaka, B. D. Patterson, T. B. Settersten, "Visible emission in hydrogen flames," *Combust. Flame*, DOI: 10.1016/j.combustflame.2009.01.011 (2009).
- V. Ebert, T. B. Settersten, D. K. Killinger, "Laser Applications to Chemical, Security, and Environmental Analysis: introduction to the feature issue," *Appl. Opt.* **48**(4), 1 (2009).
- W. D. Kulatilaka, J. H. Frank, T. B. Settersten, "Interference-free two-photon LIF imaging of atomic hydrogen in flames using picosecond excitation," *Proc. Combust. Inst.* **32**, 955 (2009).
- X. Chen, T. B. Settersten, P. P. Radi, A.P. Kouzov, "Two-color resonant four-wave mixing spectroscopy: New perspectives for direct studies of collisional state-to-state transfer," *Spectral Line Shapes* **15**, 128 (2008).
- W. D. Kulatilaka, B. D. Patterson, J. H. Frank, T. B. Settersten, "Comparison of nanosecond and picosecond excitation for interference-free two-photon laser-induced fluorescence detection of atomic hydrogen in flames," *Appl. Opt.* **47**(26), 4672 (2008).
- X. Chen, T. B. Settersten, "Investigation of OH X $^2\Pi$ collisional kinetics in a flame using picosecond two-color resonant four-wave-mixing spectroscopy," *Appl. Opt.* **46**(19), 3911 (2007).
- W. D. Kulatilaka, R. P. Lucht, S. Roy, J. R. Gord, T. B. Settersten, "Detection of atomic hydrogen in flames using picosecond two-color two-photon-resonant six-wave-mixing spectroscopy," *Appl. Opt.* **46**(19), 3921 (2007).
- C. A. Bauer, T. V. Timofeeva, T. B. Settersten, B. D. Patterson, V. H. Liu, B. A. Simmons, M. D. Allendorf, "Influence of Connectivity and Porosity on Ligand-Based Luminescence in Zinc Metal-Organic Frameworks," *J. Am. Chem. Soc.* **129**(22), 7136 (2007).

Theoretical Studies of Potential Energy Surfaces and Computational Methods

Ron Shepard

Chemical Sciences and Engineering Division,
Argonne National Laboratory, Argonne, IL 60439
[email: shepard@tcg.anl.gov]

Program Scope: This project involves the development, implementation, and application of theoretical methods for the calculation and characterization of potential energy surfaces (PES) involving molecular species that occur in hydrocarbon combustion. These potential energy surfaces require an accurate and balanced treatment of reactants, intermediates, and products. This difficult challenge is met with general multiconfiguration self-consistent field (MCSCF) and multireference single- and double-excitation configuration interaction (MR-SDCI) methods. In contrast to the more common single-reference electronic structure methods, this approach is capable of describing accurately molecular systems that are highly distorted away from their equilibrium geometries, including reactant, fragment, and transition-state geometries, and of describing regions of the potential surface that are associated with electronic wave functions of widely varying nature. The MCSCF reference wave functions are designed to be sufficiently flexible to describe qualitatively the changes in the electronic structure over the broad range of molecular geometries of interest. The necessary mixing of ionic, covalent, and Rydberg contributions, along with the appropriate treatment of the different electron-spin components (e.g. closed shell, high-spin open-shell, low-spin open shell, radical, diradical, etc.) of the wave functions are treated correctly at this level. Further treatment of electron correlation effects is included using large-scale multireference CI wave functions, particularly including the single and double excitations relative to the MCSCF reference space. This leads to the most flexible and accurate large-scale MR-SDCI wave functions that have been used to date in global PES studies.

Recent Progress: ELECTRONIC STRUCTURE CODE MAINTENANCE, DEVELOPMENT, AND APPLICATIONS: A major component of this project is the development and maintenance of the COLUMBUS Program System. The COLUMBUS Program System computes MCSCF and MR-SDCI wave functions, MR-ACPF (averaged coupled-pair functional) energies, MR-AQCC (averaged quadratic coupled cluster) energies, spin-orbit CI energies, analytic energy gradients, and nonadiabatic coupling. Geometry optimizations to equilibrium and saddle-point structures can be done automatically for both ground and excited electronic states. The COLUMBUS Program System is maintained and developed collaboratively with several researchers including Isaiah Shavitt (University of Illinois), Russell M. Pitzer (Ohio State University), Thomas Mueller (Central Institute for Applied Mathematics, Juelich, Germany), and Hans Lischka (University of Vienna, Austria). The nonadiabatic coupling and geometry optimizations for conical intersections is done in collaboration with David R. Yarkony (Johns Hopkins). The distributed development effort and software coordination uses an svn repository of source code. The parallel sections of the code are based on the single-program multiple-data (SPMD) programming model with explicit message passing using the portable MPI library, and the portable Global Array Library (distributed from PNNL) is used for data distribution. The next major release of the COLUMBUS codes will begin to incorporate the newer language features of F90/F95. This will facilitate future development and maintenance effort.

GRAPHICALLY CONTRACTED FUNCTION METHOD: We have recently developed a novel expansion basis for electronic wave functions [*J. Phys. Chem. A* **109**, 11629 (2005)]. In this approach, the wave function is written as a linear combination of *graphically contracted functions*

This work was performed under the auspices of the Office of Basic Energy Sciences, Division of Chemical Sciences, Geosciences, and Biosciences, U.S. Department of Energy, under contract number DE-AC02-06CH11357.

(GCFs), and each GCF in turn is formally equivalent to a linear combination of configuration state functions (CSFs) that comprise an underlying linear expansion space of dimension N_{csf} . The CSF coefficients that define the GCFs are nonlinear functions of a smaller number of variables $N_{\phi} \ll N_{\text{csf}}$. GCF expansions with 10 to 20 basis functions can approach the full-CI PES to within chemical accuracy (1 kcal/mole or better) [*Int. J. Quantum Chem.* **107**, 3203 (2007)]. The method is formulated in terms of spin-eigenfunctions using the Graphical Unitary Group Approach (GUGA) of Shavitt, and consequently it does not suffer from spin contamination or spin instability.

Our new method is characterized by several important features. First, open-shell spin-eigenfunctions are included in the wave function expansions. This allows our new method to be used for the reactions that are important to combustion chemistry (i.e. involving radicals and other open-shell electronic states) without introducing spin contamination. Second, we place no intrinsic restrictions on the orbital occupations, so our GCFs are not restricted to only geminals or to other preselected molecular fragments, and there are no artificial excitation-level or occupation restrictions with respect to a reference function or reference space. Third, we use linear combinations of N_{GCF} basis functions rather than a single expansion term. This allows our method to be used for both ground and excited electronic states, the increased wave function flexibility leads to more accurate wave functions, and it will allow the computation of transition moments, nonadiabatic coupling, and other properties that at present can only be computed reliably with MCSCF and MRCI approaches.

Efficient procedures to compute hamiltonian matrix elements and reduced one- and two-particle density matrices for this nonlinear expansion have been developed [*J. Phys. Chem. A* **110**, 8880 (2006)]. The effort required to construct an individual hamiltonian matrix element between two GCFs $H_{MN} = \langle M | \hat{H} | N \rangle$ scales as $\mathcal{O}(\beta n^4)$ for a wave function expanded in n molecular orbitals. The prefactor β depends on the complexity of the underlying Shavitt Graph and scales between N^0 and N^2 for N electrons. The corresponding metric matrix element $S_{MN} = \langle M | N \rangle$ requires effort that scales as $\mathcal{O}(\beta n)$, the one-particle transition density \mathbf{D}^{MN} requires $\mathcal{O}(\beta n^2)$ effort, the two-particle density \mathbf{d}^{MN} requires $\mathcal{O}(\beta n^4)$ effort. There is no component of the effort or storage for matrix element computation or wave function optimization that scales as N_{csf} . Timings with our initial implementation of this method are very promising (see Fig. 1). A hamiltonian matrix element involving GCFs corresponding to an underlying linear expansion space with dimension $N_{\text{csf}} \approx 5.5 \cdot 10^{24}$ requires only 10 to 15 seconds on a typical laptop or desktop computer. The computation of this same matrix element would require over a million times the age of the universe using traditional full-CI technology. Timings for expansions as large as $N_{\text{csf}} \approx 4.0 \cdot 10^{56}$ are shown in Fig. 1. An energy-based optimization approach has been developed and applied to the nonlinear wave function parameters; this exploits *partially contracted functions* in order to reduce the dimensionality of

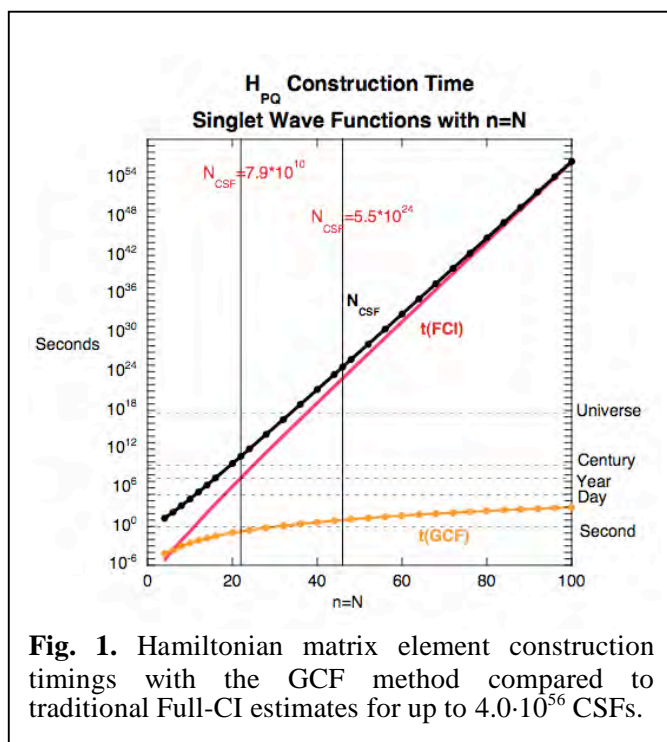


Fig. 1. Hamiltonian matrix element construction timings with the GCF method compared to traditional Full-CI estimates for up to $4.0 \cdot 10^{56}$ CSFs.

the optimization problem at each step and to minimize the number of expensive gradients that must be computed.

Many electronic structure methods expand the wave function in a basis of Slater determinants. Such methods include various SCF, MCSCF and CI methods, perturbation theory methods, coupled-cluster methods (CCSD, CCSD(T), CCSDT, etc.), DMRG methods, and many other approaches that are based on second-quantization or so-called *alpha and beta strings*. Other methods expand the wave function in a spin-symmetry-adapted CSF basis. These include those based on UGA, GUGA, the symmetric group, and other spin-coupling methods. For small wave function expansions (small numbers of electrons, orbitals, CSFs, and Slater determinants), it is straightforward to transform from one basis representation to the other. Such a transformation is useful for comparing wave functions computed with different methods, or with different approximations, comparing different states of a molecule, comparing the leading determinants of different wave functions, and for identifying the irrep label associated with a wave function computed in a subgroup of the full point group (e.g. to distinguish between Σ and Δ states of linear molecules when computed within the C_1 , C_s , C_{2v} , or D_{2h} subgroups).

However, this transformation is difficult, or practically impossible, when the determinantal expansion dimension is large, such as occurs with large numbers of electrons and orbitals. In such a situation, it is practical to compute only the expansion coefficients for some manageable number of selected determinants. In general for the GCF method, the overlap of a particular determinant is given by the expression

$$\langle D|\Psi\rangle = \sum_P^{N_{GCF}} c_P \langle D|P\rangle = \sum_P^{N_{GCF}} \sum_m^{N_{CSF}} c_P x_{mP} \langle D|\tilde{m}\rangle = \sum_m^{N_{CSF}} y_m \langle D|\tilde{m}\rangle$$

where N_{GCF} is the number of GCF expansion functions, c_P is the expansion coefficient of the GCF basis function $|P\rangle$, x_{mP} is the expansion coefficient of CSF $|\tilde{m}\rangle$ within the GCF $|P\rangle$, and y_m is the expansion coefficient of CSF $|\tilde{m}\rangle$ in the wave function $|\Psi\rangle$. If there are a large number of singly occupied spatial orbitals in a particular determinant $|D\rangle$, then $|D\rangle$ may contribute to a large number of CSFs N_{OS} , and in such a situation the determinant expansion coefficient $\langle D|\Psi\rangle$ is practically impossible to compute using the overlaps $\langle D|\tilde{m}\rangle$.

In order to sidestep this computational bottleneck, we have developed an efficient algorithm to compute the overlap $\langle D|\Psi\rangle$ directly in terms of the overlaps $\langle D|P\rangle$. This algorithm is based on two separate recursion relations. The first is that the overlaps $\langle D|\tilde{m}\rangle$ may be computed as products of Clebsch-Gordan coefficients, with one contribution from each orbital. This may be formulated recursively, where common factors are reused for several CSFs. The second recursion is inherent in the GCF basis function itself. The two recursions may be combined into a single recursive operation to compute $\langle D|P\rangle$ directly without expansion into CSFs, thereby eliminating all effort that depends on either N_{CSF} or N_{OS} . The effort for this recursive algorithm is proportional to the number of nodes in the Shavitt graph that have the same spatial orbital occupation as the determinant $|D\rangle$ and satisfy the ‘allowed area’ principle at each orbital level. Fig. 2

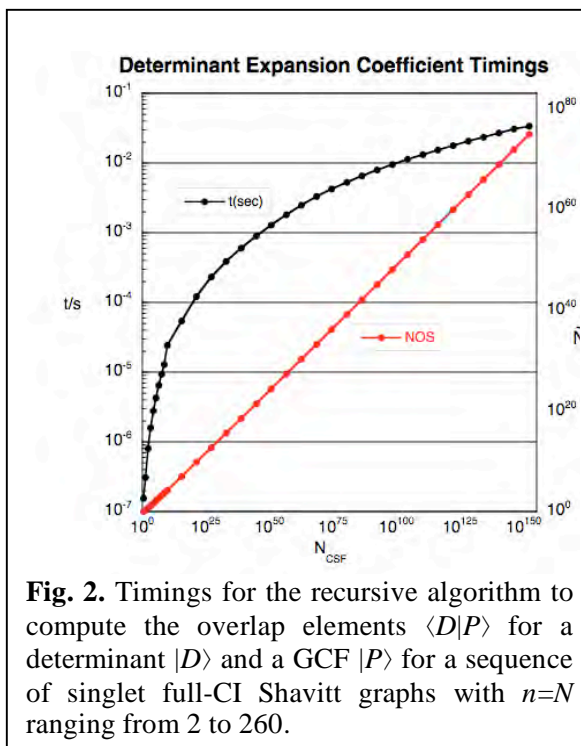


Fig. 2. Timings for the recursive algorithm to compute the overlap elements $\langle D|P\rangle$ for a determinant $|D\rangle$ and a GCF $|P\rangle$ for a sequence of singlet full-CI Shavitt graphs with $n=N$ ranging from 2 to 260.

shows timings on a laptop computer for $\langle D|P\rangle$ computation for a sequence of singlet full-CI Shavitt graphs with $n=N$ ranging from 2 to 260. The abscissa is N_{CSF} for these graphs which ranges from 1 to 10^{152} . The determinant chosen corresponds to all singly occupied spatial orbitals with alternating α and β spin factors. The number of interacting CSFs for this determinant N_{OS} ranges from 1 to 10^{75} and is also plotted in Fig. 2. Even if the overlap contribution from each interacting CSF $\langle D|\tilde{m}\rangle$ could be computed with only a single floating point operation, computing the wave function overlap in these terms for the largest expansion in Fig. 2 would require over 10^{42} times the age of the universe on a PetaFLOPS supercomputer. In contrast, using the efficient recursive algorithm to compute $\langle D|P\rangle$ directly requires only 34ms on a laptop computer.

Future Plans: GCF METHOD: Our applications have so far used single-headed Shavitt graphs appropriate for describing individual molecular states with a given number of electrons, with a particular spin state, and that belong to a particular irrep. We will generalize this in several respects. First, we will introduce state averaging over several irreps. This will allow the computation of several molecular states with essentially no additional effort over single-irrep calculations. Second, we will employ multiheaded Shavitt graphs in the state-averaging procedure. This will allow the computation of hamiltonian matrix elements corresponding to states with different numbers of electrons, different spin values, and different irreps simultaneously with only a relatively small increase in effort over the current single-state approach.

We have recently developed a new algorithm to compute the gradients of the energy with respect to the nonlinear arc factor parameters. These gradients are used during the wave function optimization. Our previous algorithm required $\mathcal{O}(\beta n^5)$ effort; the new algorithm requires $\mathcal{O}(\beta n^4)$ effort and is comparable to that of the energy evaluation itself. This is an extension of our *deferred propagation* algorithm described in last year's abstract. This will be implemented during the next year.

We have developed an efficient algorithm to compute spin-density matrices within the GCF method. This matrix may be used to compute expectation values and matrix elements of operators that depend on the M_S value of the wave function (e.g. for ESR and NMR spectra simulation). Using a straightforward approach within the spin-free GCF approach, this matrix would require $\mathcal{O}(\beta n^3)$ effort. Our algorithm exploits the recursive nature of the GCF expansion basis and requires only $\mathcal{O}(\beta n^2)$ effort. This will be implemented during the next year.

Publications:

- “Nonlinear Wave Function Expansions: A Progress Report,” R. Shepard, M. Minkoff, and S. R. Brozell, *Int. J. Quantum Chem.* **107**, 3203-3218 (2007).
- “Spin-Orbit Interaction with Nonlinear Wave Functions,” S. R. Brozell, R. Shepard and Z. Zhang, *Int. J. Quantum Chem.* **107**, 3191-3202 (2007).
- “Some Comments on the DIIS Method,” R. Shepard and M. Minkoff, *Molecular Physics* **105**, 2839-2848 (2007).
- “Advanced Software for The Calculation of Thermochemistry, Kinetics, and Dynamics,” R. Shepard, *J. Physics: Conference Series* **78**, 012067 (2007).
- “The Accuracy of Molecular Bond Lengths Computed by Multireference Electronic Structure Methods”, R. Shepard, G. S. Kedziora, H Lischka, I. Shavitt, T. Müller, P. G. Szalay, M. Kállay, M. Seth, *Chem. Phys.* **349**, 37-57 (2008).
- “Advanced Software for The Calculation of Thermochemistry, Kinetics, and Dynamics,” R. Shepard, *J. Physics: Conference Series* **125**, 012016 (2008).
- “Computation of Determinant Expansion Coefficients Within the Graphically Contracted Function Method”, G. Gidofalvi and R. Shepard, *J. Comp. Chem. (in press)*.
- “The Evaluation of Spin-Density Matrices Within the Graphically Contracted Function Method”, G. Gidofalvi and R. Shepard, (*in preparation*).

COMPUTATIONAL AND EXPERIMENTAL STUDY OF LAMINAR FLAMES

M. D. Smooke and M. B. Long
Department of Mechanical Engineering
Yale University
New Haven, CT 06520
mitchell.smooke@yale.edu

Program Scope

Our research has centered on an investigation of the effects of complex chemistry and detailed transport on the structure and extinction of hydrocarbon flames in coflowing axisymmetric configurations. We have pursued both computational and experimental aspects of the research in parallel. The computational work has focused on the application of accurate and efficient numerical methods for the solution of the boundary value problems describing the various reacting systems. Detailed experimental measurements were performed on axisymmetric coflow flames using two-dimensional imaging techniques. Spontaneous Raman scattering and laser-induced fluorescence were used to measure the temperature, and major and minor species profiles. Laser-induced incandescence (LII) has been used to measure soot volume fractions and particle sizes. A new approach to optical pyrometry has been developed to measure temperatures where the other techniques fail due to the presence of soot. Our goal has been to obtain a more fundamental understanding of the important fluid dynamic and chemical interactions in these flames so that this information can be used effectively in combustion modeling.

Recent Progress

Sooting Time-Varying Flames:

Forced, time-varying laminar flames help bridge the gap between laminar and turbulent combustion, because they reside in an ever-changing flow environment. In addition, quantitative soot volume fraction measurements in time-varying diffusion flames have shown that peak soot volume fractions can increase by factors of four to five over peak values in the equivalent steady flame [1,2]. In an effort to predict soot volume fractions as a function of time, we have started to incorporate a soot model into our time-dependent flame calculations. The governing equations are discretized using finite differences and solved implicitly using a damped modified Newton's method. However, given the size of the system of partial differential equations that must be solved (upwards of 100 chemical species and 20 soot sectional classes), the number of cycles that must be computed to eliminate start-up transients [3], and the size of the time steps that must be taken, a parallel strip domain decomposition is employed. Calculations were performed on 40 CPUs (5 nodes) of a 3.0 GHz Intel Xeon processor system with 8 cores per node and 16 GB RAM per node.

We have studied a 32% ethylene-air coflow diffusion flame in which a periodic fluctuation is imposed on the fuel velocity for forcing amplitudes of 30%, 50%, 70%, and 90%. The 50%, 70%, and 90% forcing cases display stretching and pinching of the sooting region into an isolated oval shape. In the 90% forcing case, a well-defined balloon-shaped structure of the soot volume fraction contours occurs, in which the interior of the isolated sooty region has significantly lower soot concentrations than the shell. The soot volume fraction contours for the 90% case are illustrated in Fig. 1. The peak value increases by approximately 3.3 times its minimum value between panels (b) and (j), and $f_{v,peak}$ varies by -56% and $+44\%$ from that of the equivalent steady case. In Fig. 1, a well-defined, balloon-shaped region can be seen in the contours of f_v in panel (i).

This structure is highly pronounced, having a blue and green interior region with very low f_v (as low as 0.21 ppm) between $z = 2.4$ cm and $z = 3.5$ cm. Values of f_v in this interior region increase between panels (i) and (j), at which point the balloon shape no longer exists. In the 50%, 70%, and 90% forcing cases, a secondary soot region pinches off between panels (i) and (j). This behavior contrasts with the results of Smyth *et al.* [4], which showed pinching to occur earlier in the cycle when forcing amplitude was increased. It is important to note the differences between the combustion system in the present work and the study in [4] where a methane flame with much lower inflow velocities and forcing frequency than in the present study was considered. Also, the forcing amplitudes in [4] were uncalibrated and based only on relative speaker input voltages.

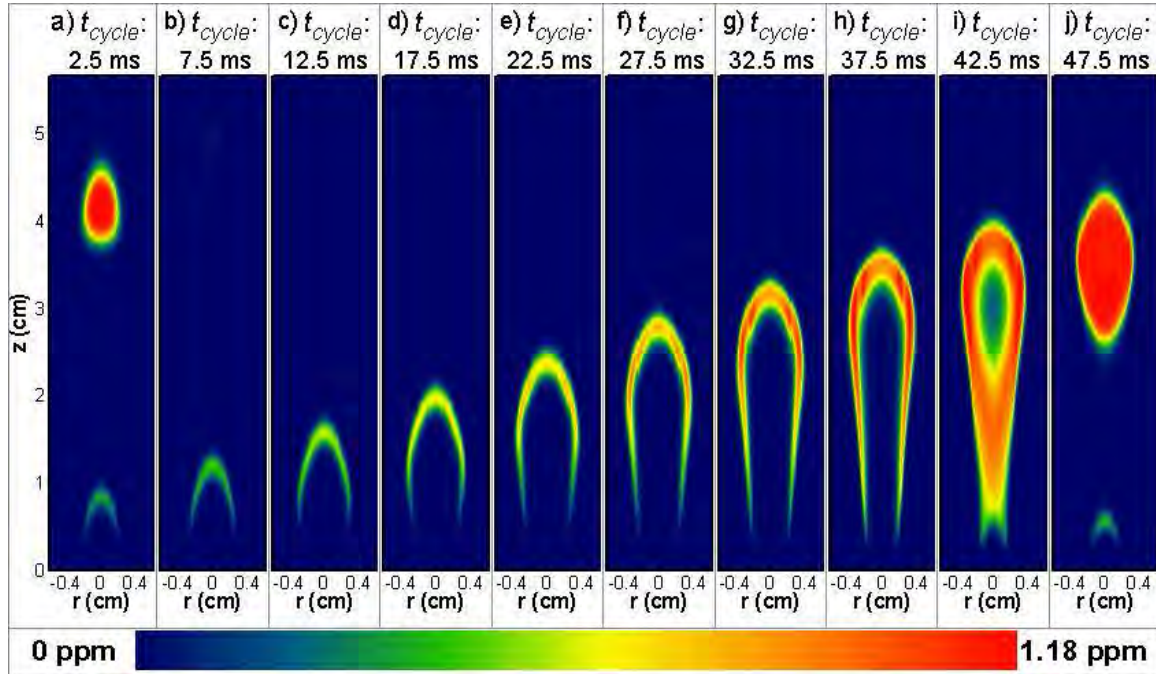


Figure 1. Computed isopleths of the soot volume fraction f_v in the coflow ethylene/air diffusion flame with 90% forcing ($\alpha = 0.9$). Panel (a) corresponds to 0.5025 seconds after initial forcing.

Measurements of Soot Particle Sizes:

Typically, particle size distributions are determined with LII using point measurements by evaluating the temporal decay of the signal as the heated soot cools back down to flame temperatures [6]. For the purpose of this study, two-dimensional measurements of particle sizes are the most practical for comparison with the computational results. For two-dimensional particle sizing, images are taken at two or more different time delays [7,8]. Care must be taken when choosing the delays because this technique suffers from a decrease in the temporal resolution and signal-to-noise characteristics that are available in point measurements.

Laser excitation is achieved using a pulsed, injection seeded, Nd:YAG laser operating at 1064 nm. Modeling of the LII process assumes that all particles in the measurement volume are heated to the same temperature, requiring a top-hat laser profile. The beam shaping lenses and apertures were carefully designed using relay imaging of the apertures to maximize the depth of field of the imaged beam sheet and to provide as uniform a beam profile as possible across the measurement volume (~2 cm tall and 300 μm wide). The LII signal is detected at a wavelength of 455 nm at discrete gate times (0, 50, 100, 200, 300, 400 and 500 ns) relative to the temporal peak of the LII

signal using a fast-gate (~5 ns) ICCD camera, and the results are analyzed to determine the optimal combination of gate delays. Gate pairs that were separated by larger times showed a larger variation in signal ratio for variations in particle size and were seen to be more robust. Benefits from increasing the variation in the signal ratio are eventually outweighed by the decline in signal at later gates. Particle sizes are determined using a library of simulated LII signals for a range of log-normal size distributions that is generated in advance and later referenced.

To refine the measurement technique, initial measurements are made in the well-characterized Santoro burner [9], and the results are compared to the values in the literature. Using an initial gate at 100 ns and a second gate at 400 ns, a particle diameter of 32.1 nm is measured on the flame centerline. This compares well with results from other studies, which are reported in [6] as: 29.3 nm, 1.18 geometric width; 35 ± 3 nm; 31 nm; 33.3 ± 3.2 nm; 32 nm. Fig. 2 shows a preliminary result comparing computed and measured particle sizes in an 80% C₂H₄. Computational particle sizes are determined by calculating the geometric mean diameter from the 20 computed size sections, assuming a log-normal distribution. It should be noted that the measurements were performed using an earlier version of the experimental apparatus that has since been improved. Also, the computational results do not properly account for bias due to the presence of aggregate structures in the larger size bins. Still, the comparison is encouraging, as the trends in the computation are captured well both qualitatively and quantitatively.

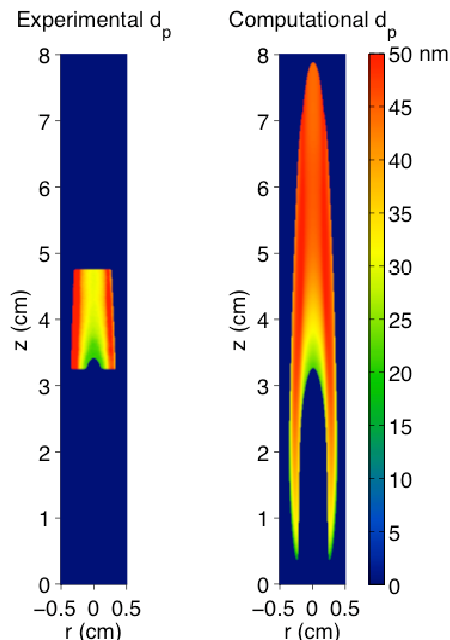


Figure 2: Experimental and computational particle sizes for an 80% C₂H₄ flame.

Future Plans

During the next year we will continue our study of sooting hydrocarbon flames with the goal of increasing our understanding of soot formation in time varying flames. Experimentally we will continue our work on improving the accuracy of our soot particle size measurement, as well as applying other diagnostic techniques that can provide information on soot aggregation. Finally, using the same techniques that we have developed for the steady sooting flames, we will perform phase-averaged measurements to characterize the soot in the time-varying flames.

References

1. J.E. Harrington, C.R. Shaddix and K.C. Smyth, "Laser imaging of chemistry-flowfield interactions: enhanced soot formation in time-varying diffusion flames," *Proceedings of SPIE-The International Society for Optical Engineering*, **2124**, 278-91 (1994).
2. K.C. Smyth, J.E. Harrington, C.R. Shaddix, W.M. Pitts and E.L. Johnson, *Flickering Flames as Testing Grounds for Reliable Models of Gas Combustion*. 1994. NIST, Gaithersburg, MD.
3. S.B. Dworkin, B.C. Connelly, A.M. Schaffer, M.B. Long and M.D. Smooke, "Computational and Experimental Study of a Forced, Time-Dependent, Methane-Air Coflow Diffusion Flame," *Proceedings of the Combustion Institute*, **31**, (2006).
4. K.C. Smyth, J.E. Harrington, E.L. Johnson, and W.M. Pitts, "Greatly Enhanced Soot Scattering in Flickering CH₄/Air Diffusion Flames," *Combust. Flame*, **95**, 229-239 (1993).
5. M.D. Smooke, M.B. Long, B.C. Connelly, M.B. Colket and R.J. Hall, "Soot Formation in Laminar Diffusion Flames," *Combustion and Flame* **143**, 613-628 (2005).

6. C. Schulz, B.F. Kock, M. Hofmann, H. Michelsen, S. Will, B. Bougie, R. Suntz and G. Smallwood, "Laser-Induced Incandescence: Recent Trends and Current Questions," *Applied Physics B-Lasers and Optics*, **83**, 333-354, (2006).
7. S. Will, S. Schraml and A. Leipertz, *Optics Letters*, "2-Dimensional Soot-Particle Sizing by Time-Resolved Laser-Induced Incandescence," **20**, 2342-2344, (1995).
8. S. Will, S. Schraml, K. Bader and A. Leipertz, "Performance Characteristics of Soot Primary Particle Size Measurements by Time-Resolved Laser-Induced Incandescence," *Applied Optics*, **37**, 5647-5658, (1998).
9. R.J. Santoro, H.G. Semerjian and R.A. Dobbins, *Combustion and Flame*, "Soot Particle Measurements in Diffusion Flames," **51**, 203, (1983).

DOE Sponsored Publications since 2007

1. G. Amantini, J. H. Frank, A. Gomez and M.D. Smooke, "Computational and Experimental Study of Standing Methane Edge Flames in the Two-Dimensional Axisymmetric Counterflow Geometry," *Comb. and Flame*, **147**, (2007).
2. G. Amantini, J. H. Frank, A. Gomez and M.D. Smooke, "Computational and Experimental Study of Steady Two-Dimensional Axisymmetric Non-Premixed Methane Counterflow Flames," *Comb. Theory and Modelling*, **11**, (2007).
3. G. Amantini, B. A. V. Bennett, J. H. Frank, A. Gomez and M. D. Smooke, "Comprehensive Study of Extinction, Re-ignition, and the Evolution of an Annular Edge Flame in a Counterflow Flame Perturbed by Vortices," *Comb. and Flame*, **150**, (2007).
4. B. A. V. Bennett, M. D. Smooke, R. J. Osborne and R. W. Pitz, "Computational and Experimental Study of Oxy-Fuel Diffusion Flames," *Comb. Theory and Modelling*, **12**, (2008).
5. B. C. Connelly, B. A. V. Bennett, M. D. Smooke, M. B. Long, "A Paradigm Shift in the Interaction of Experiments and Computations in Combustion Research," *Proceedings of the Combustion Institute*, **32**, (2008).
6. B. C. Connelly, M. B. Long, M. D. Smooke, R. J. Hall and M. B. Colket, "Computational and Experimental Investigation of the Interaction of Soot and NO_x in Coflow Diffusion Flames," *Proceedings of the Combustion Institute*, **32**, (2008).
7. S. B. Dworkin, M. D. Smooke and V. Giovangigli, "The Impact of Detailed Multicomponent Transport and Thermal Diffusion Effects on Soot Formation in Ethylene/Air Flames," *Proceedings of the Combustion Institute*, **32**, (2008).
8. J. H. Miller, B. McAndrew, M. P. Puccio, S. B. Dworkin, A. M. Schaffer, B. C. Connelly, M. B. Long and M. D. Smooke, "Measurements and Calculations of Formaldehyde Concentrations in a Methane/N₂/Air, Non-Premixed Flames," *Proceedings of the Combustion Institute*, **32**, (2008).
9. B. A. V. Bennett, C. S. McEnally, L. D. Pfefferle, M. D. Smooke and M. B. Colket, "Computational and Experimental Study of the Effects of Adding Dimethyl Ether and Ethanol to Nonpremixed Ethylene/Air Flames," accepted for publication *Comb. and Flame*, (2009).
10. H. Bufferand, L. Tosatto, B. La Mantia, M. D. Smooke and A. Gomez, "The Structure of Methane Counterflow Diffusion Flames Perturbed by Trace Amounts of Either JP-8 or a Six-Component Surrogate," accepted for publication *Comb. and Flame*, (2009).

Quantum Chemistry of Radicals and Reactive Intermediates

John F. Stanton
Institute for Theoretical Chemistry
University of Texas
Austin, TX 78712

Scope of Research

My research group works in the area of theoretical chemical physics, especially on the properties and chemistry of organic radicals and other reactive intermediates. This research follows a number of paths, including first-principles calculations of bond energies and other thermochemical information (as well as development of methodology for such calculations), methods for the simulation and analysis of molecular spectroscopy, especially relevant to those experiments that can be used to glean thermochemical information, and the development of *ab initio* methods needed for the accurate treatment of transient organic molecules.

Summary of recent major accomplishments

A principal finding in the last year has been the discovery that a simple (in principle) extension of the diabatic Hamiltonian framework of Köppel, Domcke and Cederbaum¹ can provide *quantitative* (*i.e.* potentially useful in thermochemical applications) accuracy for the energy levels of strongly coupled systems. First applied to the BNB radical, the method gives energy levels within 10 cm⁻¹ of experiment. The agreement for a system of this level of difficulty (the ²Σ_u and ²Σ_g electronic states of this system are very strongly coupled along the asymmetric stretching mode) is remarkable. And just how remarkable is clear when one investigates the intrinsic error associated with the Born-Oppenheimer approximation. For BNB, the magnitude of this “non-adiabatic” correction can be assessed as follows: one first diagonalizes the Hamiltonian expressed in the diabatic basis (these are the values that agree well with experiment), and then compares these levels with those obtained by solving the nuclear Schrödinger equation on the potential energy surface obtained from the diabatic Hamiltonian. The magnitude of the error in this case is **ca. 80 cm⁻¹**² for the ground vibronic level of the radical. This suggests that the vibronic coupling treatment can be made quantitative, and indeed more reliable *in principle* than calculations based on brute-force quantum chemistry. The method has also been applied more recently to the HCO₂ and DCO₂ radicals, a project being done in collaboration with the Neumark group at Berkeley³.

We have investigated the thermochemistry of the C₃H₂ carbenes, known from the work of Taatjes *et al.* to be present in rich cyclopentene flames⁴. These calculations, which use the so-called HEAT protocol for thermochemistry, are the most accurate to date for these systems. The HEAT approach was designed to be as accurate as possible without making sacrifices for range of application. As a result, the approach was originally only applied to very small molecules and

¹See, H. Köppel, W. Domcke and L.S. Cederbaum *Adv. Chem. Phys.* 57, 59 (1984).

²J.F. Stanton, unpublished.

³E. Garard, D.M. Neumark, K. Klein and J.F. Stanton, in progress.

⁴C.J. Taatjes, S.J. Klippenstein, N. Hansen, J.A. Miller, T.A. Cool, J. Wang, M.E. Law and P.R. Westmoreland *PCCP* 7, 806 (2005).

atoms. However, significant computational advances made in the parallelization of our CFOUR set of computer programs (formerly known as ACESII-MAB) have allowed the required and very large calculations to be run for these “large” molecules. The values of $\Delta_f H^\circ(298K)$ obtained for the isomers propadienyliene ($:C=C=CH_2$) and cyclopropenyliene ($c-C_3H_2$) were found to 556.7 and 497.1 kJ mol⁻¹, respectively, with uncertainties of *ca.* 1.0 kJ mol⁻¹. In conjunction with a parallel calculation on propargyl, for which a value in perfect agreement (within 0.1 kJ mol⁻¹) of the recent focal-point estimate⁵ of Allen and co-workers was obtained, the acetylenic bond energy of propargyl was calculated to be 416.7±1.0 kJ mol⁻¹⁶. This value agrees with, but is more precise than, that obtained by a negative-ion cycle by the Boulder group⁷.

In collaboration with the Ellison group at Colorado, we have reported the isolation and spectroscopic characterization of the propargyl peroxy ($H_2(O_2)CCCH$) radical, which is an important combustion species. We have been able to assign *all* of the fundamental bands accessible by the FTIR spectrometer (above 400 cm⁻¹), and have also been able to determine the fundamental frequencies of some of the lower-frequency modes through identification of combinations and overtones. The assignment was significantly facilitated by large-scale *ab initio* calculations of the anharmonic force field; calculated level positions agreed with experimental (Ar matrix at 10K) observations to *ca.* 5-10 cm⁻¹ for all bands except the hydrogen stretches, which are more sensitive to the matrix environment than the skeletal modes. Most important, our study indicates that of the several possible conformers amongst the two structural isomers of this molecule, the only one seen in the matrix is that in which the oxygen attaches to the terminal methylene group in an *exo* orientation⁸.

Ongoing Research and Future Plans

Currently, and made possible only because of the excellent job done by M.E. Harding in the parallelization of CFOUR, we are beginning a set of calculations on the C₆H₆ isomers and ultimately the transition states that link the various forms. This work, clearly motivated by that of Miller and Klippenstein on benzene formation from propargyl⁹, is intended to provide the best theoretical estimates possible for modelling this fundamentally important chemical process.

A study of phenyl peroxy radical (C₆H₅OO) similar to that of propargyl peroxy (above) is underway. The experimental work in Boulder has been completed, and we are currently in the process of calculating the infrared spectrum.

The equation-of-motion coupled cluster methods strongly favored and advocated by two members of this program (Stanton and Krylov) are going to be applied to study the oxidation of the vinyl radical. This work was initiated by Carpenter several years ago, but he found that the methods available at that time – notably those based on multiconfigurational Hartree-Fock theory – were not adequate to study the problem. The equation-of-motion approaches, especially the so-called EOMIP-CC variant, are ideally suited to a problem of this type. We plan to work on this problem in the coming months, in collaboration with Krylov, and in so doing, establish what might become a standard protocol for investigating the initial stages of oxidation of organic molecules.

⁵S.E. Wheeler, K.A. Robertson, W.D. Allen, H.F. Schaefer III, Y.J. Bomble and J.F. Stanton *J. Phys. Chem. A* 111, 3819 (2007).

⁶J. Vazquez, M.E. Harding, J. Gauss and J.F. Stanton, submitted to *J. Phys. Chem. A*.

⁷M.S. Robinson, M.L. Polak, V.M. Bierbaum, C.H. DePuy and W.C. Lineberger *J. Amer. Chem. Soc.* 117, 6766 (1995).

⁸E.B. Jochnowitz, M.R. Nimlos, G.B. Ellison and J.F. Stanton, submitted to *J. Chem. Phys.*

⁹J.A. Miller and S.J. Klippenstein *J. Phys. Chem. A* 107, 7783 (2003).

Universal and State-Resolved Imaging Studies of Chemical Dynamics

Arthur G. Suits
Department of Chemistry, Wayne State University
5101 Cass Ave
Detroit, MI 48202
asuits@chem.wayne.edu

Program Scope

The focus of this program is on combining universal ion imaging probes providing global insight, with high-resolution state-resolved probes providing quantum mechanical detail, to develop a molecular-level understanding of chemical phenomena. Particular emphasis is placed upon elementary reactions important in understanding and predicting combustion chemistry. This research is conducted using state-of-the-art molecular beam machines, photodissociation, reactive scattering, and vacuum ultraviolet lasers in conjunction with ion imaging techniques. An ongoing parallel effort is made to develop new tools and experimental methods with which to achieve these goals.

Recent Progress

Roaming dynamics in formaldehyde and acetone. As reported in last year's abstract, the study of formaldehyde dissociation has proved to be a rich and ongoing source of insight into roaming dynamics. In the recent *Chem. Phys.* paper, we showed the energy dependence of roaming at the energetic extremes, both below the radical threshold and up to the three body dissociation limit. This offered deep insight into the unimolecular dynamics leading to roaming, and the trajectory calculations from the Bowman group allowed us to distinguish two aspects of the roaming event, the "excursion" and the abstraction. The roaming story was summarized in a review for *Acc. Chem. Res.* And featured on the cover of the July, 2008 issue (Fig. 1).



Figure 1. Formaldehyde roaming featured in *Accounts of Chemical Research*.

We have recently studied state-resolved photodissociation dynamics of formaldehyde-d₂, i.e. D₂CO, at energies slightly above deuterium atom dissociation threshold, both experimentally and theoretically in collaboration with the Bowman group. The results show a clear bimodal distribution of energy into molecular photofragments. Substantial translational excitation at high rotational levels of CO was observed together with D₂ cofragment in moderately excited vibrational levels, whereas rather small translational energy release of CO in low rotational levels was matched by large degree of vibrational excitation in the D₂

molecule. The experimental results are entirely analogous to that for H₂CO, thereby clearly confirming roaming dynamics in this system as well. Detailed analysis of the branching is underway, but complicated in this case by greater background interference.

The photochemistry of acetone is among the most thoroughly studied of any polyatomic molecule, yet it is perhaps surprising that a unified picture of its dissociation dynamics have not yet emerged and some controversies persist. We have recently employed DC slice imaging to study the photodissociation dynamics of acetone both with one color at 230 nm, and now more recently at 193nm, with detection of the CO photoproduct via the $B (v'=0) \ ^1\Sigma^+ \leftarrow X (v''=0) \ ^1\Sigma^+$ transition. A bimodal translational energy distribution observed in the CO fragments points to two distinct dissociation pathways at both excitation energies. It is generally accepted that 193nm will access the S₂ state, while 230 nm will access S₁, but it is also believed that S₂ does not dissociate at this energy, so electronic relaxation, likely to S₁, must precede dissociation.

One pathway results in substantial translational energy release ($E_{\text{ave}} \approx 0.3$ eV) along with rather high rotational excitation (up to $J''=50$) of CO, and is attributed to the thoroughly investigated stepwise mechanism of bond cleavage in acetone. The other dissociation pathway leads to rotationally cold CO ($J''=0-20$) with very little energy partitioned into translation ($E_{\text{ave}} \approx 0.04$ eV) and in this way it is dynamically similar to the recently reported roaming mechanism found in formaldehyde and acetaldehyde dissociation. We ascribe the second dissociation pathway to an analogous roaming dissociation mechanism taking place on the ground electronic state following internal conversion. We estimate that about 15% of the total CO fragments are produced through the roaming pathway. Rotational populations were obtained using a new Doppler-free method described below.

Doppler-free spectroscopy with

masked imaging. We have recently investigated a variety of Doppler-free or reduced Doppler strategies for use with imaging, and these have led us to a novel spectroscopic technique which makes it possible to record Doppler-free resonance-enhanced multiphoton ionization (REMPI) spectra with just one laser beam, even for one-photon transitions. The approach simply involves masking the outer side of the phosphor screen under velocity map imaging conditions so that only those species having no velocity component parallel to the laser beam propagation direction are detected. The benefits of

this method were demonstrated in 1+1 ionization of hydrogen atoms in which the spin-orbit splitting in the ²P state were resolved, and in spectroscopic characterization of highly translationally and rotationally excited CO fragments resulting from the 230 nm

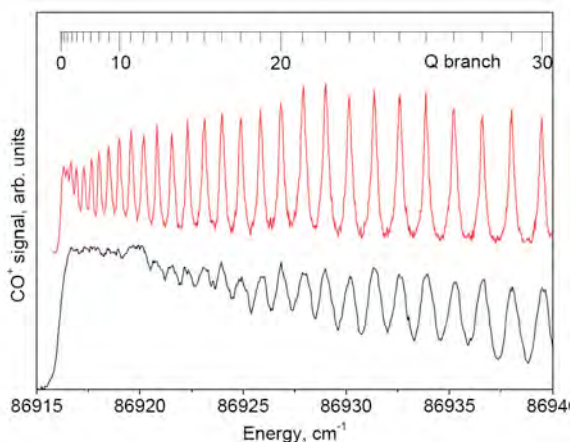


Figure 1. Masked Doppler-free REMPI spectrum (top trace) and unmasked spectrum (bottom trace) for CO from acetone dissociation on the CO B-X bandhead.

photolysis of OCS and acetone, yielding substantially improved values of the rotational constants for the B state ($v''=0$) of the CO molecule.

DC sliced imaging of CN radical reactions with alkanes. We have completed analysis of our study of the reaction of CN with butane, pentane and hexanes, at several collision energies, with detection of the alkyl radical product using single photon ionization at 157 nm. The angular distributions for these reactions show broad backward scattering clearly implying direct dynamics. Although in most cases we are blind to the most forward scattered part of the distribution owing to photochemical interference, in the one instance where it is clear, we see no evidence of forward peaking. This is perhaps a bit surprising. It is similar to the $O(^3P) + \text{alkane}$ results but very different from the widely studied $Cl + \text{alkane}$ reactions. Even for $Cl + \text{ethane}$, with only primary H atoms, broad angular distributions are seen with both forward and backward peaking components. The TS for $CN + \text{ethane}$ reported by Klippenstein et al. indicated possibly a submerged saddle point. Nevertheless, it appears these systems may yet exhibit a sufficiently tight transition state to constrain reaction to a near collinear C-H-CN geometry. This may well be a consequence of the diatomic nature of the reactant as opposed to the case for Cl atom.

For these reactions, we find the kinetic energy and the angular distribution are somewhat coupled. The reaction products have broader translational energy distributions in the backward direction than in the forward direction. The translational energy spectra of forward (0° - 90°) and backward (90° - 180°) scattering were obtained by integrating the signal in these regions separately. All results show a significant fraction of available energy in the internal excitation of either the alkyl radical or HCN. Based on the strong HCN bond and the likely abstraction dynamics, the bulk of the energy is likely in the HCN molecule. For the reaction of $CN(X^2\Sigma^+)$ with butane at collision energy of 10.8 kcal/mol, the results show a broad distribution and peaking at lower translational energy for the backward scattering.

Selected Future Plans

Roaming atom reaction dynamics. We will perform DC slice imaging a range of systems to investigate the generality of the roaming mechanism. One promising system is NO_3 radical. This is known to dissociate to yield $NO+O_2$ and an energy below the O atom loss threshold, but the dynamics responsible are not clear, and roaming is a plausible explanation. By applying state-resolved imaging of the NO product, we hope to determine the state-correlated product distributions. These will provide deep insight into the dynamics even if roaming is not responsible for the observed molecular products.

State-resolved and universal crossed-beam DC slice imaging. We have plans to continue exploring range of systems using our crossed-beam sliced imaging approach. We initially attempted some CH reactions but so far these have not proved fruitful. However, we can extend our studies of CN reactions to a range of target systems including structured alkane systems to investigate the consequences of varied stereochemistry and primary vs. secondary H atom targets.

VUV photodissociation of alkanes with universal probe. We have recently shown that one-color dissociation and ionization of heptane can be used to calibrate the relative ionization efficiency of radical isomer detection in the VUV in some cases. At the same time these results showed that photodissociation of these systems likely takes place following internal conversion to the ground state, and interesting variations in the product translational energy distributions could be traced to structural properties of the parent molecules. We intend to explore this as a means of investigating complex ground state fragmentation processes of alkanes under collisionless conditions.

DOE Publications 2007-present

S. A. Lahankar, S. D. Chambreau, X. Zhang, J. M. Bowman and A. G. Suits, "Energy dependence of the roaming atom mechanism in formaldehyde decomposition," *J. Chem. Phys.* **126**, 044314 (2007).

A. G. Suits, S. D. Chambreau, S. A. Lahankar, "State-correlated DC slice imaging of formaldehyde photodissociation: roaming atoms and multichannel branching," *Int. Rev. Phys. Chem.* **26**, 585 (2007).

S.A. Lahankar, V. Goncharov, F. Suits, J.D. Farnum, J.M. Bowman and A. G. Suits. "Further aspects of the roaming mechanism in formaldehyde dissociation," *Chem. Phys.* **347**, 288 (2008).

C. Huang, A. D. Estillore and A. G. Suits, "State-selected imaging of HCCO radical photodissociation dynamics," *J. Chem. Phys.* **128** 134301 (2008).

A. G. Suits, "Roaming atoms and radicals: A new mechanism in molecular dissociation," *Acc. Chem. Res.* **41**, 873 (2008).

V. Goncharov, N. Herath and A. G. Suits, "Roaming dynamics in acetone dissociation," *J. Phys. Chem. A* 10.2021/jp802534r (2008).

C. Huang, A. Estillore, W. Li, and A. G. Suits, "Dynamics of CN + alkane reactions by crossed-beam dc slice imaging," **129**, 074301 (2008).

V. Goncharov, N. Herath, A. Arregui, L. Banares, A. G. Suits, "Masked velocity map imaging: A one-laser-beam Doppler-free spectroscopic technique," *J. Phys. Chem A*, (2009) DOI: 10.1021/jp809711n.

Elementary Reaction Kinetics of Combustion Species

Craig A. Taatjes

*Combustion Research Facility, Mail Stop 9055, Sandia National Laboratories,
Livermore, CA 94551-0969*

cataatj@sandia.gov www.ca.sandia.gov/CRF/staff/taatjes.html

SCOPE OF THE PROGRAM

This program aims to develop new methods for studying chemical kinetics and to apply these methods to the investigation of fundamental chemistry relevant to combustion science. One central goal is to perform accurate measurements of the rates at which important free radicals react with each other and with stable molecules. Another goal is to characterize complex reactions that occur via multiple potential wells by investigating the formation of products. Increasingly, these investigations are moving towards simultaneous time-resolved detection of multiple species in well-characterized photolytically-initiated reaction systems where multiple consecutive and competing reactions may occur. Understanding the reactions in as much detail as possible under accessible experimental conditions increases the confidence with which modelers can treat the inevitable extrapolation to the conditions of real-world devices. Another area of research is the investigation and application of new detection methods for precise and accurate kinetics measurements. Absorption-based techniques and mass-spectrometric methods have been emphasized, because many radicals critical to combustion are not amenable to fluorescence detection.

An important part of our strategy, especially for complex reaction systems, is using experimental data to test and refine detailed calculations (working in close cooperation with Stephen Klippenstein at Argonne and Jim Miller at Sandia), where the calculational results offer insight into the interpretation of experimental results and to guide new measurements that will probe key aspects of potential energy surfaces. This methodology has been applied in our investigations of the reactions of alkyl radicals with O₂, where the combination of rigorous theory and validation by detailed experiments has made great strides toward a general quantitative model for alkyl oxidation.

PROGRESS REPORT

We continue to apply frequency-modulation and direct absorption spectroscopy to measurements of product formation in reactions of alkyl radicals with O₂ and kinetics of unsaturated hydrocarbon radicals. However, the multiplexed photoionization mass spectrometric reactor at the Advanced Light Source, operated in collaboration with David Osborn, has become a major part of our investigations of low-temperature hydrocarbon oxidation chemistry. Several highlights of the recent work are described briefly below.

Enol formation in OH-initiated oxidation of cycloalkenes. Photolytic OH-initiated oxidation of cyclopentene, cyclohexene, and 1,4-cyclohexadiene have been investigated using tunable synchrotron photoionization mass spectrometry. Electronic structure calculations (CBS-QB3) are employed in Franck-Condon (FC) spectral simulations of the photoionization efficiency curves (PIE) of the observed products. Cyclic products cyclopentenol (cyclopenten-1-ol, 1-*c*-C₅H₇OH) and its isomers cyclopenten-2-ol (2-*c*-C₅H₇OH) and cyclopentanone (*c*-C₅H₈=O), are detected from OH-initiated cyclopentene oxidation. In contrast, product spectra from OH-initiated oxidation of cyclohexene and cyclohexa-1,4-diene show a substantial contribution from linear aldehydes, indicating a prominent role for ring opening.

Detection of Novel Chemical Intermediates. One of the strengths of the synchrotron photoionization method is its ability to distinguish isomers and hence uncover unexpected intermediate species.¹ Carbonyl oxide species are one such intermediate. In the late 1940s Criegee^{2,3} first postulated the participation of carbonyl oxides, now often called “Criegee intermediates,” in ozonolysis of alkenes. They have also been proposed as intermediates in low-temperature combustion of dimethyl ether.^{4,5} However, despite decades of effort no gas phase Criegee intermediate had been observed until we directly detected the primary Criegee intermediate, formaldehyde oxide (CH₂OO), from Cl-initiated oxidation of dimethyl sulfoxide. This work opens the possibility for explicit kinetics studies on this critical ephemeral species and its potential detection in low-temperature hydrocarbon oxidation.

Isomeric propanol flames. The combustion of 1-propanol and 2-propanol was studied in low-pressure, premixed flat flames using molecular-beam mass spectrometry (MBMS). The ALS photoionization (PI) measurements were compared with electron ionization (EI) measurements taken in Katharina Kohse-Höinghaus’s group in Bielefeld. The quantitative agreement between the EI- and PI-datasets is good. The major-species mole fraction profiles in the 1-propanol flames and the 2-propanol flames of corresponding stoichiometry are nearly identical, and only small quantitative variations in the intermediate species pool could be detected. Differences between flames of the isomeric fuels are most pronounced for oxygenated intermediates that can be formed directly from the fuel during the oxidation process.

Vinyl radical self-reaction. Our work on the vinyl radical self-reaction has continued with photoionization mass spectrometric measurements that confirm the “low” value of the rate coefficient (less than ½ the literature value!) and demonstrate substantial branching to methyl + propargyl products (branching ratio of 0.5 at 298 K and 4 Torr).

FUTURE DIRECTIONS

Characterization of $R + O_2$ reactions will continue, both in the laser absorption work and in the ALS kinetics machine. The ability to simultaneously probe various reactants and products will play a key role in extending these measurements. The formation of OH was previously measured by LIF in the Cl-initiated oxidation of alkanes,⁶ a method that requires extensive modeling to calibrate the OH yield. The predictions of the master equation models were in only qualitative agreement with the experimental data, but the uncertainties in the experimental analysis prevent reliable modifications to the stationary point energies. Measurement of OH production by UV absorption for ethane, propane, and butane oxidations will be compared to the master-equation derived mechanisms. Oxidation of selectively deuterated alkanes will be carried out to distinguish among different internal abstraction pathways in $R + O_2$ reactions.

The application of synchrotron photoionization mass spectrometry to oxidation kinetics will also continue, exploiting the isotopic discrimination enabled by the tunability of the ALS. Characterization of OH and Cl-initiated oxidation of alkenes and aromatics will extend the previous work on alkyl + O_2 reactions to reactions relevant for low-temperature oxidation of unsaturated fuels. Initial steps in autoignition for alternative fuels, including alcohols, esters, and possible novel biofuels will also be investigated.

The most important unexplored area for autoignition chemistry is the chain branching initiated by the “second O_2 addition,” that is, the reaction of molecular oxygen with the hydroperoxyalkyl radicals QOOH. It has been a consistent goal of this program over at least the past ten years to obtain experimental information about these QOOH species and their reactions. That quest will continue.

The first strategy is to continue to search for kinetic signatures of QOOH reactions in the time-resolved product profiles of photolytically-initiated hydrocarbon oxidation. One example of such a signature is the chain branching observed in neopentane oxidation at low pressure,⁷ and more recently in the high-pressure oxidation of cyclohexane.⁸ A second strategy will be to use tunable synchrotron photoionization to try to directly detect QOOH. The more stable peroxy (ROO) isomers most often do not have stable cations but the cations in the QOOH configuration are calculated to be bound.

References

- (1) Taatjes, C. A.; Hansen, N.; McIlroy, A.; Miller, J. A.; Senosiain, J. P.; Klippenstein, S. J.; Qi, F.; Sheng, L.; Zhang, Y.; Cool, T. A.; Wang, J.; Westmoreland, P. R.; Law, M. E.; Kasper, T.; Kohse-Höinghaus, K. *Science* **2005**, *308*, 1887.
- (2) Criegee, R. *Angew. Chem. Internat. Edit.* **1975**, *14*, 745.
- (3) Criegee, R.; Wenner, G. *Liebigs. Ann. Chem.* **1949**, *564*, 9.
- (4) Andersen, A.; Carter, E. A. *J. Phys. Chem. A* **2003**, *107*, 9463.
- (5) Andersen, A.; Carter, E. A. *J. Phys. Chem. A* **2006**, *110*, 1393.
- (6) DeSain, J. D.; Klippenstein, S. J.; Miller, J. A.; Taatjes, C. A. *J. Phys. Chem. A* **2003**, *107*, 4415.
- (7) DeSain, J. D.; Klippenstein, S. J.; Taatjes, C. A. *Phys. Chem. Chem. Phys.* **2003**, *5*, 1584.
- (8) Fernandes, R. X.; Zádor, J.; Jusinski, L. E.; Miller, J. A.; Taatjes, C. A. *Phys. Chem. Chem. Phys.* **2009**, *11*, 1320.

Publications acknowledging BES support 2007-present

1. Matthew E. Law, Phillip R. Westmoreland, Terrill A. Cool, Juan Wang, Nils Hansen, Craig A. Taatjes, and Tina Kasper, "Benzene Precursors and Formation Routes in a Stoichiometric Cyclohexane Flame," *Proc. Combust. Inst.* **31**, 565-573 (2007).
2. Katharina Kohse-Höinghaus, Patrick Obwald, Ulf Struckmeier, Tina Kasper, Nils Hansen, Craig A. Taatjes, Juan Wang, Terrill A. Cool, Saugata Gon and Phillip R. Westmoreland, "The influence of ethanol addition on a premixed fuel-rich propene-oxygen-argon flame," *Proc. Combust. Inst.* **31**, 1119-1127 (2007).
3. Nils Hansen, James A. Miller, Craig A. Taatjes, Juan Wang, Terrill A. Cool, Matthew E. Law, Phillip R. Westmoreland, Tina Kasper and Katharina Kohse-Höinghaus, "Photoionization Mass Spectrometric Studies and Modeling of Fuel-Rich Allene and Propyne Flames," *Proc. Combust. Inst.* **31**, 1157-1164 (2007).
4. Sarah V. Petway, Huzeifa Ismail, William H. Green Jr., Edgar G. Estupiñán, Leonard E. Jusinski, and Craig A. Taatjes, "Measurements and Automated Mechanism Generation Modeling of OH Production in Photolytically-Initiated Oxidation of the Neopentyl Radical," *J. Phys. Chem. A* **111**, 3891-3900 (2007).
5. Edgar G. Estupiñán, Jared D. Smith, Atsumu Tezaki, Stephen J. Klippenstein, and Craig A. Taatjes, "Measurements and Modeling of DO₂ Formation in the Reactions of C₂D₅ and C₂D₇ Radicals with O₂," *J. Phys. Chem. A* **111**, 4015-4030 (2007).
6. N. Hansen, T. Kasper, S. J. Klippenstein, P. R. Westmoreland, M. E. Law, C. A. Taatjes, K. Kohse-Höinghaus, J. Wang, and T. A. Cool, "Initial Steps of Aromatic Ring Formation in a Laminar Premixed Fuel-Rich Cyclopentene Flame," *J. Phys. Chem. A* **111**, 4081-4092 (2007).
7. Huzeifa Ismail, C. Franklin Goldsmith, Paul R. Abel, Pui-Teng Howe, Askar Fahr, Joshua B. Halpern, Leonard E. Jusinski, Yuri Georgievski, Craig A. Taatjes, and William H. Green, "Temperature and Pressure Dependence of the Reaction of Vinyl Radical (C₂H₃) with Ethylene," *J. Phys. Chem. A* **111**, 6843-6851 (2007).
8. Craig A. Taatjes, "How Does the Molecular Velocity Distribution Affect Kinetics Measurements by Time-Resolved Mass Spectrometry?," *Int. J. Chem. Kinet.*, **39**, 565-570 (2007).
9. Craig A. Taatjes, Arjan Gijsbertsen, Marc J. L. de Lange, and Steven Stolte, "Measurements and Quasi-Quantum Modeling of the Steric Asymmetry and Parity Propensities in State-to-State Rotationally Inelastic Scattering of NO (²I_{1/2}) with D₂," *J. Phys. Chem. A* **111**, 7631-7639 (2007).
10. Adam M. Knepp, Giovanni Meloni, Leonard E. Jusinski, Craig A. Taatjes, Carlo Cavalotti, and Stephen J. Klippenstein, "Theory, Measurements and Modeling of OH and HO₂ Formation in the Cl-Initiated Oxidation of Cyclohexane," *Phys. Chem. Chem. Phys.* **9**, 4315 - 4331 (2007).
11. Fabien Goulay, David L. Osborn, Craig A. Taatjes, Peng Zou, Giovanni Meloni and Stephen R. Leone, "Direct detection of Polyynes Formation from the Reaction of Ethynyl Radical (C₂H) with Methylacetylene (CH₃-C≡CH) and Allene (CH₂=C=CH₂)," *Phys. Chem. Chem. Phys.* **9**, 4291-4300 (2007).
12. A. Ballast, A. Gijsbertsen, H. Linnartz, C. A. Taatjes, and S. Stolte, "A Quasi-Quantum Treatment of Inelastic Molecular Collisions," in *Rarefied Gas Dynamics: 25th International Symposium*, ed. M. S. Ivanov, A. K. Rebrov, Russian Academy of Sciences, Novosibirsk, 2007, pp. 1263-1272.
13. Alex T. Archibald, Max R. McGillen, Craig A. Taatjes, Carl J. Percival, Dudley E. Shallcross, "The atmospheric transformation of enols: a potential secondary source of carboxylic acids in the urban troposphere," *Geophys. Res. Lett.* **34**, L21801 (2007).
14. Giovanni Meloni, Talitha M. Selby, Fabien Goulay, Stephen R. Leone, David L. Osborn, and Craig A. Taatjes, "Photoionization of 1-alkenylperoxy and alkylperoxy radicals and a general rule for the stability of their cations," *J. Am. Chem. Soc.* **129**, 14019-14025 (2007).
15. Craig A. Taatjes, Nils Hansen, David L. Osborn, Katharina Kohse-Höinghaus, Terrill A. Cool, Phillip R. Westmoreland, "Imaging' Combustion Chemistry with Multiplex Synchrotron Photoionization Mass Spectrometry," *Phys. Chem. Chem. Phys.* **10**, 20-34 (2008)
16. Peng Zou, Kevin E. Strecker, Jaime Ramirez-Serrano, Leonard E. Jusinski, Craig A. Taatjes, and David L. Osborn, "Ultraviolet photodissociation of vinyl iodide: understanding the halogen dependence of photodissociation mechanisms in vinyl halides," *Phys. Chem. Chem. Phys.* **10**, 713-728 (2008).
17. Craig A. Taatjes, "Recent developments in the coupling of theory and experiment to study the elementary chemistry of autoignition," *J. Combust. Soc. Japan* **50**, 29-38 (2008).
18. Craig A. Taatjes, Giovanni Meloni, Talitha M. Selby, Adam J. Trevitt, David L. Osborn, Carl J. Percival, and Dudley E. Shallcross, "Direct Observation of the Gas-Phase Criegee Intermediate (CH₂OO)," *J. Am. Chem. Soc.* **130**, 11883-11885 (2008).
19. Craig A. Taatjes, Giovanni Meloni, Talitha M. Selby, David L. Osborn, Haiyan Fan, and Stephen T. Pratt, "Absolute Photoionization Cross Section of Methyl Radical" *J. Phys. Chem. A* **112**, 9336-9343 (2008).
20. Talitha M. Selby, Giovanni Meloni, Fabien Goulay, Stephen R. Leone, Askar Fahr, Craig Taatjes, and David L. Osborn, "Synchrotron Photoionization Mass Spectrometry Measurements of Kinetics and Product Formation in the Allyl Radical (H₂CCHCH₂) Self-Reaction," *J. Phys. Chem. A* **112**, 9366-9373 (2008).
21. David L. Osborn, Peng Zou, Howard Johnsen, Carl C. Hayden, Craig A. Taatjes, Vadim D. Knyazev, Simon W. North, Darcy S. Peterka, Musahid Ahmed, and Stephen R. Leone, "The Multiplexed Chemical Kinetic Photoionization Mass Spectrometer: A New Approach for Isomer-Resolved Chemical Kinetics," *Rev. Sci. Instrum.* **79**, 104103 (2008).
22. Giovanni Meloni, Talitha M. Selby, David L. Osborn, and Craig A. Taatjes, "Enol Formation and Ring Opening in OH-Initiated Oxidation of Cycloalkenes," *J. Phys. Chem. A* **112**, 13444-13451 (2008).
23. Judit Zádor, Ravi X. Fernandes, Yuri Georgievskii, Giovanni Meloni, Craig A. Taatjes, and James A. Miller, "The reaction of hydroxyethyl radicals with O₂: a theoretical analysis and experimental product study," *Proc. Combust. Inst.* **32**, 271-277 (2009).
24. Adam J. Trevitt, Fabien Goulay, Giovanni Meloni, David L. Osborn, Craig A. Taatjes and Stephen R. Leone, "Isomer specific product detection of CN radical reactions with ethylene and propene by tunable VUV photoionization mass spectrometry," *Int. J. Mass Spectrom.* **280**, 113-118 (2009)
25. Fabien Goulay, Adam J. Trevitt, Giovanni Meloni, Talitha M. Selby, David L. Osborn, Craig A. Taatjes, Luc Vereecken and Stephen R. Leone, "Cyclic Versus Linear Isomers Produced by Reaction of the Methylidyne (CH) Radical with Small Unsaturated Hydrocarbons," *J. Am. Chem. Soc.* **131**, 993-1005 (2009).
26. Huzeifa Ismail, Paul R. Abel, William H. Green, Askar Fahr, Leonard E. Jusinski, Adam M. Knepp, Judit Zádor, Giovanni Meloni, Talitha M. Selby, David L. Osborn, and Craig A. Taatjes, "Temperature-Dependent Kinetics of the Vinyl Radical (C₂H₃) Self Reaction," *J. Phys. Chem. A* **113**, 1278-1286 (2009).
27. T. Kasper, P. Obwald, U. Struckmeier, K. Kohse-Höinghaus, C. A. Taatjes, J. Wang, T. A. Cool, M. E. Law, A. Morel, and P. R. Westmoreland, "The combustion chemistry of propanol isomers — investigated by electron ionization and VUV-photoionization molecular-beam mass spectrometry," *Combust. Flame*, doi:10.1016/j.combustflame.2009.01.023 (2009).

Theoretical Chemical Dynamics Studies of Elementary Combustion Reactions

Donald L. Thompson

Department of Chemistry, University of Missouri, Columbia, MO 65211
thompsondon@missouri.edu

Program Scope

The objective of our research is to develop and apply methods for more accurate predictions of reaction rates based on high-level quantum chemistry. We are developing and applying efficient, robust methods for fitting global *ab initio* potential energy surfaces (PESs) for both spectroscopy and dynamics calculations and for performing direct dynamics simulations. Our approach addresses the problem that high-level quantum calculations are often too costly in computer time for practical applications resulting in the use of levels of theory that are often inadequate for reactions. A critical objective was to develop practical methods that require the minimum number of electronic structure calculations for acceptable fidelity to the *ab initio* PES. Our method does this by a procedure that determines the optimal configurations at which *ab initio* points are computed, and that ensures that the final fitted PES is uniformly accurate to a prescribed tolerance. Our fitting methods can be done automatically, with little or no human intervention, and with no prior knowledge of the topology of the PES. The methods are based on local fitting schemes using interpolating moving least-squares (IMLS).¹⁻¹¹ IMLS has advantages over the very effective modified-Shepard methods developed by Collins and others¹²⁻⁵ in that higher-order polynomials can be used and does not require derivatives but can benefit from them if available.

Recent Progress

We have developed a general three-atom code for generating a PES to a prescribed accuracy over a specified energy or coordinate range using the IMLS approach interfaced to the electronic structure codes Gaussian, Molpro, or Aces II. The code automatically takes advantage of symmetry, has three options for internal coordinates, and can be run in parallel. We used this code to develop the most accurate ground-state PESs currently available for ¹CH₂ and HCN.¹⁵ They reproduce the experimentally measured equilibrium geometries in both molecules to within 0.001 Å for the two distances and within 0.2° for the bending angle. The calculated vibrational spectra for J=0 have mean unsigned errors relative to experiment of 1.4 cm⁻¹ for ¹CH₂ below 20,000 cm⁻¹ and 2.5 cm⁻¹ for HCN:HCN 12,000 cm⁻¹.

For ¹CH₂ this level of accuracy was achieved by a complete basis set (CBS) extrapolation of augmented triple and quadruple zeta level calculations using MRCI wavefunctions, a core-valence correlation correction derived from CCSD(T) calculations with and without frozen cores, and a geometry-scaled Davidson correction where the scaling parameters are set to approximate full-CI calculations at small basis set levels. The CBS extrapolation produced significantly more accurate vibrational frequencies than those derived from the quadruple zeta basis set calculations alone. For ¹CH₂, full-CI calculations were feasible and tests of the Davidson correction led to a simple scaling of the correction with the bend that reduced error at the small basis level. Application of this scaling to the Davidson correction at the CBS level produced our best result of a 2.0 cm⁻¹ root-mean-square error relative to the 11 known experimental levels. For HCN the most accurate results were obtained by calculations analogous to those for ¹CH₂. These calculations were feasible because of our efficient and automatic PES fitting scheme that reduced

both the number of expensive calculations and the amount of human attention required to produce PESs with negligible fitting error for eigenstate calculations of the vibrational levels. We grew fitted PESs over predefined ranges of energy starting with sparse sets of *ab initio* seed points on a regular grid. Running in parallel on eight processors, a usable PES is quickly generated in an essentially automatic fashion. (On the order of twenty different individually optimized PESs were produced in about a one-month period.) The fitting accuracies of the fitted PESs were confirmed by computing a test set of vibrational levels for $^1\text{CH}_2$ using the fitted surface nominally converged to 0.33 cm^{-1} mean unsigned fitting error and using direct *ab initio* electronic structure calculation of the points required by the DVR vibrational eigenstate program. The mean unsigned and maximum differences for these two eigenstate calculations for all 216 levels below $20,000\text{ cm}^{-1}$ are 0.10 cm^{-1} and 0.41 cm^{-1} , respectively. These errors are consistent with the convergence error of the fit and they are small relative to errors produced by deficiencies in the electronic structure calculations.

We have used our automatic PES generating code to construct a global OHCl ($^3A''$) surface at the UB3LYP/aug-cc-pVTZ level of theory.¹⁶ This PES includes all reaction channels and OHCl geometries with energies up to 144 kcal/mol (6.25 eV) above the O+HCl asymptote. We have carried out a comprehensive quasiclassical trajectory study of the O+HCl reactive system for collision energies between 46 kcal/mol and 138 kcal/mol on the fitted PES. Reaction cross sections, opacity functions, and differential cross sections for all open product channels were calculated. This study improves on previous direct dynamics simulations by eliminating many of the drawbacks of that approach, such as trajectory failure due to lack of convergence of the *ab initio* calculations, relatively poor energy conservation during trajectories, and severe limitations on the level of *ab initio* theory that is feasible, and the numbers of trajectories that can be computed. The fitted PES greatly improves energy conservation during trajectory integration and eliminates problems with *ab initio* convergence, which are often encountered during direct dynamics studies.

We develop two approaches for growing IMLS-fitted PESs using classical trajectories.¹⁷ We illustrate both approaches by calculating nitrous acid (HONO) *cis*→*trans* isomerization trajectories under the control of *ab initio* forces from low-level HF/cc-pVDZ electronic structure calculations. As few as 300 *ab initio* energy/gradient calculations are required to converge the isomerization rate constant at a fixed energy to ~10%. Neither approach requires any preliminary electronic structure calculations or initial approximate representation of the PES. Hessians are not required. Both approaches rely on the fitting error estimation properties of IMLS fits. We refer to the first approach as *IMLS-accelerated direct dynamics*, in which the PES is grown “on the fly” with the computation of new *ab initio* data only when a fitting error estimate exceeds a prescribed, tight tolerance. For the isomerization of HONO a speedup over direct dynamics of ~18 was achieved while maintaining a maximum rate of drift in total energy of less than 0.1 kcal/mol·ps. The second approach, called *dynamics-driven IMLS fitting*, uses relatively inexpensive exploratory trajectories to both determine and fit the dynamically accessible configuration space. Once exploratory trajectories no longer find configurations with fitting error estimates higher than the designated accuracy, the IMLS fit is considered to be complete. A converged rate constant for *cis*→*trans* HONO isomerization was computed using between two and three hundred *ab initio* points with energy and gradient data. These methods are like the GROW method¹⁶ of the Collins’ group. The IMLS approaches can accommodate basis functions of higher order and *ab initio* derivatives of lower order (i.e., no Hessians required) than the GROW method. Our approaches may be less dynamically biased because they grow the PES

based only on the classical trajectories with no prior *ab initio* information whereas a typical GROW application fits an input string of *ab initio* energy/gradient/Hessian calculations to sustain initial trajectories that then grow the PES. The results are quite encouraging. The *dynamics-driven IMLS fitting* method appears particularly promising for both studying dynamical processes and producing fits of the dynamically relevant configuration space in large systems.

This work is being done in collaboration with Dr. Al Wagner (ANL).

Future Work

The focus of our work will now be on applying these methods to produce kinetically and spectroscopically accurate global PESs for key combustion radicals and molecules and to develop practical methods for using IMLS in direct dynamics simulations.

Publication Based on DOE-Supported Work: 2007-2009

- Y. Guo, L. B. Harding, A. F. Wagner, M. Minkoff, and D. L. Thompson, "Interpolating Moving Least-Squares Methods for Fitting Potential Energy Surfaces: An Application to the H₂CN Unimolecular Reaction," *J. Chem. Phys.* **126**, 104105(1-9) (2007).
- R. Dawes, D. L. Thompson, Y. Guo, A. F. Wagner, and M. Minkoff, "Interpolating Moving Least-Squares Methods for Fitting Potential Energy Surfaces: Computing High-Density PES Data from Low-Density *ab initio* Data Points," *J. Chem. Phys.* **126**, 184108(1-11) (2007).
- I. Tokmakov, A. F. Wagner, M. Minkoff, and D. L. Thompson, "Interpolating Moving Least-Squares Methods for Fitting Potential Energy Surfaces: Gradient Incorporation in One-Dimensional Applications," *J. Theor. Chem. Accts.* **118**, 755-767 (2007).
- Yin Guo, Igor Tokmakov, Donald L. Thompson, Albert F. Wagner, and Michael Minkoff, "Interpolating Moving Least-Squares Methods for Fitting Potential Energy Surfaces: Improving Efficiency via Local Approximants," *J. Chem. Phys.* **127**, 214106(1-8) (2007).
- Richard Dawes, Donald L. Thompson, Albert F. Wagner, and Michael Minkoff, "Interpolating Moving Least-Squares Methods for Fitting Potential Energy Surfaces: A Strategy for Efficient Automatic Data Point Placement in High Dimensions," *J. Chem. Phys.* **128**, 084107(1-10), (2008).
- Jon P. Camden, Richard Dawes, and Donald L. Thompson, "Application of Interpolating Moving Least Squares (IMLS) Fitting to Hypervelocity Collision Dynamics: O(³P) + HCl" *J. Phys. Chem. A*, in press. (Part of George C. Schatz Festschrift)
- Richard Dawes, Albert F. Wagner, and Donald L. Thompson, "*Ab Initio* Wavenumber Accurate Spectroscopy: ¹CH₂ and HCN Vibrational Levels on Automatically Generated IMLS Potential Energy Surfaces," *J. Phys. Chem. A*, in press. (Part of George C. Schatz Festschrift).
- Richard Dawes, Alessio Passalacqua, Albert F. Wagner, Thomas D. Sewell, Michael Minkoff, and Donald L. Thompson, "Interpolating Moving Least-Squares Methods for Fitting Potential Energy Surfaces: Using Classical Trajectories to Explore Configuration Space," *J. Chem. Phys.*, in press.

References

- ¹ D. H. McLain, *Comput. J.* **17**, 318 (1974).
- ² R. Farwig, in *Algorithms for Approximation*, edited by J. C. Mason and M. G. Cox (Clarendon, Oxford, 1987).
- ³ G. G. Maisuradze and D. L. Thompson, *J. Phys. Chem. A* **107**, 7118 (2003).
- ⁴ G. G. Maisuradze, D. L. Thompson, A. F. Wagner, and M. Minkoff, *J. Chem. Phys.* **119**, 10002 (2003).
- ⁵ A. Kawano, Y. Guo, D. L. Thompson, A. F. Wagner, and M. Minkoff, *J. Chem. Phys.* **120**, 6414 (2004).
- ⁶ Y. Guo, A. Kawano, D. L. Thompson, A. F. Wagner, and M. Minkoff, *J. Chem. Phys.* **121** (11), 5091 (2004).
- ⁷ G. G. Maisuradze, A. Kawano, D. L. Thompson, A. F. Wagner, and M. Minkoff, *J. Chem. Phys.* **121**, 10329 (2004).
- ⁸ A. Kawano, I.V. Tokmakov, D. L. Thompson, A. F. Wagner, and M. Minkoff, *J. Chem. Phys.* **124**, 54105 (2006).
- ⁹ Y. Guo, L. B. Harding, A. F. Wagner, M. Minkoff, and D. L. Thompson, *J. Chem. Phys.* **126**, 104105 (2007).
- ¹⁰ I. Tokmakov, A. F. Wagner, M. Minkoff, and D. L. Thompson, *J. Theor. Chem. Accts.* **118**, 755 (2007).
- ¹¹ R. Dawes, D. L. Thompson, Y. Guo, A. F. Wagner, and M. Minkoff, *J. Chem. Phys.*, **126**, 184108 (2007)
- ¹² J. Ischtwan and M. A. Collins, *J. Chem. Phys.* **100**, 8080 (1994).
- ¹³ T. Ishida and G. C. Schatz, *Chem. Phys. Letters* **314**, 369 (1999).
- ¹⁴ M. Yang, D. H. Zhang, M. A. Collins, and S.-Y. Lee, *J. Chem. Phys.* **114**, 4759 (2001).
- ¹⁵ R. Dawes, A. F. Wagner, and D. L. Thompson, “*Ab Initio Wavenumber Accurate Spectroscopy: ¹CH₂ and HCN Vibrational Levels on Automatically Generated IMLS Potential Energy Surfaces.*” *J. Phys. Chem. A*, in press.
- ¹⁶ J. P. Camden, R. Dawes, and D. L. Thompson, “*Application of Interpolating Moving Least Squares (IMLS) Fitting to Hypervelocity Collision Dynamics: O(³P) + HCl*” *J. Phys. Chem. A*, in press.
- ¹⁷ R. Dawes, A. Passalacqua, A. F. Wagner, T. D. Sewell, M. Minkoff, and D. L. Thompson, “*Interpolating Moving Least-Squares Methods for Fitting Potential Energy Surfaces: Using Classical Trajectories to Explore Configuration Space.*” *J. Chem. Phys.*, in press.

Elementary Reactions of PAH Formation

Robert S. Tranter
C.S.E. Division
Argonne National Laboratory
Argonne, IL-60439
tranter@anl.gov

Program scope

This program is focused on the experimental determination of kinetic and mechanistic parameters of elementary reactions, in particular those involved in the formation and destruction of the building blocks for aromatic species. In addition thermal sources of radicals are investigated and characterized for use in more complex reaction systems where secondary chemistry can be significant. The approach involves a shock tube (ST) equipped with laser schlieren (LS) and a time-of-flight mass spectrometer (TOF-MS) and the development of a low pressure, fast flow, reactor equipped with a quadrupole MS. The combination of these techniques permit a wide range of reaction temperatures and pressures to be access.

Recent Progress

In 2007 the shock tube was converted to a diaphragmless shock tube (DFST) and has been run exclusively in this mode since then. A primary benefit of the DFST is that it gives extremely good control over the post shock conditions generated. The ability to generate reproducible post shock conditions has been previously reported and as more experience has been gained with the DFST the variation in postshock pressure for a temperature range spanning at least 1400 K is now constrained to $< \pm 3\%$.

In the past year a number of precursors for phenyl and methyl radicals have been investigated in the shock tube and detailed studies made of the self-reactions of these radicals and subsequent secondary chemistry to try and fully characterize the radical sources at the conditions prevalent in the shock tube prior to conducting more complex radical/molecule and cross reactions

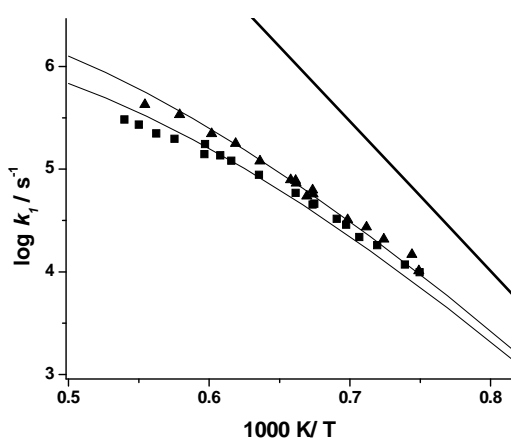


Figure 1: Initial rate coefficients derived from density gradient profiles for 2% $\text{C}_6\text{H}_5\text{I}$ in Kr and the results of Gorin model calculations. Experimental data: [▲] $P_2 = 121 \pm 6$ torr; [■] $P_2 = 57 \pm 9$ Torr; Calculations: Thin lines represent RRK calculations at the nominal pressures; Thick line = k_∞ .

Phenyl Radicals: With Kiefer the thermal dissociation of $\text{C}_6\text{H}_5\text{I}$, 2% dilute in krypton, has been studied by DFST/LS as a source of phenyl radicals over the temperature range 1300-1800 K and at 57 ± 9 Torr and 121 ± 6 Torr. The thermochemical properties for $\text{C}_6\text{H}_5\text{I}$ and several species formed in the pyrolysis of it were reevaluated by Russic and play an important role in interpreting the LS results. From the LS profiles initial rates of dissociation of phenyl iodide have been obtained. The dissociation of $\text{C}_6\text{H}_5\text{I}$ is in the fall-off region and the experimental results are well simulated with a restricted rotor Gorin model calculation using molecular parameters from a previous study by Michael et al [1]. However, it was

necessary to use a somewhat larger ΔE_{down} of 850cm^{-1} than that used by Michael et al.

Under most of the experimental conditions dissociation of phenyl radicals is unimportant. However, above about 1600 K the dissociation does contribute to the LS profiles and at the highest temperatures a small contribution from benzyne dissociation is observed. In addition to the DFST/LS experiments DFST/TOF-MS experiments were also performed. Due to experimental difficulties these latter experiments were restricted to product analysis and the order of appearance of products rather than the normal combined kinetic/product studies. Under all conditions, it was found that benzene and benzyne, C_6H_4 , were formed immediately along with biphenyl and biphenylene (C_{12}H_8). The formation of these species at low temperatures suggests that they are not due to dissociation of phenyl radicals and subsequent reactions. Furthermore, with the reagent concentrations in the LS and TOF-MS work recombination of phenyl radicals is likely. Consideration of the density gradient profiles from the LS experiments and the TOF-MS data suggested that recombination phenyl radicals follows two reaction paths: 1) Stabilization to biphenyl; 2) Disproportionation to benzene + o/m/p-benzyne. This latter path does not appear to have been considered previously. In a collaborative effort Klippenstein has investigated the $\text{C}_6\text{H}_5 + \text{C}_6\text{H}_5$ reaction theoretically and has determined results that are in reasonable agreement with the LS experiments. Over the range of experimental conditions the disproportionation route accounts for about 50% of the phenyl self reaction and becomes increasingly significant at higher temperatures. Further evidence for the disproportionation channel has been gained from DFST/TOF-MS experiments with $\text{C}_6\text{F}_5\text{I}$. In this work the perfluorinated analogs of benzyne, phenyl, benzene, biphenylene and biphenyl have been observed with similar appearance patterns to that found with phenyl iodide.

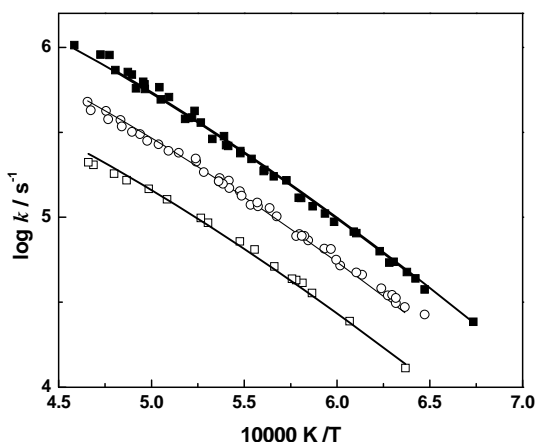


Figure 2: Initial rate coefficients derived from density gradient profiles for CH_3I dissociation in krypton and the results of Gorin model calculations. Experimental data: 2% and 4% [■] $P_2 = 280 \pm 6$ Torr; 2% and 4% [○] $P_2 = 146 \pm 3$ Torr; 2% [□] $P_2 = 66 \pm 2$ Torr; Lines are results of RRMK calculations at the nominal pressures.

experimental results.

From the CH_3I and diacetyl studies a model for recombination of methyl radicals has been developed that provides excellent simulations for all the CH_3I and diacetyl LS experiments. An important aspect of the model results from a collaborative effort with Harding and Klippenstein who examined the secondary reaction channels of $\text{CH}_3 + \text{CH}_3$. The final model

Methyl Radicals: Two sources of methyl radicals have been investigated using DFST/LS under conditions similar to those used with phenyl iodide. Methyl iodide ($66 < P_2 < 280$ Torr, $1500 < T < 2200$ K) dissociates exclusively via fission of the C-I bond and diacetyl ($55 < P_2 < 120$ Torr, $1200 < T < 1800$ K) dissociates by C-C fission to form two acetyl radicals which rapidly decompose to methyl and CO. The rates of dissociation of methyl iodide are well simulated by a Gorin model calculation, Fig. 2, that assumed a temperature dependent form for $\Delta E_{down} = 378 \times (T/298)^{0.457} \text{cm}^{-1}$ and molecular parameters from Michael et al. [1]. Similar to the $\text{C}_6\text{H}_5\text{I}$ studies the rate coefficients for CH_3I dissociation are 1.5 to 2 higher than those of Michael et al. The dissociation of diacetyl was carried out in collaboration with Kiefer and Jasper and ab-initio/master equation calculations by Jasper for diacetyl dissociation are in good agreement with the

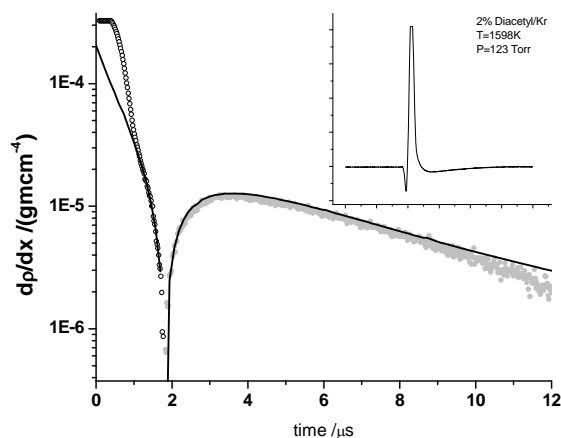


Figure 3: Example density gradient profile and raw laser schlieren signal (inset figure) for the dissociation of diacetyl. $t=0$ on the density gradient plot is located under the large spike on the inset figure which arises from passage of the shock front through the laser beam. The first few points of the plot correspond to the tail of this spike. Absolute values are plotted and open symbols represent positive values, closed symbols represent negative ones. The line is the result of simulation incorporating the methyl sub model.

of 20 ± 1 Torr and $600 < T < 2000$ K to try and resolve vibrational relaxation and obtain estimates of incubation times for inclusion in the modeling of CH_3I dissociation. Below about 1400 K pure relaxation is observed in all the experiments and above about 1400 K relaxation followed by dissociation is observed. From these latter experiments both relaxation and incubation times can be estimated. Above about 1700 K in the 10% and 20% experiments the contribution of dissociation to the density gradient is too large and relaxation times can no longer be obtained. Incubation times spanned the range 1.5 to 3 μs at 20 Torr and the ratio to the relaxation time was incorporated into the modeling of methyl iodide experiments. Attempts were made to resolve vibrational relaxation in diacetyl however it is simply too fast.

1,4-dioxane: In a previous abstract a discrepancy between LS and TOF-MS experiments on the dissociation of 1,4-dioxane had been noted. The LS experiments indicated that CH_3 radicals were formed in the dissociation of 1,4-dioxane and that a likely source was a decomposition channel leading to acetaldehyde. However, the TOF-MS studies showed no trace of acetaldehyde. Recently, in collaboration with Jasper we have explored the dissociation of 1,4-dioxane theoretically and developed a reaction mechanism that satisfies both the LS and TOF-MS observations. Currently, the model is being tested and includes the recently developed methyl radical sub mechanism.

Future Plans

Now that sources of methyl and phenyl radicals suitable for DFST/LS and DFST/TOF-MS experiments have been characterized it is intended to start to investigate radical/molecule reactions involving these species particularly with respect to molecular growth reactions. It is also planned to start studying the reactions of benzyne using particularly the self reaction and the addition of acetylinic species to benzyne to complement theoretical work by Klippenstein.

includes ($\text{CH}_3 + \text{CH}_3 = \text{C}_2\text{H}_6 + \text{H}$) and ($\text{CH}_3 + \text{CH}_3 = {}^1\text{CH}_2 + \text{CH}_4$) along with appropriate reactions of methylene and, H and CH_3 attack on the parent species. An example simulation of a diacetyl decomposition experiment is shown in Fig. 3. The model is particularly sensitive to the location of the switch from positive to negative density gradients and the depth of the well in addition to the overall shape. As an additional test of the methyl sub mechanism, a set ethane dissociation of LS experiments that encompass the range of Kiefer et al.'s [2] previous ethane pyrolysis LS experiments were performed and the data are very well simulated with the new methyl sub-model

Vibrational Relaxation in CH_3I : In some the CH_3I dissociation experiments there appeared to be an incubation delay. Consequently, a series experiments were conducted using 2, 10 and 20% mixtures of CH_3I dilute in krypton at reaction pressures

A modified DFST has been designed and will be implemented. The new design should increase the range of shock strengths available. In addition the nozzle/skimmer interface between the DFST and TOF-MS will be redesigned to allow easier access and heating which will become increasingly important as the experiments involve larger species.

References

1. S. S. Kumaran, M.-C. Su, J. V. Michael, Chem. Phys. Lett. 269, 99-106, 1997
2. J.H.Kiefer, S.Santhanam, N.K.Srinivasan, R.S.Tranter, S.J.Klippenstein and M.A.Oehlschlaeger, Proc. Combust. Inst. 30, 1129-1135, 2005

Publications 2007-

1. Giri B. R., Klippenstein S. J., Kiefer J. H. and Tranter R. S., "An Experimental and Theoretical High Temperature Kinetic Study of the Thermal Unimolecular Dissociation of Fluoroethane", Phys. Chem. Chem. Phys., 10, 6266 - 6273., 2008.
2. Tranter R. S. and Giri B. R., "A Diaphragmless Shock Tube for High Temperature Kinetic Studies", Rev. Sci. Instrum., 79, 094103, 2008
3. Xu H., Kiefer J. H., Sivaramakrishnan R., Giri B.R. and Tranter R. S., "Shock tube study of dissociation and relaxation in 1,1-difluoroethane and vinylfluoride", Phys. Chem. Chem. Phys., 9, 4164-4176, 2007.
4. Saxena S., Kiefer J. H. and Tranter R. S., "Relaxation, Incubation, and Dissociation in CO₂", J. Phys. Chem. A, 111, 3884 - 3890, 2007.
5. Tranter R. S., Giri B. G. and Kiefer J. H., "Coupling of a Shock Tube to a Time-of-Flight Mass Spectrometer for High Temperature Kinetic Studies" Rev. Sci. Instrum., 78, 034101, 2007.
6. Giri B.R. and Tranter R. S., "Dissociation of 1,1,1-Trifluoroethane Behind Reflected Shock Waves: Shock Tube/Time-of-Flight Mass Spectrometry Experiments" J. Phys. Chem. A, 111(9), 1585 – 1592, 2007.
7. Sivaramakrishnan R, Comandini A, Tranter R. S., Brezinsky K., Davis S. G. and Wang H., "Combustion of CO/H₂ Mixtures at Elevated Pressures", Proc. Combust. Inst., 31, 167-174, 2007
8. Sivaramakrishnan R., Tranter R. S. and Brezinsky K., "High Pressure Pyrolysis of Toluene. 2. Modeling Benzyl Decomposition and Formation of Soot Precursors", J. Phys. Chem. A 110(30), 9400-9404, 2006
9. Sivaramakrishnan R., Tranter R. S., Brezinsky K., "High Pressure Pyrolysis of Toluene. 1. Experiments and Modeling of Toluene Decomposition", J. Phys. Chem. A 110(30), 9388-9399, 2006
10. Gupte K. S., Kiefer J. H., Tranter R.S., Klippenstein S. J. and Harding L. B., "Decomposition of Acetaldehyde: Experiment and Detailed Theory", Proc. Combust. Inst. 31, 429-437, 2007

Variational Transition State Theory

Donald G. Truhlar

Department of Chemistry, University of Minnesota
207 Pleasant Street SE, Minneapolis, Minnesota 55455
truhlar@umn.edu

Program scope

This project involves the development of variational transition state theory (VTST) with optimized multidimensional tunneling (OMT) contributions and its application to gas-phase reactions. For overbarrier processes, we are employing both methods suitable for tight transition states, employing isoinertial minimum energy paths, variational reaction paths, and curvilinear generalized normal mode coordinates (Garrett, Truhlar 1979; Isaacson, Truhlar 1982; Jackels, Gu, Truhlar 1995; Fast, Truhlar 1998), and methods suitable for loose transition states, employing multifaceted dividing surfaces and Monte Carlo integration over transition modes (Georgievskii, Klippenstein 2003). For optimized multidimensional tunneling, we employ small curvature tunneling (Skodje, Truhlar, Garrett 1981; Liu, Lynch, Truong, Lu, Truhlar, Garrett 1993) and large curvature tunneling (Garrett, Truhlar, Wagner, Dunning 1983; Fernandez and Truhlar 2001).

The further development of VTST/OMT as a useful tool for combustion kinetics involves advancing the ability of electronic structure calculations (both wave function and density functional theory) of the required potential energy surface, which we now take as an implicit surface defined by a level of electronic structure theory (direct dynamics: Baldrige, Gordon, Steckler, Truhlar, 1989; González-Lafont, Truong, Truhlar 1991). We are developing new methods to interface reaction-path and reaction-swath dynamics calculations with electronic structure theory, for example, multiconfiguration molecular mechanics (Kim, Corchado, Villà, Xing, Truhlar 2000). We are developing and implementing of practical techniques and software for applying these theoretical methods to various classes of reactions and transition states and making applications to specific reactions, with special emphasis on combustion reactions and reactions that provide good test cases for methods needed to study combustion reactions.

Recent progress

We have completed the major project of the incorporation of the variable-reaction-coordinate multifaceted-dividing-surface algorithm for treating dividing surfaces appropriate of barrierless association reactions into a new parallel version of the freely available POLYRATE program. Using this updated program, we showed that the difficulty in efficiently generating accurate estimates for the radical-radical interaction energies is alleviated by the new M06 suite of density functionals, which are capable of accuracy as good as more expensive and more troublesome high-level wave function calculations for calculating radical association rate constants. Density functional theory is applicable to large, complex systems because of favorable cost scaling.

The diverse barrier height database DBH24 has been updated by using W4 and W3.2 data to replace previous W1 values. We used the new database to assess 348 model chemistries, each consisting of a combination of a wave function theory level or a density functional approximation with a one-electron basis set. We are also developing improved electronic structure methods and using them for rate constant calculations. One class of new methods involves wave function theory, especially generally defined electronic wave function methods with empirical elements; another class of methods is based on new density functionals. These methods are then used in direct dynamics calculations or with efficient interpolation schemes. Direct dynamics denotes that, instead of using a pre-defined potential energy function, all

required energies and forces for each geometry that is important for evaluating dynamical properties are obtained directly from electronic structure calculations. Density functional theory is very attractive as an electronic structure method for direct dynamics because of its relatively low cost and the availability of analytic gradients and Hessians. Development of improved exchange and correlation functionals is an active research area in theoretical chemistry and physics, but most of this research has neglected the important issues of barrier height prediction and noncovalent interactions, and as a consequence the functionals have not been accurate for quantitative kinetics. We have now developed new functionals, especially the M06-2X functional (Minnesota 2006 functional with double nonlocal exchange), that are quite accurate for these properties, and we have also developed multi-coefficient correlation methods for using wave function theory for these properties. A test of the M06-2X functional on DBH24 yielded a mean unsigned error of only 0.5 kcal/mol, comparable to the accuracy of CCSD(T). A key advantage of M06-2X as compared to other density functionals is the improved accuracy for attractive noncovalent interactions. This is important for barrierless reactions and for reactions with low, early saddle points (like OH + H₂S), where it is necessary to have a consistent treatment of the energy along the reactant approach coordinate.

The calculation of chemical reaction barrier heights often requires multireference methods, but well-defined and validated multireference methods for barrier height calculations have not been available. Now we have developed three model chemistries based on multireference methods, and we demonstrated their use and validated them for calculating barrier heights of chemical reactions by applying them to a new database of diverse-reaction barrier heights.

In order to generate reactive potential energy surfaces with minimal computational effort, we have introduced an algorithm called multiconfiguration molecular mechanics (MCMM). MCMM describes polyatomic potential energy surfaces by interacting molecular mechanics (MM) configurations (each of which is the analog of a valence bond configuration) and can thus be viewed as an extension of standard MM to chemical reactions or as an extension of semiempirical valence bond theory to be systematically improvable. MCMM fitting is accomplished by combining molecular mechanics potentials for the reactant and product wells with electronic structure data (energy, gradient, and Hessian) at the saddle point and a small number of non-stationary points. We have now identified the key elements required both to make MCMM more accurate and to make it more efficient, and these have been incorporated in a new non-Hermitian version of the algorithm, with very stable analytic gradients.

Software distribution

We have developed several software packages for applying variational transition state theory with optimized multidimensional tunneling coefficients to chemical reactions and for carrying out MCCM calculations, density functional theory calculations with new density functionals, direct dynamics, and MCMM applications. The URL of our software distribution site is comp.chem.umn.edu/Truhlar. The license requests that we fulfilled during the period Jan. 1, 2007–Mar. 27, 2009 for software packages developed wholly or partially under DOE support is as follows:

	<i>Total</i>	<i>academic</i>	<i>government/DoD</i>	<i>industry</i>
POLYRATE	187	175	8	4
GAUSSRATE	91	85	3	3
GAMESSPLUS	62	53	4	5
MULTILEVEL	25	25	0	0
10 others	53	50	3	0

where the 10 others are ABCRATE, GAMESSPLUSRATE, JAGUARATE, MORATE, MC-TINKER, MC-TINKERATE, MFM, MLGAUSS, MULTILEVELRATE, and MN-NWCHEMRATE.

Future plans

We have several objectives for the next few years: (1) treat the stabilization of intermediate complexes by energy transfer collisions; (2) integrate the above methods with tight transition state methods to treat multiwell reactions and reactions with inner and outer dynamical bottlenecks; (3) further improve our density functionals and multi-coefficient correlation methods for potential energy surfaces, especially for saddle point geometries, barrier heights, and vibrational frequencies at saddle points; (4) further develop the multi-configuration molecular mechanics approach as an efficient tool for the semiautomatic fitting of complex-system potential energy surfaces and apply it to calculate reaction rates for complex systems; (5) develop more reliable methods for including anharmonicity at variational transition states, especially for torsions and mode-mode coupling; (6) continue our calculations of reaction rates of peroxides and enols; (7) perform direct dynamics calculations of temperature-dependent rate constants for hydrogen-transfer isomerization of 1-pentyl and 1-hexyl radical as required for combustion modeling; (8) enhance our user-friendly computer program packages to allow more researchers to carry out calculations conveniently by the new methods.

Publications, 2007-present

Journal articles

1. "Representative Benchmark Suites for Barrier Heights of Diverse Reaction Types and Assessment of Electronic Structure Methods for Thermochemical Kinetics," J. Zheng, Y. Zhao, and D. G. Truhlar, *Journal of Chemical Theory and Computation* **3**, 569-582 (2007).
2. "Global Potential Energy Surfaces with Correct Permutation Symmetry by Multi-Configuration Molecular Mechanics," O. Tishchenko and D. G. Truhlar, *Journal of Chemical Theory and Computation* **3**, 938-948 (2007).
3. "The M06 Suite of Density Functionals for Main Group Thermochemistry, Thermochemical Kinetics, Noncovalent Interactions, Excited States, and Transition Elements: Two New Functionals and Systematic Testing of Four M06 Functionals and Twelve Other Functionals," Y. Zhao and D. G. Truhlar, *Theoretical Chemistry Accounts*, accepted Feb. 13, 2007. (Mark S. Gordon 65th Birthday Issue)
4. "Thermochemical Kinetics of Hydrogen-Atom Transfers Between Methyl, Methane, Ethynyl, Ethyne, and Hydrogen," J. Zheng, Y. Zhao, and D. G. Truhlar, *Journal of Physical Chemistry A* **111**, 4632-4642 (2007).
5. "Symmetry Numbers and Chemical Reaction Rates," A. Fernández-Ramos, B. A. Ellingson, R. Meana-Pañeda, J. M. C. Marques and D. G. Truhlar, *Theoretical Chemistry Accounts* **118**, 813-826 (2007).
6. "Multi-Coefficient Gaussian-3 Calculation of the Rate Constant for the OH + CH₄ Reaction and its ¹²C/¹³C Kinetic Isotope Effect with Emphasis on the Effects of Coordinate System and Torsional Treatment," B. A. Ellingson, J. Pu, H. Lin, Y. Zhao, and D. G. Truhlar, *Journal of Physical Chemistry A* **111**, 11706-11717 (2007).
7. "Explanation of the Unusual Temperature Dependence of the Atmospherically Important OH + H₂S → H₂O + SH Reaction and Prediction of the Rate Constant at Combustion Temperatures," B. A. Ellingson and D. G. Truhlar, *Journal of the American Chemical Society* **129**, 12765-12771 (2007).
8. "Computational Chemistry of Polyatomic Reaction Kinetics and Dynamics: The Quest for an Accurate CH₅ Potential Energy Surface," Titus V. Albu, J. Espinosa-García, D. G. Truhlar, *Chemical Reviews* **107**, 5101-5132 (2007).
9. "Reactions of Hydrogen Atom with Hydrogen Peroxide," B. A. Ellingson, D. P. Theis, O. Tishchenko, J. Zheng, and D. G. Truhlar, *Journal of Physical Chemistry A* **111**, 13554-13566 (2007).

10. "Non-Born–Oppenheimer Molecular Dynamics of Na...FH Photodissociation," A. W. Jasper and D. G. Truhlar, *Journal of Chemical Physics* **127**, 194306/1-7 (2007).
11. "A Comparative Assessment of the Perturbative and Renormalized Coupled Cluster Theories with a Non-iterative Treatment of Triple Excitations for Thermochemical Kinetics, Including a Study of Basis Set and Core Correlation Effects," J. Zheng, J. R. Gour, J. J. Lutz, M. Włoch, P. Piecuch, and D. G. Truhlar, *Journal of Chemical Physics* **128**, 44108/1-7 (2008).
12. "How Well Can New-Generation Density Functionals Describe the Energetics of Bond Dissociation Reactions Producing Radicals?" Y. Zhao and D. G. Truhlar, *Journal of Physical Chemistry A* **112**, 1095-1099 (2008).
13. "VBSM: A Solvation Model Based on Valence Bond Theory," P. Su, W. Wu, C. J. Cramer, C. P. Kelly, and D. G. Truhlar, *Journal of Physical Chemistry A* **112**, 12761-12768 (2008).
14. "Assessment of New Meta and Hybrid Meta Density Functionals for Predicting the Geometry and Binding Energy of a Challenging System: the Dimer of H₂S and Benzene," H. R. Leverentz and D. G. Truhlar, *Journal of Physical Chemistry A* **112**, 6009-6016 (2008).
15. "Multireference Model Chemistries for Thermochemical Kinetics," O. Tishchenko, J. Zheng, and D. G. Truhlar, *Journal of Chemical Theory and Computation* **4**, 1208-1219 (2008).
16. "Effects of ¹⁸O Isotopic Substitution on the Rotational Spectra and Potential Splitting in the OH–H₂O Complex: Improved Measurements for ¹⁶OH–¹⁶OH₂ and ¹⁸OH–¹⁸OH₂, New Measurements for the Mixed Isotopic Forms, and Ab Initio Calculations of the 2A' – 2A" Energy Separation," C. S. Brauer, G. Sedo, E. Dahlke, S. Wu, E. Grumstrup, K. R. Leopold, M. D. Marshall, H. O. Leunge, and D. G. Truhlar, *Journal of Chemical Physics* **129**, 104304/1-11 (2008).
17. "Density Functional Study of Methyl Radical Association Reaction Kinetics," J. Zheng, S. Zhang, and D. G. Truhlar, *Journal of Physical Chemistry A* **112**, 11509-11513 (2008).
18. "The DBH24/08 Database and Its Use to Assess Electronic Structure Model Chemistries for Chemical Reaction Barrier Heights," J. Zheng, Y. Zhao, and D. G. Truhlar, *Journal of Chemical Theory and Computation*, in press.
19. "Efficient Diffuse Basis Sets: cc-pVxZ+ and cc-pV(x+d)Z+," E. Papajak, H. R. Leverentz, J. Zheng, and D. G. Truhlar, *Journal of Chemical Theory and Computation*, in press.
20. "Thermochemical Kinetics for Multireference Systems: Addition Reactions of Ozone," Y. Zhao, O. Tishchenko, J. R. Gour, W. Li, J. J. Lutz, P. Piecuch, and D. G. Truhlar, *Journal of Physical Chemistry A*, in press.
21. "Improved methods for Feynman Path Integral Calculations of Vibrational-Rotational Free Energies and Application to Isotopic Fractionation of Hydrated Chloride Ions," *Journal of Physical Chemistry A*, Articles ASAP; DOI: 10.1021/jp900834u.

Book chapters

1. "Multilevel Methods for Thermochemistry and Thermochemical Kinetics," B. J. Lynch, D. G. Truhlar, in *Recent Advances in Electron Correlation Methodology*, edited by A. K. Wilson and K. A. Peterson (American Chemical Society Symposium Series Volume 958, Washington, DC, 2007), pp. 153-167.
2. "Variational Transition State Theory in the Treatment of Hydrogen Transfer Reactions," D. G. Truhlar and B. C. Garrett, in *Hydrogen Transfer Reactions*, edited by J. T. Hynes, J. P. Klinman, H.-H. Limbach, and R. L. Schowen (Wiley-VCH, Weinheim, Germany, 2007), Vol. 2, pp. 833-874.
3. "Variational Transition State Theory with Multidimensional Tunneling," A. Fernandez-Ramos, B. A. Ellingson, B. C. Garrett, D. G. Truhlar, in *Reviews in Computational Chemistry*, Vol. 23, edited by K. B. Lipkowitz and T. R. Cundari (Wiley-VCH, Hoboken, NJ, 2007), pp. 125-232.

Chemical Kinetic Data Base for Combustion Modeling

Wing Tsang
National Institute of Standards and Technology
Gaithersburg, MD 20899
Wing.tsang@nist.gov

Program Scope and Definition: Modern trends in technology has led to continual interest in computer simulations. This represents a cost effective solution .to empirical physical testing. Progress in the development of Computational Fluid Dynamics (CFD)[1,2] has led to the capability of handling increasingly detailed chemistry. The aim of this program is to develop the thermodynamic and kinetics information base necessary to carry out successful simulations. Especially important is information that is fundamentally correct in the sense that they are transferable to all types of combustion systems and all types of organic fuels. The last is a particularly daunting challenge. Real fuels are complex mixtures of organic compounds. Hence the database must contain not only direct studies but also sufficient information to permit the establishment of general rules that can be used as a basis for estimation. A particular advantage of this fundamental approach is that it is easily extensible to all type of organic fuels. Recent interest in alternative fuels, particularly biofuels, means that in the development of the information base of the simulation of such mixtures one can more efficiently enlarge the existing data base by adding the specific species that are introduced. Such an approach may be the only feasible one when dealing with mixtures and especially for the cases where there may be variations in the composition.

At the fundamental level for combustion kinetics applications there are only unimolecular and bimolecular processes. The situation with regard to the latter is fairly satisfactory. There are a large amount of data and the existence of correlations mean that satisfactory predictions can be made. Unimolecular processes is a more challenging area and is the focus of this program.. This involves the breakdown of the fuel and fuel radicals These are key steps in the pyrolytic breakdown of fuel molecules. It reduces the size of the fuel to the small unsaturates and fragments that are the precursors for PAH/SOOT formation. Practically all the existing fuel combustion models are for single component fuels and fitted to global results near stoichiometric conditions. The present work extends the range of existing models to cover richer systems and mixtures. Since it involves only the fuel molecule and radicals (C and H), pyrolytic systems represent the logical first step in any chemical kinetic approach to unraveling the detailed chemistry of combustion of real fuels.. It sets the stage to determining the nature of the oxidation process by treating the oxygen induced reaction as a perturbation on the pyrolytic situation.

Recent Progress:

A: Chemical activation and combustion kinetics The focus of the past years work has been on the inclusion of data chemical activation processes into combustion kinetics databases. This is an important but neglected element in existing models. They are particularly important in combustion systems due to the high concentration of reactive species in the high energy environment. Their combination with each other will lead to a vibrationally hot molecule. If

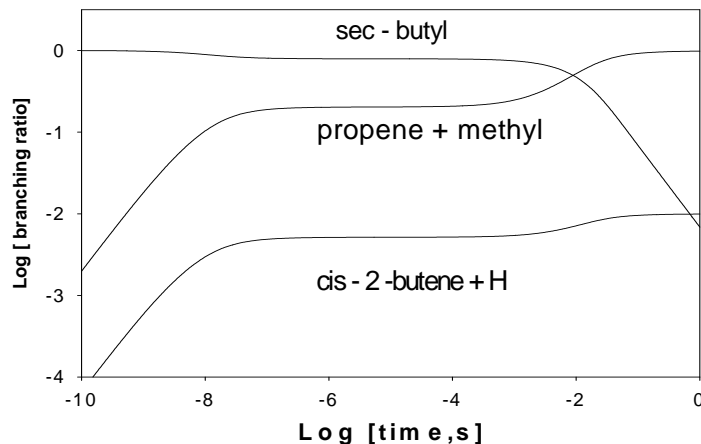


Figure 1: Branching ratios for the chemically activated sec-butyl radical formed from H-atom attack on cis-2-butene at 600 K and 1bar hydrogen molecule pressure

they are not thermalized then it is this hot molecule that will fall apart. The consequence is that the thermal rate constants usually used in combustion kinetics models can seriously under predict the actual rate constant. In order to match target global observations, adjustments must be made to fine tune the data. The consequence is a cascade of errors. The general situation is illustrated in Figure 1. This is a plot of the branching ratio for the decomposition of sec-butyl radical at 600 K and 1 bar pressure in hydrogen upon addition of H-atoms to cis-2-butene. It can be seen after an initial start-up period there is a period of time where the branching ratio is constant and therefore one can express results as a rate constant. For this situation it is simply the high pressure rate constant for the H-atom addition reaction times the branching ratio. This is the chemical activation process. Subsequently as more and more radicals are stabilized the thermal reaction begins to make contributions. Thus proper description of the system with respect to the kinetics is to add the chemically activated reaction to the thermal process. It should be noted that these branching ratios are functions of pressure. This in turn is a function of the bath molecule and represents an added complication.

B: Unimolecular rate constants from chemical activation studies Equally important is the existence of a large set of data on hydrocarbon radical decomposition carried out years ago by Rabinovitch and coworkers (3). These covered molecules with up to sixteen carbon atoms and with many types of alkyl side chains. In addition there exist data for certain reactions particularly, H-transfer isomerizations that have not been experimentally determined except from chemical activation studies.. Thus with more recent high temperature single pulse shock tube studies carried out in this laboratory with AFOSR support(4), there is the possibility of giving a complete fundamentally based picture of pyrolytic decompositions. For the present purposes the importance of the earlier work is that they are extremely clean experimentally. The first results were produced a few years after the introduction of gas chromatography and shows the importance of the capability of detecting a wide range products in dealing with complicated reaction.

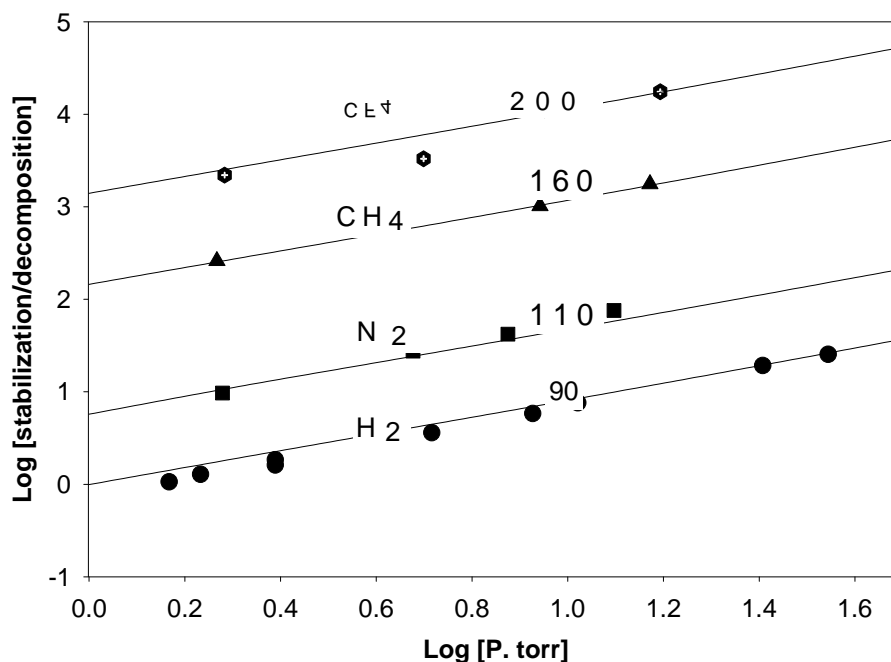


Figure 2: Step size down[cm^{-1}] for various bath molecules for the chemically activated decomposition of sec-butyl radicals for exponential model. Points are experimental results from Tardy and Rabinovitch[5]. Lines are from master equation solution using high pressure rate expressions from Tsang[6]

The original motivation of the chemically activated study was to demonstrate the connection between thermal and chemical activation processes through RRKM calculations(7) Unfortunately, due to the use of the then generally accepted values for the thermodynamic properties of the radicals the rate expressions for thermal reactions used to fit the results can no longer be accepted (6). Furthermore the energy transfer parameter the step size down appear to be considerably larger than modern day values(7). Thus although the connection between thermal and chemically activated results was in fact validated, it is suspected that these are compensating errors. This will be demonstrated to be the case. Results are plotted in Figure 1. it can be seen that using the new rate expressions the step size down necessary to fit the results have now been reduced to near by close to an order of magnitude This is in line with more recent determinations from thermal studies. The earlier chemical activation studies have indicated that at least for alkyl radicals the step down parameter does not appear to vary with molecular structure. We have now confirmed these results for the chemically activated decomposition of 2-hexyl radicals With these assumptions it is now possible to project the chemical activation results to combustion conditions and in combination with direct higher temperature studies expand considerably the data base for fuel pyrolysis. However these projections may have considerable uncertainties especially for larger fuel radicals where there

are multiple reaction channels. Clearly there is no substitute for direct measurements of branching ratios.

Future Work: We have spent considerable time on the chemically activated decomposition of heptyl radicals. The thermal reactions have been studied earlier so that there is a complete set of rate expressions. There are however problems with fitting the data of Hardwidge et al[8] on the H-transfer isomerization from the 2 to the 3 position (5-center transition state). Future work will aim at tracing the source of discrepancy. Another direction will be to analyze similar reactions for other alkyl radicals. In addition we will analyze the chemically activated decomposition of branched alkyl radicals so as to build the chemical kinetic database for the pyrolysis of the Fischer-Tropsch fuels. .

Publications 2006-2008

1. Colket M., Edward, C. T., Williams, S., Cernansky, N. P., Miller, D. L., Egolfopoulos, F., Lindstedt, P., Seshadri, K., Dryer F. L., Law, C. K., Friend, D., Lenhart, D. B., Pitsc, H., Sarofim, A, Smooke, M., Tsang, W., “Development of an Experimental Database and Kinetic Models for Surrogate Fuels”, 45th AIAAAerospace Sciences Meeting and Exhibit, Reno, Nevada, January 9, 2007
2. Tsang, W, Walker, J. A. and Manion, J. A., Proc. Comb. Institute, 31, 141-148, 2007
- 3 . Tsang, W.,Awan,I., McGovern, S., Manion, J. A., “Soot Precursors from Real Fuels: The Unimolecular Reactions of Fuel Radicals” in “Combustion Generated Fine Carbon Particles” (A. Sarofim, ed) in press
4. Tsang, W., McGovern, S., Manion, J. A., “Multichannel Decomposition and Isomerization of Octyl Radicals Proc Comb. Institute 32, submitted
5. McGivern, W. S., Iwan, I., Tsang, W, and Manion, J. A., Isomerization and Decomposition Reactions in the Pyrolysis of Branched Hydrocarbons: 4-Methyl-1-pentyl Radical, , Journal of Physical Chemistry A, 2008, 112, 6908-6917.

References

1. Kee, R. J., Coltrin, M. E. and Glarborg, P., “Chemically Reacting Flow” Theory and Practice, Wiley, Interscience, New York, 2003
2. Maas, U. and Pope, S. B., Comb. Flame 88, 2391, 1992
3. Pearson, MJ, Rabinovitch, B. S. , 42, 1624, 1965
4. Tsang, W.,Awan,I., McGovern, S., Manion, J. A., “Soot Precursors from Real Fuels: The Unimolecular Reactions of Fuel Radicals” in “Combustion Generated Fine Carbon Particles” (A. Sarofim, ed) in press
5. Tardy, D. C. and Rabinovitch, B. S., 48, J. Chem.Phys., 48, 5194, 1968
6. Tsang, W., J. Amer. Chem. Soc., 107, 2872, 1885
7. Knyazev, V. D. and Slagle, I. R., *J. Phys. Chem.*, 100, (1996), 5318-5328
8. Robinson, P. J. and Holbrook, K. A., “Unimolecular Reactions” Wiley,New York, 1972
9. Hardwidge, E. A. . Larson, C. W. And Rabinovitch, B. S., J. Amer. Chem. Soc., 92, 3278, 1970

Ultrafast Structural Dynamics as seen through Rydberg Electrons

Peter M. Weber
Department of Chemistry
Brown University, Providence, Rhode Island 02912
Peter_Weber@brown.edu

1. Program Scope

We have discovered that Rydberg electrons can serve as uniquely capable spies of the geometric structure of molecular ion cores. As a Rydberg electron passes the ion core it experiences a phase shift that determines the binding energy of the Rydberg electron. In our experiments, the Rydberg electron binding energies are observed by photoionization-photoelectron spectroscopy. Because the phase shifts are sensitively dependent on the molecular structure, we can characterize molecular structures through photoelectron spectroscopy of Rydberg states.

The spectroscopy of the structure-sensitive Rydberg electron binding energies has several intriguing characteristics. Because the spectra are purely electronic in nature, meaning that the entire Franck-Condon envelope is enclosed in a narrow band, the spectra are quite insensitive toward internal energy. The method can therefore be used to explore molecules at high temperatures, or those undergoing chemical dynamics. The complexity of the spectra does not scale with the size of the molecule because the number of Rydberg states is determined by the radial and angular momentum quantum numbers of hydrogenic systems. As a result, the method can be applied to large molecules. And because the Rydberg electron encompasses the entire molecule the shape specificity covers the global molecular structure. Consequently, it is possible to distinguish isomeric and conformeric forms even of large molecules. Finally, it is straightforward to extend the method to the time-domain, thereby providing us with a uniquely capable tool for ultrafast structural dynamics experiments.

To implement Rydberg ionization spectroscopy we use a pump-probe multi-photon ionization/photoelectron scheme in which a first laser pulse excites the molecule to a Rydberg state, and a probe pulse ionizes the molecule. We observe the photoelectron spectrum using a time-of-flight instrument. The spectrum provides the binding energy of the electron, and thereby reveals the molecule's time-dependent structural fingerprint. The ultimate time resolution of the technique is given by the duration of the laser pulses, while the spectral resolution is limited by the bandwidth of the laser and/or the spectral resolution of the photoelectron spectrometer. To measure structural dynamics in Rydberg-excited states we insert a time delay in the ionization process. To measure the dynamics in ground or excited valence states we induce the dynamics using a near UV laser pulse, and use the entire multi-photon ionization scheme as a probe process.

2. Recent Progress

Ground state Recovery upon Electronic Curve Crossing

Electronic curve crossing reactions through conical intersections are important for their ability to open or close hydrocarbon rings, and may therefore be relevant to combustion phenomena. Upon electronic excitation, the molecules quickly cross over to a 2A state that brings them through a conical intersection to the ground state surface. We have been able to follow this path from the initial excitation to the ground state surface. The sensitivity of the Rydberg spectra coupled with their narrow line shapes even when large amounts of internal energy are present allows us to interpret the time-dependent spectra in terms of the structure of the molecules.

In the cyclopentadiene systems, we find that the crossing through the conical intersections gives rise to a ground state signal that is identical to the un-excited molecules. This implies that the original molecular structure is recovered after the crossing through the electronically excited states. In the cyclohexadiene systems, we observe that the crossing through the conical intersections leads to a depletion of the original structure, and the creation of a new structure. The spectral

signature of that new structure is very broad, see figure 1 (lower panel). This implies that there is a large structural dispersion: the molecules have so much internal energy that they can convert between different conformeric forms.¹ These transformations happen very rapidly, so that we see a broad spectrum over a large range of binding energies.

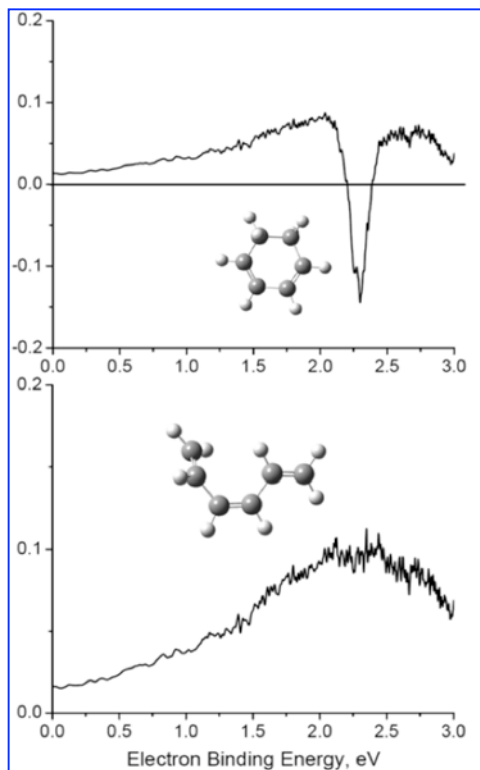


Figure 1: The pump-probe signal of cyclohexadiene after curve crossing. The dip is due to the depleted original structure. The broad band, lower panel, reflects the newly created open structure.

Conformer dynamics of hydrocarbon chains

Like all chemical reactions, conformeric transitions depend strongly on the potential energy landscape and the temperature at which the system is observed. We seek to explore conformational transformations in model systems under varying experimental conditions. Our measurements can serve as important benchmarks that can be compared to computational results. From the conformer distributions at the

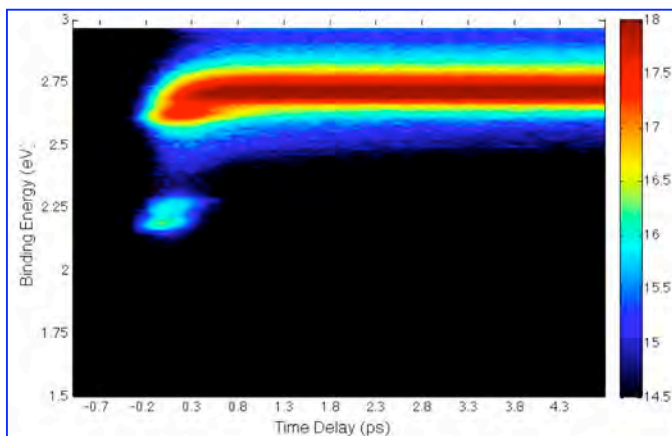


Figure 2: Time-dependent Rydberg photoelectron spectra of triethyl amine. Both the 3p peak at 2.25 eV and the 3s peak at 2.75 eV are split by the conformeric structures. The time dependence reveals the conformer transition kinetics.

beginning and the end of a reaction one can infer the relative depths of the minima in the potential landscape.

In tri-ethyl amine we observe a rapid internal conversion from 3p to 3s (figure 2). The initial conformer distribution in 3p reflects the structures present in the neutral ground state molecules (peaks at 2.25 eV). The molecules rapidly adjust their conformeric structure to reflect the planarity of the newly formed sp^2 hybridized ion core. By the time the molecules reach 3s (peaks at 2.7 eV), a new conformeric form is created that, after 1 ps, remains as the dominant geometry. The quickness of this kinetics, which is essentially complete within one picosecond, suggests that the barrier for the conformeric transition is quite small.

Sensitivity of Rydberg states toward Molecular Clustering

The typical diameter of even a low n Rydberg state such as the 3s state is on the order of 1.5 nm, much larger than molecular dimensions. As a result of this large size, the Rydberg electron can encompass an entire molecular cluster, at least for moderate cluster sizes. In our recent work we have found that the Rydberg electron binding energy is greatly depressed when a molecular ion core is clustered. For example, a 3s level of dimethyl isopropyl amine, with a binding of about 2.7 eV may get depressed to an electron binding energy of about 2.2 eV, see figure 3. This large depression arises from the shielding of the ion core's charge by the induced dipole moments of the ligand atoms and molecules. This shielding of course does not reduce the total net charge, which remains +1. However, it distributes the charge over a larger ion core volume, which has the net effect of shifting the charge outward and the Rydberg electron binding energy downward. We have observed the cluster binding energy shifts in several systems and are in the process of modeling the phenomena.

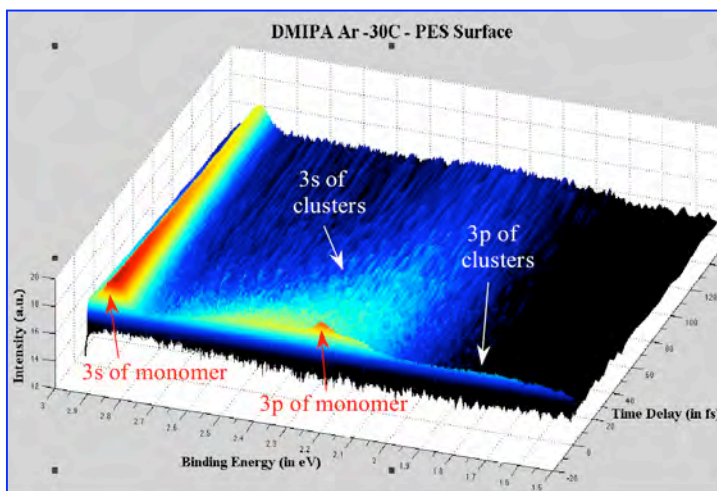


Figure 3: The time-dependent Rydberg level binding energy spectrum of N,N-dimethyl-isopropyl amine under conditions where molecular clusters form. In the clusters, the 3s and 3p Rydberg binding energies are shifted by about 0.6 eV.

This large depression arises from the shielding of the ion core's charge by the induced dipole moments of the ligand atoms and molecules. This shielding of course does not reduce the total net charge, which remains +1. However, it distributes the charge over a larger ion core volume, which has the net effect of shifting the charge outward and the Rydberg electron binding energy downward. We have observed the cluster binding energy shifts in several systems and are in the process of modeling the phenomena.

3. Future Plans

We will continue our explorations on the reaction dynamics of by focusing on model systems of relevance to combustion processes. This includes in particular the transitions between aliphatic conformeric forms, and the study of ring closing reactions of radicals.

We will also follow up on the solvation of van der Waals clusters by exploring the solvation dynamic processes.

4. Publications resulting from DOE sponsored research (2006 - 2009)

1. “Ground State Recovery and Molecular Structure upon Ultrafast Transition through Conical Intersections in Cyclic Dienes,” Fedor Rudakov and Peter M. Weber, *Chemical Physics Letters* 470, pp 187-190, (2009).
2. “Excited-state ions in femtosecond time-resolved mass spectrometry: An investigation of highly excited chloramines”, R. Y. Brogaard, N. Rusteika and T. I. Sølling, F. M. Rudakov and P. M. Weber, *J. Phys. Chem. A*, 2009, 113 (1), pp 40–43.
3. “Electronic Spectroscopy and Ultrafast Energy Relaxation Pathways in the lowest Rydberg States of Trimethylamine,” Job D. Cardoza, Fedor M. Rudakov and Peter M. Weber; *J. Phys. Chem. A*, 2008, 112 (43), pp 10736–10743.
4. “Identification of isomeric flame components by Rydberg ionization spectroscopy,” J. D. Cardoza, F. M. Rudakov, N. Hansen, P. M. Weber, *Journal of Electron Spectroscopy and Related Phenomena*, 65, 15–20 (2008).
5. “Resolved: Electronic states underneath broad absorptions,” J. D. Cardoza and P. M. Weber, *J. Chem. Phys.* 127, 036101 (2007).
6. “Ultrafast conformational dynamics in hydrocarbon chains,” Michael P. Minitti and Peter M. Weber, *Phys. Rev. Lett.*, 98, 253004 (2007).
7. “Spectroscopy and femtosecond dynamics of the ring-opening reaction of 1,3-cyclohexadiene,” N. Kuthirummal, F. M. Rudakov, C. Evans, and P. M. Weber, *J. Chem. Phys.* 125, 133307 (2006).
8. “Ultrafast time-resolved electron diffraction with megavolt electron beams,” J. B. Hastings, F. M. Rudakov, D. H. Dowell, J. F. Schmerge, J. Cardoza, J.M. Castro, S.M. Gierman, H. Loos, and P. M. Weber, *Appl. Phys. Lett.* 89, 184109 (2006).
9. “Rydberg Fingerprint Spectroscopy of Hot Molecules: Structural Dispersion in Flexible Hydrocarbons” M.P. Minitti, J.D. Cardoza and P.M. Weber, *J. Phys. Chem. A* 2006, 110, 10212-10218.
10. “The Ultrafast Photofragmentation Pathway of N,N-Dimethylisopropylamine,” M.P. Minitti, J.L. Gosselin, T.I. Sølling and P.M. Weber, *FemtoChemistry VII*, Ed. A. W. Castleman Jr & M. L. Kimble, Elsevier (2006) p. 44 - 48.
11. “Megavolt electron beams for ultrafast time-resolved electron diffraction,” F. M. Rudakov, J. B. Hastings, D. H. Dowell, J. F. Schmerge, and P. M. Weber, In “Shock Compression of Condensed Matter – 2005,” ed. M. D. Furnish, M. Elert, T. P. Russel, and C. T. White, American Institute of Physics (2006).
12. “Structure sensitive photoionization via Rydberg levels,” N. Kuthirummal and P. M. Weber, *J. Mol. Structure*, 787, 163 – 166 (2006).
13. “Energy Flow and Fragmentation Dynamics of N, N, Dimethyl-isopropyl amine,” Jaimie L. Gosselin, Michael P. Minitti, Fedor M. Rudakov, Theis I. Sølling and Peter M. Weber, *Journal of Physical Chemistry A*, 2006, 110, 4251-4255.

Probing Flame Chemistry with MBMS, Theory, and Modeling

T.J. Mountziaris, substitute PI for P. R. Westmoreland
Chemical Engineering Department, University of Massachusetts Amherst
Amherst, MA 01003-9330
tjm@ecs.umass.edu (westm@ecs.umass.edu)

I. Program Scope

Experimental and modeling research in this project is conducted by Prof. Phillip R. Westmoreland and his students. While he is on IPA leave from the university as an NSF program officer, I am his substitute PI, holding fiduciary responsibility during the period in which he is at NSF.

The objective of this research is obtaining kinetics of hydrocarbon combustion and molecular-weight growth in flames. Our approach combines molecular-beam mass spectrometry (MBMS) experiments on low-pressure flat flames; ab initio thermochemistry and transition-state structures; rate constants predicted by transition-state and chemical activation theories; and whole-flame modeling using mechanisms of elementary reactions.

MBMS is a particularly powerful technique because it can be used to measure a wide range of species quantitatively, including radicals, with minimal flame perturbation. By using two complementary instruments, we obtain remarkably complete sets of flame data that are useful for direct insights, testing of mechanistic models, and selected measurement of rate constants. Our electron-ionization quadrupole MS at UMass provides species profiles with high signal sensitivity and mass resolution. At the Advanced Light Source (ALS) at LBNL, we obtain species profiles with more precise isomer resolution and identification using time-of-flight MS with VUV photoionization. Professor Westmoreland co-developed this system with DOE-BES contractors Terry Cool, Andy McIlroy, Craig Taatjes, and Nils Hansen. Additional collaborators in making measurements include the group of Katharina Kohse-Höinghaus of Universität Bielefeld, while DOE-BES contractors Jim Miller, Stephen Klippenstein, Charlie Westbrook, and Fred Dryer have collaborated in modeling thermochemistry, kinetics, and flame structure.

II. Recent Progress

A. Data from the MBMS systems

Flames of a wide range of hydrocarbon and biomass-related fuels have been mapped by our team of researchers at the Advanced Light Source at Lawrence Berkeley National Laboratory in the past year:

- A series of fuel-rich ester flames, including ethyl formate, ethylacetate, methyl crotonate, methyl methyl propenoate, ethyl propenoate, methyl propanoate, ethyl propionate, methyl butanoate, methyl isobutanoate, methyl isobutyrate, methyl methacrylate, and methyl crotonate as model compounds for study of biofuel kinetics;
- Methylcyclohexane at $\phi=2.00$, positioning between our cyclohexane and toluene data;
- Tetrahydrofuran (THF) in a stoichiometric mixture as a cyclooxygenate;
- Dimethyl ether at $\phi=1.00, 1.20, 1.40, 1.60, 1.75, 2.0$ as a reference ether, complementing our earlier measurements;
- Ethylamine at $\phi=1.30$, again as a biofuel model compound;
- 1-Hexene at $\phi=1.00$ and 2.00 , complementing our cyclohexane data;
- Ethyne (acetylene) at $\phi=3.00$, targeting this key aromatics precursor and in a flame that provides more aromatics than the $\phi=2.41$ flame discussed below.

Temperature measurements for some of these flames were completed in our lab at UMass Amherst using Y_2O_3/BeO -coated, radiation-compensated Pt/Pt13%Rh thermocouples and others by Tina Kasper at Sandia using LIF. Mole-fraction profiles of these and prior flames have been or are being analyzed at UMass Amherst, Cornell, Sandia, and Bielefeld.

B. Modeling of DME, cyclohexane, ethyne, allene, and propyne flames reveals pathways.

Similar insights were obtained with recent modeling of our dimethylether, cyclohexane, ethyne, allene, propyne, and toluene flames. Some complementary data have been measured by Fei Qi and co-workers at the Chinese National Synchrotron Laboratory in a flame-sampling VUV-PI MBMS apparatus patterned after ours, and these data can also be used for model comparisons.

Dimethylether. DME is of interest as the simplest model compound for ethers. Our earlier work [8] and more recent publications [12,14] reveal that the dominant pathways are in line with what might be expected for the analogous alkane propane, modified for lack of H on the central heavy atom. The initial step is H-abstraction by OH, H, and O, forming a primary radical. This species beta-scissions to $\text{CH}_2\text{O} + \text{CH}_3$, and the subsequent pathways proceed as normal for these species. Blending DME into propene or ethanol into propene gives similar reductions of aromatics, but DME produces much less CH_3CHO than ethanol [12]. Combining data from the ALS system and an electron-ionization at Bielefeld with a model from collaboration with Dryer and co-workers of Princeton, we successfully modeled flames with a range of stoichiometries over $\phi=0.93, 1.16, 1.40, 1.63$ and 1.86 [14]. Minor channels appeared like homolytic thermal dissociation of DME to $\text{CH}_3\text{O} + \text{CH}_3$, but the dominant channels were little changed.

Cyclohexane. Benzene formation by cyclohexane dehydrogenation had been an interesting surprise in studying our stoichiometric cyclohexane flame [1], but in a fuel-rich flame ($\phi=2.0$), the more common $\text{C}_3\text{H}_3 + \text{C}_3\text{H}_3$ route via phenyl dominated. H-abstraction from the ring gave cyclohexyl in both cases, but the small amount of decomposition by H beta-scission to cyclohexene was much lower in the cooler $\phi=2.0$ flame. C_2H_2 thus formed more easily in the rich flame by beta-scissions and abstraction, and it reacted with CH_2 to form the C_3H_3 .

Ethyne. Fuel-rich flame studies of classical and newly measured ethyne flames show how the branching ratio of $\text{O} + \text{C}_2\text{H}_2$ between $\text{H} + \text{HCCO}$ and triplet $\text{CH}_2 + \text{CO}$ is critical to proper predictions, even at fuel-rich conditions. One reason is the impact of singlet CH_2 , which is formed from H plus the favored HCCO product of $\text{O} + \text{C}_2\text{H}_2$. As noted above, singlet CH_2 is an important precursor for C_3H_3 and thus aromatics. Growth to higher aromatics is an important part of this study. However, the uncertainties in C_3H_2 destruction chemistry have become much more important. Experimentally, C_3H_2 was identified in this $\phi=2$ flame as triplet propargylene, $\cdot\text{CH}=\text{C}=\text{CH}\cdot$, a finding that depends critically on the technique of synchrotron PI-MBMS. The UMass reaction set makes triplet C_3H_2 by abstraction, $\text{C}_3\text{H}_3 + \text{H} = \text{C}_3\text{H}_2 + \text{H}_2$, and destroys it by $\text{C}_3\text{H}_2 + \text{O}_2 = \text{H} + \text{CO} + \text{HCCO}$, compared to literature models that depend on $\text{CH} + \text{C}_2\text{H}_2 = \text{C}_3\text{H}_2 + \text{H}_2$ and destroys it by two overall reactions, $\text{C}_3\text{H}_2 + \text{O}_2 = \text{CO}_2 + \text{C}_2\text{H}_2$ or $\text{CO}_2 + \text{C}_2\text{H} + \text{H}$.

Allene and propyne. Fuel-rich flame studies [4] of these isomeric fuels have been complemented by stoichiometric studies [in review]. While $\text{C}_3\text{H}_3 + \text{C}_3\text{H}_3$ dominates benzene formation in the propyne flame, the allene flame also displays contributions from allyl + propargyl.

C. Morpholine modeling gave insights into mechanism and data.

Morpholine presented an interesting challenge: A fuel for which there was almost no kinetics or thermochemistry for constructing a flame mechanism. We had mapped a morpholine/ O_2 /Ar flame experimentally as a biofuel model compound, as it has heterocyclic ether and amine linkages. We created a reaction set that not only predicted its flame structure successfully, identifying the most important chemical pathways, but that also yielded insights into improving our data analysis.

Our mechanism were proposed in Publ. [12], starting from the fuel's cyclic $-\text{OCH}_2\text{CH}_2\text{NHCH}_2\text{CH}_2-$ molecular structure and constructing pathways with reactions analogous to those of alkanes. The radicals H, O, and OH were assumed to be present, as in alkane flames. Fuel destruction was then by H-abstraction from the C-H and N-H bonds in morpholine, followed by beta-scissions. Successive beta-scissions and abstraction steps would form a mix of C_2H_4 , $\text{CH}_2=\text{NH}$, CH_2O , C_2H_2 , HCN, CO, and their combustion reaction intermediates, as well as cyclohexane-route analogues of cyclohexene, 1,5-hexadiene, and 1,3-butadiene intermediates.

Moving beyond [12], we developed needed parameters for the reaction set. Thermochemistry came mainly from our CBS-QB3 quantum-chemistry calculations, and kinetics came from CBS-QB3 calculations or from transition-state analogies with our earlier cyclohexane model [1].

The initial predictive modeling of the flame was completed before the flame-profile data were analyzed, and we were pleased to see very good agreement with the data with the unadjusted prediction. The experimental morpholine/O₂ flame was slightly rich ($\phi=1.3$) with 25% Ar diluent, operated at 4.00 kPa and 0.33 m/s burner velocity (293 K). No temperature profile had yet been measured, so we used the cyclohexane flame's temperature profile for the modeling. Consider the major species (Fig. 1), which are largely within experimental uncertainties. The predicted profiles would be shifted slightly left or right by the position of the experimental temperature profile, which is used instead of solving an energy balance. The shift and final mole fractions will be altered somewhat by a different temperature profile, but shape, magnitude, and position were predicted remarkably well. Modeling also indicated important pathways.

The predicted N₂ profile was quite different from the initial data report, but here the prediction was of particular value. All fuel nitrogen had been assumed to go to N₂. However, the model predicted HCN and NO at significant levels as well as N₂. The combination of these species is a much better explanation.

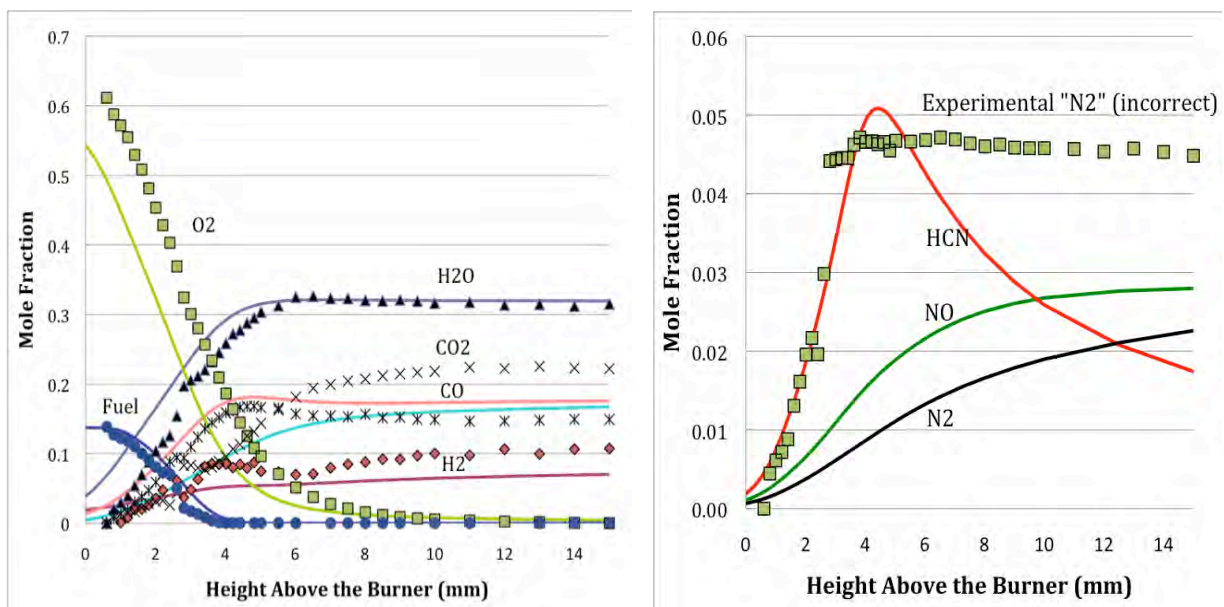


Figure 1. Experimental (symbols) and predicted (lines) mole-fraction profiles in a $\phi=1.3$ morpholine / O₂/25% Ar flame. [Left] Major species. [Right] Initial data analysis (symbols), treating all N-containing species as N₂, compared with predicted levels of HCN, NO, and N₂.

III. Future Work

We will conduct complementary experiments at UMass Amherst and at the ALS on flames of acetylene, benzene, toluene, and their mixtures along with modeling at UMass Amherst. The purpose is to establish formation and destruction chemistry of polycyclic aromatic hydrocarbons, using these fuels to focus on indene and naphthalene. The UMass system has a valuable role because it has higher signal sensitivity, especially for radicals, can be run at more fuel-rich conditions, and is more suitable for the thermocouple measurements. Professor Westmoreland will also continue to coordinate flame modeling for the research team, and we will participate in the team objectives of improving the mass and signal sensitivity of the ALS apparatus and of studying flame kinetics for other hydrocarbons, biofuel analogues, and amines.

IV. Publications and submitted journal articles supported by this project 2007-2009

1. M.E. Law, P.R. Westmoreland, T. A. Cool, J. Wang, N. Hansen, T. Kasper. "Benzene Precursors and Formation Routes in a Stoichiometric Cyclohexane Flame," *Proceedings of the Combustion Institute* **31**, 565-573 (2007); DOI: <http://dx.doi.org/10.1016/j.proci.2006.07.259>

2. T. A. Cool, J. Wang, N. Hansen, P. R. Westmoreland, F. L. Dryer, Z. Zhao, A. Kazakov, T. Kasper, K. Kohse-Höinghaus. "Photoionization mass spectrometry and modeling studies of the chemistry of fuel-rich dimethyl ether flames," *Proc. Combustion Institute* **31**, 285-293 (2007); DOI: <http://dx.doi.org/10.1016/j.proci.2006.08.044>
3. K. Kohse-Höinghaus, Patrick Oßwald, Ulf Struckmeier, T. Kasper, N. Hansen, C. A. Taatjes, J. Wang, T.A. Cool, S. Gon, P.R. Westmoreland. "The influence of ethanol addition on a premixed fuel-rich propene-oxygen-argon flame," *Proceedings of the Combustion Institute* **31**, 1119-1127 (2007); DOI: dx.doi.org/10.1016/j.proci.2006.07.007
4. N. Hansen, J.A. Miller, C. A. Taatjes, J. Wang, T.A. Cool, M.E. Law, P.R. Westmoreland. "Photoionization Mass Spectrometric Studies and Modeling of Fuel-Rich Allene and Propyne Flames," *Proc Combust Inst* **31**, 1157-64 (2007); dx.doi.org/10.1016/j.proci.2006.07.045
5. P. Oßwald, U. Struckmeier, T. Kasper, K. Kohse-Höinghaus, J. Wang, T.A. Cool, N. Hansen, P.R. Westmoreland, "Isomer-specific fuel destruction pathways in rich flames of methyl acetate and ethyl formate and consequences for the combustion chemistry of esters", *J. Phys. Chem. A* **111**(19), 4081-4092 (2007); dx.doi.org/10.1021/jp068337w
6. N. Hansen, T. Kasper, S.J. Klippenstein, P.R. Westmoreland, M.E. Law, C.A. Taatjes, K. Kohse-Höinghaus, J. Wang, T.A. Cool, "Initial steps of aromatic ring formation in a laminar premixed fuel-rich cyclopentene flame", *J Phys Chem A* **111**(19), 4093-4111 (2007); dx.doi.org/10.1021/jp0683317
7. C.A. Taatjes, N. Hansen, D.L. Osborn, K. Kohse-Höinghaus, T.A. Cool, P.R. Westmoreland. "Imaging' Combustion Chemistry via Multiplexed Synchrotron-Photoionization Mass Spectrometry." *Phys. Chem. Chem. Phys.* **10**, 20-34 (2008); dx.doi.org/10.1039/b713460f
8. N. Hansen, S.J. Klippenstein, P.R. Westmoreland, T. Kasper, K. Kohse-Höinghaus, J. Wang, T.A. Cool, "A Combined ab initio and Photoionization Mass Spectrometric Study of Polyynes in Fuel-Rich Flames," *Phy. Chem. Chem. Phys.* **10**, 366-374 (2008); dx.doi.org/10.1039/b711578d
9. J. Wang, U. Struckmeier, B. Yang, T. A. Cool, P. Osswald, K. Kohse-Höinghaus, T. Kasper, N. Hansen, P. R. Westmoreland, "Isomer-specific influences on the composition of reaction intermediates in dimethyl ether/propene and ethanol/propene flames," *J. Phys. Chem. A* **112**(39), 9255-9265 (2008); dx.doi.org/10.1021/jp8011188
10. N. Hansen, T. A. Cool, K. Kohse-Höinghaus, P. R. Westmoreland, "Recent Contributions of Flame-Sampling Molecular-Beam Mass Spectrometry to a Fundamental Understanding of Combustion Chemistry," *Prog. Energy Comb. Sci.* **35**(2) (2009) 168-191; dx.doi.org/10.1016/j.pecs.2008.10.001
11. C. K. Westbrook, W. J. Pitz, P. R. Westmoreland, F. L. Dryer, M. Chaos, Patrick Oßwald, K. Kohse-Höinghaus, T. A. Cool, J. Wang, B. Yang, N. Hansen, T. Kasper, "A Detailed Chemical Kinetic Reaction Mechanism for Oxidation of Four Small Alkyl Esters in Laminar Premixed Flames," *Proc. Combust. Inst.* **32** (2009) 221-228.
12. A. Lucassen, Patrick Oßwald, U. Struckmeier, K. Kohse-Höinghaus, T. Kasper, N. Hansen, T. A. Cool, P. R. Westmoreland, "Species identification in a laminar premixed low-pressure flame of morpholine as a model substance for oxygenated nitrogen-containing fuels," *Proc. Combust. Inst.* **32** (2009) 1268-1276.
13. N. Hansen, J. A. Miller, T. Kasper, K. Kohse-Höinghaus, P. R. Westmoreland, J. Wang, T. A. Cool, "Benzene Formation in Premixed Fuel-Rich 1,3-Butadiene Flames," *Proc. Combust. Inst.* **32** 623-630 (2009).
14. J. Wang, M. Chaos, B. Yang, T. A. Cool, F. L. Dryer, T. Kasper, N. Hansen, K. Kohse-Höinghaus, P. Oßwald, P. R. Westmoreland, "Composition of reaction intermediates for stoichiometric and fuel-rich dimethyl ether flames: Flame-sampling mass spectrometry and modeling studies," *Phys. Chem. Chem. Phys.* **11**, 1328-1339 (2009); dx.doi.org/10.1039/b815988b
15. T. Kasper, P. Oßwald, U. Struckmeier, K. Kohse-Höinghaus, C.A. Taatjes, J. Wang, T.A. Cool, M.E. Law, A. Morel, P.R. Westmoreland, "The combustion chemistry of the propanol isomers investigated by electron ionization and VUV-photoionization molecular-beam mass spectrometry," *Combustion and Flame* (accepted).

DAVID R. YARKONY

DEPARTMENT OF CHEMISTRY, JOHNS HOPKINS UNIVERSITY, BALTIMORE, MD 21218

yarkony@jhu.edu

Spectra obtained from optical and electron detachment methods are difficult to assign and interpret when they arise from states that are strongly coupled by conical intersections. The spin-orbit interaction further complicates matters. We have recently finished simulations of the photoelectron spectrum (PES) of isopropoxide and 1-propynide and are working on a similar calculation for ethoxide.

Photoelectron Spectra of States Strongly Coupled by Conical Intersections

The approach of choice for the calculation of these complex nonadiabatic spectra is the multimode vibronic coupling method. In order to simulate the spectra noted above we have developed and used state of the art techniques that greatly enhanced the power of the multimode vibronic coupling method. Very recently we have developed a normal equations based method for determining the requisite diabatic Hamiltonian that includes all second order terms in both the diagonal and all the coupling blocks and can include in the construction *ab initio* data from several regions of nuclear coordinate space to extend its domain of utility. This approach has facilitated our inclusion of nonabelian point group symmetry, which we have implemented for our study of 1-propynyl.

A. 1-Propynyl¹

1-propynyl, CH₃CC, can be viewed as acetylene, with one hydrogen replaced by a methyl group and the other hydrogen removed. The ground electronic state, which has C_{3v} symmetry is \tilde{X}^2A_1 and the lowest excited state is \tilde{A}^2E . See Fig. 1. The \tilde{X}^2A_1 state intersects the \tilde{A}^2E state, near its Jahn-Teller distorted minimum, ~2000 cm⁻¹ above the 2A_1 minimum. This intersection, which is one of three symmetry related seams of conical intersections, represents the intersection of two states of the same symmetry. The presence of not only the 2E_x - 2E_y conical intersection seam associated with the \tilde{A}^2E state, but also the three low-lying symmetry related 2A_1 - 2E seams of conical intersection, leads to significant nonadiabatic effects. Indeed the principal issue in our study was to quantify the

impact of the seams of conical intersection on the observed spectrum

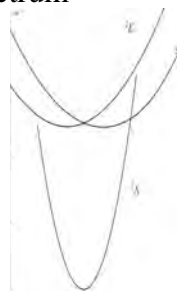


Figure 1 Schematic of the ground 2A_1 state and excited 2E state of 1-propynyl

Two experimental measurements of the spectrum of 1-propynyl are particularly relevant: a PES, Ref. ², denoted *LI-PES*; and a slow electron velocity-map imaging (SEVI) spectrum, Ref. ³, denoted *N-SEVI*.

Fig. 2 reports the simulated PES of 1-propynide, with the 2A_1 and 2E states uncoupled and compares the simulated spectrum to the measured results of *N-SEVI* and *LI-PES*. Here the height and position of the peak labeled A is scaled and positioned to agree with the peak identified in *N-SEVI* as the origin band. The lines to the red of the origin band are identified by *N-SEVI* as hot bands.

The simulated spectrum is comprised of two parts, one (blue lines) corresponds to the ejected electron leaving the molecule, 1-propynyl, in its ground 2A_1 state, and the second (green lines) corresponds to 1-propynyl in its 2E state.

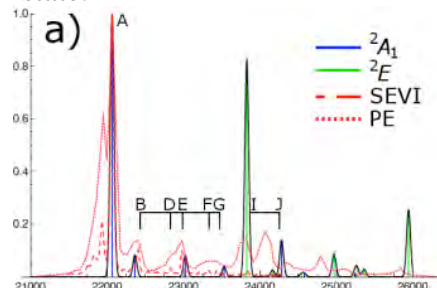


Figure 2: Simulated PES of 1-propynide neglecting the 2A_1 - 2E coupling. Here *N-SEVI* is denoted SEVI and *LI-PES* is denoted PE.

The low energy portion of the spectrum (between 22,000 cm⁻¹ and 23,500 cm⁻¹, the part due principally to the 2A_1 state) is in

reasonable agreement with the experimental results, both with regard to line positions and line intensities. This is not unexpected since the lowest energy 2A_1 - 2E conical intersection occurs at $\sim 23,800$ cm^{-1} on this energy scale. However, beyond this point agreement is poor reflecting the nonadiabatic effects due to the 2A_1 - 2E conical intersection seams.

Figure (3) compares the full nonadiabatic simulation with the results of *LI-PES*. The improvement in the intensities in the energy region greater than $\sim 23,000$ cm^{-1} is dramatic. The height of the peaks associated with the 2E state are dramatically reduced and they are spread out over this region by mixing with nominal 2A_1 vibrational levels. This is due principally to the interstate coupling induced by the 2A_1 - 2E conical intersection seams. In a time dependent picture as the wave packet enters this region on the 2E state potential energy surfaces, where in the absence of the 2A_1 - 2E conical intersection it would oscillate "creating" the intense discrete spectrum observed in Fig. 2, it is rapidly quenched to the 2A_1 state. This quenching is the principal factor leading to the absence of intense peaks in this region.

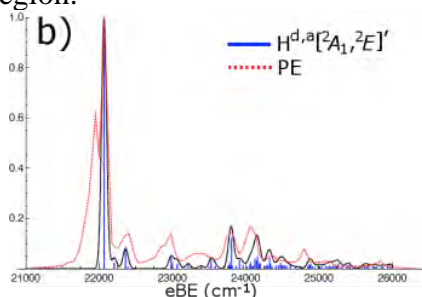


Figure 3: Simulated PES of 1-propynide including all nonadiabatic effects compared with the *LI-PES* results.

A second factor comes into play in determining the intensity of lines in the PES, the intrinsic photodetachment cross sections for ionizing 1-propynide and producing 1-propynyl in the 2A_1 or 2E states. Comparing the simulated and *LI-PES* intensities we deduced that the photodetachment cross section for producing the 2E state is $\sim 1/2$ that for the production of the 2A_1 state. This factor is included in the simulation reported in Fig. 3. In the absence of proper treatment of nonadiabatic effects a 2E state photodetachment cross section $\sim 1/10$ that of

the 2A_1 state would be required to explain the experimentally observed intensities.

Photodetachment cross sections are quite challenging to calculate owing to the fact that a free electron is produced. One of the goals of our future work will be the first principles determination of these quantities. The reliable estimates provided by the present calculations will provide valuable benchmarks.

B. Isopropoxy⁴

The isopropoxy radical, $(\text{CH}_3)_2\text{CHO}$ can be viewed as CH_3O , with two hydrogens replaced by methyl groups. In this case the 2E ground state of methoxy is split into a pair of states, nominally the $\tilde{X}{}^2A$ and $\tilde{A}{}^2A$ states. Two experimental investigations are particularly relevant to our first principles study: the negative ion PES of isopropoxide reported by Lineberger's group⁵, denoted *L2-PES* below; and the subsequent report of a dispersed fluorescence spectrum of the isopropoxy radical by Terry Miller's group⁶, denoted *M-DFS* below. As noted by *M-DFS*, a significant discrepancy between these two experiments is the inference of the \tilde{A} - \tilde{X} splitting in the isopropoxy radical.

Our calculations demonstrate the following: (i) The nominal \tilde{A} - \tilde{X} splitting reported by *M-DFS* is confirmed. (ii) The \tilde{A} - \tilde{X} splitting reported by *M-DFS* could not have been seen by *L2-PES* owing to the resolution of that experiment. (iii) The designation " \tilde{A} - \tilde{X} splitting" is a misnomer. That spectral feature is the spin-orbit induced splitting of two nearly degenerate vibronic levels. (iv) The near degeneracy results from a pseudo symmetry in which the \tilde{X} and \tilde{A} states behave like the components of a 2E state

Electronic structure calculations reveal the minimum energy point of conical intersection to be an accidental symmetry-allowed ${}^2A'$ - ${}^2A''$ intersection, \mathbf{Q}^{mex} . On the 1^2A potential energy surface, in the vicinity of \mathbf{Q}^{mex} , there are found, three minima \mathbf{Q}^{minj} , $j=1, 2, 3$ and three saddle points, \mathbf{Q}^{sj} , $j=1, 2, 3$. Key to understanding the significance of these findings is the use of intersection adapted coordinates, an orthogonal transformation of the internal coordinates, with a conical intersection as the origin. In intersection adapted coordinates, the x-coordinate points

along the direction of \mathbf{g} , the energy difference gradient vector, while the y-coordinate points along \mathbf{h} , the interstate coupling vector. These two coordinates define the branching or g - h plane. It is the explicit identification of the branching plane coordinates that gives intersection adapted coordinates their conceptual value. In the branching plane the degeneracy at the conical intersection is lifted linearly. Interestingly, we find $\|\mathbf{g}\| = 0.0211$ and $\|\mathbf{h}\| = 0.0210$. $\|\mathbf{g}\| = \|\mathbf{h}\|$ is what one would expect in a molecule with true C_{3v} symmetry.

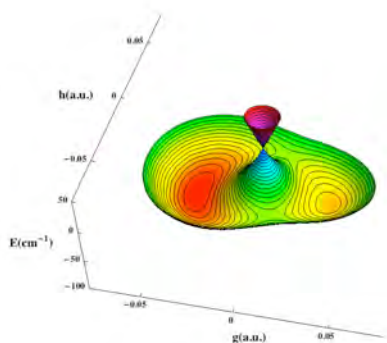


Figure 4(a) Cross section of the $1,2^2A$ potential energy surfaces in the g - h plane.

Figs. (4a) and (4b) present two representations of the adiabatic potential energy surfaces restricted to the branching plane. Fig. (4a) reports the energies $E_1(x,y)$ and $E_2(x,y)$ in a three dimensional plot, clearly depicting the conical intersection at Q^{mex} . Fig. (4b) presents $E_1(x,y)$ as a contour map. The locus of the projection of the three minima and three saddle points onto the branching plane is presented in Fig. (4b). From Fig. (4b) it is seen that the minima and saddle points reside (to a good approximation) on the vertices of equilateral triangles rotated 60° from each other. This arrangement of extrema in the g - h plane is a signature of a 2E conical intersection with significant second order terms. Thus we concluded that despite the absence of true C_{3v} symmetry the \tilde{X} and \tilde{A} states of isopropoxy closely resemble the degenerate components of a 2E state.

Figs. (5a), and (5b) compare our computed PES with the measured spectrum of $L2-PES$. As in the case of 1-propynyl, the height and position of (only) the peak labeled a is scaled

and positioned to agree with the experimental origin band. The agreement between the simulated and measured spectrum is seen to be excellent, except perhaps at the highest electron binding energies (eBEs) where the simulated spectrum somewhat over estimates the intensity.

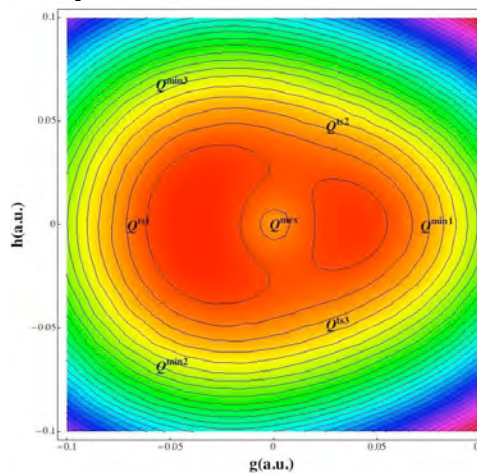


Figure 4(b) Contour map of the 1^2A potential energy surface in the g - h plane with the (projected) locations of the three minima (Q^{mini}), three saddle points (Q^{tsj}) and minimum energy conical intersection (Q^{mex}) indicated.

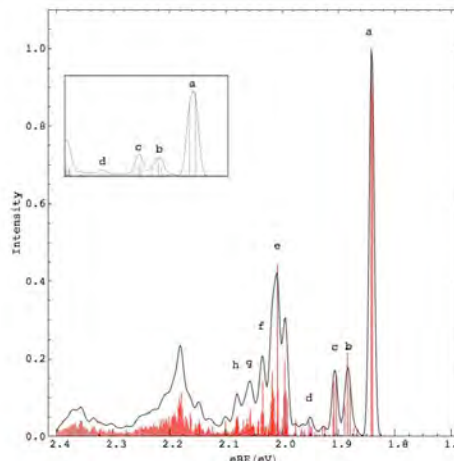


Figure 5(a): Simulated nonrelativistic PES of isopropoxy with lines broadened using 80 cm^{-1} gaussian convolution to simulate instrumental resolution of experimental spectrum of $L2-PES$. Inset gives low eBE relativistic spectrum using 80 cm^{-1} gaussian convolution.

A perusal of the simulated spectrum in this region shows that the peak labeled a is in fact two peaks separated by $\sim 17.7\text{ cm}^{-1}$. It is this feature which $M-DFS$ denote as the

$\tilde{A} - \tilde{X}$ splitting. While the computed splitting is much smaller than the $\tilde{A} - \tilde{X}$ splitting reported by *M-DFS*, analysis of the eigenvectors shows that these two vibronic states are largely the zero phonon states restricted to diabats 1 and 2 respectively. Thus these two levels are indeed related to an electronic splitting. The small separation is expected, since the two electronic states in question behave approximately like the components of a 2E state whose lowest two vibronic levels would be exactly degenerate in the nonrelativistic approximation.

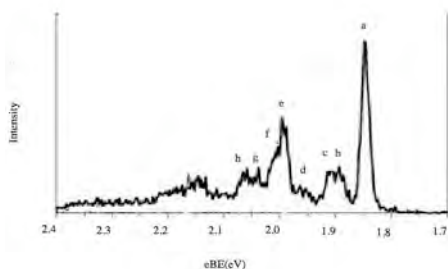


Figure 5b: *L2-PES* spectrum

The incorporation of the spin-orbit interaction (giving the relativistic spectrum) produces minor changes in the intensity patterns **except** for the two lines which comprise peak *a*. When the spin-orbit interaction is included, the separation of the first two peaks, the nominal $\tilde{A} - \tilde{X}$ splitting, increases to 60.6 (68) cm^{-1} in excellent agreement with the experimental

value of *M-DFS* given parenthetically. Finally we note that the $\tilde{A} - \tilde{X}$ splitting would not have been visible in the *L2-PES* experiment owing to the resolution available in that experiment. This is illustrated in the inset in Fig. (5) which shows the relativistic PES convoluted with a 80 cm^{-1} gaussian to simulate the *L2-PES* resolution. Only a single peak is evident at threshold in that inset.

Literature Cited

- ¹ B. N. Papas, M. S. Schuurman, and D. R. Yarkony, *J. Chem. Phys.* 130,064306 (2009).
- ² M. S. Robinson, M. L. Polak, V. M. Bierbaum, C. H. Depuy, and W. C. Lineberger, *J. Am. Chem. Soc.* 117, 6766 (1995).
- ³ J. Zhou, E. Garand, W. Einfeld, and D. M. Neumark, *J. Chem. Phys.* 127, 03430 (2007).
- ⁴ J. J. Dillon and D. R. Yarkony, *J. Chem. Phys.* (2009).
- ⁵ T. M. Ramond, G. E. Davico, R. L. Schwartz, and W. C. Lineberger, *J. Chem. Phys.* 112, 1158 (2000).
- ⁶ J. Jin, I. Sioutis, G. Tarczay, S. Gopalakrishnan, A. Bezanat, and T. A. Miller, *J. Chem. Phys.* 121, 11780 (2004).

PUBLICATIONS SUPPORTED BY DE-FG02-91ER14189: 2007 – present

1. *On the simulation of photoelectron spectra in molecules with conical intersections and spin-orbit coupling: The vibronic spectrum of CH_3S .* Michael S. Schuurman, Daniel E. Weinberg and David R. Yarkony, *J. Chem. Phys.* **127**, 104309,(12 pages)(2007)
2. *The Simulated Photoelectron Spectrum of 1-propynide.* Brian N. Papas, Michael S. Schuurman and David R. Yarkony, *J. Chem. Phys.* **130**, 064306 (12 pages) (2009)
3. *The Photoelectron Spectrum of the Isopropoxide Anion: Nonadiabatic Effects due to Conical Intersections and the Spin-orbit Interaction* Joseph J. Dillon and David R. Yarkony, *J. Chem. Phys.* **130**, (2009) to appear

Experimental Characterization of the Potential Energy Surfaces for Conformational and Structural Isomerization in Aromatic Fuels

Timothy S. Zwier

Department of Chemistry, Purdue University, West Lafayette, IN 47907-2084
zwier@purdue.edu

Program Definition and Scope

Gasoline and diesel fuels are complicated mixtures containing about 30% aromatics, including alkylbenzene, alkenylbenzene, and alkynylbenzenes of various chain lengths. The combustion of these molecules is influenced by their structural and conformational make-up, and by the rates of isomerization between them. The objective of this research program is to develop and utilize laser-based methods to characterize the spectroscopy and isomerization dynamics of conformational and structural isomers of aromatic derivatives that play a role in soot formation. As a first step in all these studies, UV-UV hole-burning and resonant ion-dip infrared (RIDIR) spectroscopy are being used to determine the number and identity of the isomers present, based on their ultraviolet and infrared spectral signatures. These structural studies then serve as a foundation for studies of the dynamics of conformational isomerization using stimulated emission pumping-population transfer (SEP-PT) spectroscopy (Figure 1a), a method developed by our group to directly measure the energy thresholds separating individual A→B reactant-product isomer pairs, thereby mapping out key stationary points on the multi-dimensional potential energy surface for isomerization. We are using these methods to study conformational isomerization in substituted benzenes spanning a range of types and degrees of conformational flexibility. From near-threshold intensity measurements we hope to explore the rate of isomerization relative to collisional cooling as a function of energy above threshold. These results can provide new tests of RRKM descriptions of isomerization in large molecules.

We have recently extended the population transfer methods to studies of structural isomerization, which require overcoming barriers significantly higher than those reached by SEP excitation. In UV-population transfer spectroscopy (Figure 1b), UV excitation occurs by counter-propagating the laser along a cooling channel affixed to the end of our pulsed valve, thereby allowing control over the number of cooling collisions simply by changing the time delay between pump and probe lasers. In this way, structural isomers absorbing an ultraviolet photon ($\sim 30,000\text{ cm}^{-1}$) and their products can be cooled to their zero-point levels prior to interrogation.

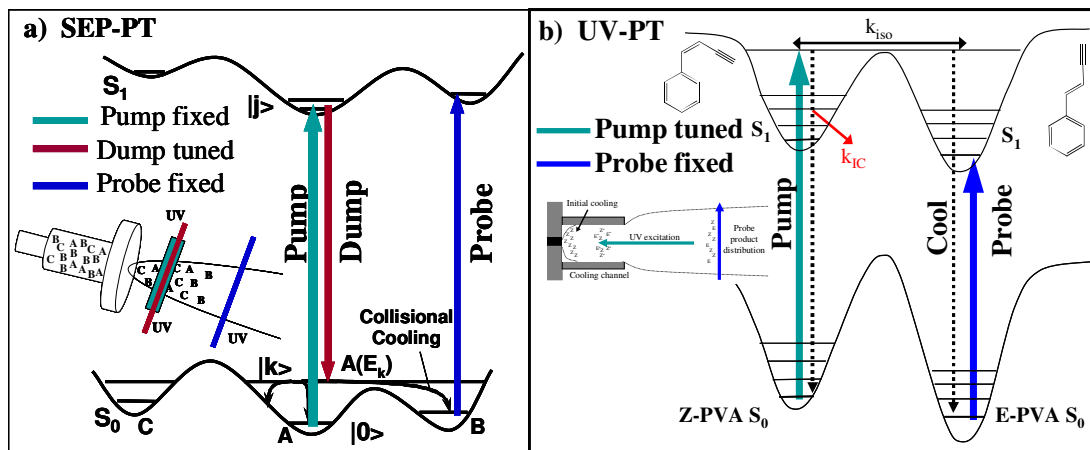


Figure 1: Schematic diagrams for SEP-PT and UV-PT spectroscopy.

Recent Progress

Over the past year, we have expanded our studies of the spectroscopy and the conformational isomerization dynamics of a series of aromatic derivatives of increasing conformational and structural complexity. Many of these studies have employed our new fluorescence-based chamber, which is pumped by a roots blower and thus is capable of the high gas throughput needed for hole-filling studies of conformational isomerization dynamics.

A. Isomerization in 5-phenyl-1-pentene

Two papers are currently in press on the single-conformation spectroscopy and conformational isomerization dynamics of 5-phenyl-1-pentene. Using rotational band contour and vibronic analysis, we have assigned transitions in the UV spectrum to five conformational isomers. SEP-PT spectroscopy (Fig. 1a) has been used to measure the energy thresholds to isomerization between 14 of the 20 X→Y reactant-product conformer pairs. The barriers are found to fall in one of two regimes: near 600 cm⁻¹ for hindered rotation of the vinyl group, and near 1200 cm⁻¹ for hindered rotation about the alkyl-alkyl C-C bonds in the pentene chain. This has the interesting consequence that pathways connecting all five observed conformers open up at 1200 cm⁻¹, associated with an ‘egg-carton’ like potential energy surface with many nearly iso-energetic minima and barriers connecting these minima that are all about the same height.

B. Internal State mixing in Diphenylmethane

Two papers on the spectroscopy and excited state internal mixing in diphenylmethane (C₆H₅-CH₂-C₆H₅, DPM) have been completed. This prototypical flexible bichromophore (with its model two-dimensional torsional surface) has fascinating spectroscopy associated with the two close-lying excited states of the two phenyl rings (with electronic origins split by only 123 cm⁻¹), in which the relative energy ordering and degree of electronic localization/delocalization depends sensitively on the relative orientation of the two phenyl rings.

We have completed a detailed study of the vibronic spectroscopy and high resolution UV spectroscopy of DPM-d₅. This is a collaborative effort with John Cable (BGSU) and David Plusquellic (NIST). By deuterating one of the phenyl rings, we partially localize the electronic excitation in S₁ and S₂. This changes both the vibronic intensities and rotational structure of the bands. The dispersed emission from the S₂(v) levels again show mixed excited state character.

C. Isomerization and vibrational cooling in bis-(2-hydroxyphenyl)methane

Two papers are currently in press describing the single-conformation rovibronic spectroscopy and SEP-PT conformational isomerization dynamics on bis-(2-hydroxyphenyl)methane, which has four flexible coordinates, two phenyl torsions and two OH torsions. Two conformational isomers are observed, one that possesses an OH···OH H-bond between the two rings, and the other two OH···π H-bonds in which the OH group on one ring H-bonds to the π cloud on the other ring. High resolution UV data (carried out in collaboration with D. Plusquellic at NIST) provide the transition dipole moment directions, and refine the structural assignments. Unusual intensity patterns in the dispersed fluorescence data highlight the extraordinary sensitivity of the transition dipole moment to the position and orientations of the two rings which cannot be accounted for by harmonic Franck-Condon analyses, even in the presence of Duschinsky mixing. SEP-population transfer (SEP-PT) spectroscopy has been used to measure the barriers to isomerization between these two isomers in both directions (E_{thresh} ~1400 cm⁻¹), thereby determining the relative energies of the two minima. The π-bound conformer is slightly lower in energy than the OH···O conformer (ΔE=14-123 cm⁻¹).

The long Franck-Condon progressions present in the OH \cdots O conformer have also been used to measure the per-collision efficiencies for vibrational cooling as a function of internal energy in the range from 30-1200 cm $^{-1}$. From this data set, three energy regimes were identified, each with a unique value of the average energy lost per collision with helium (region 1: 13 cm $^{-1}$ /collision for E=300-1200 cm $^{-1}$, region 2: 0.6 cm $^{-1}$ /collision for E=200-300 cm $^{-1}$, and region 3: 7 cm $^{-1}$ /collision for E<200 cm $^{-1}$). In region 1, the vibrational density of states is sufficient to support efficient loss of energy via $\Delta v=-1$ collisions involving the lowest frequency vibration of the conformer (with a frequency of 26 cm $^{-1}$). In region 2, the vibrational energy levels are sufficiently sparse that energy gaps exist, reducing the efficiency of relaxation. In region 3, a combination of the quantum nature of the helium, attractive forces, and orbiting resonances may be responsible for the increased efficiency at lowest energy regime. Since these rates occur in competition with isomerization, we have used this data to place bounds on the isomerization rate at threshold.

D. Ongoing work

In bis-(4-hydroxyphenyl)methane, we are in the midst of a detailed study of its conformational isomerization dynamics, using SEP-PT spectroscopy. Three conformational isomers are observed, which differ in the orientation of the two OH groups in the para positions on the phenyl rings. This will be an ideal system in which to probe the barriers, pathways, and isomerization rates under conditions in which the barriers to isomerization are exceedingly small (<100 cm $^{-1}$), as indicated by the data we are just acquiring. Under such conditions, it is clear that statistical theories are no longer appropriate, and we will search carefully for mode-specific and conformation-specific effects in the isomerization.

We are also in the midst of studies of the single-conformation spectroscopy on two of the three monomers that make up lignin, one of the most abundant biopolymers on earth. Lignin is an aromatic biopolymer that encapsulates the sugars that can serve as biofuels in plants, providing the needed structural rigidity for the plant to grow. These lignin monomers, p-coumaryl alcohol and p-coniferyl alcohol, are starting points for larger lignin oligomers that we think can be studied effectively by our methods.

Finally, we have recently successfully demonstrated UV-population transfer spectroscopy (Figure 1b) as a means to study structural isomerization, here involving isomerization between E- and Z-isomers of phenylvinylacetylene. The combined data from R2PI, UV-holeburning, UV depletion, and UV-population transfer spectra is being analyzed to understand the photophysical and photochemical pathways involved, and the sharp thresholds observed.

Publications acknowledging DOE support, 2007-present

1. Talitha M. Selby, W. Leo Meerts, and Timothy S. Zwier, "Isomer-specific Ultraviolet Spectroscopy of *meta*- and *para*-divinylbenzene", *J. Phys. Chem. A* **111**, 3697-3709 (2007).
2. Talitha M. Selby and Timothy S. Zwier, "Flexing the muscles of Divinylbenzene: Direct measurement of the barriers to conformational isomerization", *J. Phys. Chem. A* **111**, 3710-3718 (2007).
3. Nathan R. Pillsbury, Timothy S. Zwier, Richard H. Judge, Stephen Drucker, "Jet-cooled phosphorescence excitation spectrum of the $T_1(n,\pi^*) \leftarrow S_0$ transition of 2-cyclopenten-1-one", *J. Phys. Chem. A* **111**, 8357-8366 (2007).
4. Nathan R. Pillsbury, Jaime A. Stearns, Alope Das, Talitha M. Selby, David F. Plusquellic, and Timothy S. Zwier, "State-specific studies of Internal Mixing in a Prototypical Flexible Bichromophore: Diphenylmethane", *J. Chem. Phys.* **129** 114301 (2008).
5. Jaime A. Stearns, Nathan R. Pillsbury, Christian W. Müller, Kevin O. Douglass, Timothy S. Zwier, and David F. Plusquellic, "Rotationally resolved studies of S_0 and the exciton coupled S_1/S_2 origin regions of diphenylmethane and its d_{12} isotopologue", *J. Chem. Phys.* **129**, 224305 (2009).
6. Nathan R. Pillsbury and Timothy S. Zwier, "Conformation-specific spectroscopy and excited state photophysics of 5-phenyl-1-pentene", *J. Phys. Chem. A* **113**, 118-125 (2009).
7. Nathan R. Pillsbury and Timothy S. Zwier, "Conformational isomerization of 5-phenyl-1-pentene probed by SEP-population transfer spectroscopy", *J. Phys. Chem. A* **113**, 126-134 (2009).
8. Nathan R. Pillsbury, Christian W. Muller, and Timothy S. Zwier, "Conformational Effects on Excitonic Interactions in a Prototypical H-bonded Bichromophore: Bis(2-hydroxyphenyl)methane", *J. Phys. Chem. A* (in press).
9. Nathan R. Pillsbury and Timothy S. Zwier, "The Conformational Isomerization and Collisional Cooling Dynamics of Bis-(2-hydroxyphenyl)methane", *J. Phys. Chem. A* (in press).

Participant List

30th Annual Combustion Research Meeting Participation List

Last Name	First Name	Organization	Email
Ahmed	Musahid	Lawrence Berkeley National Laboratory	mahmed@lbl.gov
Allen	Wesley	University of Georgia	wdallen@uga.edu
Baer	Tomas	University of North Carolina	baer@unc.edu
Barlow	Robert	Sandia National Laboratories	barlow@sandia.gov
Bowman	Joel	Emory University	jmbowma@emory.edu
Braams	Bastiaan	Emory University	bbraams@emory.edu
Brown	Nancy	Lawrence Berkeley National Laboratory	NJBrown@lbl.gov
Butler	Laurie	The University of Chicago	L-Butler@uchicago.edu
Casassa	Michael	Office of Basic Energy Sciences, U.S. Department of Energy	michael.casassa@science.doe.gov
Chandler	David	Sandia National Laboratories	mrtargo@sandia.gov
Chen	Jacqueline	Sandia National Laboratories	jhchen@sandia.gov
Continetti	Robert	UC San Diego, Dept. of Chemistry and Biochemistry	rcontinetti@ucsd.edu
Cool	Terrill	Cornell University	tac13@cornell.edu
Crim	Fleming	University of Wisconsin-Madison	fcrim@chem.wisc.edu
Davis	Michael	Argonne National Laboratory	davis@tcg.anl.gov
Davis	Floyd	Cornell University	hfd1@cornell.edu
Ervin	Kent M.	University of Nevada, Reno	ervin@unr.edu
Field	Robert	MIT	rwfield@mit.edu
Flynn	George	Columbia University	gwf1@columbia.edu
Frank	Jonathan	Sandia National Laboratories	jhfrank@sandia.gov
Frenklach	Michael	UC Berkeley	myf@me.berkeley.edu
Green	William	MIT/Department of Chemical Engineering	balkwill@mit.edu
Guo	Hua	University of New Mexico	hguo@unm.edu

Hall	Gregory	Brookhaven National Laboratory	gehall@bnl.gov
Hansen	Nils	Sandia National Laboratories	nhansen@sandia.gov
Hanson	Ronald	Stanford University	rkhanson@stanford.edu
Harding	Lawrence	Argonne National Laboratory	harding@anl.gov
Harris	Alexander	Brookhaven National Laboratory	alexh@bnl.gov
Head-Gordon	Martin	Lawrence Berkeley National Laboratory	mhg@bastille.cchem.berkeley.edu
Hershberger	John	North Dakota State University	john.hershberger@ndsu.edu
Hirata	So	University of Florida	hirata@qtp.ufl.edu
Hoffmann	Mark	University of North Dakota	mhoffmann@chem.und.edu
Jasper	Ahren	Sandia National Laboratories	ajasper@sandia.gov
John	Kiefer	Univ. Ill. at Chicago	kiefer@uic.edu
Kaiser	Ralf	University of Hawaii at Manoa	ralfk@hawaii.edu
Kellman	Michael	University of Oregon	kellman@uoregon.edu
Kerstein	Alan	Sandia National Laboratories	arkerst@sandia.gov
Kirchhoff	William	NIST/DOE retired	william.kirchhoff@post.harvard.edu
Klippenstein	Stephen	Argonne National Laboratory	sjk@anl.gov
Kohse-Hoeinghaus	Katharina	Bielefeld University	kkh@pc1.uni-bielefeld.de
Krylov	Anna	University of Southern California	krylov@usc.edu
Leone	Stephen	Lawrence Berkeley National Laboratory	srl@berkeley.edu
Lester	Marsha	University of Pennsylvania	milester@sas.upenn.edu
Lester Jr.	William	Lawrence Berkeley National Laboratory	WALester@lbl.gov
Lucht	Robert	Purdue University	Lucht@purdue.edu
Macdonald	Robert	Argonne National Laboratory	rgmacdonald@anl.gov
Marceau	Diane	Department of Energy	diane.marceau@science.doe.gov
Matsika	Spiridoula	Temple University	smatsika@temple.edu
McIlroy	Andy	Sandia National Laboratories	mrtargo@sandia.gov
Mebel	Alexander	Florida International University	mebela@fiu.edu
Michael	Joe	Argonne National Laboratory	jmichael@anl.gov

Michelsen	Hope	Sandia National Laboratories	hamiche@sandia.gov
Miller	William H.	Lawrence Berkeley National Laboratory	millerwh@berkeley.edu
Miller	Terry	Ohio State University	tamiller@chemistry.ohio-state.edu
Miller	James	Sandia National Laboratories	jamille@sandia.gov
Muckerman	James	Brookhaven National Laboratory	muckerma@bnl.gov
Mullin	Amy	University of Maryland	mullin@umd.edu
Najm	Habib	Sandia National Laboratories	hnnajm@sandia.gov
Nesbitt	David	University of Colorado, JILA	djn@jila.colorado.edu
Neumark	Daniel	University of California at Berkeley	dneumark@berkeley.edu
Ng	Cheuk-Yiu	University of California, Davis	cyng@chem.ucdavis.edu
Oefelein	Joseph	Sandia National Laboratories	oefelei@sandia.gov
Oehlschlaeger	Matt	Renssekaer Polytechnic Institute	oehism@rpi.edu
Osborn	David	Sandia National Laboratories	dlosbor@sandia.gov
Pederson	Mark	Office of Basic Energy Sciences, U.S. Department of Energy	mark.pederson@science.doe.gov
Perry	David	The University of Akron	dperry@uakron.edu
Piecuch	Piotr	Michigan State University	piecuch@chemistry.msu.edu
Pitz	William	Lawrence Livermore National Laboratory	pitz1@llnl.gov
Pope	Stephen	Cornell University	s.b.pope@cornell.edu
Pratt	Stephen	Argonne National Laboratory	stpratt@anl.gov
Rahn	Larry	Office of Basic Energy Sciences, U.S. Department of Energy	larry.rahn@science.doe.gov
Reisler	Hanna	University of Southern California	reisler@usc.edu
Rohlfing	Eric	Office of Basic Energy Sciences, U.S. Department of Energy	eric.rohlfing@science.doe.gov
Rouson	Damian	Sandia National Laboratories	rouson@sandia.gov
Ruedenberg	Klaus	Ames Laboratory	ruedenberg@iastate.edu
Ruscic	Branko	Argonne National Laboratory	ruscic@anl.gov
Schaefer	Henry	University of Georgia	sch@uga.edu
Sears	Trevor	Brookhaven National Laboratory	sears@bnl.gov
Settersten	Thomas	Sandia National Laboratories	tbsette@sandia.gov

Shepard	Ron	Argonne National Laboratory	shepard@tcg.anl.gov
Sisk	Wade	Office of Basic Energy Sciences, U.S. Department of Energy	wade.sisk@science.doe.gov
Smooke	Mitchell	Yale University	mitchell.smooke@yale.edu
Stanton	John	University of Texas at Austin	jfstanton@gmail.com
Suits	Arthur	Wayne State University	asuits@chem.wayne.edu
Taatjes	Craig	Sandia National Laboratories	cataatj@sandia.gov
Thompson	Donald	University of Missouri - Columbia	thompsondon@missouri.edu
Tishkoff	Julian	Air Force Office of Scientific Research	julian.tishkoff@afosr.af.mil
Tranter	Robert	Argonne National Laboratory	tranter@anl.gov
Truhlar	Donald	University of Minnesota	truhlar@umn.edu
Tsang	Wing	National Institute of Standards and Technology	wing.tsang@nist.gov
Valeev	Edward F.	Virginia Tech	evaleev@vt.edu
Vasudevan	Venkatesh	ExxonMobil Research and Engineering	venkatesh.vasudevan@exxonmobil.com
Violi	Angela	University of Michigan	avioli@umich.edu
Wagner	Albert	Argonne National Laboratory	wagner@anl.gov
Weber	Peter	Brown University	Peter_Weber@brown.edu
Weber	J. Mathias	University of Colorado-Boulder	weberjm@jila.colorado.edu
Westmoreland	Phillip	University of Massachusetts Amherst	westm@ecs.umass.edu
Wittig	Curt	University of Southern California	wittig@usc.edu
Yarkony	David	Johns Hopkins University	yarkony@jhu.edu
Yu	Hua-Gen	Brookhaven National Laboratory	hgy@bnl.gov
Zwier	Timothy	Purdue University	zwier@purdue.edu